



UNIVERSITY OF

LIVERPOOL

Synthesis, Computational and Biological
Evaluation of Novel Compounds for the
Treatment of *Cryptococcus neoformans*

Thesis submitted in accordance with the requirements of the

University of Liverpool

For the degree of

Doctor in Philosophy

By

Gina Washbourn

July 2019

Declaration

This thesis is the result of my own work. The results contained within this thesis unless otherwise stated are my own. The material contained within this document has not been presented, or is currently being presented either wholly or in part of any other degree or qualification.

Gina Washbourn

This research was carried out at the University of Liverpool, Department of Chemistry

Acknowledgments

My PhD has taken what feels like a cast of thousands (too much coffee and weight gain) and whilst I'd love to mention everyone by name, that would be a book in itself! So, I'll start by saying thank you to everyone who helped me along the way!

I'd like to start by saying a massive thank you to my two supervisors Gemma Nixon and Neil Berry, for all of their support and advice, both chemical and personal. Thank you for giving me the opportunity to do my PhD and for listening to all of my ideas ... no matter how crazy. I would also like to say thank you to Paul O'Neill, Emma Shore, Neil Kershaw and Shirley Leung for all of their help solving all my chemistry problems and letting me know I was heading the right way.

A big thank you goes to all of the past and present members of the fourth floor, but particularly Mike, Nathan, Sean, Rachel, Chris, Nham, Pye, Paul M, Jack, Sophie, Josh, Monika, Nada, Charlie and Liqun for all the laughter and help you have given me. Your support, biscuits, cake and alcohol have kept me going the past 4 years and longer. Thank you for also agreeing to look over drafts of my thesis (bet you regret that now!). Also have to thank Konstantin for all of his NMR help, but mainly for helping feed my caffeine addiction.

Many thanks go to the Biology team who have run endless amounts of biological assays, and even tried to teach me how to do them! I am no biologist that's for sure! So, huge thankyou to Suzy Gore.

Big thanks to all of the people who have help me with the extra opportunities through my PhD such as my outreach and teaching, which have not only made my PhD more fun, but helped with how I carried out my research and gave me much more confidence teaching. Huge thanks here go to Gita, Helen, Cate, Lynne and Chris!

Finally, my biggest source of thanks goes to my family, perhaps my biggest supporters on this whole journey. Big thanks to my sisters, yes, I have four of them, Emma, Louise, Lorrain and Angela, who make my feel so proud every day. To my Aunty Joy and Uncle Dave who have fed me with an endless supply of bacon butties and cheesy chemistry jokes! But my biggest thanks go to Will, my best friend and partner. His support over the last 10 years has been unwavering, no matter the difficulties we have faced, I could not have completed this without him. I suppose I should also thank my cats Diego and Leo, for the 5:30 am wake up calls, but mostly for making me so happy.

My final thanks go to my Mum and Dad, the most inspiring people I have ever had the pleasure of knowing, and I know how proud you would be of us all. Thank you for teaching me to always look of the bright side of life (yes, the Monty Python version!). I love you and this PhD is all for you!

Abstract

Cryptococcus neoformans is a yeast like fungal pathogen that is relatively unknown despite causing large numbers of deaths per year. It is a disease that is prevalent in sub-Saharan Africa where the highest rate of deaths occur, at around 500,000 per year. It is particularly deadly in patients who are immunocompromised, such as those suffering from AIDS. This can lead to meningitis and encephalitis which often results in death. Current therapies are outdated and present with many issues surrounding their toxicity, efficacy and potential for resistance to emerge. *C. neoformans* as a pathogen is well adapted to the host environment, which means designing novel therapies is challenging.

Recently, focus has turned to developing novel therapies that have new mechanisms of action compared to traditional *C. neoformans* treatments. The benzimidazoles, the initial and main focus of this project, were discovered when a small number of analogues were screened against clinical isolates of *C. neoformans* and some were found to possess excellent biological activity of 0.015 - >4 mg/L. This was coupled with *in vivo* work, demonstrating the commercially available anti-helminth drug flubendazole, possessed biological activity in a mouse model (3.7 log drop in CFU when dosed at 150 mg/kg). This provided a good starting point for the project, with a large number of analogues that could be synthesised to explore the SAR. It was known that flubendazole possesses poor aqueous solubility (0.3 µM) and shows some toxicity issues due to lack of selectivity for the *C. neoformans* target versus the human protein. Extensive work has been carried out on four benzimidazole sub-templates to improve the solubility profile of this class, with some success. The lead compound, a morpholine ether derivative, has an MIC of 0.25 mg/L, *in vivo* activity showing over a 3 log drop in fungal density when dosed at 150 mg/kg orally. It also possesses an improved DMPK profile, with an aqueous solubility of 10 µM. Furthermore, detailed homology model evaluation has allowed us to understand the difference between *C. neoformans* and human targets, to allow for rationale design of selective compounds to improve the toxicology profile. Additionally, two other templates were identified; the benzisothiazolinones (BIZT) and the benzoxaboroles. A number of analogues from the BIZT class were synthesised, but showed poor activity (2 - >4 mg/L) and metabolic stability (>300 µl/min/mg in rat hepatocytes), but a reliable synthetic route was established. The benzoxaboroles were synthetically more challenging, thus only a few compounds were made and biological activity so far has been limited (0.25 - >4 mg/L), but work is ongoing to design more.

Publications

Published

Repurposing and Reformulation of the Antiparasitic Agent Flubendazole for Treatment of Cryptococcal Meningoencephalitis, a Neglected Fungal Disease

Gemma L. Nixon, Laura McEntee, Adam Johnson, Nicola Farrington, Sarah Whalley, Joanne Livermore, Cristien Natal, Gina Washbourn, Jaclyn Bibby, Neil Berry, Jodi Lestner, Megan Truong, Andrew Owen, David Laloo, Ian Charles, William Hope. *Antimicrob. Agents Chemother.*, **2018**, 62 (4) e01909-17; DOI: 10.1128/AAC.01909-17

In Progress

Synthesis and Biological Assessment of the Benzisothiazolinone Class for Treatment of the Fungal Infection *Cryptococcus neoformans*

Gina Washbourn, Matthew Pye, Caroline Vermeiren, Suzy Gore, Neil Berry, Paul O'Neill and Gemma Nixon. Submitting to *Future Med. Chem.*

Design, Synthesis and Biological Evaluation of Benzimidazoles for Treatment of the Fungal Infection *Cryptococcus neoformans*

Gina Washbourn, Emma Shore, Rachel Crick, Ryan McBerney, Benjamin Roberts, Emma McEwan, Leanne Riley, Suzanna Gore, Laura McEntee, Adam Johnson, Nicola Farrington, William Hope, Jaclyn Bibby, Neil Berry, Gemma Nixon. Submitting to *J. Med. Chem.*

Identification and Profiling of Benzimidazole Ether Derivatives; Towards a Treatment for the Fungal Infection *Cryptococcus neoformans*

Gina Washbourn, Emma Shore, Rachel Crick, Sophie Pate, Monika Lisauskaite, Lauren Gorman, Natasha Hatton, Suzanna Gore, Laura McEntee, Adam Johnson, Nicola Farrington, William Hope, Jaclyn Bibby, Neil Berry, Gemma Nixon

Stabilization of A4V mutant dimer: Development of ebselen for motor neuron disease therapy using co-crystallography

Varunya Chantadol , Gareth S.A. Wright , Kangsa Amporndanai , Munazza Shahid , Svetlana V Antonyuk , Gina Washbourn , Michael Rogers , Natalie Roberts , Mathew Pye , Paul M. O'Neill , S Samar Hasnain. Submitted to *Nat. Comms.*

Contents

Acknowledgements	iii
Abstract	iv
Publications	v
Abbreviations	vii
Chapter 1 – An Introduction to <i>C. neoformans</i>	1
1.1 <i>C. neoformans</i> History and Discovery	2
1.1 <i>C. neoformans</i> Taxonomy	2
1.3 <i>C. neoformans</i> Ecology	3
1.4 <i>C. neoformans</i> Epidemiology	4
1.5 <i>C. neoformans</i> Pathogenesis and Host Response	5
1.6 <i>C. neoformans</i> Life Cycle	6
1.6.1 Mating	6
1.6.2 Monokaryotic Fruiting	7
1.7 <i>C. neoformans</i> C. neoformans Virulence	7
1.7.1 Capsule	8
1.7.2 Melanin Formation	9
1.7.3 Growth at Mammalian Body Temperature	9
1.7.4 Degradation Enzymes	10
1.8 <i>C. neoformans</i> Current Treatments	10
1.8.1 Amphotericin B	10
1.8.2 Fluconazole	13
1.8.3 Flucytosine	15
1.9 <i>C. neoformans</i> Ideal Drug Candidate	17
1.10 Current <i>C. neoformans</i> Research	18
1.11 Project Aims	21
1.12 References	22
Chapter 2 – An Overview of the Benzimidazoles – Properties and Medicinal Uses	26
2.1 Benzimidazole Structure, Properties and Reactivity	27
2.1.1 Structure	27
2.1.2 Tautomerisation	27
2.1.3 Chemical Reactivity	28
2.1.4 Historical Synthesis of Benzimidazoles	30
2.2 Benzimidazoles as Medicines	30
2.2.1 Current Benzimidazole Containing Compounds	30
2.2.2 Benzimidazoles as Plant Fungicides	31
2.2.3 Benzimidazoles as Antihelminthics	32
2.2.4 Benzimidazoles as Antifungals	32
2.2.5 Initial SAR of Benzimidazole Analogues Against <i>C. neoformans</i>	33
2.3 Benzimidazoles and β -tubulin	34
2.3.1 Microtubule Structure and Function	34
2.3.2 Benzimidazole Mode of Action	35
2.4 Benzimidazole Metabolism	37
2.4.1 Flubendazole Metabolism	37
2.4.2 Albendazole and Fenbendazole Metabolism	38
2.5 This Project: The Benzimidazole Core	39

2.6 References	41
Chapter 3 – Synthesis and Biological Evaluation of Benzimidazole Thioether Derivatives	43
3.1 Benzimidazole Thioethers	44
3.2 Thioether Results and Discussion	45
3.2.1 Synthesis	45
3.2.1.1 Nucleophilic Aromatic Substitution	46
3.2.1.2 Tin (II) Chloride Nitro Group Reduction	46
3.2.1.3 Acid Mediated Ring Closure	47
3.2.2 Biological Data	49
3.2.3 Biological Activity	50
3.2.4 DMPK Data	52
3.2.4.1 Predicted DMPK	52
3.2.4.2 Measured DMPK	54
3.2.5 <i>In Vivo</i> Mouse Data	57
3.3 Conclusions	58
3.4 Future Work	58
3.5 Experimental	59
3.5.1 General Experimental Details	59
3.5.2 General Procedures	60
3.6 References	79
Chapter 4 – Synthesis and Biological Evaluation of Benzimidazole Ether Derivatives	80
4.1 Benzimidazole Ether Derivatives	81
4.2 Ether Results and Discussion	82
4.2.1 Synthesis	82
4.2.1.1 Nucleophilic Aromatic Substitution	82
4.2.1.2 Tin (II) Chloride Nitro Group Reduction	83
4.2.1.3 Acid Mediated Ring Closure	84
4.2.1.4 Compound Scale-Up	84
4.2.2 Biological Activity	85
4.2.3 DMPK	87
4.2.3.1 Predicted DMPK	87
4.2.3.1 Measured DMPK	88
4.2.4 <i>In Vivo</i> Mouse Data	89
4.3 Morpholine Ether Results and Discussion	90
4.3.1 Synthesis	91
4.3.1.1 Nucleophilic Substitution Reaction	91
4.3.1.2 Nucleophilic Aromatic Substitution	93
4.3.1.3 Tin (II) Chloride Nitro Group Reduction	94
4.3.1.4 Acid Mediated Ring Closure	94
4.3.3 Compound Scale-Up	96
4.3.4 Biological Activity	96
4.3.5 DMPK Data	98
4.3.5.1 Predicted DMPK	98
4.3.5.2 Measured DMPK	98
4.3.6 <i>In Vivo</i> Mouse Data	100
4.4 Conclusion	103
4.5 Future Work	103
4.6 Experimental	105
4.7 References	123

Chapter 5 – Synthesis and Biological Evaluation of Benzimidazole Ketone Derivatives	124
5.1 Benzimidazole Ketones	125
5.2 Ketone Results and Discussion	126
5.2.1 Synthesis	126
5.2.1.1 Previous Synthesis	126
5.2.1.2 Current Synthesis	129
5.2.1.2.1 Synthesis of Activated Pyridyl Ester	130
5.2.1.2.2 Pyridyl Ester Suzuki Coupling	131
5.2.1.2.3 Tin (II) Chloride Nitro Group Reduction	133
5.2.1.2.4 Acid Mediated Ring Closure	133
5.2.2 Biological Activity	134
5.2.3 DMPK	134
5.2.3.1 Predicted DMPK	135
5.2.3.2 Measured DMPK	136
5.2.4 <i>In Vivo</i> Mouse Data	137
5.4 Conclusion	141
5.5 Future Work	141
5.6 Experimental	142
5.7 References	154
Chapter 6 - Synthesis and Biological Evaluation of Benzimidazole Biphenyl Derivatives	155
6.1 Biphenyl Benzimidazole Derivatives	156
6.2 Biphenyl Results and Discussion	157
6.2.1 Synthesis	157
6.2.1.1 Suzuki Coupling Chemistry	157
6.2.1.2 Production of the Diamine	161
6.2.1.3 Acid Mediated Ring Closure	162
6.2.1.4 Compound Scale-Up	162
6.2.2 Biological Activity	163
6.2.3 DMPK Data	164
6.2.3.1 Predicted DMPK Data	164
6.2.3.2 Measured DMPK Data	166
6.2.4 <i>In Vivo</i> Mouse Data	167
6.3 Conclusion	168
6.4 Future Work	168
6.5 Experimental	169
6.6 References	187
Chapter 7 – Computational Evaluation of the Benzimidazole Scaffold	188
7.1 Computational Evaluation of the Benzimidazole Class	189
7.2 Chapter Acknowledgements	189
7.3 Molecular Modelling	190
7.3.1 Homology Models and Similarity	190
7.3.2 Identification of the Binding Site	191
7.4 Comparison of Binding Sites	192
7.5 Benzimidazole Tautomerisation	195
7.6 Docking Protocol	196
7.7 Docking Studies	197
7.7.1 Flubendazole Docking Studies	197
7.7.2 Thioether Docking Studies	202

7.7.3 Ether Docking Studies	208
7.7.4 Morpholine Ether Docking Studies	210
7.7.5 Ketone Docking Studies	212
7.7.6 Biphenyl Docking Studies	214
7.8 Correlation Between Activity and CHEMPLP Score	220
7.9 Binding Overview	221
7.10 Quantitative Structure Activity Relationship Studies	222
7.10.1 What is QSAR Modelling?	222
7.10.2 Why Do We Want to Undertake QSAR Studies?	223
7.10.3 Molecular Fingerprints	224
7.10.4 Applicability Domains	226
7.10.5 Random Forest Model	226
7.10.6 Receiver Operator Characteristic Curves	228
7.11 Design and Testing of a QSAR Model	230
7.11.1 Pipeline Pilot Protocol	230
7.11.2 Pipeline Pilot Results – Training	232
7.11.3 Pipeline Pilot Results – Testing of the Model	236
7.12 Conclusion	239
7.13 Future Work	239
7.14 Experimental	240
7.15 References	242
Chapter 8 - Synthesis and Biological Evaluation of the Benzisothiazolinone Class	244
8.1 An Introduction to the Benzisothiazolinones	245
8.1.1 Properties of Benzisothiazolinones	245
8.1.2 Previous Uses of Benzisothiazolinones	245
8.1.3 Discovery as a Potential <i>C. neoformans</i> Treatment	246
8.1.4 Biological Effects of Benzisothiazolinones	248
8.1.5 Benzisothiazolinone Metabolism	251
8.1.6 This Project: The Benzisothiazolinone Core	253
8.2 Benzisothiazolinone Results and Discussion	254
8.2.1 Benzisothiazolinones Core Amides	254
8.2.1.1 Synthesis	254
8.2.1.2 Biological Activity	258
8.2.1.3 DMPK	259
8.2.2 Benzisothiazolinone Core Alternatives	262
8.2.2.1 Synthesis	262
8.2.2.2 Biological Activity	263
8.2.2.3 DMPK	264
8.2.3 Benzisothiazolinone Core Benzyl Derivatives	266
8.2.3.1 Synthesis	266
8.2.3.2 Biological Activity	267
8.2.3.3 DMPK	268
8.3 Conclusion	271
8.4 Future Work	271
8.5 Experimental	272
8.6 References	288
Chapter 9 - Synthesis of Benzoxaboroles as Novel Treatments for <i>C. neoformans</i>	289
9.1 An Introduction to the Benzoxaboroles	290
9.1.1 Benzoxaborole Overview	289

9.1.2 Benzoxaborole Structure and Reactivity	289
9.1.3 Oxaborole Previous Uses	292
9.1.4 Identification of Oxaboroles as Antifungals	293
9.1.5 Benzoxaboroles Mode of Action	294
9.1.6 Benzoxaborole Metabolism	296
9.2 Benzoxaborole Results and Discussion	298
9.2.1 Synthesis	298
9.2.2 Biological Activity	307
9.2.3 Predicted Metabolism	308
9.3 Conclusion	309
9.4 Future Work	310
9.5 Experimental	312
9.6 References	324
Appendix	326

Abbreviations

1D	1 Dimensional
2AFC	Two Alternative Forced Choice
2D	2 Dimensional
3D	3 Dimensional
5-FC	5-Fluorocytosine
5-FU	5-Fluorouracil
AIDS	Acquired Immunodeficiency Syndrome
ALA	Alanine
AOX	Alternative Oxidase Pathway
app.	Apparent
ASN	Asparagine
ASP	Aspartic Acid
ATP	Adenosine Triphosphate
AUC	Area Under the Curve
BITZ	Benzisothiazolinone
Boc	<i>tert</i> -butyloxycarbonyl
<i>C. gatti</i>	<i>Cryptococcus gatti</i>
<i>C. neoformans</i>	<i>Cryptococcus neoformans</i>
CDCl₃	Deuterated Chloroform
CFU	Colony Forming Unit
CI	Chemical Ionisation
CLint	Intrinsic Clearance
CNA1	Calcineurin catalytic subunit A
CNS	Central Nervous System
CrAg	Cryptococcal Antigen
CYP450	Cytochrome P450
CYS	Cysteine
DCM	Dichloromethane
DFT	Density Functional Theory
DIPEA	Diisopropylethylamine
DMAP	4-Dimethylaminopyridine
DMF	<i>N,N</i> -dimethylformamide
DMPK	Drug Metabolism and Pharmacokinetics
DMSO	Dimethylsulphoxide
DNA	Deoxyribonucleic acid
DOPA	3,4-dihydroxyphenylalanine
ECFP	Extended Connectivity Fingerprint
EDC.HCl	<i>N</i> -(3-Dimethylaminopropyl)- <i>N'</i> -ethylcarbodiimide hydrochloride
eq.	Equivalents
ERG11	Sterol 14-demethylase
ES	Electrospray
EtOH	Ethanol
EUCAST	European Committee on Antimicrobial Susceptibility Testing
FDA	Food and Drug Administration
FdUMP	5-Fluorodeoxyuridine Monophosphate
FLU	Flubendazole
FMO	Flavin-containing Monooxygenase
FN	False Negative

FP	False Positive
FUDP	5-Fluorouridine Diphosphate
FUMP	5-Fluorouridine Monophosphate
GLN	Glutamine
GLU	Glutamic Acid
GLY	Glycine
GOLD	Genetic Optimisation for Ligand Docking
GORD	Gastro-oesophageal Reflux Disease
GXM	Glucuronoxylomannan
GXMGal	Glucuronoxy-mannogalactan
HATU	1-[Bis(dimethylamino)methylene]-1 <i>H</i> -1,2,3-triazolo[4,5- <i>b</i>]pyridinium 3-oxide hexafluorophosphate
Heps	Hepatocytes
HIS	Histidine
HIV	Human Immunodeficiency Virus
HPLC	High Performance Liquid Chromatography
HRMS	High Resolution Mass Spectrometry
I1	Isomer 1
I2	Isomer 2
IR	Infra-red
IV	Intravenous
kcal/mol	Kilocalories per mole
LAC1	Laccase gene
LEU	Leucine
LeuRS	Leucyl-tRNA synthetases
LRMS	Low Resolution Mass Spectrometry
LYS	Lysine
MeOH	Methanol
MET	Methionine
MIC	Minimum Inhibitory Concentration
Mics	Microsomes
MP	Melting point
NMR	Nuclear Magnetic Resonance
OOB	Out of Bag
OPS	Optimum Prediction Space
PAR	Parallel Pathway
PCR	Polymerase Chain Reaction
PD	Pharmacodynamics
PDB	Protein Data Bank
PDBE	Polybrominated Diphenyl Ethers
PK	Pharmacokinetics
PO	Per Os (by Mouth)
ppm	Parts per million
QSAR	Quantitative Structure Activity Relationship
RMSD	Root-mean-square deviation
RNA	Ribonucleic Acid
ROC	Receiver Operator Characteristic
ROS	Reactive Oxygen Species
RT	Room temperature
SAR	Structure Activity Relationship
SC	Subcutaneous

sdf	Spatial data file
SEM	Scanning Electron Microscope
SER	Serine
SET	Single Electron Transfer
S_NAr	Nucleophilic Aromatic Substitution
SSRI	Selective Serotonin Reuptake Inhibitors
TCA	Tricarboxylic Acid Cycle
TFA	Trifluoroacetic Acid
THR	Threonine
TLC	Thin Layer Chromatography
TMS	Tetramethylsilane
TP	True Positive
TUB1	Tubulin alpha-1 chain
TYR	Tyrosine
UDP	Uridine Diphosphate
VAL	Valine

Chapter 1

An Introduction to the Fungal Pathogen

C. neoformans - Biology and Current

Medicinal Chemistry

1.1 *C. neoformans* History and Discovery

It was not until 1894 that *Cryptococcus neoformans* (*C. neoformans*) began its road towards discovery. Initially, it was identified as a 'Saccharomyces-like' species that was discovered in the bone infection of a young woman. Later this unknown fungus was isolated from the fermentation of peach juice and was initially termed *Saccharomyces neoformans*. Upon later study, it was found that it didn't produce ascospores, a characteristic that defines the genus *Saccharomyces neoformans* and thus it was termed *C. neoformans*.^{1, 2} Environmentally, little was known about where this pathogen originated from. In 1951, it was reported, thanks to isolation from the soil, that the pathogen was particularly abundant within pigeon nests and droppings.³⁻⁵

Diagnosis of *C. neoformans* infection was previously difficult to distinguish from other yeast like fungal strains in patients and laboratories, particularly from other *Cryptococcus* species. However, this was made easier in the early 1960's when it was discovered that *C. neoformans* could be distinguished from other clinical yeasts by their urease activity and melanin formation.⁶⁻⁹ The 1970's brought about the discovery of the life-cycles of both *C. neoformans* and *C. gatti*. This discovery along with an increased number of cases of *Cryptococcus* in the early 1980's, allowed the disease to be considered as more of a rare, poorly researched disease, and allowed for further understanding to be garnered.^{3, 10}

1.2 *C. neoformans* Taxonomy

The two strains of *Cryptococcus* were grouped into two different varieties that were made up of 5 distinct serotypes. *C. neoformans* was made up of the serotypes A, D and AD and *C. var, gatti* has the serotypes B and C.^{3, 10, 11} Two distinct teleomorphs, or sexually reproductive stages of the two fungi, allowed *C. neoformans* and *C. gatti* to be identified as two distinct species. Initially, these fungal strains, when discovered were thought to belong to the *Basidiomycota* genus, however recent convention of one name for one fungus, means they now adopt their own genus of *Cryptococcus*.¹²⁻¹⁴

The classification of the agents of cryptococcosis was only further advanced when Polymerase Chain Reaction (PCR) and DNA sequencing became readily available in the late 1980s.^{15, 16} Genetic sequencing facilitated the understanding that each of the two main species contain subgroups, which themselves are genetically diverse. These are known as molecular types, and are thought to have diversified genetically from a single strain millions of years ago.¹⁷

1.3 *C. neoformans* Ecology

C. neoformans was initially isolated from peach juice and then further isolated from a number of other sources such as rotting vegetables and caged birds. During a study of a number of food markets in New Delhi, tomatoes were revealed to be one particular plant that was found to test positive for *C. neoformans*, as well as another similar fungal species *Candida Albicans*.¹⁸ It is also clear that there is a correlation between increased amounts of avian guano, in particular pigeon guano and the level of the fungus.^{3, 13, 19}

Due to the correlation between amounts of pigeon guano and detected levels of *C. neoformans*, pigeons have been presumed to be the major cause of fungal spread. However, only small amounts of the fungus are actually found in the pigeon. This is mostly due to the body temperature of the pigeon being 42 °C, which is higher than the normal *C. neoformans* growth range.²⁰ It was thought that pigeons were potentially carriers for the fungus, but upon the discovery of the fungus on their beaks and feet, it is possible the fungus comes from their food source. This is further validated by large concentrations of the fungus being found on weathered pigeon droppings, indicating the fungus is most likely coming from the environment.^{3, 13, 19, 21}

Despite large amounts of the fungus being found in bird guano, it is predicted that the most suitable natural environment for *C. neoformans* is actually plant based.¹⁴ It was discovered that the main source of the fungus was found in a number of species of eucalyptus tree and in the rotten wood in the hollows of other trees, though it is not known to cause plant disease.^{3, 13, 21} It is believed that trees act as a primary location for the fungus, which then facilitates its movement into the surrounding soil. Furthermore, there is evidence from amounts of *C. neoformans* in soil samples that have been exposed to bird excreta, that birds may also facilitate this transfer.²² The soil acts as an excellent growth and reproduction media for the fungus, allowing for its survival as a pathogen.²³

It is also believed the *C. neoformans* interacts with other species within the soil, most notably amoeba and bacteria including *Escherichia coli*, *Staphylococcus albus* and *Streptococcus faecalis*.¹⁴ It is believed that this interaction is what has allowed the fungus to survive and thrive within the soil and infect the amoeba using its normal pathogenic strategy.²⁴ It also helps to stimulate protective fungal virulence factors in order to survive in proximity to the bacteria, which include melanin production and capsule formation. It is believed that the adaptability of the fungus to survive different environments and hosts has allowed for greater pathogenicity when in the human host.³

1.4 *C. neoformans* Epidemiology

C. neoformans is an opportunistic yeast like fungus (Figure 1.1) and is one of the most common causes of systemic mycosis in immunosuppressed patients, such as those suffering from AIDS.^{25, 26} Systemic mycosis involves the infection of a number of organ systems, but in most patients' it presents in the lungs, as the fungal spores are breathed in.²⁷

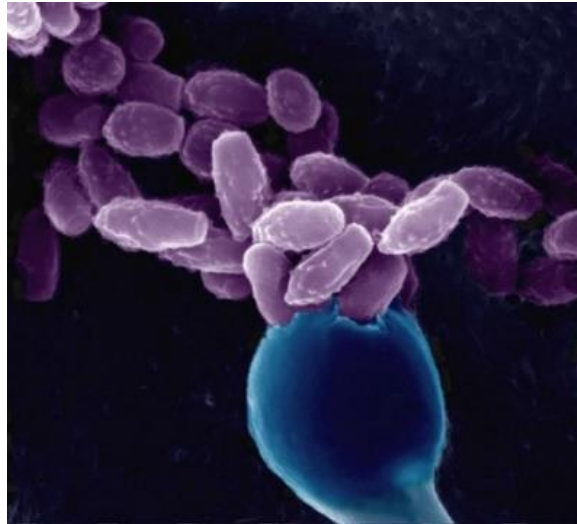


Figure 1.1. SEM image of the fungal spores produced by *C. neoformans* during the sexual reproduction stage. Reproduced from; *Scanning Electron Micrograph of Infection Yeast Spores*, C. Xue *et al.*^{28, 29}

In patients who are generally healthy, *C. neoformans* infections are rare and often do not induce illness.⁶ However, in immunosuppressed patients, manifestation of *cryptococcal* meningitis, encephalitis and less frequently pneumonia can occur.^{29, 30} *C. neoformans* generally affects the lungs and the central nervous system. Symptoms of the disease when present in the lungs include; fever, cough, shortness of breath and chest pain. If the infection spreads from the lungs to the brain, this becomes *cryptococcal* meningitis and presents itself as nausea, headaches, light sensitivity, behavioural changes and fever.^{29, 31}

Prognosis in patients who present with meningitis and pneumonia is poor, with greater than 60% of patients dying within three months of diagnosis.²⁹ Around 80% (720,000) of these cases occur in sub-Saharan Africa, where AIDS is particularly prominent (Figure 1.2A).^{32, 33} In sub-Saharan Africa it is one of the leading causes of death, causing almost half as many deaths as malaria (504,000 versus 1,135,861) and almost twice as many as tuberculosis (347,871) (Figure 1.2B).³⁴ This proves that statistically and economically, *C. neoformans* infection is a disease of great global burden.

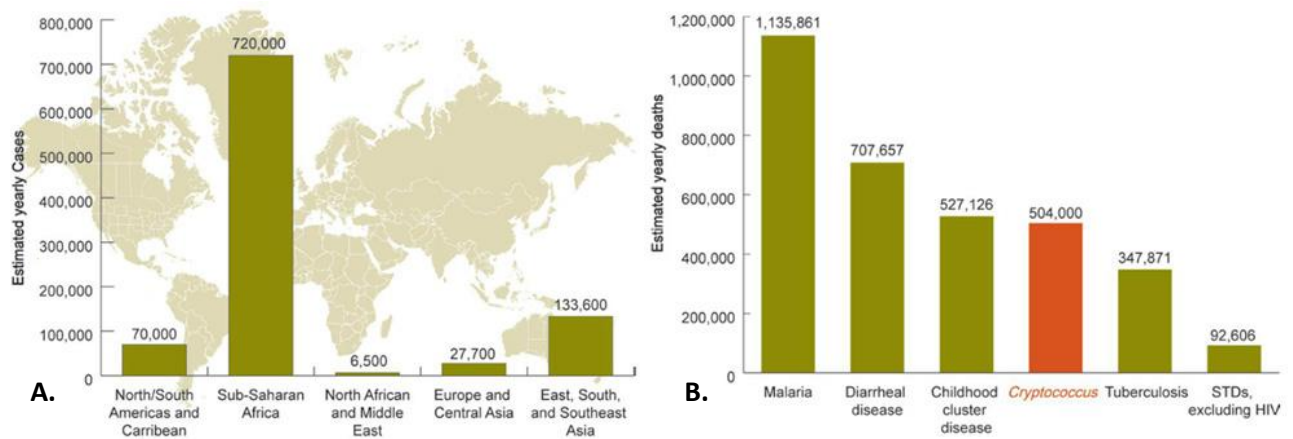


Figure 1.2A: The spread of estimated yearly cases of *C. neoformans* globally, showing sub-Saharan Africa as being the area of highest prevalence. **1.2B:** *C. neoformans* causes almost half as many deaths as malaria and more than tuberculosis, exemplifying the global impact. Reproduced from; *Estimation of the current global burden of cryptococcal meningitis among person living with HIV/AIDS*, B. J. Park *et al* and the CDC.³⁴

1.5 *C. neoformans* Pathogenesis and Host response

Infection begins when dry fungal spores are inhaled into the lungs.³⁵ They are small 1.5 - 3.5 μm , so easily navigate through the lungs to the alveoli, where they come into contact with alveolar macrophages, which recruit other immune cells, eliciting an immune response and inflammation.^{36, 37} Hosts with a normal immune response eliminate the inhaled fungus.³⁸ In immunocompromised patients, the fungus moves to the brain, crossing the blood brain barrier, adapting to the reduced oxygen and nutrient environment, where it can then multiply and cause meningoencephalitis. The most common clinical manifestation of infection are symptoms that occur in the central nervous system, though infection can occur anywhere within the body. Untreated infection, particularly within the CNS, often leads to death.^{38, 39}

Sometimes the patients inhale the spores into the lungs, where they may lay dormant, so the patient will present as asymptomatic as it does not trigger an immune response, but they will still be infected.^{40, 41} This infection can then escalate when the immune system is compromised by a variety of circumstances such as; HIV/AIDS infection, HIV progression, treatment with corticosteroids or infection with other diseases/disorders that may cause immunosuppression. Once the patient either has a reduction or loss of immunity, the yeast can then activate, travel to the CNS and then the patient can become symptomatic. This is commonly seen in patients in sub-Saharan Africa, where they are infected with AIDS and exacerbation of this disease leads to symptomatic infection.^{42, 43}

Because it has been identified that co-infection of AIDS and *C. neoformans* is very common, efforts have been focused on identifying at risk patients.³³ This is done via identification of the Cryptococcal

Antigen (CrAg) in HIV infected patients, meaning susceptible patients can receive the correct care as fast as possible. With treatment, the amount of cryptococcal antigen decreased after every therapy. However, it is still believed that small concentrations of this antigen can remain for long periods even after therapy.⁴⁴⁻⁴⁶

1.6 *C. neoformans* Life Cycle

In order for *C. neoformans* to advance into a growth state there are two different routes the cycle can take.⁴⁷ The two routes involve mating, which is carried out via a cell fusion pathway and monokaryotic fruiting which results in the doubling of the cellular DNA content. Both of these pathways are described in more detail below (Figure 1.3).⁴⁸

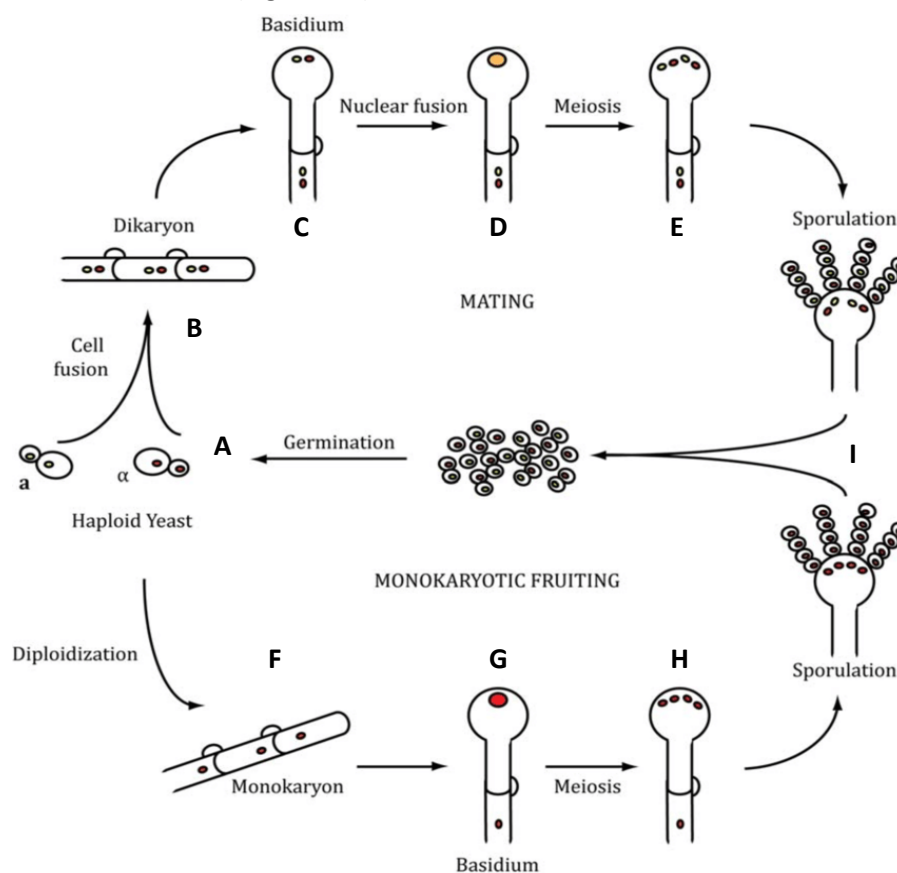


Figure 1.3. There are two different routes *C. neoformans* can use in order to generate mature pathogenic spores, which can then cause infection and reinitiate the life cycle again. Reproduced from; *Deciphering the Model Pathogenic Fungus Cryptococcus neoformans*, A. Idnorum et al and *Macrophage-Cryptococcus Interactions during Cryptococcosis* – K. Voelz.⁴⁸

1.6.1 Mating

This occurs when two haploid cells of opposite mating types fuse together (A) (Figure 1.3). The two different mating types are MATa and MATα. Initially the mating process starts when the haploids cells of the different mating types release pheromones and this promotes fusion. MATa releases MFa pheromone to attract MATα mating type and MATα release MFα to attract MATa. In response to the mating signals of the opposite mating types MATa undergoes isotropic growth, where it increases in

size in all directions. MAT α forms conjugation tubes, resulting in the connection of the two haploid cells, allowing for the fusion process to occur and the transfer of genetic information. The two cells undergo fusion, however there is no nuclear fusion and this results in the production of a dikaryon **(B)**. This is followed by basidia formation **(C)** and nuclear fusion **(D)**. There can also be the production of a haploid blastosphere, which can return to the beginning of the cycle to undergo haploid fusion once more or can follow an alternative growth pathway.^{48,49} Meiosis then occurs which produces four products, these then can undergo mitosis, which allows for multiplication **(E)**. This allows for buds to form on the surface of basidium, which gives chains of basidiospores **(I)**.^{3,48}

1.6.2 Monokaryotic Fruiting

In the environment it is also common for cells of one mating type of *C. neoformans* to double from a haploid number to a diploid number. This is most commonly the case for cells of the mating type MAT α . This process of doubling the chromosomal content of the mating cells can occur in two different ways. Firstly, there is endoduplication, which leads to the replication of the nuclear genome in the absence of mitosis occurring leading to polyploidy within the cells. The second option is nuclear fusion, which is similar to the mating process observed previously, however here this involves the fusion of two haploid nuclei of the same mating type, producing a stage known as a monokaryon **(F)**, which is a diploid cell containing only one type of genetic information. This then proceeds to another growth stage and produces a basidium **(G)**, and as with mating undergoes the processes meiosis **(H)**, mitosis and budding **(I)**, finally leading to the production of basidiospores.⁵⁰⁻⁵²

In both pathways the budding of the basidiospores allows for inhalation of the infectious agent. Release of these spores can be carried out by either dispersion or if germination occurs, haploid cells can be produced and the cycle can initiate again.

1.7 *C. neoformans* Virulence

There are four major virulence factors that are associated with the ability of *C. neoformans* to invade and repel the host's immune system (Figure 1.4). There are two structural features of the fungus, which are capsule formation and the melanin containing cell wall. They also use degradation enzymes and the ability to survive and thrive at mammalian body temperature to increase virulence in the host. These virulence factors will be discussed below.³¹

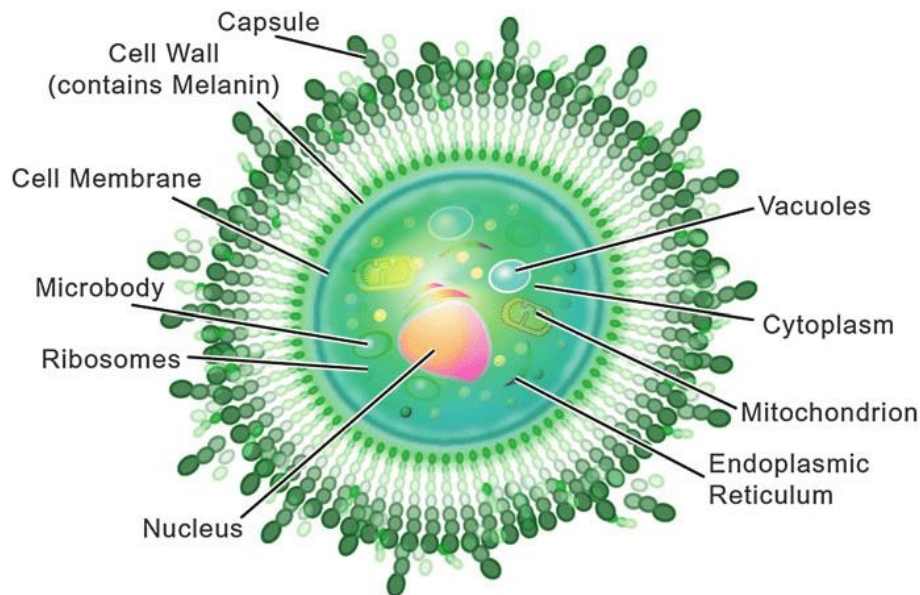


Figure 1.4. The structure of the fungus includes the capsule and melanin containing cell wall which aid the virulence of the fungus. Reproduced from; *Cryptococcus*, S. Li et al and *A Peach of a Pathogen: Cryptococcus neoformans*, Simmersecko.³¹

1.7.1 Capsule

The capsule is anchored in place by the cell wall through α -glucan, however the nature of this association is yet to be understood. It contains repeating units of the polysaccharides, glucuronoxylomannan (GXM)(1-7 million Da) and glucuronoxymannogalactan (GXMGal ~ 100,000 Da), as well as sialic acid, hyaluronic acid and manoproteins.⁵³ Polysaccharides for the capsule are most likely made in the Golgi body, which requires synthesis and polymerisation of the required polysaccharide. This is followed by movement of the product to the cell surface, where it can be expressed.⁵⁴

The size and binding specificity of the *C. neoformans* capsule is regulated by the fungus and is dynamic in response to environmental changes. *In vitro*, signals from a variety of sources are important for influencing capsule size and include; iron concentration, pH, nitrogen concentration, glucose concentration and carbon dioxide levels.⁵⁵⁻⁵⁷ *C. neoformans* uses a number of different transduction pathways and genes to adapt to a changeable environment. Activation of these pathways alters the expression of transcription factors, allowing for adaptation to the new environment. The genetic basis of capsule size has yet to be elucidated, partly because all of the transduction pathways have not been fully understood, but also it is thought that the capsule may be affected more by secretion than biosynthetic pathways.⁵⁸⁻⁶⁰ Secretion of the capsule has also not been fully understood. It is believed that polysaccharide secretion is a complex mechanism and that each pathway for secretion may result in different polysaccharides allowing for different functions to be gained. For example some

polysaccharides are involved in linkage to the cell wall and others in the secretion. This may allow for less polysaccharides overall to be produced, without compromise of the capsule size.^{3, 61-63}

1.7.2 Melanin Formation

Melanin is produced by a number of fungal species. It is a pigment that is deposited in the cell wall of the fungus and allows the cell to respond to environmental stress.⁶⁴ Some fungal strains constantly secrete melanin, however *C. neoformans* only produces melanin when in the presence of certain chemicals; 3,4-dihydroxyphenylalanine (DOPA) and other di/polyphenolic compounds.⁶⁵ The importance of melanin as a virulence factor was later validated by the deletion of the LAC1 gene.⁶⁶ LAC1 is the laccase gene and is significantly expressed when the cell is acting under normal conditions. When this gene is removed, the virulence of the fungus is significantly reduced. The laccase gene is expressed in the cell wall of the fungus and a number of other genes, all of which help with the production of melanin.⁶⁷⁻⁶⁹

It is believed the production of melanin helps to maximise fungal virulence via; the production of oxidants, protection from the immune system response of phagocytosis, killing host cells and production of microbicidal peptides.⁷⁰⁻⁷³ Furthermore, it is reported that it is melanin production that helps to provide resistance/protection for *C. neoformans* against many antifungal agents including the *C. neoformans* gold standard treatments amphotericin B, fluconazole and caspofungin.⁷⁴⁻⁷⁷

1.7.3 Growth at Mammalian Body Temperature

Growing at mammalian body temperature is insufficient for pathogens to be virulent, the ability of a pathogen to do this is however essential for them to be pathogenic. *Cryptococcus* is a large family of fungal strains where *C. neoformans* and *C. gatti* are the only successfully pathogenic strains to grow at physiological temperatures.^{78, 79} The mechanism for this is their ability to not only survive but also thrive at physiological temperatures. One reason is that other strains cannot effectively grow a polysaccharide capsule at mammalian body temperature (37 °C) but do at 24 °C. *C. neoformans* can robustly produce its polysaccharide capsule at 37 °C.⁸⁰

Studies into cryptococcal growth at mammalian temperatures show the calcineurin and calmodulin phosphatase is coded for by the gene CNA1 and when this is knocked out, the fungus shows a lack of virulence. It is believed that calcineurin in signalling cascades are required for pathogenesis.^{80, 81} This is further explained when mice are treated with cyclosporin A, a calcineurin inhibitor. Calcineurin has been found to be important for cryptococcal growth at 37 °C but not at 24 °C. Cyclosporin A inhibits

signal transduction at 37 °C and the mice treated with cyclosporin A are therefore protected from *Cryptococcus* at 37 °C. Cyclosporin A is therefore only toxic to the fungus at 37 °C rather than at 24 °C. Furthermore, genes required for cryptococcal growth at mammalian temperatures are significantly upregulated, when compared with the fungus growing at lower temperatures, which may indicate why cyclosporin A has more of an effect at mammalian temperatures for preventing cryptococcal growth. Genes that are upregulated at higher temperatures may lead to improved virulence for *C. neoformans* include; membrane integrity, stress signalling, metabolism, pre-mRNA splicing and cell-wall assembly.^{81, 82}

1.7.4 Degradation Enzymes

C. neoformans also produces a large number of degradation enzymes, including urease and phospholipase B, which have been shown to have a significant role in the pathogenicity of *C. neoformans*.⁸³⁻⁸⁶ These enzymes allow for the successful intracellular survival of the yeast via immunomodulation. This means they are more pathogenic upon infection and host cell membrane hydrolysis allows for the fungus to enter mammalian tissues.^{86, 87} The capsule has been shown to be a major virulence factor, as the absence of this completely diminishes virulence. Loss of degradation enzymes only results in a reduction in virulence.⁸⁸

1.8 *C. neoformans* Current Treatments

In patients where *C. neoformans* doesn't affect the central nervous system, the mainstay of treatment is fluconazole (**3**). In the eventuality that cryptococcal meningitis presents, amphotericin B (**1**) and flucytosine (**11**) are given for two weeks, followed by a more prolonged treatment with fluconazole.⁸⁹ No new therapies have been provided for *C. neoformans* for many years and the current therapies are dated and have a number of associated issues including toxicity, resistance and incomplete clearance of infection. These therapies and their associated issues will be discussed in this section.

1.8.1 Amphotericin B

Amphotericin B (**1**) is a hugely important antifungal therapy that has been used clinically for over 40 years. Despite having some toxicity related issues, it is a gold standard drug for the treatment of a number of life threatening fungal infections, due its broad spectrum of activity and good resistance profile.⁹⁰ It is a polyene antifungal drug that was one of the first clinically approved antifungal drugs when it was introduced in 1959.^{91, 92} It was originally extracted from the bacterium *Streptomyces nodosus* as it was found to show antifungal activity.⁹³ It is used in the treatment of a number of life-threatening fungal infections including aspergillosis, cryptococcosis and systemic candidiasis.⁹²

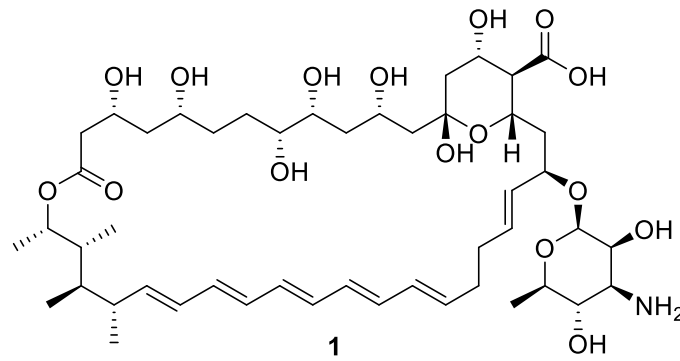


Figure 1.5. Amphotericin B (**1**) is a large molecule of the polyene class, often given intravenously to treat fungal infections.

1.8.1.1 Amphotericin Mechanism of Action

Amphotericin B (**1**) interacts with fungal membrane sterols, this results in the generation of a pore, which can cause altered permeability of ions (K^+ and Mg^{2+}). This can alter fungal cell metabolism, as well as causing leakage of essential cytoplasmic components. Evidence has shown that it also exerts its effects via production of reactive oxygen species (ROS). In this case amphotericin B (**1**) causes an ‘oxidative burst’, via as yet an unknown mechanism. Theories suggest that it could be due to the accumulation of ROS. Intracellular effects could also be due to sequestration of ergosterol.⁹⁴ Furthermore, it could be due to unfavourable interactions with the mitochondria, resulting in the loss of metabolic activity (Figure 1.6).⁹⁵⁻⁹⁷

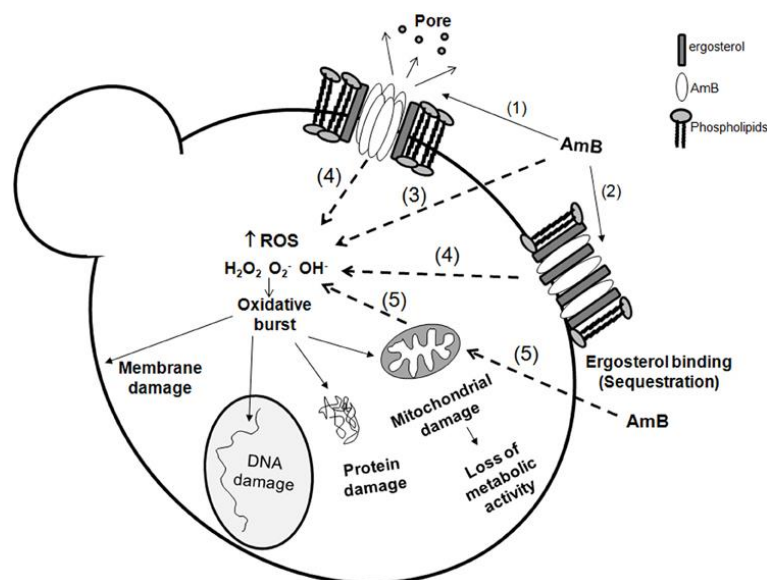


Figure 1.6. Amphotericin B (**1**) exerts its biological effects through; (1) binding to ergosterol in the membrane (sequestration), (2) generation of a pore in the membrane, (3) direct induction of ‘oxidative burst’, (4) ‘oxidative burst’ induced by changes in the membrane, (5) Damage to mitochondria. Reproduced from; *The non-mammalian host Galleria mellonella can be used to study the virulence of the fungal pathogen Candida tropicalis and the efficacy of antifungal drugs during infection by this pathogenic yeast, A. Mesa-Arango, et al* and *It only takes one to do many jobs: Amphotericin B as antifungal and immunomodulatory drug, Mesa et al.*⁹⁵

1.8.1.2 Issues with Amphotericin B

Amphotericin B (**1**) shows acute toxicity which includes nausea, vomiting, fever and hypoxia, as well as chronic effects such as nephrotoxicity.^{98, 99} These side effects are due to human ergosterol and fungal ergosterol being structurally analogous enough that amphotericin B (**1**) also binds to human membranes. This causes toxic effects such as nephrotoxicity, which is predominately due to changes in distal tubule permeability, which causes wasting of Na^+ , K^+ , and Mg^{2+} , resulting in reduced glomerular filtration.^{100, 101} Furthermore, amphotericin B (**1**) has to be given via IV infusion and requires careful monitoring due to toxicity issues; this means it has limited use in sub-Saharan Africa, where access to medical care is rare, and IV infusion not always possible.^{102, 103}

1.8.1.3 Mechanisms of Amphotericin B Resistance

Resistance to polyenes is rare and is mostly isolated to the less common species of *candida*. Recent evidence has shown there has been an increase in invasive mould infections of the non-albicans *Candida* species that have shown resistance to polyenes. It is suggested that resistance to polyenes has developed due to naturally occurring resistant cells via the production of modified sterols. Nystatin (**2**) was the original compound developed from the polyene class for antifungal use, but amphotericin B gained more popularity due to an improved toxicity profile (Figure 1.4). Nystatin (**2**) and sterol affinity is important, because the greater the affinity, the greater the rate of damage to the fungal membrane. Modification to sterols in resistant strains results in decreased nystatin (**2**) affinity and a decreased rate of membrane damage. Also the fungus can reorientate or mask the ergosterol structure, this means that polyenes will not sterically be able to bind, thus preventing antifungal activity.^{104, 105}

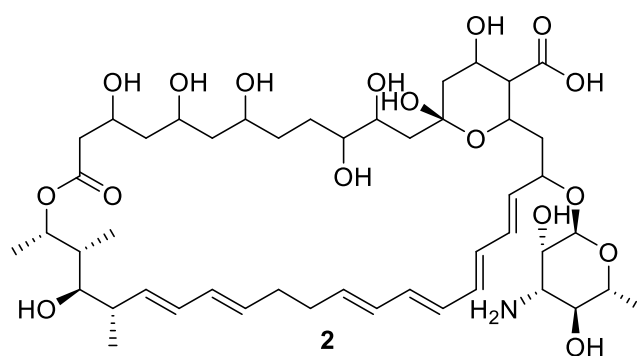


Figure 1.7. Nystatin (**2**) is a large molecule of the polyene class, often given intravenously to treat fungal infections.

1.8.2 Fluconazole

Fluconazole (**3**) was initially discovered in 1978 by Richardson *et al*, whilst working for Pfizer (Figure 1.8).^{106, 107} It was rapidly approved by the Food and Drug Administration (FDA) in 1990 due to

exhibiting good efficacy even at low doses. Fluconazole (**3**) is a compound of the azole class, characterised by the presence of the five-membered ring heterocycle that contains three nitrogen atoms. It is the lead drug in the treatment of a number of fungal infections but particularly in candidiasis.¹⁰⁸

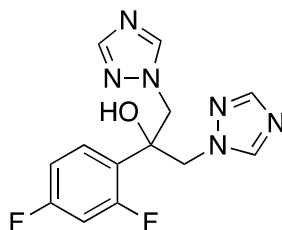


Figure 1.8. Fluconazole (**3**) is a drug of the azole class which exerts its biological effects by altering the production of ergosterol (**10**).

1.8.2.1 Fluconazole Mechanism of Action

Azole compounds like fluconazole (**3**) target the heme protein and the co-catalysed cytochrome P450 dependent demethylation of lanosterol (**4**) (Figure 1.9). This occurs at the 14 α -position, which is important as the integrity of the cell membrane is dependent on the 14 α -position being demethylated.¹⁰⁹ Normally, lanosterol (**4**) has two pathways of conversion to produce ergosterol (**10**). Both of which contain demethylation at different carbons on lanosterol (**4**). The first pathway goes via **5** being demethylated to Zymosterol (**6**). The second pathway involves demethylation of **7** to Obtusifoliol (**8**) and further demethylation to **9**. Inhibition of demethylation enzymes leads to depletion of ergosterol (**10**) and sterol precursor accumulation this therefore will alter the structure and membrane function of the fungus (Figure 1.9).¹¹⁰ It mainly inhibits CYP450-Erg11p, which catalyses the demethylation described. The azoles bind to the iron atom of the iron protoporphyrin group that is contained with the CYP450 enzyme, via a nitrogen atom in the triazole ring.^{96, 97}

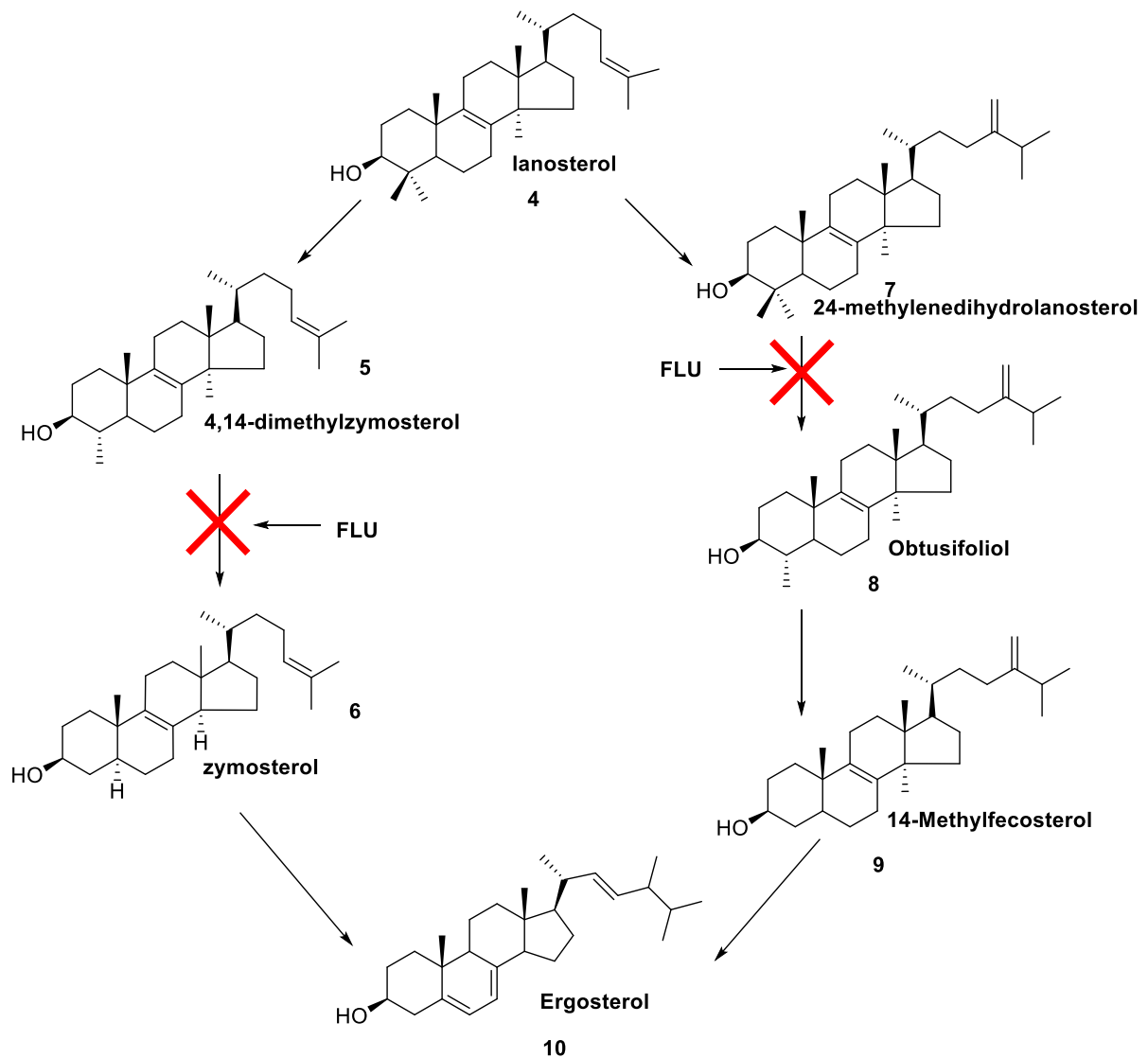


Figure 1.9. Fluconazole (3) and a number of other azoles exert their effects via interruption of two pathways that enzymatically convert lanosterol (4) to ergosterol (10). Reproduced from; *Antifungal Agents: Mode of Action, Mechanisms of Resistance, and Correlation of These Mechanisms with Bacterial Resistance*, M. Ghannoum *et al.*⁹⁶

1.8.2.2 Issues with Fluconazole

Fluconazole (3) is fungistatic, meaning that it suppresses, rather than cures the infection, this can lead to emergence of resistance.¹¹¹ Moreover, it can cause myelotoxicity, a condition in which bone marrow is suppressed, meaning that leukocytes, which are cells that are involved in the body's immune response, aren't synthesised. This effect could be hugely detrimental in patients with already suppressed immune systems, allowing for further infections. Importantly, white blood cell counts do begin to return to normal within 48 hours of discontinuation of treatment.^{112, 113}

Care must also be taken when administering this drug to patients as the drug is renally cleared, so patients with impaired renal function will need lower doses. Furthermore, given that it inhibits CYP450

enzymes, care must be taken when dosing drugs that are metabolised by CYP450 enzymes, so potentially toxic amounts of drugs aren't allowed to build up, leading to worsening of a patient's health.¹¹⁴

1.8.2.3 Mechanisms of Fluconazole Resistance

There are considered to be four biochemical mechanisms of azole resistance, these are; overexpression of the target, alteration of the target, alteration of sterol biosynthesis and increased drug efflux. Overexpression of ERG11, which is the gene that encodes the azole target, results in normal concentrations of the drug not being as effective as more ergosterol can be made, and thus resistance occurs.¹¹⁵

Alteration to the 14 α -demethylation enzyme arising from mutations, which alter how the drug binds but not how the endogenous ligand binds. This results in the target still retaining its natural biological activity, but having reduced affinity towards azoles.^{116, 117} Another method is the alteration of sterol biosynthesis, which allows the cell to bypass the production of the toxic methylated sterol intermediates such as 14 α -methylfecosterol (**9**) and still allowing the production of ergosterol (**10**), minimising the effect of fluconazole on the fungus.^{118, 119} Finally, there is reduction in the intracellular concentration of the target enzyme, which is caused by a change in the membrane sterols and lipids. This leads to poor drug permeability resulting in active drug efflux.^{96, 120}

1.8.3 Flucytosine

Flucytosine (**11**) was first synthesised in 1957 and initially intended to be used as an anti-tumour agent (Figure 1.10).^{121, 122} Efficacy was then demonstrated against *Candida albicans* and *C. neoformans* in 1963, which led to its approval for human use in 1968. It is one of the oldest antifungal therapies that is still commonly used today.¹²³⁻¹²⁵ It is a synthetically derived analogue of the DNA base cytosine that requires conversion to 5-fluorouracil in order to exhibit antifungal activity and will be discussed in a subsequent section.^{126, 127}

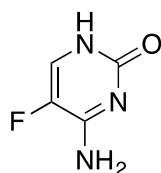


Figure 1.10. Flucytosine (**11**) is a pyrimidine analogue, which exerts its antifungal effects via interference with DNA and RNA synthesis.

1.8.3.1 Flucytosine Mechanism of Action

Flucytosine (**11**) has no intrinsic fungal activity, however on uptake by fungal cells it undergoes conversion into 5-fluorouracil (5-FU) (**12**). It is then converted into further metabolites such as 5-fluorouridine monophosphate (FUMP) (**13**) and 5-fluorodeoxyuridine monophosphate (FdUMP) (**15**). FUMP (**13**) undergoes further metabolism to FUDP (**14**) and then via incorporation into RNA, it inhibits the synthesis of proteins. FdUMP inhibits thymidylate synthetase, which leads to inhibition of DNA synthesis, which leads to fungal cell death (Figure 1.11).^{128, 129}

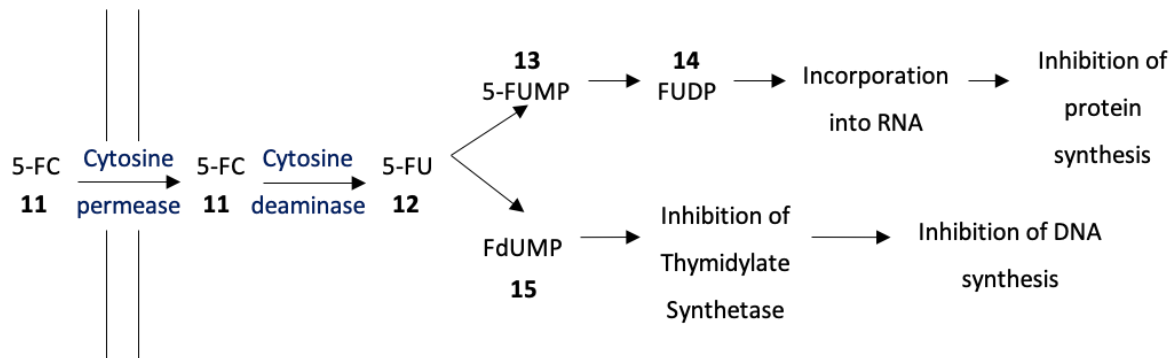


Figure 1.11. Flucytosine (**11**) passes through the membrane and once into the cell is converted to 5-FU (**12**) via cytosine deaminase. 5-FU is then further metabolised and it is these metabolites that have the biological effect on RNA and protein synthesis. Reproduced from; *Flucytosine: a review of its pharmacology, clinical indications, pharmacokinetics, toxicity and drug interaction*, A. Vermes *et al.*¹²⁹

1.8.3.2 Issues with Flucytosine

Flucytosine (**11**) has a number of associated side effects, with the most serious including hepatotoxicity and like fluconazole (**3**), bone marrow depression can occur. This is particularly problematic if given with amphotericin B, which is nephrotoxic. Given that flucytosine (**11**) relies on glomerular filtration for removal from the body, co-administration of these drugs need to be carefully monitored so that a build-up of flucytosine doesn't occur, which could induce hepatotoxicity.¹²⁹

1.8.3.3 Mechanisms of Flucytosine Resistance

Resistance described in flucytosine (**11**) occurs when it is used as a single therapy, rather than in combination.¹²⁴ There are two resistance mechanisms that are proposed. Firstly, resistance may occur due to increased synthesis of new pyrimidines, this then competes with 5-FU (**12**), resulting in an increased likelihood of a natural pyrimidine being incorporated into RNA, rather than the fluorinated version. Therefore, proteins can still be made and the fungal cell remains viable.¹³⁰ 5-FC (**11**) requires cellular uptake in order to be metabolised to 5-FU (**12**) in order to possess activity. Enzymes are used to do this and certain mutations can result in reduced amounts of these enzymes being present. This includes monophosphate pyrophosphorylase, which is the most frequently acquired type of 5-FC resistance.^{130, 131}

1.9 *C. neoformans* Ideal Drug Candidate

All drugs that are produced are required to have specific properties that will allow them to provide the best treatment (Figure 1.12). Most marketed drugs are designed so that they have good DMPK and toxicity profiles, improved activity above its predecessors and selectivity for the target versus the host. However, when assessing what properties are essential to treat *C. neoformans*, the population who most commonly suffer from this disease needs to be seriously considered. Given that this disease more commonly presents itself in sub-Saharan Africa, we need to consider more than the basic drug profile. Due to the countries where the disease is endemic having very low incomes, we need to ensure these drugs are as inexpensive as possible, this should hopefully allow them to be introduced to a wider population.

Another difficulty faced is a severe lack of access to competent health care. This means drugs like amphotericin B are hard to administer, and monitoring due to side effects is difficult. Ideally drugs that can be orally administered are of more use to the wider population, as they don't require a health care professional to provide constant administration and will often lead to better patient compliance. However, we do need a drug that is also infusible due to the need to treat seriously ill patients who may not respond to an oral dosing regimen. Finally, emergence of resistance is a huge problem with a number of drug classes such as antibiotics, antimalarials and anti-tuberculosis agents. Treatments for *C. neoformans* ideally need to be fungicidal, rather than fungistatic, that way they cure the infection, not just suppress it, which should reduce any chance of resistance emerging. Emerging resistance could further be discouraged by synthesis of a drug with a novel mechanism of action, that could be implemented in combination therapy.

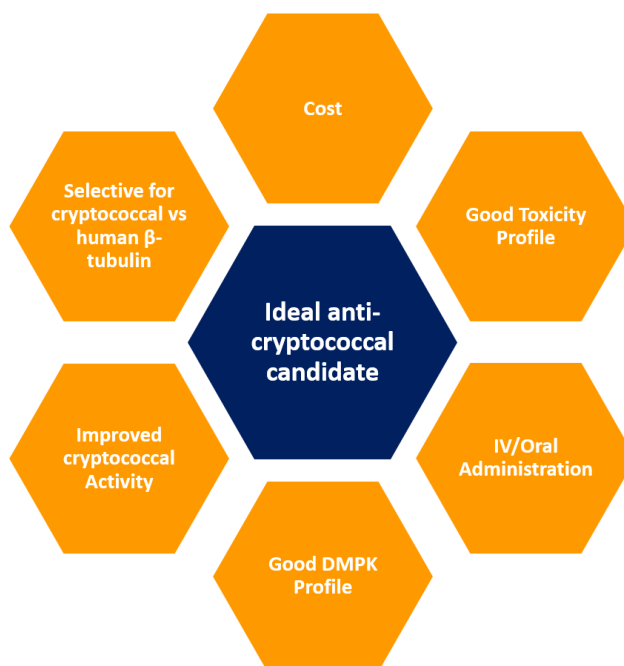


Figure 1.12. The ideal drug to treat cryptococcal infections is required to have a number of different properties. This includes cost, administration and fungicidal activity.¹³²

1.10 Current *C. neoformans* Research

Currently within the Nixon group, we are working on a number of new templates for the treatment of *C. neoformans* (Figure 1.13). This includes the three templates described in this work which are the; benzimidazoles (**16**) (Chapters 3-7), benzisothiazolinones (**17**) (Chapter 8) and benzoxaboroles (**18**) (Chapter 9). Work is also being undertaken by undergraduate students within the group on the thiazoles (**19**).

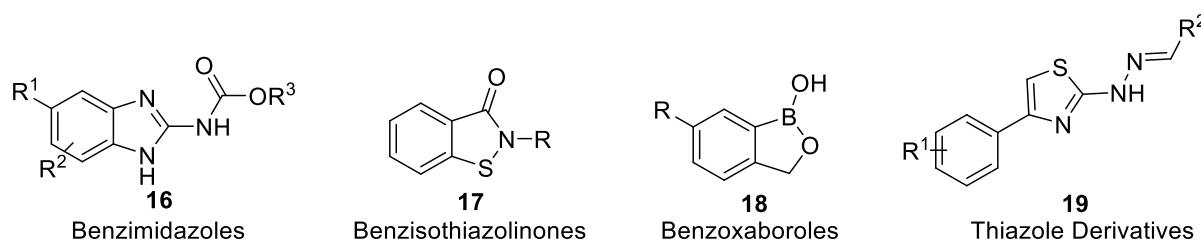


Figure 1.13. Within the Nixon group, there is ongoing development of four new classes of compounds for the treatment of *C. neoformans*. The benzimidazoles, benzisothiazolinones and benzoxaboroles are discussed in subsequent chapters.

There are also a number of the other new therapies in development, most with known mechanisms of action. This section gives a brief overview of the other compounds that are being investigated (Figure 1.14 and Table 1.1).¹³³

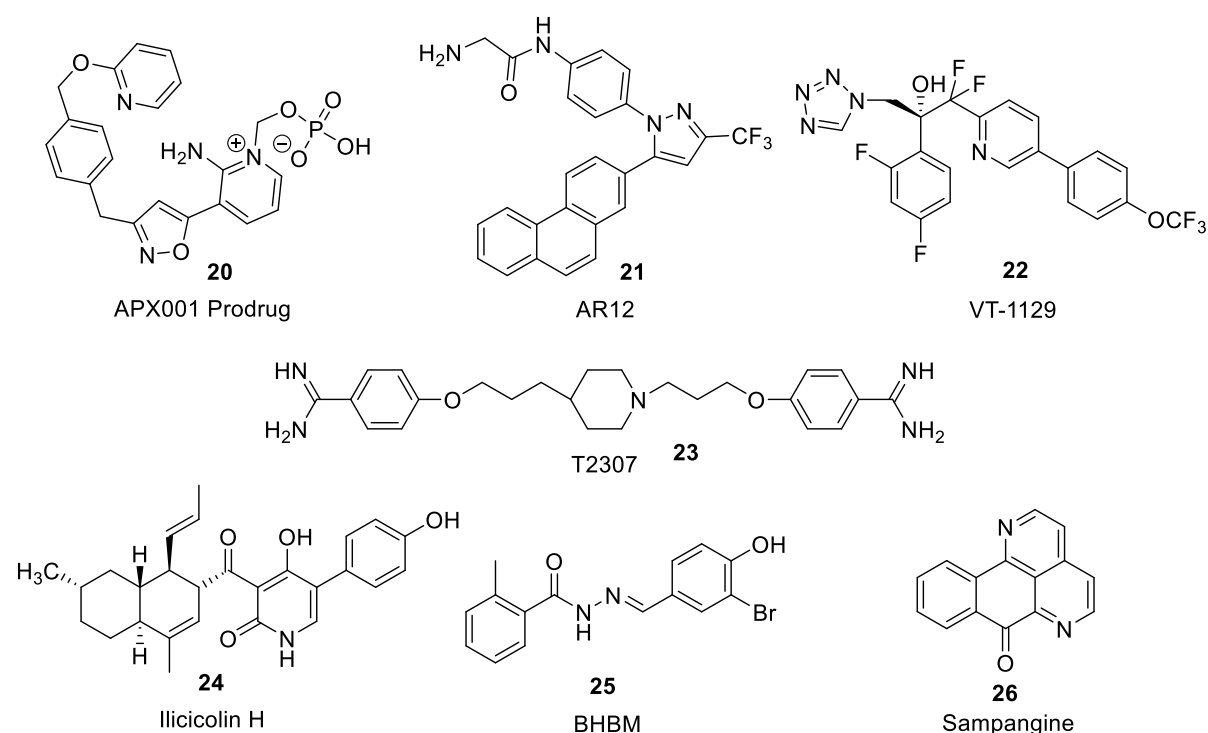


Figure 1.14. A number of novel treatments for *C. neoformans* and other fungal species are currently being investigated from a wide variety of compound classes, with differing modes of action.

Table 1.1. There are a number of novel treatment for *C. neoformans* currently under investigation, with diverse mechanisms of action.

New Agents	Mechanism of action	Potential Utilisation strategy
APX001 (20)	Inhibits the fungal protein Gwt1	Combination with existing antifungal agents, such as fluconazole
AR12 (21)	Inhibits fungal acetyl-CoA synthetase	Combination with existing antifungal agents such as fluconazole
VT-1129 (tetrazoles) (22)	Inhibits ergosterol biosynthesis	Treatment of fluconazole-resistant <i>Cryptococcus</i> strains
T2307 (allylamine) (23)	Collapses the mitochondrial membrane potential	
Illicolin H (polyketide) (24)	Inhibits fungal mitochondrial cytochrome <i>bc₁</i> reductase	
BHBM (Acylhydrazones) (25)	Targets non –mammalian sphingolipid pathway	
Sampangine derivatives (26)	Unknown	

APX001 (**20**) inhibits the fungal protein Gwt1, which is an important protein involved in the synthesis of glycolipids that anchor to the cell wall. This results in destabilisation of the fungal cell wall and consequently causes fungal cell death.^{134, 135} APX001 (**20**) as of May 2018 was undergoing Phase I clinical trials in patients with acute myeloid leukaemia and candidiasis. AR12 (**21**) inhibits fungal acetyl-

CoA synthetase, which aids in the step which allows for pyruvate to be converted and to be used in the Krebs cycle during respiration. Blockage of this pathway prevents aerobic respiration from occurring and causes fungal death. It has also been shown to improve the activity of the fluconazole in patients who aren't immunocompromised.¹³⁶ The allylamine T2307 (**23**) shows excellent activity against *C. gatti* with an MIC range of 0.0078 - 0.0625 mg/L for a number of clinical isolates. Activity is derived from collapse of the mitochondrial membrane potential, which results in disruption of mitochondrial function.¹³⁷

VT-1129 (**22**) is a tetrazole compound which shows promising activity against *C. neoformans* with an MIC 0.027 mg/L and is of great interest due to reduced drug interaction with the host CYP450 enzymes. It works via the inhibition of ergosterol biosynthesis, in a similar manner to fluconazole.¹³⁸ BHBM (**25**) is of the acylhydrazones class and targets the non-mammalian sphingolipid pathway, which plays a vital role in cell signalling, which is essential for *C. neoformans* and other fungal strains to be virulent¹³⁹. Ilicicolin H (**24**), is of the polyketide class and inhibits fungal mitochondrial cytochrome bc1 reductase, which is essential to the electron transport chain. Potent inhibition of this reductase was observed, with the compound possessing an $IC_{50} = 2-3$ ng/L.¹⁴⁰ Finally, derivatives of Sampangine (**26**), a naturally occurring compound, have been shown to have good *in vitro* activity against *C. neoformans*, with a scaffold hopping method achieving a compound with an MIC = 0.25 mg/L.¹⁴¹

Furthermore, there are current investigations into repurposing drugs to treat cryptococcosis. This includes Sertraline (**27**), which is an antidepressant of the Selective Serotonin Reuptake Inhibitor (SSRI) class, which work via interaction with fungal translation factors, and prevent protein synthesis. It shows good activity, achieving an MIC 1-8 mg/L.^{142, 143} Tamoxifen (**28**), which is an estrogen receptor antagonist, shows a synergistic effect with fluconazole and amphotericin B. This is achieved via inhibition of the calmodulin-calcineurin complex, which normally triggers an immune response when activated. This allows for fungal death via fluconazole and amphotericin B, and prevention of resistance via inhibition of the calmodulin – calcineurin pathway.¹⁴⁴

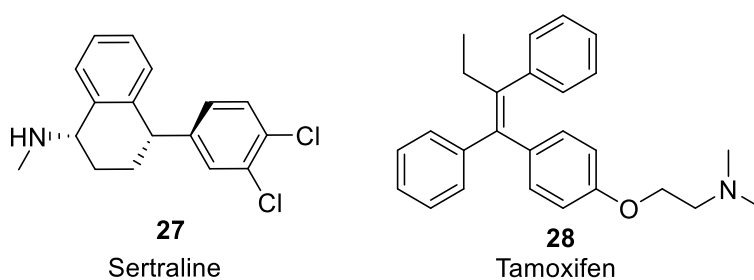


Figure 1.15. Work is ongoing to repurpose well known, commercially available drugs such as Sertraline (**27**) and Tamoxifen (**28**).

1.11 Project Aims

When starting this project there were a number of aims we wanted to achieve in order to develop new treatments for *C. neoformans*.

1. To design new compounds of the benzimidazole, benzisothiazolinones and benzoxaborole class.
2. To develop new and improve upon existing synthetic routes.
3. To continue to use learned data about activity through the project to inform design of new compounds.
4. To improve the solubility of the benzimidazole class.
5. To use computational modelling to understand the binding poses of newly designed molecules within the binding site of β -tubulin.

1.12 References

1. O. Busse, *Zentralbl. Bakteri.*, 1894, **16**, 175-180.
2. D. Srikanta, F. H. Santiago-Tirado and T. L. Doering, *Yeast.*, 2014, **31**, 47-60.
3. K. J. Kwon-Chung, J. A. Fraser, T. L. Doering, Z. Wang, G. Janbon, A. Idnurm and Y.-S. Bahn, *Cold Spring Harb Perspect Med*, **4**, a019760-a019760.
4. C. W. Emmons, *J. Bacteriol.*, 1951, **62**, 685-690.
5. C. W. Emmons, *Am. J. Epidemiol.*, 1955, **62**, 227-232.
6. M. A. Viviani and A. Maria Tortorano, in *Clinical Mycology (Second Edition)*, eds. E. J. Anaissie, M. R. McGinnis and M. A. Pfaller, Churchill Livingstone, Edinburgh, 2009, DOI: <https://doi.org/10.1016/B978-1-4160-5680-5.00009-8>, pp. 231-249.
7. L. McTaggart, S. E. Richardson, C. Seah, L. Hoang, A. Fothergill and S. X. Zhang, *J. Clin. Microbiol.*, 2011, **49**, 2522-2527.
8. H. P. Seeliger, *J. Bacteriol.*, 1956, **72**, 127-131.
9. F. Staib and M. Seibold, *Mycoses.*, 1989, **32**, 63-72.
10. K. Kwon-Chung, *Mycologia*, 1975, **67**, 1197-1200.
11. K. J. Kwon-Chung, J. E. Bennett and J. C. Rhodes, *Anton. Leeuw. Int. J. G.*, 1982, **48**, 25-38.
12. D. Hawksworth, P. Crous, S. Redhead, D. Reynolds, R. Samson, K. Seifert, J. Taylor, M. Wingfield, Ö. Catherine, F.-Y. Ahmetasan, Z. W. De Beer, Dominikbegerow, Deryaberikten, P. Teunboekhout, P. Buchanan, W. Treenaburgess, P. Leicai, J. Cannon, U. Leland and B. Weir, *IMA Fungus*, 2011, **2**, 105-112.
13. D. Ellis and T. Pfeiffer, *Eur. J. Epidemiol.*, 1992, **8**, 321-325.
14. T. G. Mitchell and J. R. Perfect, *Clin. Microbiol. Rev.*, 1995, **8**, 515-548.
15. *Can. J. Infect. Dis. Med. Microbiol.*, 1991, **2**, 89-91.
16. A. Munshi, *DNA Sequencing – Methods and Applications* Springer, New Dehli, 2014.
17. S. E. Kidd, F. Hagen, R. L. Tscharke, M. Huynh, K. H. Bartlett, M. Fyfe, L. Macdougall, T. Boekhout, K. J. Kwon-Chung and W. Meyer, *Proc. Natl. Acad. Sci. U.S.A.*, 2004, **101**, 17258-17263.
18. V. C. Misra and H. Randhawa, *The Indian journal of chest diseases & allied sciences*, 2000, **42**, 317-321.
19. T. Sorrell and D. Ellis, *Rev. Infect. Dis.*, 1997, **14**, 42-43.
20. M. Abou-Gabal and M. Atia, *Med. Mycol.*, 1978, **16**, 63-68.
21. D. Ellis and T. Pfeiffer, *Lancet.*, 1990, **336**, 923-925.
22. K. H. Bohm, E. Weiland, I. S. Abdallah and M. Sasu, *Mycopathologia.*, 1970, **42**, 57-63.
23. M. Cogliati, *Fungal. Genet. Biol.*, 2018, **1**, 1-4.
24. L. F. Mayer and W. J. Kronstad, *J. Fungi.*, 2019, **5**, 1-10.
25. J. C. Hurtado, P. Castillo, F. Fernandes, M. Navarro, L. Lovane, I. Casas, L. Quintó, F. Marco, D. Jordao, M. R. Ismail, C. Lorenzoni, A. E. Martinez-Palhares, L. Ferreira, M. Lacerda, W. Monteiro, A. Sanz, E. Letang, L. Marimon, S. Jesri, A. Cossa, I. Mandomando, J. Vila, Q. Bassat, J. Ordi, C. Menéndez, C. Carrilho and M. J. Martínez, *Sci. Rep.*, 2019, **9**, 1-10.
26. M. C. Cruz, M. S. Bartlett and T. D. Edlind, *Antimicrob. Agents. Ch.*, 1994, **38**, 378-380.
27. J. Brainard, in *Pulmonary Pathology*, eds. D. S. Zander and C. F. Farver, Philadelphia, 2nd edn., 2018, DOI: <https://doi.org/10.1016/B978-0-323-39308-9.00036-4>, pp. 713-736.
28. C. Xue and K. Carroll, Scanning Electron Micrograph of Infection Yeast Spores, <https://www.livescience.com/39541-deadly-fungus-mates-with-clones.html>).
29. W. Sabiiti and R. C. May, *Fungal. Biol. Rev.*, 2012, **7**, 1297-1313.
30. M. C. Cruz and T. Edlind, *Microbiology*, 1997, **143**, 2003-2008.
31. P. A. Spagnuolo, J. Hu, R. Hurren, X. Wang, M. Gronda, M. A. Sukhai, A. Di Meo, J. Boss, I. Ashali, R. Beheshti Zavareh, N. Fine, C. D. Simpson, S. Sharmeen, R. Rottapel and A. D. Schimmer, *Blood*, 2010, **115**, 4824-4833.
32. J. N. Jarvis, A. Boulle, A. Loyse, T. Bicanic, K. Rebe, A. Williams, T. S. Harrison and G. Meintjes, *AIDS*, 2009, **23**, 1182-1183.
33. J. N. Jarvis and T. S. Harrison, *AIDS*, 2007, **21**, 2119-2129.
34. B. J. Park, K. Wannemuehler, B. J. Marston, N. Govender, P. Pappas and T. Chiller, *AIDS*, 2009, **23**, 525-530.
35. S. S. Giles, T. R. T. Dagenais, M. R. Botts, N. P. Keller and C. M. Hull, *Infect. Immun.*, 2009, **77**, 3491-3500.
36. J. B. Neilson, R. A. Fromtling and G. S. Bulmer, *Infect. Immun.*, 1977, **17**, 634-638.
37. K. E. Powell, B. A. Dahl, R. J. Weeks and F. E. Tosh, *J. Infect. Dis.*, 1972, **125**, 412-415.
38. K. Voelz and R. C. May, *Eukaryot. Cell*, 2010, **9**, 835-846.

39. F. F. Dutra, P. C. Albuquerque, M. L. Rodrigues and F. L. Fonseca, *Fungal. Biol. Rev.*, 2018, **32**, 35-51.
40. C. Charlier, K. Nielsen, S. Daou, M. Brigitte, F. Chretien and F. Dromer, *Infect. Immun.*, 2009, **77**, 120-127.
41. F. Chrétien, O. Lortholary, I. Kansau, S. Neuville, F. Gray and F. Dromer, *J. Infect. Dis.*, 2002, **186**, 522-530.
42. F. Dromer, A. Casadevall, J. Perfect and T. Sorrell, in *Cryptococcus*, American Society of Microbiology, 2011, DOI: doi:<https://doi.org/10.1128/9781555816858.ch31>.
43. D. C. Saha, D. L. Goldman, X. Shao, A. Casadevall, S. Husain, A. P. Limaye, M. Lyon, J. Somani, K. Pursell, T. L. Pruett and N. Singh, *Clin. Vaccine Immunol.*, 2007, **14**, 1550-1554.
44. H. Lu, Y. Zhou, Y. Yin, X. Pan and X. Weng, *J. Clin. Microbiol.*, 2005, **43**, 2989-2990.
45. R. M. Wake, E. Britz, C. Sriruttan, I. Rukasha, T. Omar, D. C. Spencer, J. S. Nel, S. Mashamaite, A. Adelekan, T. M. Chiller, J. N. Jarvis, T. S. Harrison and N. P. Govender, *Clin. Infect. Dis.*, 2017, **66**, 686-692.
46. S. Antinori, A. Radice, L. Galimberti, C. Magni, M. Fasan and C. Parravicini, *J. Clin. Microbiol.*, 2005, **43**, 5828-5829.
47. X. Lin and J. Heitman, *Annu. Rev. Microbiol.*, 2006, **60**, 69-105.
48. A. Idnurm, Y.-S. Bahn, K. Nielsen, X. Lin, J. A. Fraser and J. Heitman, *Nat. Rev. Microbiol.*, 2005, **3**, 753-764.
49. C. M. McClelland, Y. C. Chang, A. Varma and K. J. Kwon-Chung, *Trends Biochem. Sci.*, 2004, **12**, 208-212.
50. J. Fu, I. R. Morris and B. L. Wickes, *Plos Path.*, 2013, **9**, 1-11.
51. B. L. Wickes, M. E. Mayorga, U. Edman and J. C. Edman, *Proc. Natl. Acad. Sci. U.S.A.*, 1996, **93**, 7327-7331.
52. A. Forsythe, A. Vogan and J. Xu, *Sci. Rep.*, 2016, **6**, 1-12.
53. T. L. Doering, *Annu. Rev. Microbiol.*, 2009, **63**, 223-247.
54. A. Yoneda and T. L. Doering, *Mol. Biol. Cell*, 2006, **17**, 5131-5140.
55. D. L. Granger, J. R. Perfect and D. T. Durack, *J. Clin. Investig.*, 1985, **76**, 508-516.
56. S. E. Vartivarian, R. E. Cowart, E. J. Anaissie, T. Tashiro and H. A. Sprigg, *J. Med. Vet. Mycol.*, 1995, **33**, 151-156.
57. T. Lian, M. I. Simmer, C. D'Souza, B. R. Steen, S. D. Zuyderduyn, S. J. M. Jones, M. Marra and J. Kronstad, *Mol. Microbiol.*, 2005, **55**, 1452-1472.
58. T. R. O'Meara and J. A. Alspaugh, *Clin. Microbiol. Rev.*, 2012, **25**, 387-408.
59. B. Haynes, M. Skowyra, S. Spencer, S. R. Gish, M. Williams, E. P. Held, M. Brent and T. Doering, *Plos Path.*, 2011, **7**, 1-15.
60. L. Kmetzsch, C. C. Staats, E. Simon, F. L. Fonseca, D. L. de Oliveira, L. Sobrino, J. Rodrigues, A. L. Leal, L. Nimrichter, M. L. Rodrigues, A. Schrank and M. H. Vainstein, *Eukaryot. Cell*, 2010, **9**, 1798-1805.
61. A. J. Reese and T. L. Doering, *Mol. Microbiol.*, 2003, **50**, 1401-1409.
62. M. L. Rodrigues, M. Alvarez, F. L. Fonseca and A. Casadevall, *Eukaryot. Cell*, 2008, **7**, 602-609.
63. M. Rodrigues and J. Djordjevic, *Mycopathologia*, 2011, **173**, 407-418.
64. J. D. Nosanchuk and A. Casadevall, *Antimicrob. Agents. Ch.*, 2006, **50**, 3519-3528.
65. S. Chaskes and R. L. Tyndall, *J. Clin. Microbiol.*, 1975, **1**, 509-514.
66. J. C. Rhodes, I. Polacheck and K. J. Kwon-Chung, *Infect. Immun.*, 1982, **36**, 1175-1184.
67. S. D. Salas, J. E. Bennett, K. J. Kwon-Chung, J. R. Perfect and P. R. Williamson, *J. Exp. Med.*, 1996, **184**, 377-386.
68. X. Zhu and P. R. Williamson, *FEMS. Yeast. Res.*, 2004, **5**, 1-10.
69. R. Pukkila-Worley, Q. D. Gerrald, P. R. Kraus, M.-J. Boily, M. J. Davis, S. S. Giles, G. M. Cox, J. Heitman and J. A. Alspaugh, *Eukaryot. Cell*, 2005, **4**, 190-201.
70. L. Liu, R. P. Tewari and P. R. Williamson, *Infect. Immun.*, 1999, **67**, 6034-6039.
71. Y. Wang, P. Aisen and A. Casadevall, *Infect. Immun.*, 1995, **63**, 3131-3136.
72. E. Blasi, R. Barluzzi, R. Mazzolla, B. Tancini, S. Saleppico, M. Puliti, L. Pitzurra and F. Bistoni, *J. Neuroimmunol.*, 1995, **58**, 111-116.
73. T. L. Doering, J. D. Nosanchuk, W. K. Roberts and A. Casadevall, *Med. Mycol.*, 1999, **37**, 175-181.
74. R. Ikeda, T. Sugita, E. S. Jacobson and T. Shinoda, *Microbiol. Immunol.*, 2003, **47**, 271-277.
75. L. R. Martinez and A. Casadevall, *Antimicrob. Agents. Ch.*, 2006, **50**, 1021-1033.
76. D. van Duin, A. Casadevall and J. D. Nosanchuk, *Antimicrob. Agents. Ch.*, 2002, **46**, 3394-3400.
77. D. van Duin, W. Cleare, O. Zaragoza, A. Casadevall and J. D. Nosanchuk, *Antimicrob. Agents. Ch.*, 2004, **48**, 2014-2020.
78. F. L. Fonseca, L. Nimrichter, R. J. B. Cordero, S. Frases, J. Rodrigues, D. L. Goldman, R. Andruszkiewicz, S. Milewski, L. R. Travassos, A. Casadevall and M. L. Rodrigues, *Eukaryot. Cell*, 2009, **8**, 1543-1553.

79. R. Petter, B. S. Kang, T. Boekhout, B. J. Davis and K. J. Kwon-Chung, *Microbiology*, 2001, **147**, 2029-2036.
80. D. S. Fox, M. C. Cruz, R. A. L. Sia, H. Ke, G. M. Cox, M. E. Cardenas and J. Heitman, *Mol. Microbiol.*, 2001, **39**, 835-849.
81. A. Odom, S. Muir, E. Lim, D. L. Toffaletti, J. Perfect and J. Heitman, *EMBO J*, 1997, **16**, 2576-2589.
82. C. H. Mody, G. B. Toews and M. F. Lipscomb, *Infect. Immun.*, 1988, **56**, 7-12.
83. G. M. Cox, H. C. McDade, S. C. A. Chen, S. C. Tucker, M. Gottfredsson, L. C. Wright, T. C. Sorrell, S. D. Leidich, A. Casadevall, M. A. Ghannoum and J. R. Perfect, *Mol. Microbiol.*, 2001, **39**, 166-175.
84. M. A. Olszewski, M. C. Noverr, G.-H. Chen, G. B. Toews, G. M. Cox, J. R. Perfect and G. B. Huffnagle, *Am. J. Pathol.*, 2004, **164**, 1761-1771.
85. R. Ganendren, E. Carter, T. Sorrell, F. Widmer and L. Wright, *Microbes. Infect.*, 2006, **8**, 1006-1015.
86. L. C. Wright, R. M. Santangelo, R. Ganendren, J. Payne, J. T. Djordjevic and T. C. Sorrell, *Eukaryot. Cell*, 2007, **6**, 37-47.
87. M. C. Noverr, G. M. Cox, J. R. Perfect and G. B. Huffnagle, *Infect. Immun.*, 2003, **71**, 1538-1547.
88. S. Chen, M. Muller, J. Zhong Zhou, L. C. Wright and T. Sorrell, *J. Infect. Dis.*, 1997, **175**, 414-420.
89. A. S. Kantarcioglu and A. Yücel, *Med. Mycol.*, 2002, **40**, 519-523.
90. D. Ellis, *J. Antimicrob. Chemother.*, 2002, **49 Suppl 1**, 7-10.
91. N.-H. Park, K.-H. Shin and M. K. Kang, in *Pharmacology and Therapeutics for Dentistry (Seventh Edition)*, eds. F. J. Dowd, B. S. Johnson and A. J. Mariotti, Mosby, 2017, DOI: <https://doi.org/10.1016/B978-0-323-39307-2.00034-5>, pp. 488-503.
92. L. D. Saravolatz, L. Ostrosky-Zeichner, K. A. Marr, J. H. Rex and S. H. Cohen, *Clin. Infect. Dis.*, 2003, **37**, 415-425.
93. J. D. Dutcher, *Chest*, 1968, **54**, 296-298.
94. S. H. Khoo, J. Bond and D. W. Denning, *J. Antimicrob. Chemother.*, 1994, **33**, 203-213.
95. A. C. Mesa-Arango, A. Forastiero, L. Bernal-Martínez, M. Cuenca-Estrella, E. Mellado and O. Zaragoza, *Med. Mycol.*, 2013, **51**, 461-472.
96. M. A. Ghannoum and L. B. Rice, *Clin. Microbiol. Rev.*, 1999, **12**, 501-517.
97. F. C. Odds, A. J. P. Brown and N. A. R. Gow, *Trends Biochem. Sci.*, 2003, **11**, 272-279.
98. R. Laniado-Laborin and M. N. Cabrales-Vargas, *Rev. Iberoam. Micol.*, 2009, **26**, 223-227.
99. R. Laniado-Laborin and M. N. Cabrales-Vargas, *Rev. Iberoam. Micol.*, 2009, **26**, 223-227.
100. T. Bicanic, C. Bottomley, A. Loyse, A. E. Brouwer, C. Muzoora, K. Taseera, A. Jackson, J. Phulusa, M. C. Hosseinipour, C. van der Horst, D. Limmathurotsakul, N. J. White, D. Wilson, R. Wood, G. Meintjes, T. S. Harrison and J. N. Jarvis, *Antimicrob. Agents. Ch.*, 2015, **59**, 7224-7231.
101. Y. W. Kim, *Electrolyte Blood Press*, 2007, **5**, 111-115.
102. R. J. Hamill, *Drugs*, 2013, **73**, 919-934.
103. M. E. Falagas, D. E. Karageorgopoulos and G. S. Tansarli, *PLoS One*, 2013, **8**, e77075-e77075.
104. H. Vanden Bossche, P. Marichal and F. C. Odds, *Trends Biochem. Sci.*, 1994, **2**, 393-400.
105. E. M. O'Shaughnessy, C. A. Lyman and T. J. Walsh, in *Antimicrobial Drug Resistance*, ed. D. L. Mayers, Humana Press, 2009, pp. 295-305.
106. K. Richardson, *Journal of chemotherapy (Florence, Italy)*, 1990, **2**, 51-54.
107. K. Richardson, K. W. Brammer, M. S. Marriott and P. F. Troke, *Antimicrob. Agents. Ch.*, 1985, **27**, 832-835.
108. C. Charlier, E. Hart, A. Lefort, P. Ribaud, F. Dromer, D. W. Denning and O. Lortholary, *J. Antimicrob. Chemother.*, 2006, **57**, 384-410.
109. H. V. Bossche, L. Koymans and H. Moereels, *Pharmacol. Ther.*, 1995, **67**, 79-100.
110. P. Marichal, J. Gorrens and H. Vanden Bossche, *Med. Mycol.*, 1985, **23**, 13-21.
111. C. J. Jessup, M. A. Pfaller, S. A. Messer, J. Zhang, M. Tumberland, E. K. Mbidde and M. A. Ghannoum, *J. Clin. Microbiol.*, 1998, **36**, 2874-2876.
112. F. H. Benkoó, A. Megyeri, A. Kiss, G. Somogyi, Z. Tegye, F. Kraicsovits, P. Kovács, *J. Antimicrob. Chemother.*, 1999, 675-681.
113. Y. Pasikhova and S. Ludlow, *Int. J. Clin. Pharmacy.*, 2014, **36**, 268-270.
114. T. D. Hilley Vensel, *Prim. Care. Update. Ob. Gyns.*, 2002, **9**, 181-183.
115. N. Dunkel, T. T. Liu, K. S. Barker, R. Homayouni, J. Morschhäuser and P. D. Rogers, *Eukaryot. Cell*, 2008, **7**, 1180-1190.
116. A. G. S. Warrilow, C. M. Martel, J. E. Parker, N. Melo, D. C. Lamb, W. D. Nes, D. E. Kelly and S. L. Kelly, *Antimicrob. Agents. Ch.*, 2010, **54**, 4235-4245.
117. D. Sanglard, F. Ischer, L. Koymans and J. Bille, *Antimicrob. Agents. Ch.*, 1998, **42**, 241-253.
118. Z. A. Kanafani and J. R. Perfect, *Clin. Infect. Dis.*, 2008, **46**, 120-128.

119. C. M. Martel, J. E. Parker, O. Bader, M. Weig, U. Gross, A. G. S. Warrilow, N. Rolley, D. E. Kelly and S. L. Kelly, *Antimicrob. Agents. Ch.*, 2010, **54**, 4527-4533.
120. E. L Berkow and S. Lockhart, *Infection and Drug Resistance*, 2017, **Volume 10**, 237-245.
121. R. Duschinsky, E. Plevan and C. Heidelberger, *J. Am. Chem. Soc.*, 1957, **79**, 4559-4560.
122. C. Heidelberger, L. Griesbach, B. Jo Montag, D. Mooren, O. Cruz, R. J Schnitzer and E. Grunberg, *Proc. Am. Assoc. Cancer. Research.*, 1958, **18**, 305-317.
123. E. Grunberg, E. Titsworth and M. Bennett, *Antimicrob. Agents. Ch.*, 1964, 566-568.
124. D. Tassel and M. A. Madoff, *J. Am. Med. Assoc.*, 1968, **206**, 830-832.
125. E. R. Block and J. E. Bennett, *Antimicrob. Agents. Ch.*, 1972, **1**, 476-482.
126. J. E. Bennett, *Ann. Intern. Med.*, 1977, **86**, 319-322.
127. A. Polak and H. Scholer, *Rev. Inst. Pasteur. Lyon*, 1980, **13**, 233-244.
128. A. R. Waldorf and A. Polak, *Antimicrob. Agents. Ch.*, 1983, **23**, 79-85.
129. A. Vermes, H.-J. Guchelaar and J. Dankert, *J. Antimicrob. Chemother.*, 2000, **46**, 171-179.
130. A. Polak, *Contrib. Microbiol. Immunol.*, 1977, **4**, 158-167.
131. M. Fasoli and D. Kerridge, *Ann. NY. Acad. Sci.*, 1988, **544**, 260-263.
132. D. J. Krysan, *Fungal Genet. Biol.*, 2015, **78**, 93-98.
133. A. Mourad and J. R. Perfect, *J. Fungi*, 2018, **4**, 1-10.
134. W. A Schell, C. Giamberardino, K. Shaw and J. R Perfect, *Journal*, 2017, **4**, S478-S478.
135. K. Shaw, W. Schell, J. Covell, G. Duboc, C. Giamberardino, M. Kapoor, M. Moloney, Q. Soltow, J. Tenor, D. Toffaletti, M. Trzoss, P. Webb and J. R. Perfect, *Antimicrob. Agents. Ch.*, 2018, **62**, e00523-00518.
136. K. Koselny, J. Green, L. DiDone, J. P. Halterman, A. W. Fothergill, N. P. Wiederhold, T. F. Patterson, M. T. Cushion, C. Rappelye, M. Wellington and D. J. Krysan, *Antimicrob. Agents. Ch.*, 2016, **60**, 7115-7127.
137. H. Nishikawa, Y. Fukuda, J. Mitsuyama, M. Tashiro, A. Tanaka, T. Takazono, T. Saijo, K. Yamamoto, S. Nakamura, Y. Imamura, T. Miyazaki, H. Kakeya, Y. Yamamoto, K. Yanagihara, H. Mukae, S. Kohno and K. Izumikawa, *J. Antimicrob. Chemother.*, 2017, **72**, 1709-1713.
138. K. Nielsen, P. Vedula, K. D. Smith, D. B. Meya, E. P. Garvey, W. J. Hoekstra, R. J. Schotzinger and D. R. Boulware, *Med. Mycol.*, 2016, **55**, 453-456.
139. C. Lazzarini, K. Haranahalli, R. Rieger, H. Ananthula, P. Desai, A. Ashbaugh, M. Linke, M. Cushion, B. Ruzsicska, J. Haley, I. Ojima and M. Del Poeta, *Antimicrob. Agents. Ch.*, 2018, **62**, e00156-00118.
140. S. B. Singh, W. Liu, X. Li, T. Chen, A. Shafiee, D. Card, G. Abruzzo, A. Flattery, C. Gill, J. R. Thompson, M. Rosenbach, S. Dreikorn, V. Hornak, M. Meinz, M. Kurtz, R. Kelly and J. C. Onishi, *ACS Med. Chem. Lett.*, 2012, **3**, 814-817.
141. Z. Jiang, N. Liu, G. Dong, Y. Jiang, Y. Liu, X. He, Y. Huang, S. He, W. Chen, Z. Li, J. Yao, Z. Miao, W. Zhang and C. Sheng, *Bioorg. Med. Chem. Lett.*, 2014, **24**, 4090-4094.
142. B. Zhai, C. Wu, L. Wang, M. S. Sachs and X. Lin, *Antimicrob. Agents. Ch.*, 2012, **56**, 3758-3766.
143. J. Rhein, B. M. Morawski, K. H. Hullsiek, H. W. Nabeta, R. Kiggundu, L. Tugume, A. Musubire, A. Akampurira, K. D. Smith, A. Alhadab, D. A. Williams, M. Abassi, N. C. Bahr, S. S. Velamakanni, J. Fisher, K. Nielsen, D. B. Meya and D. R. Boulware, *Lancet.*, 2016, **16**, 809-818.
144. A. Butts, K. Koselny, Y. Chabrier-Roselló, C. P. Semighini, J. C. S. Brown, X. Wang, S. Annadurai, L. DiDone, J. Tabroff, W. E. Childers, Jr., M. Abou-Gharbia, M. Wellington, M. E. Cardenas, H. D. Madhani, J. Heitman and D. J. Krysan, *mBio.*, 2014, **5**, e00765-00713.

Chapter 2

An Overview of the Benzimidazoles – Properties and Medicinal Uses

2.1 Benzimidazole Structure, Properties and Reactivity

2.1.1 Structure

A benzimidazole (**1**) is a bicyclic compound that is the result of fusion between a benzene ring and an imidazole ring. It is considered a benzene derivative of the imidazole class.¹ It is important to understand how benzimidazoles are numbered, as there will be numerous references to numbered positions throughout this section. Numbering starts at the NH, due to this having the highest priority and proceeds in an anti-clockwise manner towards the second nitrogen, as this is the next highest priority due to having a high atomic number and this results in the second nitrogen being numbered as position three. It then skips the bridging carbon atoms and continues numbering around the benzene ring portion of the molecule (Figure 2.1).²

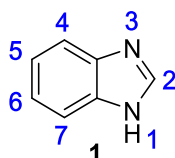


Figure 2.1. Benzimidazole numbering starts from the NH, continuing anti-clockwise so it numbers the second nitrogen third, as this has the highest atomic number.

2.1.2 Tautomerism

The position of the nitrogen atoms in the benzimidazole core mean that tautomerisation can occur as shown below. This tautomerism is also observed in imidazoles and amidines, with benzimidazoles often thought of as cyclic analogues of amidines (Figure 2.2).³

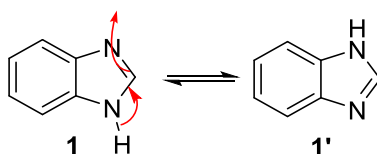


Figure 2.2. Due to the position of the two nitrogen atoms within the benzimidazole, tautomerism can occur.

Rather than producing two distinct isomers of benzimidazole, two different tautomeric forms **1** and **1'** are produced instead. Even though non-equivalent structures can be drawn, only one structure is known. This is also apparent in the Nuclear Magnetic Resonance (NMR) spectra of these compounds, given there is only one tautomer is observed, though both tautomers have been observed using solid state NMR. The benzimidazoles rapidly undergo tautomerisation, meaning the groups in the 4 and 5 positions on the benzimidazole ring are equivalent to the 6 and 7 positions (Figure 2.3). When a group is attached to the nitrogen in position one, this tautomerisation is prevented. This produces isomeric, rather than tautomeric compounds **2** and **2'** (Figure 2.3).⁴

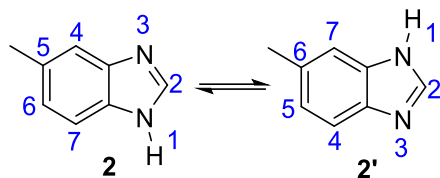


Figure 2.3. Tautomerisation means that when a group is attached in the 4 or 5 position, upon tautomerisation, this is equivalent to the 7 or 6 position respectively.

In the literature, Density Functional Theory (DFT) calculations have been carried out which show very little difference in the energies for the two tautomers of the commercially available drug omeprazole sulphoxide (**3**) and (**3'**) (Figure 2.4). This small energy difference further validates that this tautomerisation is continuously occurring and gives further understanding as to why we only see one set of peaks in NMR spectra. This is something that is important to consider when we investigate binding poses of benzimidazoles, and is discussed in detail in computational section in Chapter 7.⁵

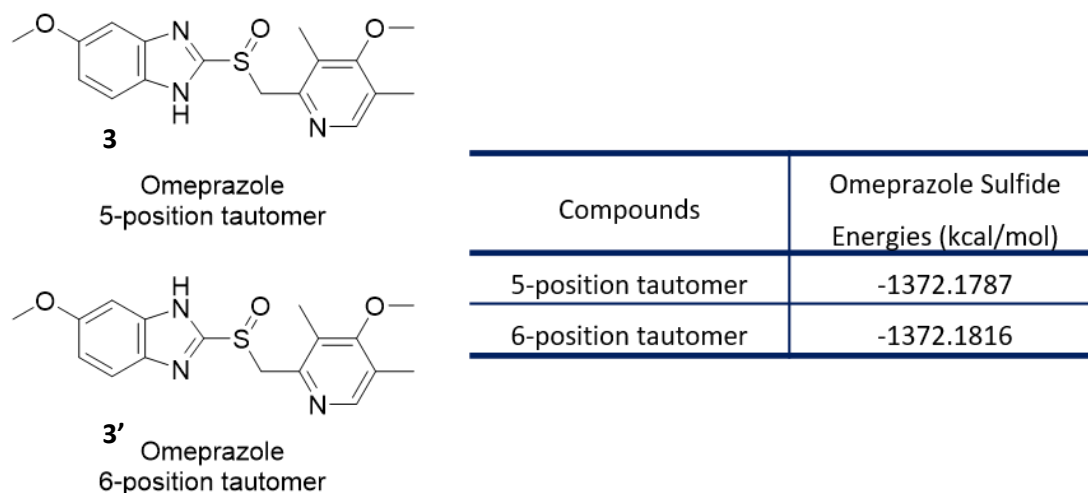


Figure 2.4. Omeprazole contains a benzimidazole moiety, which can undergo tautomerisation. DFT calculations show only a very subtle energy difference can be observed. Reproduced from; *NMR investigation and theoretical calculations on the tautomerism of benzimidazole compounds*, S. Feng *et al.*⁵

2.1.3 Chemical Reactivity

The two nitrogen atoms within the benzimidazole core are chemically distinct. Benzimidazoles have the ability to behave in both an acidic and basic manner. This is due to the differences between the two nitrogen atoms within the ring. When **1** behaves as a base it does so on the nitrogen in the 3-position. This nitrogen has a readily accessible lone pair of electrons which can attack protons to generate a salt (**4**) (Figure 2.5A). It can also react with numerous electrophiles including alkyl halides. Firstly, there is alkylation of the 3-position nitrogen to give an intermediate salt **5**, which can then lose HX to give the desired alkylated compound **6** (Figure 2.5B). Once methylation has occurred on one of the nitrogen atoms, tautomers can no longer be generated and we observe both isomers **7** and **8** of the benzimidazole, if there is substitution on the benzene ring (Figure 2.6).^{3, 6-8}

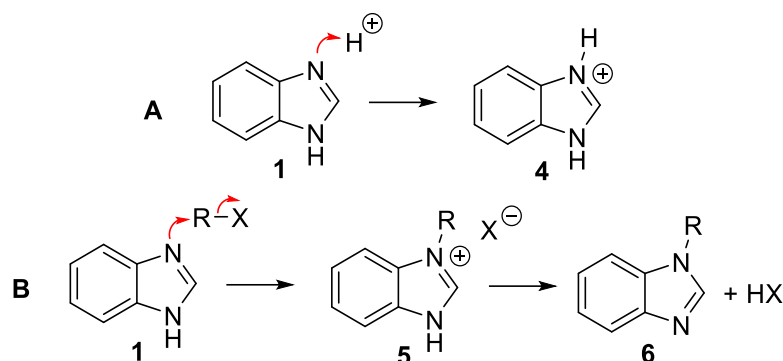


Figure 2.5 A. Benzimidazole exhibits basic properties when the nitrogen at the 3-position attacks a proton. **2.5B.** It also reacts with electrophiles in a similar manner, allowing the alkylation at the 3 position.⁸



1,5-dimethyl-1*H*-benzo[*d*]imidazole 1,6-dimethyl-1*H*-benzo[*d*]imidazole

Figure 2.6. Alkylation of one of the benzimidazole nitrogen atoms leads to two distinct compounds as the benzimidazole can no longer undergo tautomerisation.⁸

Benzimidazoles also exhibit acidic properties when they are attacked by a stronger base **9** (Figure 2.7). This is due to the nitrogen in the 1-position having a weakly acidic proton, which has a pK_a of 12.17 in water and is deprotonated by strong bases such as *n*-BuLi **10**.^{9,10} This is useful as it allows for alkylation of the benzimidazole nitrogen in the 1-position (Figure 2.8).¹¹⁻¹³

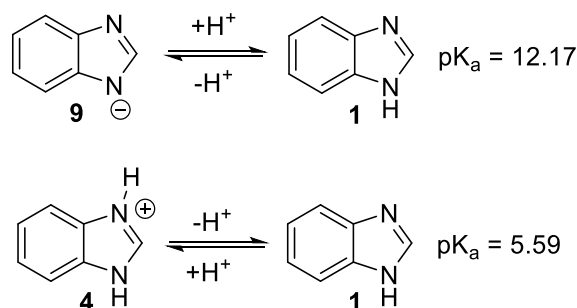


Figure 2.7. Benzimidazoles are amphoteric in nature and possess two pK_a values.¹⁰

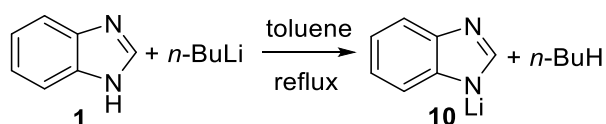


Figure 2.8. Benzimidazoles also exhibit acidic properties via the 1-position nitrogen when treated with bases such as *n*-butyllithium.⁹

2.1.4 Historical Synthesis of Benzimidazoles

Hoebrecker synthesised the first benzimidazole in 1872.¹⁴ The reduction of 2-nitro-4-methylacetanilide (**11**) to the amine derivative **12**, using tin and hydrochloric acid and then ring closure produced 2,5-dimethylbenzimidazole **13**. Ladenburg in 1875 also prepared the same compound by

starting with 3,4-diaminotoluene (**14**) and reacting with acetic acid to produce an intermediate **12**, which upon the loss of water resulted in the ring closed benzimidazole **13** (Figure 2.9).^{3, 15, 16}

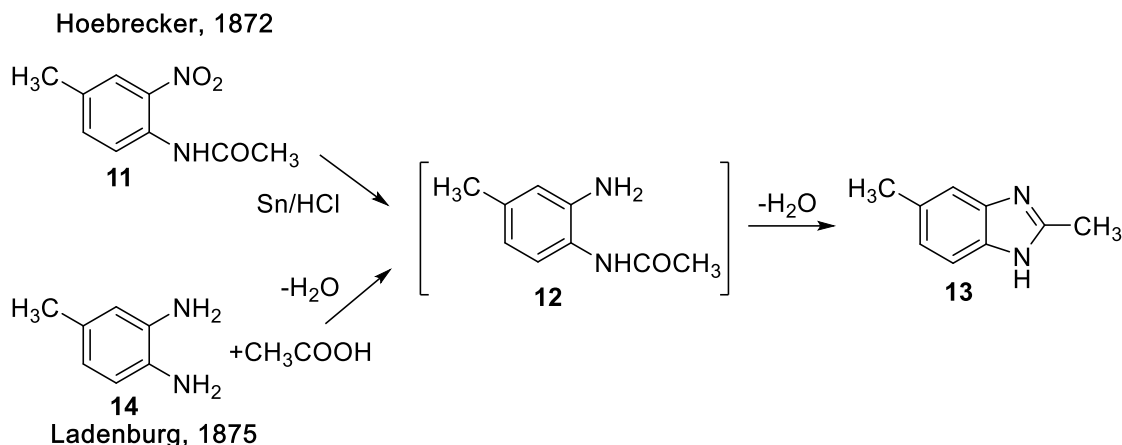


Figure 2.9. 2,5-dimethylbenzimidazole **13** was historically synthesised in the 1870's by Hoebrecker and Ladenburg.^{14, 15}

2.2 Benzimidazoles as Medicines

2.2.1 Current Benzimidazole Containing Compounds

The benzimidazole core is medicinally relevant and occurs in a number of FDA approved drugs, and occurs naturally in compounds vital to the human body.

2.2.1.1 Vitamin B12

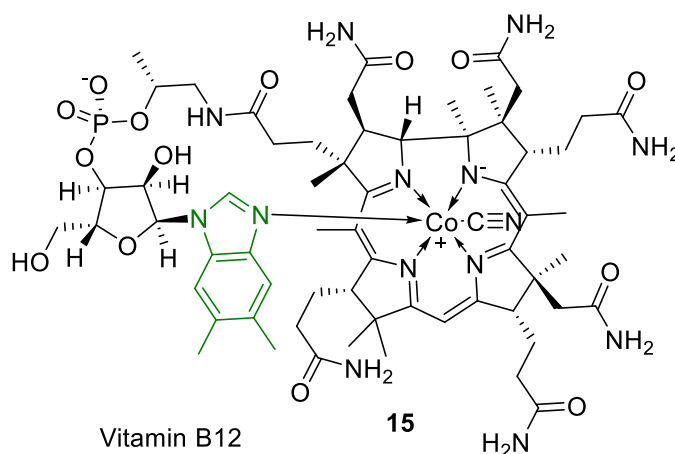


Figure 2.10. The structure of Vitamin B12 (**15**), with the benzimidazole moiety highlighted in green.

Vitamin B₁₂ (**15**), also known as cobalamin is vitally important to metabolism, DNA synthesis, synthesis of myelin and the maturation of red blood cells amongst many other processes (Figure 2.10).¹⁷⁻¹⁹ It contains a cobalt ion at its core, whereby four of the coordination sites are connected to a corrin ring. The fifth coordination site is to the benzimidazole moiety and the sixth to another moiety, which here is shown as a cyano group.²⁰ **15** deficiency causes issues with the nervous system due to lack of production of myelin which protects neurons. It also causes symptoms of fatigue and lethargy.

2.2.1.2 Omeprazole

Omeprazole (**3**) is another example of a compound containing the benzimidazole core. It is a proton-pump inhibitor that stops the secretion of gastric acid (Figure 2.11). It blocks the hydrogen/potassium adenosine triphosphatase enzyme system, which is also known as the 'proton pump'.²¹ This is important in the treatment of conditions where the patient is suffering from excessive or harmful gastric secretion, such as those suffering from dyspepsia or gastro-oesophageal reflux disease (GORD).²²

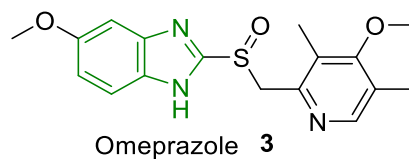


Figure 2.11. The structure of Omeprazole (**3**), a proton-pump inhibitor. The benzimidazole moiety is highlighted in green.

2.2.2 Benzimidazoles as Plant Fungicides

In 1964, it was discovered that thiabendazole (**16**) could be used to inhibit the growth of the plant fungal infection *Cercospora beticola*, which is the cause of leaf spot in sugarbeet crops.²³⁻²⁵ **16** showed broad spectrum activity and was used as a post-harvest treatment for plants to kill off a range of fungi. Benzimidazoles, including benomyl (**26**) and carbendazim (**25**) have also been tested against a number of other plant based fungal species including *Botrytis cinerea*, *Gossypium hirsutum*, *Helianthis annuus*, *Lactuca sativa* and *Pinus taeda*. In all cases, application reduced growth of these species within the plant.^{26, 27} At the time, they represented a ground breaking new class of agricultural fungicides that were used directly in soil on a huge variety of plants. Despite the emergence of resistance in some species, they are still widely used today as fungicides.²⁸

2.2.3 Benzimidazoles as Anthelmintics

Benzimidazoles have previously been used to treat helminthic infections. Helminthic infections are one of the biggest problems concerning the global production of livestock.²⁹ Initially, they were introduced to treat veterinary infections, but in 1962 the first benzimidazole, thiabendazole **16**, was developed and licensed for use in humans, and this was followed by four other benzimidazoles; mebendazole (**17**), flubendazole (**18**), albendazole (**19**) and triclabendazole (**20**) (Figure 2.12), and is a good example of a 'me-too' set of compounds, whereby chemically related compounds are produced.

^{30, 31}

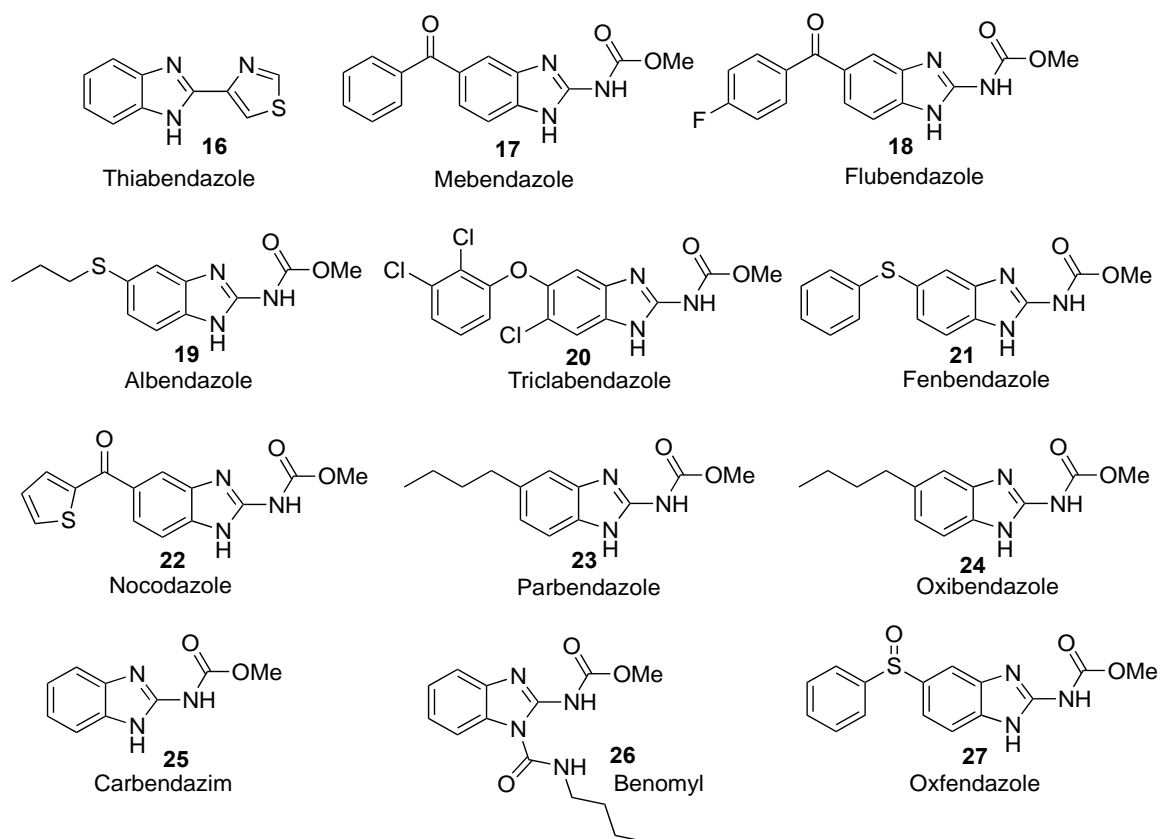


Figure 2.12. A number of benzimidazoles **16-27** have been tested as antihelminthic and antifungal agents.

2.2.4 Benzimidazoles as Antifungals

2.2.4.1 Benzimidazole Cryptococcal Data

Whilst the work surrounding benzimidazoles as anti-cryptococcal agents is limited, some research has emerged which demonstrates the activity levels of some of the benzimidazole analogues in the form of inhibitory concentration values against clinical isolates of *C. neoformans* at both 50% and 90% inhibition. These studies were carried out using a number of isolates, revealing data that will allow for the targeted design of benzimidazole analogues (Table 2.1).³²

Table 2.1: Inhibitory concentrations for a number of benzimidazole compounds tested against three clinical isolates. Reproduced from; *In vitro susceptibility of the opportunistic fungus Cryptococcus neoformans to anthelmintic benzimidazoles*, M. Cruz et al.³²

Drug	IC($\mu\text{g/mL}$) for indicated isolates					
	IU4		IU8698		ATCC 14116	
	50%	90%	50%	90%	50%	90%
Fenbendazole 21	0.019	0.028	0.011	0.014	<0.016	<0.016
Nocodazole 22	0.13	0.22	0.09	0.12	0.20	0.29
Parbendazole 23	0.16	0.23	0.16	0.23	0.16	0.22
Mebendazole 17	0.23	0.43	0.18	0.32	0.19	0.40
Albendazole 19	0.16	0.25	0.31	0.45	0.30	0.45
Oxibendazole 24	2.3	3.2	1.0	2.1	1.4	2.1
Carbendazim 25	2.0	3.6	1.5	2.0	1.6	2.3
Benomyl 26	2.3	3.7	2.8	3.8	2.0	3.5
Oxfendazole 27	2.5	>4.0	3.2	>4.0	2.8	4.0
Thiabendazole 16	>4.0	>4.0	>4.0	>4.0	>4.0	>4.0
Benzimidazole 1	>4.0	>4.0	>4.0	>4.0	>4.0	>4.0
Amphotericin B	0.035	0.064	0.024	0.065	0.011	0.045

2.2.5 Initial SAR of Benzimidazole Analogues against *C. neoformans*

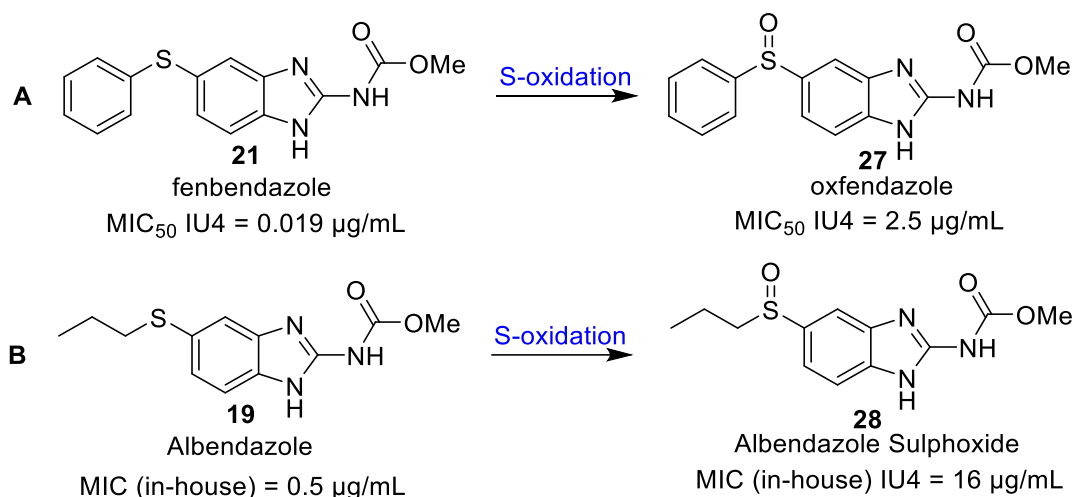


Figure 2.13A. Fenbendazole (**21**), the compound which shows the greatest activity against *C. neoformans* is metabolised to oxfendazole (**27**), which is one of the worst performing compounds, via CYP450 and FMO enzymes through the S-oxidation pathway.³³⁻³⁵ **2.13B.** Albendazole (**19**) is metabolised in the same way.

The data in Table 2.1 provide some initial SAR understanding, which with selective design of new analogues should lead to optimal activity against *C. neoformans*. From the table, it is apparent that the albendazole analogue fenbendazole (**21**) shows the lowest inhibitory concentration (0.016–0.028 $\mu\text{g/mL}$), which for most of the isolates is better than amphotericin B (0.011–0.064 $\mu\text{g/mL}$). However, oxfendazole (**27**) shows reduced inhibitory activity (Figure 2.13A). In the case of **19**, it is metabolised by CYP450 and flavin mono-oxygenases (FMO) to give albendazole sulphoxide (**28**) (Figure 2.13B).³³⁻³⁵ This is also most likely to be what is occurring with fenbendazole, meaning it could be being oxidised

to an inactive form. Furthermore, in-house testing of the synthesised albendazole sulphoxide, showed it had no activity against *C. neoformans* (Figure 2.13B).

All of the analogues that show activity against *C. neoformans* have a carbamate attached to the benzimidazole core in the 2-position, suggesting from the admittedly limited data set that this is required for activity. This is also further validated when observing the data for benzimidazole (**1**) and thiabendazole (**16**), which have virtually no activity against *C. neoformans* and have no carbamate functionality. Benomyl (**26**), which has a group attached to a ring nitrogen in the 1-position, shows reduced activity when compared with those compounds that have no groups at this position (Figure 2.14).

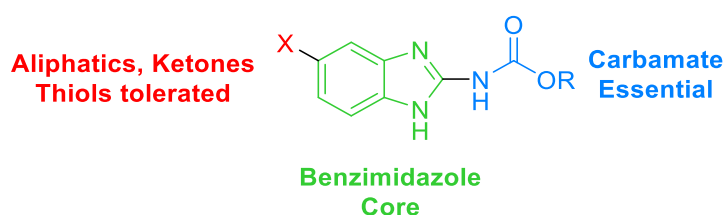


Figure 2.14. Using SAR to understand what moieties are essential to benzimidazole activity can lead to compounds with optimal activity.

The data in Table 1.1 allow for a basic structure activity profile to be observed, which includes the necessity for a carbamate group and the 2-position, and in the 5/6 position it appears a variety of groups can be introduced including; aliphatics, ketones and heteroatom linkers, with a variety of aromatic moieties tolerated. It also shows that preferentially there should be no alkylation on the NH nitrogen.

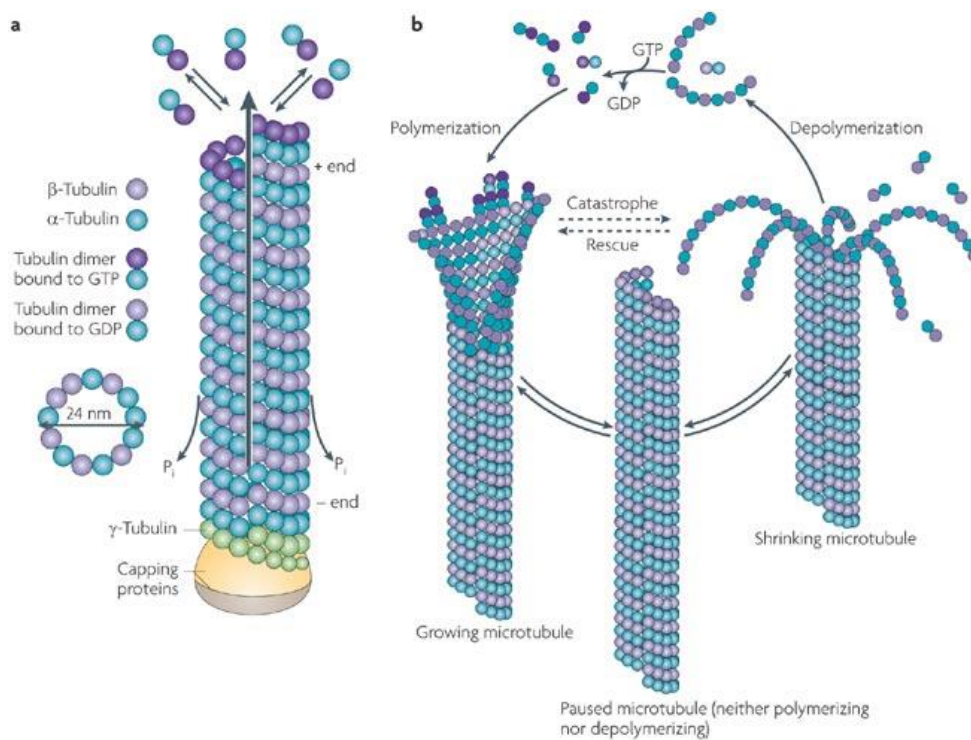
2.3 Benzimidazoles and β -Tubulin

Benzimidazoles are known to exert their biological effects by binding to the β -tubulin subunit of microtubules, which inhibits mitosis (Figure 2.15).^{36, 37}

2.3.1 Microtubule Structure and Function

Microtubules are filaments that are one of the main components of the cytoskeleton in eukaryotic cells. Tubulin is comprised of two polypeptide units (α -tubulin and β -tubulin), which dimerise to give long stranded protofilaments.^{38, 39}

Microtubules are composed of thirteen protofilaments coming together to give a characteristic hollow, tube like structure. Microtubules have a dynamic structure, whereby they are growing and shrinking all the time. At the end where the microtubules grow more rapidly, there is more polymerisation and this is designated the plus end. The other end, where depolymerisation occurs, is designated the minus end. In non-dividing cells they are used in cytoplasmic organisation, particularly of organelles. In dividing cells (mitosis) they function to segregate chromosomes in a cell, forming a mitotic spindle, which allows for cellular division (Figure 2.15).³⁸⁻⁴¹



Nature Reviews | Neuroscience

Figure 2.15. Microtubules are constantly undergoing a process of polymerisation and depolymerisation, allowing for growing and shrinking of the microtubules respectively. Microtubule depolymerisation allows for tubulin chains to be cleaved, which are then converted to tubulin dimers, which can then be reused in the polymerisation process. Reproduced from; *Microtubule assembly, organization and dynamics in axons and dendrite*, C. Conde *et al.*³⁹

2.3.2 Benzimidazole Mode of Action

Characterisation of the β -tubulin genes of *C. neoformans* has identified TUB1 as the primary target of the benzimidazole class of compounds. Comparing the biological effects of benzimidazoles with other drugs known to interact and effect polymerisation of microtubules has identified the way in which mitosis is inhibited.

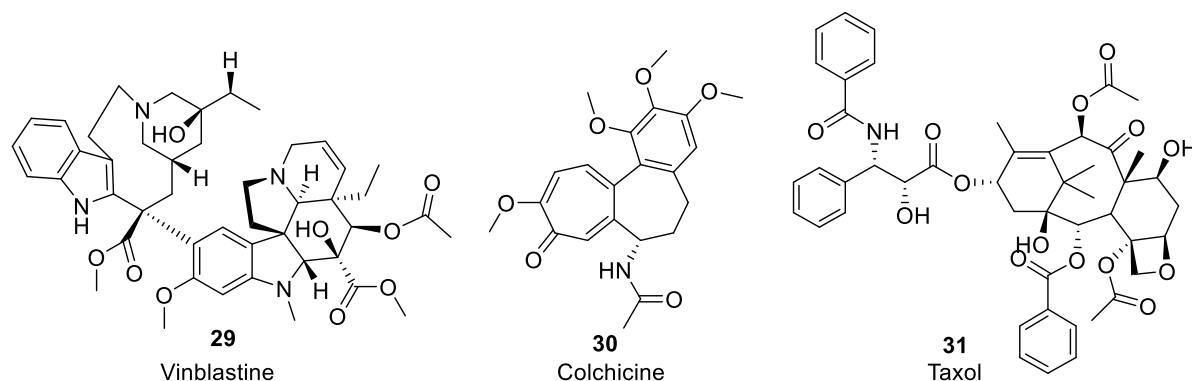


Figure 2.16. The structures of the β -tubulin bindings compounds; vinblastine **29**, colchicine **30** and taxol **31**.⁴²

Vinblastine (**29**), a well-known anticancer drug, interacts with tubulin and causes a decrease in the number of reactive cysteine residues by 8.6.⁴²⁻⁴⁴ When the same experiment was carried out using the benzimidazole analogue flubendazole (**18**), the number of reactive cysteine residues decreased by 5.2, which indicates that it interacts with tubulin, though maybe not to the same extent as vinblastine (**29**). The interaction of a drug with tubulin can either cause an increase or decrease in polymerisation, both of which can affect mitosis. Comparisons were drawn with colchicine (**30**),^{44, 45} which inhibits microtubule polymerisation and taxol (paclitaxel) (**31**), which increases microtubule polymerisation.^{44, 46} It was found that flubendazole (**18**) and mebendazole (**17**) behaved similarly to **30** and inhibited microtubule polymerisation, thus inhibiting mitosis (Figure 2.17).^{41, 47} They are also proposed to bind to the β -tubulin at the colchicine binding site, which will be discussed in more detail in Chapter 7.⁴⁸

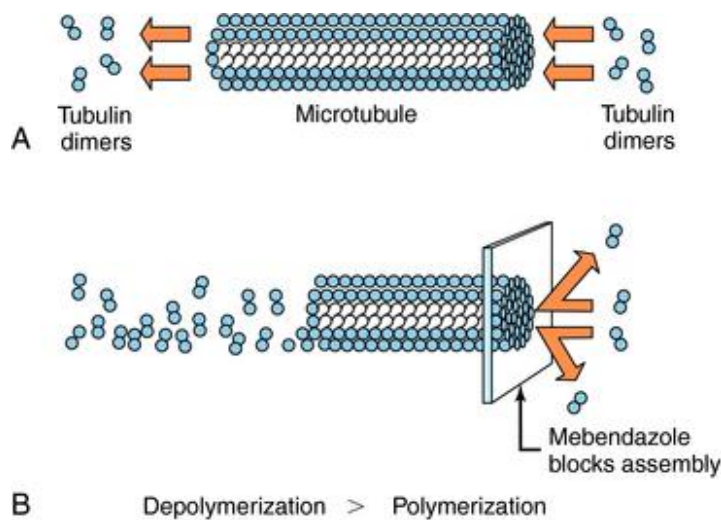


Figure 2.17. Mebendazole (**17**), a derivative of the benzimidazole being investigated inhibits cellular mitosis via blocking polymerisation within the microtubule, meaning the rate of depolymerisation is greater than polymerisation, resulting in a shortening of the microtubule and inhibited mitosis. Reproduced from; *Brody's Human Pharmacology, Chapter 52 Drugs to Treat Parasitic Infection*, S. Watts et al.⁴⁷

2.4 Benzimidazole Metabolism

From literature predictions and biological evaluation, there are multiple ways in which benzimidazoles are metabolised, and this varies depending on whether they are flubendazole (**18**) or albendazole (**19**) derivatives.

2.4.1 Flubendazole Metabolism

A group at Charles University, Prague, conducted *in vitro* and *ex vivo* experiments on **18** and identified via HPLC, utilising mass-spectrometric and spectrofluorimetric detection, that four flubendazole metabolites were present. One metabolite was formed via the reduction of the ketone to the alcohol **32** (FLU-OH) carried out via a reductase enzyme. Further metabolism of the alcohol lead to a glucoside analogue (FLU-O-glucoside) **33** and two other glucoside conjugates of flubendazole **34** and **35**, carried out via a UDP-glucosyl transferase enzyme (Figure 2.18).⁴⁹

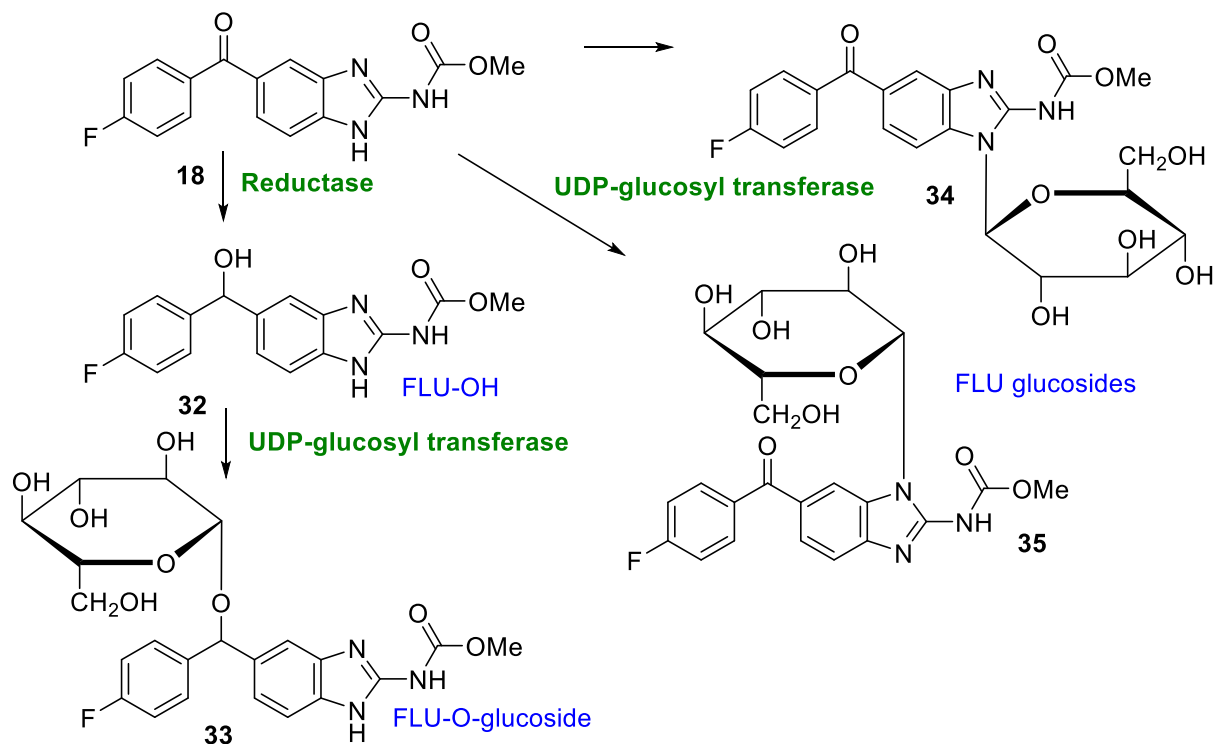


Figure 2.18. Previous research to investigate the metabolism of flubendazole revealed four metabolites; a reduced ketone analogue (FLU-OH) **32** and alcohol-glucoside conjugate (FLU-O-glucoside) **33** and two flubendazole glucoside conjugates **34** and **35**. Reproduced from; *The metabolism of flubendazole and the activities of selected biotransformation enzymes in Haemonchus contortus strains susceptible and resistant to anthelmintics*, I. Vokřál *et al.*⁴⁹

Another paper published by Moreno *et al* also discovered that **18** can undergo a hydrolysis or decarboxylation reaction, which cleaves the carbamate group, leaving behind a primary amine **36** (Figure 2.19). When sheep were dosed at 5 mg/kg, the FLU-NH₂ metabolite **36** exhibited very low plasma concentrations of 0.103 – 0.016 µg/ml over 36 hours. It also showed that the reduced FLU-OH

32 metabolite was the main metabolite, showing a rate of production of this metabolite of 9.46 ± 2.72 nmol/mg/h.⁵⁰ However, in pigs the opposite is true and FLU-NH₂ (**36**) is the predominant metabolite.⁵¹

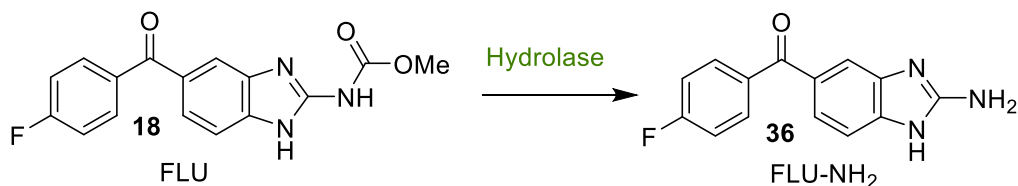


Figure 2.19. Carbamate hydrolysis of flubendazole by hydrolases generates a primary amine.⁵⁰

2.4.2 Albendazole and Fenbendazole Metabolism

The metabolism of albendazole (**19**) differs from flubendazole (**18**). The first instance is the oxidation of the sulphur atom, initially to the sulphoxide **28** and then to the sulphone **37** (Figure 2.20). The drug undergoes almost full first-pass metabolism in the gut or liver to give mixture of *R* and *S* enantiomers of **28**. This same sulphur metabolism is observed in fenbendazole (**21**), producing fenbendazole sulphoxide and fenbendazole sulphone.⁵²

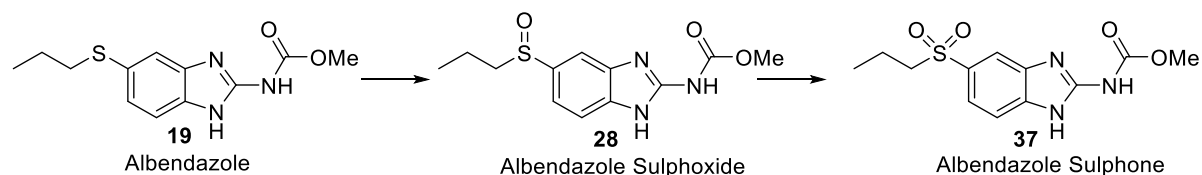


Figure 2.20. The oxidation of albendazole **19** is mediated by FMO and CYP450 enzymes within the liver to give the sulphoxide **28** and subsequently the sulphone **37**.^{33, 53}

Albendazole sulphoxidation in humans is mediated by Flavin Mono-oxygenase (FMO) enzymes and Cytochrome P450 (CYP450) enzymes, in particular CYP3A4, within the liver microsomes. It is reported that rat liver FMO's mediate the formation of (*R*)-albendazole sulphoxide (**28a**) and CYP3A enzymes promote formation of (*S*)-albendazole sulphoxide (**28b**).^{33, 53, 54}

21 undergoes CYP450 mediated hydroxylation of the thiol benzene to give a *para*-hydroxyl metabolite **38**, which can then undergo further metabolism to produce glucuronides and other phase II metabolites (Figure 2.21).^{55, 56} **19** undergoes hydroxylation of the carbamate **39**, as well as hydroxylation of the aliphatic chain attached to the sulphur, this like **21** can then undergo further metabolism, often phase II in nature, utilising enzymes such as UDP-glucosyltransferases. (Figure 2.22).⁵²

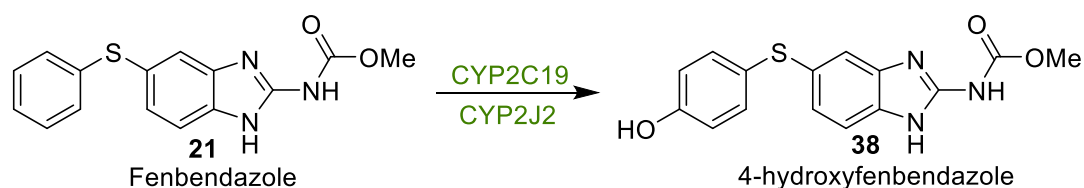


Figure 2.21. Fenbendazole (**21**) is metabolised to the 4-hydroxy metabolite **38** via CYP450 enzymes.⁵⁵

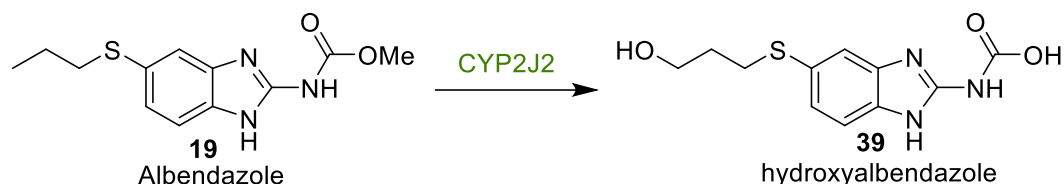


Figure 2.22. Albendazole (**19**) is metabolised to its hydroxylated metabolite **39** via hydroxylation of the alkane chain and the carbamate.⁵⁵

2.5 This Project: The Benzimidazole Core

The data for the small number of benzimidazole compounds above is promising and has led to a benzimidazole template being developed that will allow us to probe the structure activity relationship surrounding flubendazole. Medicinal chemistry will be employed to alter a number of sites on flubendazole to optimise activity against *C. neoformans* (Figure 2.23)

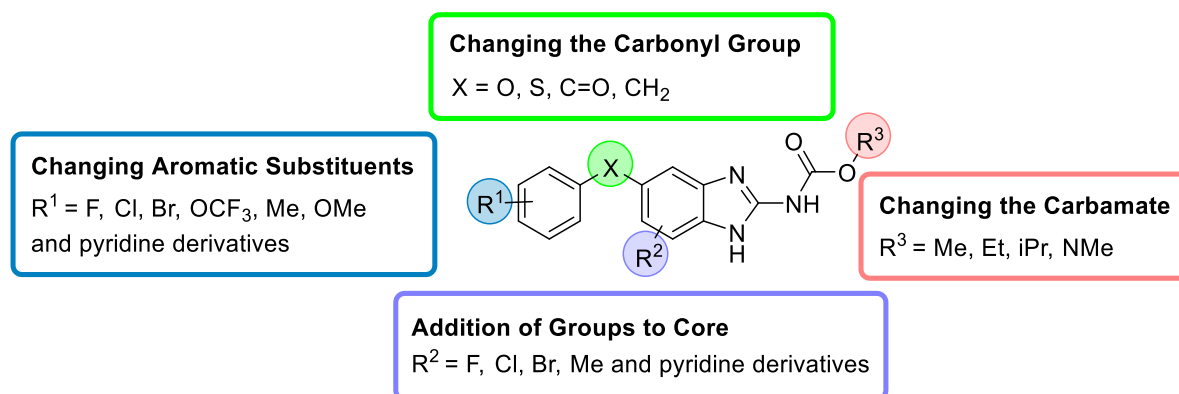


Figure 2.23. Diversifying the molecule at a variety of positions will allow exploration of SAR.

Activity at the R¹ and R² position will be investigated to see if activity can be improved via altering type and position of substituents. A variety of aromatic substituents will be investigated to understand the trends in activity based on size and the electronic properties. It is known in the literature that benzimidazole carbamate derivatives have low aqueous solubility (Table 2.2).^{57, 58} Pyridine groups are often introduced into molecules to enhance water solubility and binding interactions. The benzimidazole carbamates are known for having particularly low water solubility (Table 2.2), so the introduction of pyridine at the R¹ and R² positions could help to enhance water solubility.⁵⁹

Table 2.2. The water solubility data for four benzimidazole compounds.

Compound	Solubility (mg/L)
Albendazole ⁵⁷	1.4
Fenbendazole ⁵⁷	0.9
Carbendazim ⁵⁸	8
Thiazbendazole ⁵⁸	30

The rationale behind the alteration of the carbonyl group at position X derives from literature precedence for synthesis of some of these analogues, mainly of the thiol and ether classes. Furthermore, compounds like fenbendazole, a thioether derivative, have been shown already to possess excellent activity against *C. neoformans*. Finally, alteration of the carbamate end will be carried out to see if potency can still be maintained with expansion or alteration to this group. This includes lengthening the chain to ethyl and isopropyl groups, as well as swapping to a urea moiety, as the addition of urea groups is widely known to increase solubility.⁶⁰

Retrosynthetic analysis suggested that building the core and then carrying out late stage functionalisation was an attractive possibility. Synthesis of the core with a bromine in the 5-position showed potential for a number of palladium coupling reactions, which would allow for this functionalisation. This was attempted for the biphenyl but was unsuccessful. This was thought to be due to the poor solubility of the benzimidazole starting material.

2.6 References

1. B. A. Reddy, *E. J. Chem.*, 2010, **7**, 222-226.
2. Salahuddin, M. Shaharyar and A. Mazumder, *Arab. J. Chem.*, 2017, **10**, S157-S173.
3. J. B. Wright, *Chem. Rev.*, 1951, **48**, 397-541.
4. C. I. Nieto, P. Cabildo, M. Á. García, R. M. Claramunt, I. Alkorta and J. Elguero, *Beilstein J. Org. Chem.*, 2014, **10**, 1620-1629.
5. F. Su, Z. Sun, W. Su and X. Liang, *J. Mol. Struct.*, 2018, **1173**, 690-696.
6. B. B. Ivanova and L. I. Pindeva, *J. Mol. Struct.*, 2006, **797**, 144-153.
7. N. Siddiqui, M. Faiz Arshad, W. Ahsan and M. Alam, *Int. J. Pharm. Sci. Res.*, 2008, **1**, 136-143.
8. K. K. Reddy and N. V. S. Rao, *Proc. Indian Acad. Sci.*, 1969, **70**, 292-299.
9. T. J. Barbarich, P. F. Driscoll, S. Izquierdo, L. N. Zakharov, C. D. Incarvito and A. L. Rheingold, *Inorg. Chem.*, 2004, **43**, 7764-7773.
10. H. Sari and A. K. Covington, *J. Chem. Eng. Data.*, 2005, **50**, 1425-1429.
11. P. N. Preston, *Chem. Rev.*, 1974, **74**, 279-314.
12. R. C. Elderfield, *J. Am. Pharm. Assoc.*, 1951, **40**, 302-302.
13. J. G. Cannon, *Journal of Medicinal Chemistry*, 1997, **40**, 4165-4166.
14. F. Hobrecker, *Ber. Dtsch. Chem. Ges.*, 1872, **5**, 920-924.
15. A. Ladenburg, *Berichte der deutschen chemischen Gesellschaft*, 1875, **8**, 677-678.
16. V. Yerragunta, P. Patil, S. Srujana, R. Devi, R. Gayathri, Srujana and A. Divya, *PharmaTutor*, 2014, **2**, 10-113.
17. K. Yamada, in *Interrelations between Essential Metal Ions and Human Diseases*, eds. A. Sigel, H. Sigel and R. K. O. Sigel, Springer Netherlands, Dordrecht, 2013, DOI: 10.1007/978-94-007-7500-8_9, pp. 295-320.
18. R. Carmel, Megaloblastic anemias: Disorders of impaired DNA synthesis, <https://oncohemakey.com/megaloblastic-anemiasdisorders-of-impaired-dna-synthesis/>, June 2019).
19. A. Miller, M. Korem, R. Almog and Y. Galboiz, *J. Neurol. Sci.*, 2005, **233**, 93-97.
20. M. M. Lubran, *Annals Clin. Lab. Sci.*, 1971, **1**, 236-244.
21. Y. M. Choi-Sledeski and C. G. Wermuth, in *The Practice of Medicinal Chemistry (Fourth Edition)*, eds. C. G. Wermuth, D. Aldous, P. Raboisson and D. Rognan, Academic Press, San Diego, 2015, DOI: <https://doi.org/10.1016/B978-0-12-417205-0.00028-6>, pp. 657-696.
22. A. A. Al-Badr, in *Profiles of Drug Substances, Excipients and Related Methodology*, ed. H. G. Brittain, Academic Press, 2010, vol. 35, pp. 151-262.
23. Z. Solel, *Phytopathology*, 1970, **60**, 1186-1190.
24. G. Stallknecht and G. Crane, *Phytopathology*, 1969, **59**, 393.
25. N. Trkulja, Ž. Ivanović, E. Pfaf-Dolovac, N. Dolovac, M. Mitrović, I. Toševski and J. Jović, *Eur. J. Plant Pathol.*, 2013, **135**, 889-902.
26. J. A. LaMondia and S. M. Douglas, *Plant Dis.*, 1997, **81**, 729-732.
27. M. C. Dias, *J. Bot.*, 2012, DOI: 10.1155/2012/135479, 1-4.
28. H. Ishii, *JARQ*, 2006, **40**, 205-2011.
29. B. Munguía, M. Michelena, E. Melian, J. Saldaña, X. Ures, E. Manta and L. Domínguez, *Exp. Parasitol.*, 2015, **153**, 75-80.
30. O. J. Stone, C. T. Stone, Jr. and J. F. Mullins, *JAMA.*, 1964, **187**, 536-538.
31. S. Régnier, *Health Care Manag. Sci.*, 2013, **16**, 300-313.
32. M. C. Cruz, M. S. Bartlett and T. D. Edlind, *Antimicrob. Agents Chemother.*, 1994, **38**, 378-380.
33. M. P. Marques, O. M. Takayanagui and V. L. Lanchote, *Braz. J. Med. Biol. Res.*, 2002, **35**, 261-269.
34. O. M. Takayanagui, P. S. Bonato, S. A. C. Dreossi and V. L. Lanchote, *Br. J. Clin. Pharmacol.*, 2002, **54**, 125-130.

35. Q. A. McKellar, C. Gokbulut, K. Muzandu and H. Benchaoui, *Drug Metab. Dispos.*, 2002, **30**, 1230-1239.
36. M. E. Oxberry, T. G. Geary and R. K. Prichard, *Parasitology*, 2001, **122**, 683-687.
37. M. Robinson, A. Trudgett, I. Fairweather and N. McFerran, *Trends Parasitol.*, 2002, **18**, 153-154.
38. E. Mandelkow and E.-M. Mandelkow, *Curr. Opin. Struct. Biol.*, 1994, **4**, 171-179.
39. C. Conde and A. Cáceres, *Nat. Rev. Neurosci.*, 2009, **10**, 319-332.
40. M. W. Rochlin, M. E. Dailey and P. C. Bridgman, *Mol. Biol. Cell*, 1999, **10**, 2309-2327.
41. P. A. Spagnuolo, J. Hu, R. Hurren, X. Wang, M. Gronda, M. A. Sukhai, A. Di Meo, J. Boss, I. Ashali, R. Beheshti Zavareh, N. Fine, C. D. Simpson, S. Sharmeen, R. Rottapel and A. D. Schimmer, *Blood*, 2010, **115**, 4824-4833.
42. J. J. Field, A. B. Waight and P. D. Senter, *Proc. Natl. Acad. Sci. U.S.A.*, 2014, **111**, 13684-13685.
43. S. S. Rai and J. Wolff, *J. Biol. Chem.*, 1996, **271**, 14707-14711.
44. Y. Lu, J. Chen, M. Xiao, W. Li and D. D. Miller, *Pharm. Res.*, 2012, **29**, 2943-2971.
45. J. Wolff and L. Knipling, *J. Biol. Chem.*, 1995, **270**, 16809-16812.
46. S. Rao, L. He, S. Chakravarty, I. Ojima, G. A. Orr and S. B. Horwitz, *J. Biol. Chem.*, 1999, **274**, 37990-37994.
47. S. Watts, C. Faingold, G. Dunaway and L. Crespo, in *Brody's Human Pharmacology*, eds. S. Watts, C. Faingold, G. Dunaway and L. Crespo, Elsevier Health Sciences, 2009.
48. R. Aguayo-Ortiz, O. Méndez-Lucio, J. L. Medina-Franco, R. Castillo, L. Yépez-Mulia, F. Hernández-Luis and A. Hernández-Campos, *J. Mol. Graph. Model.*, 2013, **41**, 12-19.
49. I. Vokřál, H. Bártíková, L. Prchal, L. Stuchlíková, L. Skálová, B. Szotáková, J. Lamka, M. Várady and V. Kubíček, *Parasitology*, 2012, **139**, 1309-1316.
50. L. Moreno, L. Alvarez, L. Mottier, G. Virkel, S. Sanchez Bruni and C. Lanusse, *J. Vet. Pharmacol. Ther.*, 2004, **27**, 299-308.
51. L. Ceballos, L. Alvarez, C. Mackenzie, T. Geary and C. Lanusse, *Int. J. Parasitol. Drugs. Drug Resist.*, 2015, **5**, 178-184.
52. E. Syslová, P. Landa, L. R. Stuchlíková, P. Matoušková, L. Skálová, B. Szotáková, M. Navrátilová, T. Vaněk and R. Podlipná, *Chemosphere*, 2019, **218**, 662-669.
53. J. S. McCarthy and T. A. Moore, in *Mandell, Douglas, and Bennett's Principles and Practice of Infectious Diseases*, eds. J. E. Bennett, R. Dolin and M. J. Blaser, Elsevier, Philadelphia, 8th edn., 2015, DOI: <https://doi.org/10.1016/B978-1-4557-4801-3.00042-4>.
54. G. Virkel, A. Lifschitz, J. Sallovitz, A. Pis and C. Lanusse, *Drug Metab. Dispos.*, 2004, **32**, 536-544.
55. Z. Wu, D. Lee, J. Joo, J.-H. Shin, W. Kang, S. Oh, D. Y. Lee, S.-J. Lee, S. S. Yea, H. S. Lee, T. Lee and K.-H. Liu, *Antimicrob. Agents. Chemother.*, 2013, **57**, 5448-5456.
56. M. Murray, A. M. Hudson and V. Yassa, *Chemical research in toxicology*, 1992, **5**, 60-66.
57. Aqueous Solubility from MLSMR Stock Solutions, <https://pubchem.ncbi.nlm.nih.gov/bioassay/1996>, June 2019).
58. C. Coscollà, V. Yusà, M. I. Beser and A. Pastor, *J. Chromatogr. A*, 2009, **1216**, 8817-8827.
59. Y. Hamada, *Intechopen*, 2018, DOI: 10.5772/intechopen.74719, 9-26.
60. L. A. Pinck and M. A. Kelly, *J. Am. Chem. Soc.*, 1925, **47**, 2170-2172.

Chapter 3

Synthesis and Biological Evaluation of Benzimidazole Thioether Derivatives

3.1 Benzimidazole Thioethers

As stated in Chapter 2, some thioether benzimidazole derivatives, including fenbendazole (**1**) and albendazole (**2**) were tested against *C. neoformans*, with fenbendazole possessing the best activity with an MIC range of 0.011 – 0.028 mg/L across a range of *C. neoformans* clinical isolates. Furthermore, there were already established synthetic routes within the literature, with further room for optimisation.¹ There is also a wide variety of commercially and most importantly inexpensive thiol starting materials available, which makes the design of these compounds more attractive. Fenbendazole (**1**) was the more attractive starting point for this project due to starting with a ten-fold higher activity against *C. neoformans* than albendazole and the opportunity for greater synthetic diversity.¹

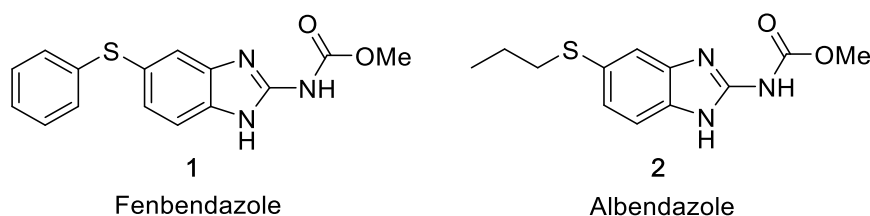


Figure 3.1. Two benzimidazoles of the thioether class were identified as having good activity against *C. neoformans* in the literature.

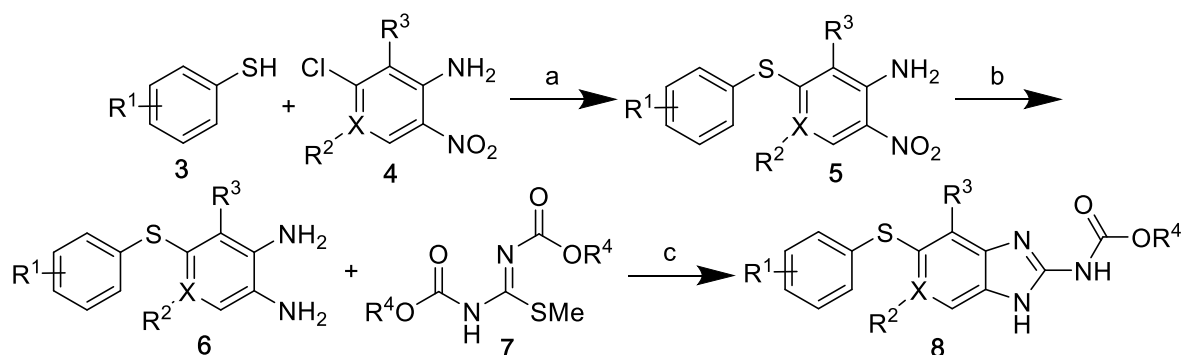
From Chapter 2, we also identified that the bridging sulphur atom could be oxidised to give the sulphoxide, which was biologically inactive against *C. neoformans*.^{2,3} With this in mind, the aims for the project were;

1. To design and synthesise a number of thioether analogues to be tested against *C. neoformans* in order to allow for structure activity relationship (SAR) development.
2. To design fenbendazole derivatives that are less rapidly metabolised to the sulphoxide, allowing for higher concentrations of the biologically active drug to remain in the body.^{2,4}
3. Obtain Drug Metabolism and Pharmacokinetic (DMPK) data and allow this to inform whether we have improved metabolic stability and observed any improvement in solubility.⁵

3.2 Discussion

3.2.1 Synthesis

The synthesis of the thioether derivatives followed a three-step route. This route has been reported on numerous occasions in the literature to make compounds of the thioether benzimidazole class. Similar chemistry was used here, with some modifications to solvents, reaction time and temperatures, to ensure the best possible yields (Scheme 3.1 and Table 3.1).⁶⁻⁸



Scheme 3.1. Reagents and Conditions: (a) K₂CO₃ (2 eq.), DMF, reflux, overnight (57 – 97% yield); (b) SnCl₂ (5 eq.), ethanol, reflux, overnight (42 – 90% yield); (c) 1,3-Bis(carbonyl)-2-methyl-2-thiopseudourea (**7**) (1 eq.), acetic acid (2 M), methanol (0.4 M), sealed tube, 65 °C, overnight (22 – 80% yield).

Table 3.1. Percentage yields obtained for all compounds created within the thioether template, including intermediates and final products.

	R ¹	R ²	R ³	R ⁴	X	Step A % yield (5)	Step B % yield (6)	Step C % yield (8)
a	4-F	H	H	Me	C	72	60	50
b	2-F	H	H	Me	C	70	98	Not finished
c	4-OMe	H	H	Me	C	57	90	35
d	2-Br	H	H	Me	C	97	72	55
e	2-CF ₃	H	H	Me	C	87	51	50
f	2-OMe	Me	H	Me	C	87	45	61
g	4-F	F	H	Me	C	57	60	72
h	4-F	F	H	Et	C	57	60	60
i	4-F	Me	H	Me	C	62	70	60
j	4-F	Me	H	Et	C	62	70	60
k	4-F	Me	H	Bn	C	62	70	22
l	2-iPr	H	H	Me	C	87	42	43
m	2-iPr	H	H	Et	C	87	42	24
n	4-OMe		H	Me	N	77	78	56
o	2-F	F	H	Me	C	88	70	68
p	2-F	F	H	Et	C	88	70	29
q	2-F	H	F	Me	C	85	65	54
r	2-F	H	F	Et	C	85	65	24
s	2-F	Br	H	Me	C	97	83	53
t	2-F	Br	H	Et	C	97	83	80

3.2.1.1 Nucleophilic Aromatic Substitution (S_NAr)

The first step involved a nucleophilic aromatic substitution (S_NAr) of the substituted thiol (**3**) with the desired chloronitroaniline (**4**) to give the nitroaniline intermediate **5**.⁷ This generally occurred in good yields due to the thiol (**3**) being highly nucleophilic.⁹⁻¹¹ More electron donating substituents generally gave the best yields, which is due to the enhanced nucleophilicity of the thiol, as observed with the majority of the methoxy derivatives (**5f**) and (**5n**), bromine (**5d**) and isopropyl (**5l**) and (**5m**) (Table 3.1).¹² The first 4-OMe (**5c**) derivative showed a lower yield, but this was due to experimental error as it was one of the first derivatives synthesised and at this point in the project optimisation of reaction conditions, work-up procedures and purification was not complete.

These molecules were characterised by 1H NMR. When the sample was run in chloroform there was the key appearance of 7 aromatic protons, with the nitroaniline aromatic ring protons being observed up-field towards 6 ppm and the thiol ring protons down-field towards 8 ppm. There was also the additional presence of a broad singlet around 6 ppm, which correspond to the 2 protons of the amine (See Figure 1A in Appendix). Generally, these compounds were purified by column chromatography, which sometimes proved difficult if the reaction had not gone to completion. This was because the R_f values of the starting material and product were almost identical and thus separation was very difficult. In order to ensure the reaction went to completion, TLC monitoring was employed to check the consumption of the starting nitroaniline. Also, slight excess of the thiol was used, as this could be easily separated out. A large number of these compounds were made, with the only limitation being the availability of the thiol starting materials, as more obscure derivatives were either expensive or unobtainable, when compared with the phenol derivatives (Discussed in Chapter 4).

3.2.1.2 Tin (II) Chloride Nitro Group Reduction

The second step involved a reduction which was carried out by dissolving **5** in ethanol, followed by the addition of five equivalents of tin (II) chloride and reflux overnight.^{13, 14} The precise mechanism of how tin and other reducing agents such as zinc perform this reduction is not confirmed, but the most popular mechanism is that of single electron transfer (SET) (Figure 3.2). The nitro group (**A**) is first acidified, and then following two single electron transfers to oxygen and subsequent protonation, the nitroso intermediate (**B**) can be formed. A similar procedure of protonation and reduction via SET then occurs to give the hydroxylamine (**C**), and then repeated again to provide the final amine product (**D**).¹⁵⁻¹⁷ Due to the presence of protons in the reaction the finally amine is then readily protonated, so during the work up aqueous NaOH is added to neutralise the acid and yield the free amine (**6**).

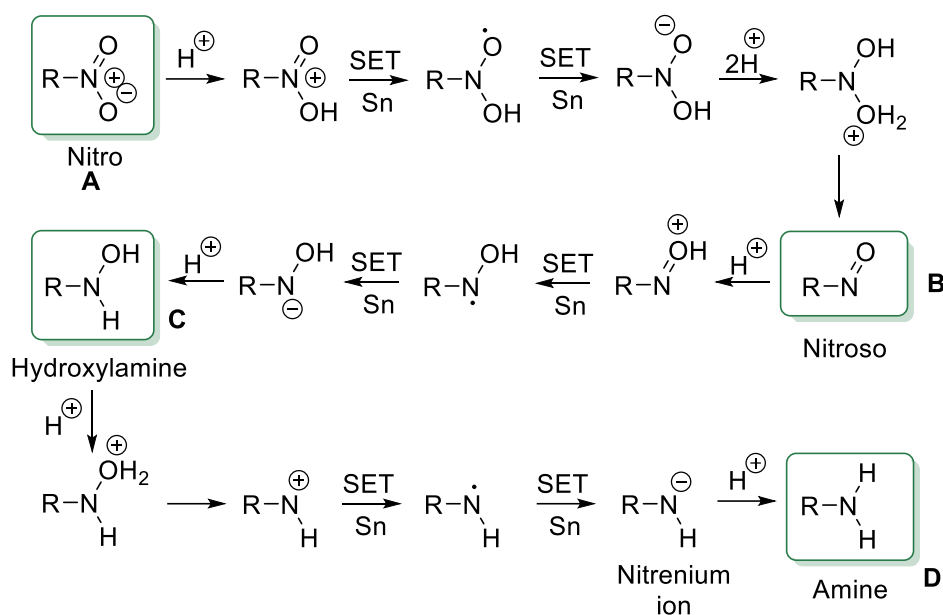


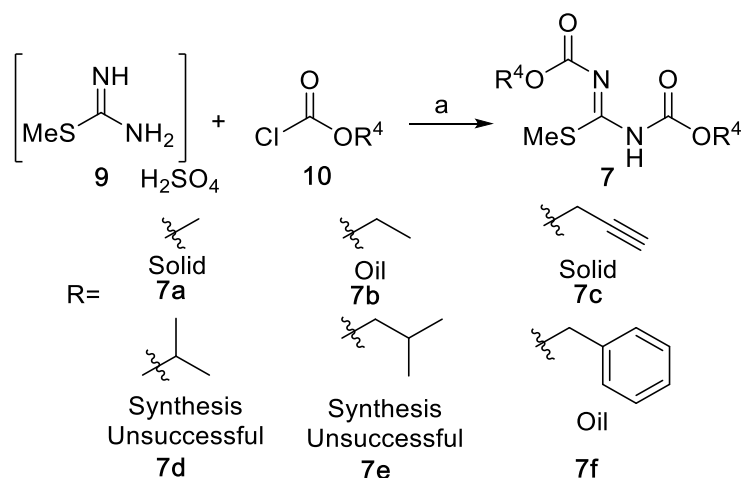
Figure 3.2. A plausible proposed pathway for the reduction of a nitro group to an amine via single electron transfer (SET). Reproduced from; *March's Advanced Organic Chemistry*, J. March et al.¹⁵⁻¹⁷

The initial work up conditions were optimised to increase the concentration of NaOH to 25% for basifying the reaction, ensuring that the free amine could be obtained, it also minimised excess water, which made filtration easier. Furthermore, 10% Pd/C hydrogenation was attempted, however no product was obtained. This was thought to be due potential sulphur poisoning of the palladium catalyst.¹⁸⁻²¹ The product was characterised by NMR and mass spectrometry, with the most noticeable changes being observed in the 1H NMR spectrum. When the NMR sample was taken in chloroform, then either one large broad peak, or two broad peaks were observed, which indicate the four NH_2 protons of the diamine. The proton that was adjacent to the nitro group shows a significant shift from around 8 ppm to closer to 6.5 ppm on reduction to the amine (**6**) (Appendix – Figure 1B).

3.2.1.3 Acid Mediated Ring Closure to Establish the Benzimidazole Core

The final step in the synthetic route involved a ring closure to give the benzimidazole core with the carbamate installed at the same time and proved to be a significant challenge. Firstly, synthesis of the dimethyl ((methylthio)methylene)dicarbamate (**7**) used for the ring closure was a very difficult reaction to carry out consistently (Scheme 3.2). The thio urea starting material (**9**) and chloroformate (**10**) are stirred in water at 0 °C for 15 minutes and then 25% NaOH added until the product precipitates out as a white solid, which is obtained through filtration. The use of 4.3 equivalents of **10** is excessive, however for every molecule of **9**, two molecules of **10** are used, but also excess is used due to the spontaneous hydrolysis of **10** into methanol, carbon dioxide and hydrochloric acid upon

reaction with water. This highlights the need for the reaction to be carried out as quickly as possible, to ensure that **7** is obtained.^{22, 23}



Scheme 3.2. Reagents and Conditions: (a) chloroformate (4.3 eq.), water, 0 °C to room temperature, 15 minutes, 25% NaOH, pH 9-10 (% yield);

Reproducibility of this reaction was initially problematic. Where some reactions would give excellent yields, with others no solid would precipitate, even when a workup was undertaken. Within the group a number of other methods were attempted, including adjusting concentrations of water and sodium hydroxide added, equivalents of methyl chloroformate added and even attempting the whole reaction at room temperature. Eventually, it was found that fast addition of **10** and vigorous stirring, followed by dropwise addition of 25% sodium hydroxide resulted in reliable synthesis of the product (**7a**).

For other analogues, where the chloroformate was changed to ethyl (**7b**), benzyl (**7f**) and other alkyl chains, the urea synthesis behaved differently, whereby compounds with larger side chains would not precipitate and required work-up procedures to obtain the products as either oils or sticky solids. In the case of the isopropyl (**7d**) and isobutyl (**7e**) groups, no confirmed product was isolated from this reaction.

The ring closure reaction implemented **6** and **7** to produce the final product (**8**). It was easy to observe the progress of the reaction due to pale solid precipitating out of the brown solution in the tube. For some analogues such as 2-iPr, and methyl containing analogues this reaction took overnight. For the majority of fluorinated analogues, solid precipitated after only 1 hour, but the reaction was left for longer to ensure maximum yield. Finally, the product was filtered and washed with diethyl ether to obtain the desired product as either a white, cream or yellow solid. Thioethers generally behaved well in the final ring closure step, with the majority of yields being obtained at around 50%.

Reduced yields were attributed to two potential factors. Firstly, different solubilities of the final products in methanol and acetic acid often resulted in different amounts of the products being obtained. Alterations to this were attempted, by adjusting the concentration of methanol in the sealed tube, however too little meant the reaction did not stir effectively and too much caused the product to dissolve further. Secondly, was the stability of the urea. It was noted that over a longer period of time, yields for the reaction dropped as the thiourea material aged, and this was especially pronounced when it was kept at room temperature. This problem was solved by storing the urea in the freezer and sealing the flask, slowing its decomposition, as well as running a number of parallel ring closures, to ensure that the urea was used immediately.

Also, slight differences in how the thio urea (**7**) is made each time due to differences in how much NaOH each time is added for the solid to precipitate. If more NaOH was used in the previous step, then there may not be enough acid remaining to carry out a higher yielding ring closure. Additional acid was added (0.5 eq.) and the reaction re-heated and in some cases, this helped **8** to precipitate. Sometimes, when too little NaOH was added in the previous step, the concentration of acid was too high. In this case the ring closure is likely to have worked, but the excess acetic acid is aiding the solubility of the product (**8**). Careful addition of a small amount of 1M NaOH allowed for the compounds to precipitate and be filtered. Finally, the powder product obtained was difficult to remove from the sinter funnel and due to the lack of solubility in anything but DMSO it was difficult to transfer. This was particularly pronounced in small scale reactions, where a lot of the product remained in the funnel. The funnel was changed to a Buchner funnel, but this did not allow for a thorough drying of the product.

Compounds were identified by ^1H and ^{13}C NMR spectroscopy, with a peak at around 148 ppm in the ^{13}C NMR being indicative of product formation as this corresponding to the carbon in the 2-position of the benzimidazole core. Purity was confirmed by HPLC, with all analogues achieving over 94% purity apart from **8a**, which was the first compound synthesised and whose purification was not optimised (Appendix - Figure 1C – 1E).

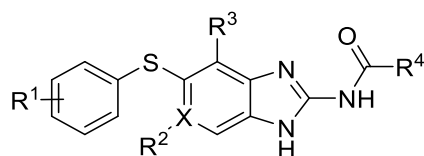
3.2.2 Biological Data

All compounds were tested for biological activity against whole cell *C. neoformans* using the European Committee on Antimicrobial Susceptibility Testing (EUCAST) method, which is a standardised method to make results more comparable from different research projects.²⁴ Fungal cells were grown on agar plates and the media used for Minimum Inhibitory Concentration (MIC) testing was a dextrose

solution containing DMSO. The plates, once inoculated, were incubated for 48 hours, and the MIC value given at the lowest concentration where there was no observable growth.^{25, 26}

3.2.3 Biological Activity

Table 3.2. The thioether class of compound show generally good MIC testing data. **Green** – good - 0.015 – 0.25 mg/L, **yellow** – acceptable - 0.5 – 4 mg/L, **red** – poor - >4 mg/L. * w made by Leanne Riley, x and y made by Dr Emma Shore, z made by Ben Roberts.



	R ¹	R ²	R ³	R ⁴	X	MIC (mg/L)
Flubendazole						0.125
Fenbendazole						0.03
8a	4-F	H	H	OMe	C	0.03
8b	2-F	H	H	OMe	C	0.06
8c	4-OMe	H	H	OMe	C	0.03
8d	2-Br	H	H	OMe	C	0.03
8e	2-CF ₃	H	H	OMe	C	>4
8f	2-OMe	Me	H	OMe	C	>4
8g	4-F	F	H	OMe	C	0.06
8h	4-F	F	H	OEt	C	>4
8i	4-F	Me	H	OMe	C	>4
8j	4-F	Me	H	OEt	C	>4
8k	4-F	Me	H	OBn	C	>4
8l	2-iPr	H	H	OMe	C	0.25
8m	2-iPr	H	H	OEt	C	>4
8n	4-OMe		H	OMe	N	>4
8o	2-F	F	H	OMe	C	0.06
8p	2-F	F	H	OEt	C	>4
8q	2-F	H	F	OMe	C	1
8r	2-F	H	F	OEt	C	>4
8s	2-F	Br	H	OMe	C	0.5
8t	2-F	Br	H	OEt	C	>4
8u	2-Me, 6-Me	H	H	OMe	C	0.125
8v	2-Me, 6-Me	H	H	OEt	C	0.5
8w	3-OMe	H	H	OMe	C	0.015
8x	4-OMe	H	H	NHMe	C	1
8y	3-OMe	H	H	NHMe	C	>4
8z	2-OMe	H	H	OMe	C	1

The thioether sub-compound class showed overall excellent activity in the whole cell MIC testing, with an activity range of 0.015 - >4 mg/L. From this we can observe some general trends as to what may infer activity on this class of compound (Table 3.2).

A number of groups are well tolerated at position R¹. Compounds **8g-k** and **8o-t** with fluorine in any position on the ring were generally well tolerated, with a slight preference for the 4-position which showed a slight improvement in activity. Fluorine based analogues only showed a loss of activity upon addition of groups such as methyl **8i-k** to the core and alteration of the carbamate via changing from methyl to ethyl **8h, 8r, 8t**. 2-position substituents were particularly valuable as these could potentially sterically block or minimise metabolism of the adjacent sulphur atom. Activity of the compounds substituted at the *ortho* position gives some information about what may drive biological activity. As a general trend, the larger the volume of the group at the 2-position, the greater the reduction in activity is (Table 3.2). This holds true until we reach 2-iPr, which has the largest volume of all the 2-substituents indicated below (Table 3.3). This indicates that the interplay between steric and electronic effects is important to understand activity.

Table 3.3. Calculated areas for substituted benzene derivatives. Calculations carried out using Molecular Mechanism MMFF, Spartan.

Group (on benzene)	Surface Area (Å ³)	MIC (mg/L)
F	104	0.06
Br	117	0.03
OMe	127	1
OCF ₃	132	>4
iPr	154	0.25

Fluorine is the smallest group, with a volume for fluorobenzene of 104 Å³, and possesses an excellent activity of 0.06 mg/L. This is only slightly lower than the 2-Br derivative (**8d**) which has an MIC of 0.03 mg/L but a larger surface area of 117 Å³. This could be that this slightly larger atom facilitates more Van der Waals interactions in the binding site, resulting in better activity. The OCF₃ and OMe derivatives (**8e** and **8z**) show MIC values of 1 and >4 mg/L respectively, with increasing surface from 132 Å³ to 154 Å³. The decrease in activity could be due to both being larger groups. The iPr derivative (**8l**) however possesses good activity with an MIC of 0.25 mg/L, but as stated previously has the largest volume of 154 Å³. This larger volume has led to a reduced activity value compared with the bromo and fluoro compounds. OMe and OCF₃ are both mesomerically electron donating, which may push additional electron density onto the sulphur atom, which may reduce activity. The iPr group is less electron donating, and thus pushes less electron density onto sulphur, which may help to balance out steric and electronic factors. At the 2 and 4 positions, whilst there is still some electronic influence, size of the substituent does not show as much of an effect, leading to less discernible differences in activity.²⁷

The pyridine moiety was incorporated in an attempt to improve solubility.²⁸ In a screen at Glaxo Smith Kline (GSK) they looked at the impact of having heterocycles in compounds and their effect on solubility. Pyridine came in the middle of ranking in terms of increasing solubility, after groups such as triazoles, pyrazoles, tetrazoles and pyrazines, all of which are synthetically more difficult to incorporate into the molecules. This pyridine compound (**8n**) showed no activity with an MIC of >4 mg/L.²⁸ The Log D for **8n** is 2.51, which is significantly lower than any of the other compounds of this class and indicates that the molecules might not be lipophilic enough to penetrate the cell effectively, thus giving poor MIC activity.

Finally, we synthesised an analogue in which the aryl ring was moved from the 5-position to the 4-position to see if activity was retained. This analogue (**11**) gave a poor MIC value of >4 mg/L, which can be explained by poor binding due to having a more compact shape compared to the other linear analogues (Figure 3.3).

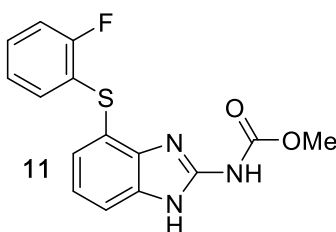


Figure 3.3. Moving the aryl group round the benzimidazole core resulting in no biological activity.

3.2.4 DMPK Data

3.2.4.1 Predicted DMPK

Predicted DMPK was calculated through Astra Zeneca's predictive screen for all compounds synthesised in the thioether compound class (Table 3.4) and general trends can be observed. Firstly, Log D for these compounds is generally quite high, with this being increased upon the addition of bromine (**8d**, **8s** and **8t**), addition of phenyl (**8k**) and other alkyl chains (**8h** and **8j**). However, for the thioether class of compound, it does not appear that high LogD is a problem, as these compounds generally have good activity, especially for **8d** where the addition of bromine has resulted in an excellent MIC value of 0.03 mg/ml (Table 3.2). This indicates that higher Log D maybe beneficial for these compounds as it leads to better cell permeation.²⁹

Fenbendazole (**1**) possesses an aqueous solubility of 0.3 μ M, and sets a low starting point for improvement. Aqueous solubility across the thioether class is predicted to be very poor, which is no surprise, as no solubilising groups have been added and no large changes to the core or carbamate

could have caused an increase in solubility. Carbamates are known for possessing sparing aqueous solubility, especially when in combination with the benzimidazole core.^{30, 31} Morpholine is commonly introduced into molecules in order to improve their aqueous solubility. No incorporation of solubilising groups such as morpholine was undertaken due to difficulties acquiring starting materials and a feasible synthetic route.^{32, 33} Compound **8n**, which has a pyridine ring introduced to the benzimidazole core, shows a small increase in solubility of 3.0 μM , which is a factor of ten higher than the rest of the compounds in the class, but still does not possess the solubility required to make this an ideal drug candidate and is poorly active.

Table 3.4. Predicted DMPK data for the thioether class of compounds show good metabolic properties overall, but poor solubility and Log D values. Values are colour coded with a traffic light system according to how good or bad a particular value is. **Green** – good, **amber** – acceptable/medium, **red** – poor. MPO – Multiparamater Optimisation.

Compound	LogD _{7.4}	CLogP	Aqueous Solubility (μM)	Rat Heps CLint ($\mu\text{l}/\text{min}/\text{mg}$)	Human Mics CLint ($\mu\text{l}/\text{min}/\text{mg}$)	MPO Score
Flubendazole	2.9	1.50	0.8	39	44	5.1
1	3.9	2.65	0.3	20	33	4.7
8a	4.0	2.80	Not obtained	12	11	4.7
8c	3.70	2.57	0.7	28	21	4.5
8d	4.35	3.52	0.2	34	19	4.1
8f	3.92	2.67	0.8	21	48	4.5
8g	4.15	2.94	0.8	8	21	4.8
8h	4.51	3.47	0.7	12	37	4.3
8i	4.18	3.29	0.8	9	25	4.4
8j	4.5	3.82	0.8	13	51	4.1
8k	5.36	3.92	0.1	33	83	3.7
8l	4.71	3.38	0.4	56	55	4.3
8m	5.0	3.91	0.4	95	113	4.0
8n	2.51	1.47	3.0	18	38	5.4
8o	3.98	2.94	1.0	16	32	4.7
8p	4.31	3.47	1.1	24	60	4.3
8q	4.37	2.94	0.4	17	30	4.7
8r	4.72	3.47	0.5	28	53	4.3
8s	3.72	3.66	1.7	25	26	3.9
8t	4.09	4.19	1.8	41	47	3.5

Metabolism within both human microsomes and rat hepatocytes is generally acceptable across the thioether series, with most compounds showing good to medium values. The worst values were observed for compound **8m**, with has both an isopropyl and ethyl group in the molecule, both of which are readily metabolised to aliphatic alcohols, which can then undergo further phase II metabolism to glucuronides and glucosides amongst many others. MPO scores were calculated for these compounds

as this can indicate whether a compound is likely to penetrate into the CNS. This is based on six parameter; molecular weight, ClogP, ClogD, pKa, hydrogen bond donors (HBD) and TPSA (Topological Polar Surface Area).^{34, 35} Each of these are given an equal weight and are assigned a value between 0 and 1 depending on how favourable the property is for a CNS penetrable drug. Ideally, a lower ClogP and ClogD is preferred, low pKa, one or less hydrogen bond donors, a molecular weight that is higher, but not too high that it disobeys Lipinski's rules and a TPSA that is also higher. Generally, MPO scores of >4 are considered to be CNS penetrable compounds. The majority of the compounds in this project have good MPO scores, with only three compounds **8k**, **8s** and **8t** possessing sub-optimal scores, mainly due to possessing a higher molecular weight.

3.2.4.2 Measured DMPK

Whilst predictive DMPK gave us an idea about the potential properties our compounds could have, they were also outsourced to Astra Zeneca for measured DMPK properties. This serves two purposes;

1. Obtaining measured DMPK can identify a compound with suitable properties
2. Compare this to the predictive data. If the values are similar then predictive data can be used in conjunction with SAR and computational modelling to design additional compounds.

Table 3.5. Measured DMPK data for the thioether class of compounds show good to acceptable metabolic properties overall, but poor solubility. Values are colour coded with a traffic light system according to how good or bad a particular value is. **Green** – good, **amber** – acceptable/medium, **red** – poor.

Compound	LogD _{7.4}	Aqueous Solubility (μM)	Rat Heps CLint (μl/min/mg)	Human Mics CLint (μl/min/mg)
1	3.9	0.3	20	33
8a	4.2	0.5	10	32
8c	4	0.3	12	17
8d	4.8	0.1	22	9
8g	4.1	0.1	11	54
8h	4.6	0.1	26	59
8o	2.8	0.4	56	44
8q	3.5	1	46	37

Importantly, one of the main concerns regarding the development of the thioether derivatives was the potential metabolism of sulphur to sulphoxide, which is a known metabolic route, and leads to reduced activity of the metabolites (MIC >4 mg/L). From the data, it is observed that whilst metabolism is present, it's not as high as initially expected. Compounds **8g**, **8h** and **8o** showed the addition of fluorines to the core in an attempt to block metabolism. This showed no improvement with microsomal clearance values indicating a slight increase in metabolism.

We also investigated metabolism using the prediction module of Stardrop.³⁶ This module carries out quantum mechanical simulations to predict which CYP450 enzymes are likely to carry out metabolism at certain points on each molecule. This calculation looks at the seven major isoforms of CYP450 that carry out the metabolism of most approved drug compounds. Four compounds are displayed in Figure 3.4 below. CYP1A2, 2C9 and 3A4 are major isoforms implicated in the metabolism of the benzimidazole thioethers. Interestingly, the calculation does identify some very minor metabolism on the sulphur atom of around 1-2%, which increase to 4% upon the addition of the two fluorine atoms adjacent to the sulphur atom (**8q** and **8r**). **8c** shows metabolism at the 4-OMe, however in the measured DMPK screen the metabolic values are excellent. Compound **8l** shows that the isopropyl group has been indicated as a metabolic weak point, which helps to verify its increased metabolic clearance. Compounds **8q** and **8r** show the difference in metabolism between the methyl and ethyl carbamate groups. The metabolic profiles look very similar, with greater metabolism occurring on the methyl group alone, but similar combined metabolism on both of the carbons of the ethyl group. This agrees with the measured DMPK data for these compounds, where no significant difference in metabolic data is observed.

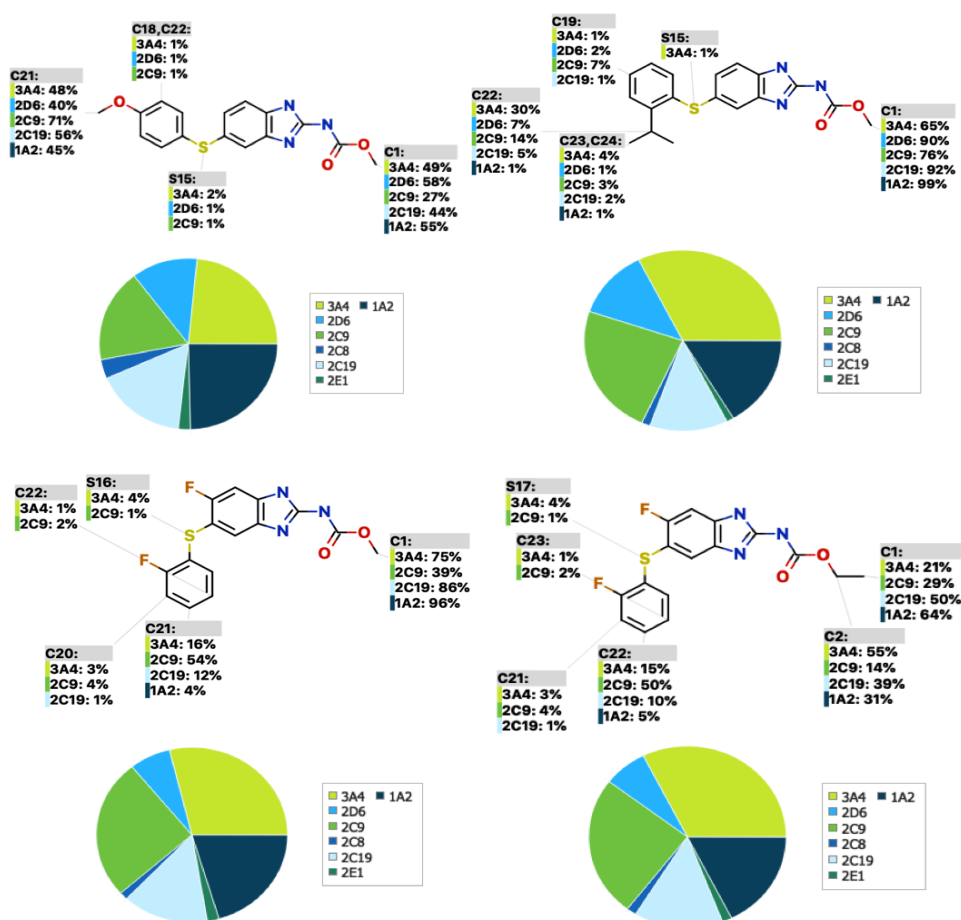


Figure 3.4. Metabolism predictions for four compounds from the thioether series. Calculations run on Stardrop.

Based on the plot of predicted Log D against measured Log D it is apparent that there is some correlation between the two, with an R^2 value of 0.29 (Figure 3.5). Inspection of the data shows the numbers aren't always similar for measured and predicted, however the colour categories are. Therefore, predicted Log D can be used as a good estimate, with measured DMPK to gain more precise data. Aqueous solubility shows a good correlation, with an R^2 value of 0.84. This suggests that the solubility predictions should be reliable, and can be used to help aid design of analogues. Both metabolic correlations are quite poor, and it's worth noting that this correlation is shown on a small number of analogues. For human microsomal clearance, we can observe an R^2 value of 0.18, which shows a small positive correlation. Viewing the data, it is clear the colour categories are generally the same, but there are some differences in numbers. Rat hepatic clearance values show almost no correlation with an R^2 value of 0.099. This shows that some of the compounds aren't even predicted to be in the same colour categories, with some big differences in number and is most noticeable for **8d** and **8o**.

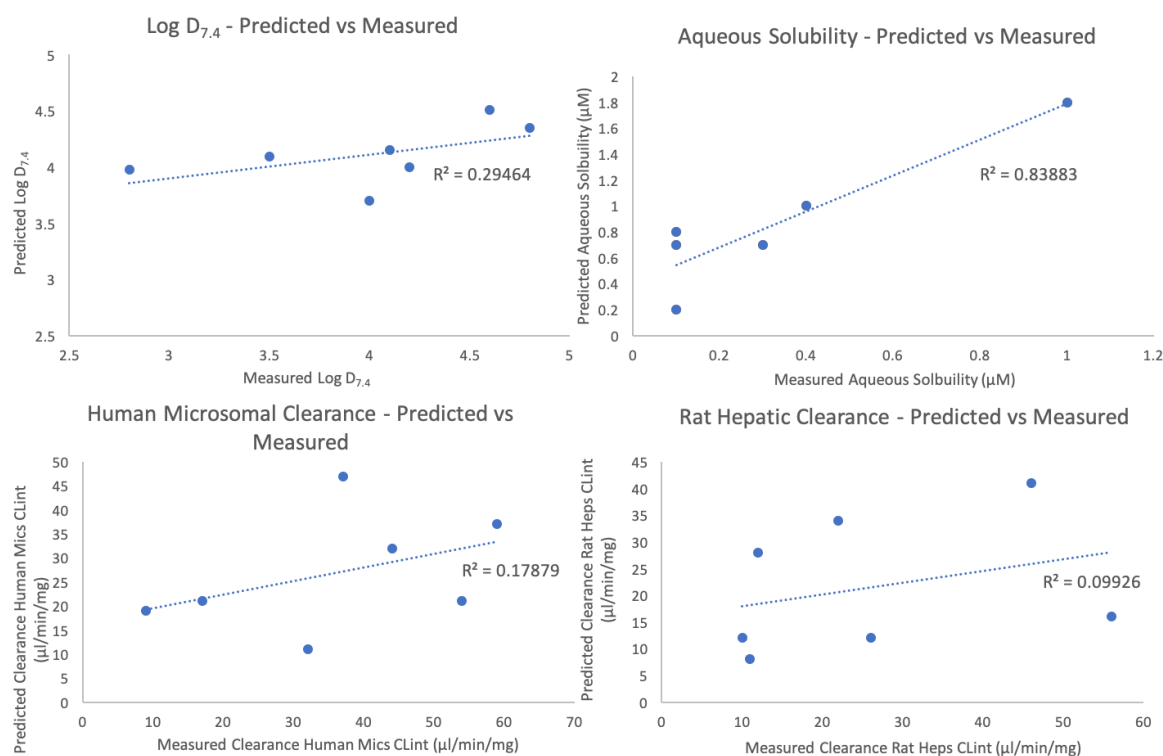


Figure 3.5. Each of the parameters obtained from measured DMPK testing was plotted against the numbers obtained from predicted DMPK analysis.

Ideally, we would prefer to carry out measured DMPK analysis for all compounds, but this is expensive and requires compounds to be made first. Predictive DMPK is useful as it allows for the identification of compounds with desirable DMPK properties, but also may allow us to screen out compounds with undesirable properties. Whilst predictive DMPK calculations are a useful tool for guidance, this section

has proven they are not 100% accurate, but do provide a reasonable approximation of values or colour categories. It is therefore essential to use predictive and measured DMPK analysis together to confirm results.

3.2.5 *In Vivo* Mouse Data

In vivo mouse studies were carried out in Prof. William Hope's Group by Suzy Gore.³⁷ Two thioethers, compound **8o** and **8q**, were chosen for *in vivo* testing due to possessing good activity values, 0.06 mg/L and 1 mg/L respectively and having a good balance of DMPK properties. Extensive work was carried out surrounding vehicles to be used for *in vivo* testing, and for these compounds 10% DMSO, 10% ethanol and 80% castor oil was chosen due to its ability to solubilise these compounds with minimal heating. Both compounds were given orally at a dose of 150 mg/kg (Figure 3.6).

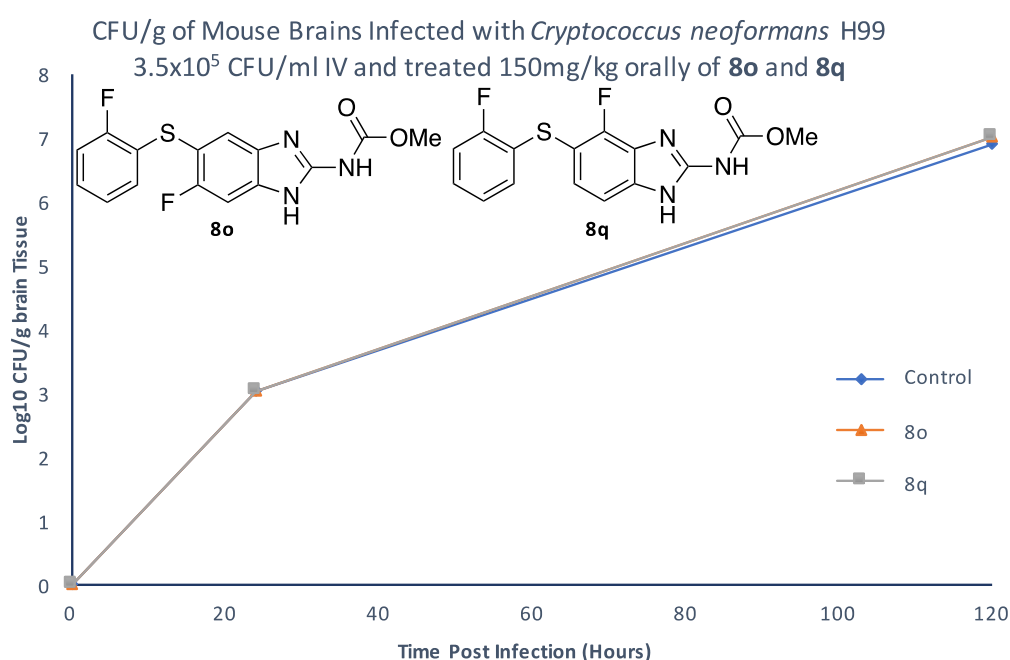


Figure 3.6. Selected thioethers, compounds **8o** and **8q**, were chosen for *in vivo* testing using mouse models. The control shows an increase in fungal density in the brain when no drug is given. Both thioether derivatives show no *in vivo* activity, as observed by possessing a similar shape plot to the control.

All *in vivo* tests are run using a control set of mice to ensure the *C. neoformans* strain is growing correctly, so that results when administering the drug compound are not biased. Figure 3.6 shows both of the thioether compounds administered showed no activity at the dose administered, this is concluded from no observable decrease in fungal density in the brain tissue. Despite having excellent MIC results, these compounds possess no *in vivo* activity. This is hypothesised to be due to either poor absorption of the drug from the gut as they are very lipophilic, and are also administered in an oil based vehicle, or that they are being rapidly metabolised to an inactive metabolite before they reach the brain.³⁸ The second hypothesis is less likely due to good metabolic clearance values observed for

these compounds. Using a dose of greater than 150 mg/kg is not possible for these compounds due to difficulty dissolving the compounds in the vehicle, due to inherent poor solubility.

3.3 Conclusions

This project has resulted in the synthesis of around 35 thioether analogues, with 27 discussed in this chapter. The synthetic route from the literature has been further developed to improve reaction yields and purification, which has allowed for successful syntheses of these analogues and a SAR profile to be developed (Figure 3.7). The thioether class on the whole possesses excellent activity, with **8w** providing the best activity for the entire project giving an MIC of 0.015 mg/L. DMPK data shows that these compounds are surprisingly metabolically stable, even at the oxidisable sulphur group. However, aqueous solubility is still an issue (range 0.1 – 3.0 μM), with no significant improvement on fenbendazole (**1**) (0.3 μM) or flubendazole (0.8 μM). Unfortunately, there was no *in vivo* activity for these analogues, though this is suspected to be a gut penetration issue and may be traversed.

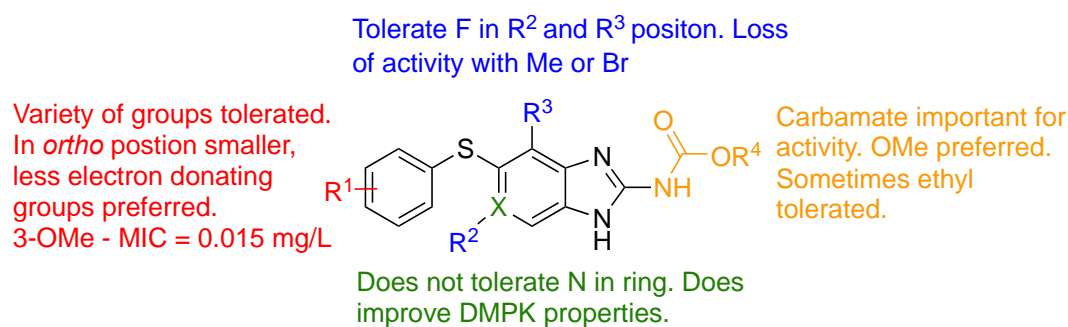


Figure 3.7. An overall SAR conclusion.

3.4 Future Work

The thiol class possesses potent activity, so this does not require significant improvement. There is a need to increase aqueous solubility and *in vivo* activity for this class. This could be achieved via synthesis of a morpholine derived compound (**12**), analogous to a compound made as part of the ether class (Figure 3.8), which is discussed in Chapter 4. This compound possessed good *in vivo* activity and improved aqueous solubility. This compound would require a new synthetic route, due to similar starting materials not being available for the thiol class.

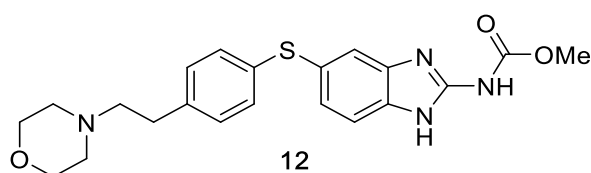


Figure 3.8. Design of a novel compound (**12**), analogous to a biologically ether compound.

3.5 Experimental

3.5.1 General Experimental Details

3.5.1.1 Chemicals

All chemicals and solvents were purchased from Fluorochem, Aldrich, TCI, Fischer or Alfa Aesar with no additional purification required before use. DMF was obtained from an MBRAUN MBSPS5 solvent purification system, though anhydrous solvent was not required for reaction.

3.5.1.2 Thin Layer Chromatography (TLC)

Carried out on Merck silica gel 60 F-254 aluminium backed plates. Compounds were observed via exposure to UV light or treatment with appropriate staining solutions such as potassium permanganate and ninhydrin and then developed via heat gun.

3.5.1.3 Flash Column Chromatography

Performed using silica (40 – 63 μm) supplied by Aldrich. Made into a slurry to provide the column mobile phase and layered onto sand. Product was absorbed onto silica and loaded onto top of mobile phase. Column was then eluted using the desired eluent and desired fractions collected.

3.5.1.4 Characterisation of Compounds

^1H (400MHz) and ^{13}C (100MHz) NMR spectra were recorded on a Bruker AMX400 spectrometer (^1H 400 MHz; ^{13}C 101 MHz) in the deuterated solvents described in each experimental procedure. Deuterated solvents obtained from Aldrich. Chemical shifts are reported as ppm (parts per million). Internal standard tetramethylsilane (TMS) and reported from downfield to upfield. Coupling constant (J) are reported in Hz. Splitting reported as singlet – s, broad singlet – bs, multiplet – m, d – doublet, t – triplet, q – quartet, s – septet, dd – doublet of doublets, ddd – doublet of doublet of doublets, app. t – apparent triplet. Low Resolution Mass spectrometry (LRMS) and High Resolution Mass Spectrometry (HRMS) were recorded using the analytical service within the Chemistry Department at the University of Liverpool. LRMS and HRMS was conducted on a VG analytical 7070E machine, Frisons TRIO mass spectrometers or Agilent QTOF 7200 using chemical ionisation (CI) or electrospray (ESI). Elemental analysis (%C, %H, %N and %S where specified) were determined by the University of Liverpool Microanalysis Laboratory. Infra-red spectra were recorded in the range of 4000-600 cm^{-1} using a JASCO FT/IR 4200 spectrometer, or Bruker ALPHA FT-IR platinum ATR spectrometer. Melting points were carried out using a Gallenkamp melting point machine and values are recorded in degrees Celsius. HPLC was carried out using Agilent 1200 HPLC equipped with a ZORBAX Eclipse Plus C18 column (4.6mm x 10 mm, 3.5 μm) at 25 $^\circ\text{C}$. Flow rate 1 ml/min for 15 minutes using MeCN/Water with compounds dissolved in methanol. UV detector recorded signals at 254 nm. Method A: min, gradient: 2% MeCN hold to 1 min, 2-98% MeCN in 11 min, then hold at 98% MeCN to 15 min.

3.5.2 General Procedures

General Procedure A – S_NAr Coupling (5)

To a flask at room temperature was added a 2-nitroaniline derivative (**4**) (1.0 eq.), *N,N*-dimethylformamide (0.35 M), potassium carbonate (2.0 eq.) and the substituted thiol (**3**) (1.5 eq.) and the reaction heated to reflux overnight. The reaction was cooled to room temperature and then diluted with ethyl acetate, washed with water, saturated aq. NaHCO_3 solution, brine, dried over magnesium sulphate and concentrated to give a crude orange oil, which was purified by column chromatography eluting with 10% ethyl acetate in hexane increasing to 20% to obtain the product, or triturating with *n*-Hexane to yield the pure product. Often these compounds were an oil after fraction collection and concentration. Precipitation of the solid was brought about by adding diethyl ether and concentration under air flow.

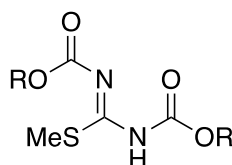
General Procedure B – Single Nitro reduction (6)

To a flask at room temperature was added 2-nitro-5-(phenylthio)aniline (**5**) (1.0 eq.), ethanol (0.15 M) and tin (II) chloride dihydrate (5.0 eq.) and the reaction refluxed (65 °C) overnight. The reaction was cooled to room temperature and the volume reduced. The solution was adjusted to pH 10 with 25% sodium hydroxide and filtered with water and ethyl acetate. The water layer was then washed twice more with ethyl acetate, the combined organic layers washed with brine, dried over magnesium sulphate and concentrated. The product was purified by column chromatography eluting with 50% ethyl acetate in *n*-hexane, increasing to 100% ethyl acetate, to elute the product.

General Procedure C – Acid Mediated Ring Closure (8)

To a flask at room temperature was added 4-(Phenylthio)benzene-1,2-diamine derivative (**6**) (1.0 eq.), acetic acid (2 M), methanol (0.4 M), (thio)methylene dicarbamate derivative (**7**) (1.0 eq.) and the reaction heated to 65 °C overnight. The reaction was cooled to room temperature and the resulting solid filtered and washed using diethyl ether to give the final product.

dimethyl ((methylthio)methylene)dicarbamate (7)

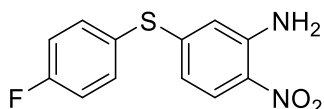


To a flask at 0 °C was added 2-methyl-2-thiopseudourea hemisulphate salt (**9**) (1 eq.), distilled water (1M). Chloroformate (**10**) (4.3 eq.) was added and the reaction vigorously stirred at 0 °C for 15 mins. The reaction was then warmed to room temperature, still maintaining vigorous stirring and then

slowly basified to pH 9-10 using 25 % sodium hydroxide. The resulting white precipitate was then filtered and washed with cold water to yield the product as a white solid, which was carried through crude into the next step. If no solid precipitated, then extracted with ethyl acetate, dried over magnesium sulphate and concentrated to yield the product.

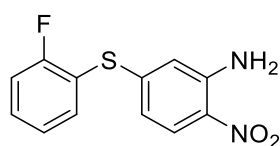
3.5.2.1 2-Nitro-5-(phenylthio)aniline Derivatives

5-((4-Fluorophenyl)thio)-2-nitroaniline (**5a**)⁷



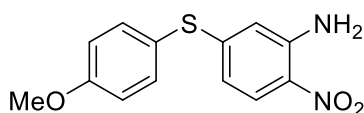
General Procedure A - Employed 5-chloro-2-nitroaniline and 4-fluorothiophenol to give the title compound (**5a**) (0.63 g, 72% yield) as a yellow solid. ¹H NMR (400 MHz, CDCl₃) δ 7.97 (d, 1H, *J* = 9.1 Hz), 7.56-7.51 (m, 2H), 7.19 - 7.11 (m, 2H), 6.38 (dd, 1H, *J* = 9.1 Hz), 6.31 (d, 1H, *J* = 1.92 Hz), 6.05 (bs, 2H). ¹³C NMR (100 MHz, CDCl₃) δ 163.6 (d, *J* = 252.0 Hz), 149.3, 144.9, 137.4 (d, *J* = 8.7 Hz), 136.0 (d, *J* = 8.3 Hz), 135.3, 126.7, 117.2 (d, *J* = 21.9 Hz), 115.1, 114.0.

5-((2-Fluorophenyl)thio)-2-nitroaniline (**5b**)



General Procedure A - Employed 5-chloro-2-nitroaniline and 2-fluorothiophenol to give the title compound (**5b**) (1.19 g, 70% yield) as a brown oil. ¹H NMR (400 MHz, CDCl₃) δ 7.99 (d, 1H, *J* = 8.9 Hz), 7.60 – 7.53 (m, 1H), 7.51 – 7.45 (m, 1H), 7.28 – 7.19 (m, 2H), 6.44 – 6.38 (m, 2H), 6.04 (bs, 2H). ¹³C NMR (100 MHz, CDCl₃) δ 162.7 (d, *J* = 249.9 Hz), 147.2, 144.8, 137.0, 132.2 (d, *J* = 8.4 Hz), 130.2, 126.8, 125.3 (d, *J* = 4.1 Hz), 117.5 (d, *J* = 18.2 Hz), 116.7 (d, *J* = 22.9 Hz), 115.4, 114.4. HRMS: (Cl⁺, CH₄) *m/z* Calculated for C₁₂H₁₀FN₂O₂S: 265.0442. Found [M+H]⁺: 265.0441 (Diff – 0.05 ppm).

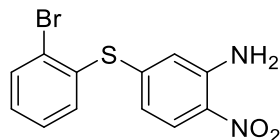
5-((4-Methoxyphenyl)thio)-2-nitroaniline (**5c**)⁷



General Procedure A - Employed 5-chloro-2-nitroaniline and 4-methoxythiophenol to give the title compound (**5c**) (0.27 g, 57% yield) as a yellow solid. ¹H NMR (400 MHz, CDCl₃) δ 7.95 (dd, 1H, *J* = 9.1 & 2.0 Hz), 7.47 (d, 2H, *J* = 8.6 Hz), 6.98 (d, 2H, *J* = 8.6 Hz), 6.37 (d, 1H, *J* = 9.1 Hz), 6.25 (d, 1H, *J* = 2.0 Hz), 4.86 (s, 3H), 6.02 (bs, 2H). ¹³C NMR (100 MHz, CDCl₃) δ 161.0, 150.9, 144.9, 137.3, 129.7, 126.5,

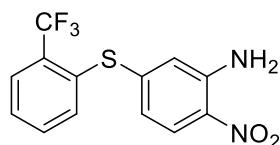
120.1, 115.5, 114.8, 113.2, 55.5. HRMS: (ES+) m/z Calculated for $C_{13}H_{13}N_2O_3S$: 277.0641. Found $[M+H]^+$: 277.0641 (Diff – 0 ppm).

4-((2-Bromophenyl)thio)-2-nitroaniline (**5d**)⁷



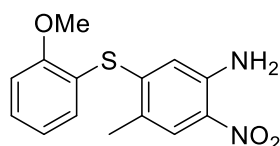
General Procedure A - Employed 5-Chloro-2-nitroaniline and 2-Bromothiophenol to give the title compound (**5d**) (0.91 g, 97% yield) as a yellow solid. 1H NMR (400 MHz, $CDCl_3$) δ 7.94 (d, 1H, $J = 7.5$ Hz), 7.65 (dd, 1H, $J = 7.7$ & 1.4 Hz), 7.49 (dd, 1H, $J = 7.5$ & 1.7 Hz), 7.29 (ddd, 1H, $J = 8.3, 7.5$ & 1.4 Hz), 7.21 (ddd, 1H, $J = 8.3, 7.7$ & 1.7 Hz), 6.36 (dd, 1H, $J = 7.5$ & 2.0 Hz), 6.34 (d, 1H, $J = 2.0$ Hz), 5.98 (s, 2H). ^{13}C NMR (100 MHz, $CDCl_3$) δ 146.7, 144.9, 136.2, 134.0, 132.4, 130.8, 130.4, 129.2, 128.5, 126.9, 116.2, 115.5. HRMS: (ES+) m/z Calculated for $C_{12}H_{10}BrN_2O_2S$: 324.9641. Found $[M+H]^+$: 324.9654 (Diff -3.94 ppm).

2-Nitro-5-((2-(trifluoromethyl)phenyl)thio)aniline (**5e**)



General Procedure A - Employed 5-chloro-2-nitroaniline and 2-(trifluoromethyl)benzenethiol to give the title compound (**5e**) (0.52 g, 87% yield) as a brown oil. 1H NMR (400 MHz, $CDCl_3$) δ 7.99 (d, 1H, $J = 9.0$ Hz), 7.86 (dd, 1H, $J = 7.2$ & 1.6 Hz), 7.65 – 7.51 (m, 3H), 6.43 (d, 1H, $J = 1.9$ Hz), 6.39 (dd, 1H, $J = 9.0$ & 1.9 Hz), 6.04 (bs, 2H). ^{13}C NMR (100 MHz, $CDCl_3$) δ 147.6, 144.8, 137.9, 133.5, 133.2, 132.8, 130.4, 129.5, 127.4, 126.8, 123.3 (q, $J = 272.3$ Hz), 116.4, 115.9. HRMS: (CI+, CH_4) m/z Calculated for $C_{13}H_{10}F_3N_2O_2S$: 315.0410. Found $[M+H]^+$: 315.0417 (Diff -2.35 ppm).

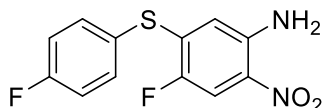
4-((2-Methoxyphenyl)thio)-5-methyl-2-nitroaniline (**5f**)



General Procedure A - Employed 5-chloro-4-methyl-2-nitroaniline and 2-methoxythiophenol to give the title compound (**5f**) (0.41 g, 87% yield) as a yellow solid. 1H NMR (400 MHz, $CDCl_3$) δ 7.89 (s, 1H), 7.50 – 7.43 (m, 2H), 7.06 – 7.01 (m, 2H), 5.98 (s, 1H), 5.79 (bs, 2H), 3.86 (s, 3H), 2.33 (s, 3H). ^{13}C NMR (100 MHz, $CDCl_3$) δ 159.9, 148.7, 143.1, 136.9, 131.7, 129.6, 126.0, 124.3, 121.8, 117.9, 114.0, 111.8,

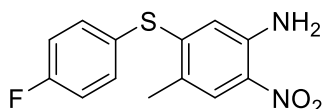
56.1, 18.7. HRMS: (Cl⁺, CH₄) *m/z* Calculated for C₁₄H₁₅N₂O₃S: 291.0798. Found [M+H]⁺: 291.0810 (Diff 4.12 ppm).

4-Fluoro-5-((4-fluorophenyl)thio)-2-nitroaniline (5g/5h)



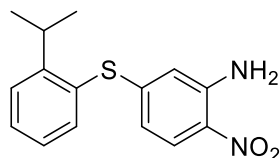
General Procedure A - Employed 5-chloro-4-fluoro-2-nitroaniline and 4-fluorothiophenol to give the title compound **(5g/5h)** (0.33 g, 57% yield) as a yellow solid. ¹H NMR (400 MHz, CDCl₃) δ 7.80 (d, 1H, *J* = 10.0 Hz), 7.56 (dd, 2H, *J* = 8.5 & 7.8 Hz), 7.19 (dd, 2H, *J* = 9.0 & 8.5 Hz), 5.97 (d, 1H, *J* = 6.3 Hz), 5.87 (s, 2H). ¹³C NMR (100 MHz, CDCl₃) δ 164.0 (d, *J* = 251.5 Hz), 149.6 (d, *J* = 240.1 Hz), 141.6, 137.7 (d, *J* = 9.1 Hz), 130.2, 128.7, 123.5, 117.5 (d, *J* = 21.9 Hz), 115.0, 111.0 (d, *J* = 26.1 Hz). HRMS: (Cl⁺, CH₄) *m/z* Calculated for C₁₂H₉F₂N₂O₂S: 283.0347. Found [M+H]⁺: 283.0354 (Diff – 2.53 ppm).

5-((4-Fluorophenyl)thio)-4-methyl-2-nitroaniline (5i/5j/5k)

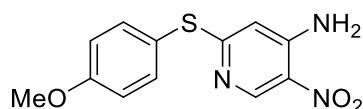


General Procedure A - Employed 5-chloro-4-methyl-2-nitroaniline and 4-fluorothiophenol to give the title compound **(5i/5j/5k)** (0.36 g, 62% yield) as a yellow solid. ¹H NMR (400 MHz, CDCl₃) δ 7.90 (s, 1H), 7.52 (dd, 2H, *J* = 8.7 & 7.5 Hz), 7.18 (dd, 2H, *J* = 8.7 & 9.6 Hz), 6.00 (s, 1H), 5.82 (s, 2H), 2.29 (s, 2H). ¹³C NMR (100 MHz, CDCl₃) δ 163.4 (d, *J* = 257.3 Hz), 143.1, 138.6, 137.5 (d, *J* = 8.4 Hz), 132.1, 126.2, 125.4, 123.8, 117.5 (d, *J* = 22.4 Hz), 113.9, 22.6. HRMS: (Cl⁺, CH₄) *m/z* Calculated for C₁₃H₁₂FN₂O₂S: 279.0598. Found [M+H]⁺: 279.0604 (Diff – 2.02 ppm).

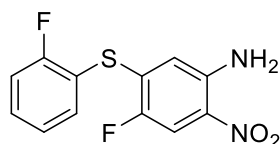
5-((2-Isopropylphenyl)thio)-2-nitroaniline (5l/5m)



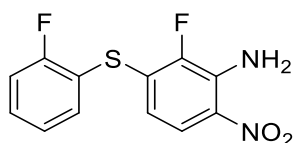
General Procedure A - Employed 5-chloro-2-nitroaniline and 2-isopropylthiophenol to give the title compound **(5l/5m)** (0.40 g, 87% yield) as a yellow solid. ¹H NMR (400 MHz, CDCl₃) δ 7.93 (d, 1H, *J* = 8.9 Hz), 7.54 – 7.50 (m, 1H), 7.49 – 7.43 (m, 2H), 7.28 – 7.22 (m, 1H), 6.35 (dd, 1H, *J* = 8.9 & 1.8 Hz), 6.22 (d, 1H, *J* = 1.8 Hz), 5.98 (bs, 2H), 3.48 (sept, 1H, *J* = 6.9 Hz), 1.91 (d, 6H, *J* = 6.9 Hz). ¹³C NMR (100 MHz, CDCl₃) δ 152.5, 149.2, 145.6, 145.4, 136.6, 130.3, 126.8, 126.5, 125.9, 116.2, 113.9, 113.4, 23.5, 22.4. HRMS: (Cl⁺, CH₄) *m/z* Calculated for C₁₅H₁₇N₂O₂S: 289.1005. Found [M+H]⁺: 289.1012 (Diff – 2.38 ppm).

2-((4-Methoxyphenyl)thio)-5-nitropyridin-4-amine (5n)

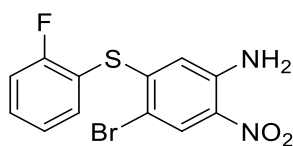
General Procedure A - Employed 2-chloro-5-nitropyridin-4-amine and 4-methoxythiophenol to give the title compound (**5n**) (0.36 g, 77% yield) as a yellow solid. ^1H NMR (400 MHz, CDCl_3) δ 9.04 (s, 1H), 7.52 (d, 2H, $J = 9.0$ Hz), 7.00 (d, 2H, $J = 9.0$ Hz), 5.94 (s, 1H), 3.87 (s, 3H). ^{13}C NMR (100 MHz, CDCl_3) δ 169.5, 161.2, 148.8, 148.7, 137.4, 127.9, 119.7, 115.6, 105.7, 55.4. HRMS: (Cl^+ , CH_4) m/z Calculated for $\text{C}_{12}\text{H}_{12}\text{N}_3\text{O}_3\text{S}$: 278.0594. Found $[\text{M}+\text{H}]^+$: 278.0595 (Diff – 0.26 ppm).

4-Fluoro-5-((2-fluorophenyl)thio)-2-nitroaniline (5o/5p)

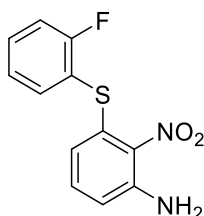
General Procedure A - Employed 5-chloro-4-fluoro-2-nitroaniline and 2-fluorothiophenol to give the title compound (**5o/5p**) (1.43 g, 88% yield) as an orange solid. ^1H NMR (400 MHz, CDCl_3) δ 7.81 (d, 1H, $J = 10.1$ Hz), 7.61 – 7.48 (m, 2H), 7.30 – 7.21 (m, 2H), 6.08 (d, 1H, $J = 6.5$ Hz), 5.89 (bs, 2H). ^{13}C NMR (100 MHz, CDCl_3) δ 162.8 (d, $J = 246.6$ Hz), 149.9 (d, $J = 240.4$ Hz), 141.2, 137.2, 136.9 (d, $J = 20.7$ Hz), 132.8 (d, $J = 8.3$ Hz), 128.8, 125.6 (d, $J = 4.1$ Hz), 116.9 (d, $J = 21.7$ Hz), 115.5, 111.2 (d, $J = 26.4$ Hz) not all carbons visible. HRMS: (Cl^+ , CH_4) m/z Calculated for $\text{C}_{12}\text{H}_9\text{F}_2\text{N}_2\text{O}_2\text{S}$: 283.0347. Found $[\text{M}+\text{H}]^+$: 283.0358 (Diff – 3.83 ppm).

2-Fluoro-3-((2-fluorophenyl)thio)-6-nitroaniline (5q/5r)

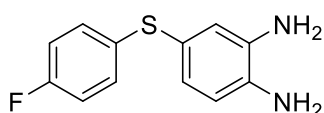
General Procedure A - Employed 2,3-difluoro-6-nitroaniline and 2-fluorothiophenol to give the title compound (**5q/5r**) (0.35 g, 85% yield) as an orange solid. ^1H NMR (400 MHz, CDCl_3) δ 7.76 (dd, 1H, $J = 9.4$ & 1.5 Hz), 7.55 (ddd, 1H, $J = 8.2$ & 7.4 & 1.5 Hz), 7.52 – 7.45 (m, 1H), 7.22 – 7.18 (m, 2H), 6.16 (bs, 2H), 6.08 (dd, 1H, $J = 9.8$ & 7.4 Hz). ^{13}C NMR (100 MHz, CDCl_3) δ 162.8 (d, $J = 249.2$ Hz), 147.5 (d, $J = 238.4$ Hz), 136.7, 134.7 (d, $J = 15.5$ Hz), 132.4 (d, $J = 7.8$ Hz), 131.6 (d, $J = 15.6$ Hz), 131.1, 125.3 (d, $J = 4.2$ Hz), 121.2 (d, $J = 3.4$ Hz), 116.7 (d, $J = 22.3$ Hz), 116.2 (d, $J = 19.0$ Hz), 113.4 (d, $J = 1.9$ Hz). HRMS: (Cl^+ , CH_4) m/z Calculated for $\text{C}_{12}\text{H}_9\text{F}_2\text{N}_2\text{O}_2\text{S}$: 283.0347. Found $[\text{M}+\text{H}]^+$: 283.0360 (Diff -4.65 ppm).

4-Bromo-5-((2-fluorophenyl)thio)-2-nitroaniline (5s/5t)

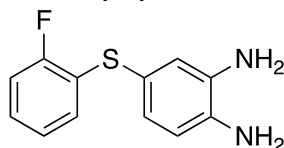
General Procedure A - Employed 4-bromo-5-chloro-2-nitroaniline and 2-fluorothiophenol to give the title compound (**5s/5t**) (0.34 g, 97% yield) as an orange solid. ^1H NMR (400 MHz, CDCl_3) δ 8.30 (s, 1H), 7.58 (m, 2H), 7.27 (m, 2H), 5.93 (s, 3H). ^{13}C NMR (100 MHz, CDCl_3) δ 163.0 (d, $J = 251.5$ Hz), 148.8, 143.7, 137.7, 133.1 (d, $J = 8.0$ Hz), 130.3, 129.6, 125.8 (d, $J = 4.0$ Hz), 117.0 (d, $J = 22.6$ Hz), 114.4, 106.5. Not all carbons visible. HRMS: (Cl $^+$, CH_4) m/z Calculated for $\text{C}_{12}\text{H}_9\text{BrFN}_2\text{O}_2\text{S}$: 342.9547. Found [M+H] $^+$: 342.9547 (Diff -1.38 ppm).

3-((2-Fluorophenyl)thio)-2-nitroaniline (11a)

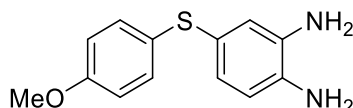
General Procedure A - Employed 3-chloro-2-nitroaniline and 2-fluorothiophenol to give the title compound (**11a**), which was carried through crude into the next reaction.

3.5.2.2 4-(Phenylthio)benzene-1,2-diamine Derivatives**4-((4-Fluorophenyl)thio)benzene-1,2-diamine (6a)⁷**

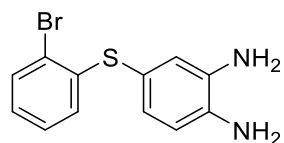
General Procedure B - Employed 5-((4-fluorophenyl)thio)-2-nitroaniline (**5a**) to give the title compound (**6a**) (0.21 g, 60% yield) as a brown oil. ^1H NMR (400 MHz, CDCl_3) δ 7.20 – 7.15 (m, 2H), 6.95 – 6.91 (m, 2H) 6.83 (dd, 1H, $J = 7.9$ & 2.0 Hz), 6.80 (d, 1H, $J = 2.0$ Hz), 6.66 (d, 1H, $J = 7.9$ Hz), 3.43 (bs, 4H); ^{13}C NMR (100 MHz, CDCl_3) δ 161.3 (d, $J = 244.0$ Hz), 133.9, 133.4, 131.1, 130.6 (d, $J = 8.1$ Hz), 125.9, 123.5, 121.6, 117.1, 115.9 (d, $J = 23.8$ Hz). HRMS: (Cl, CH_4) m/z Calculated for $\text{C}_{12}\text{H}_{12}\text{FN}_2\text{O}_2\text{S}$: 235.0700. Found [M+H] $^+$: 235.0710 (Diff -4.46 ppm).

4-((2-Fluorophenyl)thio)benzene-1,2-diamine (6b)

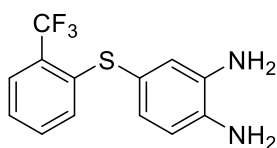
General Procedure B - Employed 5-((2-fluorophenyl)thio)-2-nitroaniline (**5b**) to give the title compound (**6b**) (0.21 g, 60% yield) as a brown oil. ^1H NMR (400 MHz, CDCl_3) δ 7.13 – 7.08 (m, 1H), 7.04 – 6.99 (m, 1H), 6.97 – 6.95 (m, 2H), 6.89 (dd, 1H, $J = 7.8$ & 2.2 Hz), 6.86 (d, 1H, $J = 2.2$ Hz), 6.69 (d, 1H, $J = 7.8$ Hz), 3.44 (bs, 4H). ^{13}C NMR (100 MHz, CDCl_3) δ 159.4 (d, $J = 244.3$ Hz), 135.9, 135.4, 129.9 (d, $J = 2.2$ Hz), 127.1 (d, $J = 8.3$ Hz), 127.0, 126.6 (d, $J = 16.9$ Hz), 124.4 (d, $J = 3.7$ Hz), 122.6, 120.6, 117.1, 115.3 (d, $J = 21.6$ Hz). HRMS: (CI, CH_4) m/z Calculated for $\text{C}_{12}\text{H}_{12}\text{FN}_2\text{O}_2\text{S}$: 235.0700. Found $[\text{M}+\text{H}]^+$: 235.0697 (Diff 1.16 ppm).

4-((4-Methoxyphenyl)thio)benzene-1,2-diamine (6c)⁷

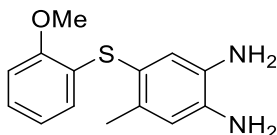
General Procedure B - Employed 5-((4-methoxyphenyl)thio)-2-nitroaniline (**5c**) to give the title compound (**6c**) (0.20 g, 90% yield) as a yellow oil. ^1H NMR (400 MHz, CDCl_3) δ 7.17 (d, 2H, $J = 9.1$ Hz), 6.74 (d, 2H, $J = 9.1$ Hz), 6.68 (dd, 1H, $J = 8.0$ & 1.8 Hz), 6.66 (d, 1H, $J = 1.8$ Hz), 6.55 (d, 1H, $J = 8.0$ Hz), 3.71 (s, 3H), 3.31 (bs, 4H); ^{13}C NMR (100 MHz, CDCl_3) δ 158.7, 135.4, 134.6, 132.1, 128.3, 125.9, 124.2, 120.1, 117.1, 114.6, 55.4. HRMS: (CI+, CH_4) m/z Calculated for $\text{C}_{13}\text{H}_{13}\text{N}_2\text{OS}$: 247.0900. Found $[\text{M}+\text{H}]^+$: 247.0896 (Diff 1.35 ppm).

4-((2-Bromophenyl)thio)benzene-1,2-diamine (6d)⁷

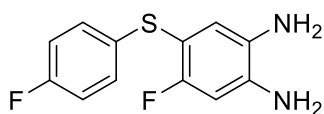
General Procedure B - Employed 4-((2-bromophenyl)thio)-2-nitroaniline (**5d**) to give the title compound (**6d**) (0.58 g, 72% yield) as a yellow solid. ^1H NMR (400 MHz, CDCl_3) δ 7.47 (d, 1H, $J = 8.0$ Hz), 7.10 – 7.05 (m, 1H), 6.96 – 6.90 (m, 3H), 6.73 (d, 1H, $J = 8.0$ Hz), 6.71 (dd, 1H, $J = 8.0$ & 1.7 Hz), 3.56 (s, 2H), 3.44 (s, 2H). ^{13}C NMR (100 MHz, CDCl_3) δ 141.6, 136.6, 135.4, 132.5, 128.4, 127.7, 127.0, 125.5, 123.9, 123.5, 120.2, 117.5. HRMS: (CI+, CH_4) m/z Calculated for $\text{C}_{12}\text{H}_{12}\text{BrN}_2\text{S}$: 294.9899. Found $[\text{M}+\text{H}]^+$: 294.9912 (Diff -4.43 ppm).

4-((2-(Trifluoromethyl)phenyl)thio)benzene-1,2-diamine (6e)

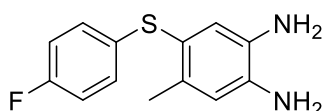
General Procedure B - Employed 2-nitro-5-((2-(trifluoromethyl)phenyl)thio)aniline (**5e**) to give the title compound (**6e**) (0.24 g, 51% yield) as a yellow solid. ^1H NMR (400 MHz, CDCl_3) δ (400 MHz, CDCl_3) δ 7.60 (d, 1H, $J = 7.6$ Hz), 7.29 – 7.22 (m, 1H), 7.17 – 7.10 (m, 1H), 7.00 (d, 1H, $J = 8.0$ Hz), 6.93 (dd, 1H, $J = 8.0$ Hz), 6.88 (s, 1H), 6.72 (d, 1H, $J = 7.9$ Hz). ^{13}C NMR (100 MHz, CDCl_3) δ 140.0, 136.6, 135.5, 131.8, 129.1, 128.2, 125.4, 124.6, 124.0 (q, $J = 273.0$ Hz), 123.5, 120.4, 120.3, 117.1. HRMS: (Cl^+ , CH_4) m/z Calculated for $\text{C}_{13}\text{H}_{12}\text{F}_3\text{N}_2\text{S}$: 285.0668. Found $[\text{M}+\text{H}]^+$: 285.0664 (Diff 1.38 ppm).

4-((2-Methoxyphenyl)thio)-5-methylbenzene-1,2-diamine (6f)

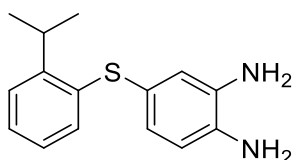
General Procedure B - Employed 5-((2-methoxyphenyl)thio)-4-methyl-2-nitroaniline (**5f**) to give the title compound (**6f**) (0.16 g, 45% yield) as a yellow solid. ^1H NMR (400 MHz, CDCl_3) δ 7.05 (ddd, 1H, 8.3, 8.2 & 1.7 Hz), 6.91 (s, 1H), 6.82 (dd, 1H, $J = 8.2$ & 1.0 Hz), 6.76 (ddd, 1H, $J = 8.3$, 7.6 & 1.0 Hz), 6.68 (s, 1H), 6.53 (dd, 1H, $J = 7.6$ & 1.7 Hz), 3.92 (s, 3H), 2.24 (s, 3H). ^{13}C NMR (100 MHz, CDCl_3) δ 155.1, 137.0, 135.6, 132.8, 127.9, 125.8, 125.4, 125.3, 121.2, 118.6, 118.3, 110.1, 55.8, 19.8. LRMS: (Cl^+ , CH_4) m/z Calculated for $\text{C}_{14}\text{H}_{17}\text{N}_2\text{O}_2\text{S}$: 261.36. Found $[\text{M}+\text{H}]^+$: 261.1.

4-Fluoro-5-((4-fluorophenyl)thio)benzene-1,2-diamine (6g/6h)

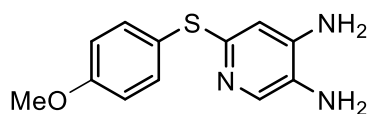
General Procedure B - Employed 4-fluoro-5-((4-fluorophenyl)thio)-2-nitroaniline (**5g/5h**) to give the title compound (**6g/6h**) (0.17 g, 60% yield) as a yellow solid. ^1H NMR (400 MHz, CDCl_3) δ 7.16 (dd, 2H, $J = 8.7$ & 7.5 Hz), 6.93 (dd, 2H, $J = 8.7$ Hz & 9.8 Hz), 6.79 (d, 1H, $J = 6.8$ Hz), 6.49 (d, 1H, $J = 9.5$ Hz), 3.71 (s, 2H), 3.19 (s, 2H). ^{13}C NMR (400 MHz, CDCl_3) δ 162.6 (d, $J = 245.6$ Hz), 158.9 (d, $J = 237.1$ Hz), 138.6 (d, $J = 11.1$ Hz), 132.7 (d, $J = 3.7$ Hz), 130.2 (d, $J = 3.0$ Hz), 130.0 (d, $J = 7.7$ Hz), 124.0 (d, $J = 1.6$ Hz), 116.0 (d, $J = 21.5$ Hz), 108.1 (d, $J = 20.1$ Hz), 103.6 (d, $J = 25.1$ Hz). HRMS: (Cl^+ , CH_4) m/z Calculated for $\text{C}_{12}\text{H}_{11}\text{F}_2\text{N}_2\text{S}$: 253.0606. Found $[\text{M}+\text{H}]^+$: 253.0608 (Diff -0.97 ppm).

4-((4-Fluorophenyl)thio)-5-methylbenzene-1,2-diamine (6i/6j/6k)

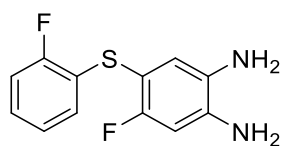
General Procedure B - Employed 5-((4-fluorophenyl)thio)-4-methyl-2-nitroaniline (**5i/5j/5k**) to give the title compound (**6i/6j/6k**) (0.26 g, 70% yield) as a yellow solid. ^1H NMR (400 MHz, CDCl_3) δ 7.03 (dd, 2H, $J = 8.7$ & 9.0 Hz), 6.91 (dd, 2H, $J = 8.7$ & 10.6 Hz), 6.86 (s, 1H), 6.63 (s, 1H), 3.38 (s, 4H), 2.22 (s, 3H). ^{13}C NMR (100 MHz, CDCl_3) δ 161.0 (d, $J = 244.0$ Hz), 136.6, 134.2, 134.0, 132.7, 128.7 (d, $J = 7.8$ Hz), 124.2, 120.9, 118.4, 116.0 (d, $J = 21.9$ Hz), 19.7. HRMS: (Cl^+ , CH_4) m/z Calculated for $\text{C}_{13}\text{H}_{14}\text{FN}_2\text{S}$: 249.0856. Found $[\text{M}+\text{H}]^+$: 249.0861 (Diff 2.01 ppm).

4-((2-Isopropylphenyl)thio)benzene-1,2-diamine (6l/6m)

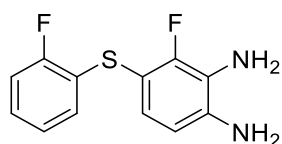
General Procedure B - Employed 5-((2-isopropylphenyl)thio)-2-nitroaniline (**5l/5m**) to give the title compound (**6l/6m**) (0.15 g, 42% yield) as a yellow solid. ^1H NMR (400 MHz, CDCl_3) δ 7.25 (d, 1H, $J = 1.9$ Hz), 7.17 – 7.13 (m, 1H), 7.03 – 6.98 (m, 2H), 6.80 (dd, 1H, $J = 7.6$ & 1.9 Hz), 6.79 – 6.74 (m, 1H), 6.66 (d, 1H, $J = 7.6$ Hz), 3.49 (sep, 1H, $J = 6.8$ Hz), 3.41 (s, 4H), 1.26 (d, 6H, $J = 6.8$ Hz). ^{13}C NMR (100 MHz, CDCl_3) δ 147.0, 136.6, 135.4, 135.1, 129.3, 126.2, 126.1, 125.9, 125.3, 123.7, 121.7, 117.2, 30.2, 23.4. HRMS: (Cl^+ , CH_4) m/z Calculated for $\text{C}_{15}\text{H}_{19}\text{N}_2\text{S}$: 259.1263. Found $[\text{M}+\text{H}]^+$: 259.1262 (Diff 0.6 ppm).

6-((4-Methoxyphenyl)thio)pyridine-3,4-diamine (6n)

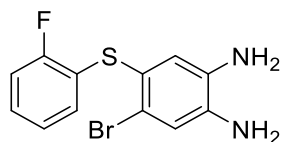
General Procedure B - Employed 2-((4-methoxyphenyl)thio)-5-nitropyridin-4-amine (**5n**) to give the title compound (**6n**) (0.25 g, 78% yield) as a yellow oil. ^1H NMR (400 MHz, CDCl_3) δ 7.80 (s, 1H), 7.49 (d, 2H, $J = 8.9$ Hz), 6.91 (d, 2H, $J = 8.9$ Hz), 6.18 (s, 1H), 3.89 (s, 2H), 3.83 (s, 3H), 3.04 (s, 2H). ^{13}C NMR (100 MHz, CDCl_3) δ 160.1, 153.7, 144.6, 138.6, 136.3, 127.0, 123.3, 115.0, 107.6, 55.2. HRMS: (Cl^+ , CH_4) m/z Calculated for $\text{C}_{12}\text{H}_{14}\text{N}_3\text{OS}$: 248.0852. Found $[\text{M}+\text{H}]^+$: 248.0861 (Diff – 3.76 ppm).

4-Fluoro-5-((2-fluorophenyl)thio)benzene-1,2-diamine (6o/6p)

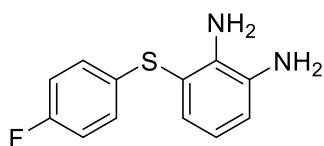
General Procedure B - Employed 4-fluoro-5-((2-fluorophenyl)thio)-2-nitroaniline (**5o/5p**) to give the title compound (**6o/6p**) (0.30 g, 70% yield) as a yellow solid. ^1H NMR (400 MHz, CDCl_3) δ 7.14 – 7.08 (m, 1H), 7.04 – 7.00 (m, 1H), 6.99 – 6.91 (m, 2H), 6.83 (d, 1H, $J = 7.2$ Hz), 6.51 (d, 1H, $J = 9.7$ Hz), 3.77 (s, 2H), 3.18 (s, 2H). ^{13}C NMR (100 MHz, CDCl_3) δ 159.5 (d, $J = 244.4$ Hz), 158.2 (d, $J = 239.3$ Hz), 139.3 (d, $J = 10.3$ Hz), 130.3 (d, $J = 2.4$ Hz), 129.4 (d, $J = 2.1$ Hz), 127.2 (d, $J = 1.7$ Hz), 125.1 (d, $J = 17.0$ Hz), 124.6 (d, $J = 1.7$ Hz), 124.5 (d, $J = 3.5$ Hz), 115.4 (d, $J = 22.1$ Hz), 105.1 (d, $J = 18.0$ Hz), 103.4 (d, $J = 27.1$ Hz). HRMS: (ES+) m/z Calculated for $\text{C}_{12}\text{H}_{11}\text{F}_2\text{N}_2\text{S}$: 253.0606. Found $[\text{M}+\text{H}]^+$: 253.0608 (Diff -0.97 ppm).

3-Fluoro-4-((2-fluorophenyl)thio)benzene-1,2-diamine (6q/6r)

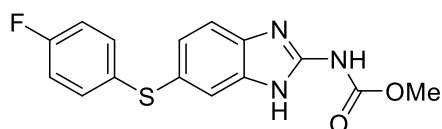
General Procedure B - Employed 2-fluoro-3-((2-fluorophenyl)thio)-6-nitroaniline (**5q/5r**) to give the title compound (**6q/6r**) (0.20 g, 65% yield) as a brown oil. ^1H NMR (400 MHz, CDCl_3) δ 7.14 – 7.06 (m, 1H), 7.04 – 6.98 (m, 1H), 6.98 – 6.90 (m, 2H), 6.87 (dd, 1H, $J = 8.4$ & 7.9 Hz), 6.50 (d, 1H, $J = 8.4$). ^{13}C NMR (100 MHz, CDCl_3) δ 159.6 (d, $J = 248.1$ Hz), 153.0 (d, $J = 239.6$ Hz), 139.2 (d, $J = 5.9$ Hz), 129.5 (d, 1.9 Hz), 127.3, 127.2, 125.1 (d, $J = 17.1$ Hz), 124.5 (d, $J = 3.3$ Hz), 122.9 (d, $J = 16.8$ Hz), 115.4 (d, $J = 21.4$ Hz), 11.8 (d, $J = 2.4$ Hz), 106.8 (d, $J = 18.0$ Hz). HRMS: (CI+, CH_4) m/z Calculated for $\text{C}_{12}\text{H}_{11}\text{F}_2\text{N}_2\text{S}$: 253.0606. Found $[\text{M}+\text{H}]^+$: 253.0615 (Diff -3.73 ppm).

4-Bromo-5-((2-fluorophenyl)thio)benzene-1,2-diamine (6s/6t)

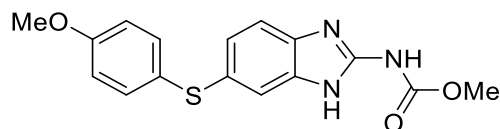
General Procedure B - Employed 4-bromo-5-((2-fluorophenyl)thio)-2-nitroaniline (**5s/5t**) to give the title compound (**6s/6t**) (0.24 g, 83% yield) as a brown oil. ^1H NMR (400 MHz, CDCl_3) δ 7.16 (m, 1H), 7.00 (m, 4H), 6.83 (s, 1H), 3.46 (s, 4H). ^{13}C NMR (100 MHz, CDCl_3) δ 159.8 (d, $J = 246.8$ Hz), 137.3, 134.6, 130.5 (d, $J = 2.1$ Hz), 127.8 (d, $J = 7.9$ Hz), 127.0, 124.6 (d, $J = 3.5$ Hz), 123.1, 122.7 (d, $J = 22.3$ Hz), 120.4, 118.7, 115.6 (d, $J = 22.0$ Hz).

3-((4-Fluorophenyl)thio)benzene-1,2-diamine (11b)

General Procedure A - Employed 3-((2-fluorophenyl)thio)-2-nitroaniline (**11a**) to give the title compound (**11b**) (0.26 g, 50% yield) as a brown oil. ^1H NMR (400 MHz, CDCl_3) δ 7.14 – 7.01 (m, 3H), 6.95 (dd, 1H, $J = 8.4$ & 7.3 Hz), 6.82 – 6.76 (m, 2H), 6.71 (dd, 1H, $J = 8.4$ & 8.1 Hz), 4.08 (s, 2H), 3.44 (s, 2H). ^{13}C NMR (100 MHz, CDCl_3) δ 159.3 (d, $J = 246.0$ Hz), 138.6, 134.8, 128.5, 128.4 (d, $J = 2.4$ Hz), 127.0 (d, $J = 7.6$ Hz), 125.7 (d, $J = 3.4$ Hz), 119.6, 118.4, 115.7, 115.4 (d, $J = 21.3$ Hz), 114.4. HRMS: (Cl^+ , CH_4) m/z Calculated for $\text{C}_{12}\text{H}_{11}\text{F}_2\text{N}_2\text{S}$: 253.0606. Found $[\text{M}+\text{H}]^+$: 253.0615 (Diff -3.73 ppm).

3.5.2.3 Methyl (6-(phenylthio)-1H-benzo[d]imidazol-2-yl)carbamate Derivatives**Methyl (6-((4-fluorophenyl)thio)-1H-benzo[d]imidazol-2-yl)carbamate (8a)⁷**

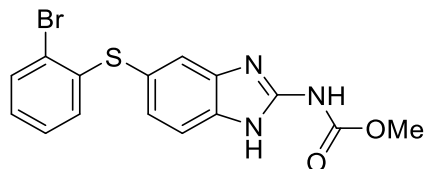
General Procedure C - Employed 4-((4-fluorophenyl)thio)benzene-1,2-diamine (**6a**) to give the title compound (**8a**) (0.13 g, 50% yield) as a cream solid. ^1H NMR (400MHz, DMSO) δ 11.63 (bs, 2H), 7.50 (d, 1H, $J = 1.6$ Hz), 7.45 (d, 1H, $J = 8.2$ Hz), 7.24 – 7.20 (m, 2H), 7.17 (dd, 1H, $J = 8.2$ & 1.6 Hz), 7.19 – 7.14 (m, 2H), 3.77 (s, 3H); ^{13}C NMR (100 MHz, DMSO) δ 161.4 (d, $J = 246.5$ Hz), 155.0, 148.7, 137.6, 134.0 (d, $J = 3.7$ Hz), 133.9, 131.1 (d, $J = 8.6$ Hz), 126.7, 124.8, 118.8, 116.7 (d, $J = 18.3$ Hz), 115.4, 53.0. HRMS: (ES^+) m/z Calculated for $\text{C}_{15}\text{H}_{13}\text{FN}_3\text{O}_2\text{S}$: 318.0713. Found $[\text{M}+\text{H}]^+$: 318.0712 (Diff – 0.2 ppm). $\nu_{\text{max}}/\text{cm}^{-1}$: (solid) 3656 (s), 2980 (m), 2888 (m), 1506 (m), 1462 (m), 1263 (m). MP: 230 - 232 °C. Purity HPLC (Method A) 89.5%, $R_t = 9.69$ min.

Methyl (6-((4-methoxyphenyl)thio)-1H-benzo[d]imidazol-2-yl)carbamate (8c)⁷

General Procedure C - Employed 4-((4-fluorophenyl)thio)benzene-1,2-diamine (**6c**) to give the title compound (**8c**) (0.095 g, 35% yield) as a cream solid. ^1H NMR (400MHz, DMSO) δ 11.71 (bs, 2H), 7.44 (d, 1H, $J = 8.3$ Hz), 7.42 (d, 1H, $J = 1.7$ Hz), 7.34 (d, 2H, $J = 8.8$ Hz), 7.14 (dd, 1H, $J = 8.3$ & 1.7 Hz), 7.00 (d, 2H, $J = 8.8$ Hz), 3.82 (s, 3H), 3.81 (s, 3H); ^{13}C NMR (100 MHz, DMSO) δ 158.1, 154.0, 153.0, 147.4, 135.4, 131.9, 126.4, 123.8, 114.4, 54.6, 51.9. HRMS: (ES^+) m/z Calculated for $\text{C}_{16}\text{H}_{16}\text{N}_3\text{O}_3\text{S}$: 330.0912.

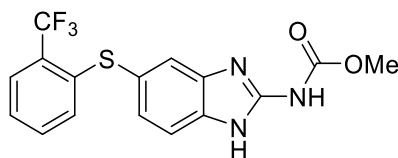
Found $[M+H]^+$: 330.0911 (Diff – 0.4ppm). $\nu_{\max}/\text{cm}^{-1}$: (solid) 3356 (s), 2978 (m), 2888 (m), 1713 (s), 1521 (s), 1490 (m), 1261 (m). MP: 232 - 235 °C. Purity HPLC (Method A) 95.1%, R_t = 9.54 min.

Methyl (5-((2-bromophenyl)thio)-1H-benzo[d]imidazol-2-yl)carbamate (8d)⁷

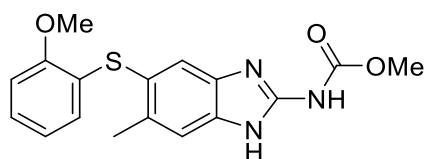


General Procedure C - Employed 4-((2-bromophenyl)thio)benzene-1,2-diamine (**6d**) to give the title compound (**8d**) (0.035 g, 55% yield) as a cream solid. ¹H NMR (400MHz, DMSO) δ 11.69 (s, 2H), 7.60 (d, 1H, J = 8.1 Hz), 7.59 (s, 1H), 7.53 (d, 1H, J = 8.0 Hz), 7.24 (d, 1H, J = 8.1 Hz), 7.19 (dd, 1H, J = 7.7 & 7.9 Hz), 7.05 (dd, 1H, J = 8.0 & 7.7 Hz), 6.59 (d, 1H, J = 7.9 Hz), 3.77 (s, 3H). ¹³C NMR (100 MHz, DMSO) δ 153.3, 146.0, 145.2, 142.2, 141.1, 139.2, 128.8, 128.4, 127.6, 127.5, 127.2, 120.1, 116.6, 115.6, 52.9. HRMS: (ES+) m/z Calculated for C₁₅H₁₃⁷⁹BrN₃O₂S: 377.9912. Found $[M+H]^+$: 377.9904 (Diff - 2.12 ppm). $\nu_{\max}/\text{cm}^{-1}$: (solid) 3395 (s), 2979 (m), 2956 (m), 1639 (s), 1457 (m), 1267 (m). MP: 240 °C decomposed. Microanalysis: Predicted C(47.63%), H(3.20%), N (11.11%), S(8.48%); Obtained C(47.48%), H(3.22%), N (11.06%), S(8.61%). Purity HPLC (Method A) 98.4%, R_t = 10.22 min.

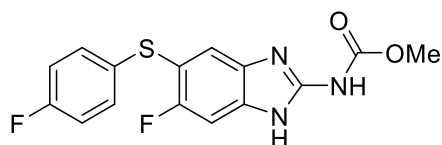
Methyl (5-((2-(trifluoromethyl)phenyl)thio)-1H-benzo[d]imidazol-2-yl)carbamate (8e)



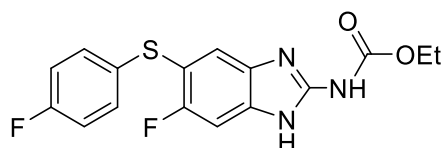
General Procedure C – Employed 4-((2-(trifluoromethyl)phenyl)thio)benzene-1,2-diamine (**6e**) to give the title compound (**8e**) (0.052 g, 50% yield) as a cream solid. ¹H NMR (400MHz, DMSO) δ 11.80 (bs, 2H), 7.74 (d, 1H, J = 8.0 Hz), 7.59 (s, 1H), 7.52 (d, 1H, J = 8.3 Hz), 7.46 (dd, 1H, J = 8.5 & 7.6 Hz), 7.33 (dd, 1H, J = 8.3 & 7.6 Hz), 7.24 (d, 1H, J = 8.0 Hz), 6.95 (d, 1H, J = 8.6 Hz), 6.95 (d, 1H, J = 8.6 Hz), 3.78 (s, 3H). ¹³C NMR (100 MHz, DMSO) δ 154.9, 150.0, 139.2, 133.4, 132.6, 129.8, 128.5, 128.3, 127.12, 127.06, 126.2, 125.8, 122.4 (d, J = 154.3 Hz), 52.8. ¹⁹F NMR (376 MHz) δ -59.9. HRMS: (ES+) m/z Calculated for C₁₆H₁₃F₃N₃O₂S: 368.0675. Found $[M+H]^+$: 368.0679 (Diff – 1.15 ppm). $\nu_{\max}/\text{cm}^{-1}$: (solid) 3045 (s), 2980 (m), 2959 (m), 1719 (s), 1594 (m), 1455 (m), 1271 (s). MP: 230 - 233 °C decomposed. Purity HPLC (Method A) 100%, R_t = 10.26 min.

Methyl (5-((2-methoxyphenyl)thio)-6-methyl-1H-benzo[d]imidazol-2-yl)carbamate (8f)

General Procedure C - Employed 4-((2-methoxyphenyl)thio)-5-methylbenzene-1,2-diamine (**6f**) to give the title compound (**8f**) (0.056 g, 61% yield) as a white solid. ^1H NMR (400MHz, DMSO) δ 11.76 (s, 2H), 7.50 (s, 1H), 7.46 – 7.41 (m, 1H), 7.14 - 7.10 (m, 1H), 7.02 (s, 1H), 6.79 - 6.75 (m, 1H), 6.40 – 6.36 (m, 1H), 3.88 (s, 3H), 3.78 (s, 3H), 2.34 (s, 3H). ^{13}C NMR (100 MHz, DMSO) δ 155.5, 154.2, 146.6, 140.5, 137.4, 134.6, 131.7, 126.8, 126.6, 126.3, 121.6, 116.9, 115.7, 111.3, 56.1, 52.9, 20.7. HRMS: (ES+) m/z Calculated for $\text{C}_{17}\text{H}_{18}\text{N}_3\text{O}_3\text{S}$: 344.1069. Found $[\text{M}+\text{H}]^+$: 344.1061 (Diff -2.32 ppm). $\nu_{\text{max}}/\text{cm}^{-1}$: (solid) 3330 (s), 2979 (m), 2951 (m), 2832 (m), 1621 (s), 1460 (m), 1270(s). MP: 240 °C. Purity HPLC (Method A) 94.4%, R_t = 9.56 min.

Methyl (6-fluoro-5-((4-fluorophenyl)thio)-1H-benzo[d]imidazol-2-yl)carbamate (8g)

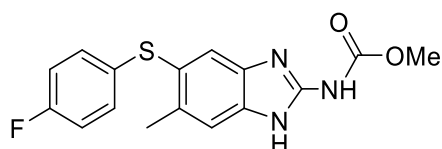
General Procedure C - Employed 4-fluoro-5-((4-fluorophenyl)thio)benzene-1,2-diamine (**6g**) to give the title compound (**8g**) (0.079 g, 72% yield) as a white solid. ^1H NMR (400MHz, DMSO) δ 11.72 (s, 2H), 7.50 (s, 1H, J = 6.8 Hz), 7.33 (d, 1H, J = 10.2 Hz), 7.23 - 7.17 (m, 4H), 3.77 (s, 3H). ^{13}C NMR (100 MHz, DMSO) δ 161.5 (d, J = 244.9 Hz), 157.0 (d, J = 244.7 Hz), 154.6, 148.5, 140.6, 134.7, 132.2 (d, J = 3.6 Hz), 130.8 (d, J = 5.5 Hz), 118.7, 116.0 (d, J = 21.3 Hz), 115.4, 104.5 (d, J = 21.3 Hz), 53.1. HRMS: (ES+) m/z Calculated for $\text{C}_{15}\text{H}_{12}\text{F}_2\text{N}_3\text{O}_2\text{S}$: 336.0618. Found $[\text{M}+\text{H}]^+$: 336.0620 (Diff 0.60 ppm). $\nu_{\text{max}}/\text{cm}^{-1}$: (solid) 3334 (s), 2959 (m), 2667 (m), 1702 (s), 1456 (m), 1273 (s). MP: 256 °C decomposed. Purity HPLC (Method A) 98.8%, R_t = 9.65 min.

Ethyl (6-fluoro-5-((4-fluorophenyl)thio)-1H-benzo[d]imidazol-2-yl)carbamate (8h)

General Procedure C - Employed 4-fluoro-5-((4-fluorophenyl)thio)benzene-1,2-diamine (**6h**) to give the title compound (**8h**) (0.066 g, 60% yield) as a white solid. ^1H NMR (400MHz, DMSO) δ 11.69 (s, 2H), 7.50 (d, 1H, J = 6.6 Hz), 7.33 (d, 1H, J = 9.7 Hz), 7.23 - 7.17 (m, 4H), 4.23 (q, 2H, J = 7.1 Hz), 1.28 (t, 3H, J = 7.1 Hz). ^{13}C NMR (100 MHz, DMSO) δ 162.4 (d, J = 244.1 Hz), 160.5 (d, J = 246.4 Hz), 154.2,

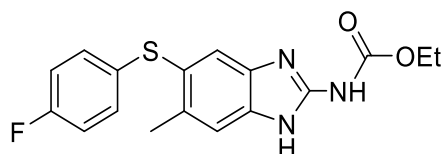
149.5, 140.0, 133.5, 132.4, 130.7 (d, $J = 9.2$ Hz), 120.9, 116.9 (d, $J = 22.7$ Hz), 114.8, 104.3, 61.9, 14.7. HRMS: (ES+) m/z Calculated for $C_{16}H_{14}F_2N_3O_2S$: 350.0775. Found $[M+H]^+$: 350.0768 (Diff -2.0 ppm). $\nu_{\max}/\text{cm}^{-1}$: (solid) 3361 (s), 2981 (m), 2881 (m), 2723 (m), 1692 (s), 1451 (m), 1272 (s). MP: 258 °C decomposed. Purity HPLC (Method A) 98.0%, $R_t = 10.26$ min.

Methyl (5-((4-fluorophenyl)thio)-6-methyl-1H-benzo[d]imidazol-2-yl)carbamate (8i)



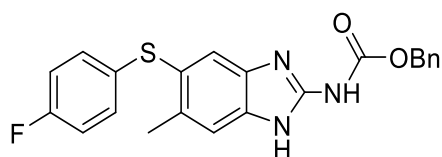
General Procedure C - Employed 4-((4-fluorophenyl)thio)-5-methylbenzene-1,2-diamine (**6i**) to give the title compound (**8i**) (0.053 g, 60% yield) as a white solid. ^1H NMR (400MHz, DMSO) δ 11.68 (s, 2H), 7.49 (s, 1H), 7.39 (s, 1H), 7.15 (dd, 2H, $J = 9.2$ & 8.3 Hz), 7.07 (dd, 2H, $J = 9.2$ & 8.3 Hz), 3.75 (s, 3H), 2.35 (s, 3H). ^{13}C NMR (100 MHz, DMSO) δ 161.1 (d, $J = 243.4$ Hz), 155.1, 148.6, 143.9, 139.9, 133.5 (d, $J = 2.9$ Hz), 133.5, 129.7 (d, $J = 9.7$ Hz), 123.4, 119.1, 116.8 (d, $J = 21.6$ Hz), 113.3, 52.8, 21.1. HRMS: (ES+) m/z Calculated for $C_{16}H_{15}FN_3O_2S$: 332.0869. Found $[M+H]^+$: 332.0868 (Diff -0.30 ppm). $\nu_{\max}/\text{cm}^{-1}$: (solid) 3335 (s), 2656 (m), 1634 (s), 1457 (m), 1276 (s). MP: 262 °C decomposed. Purity HPLC (Method A) 100%, $R_t = 10.12$ min.

Ethyl (5-((4-fluorophenyl)thio)-6-methyl-1H-benzo[d]imidazol-2-yl)carbamate (8j)



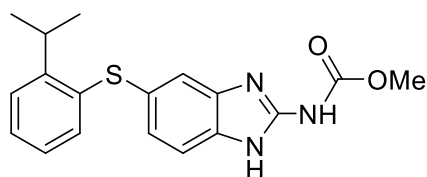
General Procedure C - Employed 4-((4-fluorophenyl)thio)-5-methylbenzene-1,2-diamine (**6j**) to give the title compound (**8j**) (0.066 g, 60% yield) as a white solid. ^1H NMR (400MHz, DMSO) δ 11.70 (s, 2H), 7.50 (s, 1H), 7.40 (s, 1H), 7.14 (m, 2H), 7.07 (m, 2H), 4.22 (q, 2H, $J = 7.0$ Hz), 2.35 (s, 3H), 1.28 (t, 3H, $J = 7.0$ Hz). ^{13}C NMR (100 MHz, DMSO) δ 161.1 (d, $J = 239.5$ Hz), 154.7, 148.6, 136.2, 135.5, 135.7 (d, $J = 2.5$ Hz), 133.5, 129.7 (d, $J = 7.6$ Hz), 123.3, 118.8, 116.7 (d, $J = 22.5$ Hz), 112.7, 61.8, 21.1, 14.8. HRMS: (ES+) m/z Calculated for $C_{17}H_{17}FN_3O_2S$: 346.1026. Found $[M+H]^+$: 346.1019 (diff -2.02 ppm).

Benzyl (5-((4-fluorophenyl)thio)-6-methyl-1H-benzo[d]imidazol-2-yl)carbamate (8k)



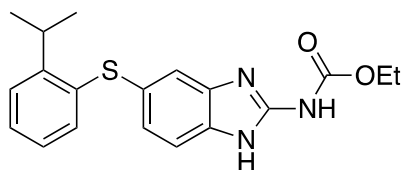
General Procedure C - Employed 4-((4-fluorophenyl)thio)-5-methylbenzene-1,2-diamine (**6k**) to give the title compound (**8k**) (0.028 g, 22% yield) as a white solid. ^1H NMR (400MHz, DMSO) δ 11.78 (s, 2H), 7.47 – 7.41 (m, 7H), 7.15 (dd, 2H, $J = 9.4$ & 8.6 Hz), 7.07 (dd, 2H, $J = 8.6$ & 8.4 Hz), 5.24 (s, 2H), 2.34 (s, 3H). ^{13}C NMR (100 MHz, DMSO) δ 161.1 (d, $J = 242.8$ Hz), 156.4, 148.0, 137.6, 136.7, 136.6, 133.6 (d, 3.1 Hz) 132.4, 129.8, (d, $J = 7.7$ Hz), 12.90, 128.6, 128.5, 123.6, 119.9, 116.8 (d, $J = 22.1$ Hz), 114.0, 67.1, 21.0. HRMS: (ES+) m/z Calculated for $\text{C}_{22}\text{H}_{19}\text{FN}_3\text{O}_2\text{S}$: 408.1182. Found $[\text{M}+\text{H}]^+$: 408.1179 (diff – 0.74 ppm). MP 232 – 235 °C. Purity HPLC (Method A) 98.5%, $R_t = 11.67$ min.

Methyl (5-((2-isopropylphenyl)thio)-1H-benzo[d]imidazol-2-yl)carbamate (8l)



General Procedure C - Employed 4-((2-isopropylphenyl)thio)benzene-1,2-diamine (**6l**) to give the title compound (**8l**) (0.040 g, 43% yield) as a white solid. ^1H NMR (400MHz, DMSO) δ 11.66 (s, 2H), 7.43 (m, 1H), 7.40 (s, 1H), 7.35 (d, 1H, $J = 7.2$ Hz), 7.21 (m, 1H), 7.10 (m, 2H), 6.93 (d, 1H, $J = 7.2$ Hz), 3.76 (s, 3H), 3.45 (sep, 1H, $J = 6.2$ Hz), 1.20 (d, 6H, $J = 6.2$ Hz). ^{13}C NMR (100 MHz, DMSO) δ 158.4, 155.1, 147.5, 139.5, 135.9, 130.3, 127.4, 126.2, 126.1, 125.2, 124.3, 118.4, 113.4, 53.0, 30.3, 23.7. HRMS: (ES+) m/z Calculated for $\text{C}_{18}\text{H}_{20}\text{N}_3\text{O}_2\text{S}$: 342.1276. Found $[\text{M}+\text{H}]^+$: 342.1285 (Diff 2.6 ppm). $\nu_{\text{max}}/\text{cm}^{-1}$: (solid) 3394 (s), 3064 (m), 2956 (m), 2869 (m), 1644 (s), 1456 (m), 1261 (s). MP: 210 - 212 °C. Purity HPLC (Method A) 99.4%, $R_t = 11.00$ min.

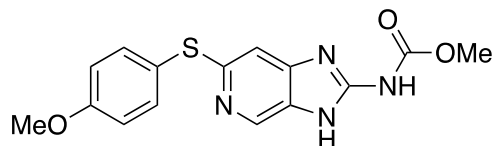
Ethyl (5-((2-isopropylphenyl)thio)-1H-benzo[d]imidazol-2-yl)carbamate (8m)



General Procedure C - Employed 4-((2-isopropylphenyl)thio)benzene-1,2-diamine (**6m**) to give the title compound (**8m**) (0.023 g, 24% yield) as a white solid. ^1H NMR (400MHz, DMSO) δ 11.68 (s, 2H), 7.45 – 7.41 (m, 2H), 7.34 (d, 1H, $J = 7.4$ Hz), 7.20 (dd, 1H, $J = 8.4$ & 7.4 Hz), 7.10 (d, 1H, $J = 8.2$ Hz), 7.06 (d, 1H, $J = 8.4$ Hz), 6.93 (d, 1H, $J = 8.2$ Hz), 4.22 (q, 2H, $J = 6.9$ Hz), 3.45 (sep, 1H, $J = 7.1$ Hz), 1.28 (t, 3H, $J = 6.9$ Hz), 1.20 (d, 6H, $J = 7.1$ Hz). ^{13}C NMR (100 MHz, DMSO) δ 154.6, 152.3, 148.5, 147.4, 136.0, 132.4, 127.4, 127.0, 126.2, 126.1, 125.1, 120.6, 114.7, 61.8, 30.4, 23.6, 14.8. HRMS: (ES+) m/z Calculated for $\text{C}_{19}\text{H}_{21}\text{N}_3\text{O}_2\text{S}^{23}\text{Na}$: 378.1252. Found $[\text{M}+\text{Na}]^+$: 378.1248 (Diff – 1.06 ppm). $\nu_{\text{max}}/\text{cm}^{-1}$:

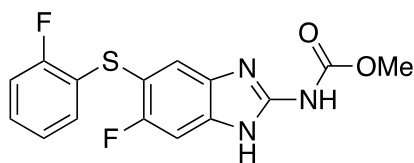
(solid) 3334 (s), 3056 (m), 2955 (m), 2927 (m), 2866 (m), 1636 (s), 1467 (m), 1265 (s). MP: 206-208 °C. Purity HPLC (Method A) 100%, R_t = 11.53 min.

Methyl (6-((4-methoxyphenyl)thio)-3H-imidazo[4,5-c]pyridin-2-yl)carbamate (8n)



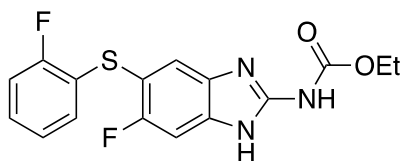
General Procedure C - Employed 6-((4-methoxyphenyl)thio)pyridine-3,4-diamine (**6n**) to give the title compound (**8n**) (0.057 g, 56% yield) as a white solid. ^1H NMR (400MHz, DMSO) δ 12.01 (bs, 1H), 11.48 (bs, 1H), 8.48 (s, 1H), 7.51 (d, 2H, J = 8.5 Hz), 7.06 (d, 2H, J = 8.5 Hz), 6.87 (s, 1H), 3.82 (s, 3H), 3.75 (s, 3H). ^{13}C NMR (100 MHz, DMSO) δ 160.4, 154.6, 152.5, 150.6, 146.4, 141.0, 137.0, 125.8, 123.5, 118.6, 115.9, 55.6, 53.0. HRMS: (ES+) m/z Calculated for $\text{C}_{15}\text{H}_{15}\text{N}_4\text{O}_3\text{S}$: 331.0859. Found $[\text{M}+\text{H}]^+$: 331.0852 (Diff 2.09 ppm). MP: 240 °C. Purity HPLC (Method A) 98.3%, R_t = 8.13 min.

Methyl (6-fluoro-5-((2-fluorophenyl)thio)-1H-benzo[d]imidazol-2-yl)carbamate (8o)



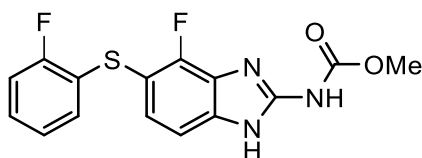
General Procedure C - Employed 4-fluoro-5-((2-fluorophenyl)thio)benzene-1,2-diamine (**6o**) to give the title compound (**8o**) (0.94 g, 68% yield) as a cream solid. ^1H NMR (400MHz, DMSO) δ 11.82 (bs, 2H), 7.54 (d, 1H, J = 6.6 Hz), 7.37 (d, 1H, J = 9.6 Hz), 7.31 – 7.24 (m, 2H), 7.15 – 7.08 (m, 1H), 6.92 (dd, 1H, J = 8.8 & 7.7 Hz), 3.78 (s, 3H). ^{13}C NMR (100 MHz, DMSO) δ 159.5 (d, J = 242.3 Hz), 157.9, (d, J = 238.0 Hz), 154.7, 149.5, 130.1, 128.9 (d, J = 7.6 Hz), 125.8 (d, J = 3.1 Hz), 124.0 (d, J = 16.1 Hz), 116.2 (d, J = 21.9 Hz), 109.0 (d, J = 20.2 Hz), 53.2. ^{19}F NMR (376 MHz, DMSO) δ -112.9, -117.3. HRMS: (ES+) m/z Calculated for $\text{C}_{15}\text{H}_{12}\text{F}_2\text{N}_3\text{O}_2\text{S}$: 336.0613. Found $[\text{M}+\text{H}]^+$: 336.0615 (Diff – 0.8 ppm). $\nu_{\text{max}}/\text{cm}^{-1}$: (solid) 3348 (m), 3070 (m), 2980 (m), 2888 (m), 1699 (s), 1636 (m), 1457 (m), 1271 (m). MP: 294 -296 °C. Purity HPLC (Method A) 97.5%, R_t = 9.65 min.

Ethyl (6-fluoro-5-((2-fluorophenyl)thio)-1H-benzo[d]imidazol-2-yl)carbamate (8p)



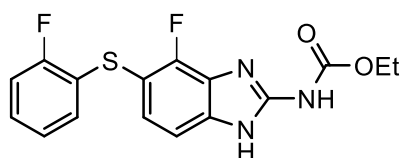
General Procedure C - Employed 4-fluoro-5-((2-fluorophenyl)thio)benzene-1,2-diamine (**6p**) to give the title compound (**8p**) (0.21 g, 29% yield) as a cream solid. ^1H NMR (400MHz, DMSO) δ 11.80 (s, 2H), 7.55 (d, $J = 6.5$ Hz), 7.37 (d, 1H, $J = 9.6$ Hz), 7.30 - 7.24 (m, 2H), 7.14 - 7.09 (m, 1H, $J = 7.9$ Hz), 6.94 - 6.89 (m, 1H), 4.25 (q, 2H, $J = 7.3$ Hz), 1.28 (t, 3H, $J = 7.3$ Hz). ^{13}C NMR (100 MHz, DMSO) δ 159.2 (d, $J = 244.7$ Hz), 158.5 (d, $J = 243.7$ Hz), 154.2, 149.5, 130.0, 128.8 (d, $J = 7.6$ Hz), 125.8 (d, $J = 3.7$ Hz), 124.9 (d, $J = 16.3$ Hz), 118.2, 116.2 (d, $J = 22.1$ Hz), 112.1, 108.7, 62.0, 14.6. ^{19}F NMR (376 MHz, DMSO) δ -112.3, -116.7. HRMS: (ES+) m/z Calculated for $\text{C}_{16}\text{H}_{14}\text{F}_2\text{N}_3\text{O}_2\text{S}$: 350.0769. Found $[\text{M}+\text{H}]^+$: 350.0771 (Diff - 0.5 ppm). $\nu_{\text{max}}/\text{cm}^{-1}$: (solid) 3347 (m), 2980 (m), 2888 (m), 2658 (m), 1688 (s), 1593 (m), 1461 (m), 1268 (s). MP 300 - 302°C. Purity HPLC (Method A) 98.5%, $R_t = 10.20$ min.

Methyl (4-fluoro-5-((2-fluorophenyl)thio)-1H-benzo[d]imidazol-2-yl)carbamate (8q)



General Procedure C - Employed 3-fluoro-4-((2-fluorophenyl)thio)benzene-1,2-diamine (**6q**) to give the title compound (**8q**) (0.68 g, 54% yield) as a white solid. ^1H NMR (400MHz, DMSO) δ 12.30 (bs, 1H), 11.57 (bs, 1H), 7.38 (d, 1H, $J = 8.3$ Hz), 7.27 - 7.20 (m, 3H), 7.12 - 7.04 (m, 1H), 6.84 (dd, 1H, $J = 8.8$ & 7.6 Hz), 3.79 (s, 3H). ^{13}C NMR (100 MHz, DMSO) δ 159.2 (d, $J = 243.4$ Hz), 154.5, 152.5 (d, $J = 242.0$ Hz), 148.5, 138.2, 130.3, 129.5, 128.5, 128.4 (d, $J = 4.3$ Hz), 125.7 (d, $J = 3.3$ Hz), 124.6 (d, $J = 16.6$ Hz), 116.1 (d, $J = 20.8$ Hz), 109.5, 107.4 (d, $J = 16.2$ Hz), 53.2. ^{19}F NMR (367 MHz, DMSO) -112.6, -124.6. HRMS: (ES+) m/z Calculated for $\text{C}_{15}\text{H}_{12}\text{F}_2\text{N}_3\text{O}_2\text{S}$: 336.0613. Found $[\text{M}+\text{H}]^+$: 336.0615 (Diff - 0.8 ppm). $\nu_{\text{max}}/\text{cm}^{-1}$: (solid) 3341 (s), 2967 (m), 2887 (m), 2735 (m), 1709 (s), 1442 (m), 1258 (m), 1201 (m). MP: 250 - 252 °C. Purity HPLC (Method A) 99.1%, $R_t = 9.76$ min.

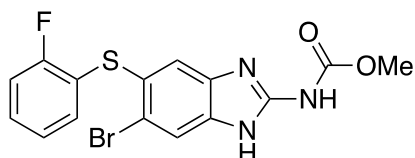
Ethyl (4-fluoro-5-((2-fluorophenyl)thio)-1H-benzo[d]imidazol-2-yl)carbamate (8r)



General Procedure C - Employed 3-fluoro-4-((2-fluorophenyl)thio)benzene-1,2-diamine (**6r**) to give the title compound (**8r**) (0.023 g, 24% yield) as a white solid. ^1H NMR (400MHz, DMSO) δ 12.33 (bs, 1H), 11.47 (bs, 1H), 7.37 (dd, 1H, $J = 8.3$ & 1.7 Hz), 7.28 - 7.21 (m, 3H), 7.12 - 7.06 (m, 1H), 6.87 (dd, 1H, $J = 8.3$ & 7.7 Hz), 4.25 (q, 2H, $J = 7.1$ Hz), 1.29 (t, 3H, $J = 7.1$ Hz). ^{13}C NMR (100 MHz, DMSO) δ 159.1 (d, $J = 244.0$ Hz), 155.8 (d, $J = 266.7$ Hz), 154.1, 148.5, 138.2, 129.4, 128.8 (d, $J = 7.7$ Hz), 128.4 (d, $J = 6.3$ Hz), 127.3, 125.8 (d, $J = 3.2$ Hz), 125.6 (d, $J = 16.2$ Hz), 116.1 (d, $J = 21.2$ Hz), 109.3, 62.0, 14.8. Not

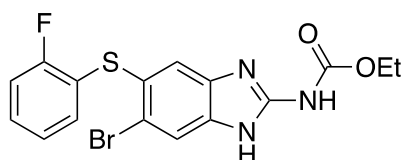
all quaternary carbons visible. HRMS: (ES+) m/z Calculated for $C_{16}H_{14}F_2N_3O_2S$: 350.0769. Found $[M+H]^+$: 350.0780 (Diff -2.97 ppm). $\nu_{\max}/\text{cm}^{-1}$: (solid) 3370 (s), 3175 (m), 2980 (m), 1689 (s), 1440 (m), 1261 (m). MP: 264 – 266 °C.

Methyl (6-bromo-5-((2-fluorophenyl)thio)-1H-benzo[d]imidazol-2-yl)carbamate (8s)

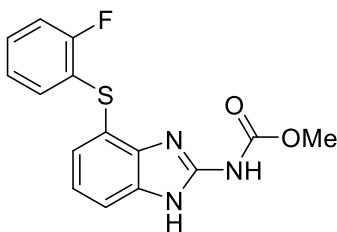


General Procedure C - Employed 4-bromo-5-((2-fluorophenyl)thio)benzene-1,2-diamine (**6s**) to give the title compound (**8s**) (0.080 g, 53% yield) as a pale pink solid. ^1H NMR (400MHz, DMSO) δ 11.75 (s, 2H), 7.78 (s, 1H), 7.44 (s, 1H), 7.40 – 7.29 (m, 2H), 7.21 – 7.15 (m, 1H), 7.00 (dd, 1H, $J = 8.9$ & 8.0 Hz), 3.76 (s, 3H). ^{13}C NMR (100 MHz, DMSO) δ 160.0 (d, $J = 245.4$ Hz), 154.6, 149.3, 131.7, 130.5, 129.7 (d, $J = 7.9$ Hz), 126.0 (d, $J = 3.6$ Hz), 123.4, 123.1 (d, $J = 17.5$ Hz), 118.3, 116.4 (d, $J = 22.4$ Hz), 53.2 not all carbons observed. HRMS: (ES+) m/z Calculated for $C_{15}H_{12}BrFN_3O_2S$: 395.9812. Found $[M+H]^+$: 395.9807 (Diff 1.22 ppm). $\nu_{\max}/\text{cm}^{-1}$: (solid) 3334 (m), 2980 (m), 2888 (m), 1697 (s), 1449 (m), 1262 (s). MP: 243 - 246 °C Purity HPLC (Method A) 89.5%, $R_t = 10.16$ min.

Ethyl (6-bromo-5-((2-fluorophenyl)thio)-1H-benzo[d]imidazol-2-yl)carbamate (8t)



General Procedure C - Employed 4-bromo-5-((2-fluorophenyl)thio)benzene-1,2-diamine (**6t**) to give the title compound (**8t**) (0.12 g, 80% yield) as a cream solid. ^1H NMR (400MHz, DMSO) δ 11.85 (s, 2H), 7.78 (s, 1H), 7.42 (s, 1H), 7.40 – 7.29 (m, 2H), 7.21 – 7.14 (m, 1H), 7.02 – 6.97 (m, 1H), 4.23 (q, 2H, $J = 6.9$ Hz), 1.28 (t, 3H, $J = 6.9$ Hz). ^{13}C NMR (100 MHz, DMSO) δ 159.8 (d, $J = 243.9$ Hz), 154.2, 149.3, 131.7, 129.7 (d, $J = 7.4$ Hz), 127.2, 126.0 (d, $J = 3.7$ Hz), 125.7, 123.3, 123.1 (d, $J = 14.7$ Hz), 118.3, 116.4 (d, $J = 22.1$ Hz), 62.1, 14.7. HRMS: (ES+) m/z Calculated for $C_{16}H_{14}BrFN_3O_2S$: 409.9969. Found $[M+H]^+$: 409.9962 (Diff -1.54 ppm). $\nu_{\max}/\text{cm}^{-1}$: (solid) 3350 (s), 2982 (m), 2757 (m), 1688 (s), 1447 (m), 1255 (s). MP: 254 - 256 °C decomposed. Purity HPLC (Method A) 90.5%, $R_t = 10.7$ min.

Methyl (4-((2-fluorophenyl)thio)-1H-benzo[d]imidazol-2-yl)carbamate (11)

General Procedure C - Employed 3-((4-fluorophenyl)thio)benzene-1,2-diamine (**11b**) to give the title compound (**11**) (0.25 g, 71% yield) as a white solid. ^1H NMR (400MHz, DMSO) δ 12.08 (s, 1H), 11.48 (s, 1H), 7.49 (d, 1H, $J = 7.5$ Hz) 7.33 – 7.24 (m, 2H), 7.13 – 7.05 (m, 2H), 7.00 – 6.91 (m, 2H), 3.76 (s, 3H). ^{13}C NMR (100 MHz, DMSO) δ 160.3 (d, $J = 243.0$ Hz), 154.8, 147.6, 139.3, 136.2, 129.7 (d, $J = 7.7$ Hz), 125.7 (d, $J = 3.5$ Hz), 125.2, 124.7, 122.1 (d, $J = 17.2$ Hz), 122.0, 119.1, 116.3 (d, $J = 22.1$ Hz), 114.8, 53.3. ^{19}F NMR (376 MHz, DMSO) δ -111.3. HRMS: (ES+) m/z Calculated for $\text{C}_{15}\text{H}_{13}\text{FN}_3\text{O}_2\text{S}$: 318.0707. Found $[\text{M}+\text{H}]^+$: 318.0714 (Diff -2.31ppm). $\nu_{\text{max}}/\text{cm}^{-1}$: (solid) 3391 (m), 2980 (m), 2884 (m), 2755 (m), 1718 (s), 1444 (m), 1261 (m). MP: 222 – 225 °C. Purity HPLC (Method A) 98.3%, $R_t = 9.71$ min.

3.6 References

1. M. C. Cruz, M. S. Bartlett and T. D. Edlind, *Antimicrob. Agents Chemother.*, 1994, **38**, 378-380.
2. M. P. Marques, O. M. Takayanagui and V. L. Lanchote, *Braz. J. Med. Biol. Res.*, 2002, **35**, 261-269.
3. E. Syslová, P. Landa, L. R. Stuchlíková, P. Matoušková, L. Skálová, B. Szotáková, M. Navrátilová, T. Vaněk and R. Podlipná, *Chemosphere*, 2019, **218**, 662-669.
4. Q. A. McKellar, C. Gokbulut, K. Muzandu and H. Benchaoui, *Drug Metab. Dispos.*, 2002, **30**, 1230-1239.
5. L. Fernández, E. Sigal, L. Otero, J. J. Silber and M. Santo, *Brazilian Journal of Chemical Engineering*, 2011, **28**, 679-689.
6. E. C. Cortés and L. A. A. Anaya, *J. Heterocycl. Chem.*, 1997, **34**, 745-748.
7. E. C. Cortés, R. S. Mendoza, M. S. Gutiérrez and O. G.-M. De Cortés, *J. Heterocycl. Chem.*, 2004, **41**, 273-276.
8. *US Pat.*, US20030612163, 2003.
9. R. F. Hudson and G. Klopman, *J. Chem. Soc.*, 1962, DOI: 10.1039/JR9620001062, 1062-1067.
10. P. M, in *The Thiol Group (1974)*, 1974, DOI: 10.1002/9780470771327.ch6, pp. 721-784.
11. M. S. Ning, S. E. Price, J. A. Ta and K. M. Davies, *J. Phys. Org. Chem.*, 2010, **23**, 220-226.
12. S. K. Giri, R. Gour and K. P. R. Kartha, *RSC Adv.*, 2017, **7**, 13653-13667.
13. T. T. Martinez, R. W. Jaeger, F. J. deCastro, M. W. Thompson and M. F. Hamilton, *Vet. Hum. Toxicol.*, 1986, **28**, 233-236.
14. E. C. Cortés, A. M. H. Sanabria and O. G. Mellado, *J. Heterocycl. Chem.*, 2002, **39**, 55-59.
15. Y. Ogata, *J. Org. Chem.*, 1982, **47**, 3577-3581.
16. M. B. Smith and J. March, *March's Advanced Organic Chemistry: Reactions, Mechanisms, and Structure*, Wiley, 5th edn., 2001.
17. D. Widdowson, The Chemistry of Nitrogen Compounds, http://www.ch.ic.ac.uk/widdowson/teach_files/nitrogen/dw1.html, (accessed June 2019).
18. D. B. Tiedtke, T. T. Peter Cheung, J. Leger and S. A. Zisman, *Chemicals Influencing The Activity of Palladium-Based Catalysts For The Selective Hydrogenation Of Acetylene To Ethylene in Acetylene Converters*, 2001.
19. D. E. Grove, *Platinum Metals Rev.*, 2003, **47**, 44-44.
20. J. Dunleavy, *Platinum Metals Rev.*, 2006, **50**, 110.
21. M. Argyle and C. Bartholomew, *Catalysts*, 2015, **5**, 145-269.
22. O. A. El Seoud and K. Takashima, *J. Chem. Educ.*, 1998, **75**, 1625-1627.
23. A. R. Butler, I. H. Robertson and R. Bacaloglu, *J. Chem. Soc., Perkin Trans. 2*, 1974, **1**, 1733-1736.
24. EUCAST, European Committee on Antimicrobial Susceptibility Testing (EUCAST), <http://www.eucast.org/documents/sops/>, (accessed June 2019, 2019).
25. H. Nishikawa, Y. Fukuda, J. Mitsuyama, M. Tashiro, A. Tanaka, T. Takazono, T. Saijo, K. Yamamoto, S. Nakamura, Y. Imamura, T. Miyazaki, H. Kakeya, Y. Yamamoto, K. Yanagihara, H. Mukae, S. Kohno and K. Izumikawa, *J. Antimicrob. Chemother.*, 2017, **72**, 1709-1713.
26. T. Shibata, T. Takahashi, E. Yamada, A. Kimura, H. Nishikawa, H. Hayakawa, N. Nomura and J. Mitsuyama, *Antimicrob Agents Chemother*, 2012, **56**, 5892-5897.
27. Spartan, *Wavefunction*, 2016.
28. Y. Hamada, in *Pyridine*, Intechopen, 1st edn., 2018, DOI: 10.5772/intechopen.74719.
29. A. Kokate, X. Li and B. Jasti, *AAPS PharmSciTech.*, 2008, **9**, 501-504.
30. V. H. Freed, R. Haque and J. Verneti, *J. Agric. Food Chem.*, 1967, **15**, 1121-1123.
31. J. E. Cheong, M. Zaffagni, I. Chung, Y. Xu, Y. Wang, F. E. Jernigan, B. R. Zetter and L. Sun, *Eur. J. Med. Chem.*, 2018, **144**, 372-385.
32. M. A. Walker, *Expert Opin. Drug Discov.*, 2014, **9**, 1421-1433.
33. A. Zafar, L. I. Pilkington, N. A. Haverkate, M. Van Rensburg, E. Leung, S. Kumara, W. A. Denny, D. Barker, A. Alsuraifi, C. Hoskins and J. Reynisson, *Molecules*, 2018, **23**, 145-158.
34. T. T. Wager, X. Hou, P. R. Verhoest and A. Villalobos, *ACS Chem. Neurosci.*, 2016, **7**, 767-775.
35. W. P. Walters, *Expert Opin. Drug Discov.*, 2012, **7**, 99-107.
36. Stardrop, *Optibrium*, 2018.
37. S. Gore, Personal communication, 2019.
38. P. Wils, A. Warnery, V. Phung-Ba, S. Legrain and D. Scherman, *J. Pharmacol. Exp. Ther.*, 1994, **269**, 654-658.

Chapter 4

Synthesis and Biological Evaluation of Benzimidazole Ether Derivatives

4.1 Benzimidazole ether derivatives

Unlike the thioether and ketone derivatives fenbendazole and flubendazole, which have been reported in the literature as commercially available compounds, the ether class, whereby the sulphur group is swapped for an oxygen is not. Having an oxygen atom in the bridging group is interesting as the thioether metabolism we were concerned about (Chapter 2, Section 2.4.2) is no longer present in this molecule (Figure 4.1). It was also proposed that the same synthetic route used for the thiol class could be applied to the ether class, so this was advantageous as no new routes needed to be developed. Furthermore, before undertaking any synthesis, a search of the literature unveiled a large number of phenol starting materials, significantly larger than the thiophenol starting materials, allowing greater potential for template expansion if these compounds were active. Addition of solubilising groups, using the larger range of starting materials is essential and should provide a significant benefit.

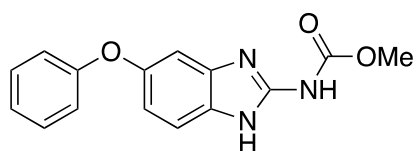


Figure 4.1. Ether derivatives of fenbendazole are not reported in the literature as commercially available compounds.

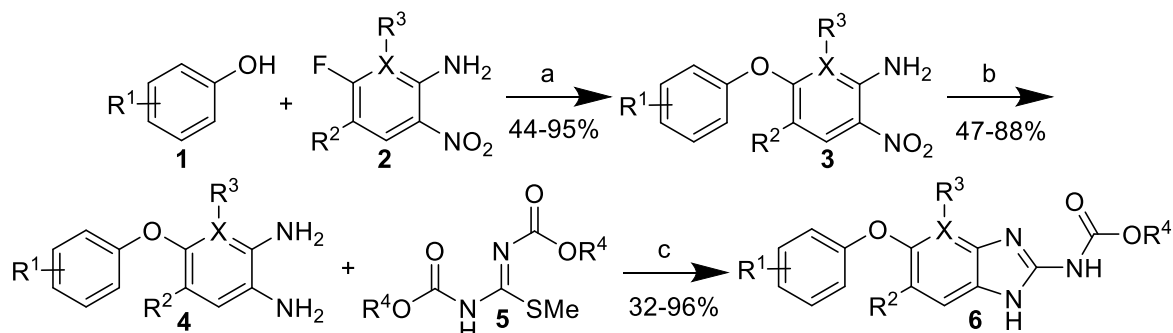
Using the synthetic route established in Chapter 3, the aims for the benzimidazole ether project were;

1. To design and synthesise a number of ether derivatives for biological testing against *C. neoformans*, to understand and develop an SAR relationship
2. To obtain DMPK data to allow this to inform what compounds show suitable properties and allow this to inform design of other analogues.
3. To add solubilising groups to improve aqueous solubility by taking advantage of the large range of commercially available phenols.

4.2 Ether Derivatives Discussion

Like the thioether derivatives described in Chapter 3, synthesis of the ether derivatives followed a three-step route (Scheme 4.1). This route was adapted from the thioether route reported, with some modification of the chemistry to improve yields and purification. There is also a paper by Wang, *W et al*, that reports the synthesis of some similar phenol derivatives.¹⁻⁴

4.2.1 Synthesis



Scheme 4.1. Reagents and Conditions: (a) K_2CO_3 (2.0 eq.), DMF, reflux, overnight (44 – 95% yield); (b) $SnCl_2$ (5.0 eq.), ethanol, reflux, overnight (47 – 88% yield); (c) 1,3-Bis(methoxycarbonyl)-2-methyl-2-thiopseudourea (**5**) (1.0 eq.), acetic acid (2 M), methanol (0.4 M), sealed tube, 65 °C, overnight (32 – 96% yield).

Table 4.1. Percentage yields obtained for all compounds created within the ether template, including intermediates and final products.

	R ¹	R ²	R ³	R ⁴	X	Step A % yield (3)	Step B % yield (4)	Step C % yield (6)
6a	4-F	H	H	Me	C	95	76	78
6b	4-F		H	Me	N	44	54	32
6c	4-F	Br	H	Me	C	73	68	35
6d	4-F	Br	H	Et	C	73	68	96
6e	4-F	H	F	Me	C	79	88	55
6f	4-F	H	F	Et	C	79	88	57
6g	4-F	F	F	Me	C	57	41	65

4.2.1.1 Nucleophilic Aromatic Substitution (S_NAr)

This occurred via the same reaction described for the thiols, however proved to be more problematic at first. Phenols (**1**) as nucleophiles are generally less reactive because the sulphur atom is bigger, more acidic and it is more easily polarisable, thus making it a better nucleophile.⁵⁻⁷ The phenoxy anion produced during the reaction also has a reduction in nucleophilicity because the lone pair of electrons resonates throughout the ring. The first approach to improving yields was to use sodium hydride instead of potassium carbonate, this showed no change in the yield observed for the synthesis of **6a**. It was decided not to continue with the use of sodium hydride, as it is more difficult to handle than the potassium carbonate and didn't afford improved yields.

As with the thiol derivatives, the starting nitroaniline (**2**) has a very similar R_f value to the product (**3**), and there is even more R_f overlap observed when compared with the thiols. Because of the reduced nucleophilicity of the phenol starting material (**1**), the starting material was not fully consumed and purification was then very difficult, even with multiple columns, the starting material and product couldn't be efficiently separated. Realising the need for reaction completion, we started using 5-fluoro-2-nitroaniline instead of 5-chloro-2-nitroaniline that had been used with the thiol. Fluorine is known to be much more reactive in nucleophilic aromatic substitution reactions, making it easier for the nucleophile to attack.⁸⁻¹¹ This resulted in complete conversion of the starting material to the product and greatly improved reaction yields and where possible fluoro derivatives were used in combination with phenol starting materials.

These compounds were characterised by mass spectrometry, as well as the upfield shift of the aromatic peaks belonging to the aryl ring possessing the NH_2 and nitro group. ^{19}F NMR was also analysed for these compounds. The starting material contains a fluorine, which gives a sharp peak at around -102 ppm in the ^{19}F NMR spectrum, consistent with the single fluorine atom in the 5-position of the starting material. The absence of this peak in the product NMR spectrum, showed the appearance of the product, indicating there had been full conversion to the product and that it was of high purity (See Appendix, Figure 2A).

4.2.1.2 Tin (II) Chloride Nitro Group Reduction

The tin (II) chloride mediated nitro reduction occurred in a similar manner to that described in the thiol section (Chapter 3, Section 3.2.1.2) occurring in 47 – 88% yield. This shows similar to lower yields than observed for the thiol derivatives. Purification for some of the ether analogues proved to be more difficult, this was mainly due to carrying over impurities from the first step when full conversion of the reaction was not observed. Reduction of the nitroaniline starting material (**2**) gave rise to an impurity which was difficult to separate from the desired product. This often resulted in the need for a second column purification and loss of material in order to gain purer product (**4**), which is important for the final step.^{1, 12, 13}

The products (**4**) of this reaction were identified by the upfield shift of a proton from around 8.10 ppm, when adjacent to a nitro group, to around 6.65 ppm when adjacent to an amine group after the reduction. The nitro group is electron withdrawing, which results in neighbouring protons appearing more downfield. The reduction to **4**, provides the ring with an additional electron donating group, which shifts the neighbouring proton more upfield (Figure 4.2) (See Appendix, Figure 2B).

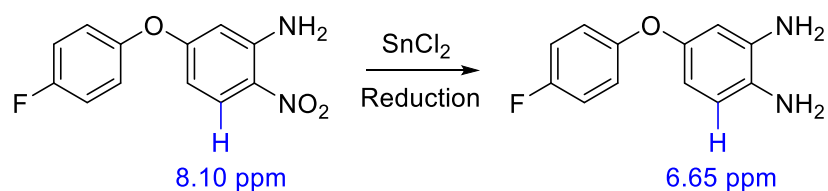


Figure 4.2. Due to the electron withdrawing nature of the nitro group, the neighbouring proton highlighted in blue is found downfield at 8.10 ppm. Reduction to the diamine results in an obvious NMR change to a more downfield position of 6.65 ppm.

4.2.1.3 Acid Mediated Ring Closure to Establish the Benzimidazole Core

The acid mediated ring closure to generate the five-membered ring (**6**) was similar to that observed in the thiol class (Chapter 3, Section 3.2.1.3) with yields of up to 78% generally observed. It is proposed that the ethers possess slightly higher solubility in the reaction medium than the thiol compounds. This moderate increase may have reduced the precipitation of the final compound, resulting in greater difficulty during filtration and purification. Compounds that had trace impurities from the previous step due to lack of full conversion sometimes remained in the product. These impurities were removed via washing with a solvent such as ethyl acetate or methanol, but did result in some loss of the less soluble desired product (**6**). Purity was confirmed by HPLC (See Appendix, Figure 2C - 2E).

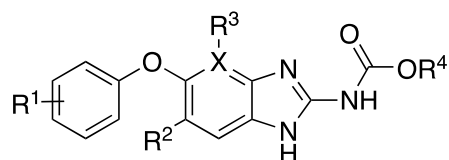
4.2.1.4 Compound Scale Up

Compound **6a** was sent for testing in mice due to its promising *in vitro* efficacy and DMPK properties (See Section 4.2.3 below), which required more material. A scale up procedure starting from 0.30 g of 5-fluoro-2-nitroaniline (**2**) was increased to 2.0 g of starting material. For the initial two steps the yields were similar, however the SnCl₂ reduction work-up is considerably more difficult when carried out on larger scale due to the amount of 25% NaOH that is required to be added and the difficulty with filtering the NaCl and Sn waste solids produced. This required much more extensive washing of the solid, to ensure as much diamine was obtained in the filtrate for purification. This was balanced out by larger scale reactions performing better in the final ring-closure step, which in the case of **6a** resulted in 1.30 g of final product being obtained in 78% yield, which is an improvement from 47% yield seen with the smaller scale. Whilst this is not an industrial size scale up, it has indicated potential issues and benefits of the scale up of compound **6a**.

4.2.2 Biological Activity

Biological testing carried out as stated in Chapter 3, Section 3.2.3 and data given in Table 4.2.

Table 4.2. The ether class of compound show generally good MIC testing data. Green – good - 0.015 – 0.25 mg/L, yellow – acceptable - 0.5 – 4 mg/L, red – poor - >4 mg/L. * 6h-s made by Dr Emma Shore, 6t made by Monika Lisauskaite, 6u made by Rachel Crick and 6v – 6ae made by Natasha Hatton.



Compound	R ¹	R ²	R ³	R ⁴	X	MIC (mg/L)
Flubendazole						0.125
Fenbendazole						0.03
6a	4-F	H	H	OMe	C	0.06
6b	4-F	H		OMe	N	>4
6c	4-F	Br	H	OMe	C	>4
6d	4-F	Br	H	OEt	C	>4
6e	4-F	H	F	OMe	C	>4
6f	4-F	H	F	OEt	C	>4
6g	4-F	F	F	OMe	C	>4
6h	3-F	H	H	OMe	C	0.125
6i	2-F	H	H	OMe	C	0.06
6j	4-Cl	H	H	OMe	C	0.125
6k	3-Cl	H	H	OMe	C	0.06
6l	4-CN	H	H	OMe	C	1
6m	4-OMe	H	H	OMe	C	0.125
6n	3-OMe	H	H	OMe	C	0.06
6o	4-Br	H	H	OMe	C	0.125
6p	2-F	F	H	OMe	C	0.25
6q	4-F	F	H	OMe	C	0.5
6r	3-Cl, 4-F	H	H	OMe	C	0.25
6s	3-Cl, 4-F	H	H	OBn	C	>4
6t	4-F	H	H	NMe	C	>4
6u	4-F	H	H	Propargyl	C	0.25
6v	H	H	H	OMe	C	0.5
6w	2-Cl	H	H	OMe	C	1
6x	2-CN	H	H	OMe	C	>4
6y	2-OMe	H	H	OMe	C	>4
6z	2-Br	H	H	Me	C	>4
6aa	2-OCF ₃	H	H	Me	C	>4
6ab	2-F, 4-F	H	H	OMe	C	0.5
6ac	2-F, 5-F	H	H	OMe	C	0.5
6ad	2-F, 6-F	H	H	OMe	C	>4
6ae	3-F, 5-F	H	H	OMe	C	0.125

The ether class, whilst possessing some of the best biological activity of all the templates, was not as good in comparison to the thioether analogues overall (Table 4.2). The 2-Br thiol derivative showed an activity value of 0.03 mg/L, whereas the ether derivative (**6z**) showed no activity. This was also true for a number of other compounds, which showed excellent activity in the thiol class, but reduced

activity in the ether class. However, it's important to note that whilst these compounds do have reduced activity, it is still improved versus the other classes and templates within the project.

However, there are some trends for activity that can be observed. For the mono-substituted fluorine derivatives **6a**, **6h** and **6i**, fluorine in the 2 and 4-position leads to an increase in activity, whereby both have an MIC value of 0.06 mg/L, versus the 3-position analogue (**6h**) which has a value of 0.25 mg/L. Fluorine is electron withdrawing from the *ortho* and *para* positions, which may result in less electron density on the ether, leading to improved activity. This appears to also be the case when comparing less electron withdrawing functionalities such as Cl and Br, whereby the activity for the *ortho* (**6w** and **6z**) and *para* (**6j** and **6o**) positions is reduced compared to the fluorine analogues. This potentially has a two-fold reason. Firstly, the size of the halogen atoms increases down the group, so steric factors may impede activity. Secondly, whilst halogens are electron withdrawing, Cl and Br are also mesomerically electron donating, whereas fluorine is inductively electron withdrawing. This would result in extra electron density on the ether from those analogues in the *ortho* and *para* positions, explaining the lower activity. The *meta*-Cl analogue (**6k**) shows better activity than the *meta*-F derivative (**6h**). This is because at this position they don't donate electrons onto the ether due to being *ortho/para* directing. For the (**6h**), there is no electron withdrawing ability at this position, so activity is lower.¹⁴ We also synthesised a derivative (**7**) whereby the aryl group has been moved to the 4-position, but like the thiol derivative it presented with a poor MIC of >4 mg/L (Figure 4.3).

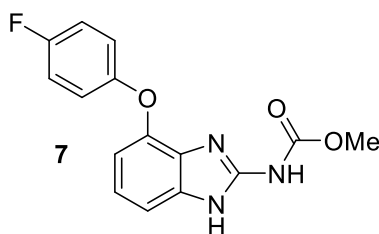


Figure 4.3. A 4-position derivative was synthesised but showed no activity.

4.2.3 DMPK

4.2.3.1 Predicted DMPK

The ethers show properties that are very comparable to the thioethers (Table 4.3). Log D is poor, meaning these compounds will be lipophilic.¹⁵ This is good as it is more likely to penetrate the blood brain barrier, but does mean they are less likely to be absorbed from the gut.¹⁶ Aqueous solubility shows no improvement via the predictive screen, with compound **6b** showing the highest value due to the presence of a pyridine ring in the core. Metabolic data is predicted to be excellent and generally lower than the thiol derivatives. One of the attractions of synthesising the ether template was the lack of metabolism at the oxygen linker, versus the potential oxidation of the sulphur. The predicted data indicates that the ethers are better in terms of metabolism. MPO scores are also mostly above 4, indicating these compounds will have good CNS penetration. **6c** and **6d** have lower MPO scores due to the addition of the bromine group driving CLogP, CLogD and molecular weight up.

Table 4.3. Predicted data shows the ether class has excellent metabolic properties but no further improvement in solubility. Values are colour coded with a traffic light system according to how good or bad a particular value is. **Green** – good, **amber** – acceptable/medium, **red** – poor.

	LogD _{7.4}	ClogP	Aqueous Solubility (μM)	Rat Heps CLint (μl/min/mg)	Human Mics CLint (μl/min/mg)	MPO
6a	3.54	3.95	2.7	10	18	4.6
6b	2.86	3.22	10.6	6	9	5.3
6c	4.06	4.66	1.0	10	16	3.7
6d	4.44	5.19	1.0	16	31	3.3
6e	3.51	3.97	2.7	12	15	4.7
6f	3.85	4.50	2.3	20	29	4.2
6u	2.67	4.37	15.96	56	29	4.3

Metabolism investigation was carried out using Stardrop (Figure 4.4).¹⁷ Two examples of the ether class are shown here and show that the major isoforms for metabolism are 3A4, 2C9 and 1A2, which shows agreement with the literature and the thiol class. Metabolism on the aryl ring to an epoxide and then alcohol is predicted to occur, but given the low measured metabolic clearance values, this does not appear to have a major influence. The carbamate group metabolism to produce the demethylated metabolite is also indicated, which is likely the major metabolic hit-point and is widely reported in the literature.^{18,19}

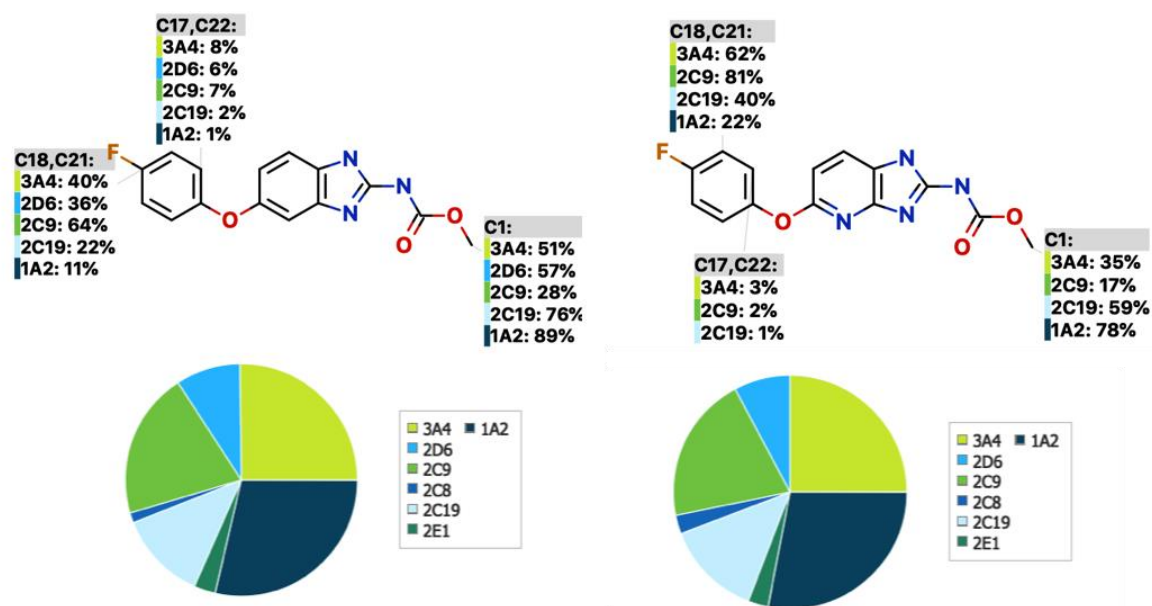


Figure 4.4. Metabolism predictions for two compounds from the ether series. Calculations run on Stardrop.¹⁷

4.2.3.2 Measured DMPK

Table 4.4. Measured data shows the ether class has excellent metabolic properties but no further improvement in solubility. Values are colour coded with a traffic light system according to how good or bad a particular value is. **Green** – good, **amber** – acceptable/medium, **red** – poor.

Compound	LogD _{7.4}	Aqueous Solubility (μM)	Rat Heps CLint (μl/min/mg)	Human Mics CLint (μl/min/mg)
6a	3.6	0.3	8	26
6b	2.6	18	2	15
6h	3.7	0.5	10	13
6i	3.4	1	22	23
6j	4.1	0.7	11	32
6q	3.7	1	8	71
6r	4.2	0.1	4	10
6u	4	0.3	25	35
6ab	3.5	0.3	5	72
6ae	4	14	4	12

Measured data shows agreement with the predicted data overall. Some of the numbers aren't identical, but the general magnitude of these numbers is comparable. Log D and aqueous solubility are very poor, however this appears to be inherent to the core of this template. Addition of solubilising groups has been attempted and will be discussed in Section 4.3. Metabolism values confirm what was predicted. **6a** shows excellent metabolic values, which are improved when compared to the thiol analogue. This validates the ether as a lead template due to less metabolic risk, despite having moderately reduced activity. It also indicates that the measured DMPK screen is highlighting potential metabolism of the sulphur, providing a better level of confidence in the screening of our compounds.

4.2.4 *In Vivo* Mouse Data

A larger scale batch of compound **6a** was produced, yielding around 2 g of final material in total. This was used to carry out *in vivo* mouse testing on **6a**, which had an excellent MIC value of 0.06 mg/L. Initially, this was tested *in vivo* via an oral dosing method using 10% DMSO in 90% castor oil and dosing once a day. From Figure 4.5, it is apparent that **6a** has no effect *in vivo* via the dosing method as there is no drop in fungal density in the brain when compared with the control. Furthermore, when this testing was carried out, it was noticed that the mice had issues with diarrhoea, which is a known issue when using large amounts of castor oil in vehicles.²⁰

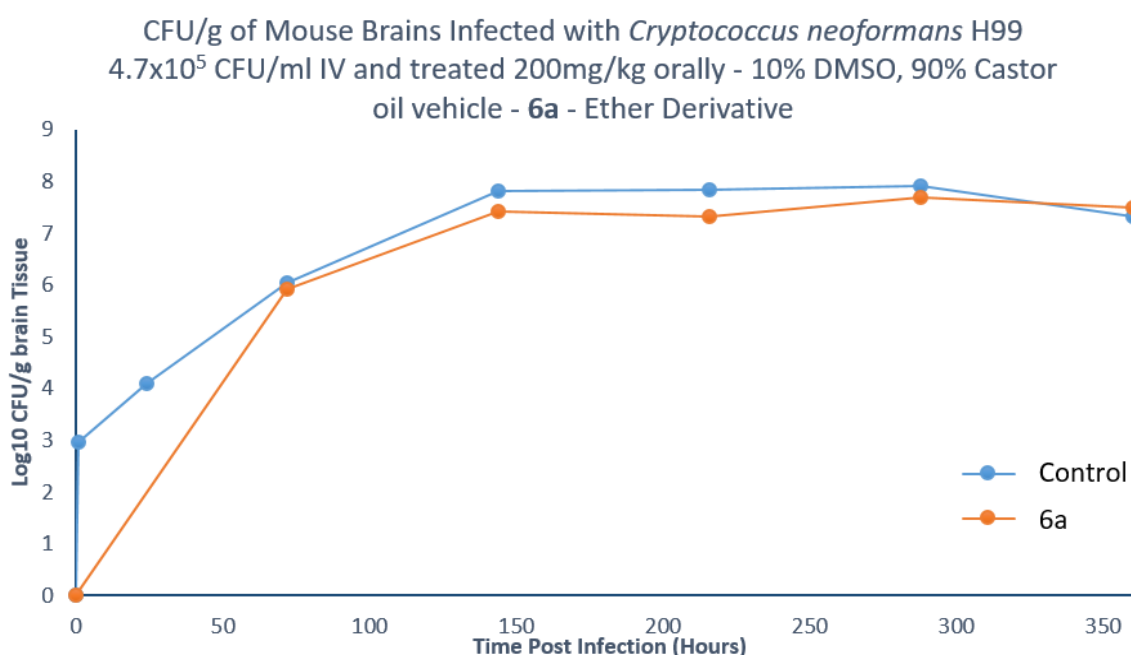


Figure 4.5. Compound **6a** was chosen for *in vivo* testing using a mouse model. The control shows an increase in fungal density in the brain when no drug is given. The ether derivative shows no fungal density drop when compared to the control and is considered inactive via this dosing method and vehicle.

6a also underwent subcutaneous testing using a different vehicle. One of the problems with using 90% castor oil in the previous vehicle was consistency. Castor oil is very viscous, and whilst it could be dosed orally, was too viscous to be dosed subcutaneously, so the vehicle was modified to include 10% ethanol, which made the solution less viscous and easier to dose. Figure 4.6 shows that even with subcutaneous dosing, **6a** shows no drop in fungal density. This is hypothesised to be due to poor solubility, and may be navigated in future trials by using a different vehicle.

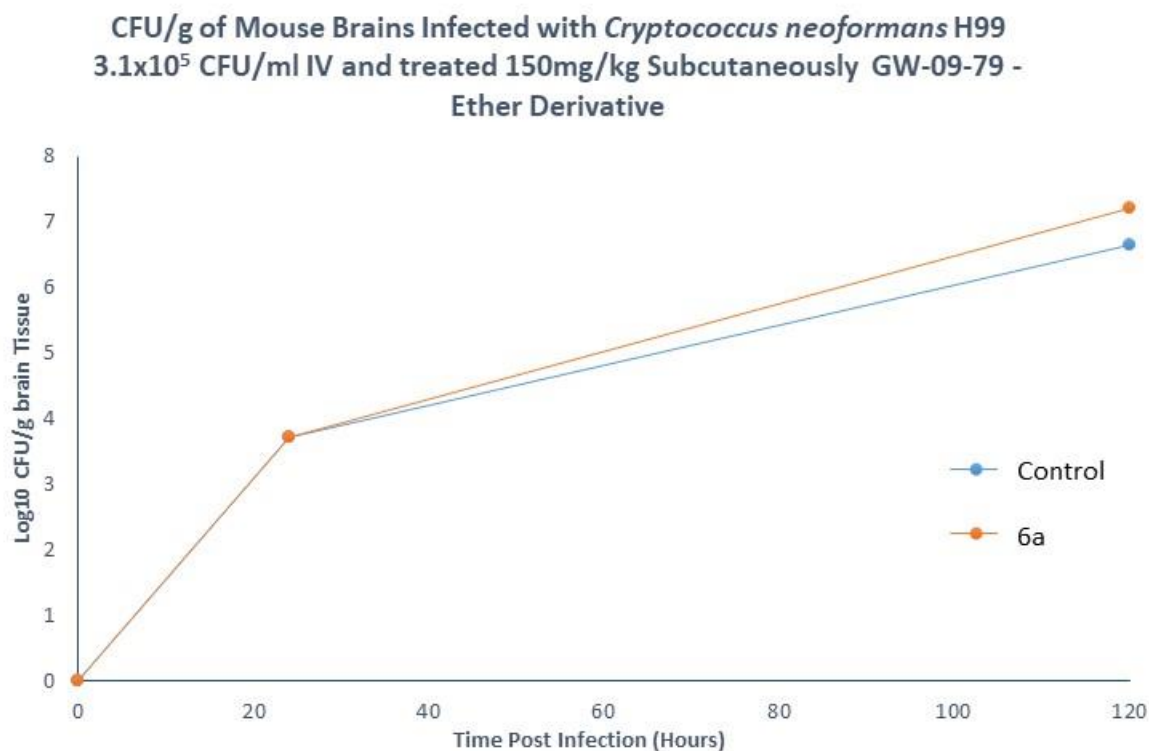


Figure 4.6. Compound **6a** was chosen for *in vivo* testing using a mouse model. The control shows an increase in fungal density in the brain when no drug is given. The ether derivative shows no fungal density drop when compared to the control and is considered inactive via this dosing method and vehicle.

4.3 Morpholine Ether Derivatives Discussion

It was apparent, from the measured and predicted DMPK data obtained, that solubility was an issue with this template. With this in mind, addition of solubilising groups such as morpholine was attempted.²¹ This has been observed in the literature in a paper by A. Zafar *et al*, incorporation of a morpholine can significantly improve solubility (Figure 4.2).²² Design of these compounds was limited due to the availability of starting materials. Ether analogues could be synthesised due to ready availability of starting materials, however this was not possible for the corresponding thiol derivatives.

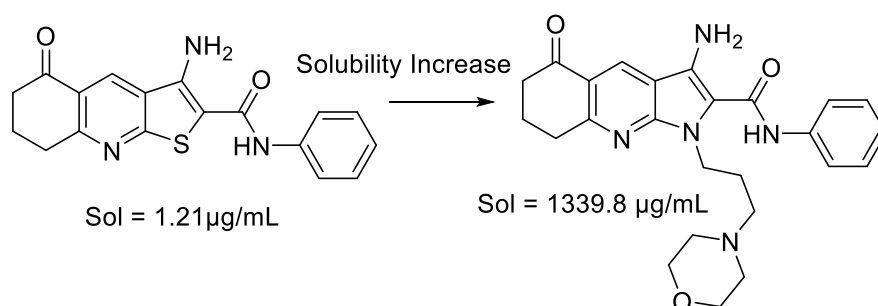
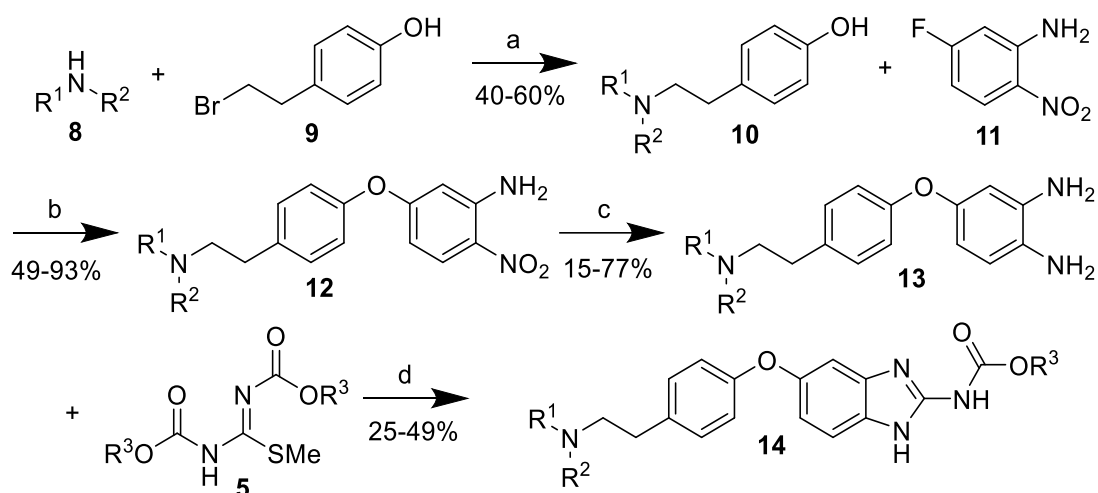


Figure 4.7. An example of the solubility increase observed from the addition of a morpholine group.²²

4.3.1 Synthesis



Scheme 4.2. Reagents and Conditions: (a) K_2CO_3 (2.0 eq.), DMF or MeCN, reflux, overnight (40 – 66% yield); (b) K_2CO_3 (2.0 eq.), DMF, reflux, overnight (49 – 93% yield); (c) $SnCl_2$ (5.0 eq.), ethanol, reflux, overnight (15 -77% yield); (d) 1,3-Bis(methoxycarbonyl)-2-methyl-2-thiopseudourea (**5**) (1.0 eq.), acetic acid (2 M), methanol (0.4 M), sealed tube, 65 °C, overnight (25 – 49% yield).

Table 4.5. Percentage yields obtained for all compounds created within the ether template, including intermediates and final products.

	R ¹	R ²	R ³	Step A % yield (10)	Step B % yield (11)	Step C % yield (13)	Step D% yield (14)
14a	Morpholine		Me	66	85	77	49
14b	Benzyl	Me	Me	56	54	46	37
14c	4-fluoropiperidine		Me	40	80	44	25
14d	Piperazine		Me	64	49	15	44
14e	Thiomorpholine		Me	63	75	50	43

4.3.1.1 Nucleophilic Substitution to generate morpholine phenol derivatives

The first step of the reaction sequence involved a nucleophilic substitution of **9** with the desired amine (**8**). The reaction occurred in moderate yields of 40 - 65%, with a number of other analogues not being synthesised due to very poor yields obtained from the first step. Most of the analogues synthesised involved a morpholine-like derivative, in order to improve solubility. This did require the addition of secondary amines, which are more sterically demanding in the reaction and were a contributing factor to the reduced yield.

The reaction required a phenol derivatives (**9**), DMF and amine (**8**) being stirred with potassium carbonate. In DMF it is believed that **9** is potentially undergoing a self-coupling reaction, producing dimers (Figure 4.8). These have been observed in small amounts within ¹H NMR spectra and can be seen on the TLC, whereby additional, more polar spots have been present and are observed with

higher mass numbers in the mass spectrum. This is because in DMF the pK_a of phenol is 15.40 (Table 4.6) and this is still moderately acidic and is deprotonated readily by the potassium carbonate, hence a competing nucleophilic substitution reaction with morpholine.

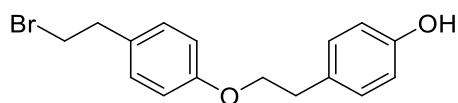


Figure 4.8. Reaction in DMF resulted in multiple by-products being formed. From NMR data it was hypothesised that self-coupling products were being produced.

Table 4.6. Changes in pK_a of both phenol and morpholine can help to improve the reaction yields through selective deprotonation.

	Phenol	Morpholine
Water	9.89 ²³	8.49 ²⁴
DMF	15.40 ²⁵	Not Found in Lit.
DMSO	16.47 ²⁶	9.15 ²⁴
MeCN	26.60 ²⁷	16.61 ²⁸

When the solvent was changed to acetonitrile, a high yield was observed and the product was easier to purify due to the lack of other side products being produced. In the 1H NMR spectrum there was no observation of self-coupling products. This can be rationalised if we considered the literature reported values for both phenol and morpholine in acetonitrile (Table 4.6). Morpholine shows a small increase to a pK_a of 16.61. However, phenol sees a sharp increase to 26.60, making it far less acidic and less likely to be deprotonated by potassium carbonate. This will reduce the phenol self-coupling reaction improving the yield.

Furthermore, literature suggested that carrying this reaction out in acetonitrile actually helped with purification as the product was only sparingly soluble in the reaction solvent. Thus concentration and filtration with diethyl ether yielded the product as a white solid, and removed the need for column purification, which resulted in a loss of yield due to polarity of the compound.²⁹ Whilst this did produce a white solid when tried on the morpholine analogue, 1H NMR confirmed the presence of unreacted morpholine, which couldn't be easily washed out with diethyl ether. An aqueous workup was attempted, however due to morpholine addition enhancing water solubility, some product transitioned to the aqueous layer and yield was reduced. We attempted to reduce the equivalents of the morpholine so that less would remain, which did improve purity but some remained. The morpholine did result in some further purification issues, which will be discussed in the next section. Furthermore, it was advantageous to use *N,N*-diisopropylethylamine as the base in these reaction, as potassium carbonate was soluble in acetonitrile and during the filtration step would be filtered off with the product. DIPEA had enhanced solubility in acetonitrile and was mostly washed out with the

diethyl ether during the filtration, however small traces did remain in the NMR, though it was unlikely to effect the next step.

These compounds (**10**) were characterised by ^1H and ^{13}C NMR, and additional morpholine aliphatic protons were observed, but the clearest evidence provided that these reactions had worked was the lack of bromine splitting pattern observed in the mass spectrometry data, along with the correct mass, which indicated the nucleophilic substitution has occurred to produce an isolatable product (**10**) (See Appendix, Figure 3A).

4.3.1.2 Nucleophilic Aromatic Substitution ($\text{S}_{\text{N}}\text{Ar}$)

This reaction occurred in the same manner as observed in previous templates, however due to the higher polarity of the compound (**11**), and the addition of water solubilising groups, purification proved to be more difficult due to the product partially partitioning into the water layer, or being lost on the column. The appearance of an additional three aromatic peaks corresponding to the protons on the nitroaniline ring, as well as the downfield shift of the phenol protons from 7.04 ppm and 6.72 ppm to 7.25 ppm and 7.02 ppm, due to the addition of an electron withdrawing ring being added, confirmed the product (See Appendix, Figure 3B). Furthermore, amine based impurities such as morpholine from the first step were also found to react and produce by-products in this step, which displayed similar polarity on the TLC plate to the desired product, meaning it was difficult to obtain pure compound. The morpholine was observed via NMR to be adding in to the nitroaniline and completing the $\text{S}_{\text{N}}\text{Ar}$ coupling to produce **15** (Figure 4.9). This was identified by having both nitroaniline peaks and morpholine peaks in the ^1H NMR spectrum, but no peaks belonging to the ethyl linkage.

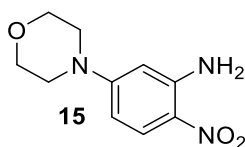


Figure 4.9. Residual morpholine from the initial nucleophilic substitution reaction can also react in the $\text{S}_{\text{N}}\text{Ar}$ reaction to produce a by-product (**15**) that is difficult to separate from the desired product.

4.3.1.3 Tin (II) Chloride Nitro Group Reduction

Tin (II) chloride reduction generally showed moderate yields for this reaction of 44 – 77%. Reduced yields were observed due to the diamine (**13**) being very water soluble, with a large amount of compounds needing to be removed from the water layer. Higher yields were observed when more extensive washing and ‘salting out’ was employed. The aqueous workup was essential in order to separate out Sn waste from the product, as small amounts did filter through into the filtrate. Iron reduction was also attempted with the addition of acid, and this encountered the same issues with

the need for water washes, and the work-up was actually more problematic with the iron, due to greater difficult filtering off the waste.

One reaction showed a very poor yield, where a piperazine analogue **13d** was produced. Up until this stage the piperazine analogue possessed a *t*-butyl carbonate protecting group on one of the amines and the acidic conditions of the tin (II) chloride reaction causes its deprotection. Deprotection of this amine resulted in a particularly polar amine, which was very water soluble and only a small amount could be extracted, resulting in a yield of 14%.

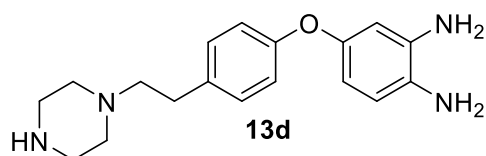


Figure 4.10. The piperazine derivative produced was particularly polar, and thus a lot of this compound was lost in the water layer during extraction, results in a low yield of 15%.

These samples required methanol-D₄ as an NMR solvent, given their very poor solubility in other organic solvents. Previously, identification of the diamine (**13**) could have been validated via the presence of a peak around 3.5 ppm, for the four N-H protons, as observed in other diamine analogues. Instead, an upfield shift was observed for the proton that was previously adjacent to the nitro group. This shift was due to removal of the electron withdrawing influence of the nitro group (Figure 4.11) (See Appendix, Figure 3C).

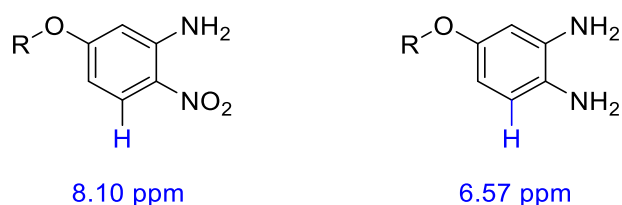


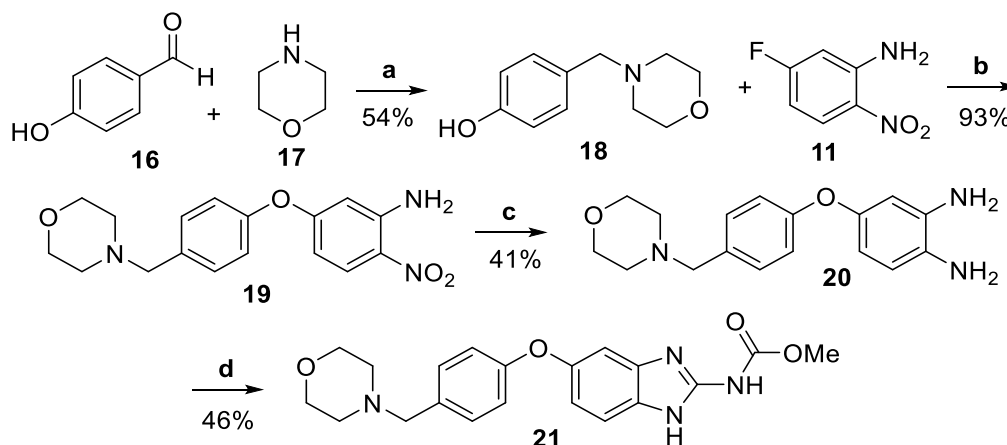
Figure 4.11. Upfield shift of the proton highlight in blue, was used to identify the product was obtained.

4.3.1.4 Acid Mediated Ring Closure to Establish the Benzimidazole Core

Yields for this final ring closure reaction were much more variable than for other sub-templates, with a range of 25 – 49%. Predicted DMPK data suggested these compounds had greater aqueous solubility and it is believed for this reason that the final compounds are slightly more soluble in the methanol used in the final ring closure. Subsequently, not all of the final compound precipitated, and therefore could not be obtained via filtration. Whilst these compounds do have improved solubility, they were not soluble enough to allow purification via column chromatography, using normal phase solvents and silica. A further issue with this reaction was due to reduced yields throughout the synthesis, only a small amount of final compound was obtained, and like all final carbamate compounds solubility is

poor and thus DMSO was used as the NMR solvent, which resulted in the product being submitted for NMR analysis that couldn't be recovered (See Appendix 3D - F).

4.3.2 Synthesis of methyl (5-(4-(morpholinomethyl)phenoxy)-1H-benzo[d]imidazol-2-yl)carbamate



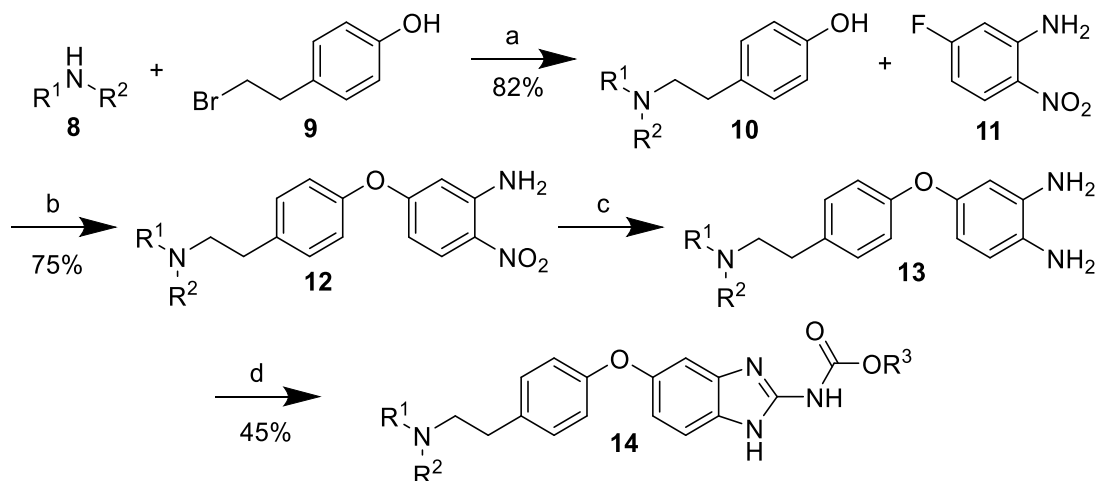
Scheme 4.3. Hit compound **14a** led to the design of a shorter linker chain and compound **21**. *Reagents and Conditions:* (a) methanol, reflux, 2 hours, NaBH₄ (5.0 eq.), methanol, 0 °C to room temperature, overnight (54% yield); (b) K₂CO₃ (2.0 eq.), *N,N*-dimethylformamide, reflux, overnight (93% yield); (c) SnCl₂ (5.0 eq.), ethanol, reflux, overnight (41% yield); (d) 1,3-Bis(methoxycarbonyl)-2-methyl-2-thiopseudourea (**5**) (1.0 eq.), acetic acid (2 M), methanol (0.4 M), sealed tube, 65 °C, overnight (46% yield).

Given the initial activity observed with the morpholine hit compound (**14a**), changing the carbon linker attached to the nitrogen of the morpholine was an obvious choice. Firstly, we looked at shortening the chain by one carbon and produced compound **21**.

The first step of this reaction involved reacting 4-hydroxybenzaldehyde and using reductive amination reaction conditions to remove the aldehyde and replace it with a morpholine. After acid-base work-up and purification the desired compound (**18**) was produced in a moderate 54% yield. A one-pot condition was tried at 0 °C and then heating to reflux to provide faster and easier reaction conditions, however this proved unsuccessful with both morpholine and thiomorpholine derivatives. This reaction was characterised via the disappearance of the aldehyde peak observed in the starting material (**16**) which appears around 9.8 ppm and the appearance of a CH₂ peak at 3.44 ppm indicating the aldehyde has been reduced. Finishing this route utilised the same reaction conditions as above; Step b) S_NAr of **18** with **11** to give the nitroaniline intermediate (**19**), Step c) SnCl₂ reduction to give the diamine (**20**), Step d) Ring closure to give the final product (**21**).

4.3.3 Compound Scale-Up

Compound **14a**, based on its original MIC value of 0.25 mg/L and improved solubility, was chosen as a candidate for *in vivo* testing. This resulted in large amounts of this compound needing to be synthesised. For the morpholine derivative this was more difficult than other analogues as the higher polarity and more aqueous solubility of these compounds meant that work-up and purification conditions were less successful. This was more than what was synthetically feasible in our laboratory set-up and was therefore outsourced to WUXI and followed the route detailed in Scheme 4.4.



Scheme 4.4. Updated WUXI conditions. *Reagents and Conditions:* (a) DIPEA (2.0 eq.), MeCN, reflux, overnight (82% yield); (b) K_2CO_3 (2.0 eq.), DMF, reflux, overnight (75% yield); (c) H_2 , Pd/C (10%), DMF/ethanol, reflux, overnight; (d) 1,3-Bis(methoxycarbonyl)-2-methyl-2-thiopyridone (1.0 eq.), acetic acid (2 M), methanol (0.4 M), sealed tube, 65 °C, overnight (45% yield).

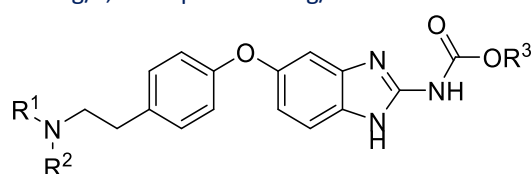
The route used by WUXI largely followed what was detailed earlier in Scheme 2.2. The main differences were; the initial coupling step was carried out using acetonitrile, as indicated in the discussion and led to improved yields. The nitro reduction step was carried out using 10% Pd/C, which is a superior reaction condition given the removal of tin from the route. At the end of this scale up process 27.1 g of final product was made in 98.5% purity.

4.3.4 Biological Activity

Initially, minimum inhibitory concentration testing identified the morpholine analogue as having a good activity value of 0.25 mg/L, and the predicted improvement in solubility made it an attractive template, thus we sought to make other analogues which can be seen in Table 4.7. All other analogues showed minimal or no activity, with a value of >4 mg/L being observed. The morpholine analogue by this point had been selected for *in vivo* mice testing, which will be described in the subsequent section and was found to have activity. This led us to re-test the morpholine and it was found to have a lower MIC than initially tested.

Particularly for the morpholine analogues, there appeared to be discrepancies with MIC data that weren't observed for other templates. This occurred regardless of whether compound came from identical batches or when fresh compounds were made. Furthermore, because we realised that the compounds weren't obtaining the higher MIC values we expected, they were re-tested again at higher concentration allowing the range to run up to 32 mg/L rather than the previous 4 mg/L. This data showed no change in MIC across the compound class despite the morpholine having good activity *in vivo*.

Table 4.7. Biological activity observed for the morpholine compound class. Higher concentration MIC's were also observed for this class to detect any possible structure activity relationships. **Green** – good - 0.015 – 0.25 mg/L, **yellow** – acceptable - 0.5 – 4 mg/L, **red** – poor - >4 mg/L.



Compound	R ¹	R ²	R ³	n	Standard MIC (mg/L)	Higher Concentration MIC (mg/L)
14a	Morpholine		Me	2	0.25(4)	ND
14b	Benzyl	Me	Me	2	>4	>32
14c	4-fluoropiperidine		Me	2	>4	32
14d	Piperazine		Me	2	4	>32
14e	Thiomorpholine		Me	2	1-2	>32
21	Morpholine			1	4	>32

The biology testing for these compounds actually highlighted something important about compound storage. To ensure no decomposition of these compounds occurred when they were made up in solution for biological testing, they were plated up at varying concentrations and frozen, so that repeats could be done at a later time. Due to the insolubility of these compounds, they were often heated slightly to ensure full dissolution. Freezing actually caused the compounds to precipitate and were therefore not fully dissolved in the testing medium. This means when the MIC test was carried out, the concentration in DMSO was not correct and thus incorrect MIC values obtained. This resulted in smaller amounts of compounds being used and fresh batches being made up for biological testing each time. We are currently awaiting retesting of MIC data, but the most consistent values have been given in Table 4.7.

4.3.5 DMPK

4.3.5.1 Predicted DMPK

Predicted DMPK showed that these compounds generally would possess good log D values, except compound **14b** that contained an *N*-Benzylmethylamine group, which is known to drive log D up. Aqueous solubility showed no improvement, apart from compound **14d**, a piperazine derivative which showed an excellent predicted solubility value.

Table 4.8. Predicted DMPK data for the morpholine ether class of compounds show good metabolic properties overall, but poor clearance. Values are colour coded with a traffic light system according to how good or bad a particular value is. **Green** – good, **amber** – acceptable/medium, **red** – poor.

	LogD _{7.4}	CLogP	Aqueous Solubility (μM)	Rat Heps CLint (μl/min/mg)	Human Mics CLint (μl/min/mg)	MPO
14a	3.04	3.93	3.8	10	20	4.5
14b	4.25	5.74	2.2	33	54	3.0
14c	3.38	4.84	7.8	14	49	3.9
14d	1.54	3.52	106.4	2	8	4.7
14e	3.67	4.66	4.3	23	45	4.0
21	2.91	3.55	6.6	13	18	5.0

4.3.5.2 Measured DMPK

Measured DMPK obtained for the morpholine class showed two things. Firstly, that the addition of morpholine-like groups to the benzimidazole did not increase solubility as significantly as expected. However, values were better than the predictions and better when compared with other classes. Secondly, the thiomorpholine **14e**, which was predicted to have reasonable metabolic clearance values, behaved very poorly when measured, mostly due to extensive oxidation of the sulphur.³⁰

Table 4.9. Measured DMPK data for the thiol class of compounds show good metabolic properties overall, but poor clearance. Values are colour coded with a traffic light system according to how good or bad a particular value is. **Green** – good, **amber** – acceptable/medium, **red** – poor.

Compound	LogD _{7.4}	Aqueous Solubility (μM)	Rat Heps CLint (μl/min/mg)	Human Mics CLint (μl/min/mg)
14a	2.9	10	30	48
14c	3	12	<3	10
14e	3.7	0.6	>300	127
21	2.6	27	16	7

Stardrop calculations show that the morpholine derivatives are extensively metabolised by the CYP3A4 enzyme particularly on the morpholine ring and in the case of compound **14e**, and on the sulphur atom via oxidation (Figure 4.13). As with other templates the carbamate is also indicated for

metabolism.³¹ CYP2D6 is also indicated as being a major isoform for metabolism, which is different to the other templates and helps to facilitate metabolism of the carbamate of the morpholine compound **14a** and the sulphur of **14e**.

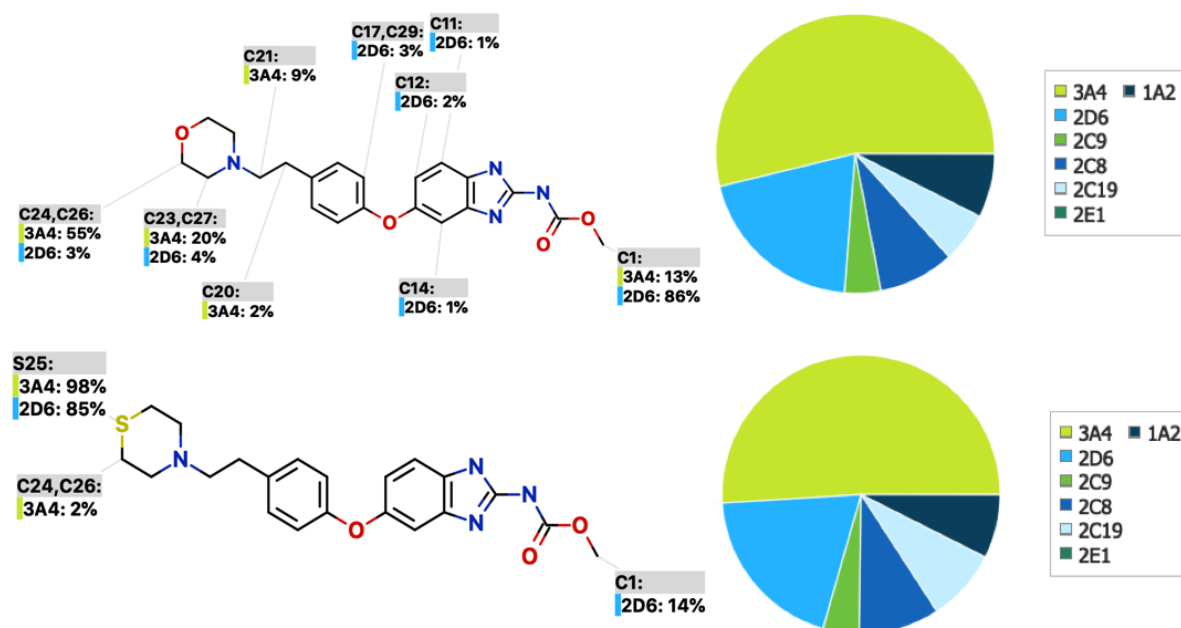


Figure 4.13. Metabolism predictions for two compounds from the morpholine series. Calculations run on Stardrop.¹⁷

Measured and predicted DMPK properties were plotted against each other for both the ether and morpholine ether derivatives combined and show very little correlation for all of the properties investigated (Figure 4.14). This means whilst the predicted DMPK may help indicate the general direction of change for a property, it is not reliable enough to make a decision as to whether a compound will be stable or more soluble for this particular group of compounds.

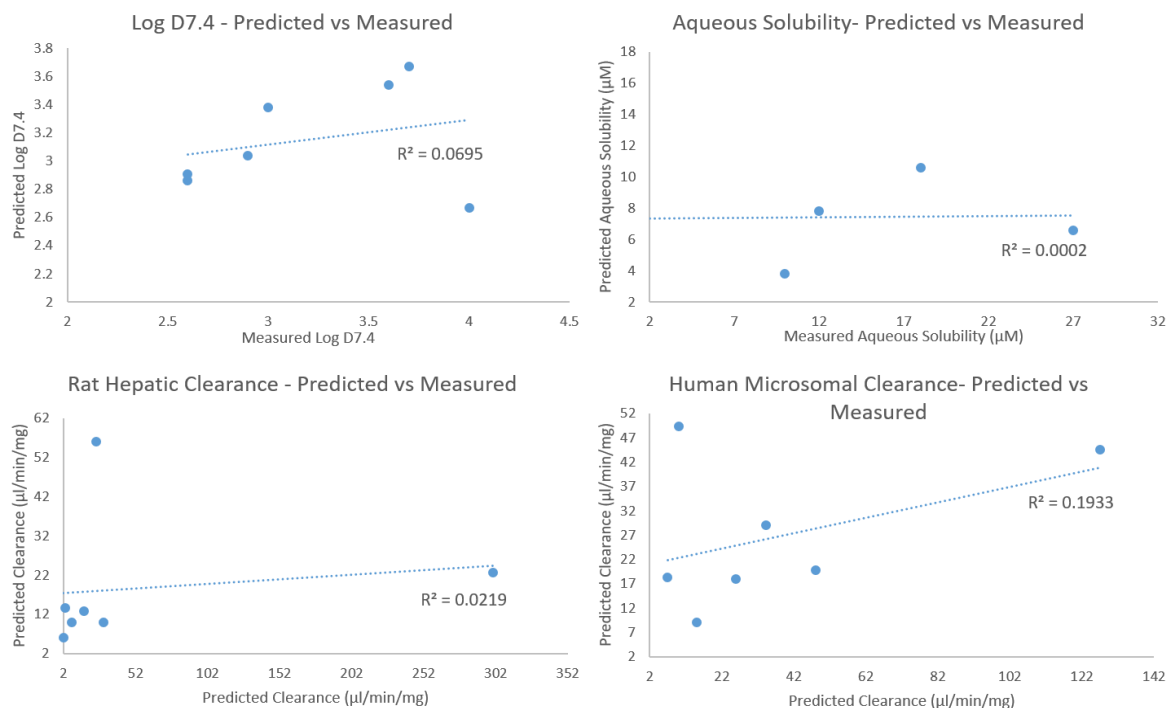


Figure 4.14. Each of the parameters obtained from measured DMPK testing was plotted against the numbers obtained from predicted DMPK analysis.

4.3.6 *In Vivo* Mouse Data

When compound **14a** was tested initially it possessed a moderate MIC value of 0.25 mg/L. Measured DMPK showed it was slightly more soluble, and this was further validated by its ease of dissolution in a number of vehicles. **14a** was tested subcutaneously and showed a very small decrease in fungal density, which was better than other templates but not as significant as flubendazole (Figure 4.15). Oral administration using **14a** was also investigated and showed the dependency of efficacy on the dosage vehicle used. When an oil based vehicle of 10% DMSO, 10% ethanol and 80% castor oil was used, there was no increase in fungal density observed. When an aqueous based vehicle was used, made up of 10% DMSO, 10% Tween and 80% PBS, there was a much more significant decrease in fungal density (Figure 4.15). This was thought to be due to improved intestinal absorption due to being in an aqueous vehicle and the mice not suffering from diarrhoea, so less compound was lost.

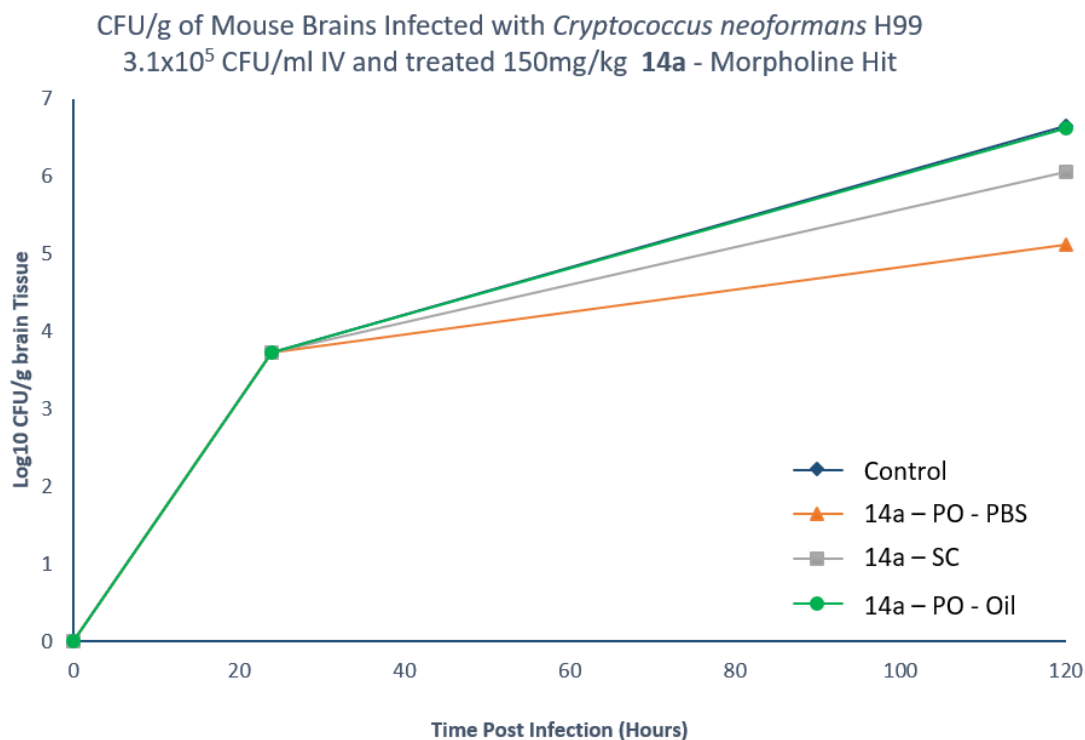


Figure 4.15. Compound **14a**, was selected as the new hit compound for *in vivo* testing and was tested in a range of vehicles and administration routes to obtain efficacy data. Given orally and using a 10% DMSO, 10% Tween and 80% PBS solutions showed the most significant drop in fungal density.

Given that compound **14a** was exhibiting a decrease in fungal density, it was outsourced to WUXI to be made on a larger scale to allowing for more *in vivo* testing to be carried out. The compound was tested both subcutaneously and orally using 10% DMSO, 10% Tween 80 and 80% PBS. Figure 4.16 shows that the WUXI compound showed a similar slight decrease in fungal density but when dosed orally, the WUXI compound showed a much more significant drop in fungal density. From the data, it appears that oral dosing of **14a** results in better efficacy. This is hypothesised to be due to the drug encountering the acidic environment of the stomach, meaning that the morpholine becomes protonated, generating a salt which enhances solubility, resulting in a bigger reduction in fungal density.

CFU/g of Mouse Brains Infected with *Cryptococcus neoformans* H99
4.2x10⁵ CFU/ml IV and treated with 150 mg/kg Morpholine - WUXI
Derivative

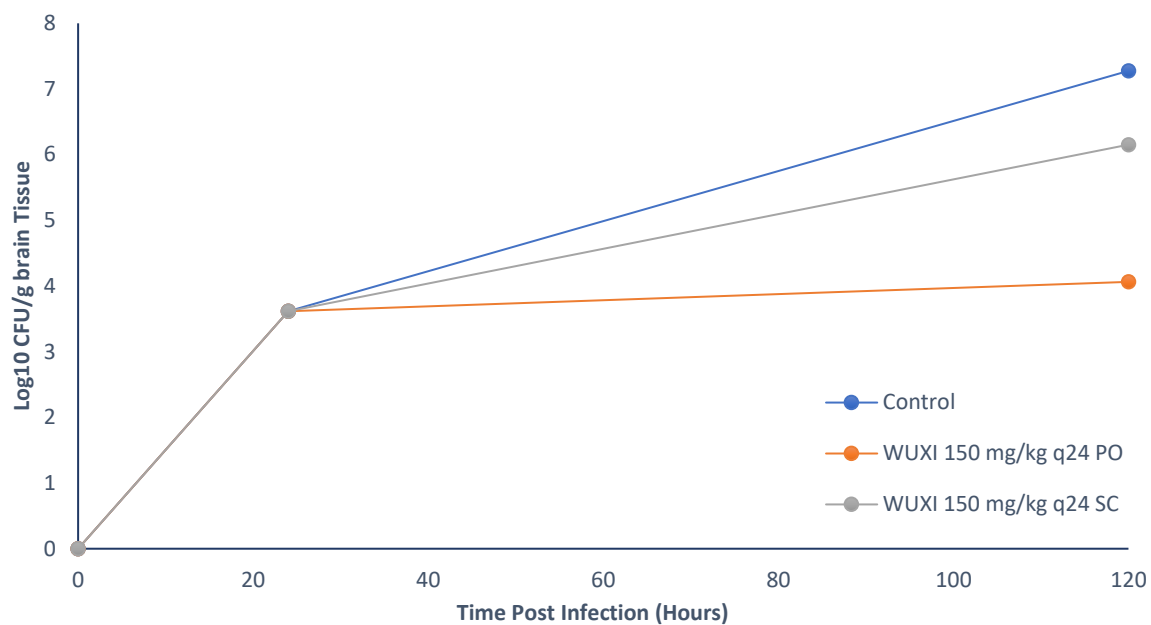


Figure 4.16. Compound **14a** was made on large scale by WUXI and was tested *in vivo*. It showed improved activity versus the in-house sample of **14a** produced and was more soluble

4.4 Conclusion

Synthetic routes for both the ether and morpholine class have been achieved, with significant work carried out to improve the original low yielding route for the morpholine, with the new route being implemented into scale-up reactions. Biological data for the ether class shows generally good activity with an MIC range of 0.06 - >4 mg/L, with a number of compounds showing activity of 0.06 mg/L. From this information, a basic SAR profile has been established as shown in Figure 4.17. However, these compounds showed no activity *in vivo*, even with a change in dosing vehicle. For the morpholine derivatives, MIC data is not consistent, but these compounds do show good activity *in vivo*, exhibiting over a three-log drop in fungal density in the brain tissue.

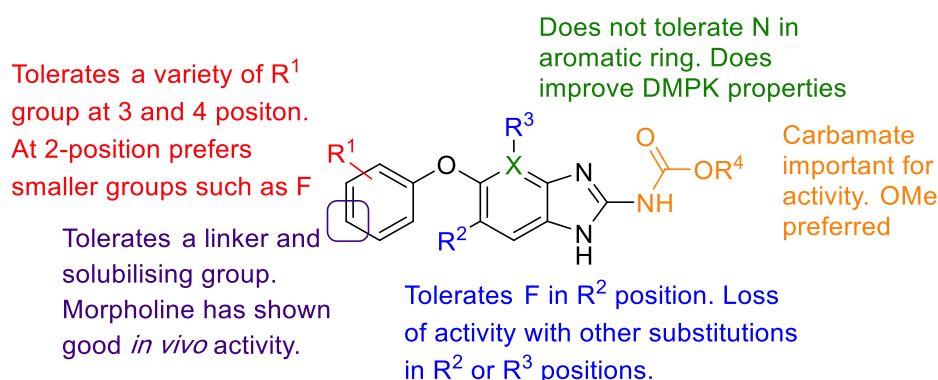


Figure 4.17. An overall SAR conclusion.

4.5 Future Work

Given that we believe solubility could play a role in both *in vitro* and *in vivo* activity, more soluble versions of these compounds will be synthesised by making salt of the active compounds, such as the HCl salt. This should improve the aqueous solubility, rendering it easier to administer and hopefully more likely to be absorbed. We are also working on the synthesis of additional analogues with shorter and longer chains lengths, to understand what is tolerated when adding the morpholine for additional solubility (Figure 4.18).

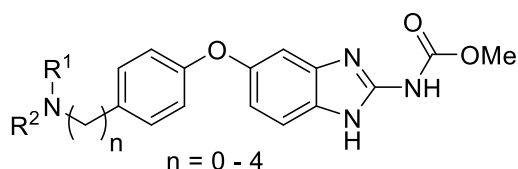


Figure 4.18. Additional morpholine analogues are being synthesised to probe SAR.

We are also investigating alternative morpholine derivatives. This includes alkylation of the ring, looking at both *R* and *S* enantiomers to see if this confers any activity advantage. We are also investigating the spiro morpholine given its structural similarity to morpholine but more compact shape (Figure 4.19).

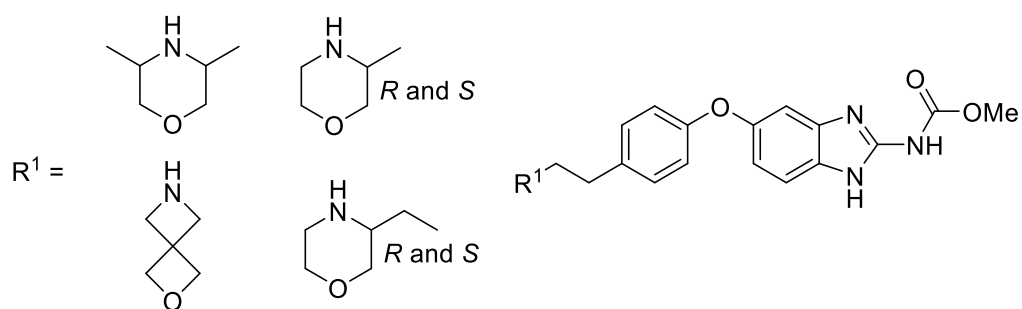


Figure 4.19. Alternative morpholine derivatives to be synthesised.

Work is also ongoing to carry out PK/PD studies to understand the outcomes of administration of these compounds. This will allow for the identification of any routes of metabolism and whether the drug is orally bioavailable. This is important for both the active morpholine **14a**, but also for the compounds that are inactive as this will allow understanding of why good MIC activity does not translate into good *in vivo* activity.

4.6 Experimental

4.6.1 General Experimental Details

For general experimental details please see Section 3.5.1, Chapter 3. For synthesis of dimethyl ((methylthio)methylene)dicarbamate please see Section 3.5.2, Chapter 3.

4.6.1.1 HPLC

Flow rate 1 ml/min for 15 minutes using MeCN/Water with compounds dissolved in methanol. UV detector recorded signals at 254 nm. **HPLC Method A:** min, gradient: 2% MeCN hold to 1 min, 2-98% MeCN in 11 min, then hold at 98% MeCN to 15 min. **HPLC Method B:** min, gradient: 2% MeCN (0.05% Formic acid) hold to 1 min, 2-98% MeCN (0.05% Formic acid) in 11 min, then hold at 98% MeCN (0.05% Formic acid) to 15 min.

4.6.2 General Procedures

General Procedure A – S_NAr Coupling

To a flask at room temperature was added a 2-nitroaniline derivative (1.0 eq.), DMF (0.35 M), K₂CO₃ (2.0 eq.) and the substituted phenol (1.5 eq.) and the reaction heated to reflux overnight. The reaction was cooled to room temperature then diluted with ethyl acetate, washed with water, brine, dried over magnesium sulphate and concentrated to give a crude orange or yellow oil, which was purified by column chromatography eluting with 10% ethyl acetate in *n*-hexane increasing to 20% to obtain the product, or triturating with *n*-Hexane to yield the pure product.

General Procedure B – Single Nitro reduction

To a flask at room temperature was added 2-nitro-5-phenoxyaniline derivative (1.0 eq.), EtOH (0.15 M) and SnCl₂ (5.0 eq.) and the reaction heated to reflux overnight. The reaction was then cooled to room temperature. The reaction volume was then reduced, adjusted to pH 10 with 25% NaOH and filtered, washing with water and ethyl acetate. The water layer was then washed twice more with ethyl acetate, the combined organic layers washed with brine, dried over magnesium sulphate and concentrated. The product was purified by column chromatography eluting with 50% Ethyl acetate in *n*-hexane, increasing to 100% Ethyl acetate, to elute the product.

General Procedure C – Acid Mediated Ring Closure

To a flask at room temperature was added 4-phenoxybenzene-1,2-diamine derivative (1.0 eq.), acetic acid (2.0 M), MeOH (0.4 M), dimethyl ((methylthio)methylene)dicarbamate (1.0 eq.) and the reaction

heated to 65 °C overnight. The reaction was allowed to cool to room temperature and the resulting solid filtered using diethyl ether to give the final product.

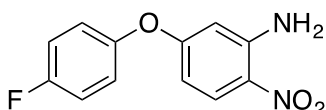
General Procedure D – Nucleophilic Substitution

To a flask at room temperature was added 4-(2-bromoethyl)phenol (1.0 eq.), *N,N*-dimethylformamide (0.64 M), potassium carbonate (2.0 eq.) and the desired amine (1.0 eq.) and the reaction heated to 90 °C overnight. The reaction was then cooled to room temperature and diluted with ethyl acetate, washed with saturated aq. NaHCO₃ solution, water, brine, dried over magnesium sulphate and concentrated. The product was purified by column chromatography, eluting in 50% ethyl acetate/*n*-hexane.

4.6.3 Ether Derivatives

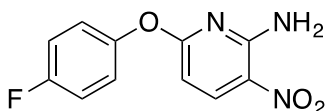
4.6.3.1 Synthesis of 2-nitro-5-phenoxyaniline Derivatives

5-(4-Fluorophenoxy)-2-nitroaniline (3a)

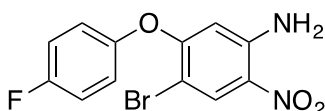


General Procedure A - Employed 5-fluoro-2-nitroaniline and 4-fluorophenol to give the product (**3a**) (1.52 g, 95% yield) as a pale yellow solid. ¹H NMR (400 MHz, CDCl₃) δ 8.10 (d, 1H, *J* = 9.6 Hz), 7.10 – 7.07 (m, 4H), 6.31 (dd, 1H, *J* = 9.6 and 2.5 Hz), 6.13 (d, 1H, *J* = 2.5 Hz), 6.12 (s, 2H). ¹³C NMR (100 MHz, CDCl₃) δ 164.2, 160.0 (*J* = 254.0 Hz), 150.2, 146.7, 128.9, 127.9, 122.4 (d, *J* = 8.4 Hz), 116.8 (d, *J* = 24.0 Hz), 107.4, 103.3. HRMS: (Cl⁺, CH₄) *m/z* Calculated for C₁₂H₁₀FN₂O₂: 249.0670. Found [M+H]⁺: 259.0678 (Diff – 3.3 ppm).

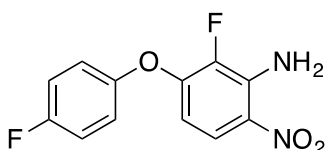
6-(4-Fluorophenoxy)-3-nitropyridin-2-amine (3b)



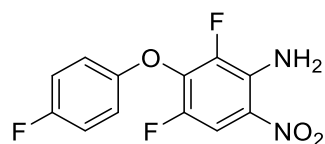
General Procedure A - Employed 6-chloro-3-nitropyridin-2-amine and 4-fluorophenol to give the product (**3b**) (0.32g, 44% yield) as a yellow solid. ¹H NMR (400 MHz, CDCl₃) δ 8.41 (d, 1H, *J* = 8.9 Hz), 7.90 (s, 1H), 7.12 - 7.08 (m, 4H), 6.28 (d, 1H, *J* = 8.9 Hz), 5.61 (s, 1H). ¹³C NMR (100 MHz, CDCl₃) δ 166.1, 160.1 (d, *J* = 248.4), 153.6, 148.4, 138.9, 128.9, 123.2 (d, *J* = 8.7 Hz), 116.3 (d, *J* = 25.2 Hz), 101.5. HRMS: (Cl⁺, CH₄) *m/z* Calculated for C₁₁H₉FN₃O₃: 250.0622. Found [M+H]⁺: 250.0627 (Diff – 1.64 ppm).

4-Bromo-5-(4-fluorophenoxy)-2-nitroaniline (3c/3d)

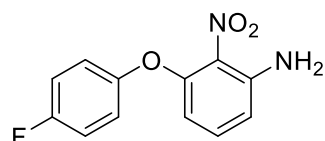
General Procedure A - Employed 4-bromo-5-fluoro-2-nitroaniline and 4-fluorophenol to give the product (**3c/3d**) (0.24 g, 73% yield) as an orange solid. ^1H NMR (400 MHz, CDCl_3) δ 8.43 (s, 1H), 7.14 - 7.09 (m, 4H), 6.06 (s, 2H), 5.96 (s, 1H). HRMS: (Cl^+ , CH_4) m/z Calculated for $\text{C}_{12}\text{H}_9\text{BrFN}_2\text{O}_3$: 326.9775. Found $[\text{M}+\text{H}]^+$: 326.9784 (Diff - 2.67 ppm).

2-Fluoro-3-(4-fluorophenoxy)-6-nitroaniline (3e/3f)

General Procedure A - Employed 2,3-difluoro-6-nitroaniline and 4-fluorophenol to give the product (**3e/3f**) (0.3 g, 79% yield) as an orange solid. ^1H NMR (400 MHz, CDCl_3) δ 7.89 (dd, 1H, $J = 9.7$ & 2.1 Hz), 7.12 - 7.03 (m, 4H), 6.27 - 6.15 (m, 3H). ^{13}C NMR (100 MHz, CDCl_3) δ 159.7 (d, $J = 245.0$ Hz), 150.9, 149.6 (d, $J = 8.9$ Hz), 141.4 (d, $J = 214.2$ Hz), 136.6 (d, $J = 12.5$ Hz), 128.5, 122.1 (d, $J = 4.0$ Hz), 121.1 (d, $J = 8.8$ Hz), 116.8 (d, $J = 23.8$ Hz), 105.3. HRMS: (Cl^+ , CH_4) m/z Calculated for $\text{C}_{12}\text{H}_9\text{F}_2\text{N}_2\text{O}_3$: 267.0576. Found $[\text{M}+\text{H}]^+$: 267.0581 (Diff -1.98 ppm).

2,4-Difluoro-3-(4-fluorophenoxy)-6-nitroaniline (3g)

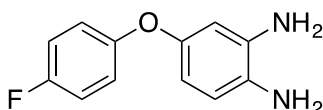
General Procedure A - Employed 2,3,4-trifluoro-6-nitroaniline and 4-fluorophenol to give the product (**3g**) (0.23 g, 57% yield) as an orange solid. ^1H NMR (400 MHz, CDCl_3) δ 7.84 (dd, 1H, $J = 10.9$ & 2.2 Hz), 7.05 - 7.01 (m, 2H), 6.9 - 6.95 (m, 2H), 6.08 (s, 2H). HRMS: (Cl^+ , CH_4) m/z Calculated for $\text{C}_{12}\text{H}_8\text{F}_2\text{N}_3\text{O}_3$: 285.0482. Found $[\text{M}+\text{H}]^+$: 285.0493 (Diff -3.92 ppm)

3-(4-Fluorophenoxy)-2-nitroaniline (7a)

General Procedure A - Employed 4-fluorophenol and 3-fluoro-2-nitroaniline to give the crude product (**7a**) as a brown oil. This was mixed with the starting nitroaniline in a ratio of 1: 0.47 in favour of the desired product, indicated via the presence of the following peaks. $^1\text{H NMR}$ (400 MHz, CDCl_3) δ 7.12 (dd, 1H, $J = 8.5$ & 8.2 Hz), 7.05 – 7.02 (m, 4H), 6.51 (d, 1H, $J = 8.5$ Hz), 6.17 (d, 1H, $J = 8.2$ Hz), 5.13 (s, 2H).

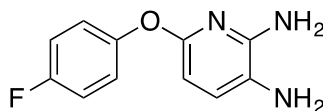
4.6.3.2 Synthesis of 4-phenoxybenzene-1,2-diamine Derivatives

4-(4-Fluorophenoxy)benzene-1,2-diamine (**4a**)



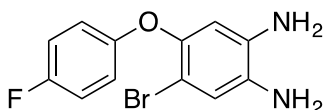
General Procedure B - Employed 5-(4-fluorophenoxy)-2-nitroaniline (**3a**) to give the product (**4a**) (0.8 g, 76% yield) as a brown solid. $^1\text{H NMR}$ (400 MHz, CDCl_3) δ 6.95 - 6.92 (m, 4H), 6.65 (d, 1H, $J = 8.7$ Hz), 6.39 (d, 1H, $J = 2.7$ Hz), 6.34 (dd, 1H, $J = 8.7$ & 2.7 Hz), 3.30 (s, 4H). $^{13}\text{C NMR}$ (100 MHz, CDCl_3) δ 158.3 (d, $J = 239.9$ Hz), 154.4 (d, $J = 2.4$ Hz), 151.0, 136.7, 130.0, 119.1 (d, $J = 8.6$ Hz), 117.9, 116.0 (d, $J = 23.3$ Hz), 110.3, 107.7. HRMS: (Cl^+ , NH_3) m/z Calculated for $\text{C}_{12}\text{H}_{12}\text{FN}_2\text{O}$: 219.0928. Found $[\text{M}+\text{H}]^+$: 219.0931 (Diff – 1.13 ppm).

6-(4-Fluorophenoxy)pyridine-2,3-diamine (**4b**)



General Procedure B - Employed 6-(4-fluorophenoxy)-3-nitropyridin-2-amine (**3b**) to give the product (**4b**) (0.15 g, 54% yield) as a brown oil. $^1\text{H NMR}$ (400 MHz, CDCl_3) δ 7.03 - 7.00 (m, 4H), 6.93 (d, 1H, $J = 8.2$ Hz), 6.09 (d, 1H, $J = 8.2$ Hz), 4.30 (s, 2H), 3.08 (s, 2H). $^{13}\text{C NMR}$ (100 MHz, CDCl_3) δ 158.9 (d, $J = 244.5$ Hz), 156.2, 151.7, 148.6, 127.5, 123.6, 121 (d, $J = 8.8$ Hz), 116.0 (d, $J = 24.7$ Hz), 100.6. HRMS: (Cl^+ , CH_4) m/z Calculated for $\text{C}_{11}\text{H}_{11}\text{FN}_3$: 220.0881. Found $[\text{M}+\text{H}]^+$: 220.0887 (Diff 2.73).

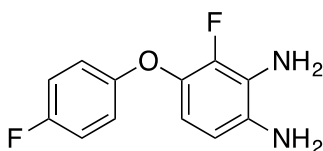
4-Bromo-5-(4-fluorophenoxy)benzene-1,2-diamine (**4c/4d**)



General Procedure B - Employed 4-bromo-5-(4-fluorophenoxy)-2-nitroaniline (**3c/3d**) to give the product (**4c/4d**) (0.15 g, 68% yield) as a brown solid. $^1\text{H NMR}$ (400 MHz, CDCl_3) δ 7.00 – 6.94 (m, 2H), 6.92 (s, 1H), 6.87 – 6.83 (m, 2H), 6.40 (s, 1H), 3.39 (s, 4H). $^{13}\text{C NMR}$ (100 MHz, CDCl_3) δ 158.2 (d, $J =$

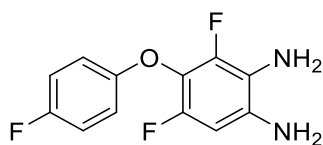
241.6 Hz), 154.0, 146.4, 135.9, 132.2, 120.7, 118.0 (d, $J = 8.6$ Hz), 116.0 (d, $J = 23.6$ Hz), 109.6, 103.9. HRMS: (Cl⁺, CH₄) m/z Calculated for C₁₂H₁₂BrFN₂O: 297.0033. Found [M+H]⁺: 297.0039 (Diff – 1.76 ppm).

3-Fluoro-4-(4-fluorophenoxy)benzene-1,2-diamine (4e/4f)



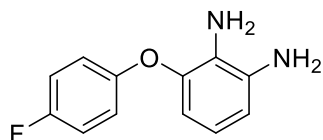
General Procedure B - Employed 2-fluoro-3-(4-fluorophenoxy)-6-nitroaniline (**3e/3f**) to give the product (**4e/4f**) (0.23 g, 88% yield) as a brown oil. ¹H NMR (400 MHz, CDCl₃) δ 6.99 – 6.93 (m, 2H), 6.91 – 6.87 (m, 2H), 6.45 (dd, 1H, $J = 8.5$ & 1.1 Hz), 6.41 (dd, 1H, $J = 8.5$ & 7.7 Hz), 3.46 (s, 4H). ¹³C NMR (100 MHz, CDCl₃) δ 158.1 (d, $J = 238.1$ Hz), 154.5, 144.9 (d, $J = 238.1$ Hz), 136.8 (d, $J = 11.0$ Hz), 132.8 (d, $J = 4.5$ Hz), 124.7 (d, $J = 13.5$ Hz), 117.5 (d, $J = 7.8$ Hz), 115.9 (d, $J = 23.5$ Hz), 111.8 (d, $J = 1.2$ Hz), 111.3 (d, $J = 3.0$ Hz). HRMS: (Cl⁺, CH₄) m/z Calculated for C₁₂H₁₁F₂N₂O₂: 237.0834. Found [M+H]⁺: 237.0845 (Diff – 4.7 ppm).

3,5-Difluoro-4-(4-fluorophenoxy)benzene-1,2-diamine (4g)



General Procedure B - Employed 3-(4-fluorophenoxy)-2-nitroaniline (**3g**) to give the product (**4g**) (0.14 g, 41% yield) as a brown solid. ¹H NMR (400 MHz, CDCl₃) δ 6.98 – 6.94 (m, 2H), 6.37 (dd, 1H, $J = 11.2$ & 1.9 Hz), 3.34 (s, 4H). ¹³C NMR (100 MHz, CDCl₃) δ 158.2 (d, $J = 240.3$ Hz), 154.5, 149.7 (d, $J = 239.8$ Hz), 146.7 (d, $J = 240.6$ Hz), 133.9 (dd, $J = 6.6$ & 6.5 Hz), 124.8, 119.0 (dd, $J = 14.0$ & 3.3 Hz), 116.2 (d, $J = 8.6$ Hz), 115.9 (d, $J = 23.7$ Hz), 99.0 (dd, $J = 22.4$ & 2.9 Hz). HRMS: (Cl⁺, CH₄) m/z Calculated for C₁₂H₁₀F₃N₂O: 255.0740. Found [M+H]⁺: 255.0743 (Diff -1.32 ppm).

3-(4-fluorophenoxy)benzene-1,2-diamine (7b)

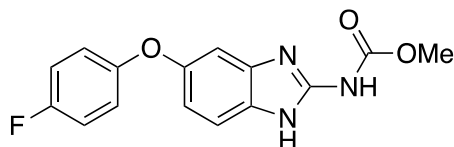


General Procedure B - Employed 3-(4-fluorophenoxy)-2-nitroaniline (**7a**) to give the product (**7b**) (0.17 g, 47% yield) as a brown solid. ¹H NMR (400 MHz, CDCl₃) δ 7.03 – 6.90 (m, 4H), 6.64 (dd, 1H, $J = 8.3$ & 7.9 Hz), 6.53 (d, 1H, $J = 7.9$ Hz), 6.36 (d, 1H, $J = 8.3$ Hz), 3.50 (s, 4H). ¹³C NMR (100 MHz, CDCl₃) δ 158.6

(d, $J = 242.2$ Hz), 153.4, 145.1, 136.4, 126.7, 119.4, 118.8 (d, $J = 8.5$ Hz), 116.1 (d, $J = 23.7$ Hz). HRMS: (Cl⁺, CH₄) m/z Calculated for C₁₂H₁₂FN₂O: 219.0928. Found [M+H]⁺: 219.0920 (Diff – 0.29 ppm).

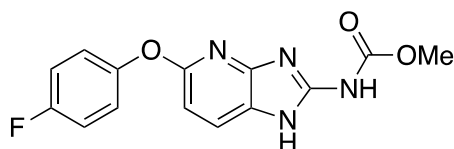
4.6.3.3 Synthesis of (5-phenoxy-1H-benzo[d]imidazol-2-yl)carbamate Derivatives

Methyl (5-(4-fluorophenoxy)-1H-benzo[d]imidazol-2-yl)carbamate (6a)



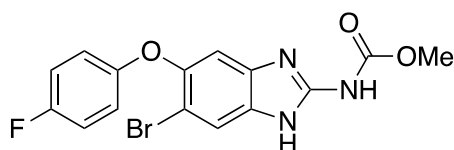
General Procedure C - Employed 4-(4-fluorophenoxy)benzene-1,2-diamine (**4a**) to give the product (**6a**) (1.29 g, 78% yield) as a pale pink solid. ¹H NMR (400 MHz, DMSO) δ 11.62 (s, 2H), 7.40 (d, 1H, $J = 8.5$ Hz), 7.19 – 7.17 (m, 2H), 7.03 (d, 1H, $J = 2.1$ Hz), 7.04 – 6.99 (m, 2H), 6.80 (dd, 1H, $J = 8.5$ & 2.1 Hz), 3.75 (s, 3H). ¹³C NMR (100 MHz, DMSO) δ 158.1 (d, $J = 239.9$ Hz), 155.2, 154.9, 151.7, 148.5, 137.9, 130.9, 119.7 (d, $J = 8.0$ Hz), 116.8 (d, $J = 23.6$ Hz), 114.9, 113.5, 105.2, 52.9. ¹⁹F NMR (367 MHz, DMSO) δ -121.3. HRMS: (ES⁺) m/z Calculated for C₁₅H₁₃FN₃O₃: 302.0935. Found [M+H]⁺: 302.0945 (Diff -3.27 ppm). $\nu_{\max}/\text{cm}^{-1}$: (solid) 3354 (s), 2980 (m), 2640 (m), 1627 (s), 1141 (m), 1276 (s). MP: 229-231 °C. Purity HPLC (Method A) 97.3%, $R_t = 9.15$ min.

Methyl (5-(4-fluorophenoxy)-1H-imidazo[4,5-b]pyridin-2-yl)carbamate (6b)



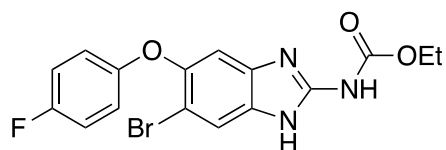
General Procedure C - Employed 6-(4-fluorophenoxy)pyridine-2,3-diamine (**4b**) to give the product (**6b**) (0.060 g, 32% yield) as a cream solid. ¹H NMR (400 MHz, DMSO) δ 12.00 (s, 1H), 11.4 (s, 1H), 7.80 (d, 1H, $J = 7.9$ Hz), 7.26 – 7.18 (m, 2H), 7.15 – 7.09 (m, 2H), 6.74 (d, 1H, $J = 7.9$ Hz), 3.77 (s, 3H). ¹³C NMR (100 MHz, DMSO) δ 158.9, 158.8 (d, $J = 238.9$ Hz), 154.5, 151.8 (d, $J = 2.3$ Hz), 149.0, 122.5 (d, $J = 7.9$ Hz), 116.5 (d, $J = 22.9$ Hz), 104.8, 53.1 not all carbons visible. ¹⁹F NMR (376 MHz, DMSO) – 120.0 HRMS: (ES⁺) m/z Calculated for C₁₄H₁₂FN₄O₃: 303.0888. Found [M+H]⁺: 303.0894 (Diff – 1.83 ppm). MP: 278 – 280 °C. Purity HPLC (Method A) 94.9%, $R_t = 8.24$ min.

Methyl (6-bromo-5-(4-fluorophenoxy)-1H-benzo[d]imidazol-2-yl)carbamate (6c)



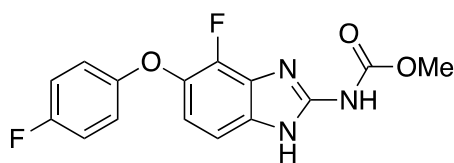
General Procedure C - Employed 4-bromo-5-(4-fluorophenoxy)benzene-1,2-diamine (**4c**) to give the product (**6c**) (0.32 g, 35% yield) as a pale pink solid. ^1H NMR (400 MHz, DMSO) δ 11.44 (s, 2H), 7.71 (s, 1H), 7.22 – 7.14 (m, 3H), 6.95 – 6.88 (m, 2H), 3.77 (s, 3H). ^{13}C NMR (100 MHz, DMSO) δ 158.2 (d, $J = 240.4$ Hz), 154.7, 154.6, 149.0, 147.0, 137.9, 133.2, 119.8, 118.5 (d, $J = 8.1$ Hz), 116.8 (d, $J = 23.6$ Hz), 107.3, 53.1 not all carbons visible. HRMS: (ES+) m/z Calculated for $\text{C}_{15}\text{H}_{12}\text{BrFN}_3\text{O}_3$: 380.0041. Found $[\text{M}+\text{H}]^+$: 380.0048 (Diff -1.94 ppm). $\nu_{\text{max}}/\text{cm}^{-1}$: (solid) 3346 (m), 2954 (m), 2654 (m), 1625 (m), 1593 (m), 1272 (s). MP 252 – 254 °C. Purity HPLC (Method A) 91.0%, $R_t = 9.82$ min.

Ethyl (6-bromo-5-(4-fluorophenoxy)-1H-benzo[d]imidazol-2-yl)carbamate (6d)

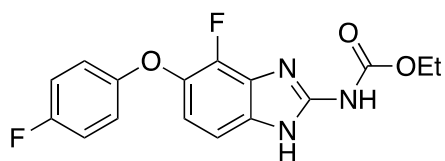


General Procedure C - Employed 4-bromo-5-(4-fluorophenoxy)benzene-1,2-diamine (**4d**) to give the product (**4d**) (0.090g, 96% yield) as a white solid. ^1H NMR (400 MHz, DMSO) δ 11.78 (bs, 2H), 7.70 (s, 1H), 7.22 – 7.13 (m, 3H), 6.95 – 6.87 (m, 2H), 4.23 (q, 2H, $J = 6.6$ Hz), 1.28 (t, 3H, $J = 6.6$ Hz). ^{13}C NMR (100 MHz, DMSO) δ 158.1 (d, $J = 238.5$ Hz), 154.6, 154.3, 149.0, 147.0, 137.1, 133.6, 118.7, 118.5 (d, $J = 8.6$ Hz), 116.8 (d, $J = 22.4$ Hz), 107.3, 106.3, 61.8, 14.6. HRMS: (ES+) m/z Calculated for $\text{C}_{16}\text{H}_{14}\text{BrFN}_3\text{O}_3$: 394.0197. Found $[\text{M}+\text{H}]^+$: 394.0205 (Diff -2.07 ppm). $\nu_{\text{max}}/\text{cm}^{-1}$: (solid) 3346 (m), 2954 (m), 2654 (m), 1625 (m), 1593 (m), 1272 (s). MP: 270 °C decomposed. Purity HPLC (Method A) 93.2%, $R_t = 10.32$ min.

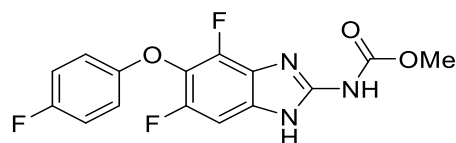
Methyl (4-fluoro-5-(4-fluorophenoxy)-1H-benzo[d]imidazol-2-yl)carbamate (6e)



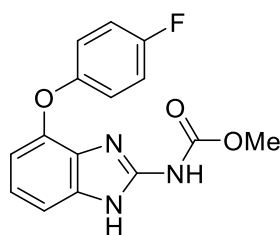
General Procedure C - Employed 3-fluoro-4-(4-fluorophenoxy)benzene-1,2-diamine (**4e**) to give the product (**6e**) (0.077 g, 55% yield) as a white solid. ^1H NMR (400 MHz, DMSO) δ 11.76 (bs, 2H), 7.28 (d, 2H, $J = 8.6$ Hz), 7.19 – 7.12 (m, 2H), 6.97 – 6.89 (m, 3H), 3.78 (s, 3H). ^{13}C NMR (100 MHz, DMSO) δ 157.9 (d, $J = 238.8$ Hz), 155.2, 154.5, 148.5, 136.7 (d, $J = 8.6$ Hz), 133.3, 117.6 (d, $J = 8.4$ Hz), 116.7 (d, $J = 23.0$ Hz), 115.5, 108.0, 53.1. Not all quaternary carbons visible. HRMS: (ES+) m/z Calculated for $\text{C}_{15}\text{H}_{12}\text{F}_2\text{N}_3\text{O}_3$: 320.0841. Found $[\text{M}+\text{H}]^+$: 320.0841 (Diff 0.14 ppm). $\nu_{\text{max}}/\text{cm}^{-1}$: (solid) 3321 (s), 2970 (m), 2742 (m), 1659 (s), 1450 (m), 1274 (s). MP: 245 °C decomposed. Purity HPLC (Method A) 99.4%, $R_t = 9.37$ min.

Ethyl (4-fluoro-5-(4-fluorophenoxy)-1H-benzo[d]imidazol-2-yl)carbamate (6f)

General Procedure C - Employed 3-fluoro-4-(4-fluorophenoxy)benzene-1,2-diamine (**4f**) to give the product (**6f**) (0.083 g, 57% yield) as a white solid. ^1H NMR (400 MHz, DMSO) δ 12.13 (bs, 1H), 11.41 (bs, 1H), 7.28 (d, 1H, $J = 8.5$ Hz), 7.19 – 7.12 (m, 2H), 3.96 – 6.88 (m, 3H), 4.25 (q, 2H, $J = 7.1$ Hz), 1.29 (t, 3H, $J = 7.1$ Hz). ^{13}C NMR (100 MHz, DMSO) δ 157.8 (d, $J = 237.5$ Hz), 155.2 (d, $J = 1.8$ Hz), 154.1, 148.5, 136.7 (d, $J = 9.1$ Hz), 133.1, 117.6 (d, $J = 8.1$ Hz), 116.7 (d, $J = 23.5$ Hz), 115.5, 107.9, 61.7, 14.8. Not all carbons visible. HRMS: (ES+) m/z Calculated for $\text{C}_{16}\text{H}_{14}\text{F}_2\text{N}_3\text{O}_3$: 334.0998. Found $[\text{M}+\text{H}]^+$: 334.1001 (Diff -0.96ppm). $\nu_{\text{max}}/\text{cm}^{-1}$ (solid): 3376 (s), 2984 (m), 2834 (m), 1689 (s), 1499 (s), 1224 (m). MP: 252 °C decomposed. Purity HPLC (Method A) 91.8%, $R_t = 10.32$ min.

Methyl (4,6-difluoro-5-(4-fluorophenoxy)-1H-benzo[d]imidazol-2-yl)carbamate (6g)

General Procedure C - Employed 3,5-difluoro-4-(4-fluorophenoxy)benzene-1,2-diamine (**4g**) to give the product (**6g**) (0.15 g, 65% yield) as a white solid. ^1H NMR (400 MHz, DMSO) δ 12.28 (s, 1H), 11.52 (s, 1H), 7.29 (d, 1H, $J = 9.9$ Hz), 7.20 - 7.13 (m, 2H), 7.00 – 6.94 (m, 2H), 3.77 (s, 3H). ^{13}C NMR (100 MHz, DMSO) δ 158.0 (d, $J = 246.1$ Hz), 154.8, 154.5, 150.8 (d, $J = 238.5$ Hz), 148.5, 131.2, 126.6, 125.6, 116.8 (d, $J = 25.1$ Hz), 116.6 (d, $J = 8.5$ Hz), 95.8, 53.1. One C-F carbon not visible. HRMS: (ES+) m/z Calculated for $\text{C}_{15}\text{H}_{11}\text{F}_3\text{N}_3\text{O}_3$: 338.0747. Found $[\text{M}+\text{H}]^+$: 338.0748 (Diff -0.22 ppm). $\nu_{\text{max}}/\text{cm}^{-1}$ (solid): 3318 (m), 2971 (m), 2767 (m), 2689 (m), 1710 (s), 1614 (m), 1466 (m), 1270 (s). MP: > 300 °C decomposed. Purity HPLC (Method A) 99.3%, $R_t = 9.57$ min.

Methyl (4-(4-fluorophenoxy)-1H-benzo[d]imidazol-2-yl)carbamate (7)

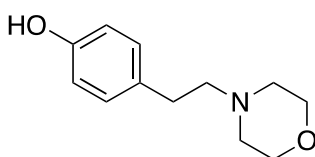
General Procedure C - Employed 3-(4-fluorophenoxy)benzene-1,2-diamine (**7b**) to give the product (**7**) (0.11 g, 47% yield) as a white solid. ^1H NMR (400 MHz, DMSO) δ 12.00 (s, 1H), 11.30 (s, 1H), 7.45 –

6.61 (m, 7H), 3.74 (s, 3H). ^{13}C NMR (100 MHz, DMSO) δ 157.8 (d, $J = 237.2$ Hz), 154.7, 154.6, 147.2, 144.6, 140.0, 135.9, 121.7, 118.5 (d, $J = 7.9$ Hz), 116.5 (d, $J = 23.4$ Hz), 112.5, 108.8, 52.8. HRMS: (ES+) m/z Calculated for $\text{C}_{15}\text{H}_{13}\text{FN}_3\text{O}_3$: 302.0935. Found $[\text{M}+\text{H}]^+$: 302.0935 (Diff -2.26 ppm). $\nu_{\text{max}}/\text{cm}^{-1}$ (solid): 3338 (m), 2980 (m), 2885 (m), 1632 (s), 1439 (m), 1262 (s). MP: 222 – 225 °C. Purity HPLC (Method A) 97.0%, $R_t = 9.28$ min.

4.6.4 Morpholine Derivatives

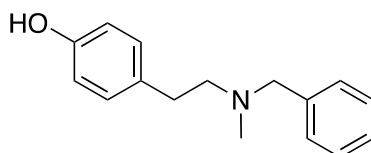
4.6.4.1 Synthesis of 4-(2-aminoethyl)phenol Derivatives

4-(2-Morpholinoethyl)phenol (**10a**)



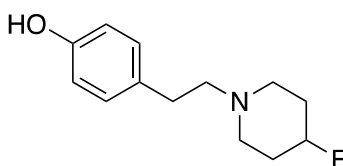
General Procedure D - Employed morpholine to give the product (**10a**) (0.52 g, 66% yield) as a pale pink solid. ^1H NMR (400 MHz, CD_3OD) δ 7.04 (d, 2H, $J = 8.1$ Hz), 6.72 (d 2H, $J = 8.1$ Hz), 3.75 – 3.72 (m, 4H), 2.76 - 2.73 (m, 2H), 2.59 – 2.56 (m, 6H). ^{13}C NMR (100 MHz, CD_3OD) δ 155.4, 130.3, 129.1, 114.8, 66.1, 60.8, 53.5, 31.5. HRMS: (Cl^+ , CH_4) m/z Calculated for $\text{C}_{12}\text{H}_{18}\text{NO}_2$: 208.1332. Found $[\text{M}+\text{H}]^+$: 208.1325 (Diff 3.32 ppm).

4-(2-(Benzyl(methyl)amino)ethyl)phenol (**10b**)



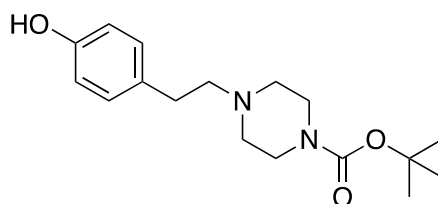
General Procedure D - Employed *N*-benzylmethylamine to give the product (**10b**) (0.51 g, 56% yield) as a white solid. ^1H NMR (400 MHz, CDCl_3) δ 7.27 (m, 5H), 7.00 (d, 2H, $J = 8.2$ Hz), 6.70 (d, 2H, $J = 8.2$ Hz), 3.59 (s, 2H), 2.79 – 2.75 (m, 2H), 2.65 - 2.61 (m, 2H), 2.30 (s, 3H). ^{13}C NMR (100 MHz, CDCl_3) δ 154.3, 138.1, 132.0, 129.8, 129.3, 128.3, 127.2, 115.4, 62.1, 59.3, 42.0, 32.7. HRMS: (Cl^+ , CH_4) m/z Calculated for $\text{C}_{16}\text{H}_{20}\text{NO}$: 242.1539. Found $[\text{M}+\text{H}]^+$: 242.1548 (Diff – 3.73 ppm).

4-(2-(4-Fluoropiperidin-1-yl)ethyl)phenol (**10c**)



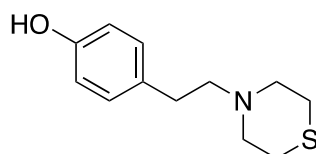
General Procedure D - Employed 4-fluoropiperidine to give the product (**10c**) (0.35 g, 40% yield) as a pale white solid. ^1H NMR (400 MHz, DMSO) δ 9.12 (s, 1H), 6.99 (d, 2H, $J = 8.7$ Hz), 6.65 (d, 2H, $J = 8.7$ Hz), 4.68 – 4.64 (m, 1H, $J = 49.6$ Hz), 2.60 – 2.57 (m, 4H), 2.46 – 2.43 (m, 2H), 2.35 - 2.32 (m, 2H), 1.87 – 1.82 (m, 2H), 1.71 – 1.68 (m, 2H). ^{13}C NMR (100 MHz, CD_3OD) δ 155.9, 131.0, 129.9, 115.5, 89.2 (d, $J = 170.4$ Hz), 60.5, 49.7 (d, $J = 6.9$ Hz), 32.7, 31.7 (d, $J = 19.7$ Hz). HRMS: (Cl^+ , CH_4) m/z Calculated for $\text{C}_{13}\text{H}_{19}\text{FNO}$: 224.1445. Found $[\text{M}+\text{H}]^+$: 224.1441 (Diff 1.85 ppm).

***tert*-Butyl 4-(4-hydroxyphenethyl)piperazine-1-carboxylate (**10d**)**



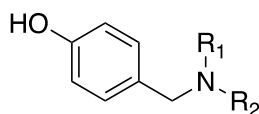
General Procedure D - Employed to give the product (**10d**) (0.49 g, 64% yield) as a yellow oil. ^1H NMR (400 MHz, CD_3OD) δ 7.04 (d, 2H, $J = 8.5$ Hz), 6.71 (d, 2H, $J = 8.5$ Hz), 3.48 – 3.44 (m, 4H), 2.78 - 3.72 (m, 2H), 2.59 – 2.56 (m, 2H), 2.53 – 2.49 (m, 4H), 1.46 (s, 9H). ^{13}C NMR (100 MHz, CD_3OD) δ 155.4, 155.0, 130.4, 129.2, 114.8, 79.8, 60.4, 52.5, 42.9, 31.7, 27.2. HRMS: (ES^+) m/z Calculated for $\text{C}_{17}\text{H}_{27}\text{N}_2\text{O}_3$: 307.2016. Found $[\text{M}+\text{H}]^+$: 307.2025 (Diff -3.00 ppm)

4-(2-thiomorpholinoethyl)phenol (10e**)**



General Procedure D - Employed thiomorpholine to give the product (**10e**) (0.35 g, 63% yield) as a yellow solid. ^1H NMR (400 MHz, CD_3OD) δ 7.02 (d, 2H, $J = 8.5$ Hz), 6.72 (d, 2H, $J = 8.5$ Hz), 2.83 – 2.79 (m, 4H), 2.73 – 2.68 (m, 6H), 2.60 - 2.57 (m, 2H). ^{13}C NMR (100 MHz, CD_3OD) δ 155.3, 130.5, 129.2, 114.8, 61.2, 54.6, 31.1, 26.8. HRMS: (Cl^+ , CH_4) m/z Calculated for $\text{C}_{12}\text{H}_{18}\text{NOS}$: 224.1104. Found $[\text{M}+\text{H}]^+$: 224.1109 (Diff -2.43 ppm).

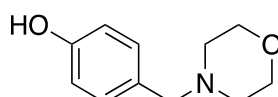
4.6.4.2 4-((amino)methyl)phenol Derivatives



To a flask at room temperature was added the desired aldehyde (1.0 eq.) and amine (1.0 eq.), along with anhydrous methanol and the reaction refluxed for two hours. The reaction was cooled and then

concentrated. The compound was then redissolved in methanol at 0 °C and NaBH₄ (5.0 eq.) added portion-wise. The reaction was left to stir at 0 °C for an hour and then overnight at room temperature. The reaction was then acidified to pH 3 using 3M HCl, basified to pH 9 using 25% NaOH. Extracted using DCM. The organic layer dried over magnesium sulphate, filtered and concentrated. The product was purified via column chromatography, eluting with 50% ethyl acetate in hexane, increasing to 66% ethyl acetate in hexane to give the product as a white solid.

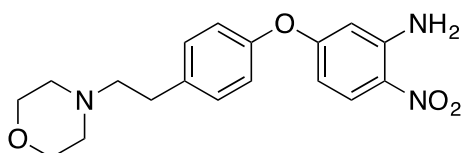
4-(Morpholinomethyl)phenol (**18**)



Reaction carried out using 4-hydroxybenzaldehyde and morpholine to give the product (**18**) (0.27 g, 54% yield) as a white solid. ¹H NMR (400 MHz, CD₃OD) δ 7.16 (d, 2H), 6.76 (d, 2H, *J* = 8.4 Hz), 3.72 - 3.67 (m, 4H), 3.44 (s, 2H), 2.48 - 2.45 (m, 4H). ¹³C NMR (100 MHz, CD₃OD) δ 156.5, 130.6, 127.1, 114.6, 66.3, 62.5, 52.9. HRMS: (ES+) *m/z* Calculated for C₁₂H₁₆NO₂: 194.1176. Found [M+H]⁺: 194.1182 (Diff - 3.45 ppm).

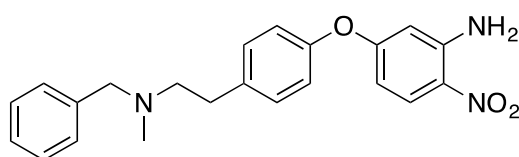
4.6.4.3 Synthesis of 5-(4-(2-(amine)ethyl)phenoxy)-2-nitroaniline

5-(4-(2-Morpholinoethyl)phenoxy)-2-nitroaniline (**12a**)



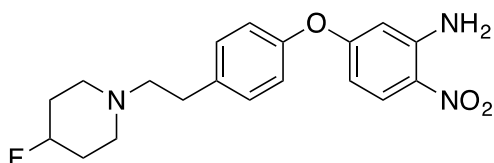
General Procedure A - Employed 5-fluoro-2-nitroaniline and 4-(2-morpholinoethyl)phenol (**10a**) to give the product (**12a**) (1.02. g, 85% yield) as a yellow oil. ¹H NMR (400 MHz, CD₃OD) δ 8.10 (d, 1H, *J* = 9.7 Hz), 7.25 (d, 2H, *J* = 8.3 Hz), 7.00 (d, 2H, *J* = 8.3 Hz), 6.31 (dd, 1H, *J* = 9.7 & 2.4 Hz), 6.14 (d, 1H, *J* = 2.4 Hz), 6.11 (s, 2H), 3.78 - 3.74 (m, 4H), 2.86 - 2.83 (m, 2H), 2.64 - 2.61 (m, 2H), 2.57 - 2.53 (m, 4H). ¹³C NMR (100 MHz, CD₃OD) δ 164.2, 152.7, 146.7, 137.3, 130.3, 128.7, 127.7, 120.8, 107.7, 103.3, 66.9, 50.7, 53.7, 32.6. HRMS: (ES+) *m/z* Calculated for C₁₈H₂₂N₃O₄: 344.1605. Found [M+H]⁺: 344.1601 (Diff 0.97 ppm).

5-(4-(2-(Benzyl(methyl)amino)ethyl)phenoxy)-2-nitroaniline (**12b**)



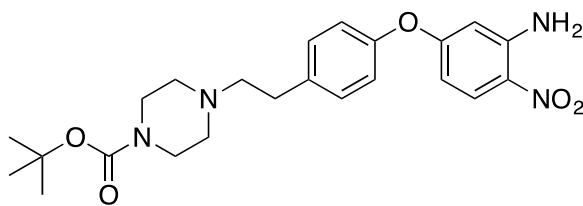
General Procedure A - Employed 5-fluoro-2-nitroaniline and 4-(2-(benzyl(methyl)amino)ethyl)phenol (**10b**) to give the product (**12b**) (0.35 g, 54% yield) as a yellow solid. ^1H NMR (400 MHz, CDCl_3) δ 8.10 (d, 1H, $J = 9.6$ Hz), 7.31 – 7.26 (m, 5H), 7.22 (d, 2H, $J = 8.2$ Hz), 6.98 (d, 2H, $J = 8.2$ Hz), 6.33 (dd, 1H, $J = 9.6$ & 2.8 Hz), 6.12 (d, 1H, $J = 2.8$ Hz), 6.08 (s, 2H), 3.57 (s, 2H), 2.86 – 2.82 (m, 2H), 2.67 – 2.63 (m, 2H), 2.30 (s, 3H). ^{13}C NMR (100 MHz, CDCl_3) δ 164.5, 152.5, 146.8, 138.9, 137.8, 130.4, 129.0, 128.7, 128.2, 127.7, 126.9, 120.7, 107.7, 103.2, 62.3, 58.9, 42.2, 33.2. HRMS: (ES+) m/z Calculated for $\text{C}_{22}\text{H}_{24}\text{N}_3\text{O}_3$: 378.1812. Found $[\text{M}+\text{H}]^+$: 378.1822 (Diff -2.54 ppm).

5-(4-(2-(4-Fluoropiperidin-1-yl)ethyl)phenoxy)-2-nitroaniline (12c)

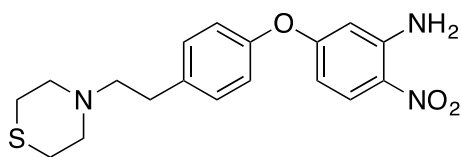


General Procedure A - Employed 5-fluoro-2-nitroaniline and 4-(2-(4-fluoropiperidin-1-yl)ethyl)phenol (**10c**) to give the product (**12c**) (0.36 g, 80% yield) as a yellow solid. ^1H NMR (400 MHz, CD_3OD) δ 8.10 (d, 1H, $J = 9.3$ Hz), 7.24 (d, 2H, $J = 8.5$ Hz), 6.99 (d, 2H, $J = 8.5$ Hz), 6.32 (dd, 1H, $J = 9.3$ & 2.4 Hz), 6.14 (d, 1H, $J = 2.4$ Hz), 6.10 (s, 2H), 4.73 – 4.70 (m, $J = 48.1$ Hz), 2.85 – 2.82 (m, 2H), 2.68 – 2.66 (m, 6H), 2.51 – 2.48 (m, 2H). ^{13}C NMR (100 MHz, CD_3OD) δ 164.3, 152.7, 146.8, 137.5, 130.3, 129.8, 128.7, 120.8, 107.7, 103.4, 90.1 (d, $J = 175.0$ Hz), 60.3, 49.5 (d, $J = 5.0$ Hz), 33.1, 31.4 (d, $J = 20.2$ Hz). HRMS: (ES+) m/z Calculated for $\text{C}_{19}\text{H}_{23}\text{FN}_3\text{O}$: 360.1718. Found $[\text{M}+\text{H}]^+$: 360.1728 (Diff – 2.65 ppm).

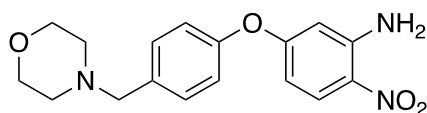
tert-Butyl 4-(4-(3-amino-4-nitrophenoxy)phenethyl)piperazine-1-carboxylate (12d)



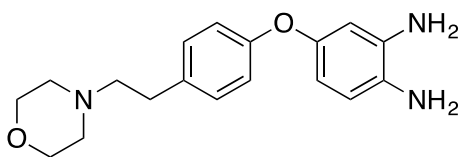
General Procedure A - Employed 5-fluoro-2-nitroaniline and *tert*-butyl 4-(4-hydroxyphenethyl)piperazine-1-carboxylate (**10d**) to give the product (**12d**) (0.34 g, 49% yield) as a yellow oil. ^1H NMR (400 MHz, CD_3OD) δ 8.03 (d, 1H, $J = 9.3$ Hz), 7.29 (d, 2H, $J = 8.4$ Hz), 7.01 (d, 2H, $J = 8.4$ Hz), 6.27 (s, 1H, $J = 2.6$ Hz), 6.24 (dd, 1H, $J = 9.3$ & 2.6 Hz), 3.47 – 3.44 (m, 4H), 2.86 – 2.82 (m, 2H), 2.65 – 2.63 (m, 2H), 2.53 – 2.49 (m, 4H). ^{13}C NMR (100 MHz, CD_3OD) δ 164.3, 155.0, 153.0, 148.2, 137.0, 130.1, 129.2, 128.0, 120.5, 106.5, 102.8, 80.0, 60.1, 60.0, 52.5, 31.9, 27.2.

2-Nitro-5-(4-(2-thiomorpholinoethyl)phenoxy)aniline (12e)

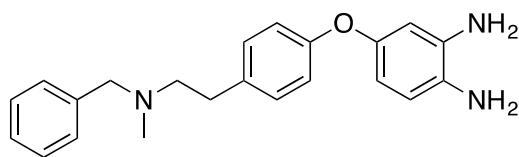
General Procedure A – Employed 5-fluoro-2-nitroaniline and 4-(2-thiomorpholinoethyl)phenol (**10e**) to give the product (**12e**) (0.42 g, 75% yield) as a brown oil. ^1H NMR (400 MHz, CD_3OD) δ 8.00 (d, 1H, $J = 9.5$ Hz), 7.32 (d, 2H, $J = 8.3$ Hz), 7.07 (d, 2H, $J = 8.3$ Hz), 6.34 (d, 1H, $J = 2.5$ Hz), 6.27 (dd, 1H, $J = 8.3$ & 2.5 Hz), 2.75 – 2.72 (m, 6H), 2.63 – 2.57 (m, 8H). ^{13}C NMR (100 MHz, CD_3OD) δ 164.0, 152.9, 148.7, 138.0, 131.2, 128.7, 126.5, 120.9, 107.1, 103.0, 60.7, 54.9, 32.1, 27.7. HRMS: (ES+) m/z Calculated for $\text{C}_{18}\text{H}_{22}\text{N}_3\text{O}_3\text{S}$: 360.1376. Found $[\text{M}+\text{H}]^+$: 360.1389 (Diff – 3.48 ppm).

5-(4-(Morpholinomethyl)phenoxy)-2-nitroaniline (19)

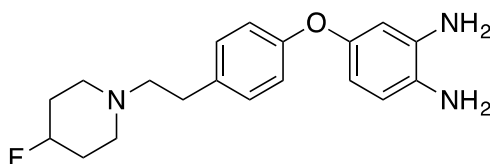
General Procedure A - Employed 5-fluoro-2-nitroaniline and 4-(morpholinomethyl)phenol (**18**) to give the product (**19**) (0.39 g, 93% yield) as a yellow solid. ^1H NMR (400 MHz, CD_3OD) δ 8.07 (d, 1H, $J = 9.4$ Hz), 7.44 (d, 2H, $J = 8.5$ Hz), 7.09 (d, 2H, $J = 8.5$ Hz), 6.33 (d, 1H, $J = 2.5$ Hz), 6.29 (dd, 1H, $J = 9.4$ & 2.5 Hz), 3.74 – 3.71 (m, 4H), 3.59 – 3.55 (s, 2H), 2.52 – 2.49 (m, 4H). ^{13}C NMR (100 MHz, CD_3OD) δ 163.4, 153.9, 148.2, 134.2, 130.9, 129.0, 120.2, 106.5, 103.0, 66.4, 52.1, 53.2. Not all quaternary carbons visible. HRMS: (ES+) m/z Calculated for $\text{C}_{17}\text{H}_{20}\text{N}_3\text{O}_4$: 330.1448. Found $[\text{M}+\text{H}]^+$: 330.1454 (Diff – 1.81 ppm).

4.6.4.4 4-(4-(amino)phenoxy)benzene-1,2-diamine Derivatives**4-(4-(2-Morpholinoethyl)phenoxy)benzene-1,2-diamine (13a)**

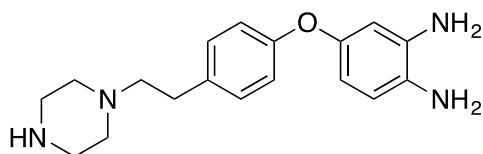
General Procedure B - Employed 5-(4-(2-morpholinoethyl)phenoxy)-2-nitroaniline (**12a**) to give the product (**13a**) (0.60 g, 77% yield) as a brown oil. ^1H NMR (400 MHz, CD_3OD) δ 7.01 (d, 2H, $J = 8.6$ Hz), 6.71 (d, 2H, $J = 8.6$ Hz), 6.57 (d, 1H, $J = 8.3$ Hz), 6.30 (d, 1H, $J = 2.7$ Hz), 6.13 (dd, 1H, $J = 8.3$ & 2.7 Hz), 3.64 – 3.60 (m, 4H), 2.68 – 2.63 (m, 2H), 2.48 – 2.42 (m, 6H). ^{13}C NMR (100 MHz, CD_3OD) δ 157.3, 150.2, 136.7, 133.2, 130.8, 129.3, 117.1, 117.0, 109.6, 107.5, 66.2, 60.6, 53.2, 31.5. HRMS: (ES+) m/z Calculated for $\text{C}_{18}\text{H}_{24}\text{N}_3\text{O}_2$: 314.1863. Found $[\text{M}+\text{H}]^+$: 314.1874 (Diff -.35 ppm).

4-(4-(2-(Benzyl(methyl)amino)ethyl)phenoxy)benzene-1,2-diamine (13b)

General Procedure B - Employed 5-(4-(2-(benzyl(methyl)amino)ethyl)phenoxy)-2-nitroaniline (**12b**) to give the product (**13b**) (0.33 g, 46% yield) as a brown oil. ^1H NMR (400 MHz, CD_3OD) δ 7.33 – 7.21 (m, 5H), 7.08 (d, 2H, $J = 8.4$ Hz), 6.86 (d, 2H, $J = 8.4$ Hz), 6.65 (d, 1H, $J = 8.2$ Hz), 6.41 (d, 1H, $J = 2.6$ Hz), 6.37 (dd, 1H, $J = 8.2$ & 2.6 Hz), 3.56 (s, 2H), 2.82 – 2.75 (m, 2H), 2.65 – 2.60 (m, 2H), 2.27 (s, 3H). ^{13}C NMR (100 MHz, CD_3OD) δ 156.6, 151.0, 139.0, 136.6, 134.4, 130.0, 129.7, 129.0, 128.2, 127.0, 117.9, 117.7, 110.6, 108.0, 62.2, 59.3, 42.2, 33.1. HRMS: (ES+) m/z Calculated for $\text{C}_{22}\text{H}_{26}\text{N}_3\text{O}$: 348.0270. Found $[\text{M}+\text{H}]^+$: 348.2063 (Diff 2.08 ppm).

4-(4-(2-(4-Fluoropiperidin-1-yl)ethyl)phenoxy)benzene-1,2-diamine (13c)

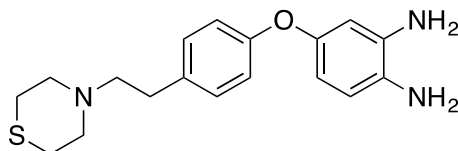
General Procedure B - Employed 5-(4-(2-(4-fluoropiperidin-1-yl)ethyl)phenoxy)-2-nitroaniline (**12c**) to give the product (**13c**) (0.14 g, 44% yield) as a brown oil. ^1H NMR (400 MHz, CD_3OD) δ 7.10 (d, 2H, $J = 8.8$ Hz), 6.87 (d, 2H, $J = 8.8$ Hz), 6.66 (d, 1H, $J = 7.9$ Hz), 6.42 (d, 1H, $J = 2.6$ Hz), 6.37 (dd, 1H, $J = 7.9$ & 2.6 Hz), 4.71 – 4.69 (m, 1H, $J = 48.4$ Hz), 2.79 – 2.76 (m, 2H), 2.70 – 2.66 (m, 4H), 2.62 – 2.59 (m, 2H), 2.53 – 2.49 (m, 4H), 1.95 – 1.90 (m, 4H). ^{13}C NMR (100 MHz, CD_3OD) δ 156.9, 150.8, 136.6, 133.9, 130.0, 129.6, 117.9, 117.8, 110.6, 108.1, 88.2 (d, $J = 164.7$ Hz), 60.1, 49.4 (d, $J = 5.2$ Hz), 32.8, 31.3 (d, $J = 19.6$ Hz). HRMS: (ES+) m/z Calculated for $\text{C}_{19}\text{H}_{25}\text{FN}_3\text{O}$: 330.1976. Found $[\text{M}+\text{H}]^+$: 330.1986 (Diff – 2.87 ppm).

4-(4-(2-(Piperazin-1-yl)ethyl)phenoxy)benzene-1,2-diamine (13d)

General Procedure B - Employed *tert*-butyl 4-(4-(3-amino-4-nitrophenoxy)phenethyl)piperazine-1-carboxylate (**12d**) to give the product (**13d**) (0.050 g, 15% yield) as a brown oil. ^1H NMR (400 MHz, CD_3OD) δ 7.01 (d, 2H, $J = 8.7$ Hz), 6.71 (d, 2H, $J = 8.7$ Hz), 6.56 (d, 1H, $J = 8.4$ Hz), 6.30 (d, 1H, $J = 2.8$ Hz), 6.13 (dd, 1H, $J = 8.4$ & 2.8 Hz), 2.79 – 2.75 (m, 4H), 2.67 – 2.65 (m, 2H), 2.48 – 2.43 (m, 6H). ^{13}C

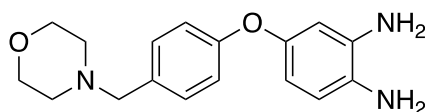
NMR (100 MHz, CD₃OD) δ 157.3, 150.2, 136.7, 133.4, 130.1, 129.3, 117.1, 117.0, 109.5, 107.5, 60.8, 53.3, 44.6, 31.5. HRMS: (ES+) m/z Calculated for C₁₈H₂₅N₄O: 313.2023. Found [M+H]⁺: 313.2025 (Diff - 0.72 ppm).

4-(4-(2-Thiomorpholinoethyl)phenoxy)benzene-1,2-diamine (13e)



General Procedure B - Employed 2-nitro-5-(4-(2-thiomorpholinoethyl)phenoxy)aniline to give the product **(13e)** (0.18 g, 50% yield) as a brown oil. ¹H NMR (400 MHz, CD₃OD) δ 7.10 (d, 2H, J = 8.3 Hz), 6.82 (d, 2H, J = 8.3 Hz), 6.68 (d, 1H, J = 8.4 Hz), 6.41 (d, 1H, J = 2.5 Hz), 6.24 (dd, 1H, J = 8.4 & 2.5 Hz), 2.83 – 2.79 (m, 4H), 2.76 – 2.73 (m, 2H), 2.71 – 2.66 (m, 4H), 2.62 – 2.59 (m, 2H). ¹³C NMR (100 MHz, CD₃OD) δ 157.3, 150.2, 137.7, 133.4, 130.1, 129.4, 117.2, 117.1, 109.6, 107.5, 61.0, 54.6, 313.3, 26.9. HRMS: (ES+) m/z Calculated for C₁₈H₂₄N₃OS: 330.1635. Found [M+H]⁺: 330.1636 (Diff -0.55 ppm).

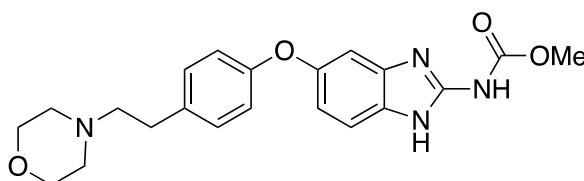
4-(4-(Morpholinomethyl)phenoxy)benzene-1,2-diamine (20)



General Procedure B - Employed 5-(4-(morpholinomethyl)phenoxy)-2-nitroaniline (**19**) to give the product **(20)** (0.14 g, 41% yield) as a brown solid. ¹H NMR (400 MHz, CD₃OD) δ 7.25 (d, 2H, J = 8.5 Hz), 6.86 (d, 2H, J = 8.5 Hz), 6.71 (d, 1H, J = 8.1 Hz), 6.44 (d, 1H, J = 2.6 Hz), 6.27 (dd, 1H, J = 8.1 & 2.6 Hz), 3.72 – 3.69 (m, 4H), 3.48 (s, 2H), 2.48 – 2.43 (m, 4H). ¹³C NMR (100 MHz, CD₃OD) δ 158.4, 149.8, 136.6, 130.5, 130.3, 130.0, 117.0, 116.6, 109.8, 107.7, 66.3, 62.2, 53.1. HRMS: (CI+, NH₃) m/z Calculated for C₁₇H₂₂N₃O₂: 300.1707. Found [M+H]⁺: 300.1710 (Diff – 3.06 ppm).

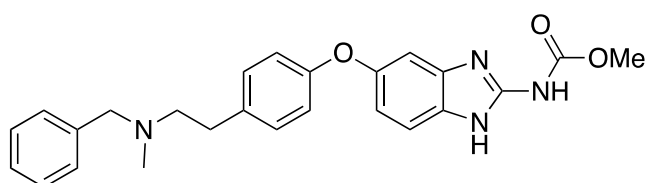
4.6.4.5 Synthesis of methyl (5-(4-(amine)phenoxy)-1H-benzo[d]imidazol-2-yl)carbamate Derivatives

Methyl (5-(4-(2-morpholinoethyl)phenoxy)-1H-benzo[d]imidazol-2-yl)carbamate (14a)



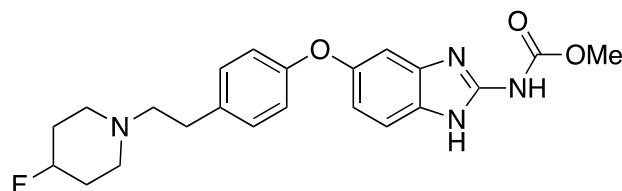
General Procedure C - Employed 4-(4-(2-morpholinoethyl)phenoxy)benzene-1,2-diamine (**13a**) to give the product (**14a**) (0.38 g, 49% yield) as a white solid. ^1H NMR (400 MHz, DMSO) δ 11.66 (bs, 2H), 7.39 (d, 1H, $J = 8.4$ Hz), 7.19 (d, 2H, $J = 7.8$ Hz), 7.03 (s, 1H), 6.86 (d, 2H, $J = 7.8$ Hz), 6.79 (d, 1H, $J = 8.4$ Hz), 3.74 (s, 3H), 3.64 – 3.54 (m, 4H), 2.74 – 2.66 (m, 2H), 2.51 – 2.39 (m, 6H). ^{13}C NMR (100 MHz, DMSO) δ 156.9, 155.2, 151.6, 148.4, 134.8, 130.4, 117.9, 114.6, 113.8, 105.0, 66.6, 60.5, 53.7, 52.9, 31.9 not all quaternary carbons visible. HRMS: (ES+) m/z Calculated for $\text{C}_{21}\text{H}_{25}\text{N}_4\text{O}_4$: 397.1870. Found $[\text{M}+\text{H}]^+$: 397.1871 (Diff -0.21 ppm). $\nu_{\text{max}}/\text{cm}^{-1}$: (solid) 3328 (s), 2947 (m), 1626 (s), 1472 (m), 1225 (s). MP: 198 – 201 °C. Purity HPLC (Method B) 97.3%, $R_t = 9.15$ min.

Methyl (5-(4-(2-(benzyl(methyl)amino)ethyl)phenoxy)-1H-benzo[d]imidazol-2-yl)carbamate (14b)



General Procedure C - Employed 4-(4-(2-(benzyl(methyl)amino)ethyl)phenoxy)benzene-1,2-diamine (**13b**) to give the product (**14b**) (0.069 g, 37% yield) as a pale pink solid. ^1H NMR (400 MHz, DMSO) δ 10.65 (s, 2H), 7.38 (d, 1H, $J = 8.3$ Hz), 7.27 (m, 5H), 7.16 (d, 2H, $J = 8.8$ Hz), 7.02 (d, 1H, $J = 2.4$ Hz), 6.86 (d, 2H, $J = 8.8$ Hz), 6.79 (dd, 1H, $J = 8.3$ & 2.4 Hz), 3.75 (s, 3H), 3.52 (s, 2H), 2.75 – 2.72 (m, 2H), 2.57 – 2.54 (m, 2H), 2.20 – 2.17 (m, 3H). ^{13}C NMR (100 MHz, DMSO) δ 156.9, 154.1, 151.7, 148.4, 140.8, 139.6, 136.0, 130.4, 129.8, 129.1, 128.6, 127.2, 117.9, 113.7, 113.6, 104.7, 61.7, 59.1, 52.9, 42.4, 32.6. HRMS: (ES+) m/z Calculated for $\text{C}_{25}\text{H}_{27}\text{N}_4\text{O}_3$: 431.2078. Found $[\text{M}+\text{H}]^+$: 431.2070 (Diff 1.76 ppm). $\nu_{\text{max}}/\text{cm}^{-1}$: (solid) 3331 (s), 3028 (m), 2943 (m), 2839 (m), 1625 (s), 1474 (m), 1277 (s). MP: 180 - 183 °C decomposed. Purity HPLC (Method B) 97.3%, $R_t = 6.28$ min.

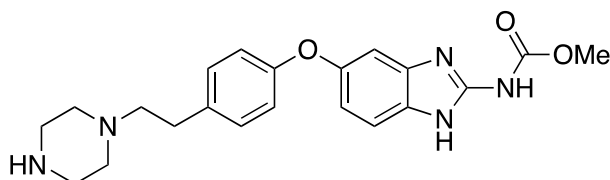
Methyl (5-(4-(2-(4-fluoropiperidin-1-yl)ethyl)phenoxy)-1H-benzo[d]imidazol-2-yl)carbamate (14c)



General Procedure C - Employed 4-(4-(2-(4-fluoropiperidin-1-yl)ethyl)phenoxy)benzene-1,2-diamine (**13c**) to give the product (**14c**) (0.043 g, 25% yield) as an orange solid. ^1H NMR (400 MHz, DMSO) δ 11.60 (d, 2H), 7.38 (d, 1H, $J = 8.4$ Hz), 7.18 (d, 2H, $J = 7.8$ Hz), 7.02 (s, 1H), 6.86 (d, 2H, $J = 7.8$ Hz), 6.79 (d, 1H, $J = 8.4$ Hz), 4.69 – 4.66 (m, 1H, $J = 49.6$ Hz), 3.75 (s, 3H), 2.71 – 2.68 (m, 2H), 2.63 – 2.59 (m, 6H), 1.87 – 1.85 (m, 2H), 1.72 – 1.69 (m, 2H). ^{13}C NMR (100 MHz, DMSO) δ 156.7, 155.3, 151.6, 148.4,

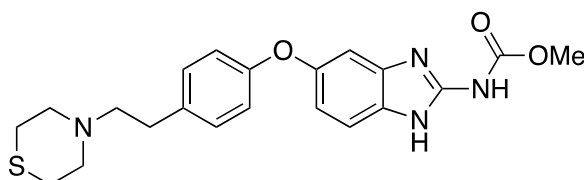
137.1, 135.0, 130.4, 117.9, 114.8, 113.7, 105.0, 89.3 (d, $J = 163.2$ Hz), 60.2, 52.9, 49.6 (d, $J = 6.6$ Hz), 32.6, 31.7 (d, $J = 18.7$ Hz), not all quaternary carbons visible. HRMS: (ES+) m/z Calculated for $C_{22}H_{26}FN_4O_3$: 413.1983. $\nu_{\max}/\text{cm}^{-1}$: (solid) 3357 (m), 2980 (m), 2768 (m), 1627 (s), 1473 (m), 1262 (s). Found $[M+H]^+$: 413.1982 (Diff - 0.35 ppm). MP: 218 – 220 °C. Purity HPLC (Method B) 96.7%, $R_t = 5.68$ min.

Methyl (5-(4-(2-(piperazin-1-yl)ethyl)benzyl)-1H-benzo[d]imidazol-2-yl)carbamate (14d)

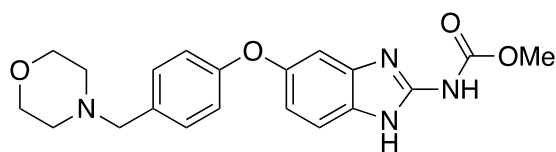


General Procedure C - Employed 4-(4-(2-(piperazin-1-yl)ethyl)phenoxy)benzene-1,2-diamine (**13d**) to give the product (**14d**) (0.028 g, 44% yield) as a cream solid. ^1H NMR (400 MHz, DMSO) δ 7.38 (d, 1H, $J = 8.5$ Hz), 7.18 (d, 2H, $J = 8.8$ Hz), 7.01 (d, 1H, $J = 2.3$ Hz), 6.85 (d, 2H, $J = 8.8$ Hz), 6.78 (dd, 1H, $J = 8.5$ & 2.3 Hz), 3.75 (s, 3H), 2.76 – 2.71 (m, 4H), 2.69 – 2.65 (m, 2H), 2.48 – 2.46 (m, 2H), 2.41 – 2.37 (m, 4H). ^{13}C NMR (100 MHz, DMSO) δ 156.9, 155.3, 151.6, 148.4, 135.0, 133.3, 130.4, 130.0, 117.9, 114.7, 113.7, 104.9, 60.9, 53.8, 52.9, 45.5, 32.2. HRMS: (ES+) m/z Calculated for $C_{12}H_{26}N_5O_3$: 396.2030. Found $[M+H]^+$: 396.2039 (Diff -2.13 ppm). $\nu_{\max}/\text{cm}^{-1}$: (solid) 3655 (m), 3331 (m), 2980 (m), 2888 (m), 1626 (s), 1473 (m), 1261 (s). MP: 228 - 230 °C decomposed.

Methyl (5-(4-(2-thiomorpholinoethyl)benzyl)-1H-benzo[d]imidazol-2-yl)carbamate (14e)



General Procedure C - Employed 4-(4-(2-thiomorpholinoethyl)phenoxy)benzene-1,2-diamine (**13e**) to give the product (**14e**) (0.10 g, 43% yield) as a cream solid. ^1H NMR (400 MHz, DMSO) δ 11.59 (s, 2H), 7.38 (d, 1H, $J = 8.6$ Hz), 7.18 (d, 2H, $J = 8.9$ Hz), 7.02 (d, 1H, $J = 2.1$ Hz), 6.87 (d, 2H, $J = 8.9$ Hz), 6.79 (dd, 1H, $J = 8.6$ & 2.1 Hz), 3.75 (s, 3H), 2.73 – 2.68 (m, 6H), 2.62 – 2.58 (m, 4H), 2.54 – 2.52 (m, 2H). ^{13}C NMR (100 MHz, DMSO) δ 156.9, 155.3, 151.6, 148.4, 137.5, 134.9, 130.4, 129.9, 117.9, 114.9, 113.7, 104.8, 61.0, 54.9, 52.5, 31.9, 27.6. HRMS: (ES+) m/z Calculated for $C_{21}H_{26}N_4O_3S$: 413.1642. Found $[M+H]^+$: 413.1652 (Diff -2.43 ppm). $\nu_{\max}/\text{cm}^{-1}$: (solid) 3339 (m), 2980 (m), 2888 (m), 2805 (m), 1632 (s), 1458 (m), 1263 (s). MP: 220 - 222 °C decomposed. Purity HPLC (Method B) 93.7%, $R_t = 5.23$ min.

methyl (5-(4-(morpholinomethyl)phenoxy)-1H-benzo[d]imidazol-2-yl)carbamate (21)

General Procedure C – Employed 4-(4-(morpholinomethyl)phenoxy)benzene-1,2-diamine (**20**) to give the product (**21**) (0.082 g, 46% yield) as a white solid. ^1H NMR (400 MHz, DMSO) δ 11.67 (s, 2H), 7.40 (d, 1H, $J = 8.5$ Hz), 7.26 (d, 2H, $J = 8.2$ Hz), 7.05 (d, 1H, $J = 1.7$ Hz), 6.90 (d, 2H, $J = 8.2$ Hz), 6.81 (dd, 1H, $J = 8.5$ & 1.7 Hz), 3.75 (s, 3H), 3.59 - 3.55 (m, 4H), 3.43 - 3.41 (s, 2H), 2.38 - 2.33 (m, 4H). ^{13}C NMR (100 MHz, DMSO) δ 157.9, 155.2, 152.9, 151.3, 148.4, 132.1, 131.0, 117.6, 114.9, 113.9, 105.3, 66.6, 62.2, 53.5, 52.9. Not all quaternary carbons visible. HRMS: (ES+) m/z Calculated for $\text{C}_{20}\text{H}_{23}\text{N}_4\text{O}_4$: 383.1714. Found $[\text{M}+\text{H}]^+$: 383.1721 (Diff -1.75 ppm). $\nu_{\text{max}}/\text{cm}^{-1}$: (solid) 3382 (m), 2970 (m), 2929 (m), 2853 (m), 1705 (s), 1599 (m), 1476 (m), 1323 (m), 1271 (m). MP: 222 - 225 °C decomposed. Purity HPLC (Method B) 100%, $R_t = 5.19$ min.

4.7 References

1. E. C. Cortés and L. A. A. Anaya, *J. Heterocycl. Chem.*, 1997, **34**, 745-748.
2. E. C. Cortés, R. S. Mendoza, M. S. Gutiérrez and O. G.-M. De Cortés, *J. Heterocycl. Chem.*, 2004, **41**, 273-276.
3. *US Pat.*, US20030612163, 2003.
4. W. Wang, D. Kong, H. Cheng, L. Tan, Z. Zhang, X. Zhuang, H. Long, Y. Zhou, Y. Xu, X. Yang and K. Ding, *Bioorg. Med. Chem. Lett.*, 2014, 4250-4253.
5. R. F. Hudson and G. Klopman, *J. Chem. Soc.*, 1962, **1**, 1062-1067.
6. S. K. Giri, R. Gour and K. P. R. Kartha, *RSC Adv.*, 2017, **7**, 13653-13667.
7. J. McMurry, *Organic Chemistry*, Brooks Cole, 7th edn., 2009.
8. V. M. Vlasov, *Russ. Chem. Rev.*, 2003, **72**, 681-703.
9. G. P. Stahly, *J. Org. Chem.*, 1985, **50**, 3091-3094.
10. H. Amii and K. Uneyama, *Chem. Rev.*, 2009, **109**, 2119-2183.
11. N. A. Senger, B. Bo, Q. Cheng, J. R. Keeffe, S. Gronert and W. Wu, *J. Org. Chem.*, 2012, **77**, 9535-9540.
12. Y. Ogata, *J. Org. Chem.*, 1982, **47**, 3577-3581.
13. M. B. Smith and J. March, *March's Advanced Organic Chemistry: Reactions, Mechanisms, and Structure*, Wiley, 2001.
14. I. Hunt, Chapter 12 : Reactions of Arenes. Electrophilic Aromatic Substitution (<http://www.chem.ucalgary.ca/courses/350/Carey5th/Ch12/ch12-8b.html>, June 2019).
15. M. Kah and C. D. Brown, *Chemosphere*, 2008, **72**, 1401-1408.
16. M. Remko, *Chemical Papers- Slovak Academy of Sciences*, 2007, **61**, 133-141.
17. Optibrium, *Stardrop*, 2018.
18. P.-G. Forkert, R. P. Lee and K. Reid, *Drug Metab. Dispos.*, 2001, **29**, 258-263.
19. A. K. Ghosh and M. Brindisi, *J. Med. Chem.*, 2015, **58**, 2895-2940.
20. P. Girard, Y. Pansart, I. Lorette and J.-M. Gillardin, *Dig. Dis. Sci.*, 2003, **48**, 770-774.
21. M. A. Walker, *Expert Opin. Drug Discov.*, 2014, **9**, 1421-1433.
22. A. Zafar, L. I. Pilkington, N. A. Haverkate, M. Van Rensburg, E. Leung, S. Kumara, W. A. Denny, D. Barker, A. Alsuraifi, C. Hoskins and J. Reynisson, *Molecules*, 2018, **23**, 145-169.
23. A. Zhai, *Determination of Phenols in Drinking Water with Agilent Bond Elut Plexa SPE and HPLC*, Agilent Technologies, 2012.
24. M. R. Crampton and I. A. Robotham, *J. Chem. Res.*, 1997, DOI: 10.1039/A606020J, 22-23.
25. F. Maran, D. Celadon, M. G. Severin and E. Vianello, *J. Am. Chem. Soc.*, 1991, **113**, 9320-9329.
26. F. G. Bordwell, R. J. McCallum and W. N. Olmstead, *J. Org. Chem.*, 1984, **49**, 1424-1427.
27. K. Roy and P. L. A. Popelier, *J. Phys. Org. Chem.*, 2009, **22**, 186-196.
28. J. D. Soper, E. Saganic, D. Weinberg, D. A. Hrovat, J. B. Benedict, W. Kaminsky and J. M. Mayer, *Inorganic Chemistry*, 2004, **43**, 5804-5815.
29. C. A. Grice, K. L. Tays, B. M. Savall, J. Wei, C. R. Butler, F. U. Axe, S. D. Bembenek, A. M. Fourie, P. J. Dunford, K. Lundeen, F. Coles, X. Xue, J. P. Riley, K. N. Williams, L. Karlsson and J. P. Edwards, *J. Med. Chem.*, 2008, **51**, 4150-4169.
30. B. Combourieu, P. Besse, M. Sancelme, J. P. Godin, A. Monteil, H. Veschambre and A. M. Delort, *Appl. Environ. Microbiol.*, 2000, **66**, 3187-3193.
31. R. Gao, L. Li, C. Xie, X. Diao, D. Zhong and X. Chen, *Drug Metab. Dispos.*, 2012, **40**, 556-567.

Chapter 5

Synthesis and Biological Evaluation of Benzimidazole Ketone Derivatives

5.1 Benzimidazole Ketones

As stated in previous chapters, Flubendazole (**1**), a ketone derivative of the benzimidazoles, served as the starting analogue for this project, with established activity against *C. neoformans* and an MIC value of 0.125 mg/L. Whilst **1** has good activity against *C. neoformans*, it possesses a very poor aqueous solubility profile (0.8 μM). In order to be used more effectively in clinical treatment solubility needs to be improved to allow for gut permeation. Flubendazole (**1**) is made commercially for its use in the veterinary clinic and as a fungicide, however very little is reported in the literature regarding its precise synthesis, or synthesis of its derivatives. This brings a further challenge in making compounds of this type. **1** has also been reported recently in the literature as exhibit a poor toxicity profile, which is mainly due to its mechanism of action at β -tubulin, which is present in both *C. neoformans* and humans. This causes gastrointestinal issues at the site of absorption and where intestinal cells are undergoing rapid mitosis, thus experiencing the toxicity effects of flubendazole more rapidly.¹⁻³

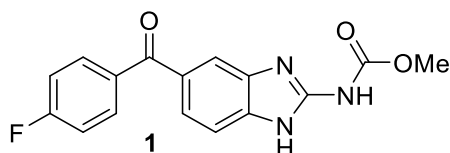


Figure 5.1. The commercially available therapeutic, Flubendazole. A ketone derivative of the benzimidazole class.

Knowing the challenges presented by developing new flubendazole analogues, means medicinal chemistry can be targeted to attempted to overcome these issues. With this in mind the aims of the ketone project were;

1. To develop new synthetic routes to generate new derivatives of the ketone class. This would allow for SAR exploration and better design of future analogues.
2. To understand whether selectivity for *C. neoformans* β -tubulin can be achieved allowing for a potentially reduced toxicity profile.
3. To improve aqueous solubility resulting in better absorption, allowing for better *in vivo* efficacy.

5.2 Ketone Discussion

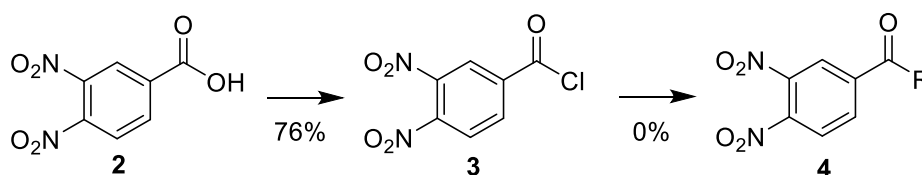
5.2.1 Synthesis

5.2.1.1 Previous Synthesis

Literature methods for the synthesis of flubendazole are somewhat limited. There is one key synthetic route used and this was attempted first for the initial analogues.

5.2.1.1.1 Friedel-Crafts Acylations

The initial synthetic route involved conversion of the commercially available 3,4-dinitrobenzoic acid (**2**) into the acid chloride derivative **3**, via widely reported SOCl_2 conditions, and this was carried out in a good yield of 76% (Scheme 5.1).⁴⁻⁷ Using standard Friedel-Crafts acylation conditions, whereby the catalyst aluminium chloride was used and the desired benzene derivative, installation of the ketone with the required R group was attempted.⁵ Apart from making the 4-F derivative, no other analogues were made as the *para* were the most favourable, due to electronic and steric effects. Analogues such as CN and OCF_3 are electron withdrawing, removing electron density away from the benzene ring, resulting in an inability to react in the electrophilic substitution reaction as the nucleophile, despite the acid chloride being an excellent electrophile.



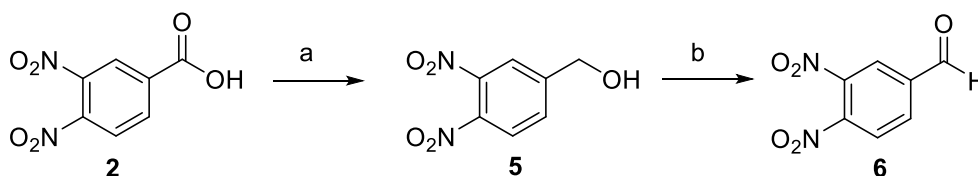
Scheme 5.1. The failed Friedel-Crafts acylation route that was initially employed for the synthesis of the ketone class of compound. *Reagents and Conditions:* (a) SOCl_2 (xs), DMF (cat.), 65 °C, 4 hours, 76% Yield; (b) AlCl_3 (1.0 eq.), ArX (1.0 eq.), DCM, reflux, 4 hours, no reaction.

A number of other Friedel-Crafts style routes were attempted over the course of the project, with the main issue being the necessity for the two nitrogen atoms on the benzene ring, in order for a ring closure to occur later. Main routes involved masking or protecting these nitrogen groups, or even omitting them and facilitating their later installation through *tert*-butylcarbamate Buchwald-Hartwig chemistry, but all of these were unsuccessful.⁸ This is predominantly due to the directing effects of the amine/nitro substituents preventing the reaction occurring in the desired position and Friedel-Crafts acylation reactions often presenting with reduced yields.

5.2.1.1.2 Weinreb Amide – Grignard Chemistry

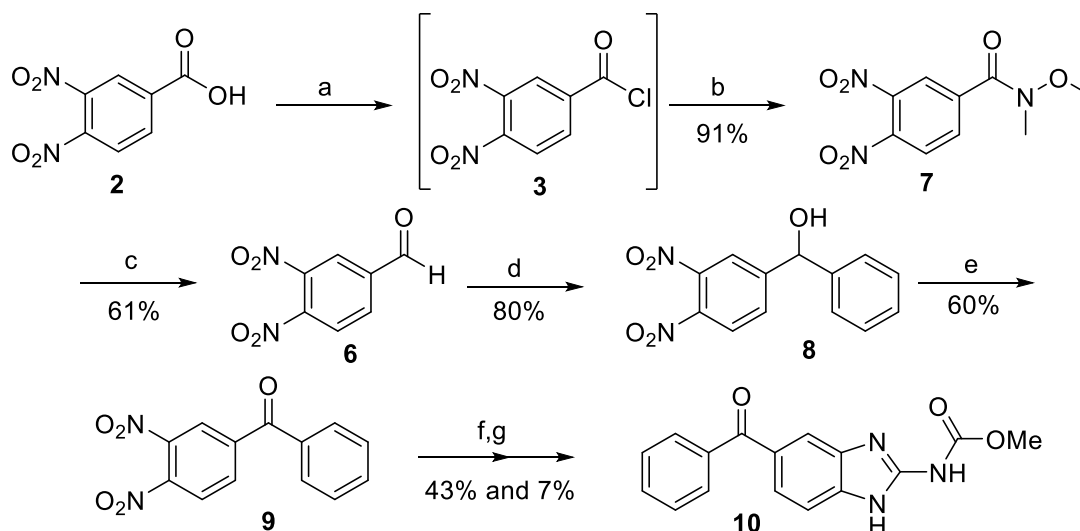
Generation of biaryl ketones is commonly carried out using the addition of a Grignard reagent into an aldehyde. This produces an alcohol, which can then be re-oxidised to the ketone using an oxidising

agent such as pyridinium chlorochromate (PCC) or MnO_2 .⁹⁻¹¹ This route was also attempted. 3,4-dinitrobenzaldehyde (**6**) is not commercially available and neither is the precursor alcohol, so we started with 3,4-dinitrobenzoic acid (**2**) (Scheme 5.2). This was reduced using borane dimethylsulfide, to give the intermediate alcohol (**5**), as reported in the literature.^{11,12} MnO_2 was then used to attempt to oxidise the alcohol to the aldehyde, however there was no conversion of **5** to the aldehyde, as would be observed via a less polar spot on the TLC plate.⁹



Scheme 5.2. Reagents and conditions: (a) $\text{BH}_3 \cdot \text{SMe}_2$ (2.0 eq.), THF, 0 °C to RT, hours, (b) MnO_2 (10 eq.), THF, RT, Overnight, no reaction.

An alternative to this route was to generate a Weinreb Amide (Scheme 5.3). This involved the generation of the 3,4-dinitrobenzoyl chloride (**3**) using thionyl chloride and then coupling with dimethylhydroxylamine hydrochloride to give the desired amide (**7**).^{7,13-15} Initially, direct coupling of a Grignard reagent was attempted with **7**, as reported in the literature, however this resulted in no product formation. Therefore, the Weinreb amide was reduced using DIBAL to give the aldehyde (**6**), which was reacted with the Grignard reagent to give an alcohol (**8**). Subsequent oxidation to yield the ketone (**9**) was followed by SnCl_2 reduction and ring closure to give the desired final benzimidazole compound (**10**).

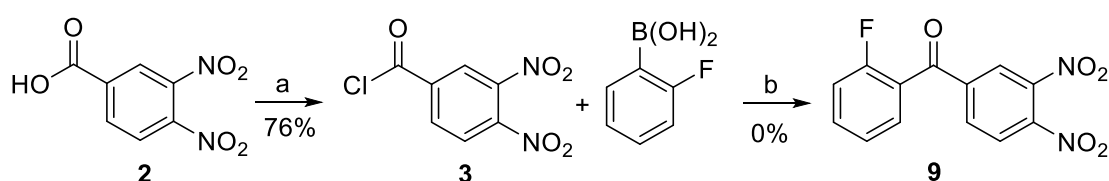


Scheme 5.3. Reagents and conditions: (a) thionyl chloride (xs), 65 °C, 4 hours; (b) *N,O*-dimethylhydroxylamine hydrochloride (1.1 eq.), NEt_3 (1.5 eq.), DCM, 0°C to room temperature, overnight (91% yield); (c) DIBAL (3.0 eq.), THF, -20 °C to room temperature, 1 hour (61% yield); (d) Mg (10 eq.), I_2 , bromobenzene derivative (1.1 eq.), 0°C to reflux, 1 hour (80% yield); (e) PDC (1.5 eq.), DCM, room temperature, 4 hours (60% yield). (f) H_2 , 10% Pd/C, ethanol, room temperature, overnight (48% yield), 1,3-Bis(methoxycarbonyl)-2-methyl-2-thiopseudourea (1.0 eq.), DME (0.55 M), methanol (2.2 M), sealed tube, 65 °C, overnight (7 % yield).

This synthetic route only worked for one the 3-F ketone analogue. It required a number of repeats of the route to obtain enough compound for the final step. It also contains a number of steps in comparison to the routes for other templates.

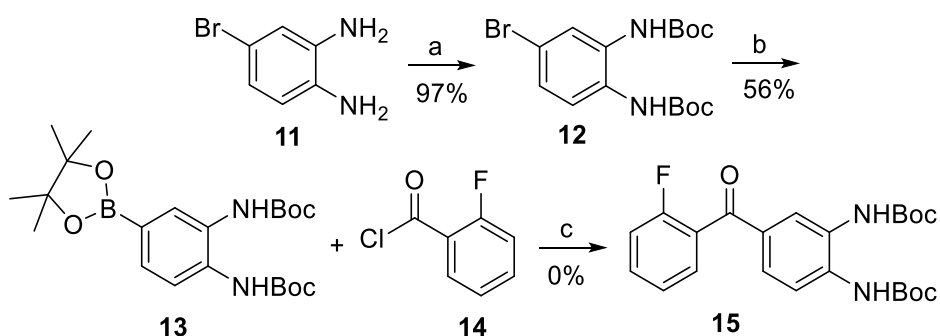
5.2.1.1.3 Initial Suzuki Chemistry Routes

Literature investigation uncovered that a ketone could be formed from a Suzuki cross coupling reaction between a ketone and an acid chloride (Scheme 5.4).^{16, 17} Initially, the route involved synthesising the already established 3,4-dinitrobenzoyl chloride (**3**), with the desired boronic acid, however no product (**9**) was observed. A test reaction using 4-fluorobenzoyl chloride and 4-chlorobenzeneboronic acid, yielded the product in poor yield, along with an ester product.



Scheme 5.4. Reagents and conditions: (a) SOCl_2 (xs), 65 °C, 4 hours, 76% Yield; (b) Pd(PPh₃)₂Cl₂ (0.10 eq.), K₃PO₄·H₂O (1.5 eq.), toluene, 110 °C, overnight, no reaction.

Next, we chose to synthesise the boronic ester **13**, due to the high commercial availability of derivatised acid chlorides (**14**) (Scheme 5.5). The reaction involved using 5-bromo-benzenediamine (**11**) and *tert*-butyl carbamate protection of the primary amines to give **12**. Carrying out a Suzuki-Miyaura Borylation using bis(pinacolato)diboron yielded **13**, which was then employed in the Suzuki coupling step, however again this yielded no results.¹⁸

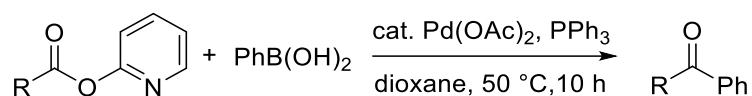


Scheme 5.5. Reagents and conditions: (a) Di-*tert*-butyl dicarbonate (2.4 eq.), ethanol, room temperature, Overnight, 97% yield; (b) Pd(PPh₃)₂Cl₂ (0.20 eq.), bis(pinacolato)diboron (6.0 eq.), KOAc (6.0 eq.), toluene, 100 °C, overnight (56% yield); (c) Pd(PPh₃)₂Cl₂ (0.10 eq.), K₃PO₄·H₂O (1.5 eq.), toluene, 100 °C, overnight.

It is believed for both of the routes described, that the acid chloride was not reactive enough and the reaction may be more substrate specific, so an alternative route was envisaged.

5.2.1.2 Current Synthesis

Due to the lack of success with Freidel-Crafts Acylation and other Suzuki chemistry routes, as well as the long synthesis for the Weinreb Amide, finding a new route was imperative.



Scheme 5.6. Suzuki couplings using activated esters to generate ketones.¹⁹

Literature investigation led to the discovery of a pyridine activating group, which had been used in a Suzuki style reaction, albeit with very simplified analogues (Scheme 5.6). Four ester analogues were synthesised and evaluated in the Suzuki reaction based on reaction yields. All four of these analogues showed similar electronic properties, but two possessed additional methyl groups on the pyridine ring or movement of the pyridine nitrogen (Figure 5.2).¹⁹

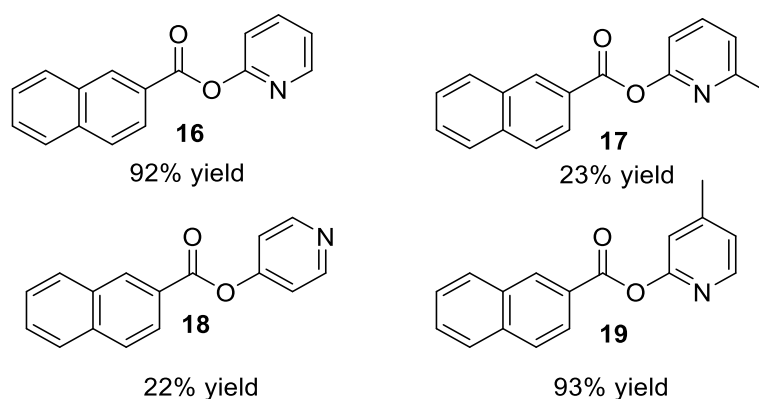
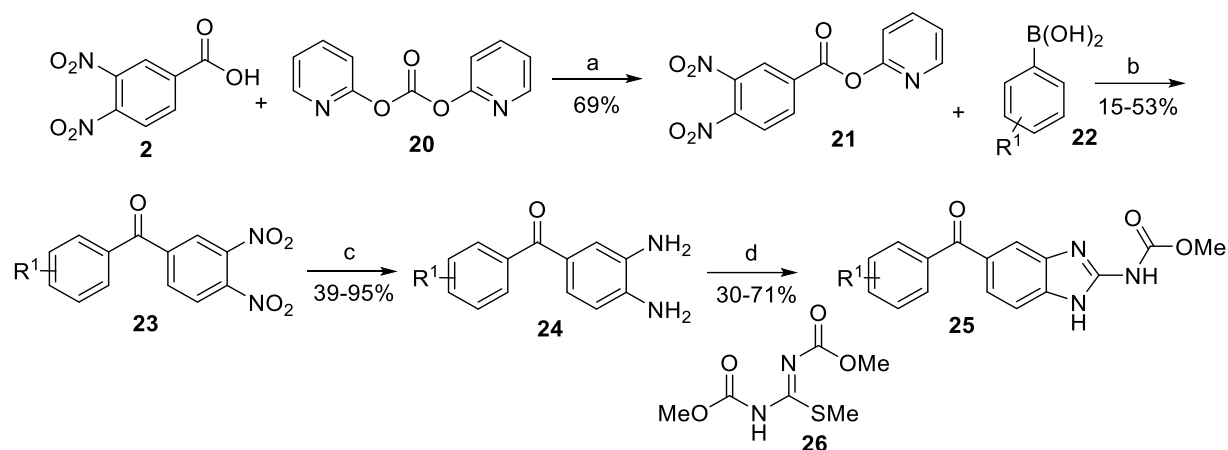


Figure 5.2. Structure and yields of different pyridyl analogues used in the Suzuki cross coupling.

The 2-pyridine ester **16** gave an excellent yield, as does its 4-methylated derivative compound **19**. However, despite being electronically similar, compounds **17** and **18** showed a sharp reduction in yield. **17** shows the 2-methylated pyridine ring, which is proposed to be sterically blocking the pyridine nitrogen from co-ordinating to the palladium catalyst, thus reducing yield. **18** shows the movement of the pyridine nitrogen around the ring, into a position that cannot easily co-ordinate to the palladium catalyst and still carry out the coupling reaction.¹⁹

Use of an activated pyridine ester under Suzuki coupling conditions was attempted for the synthesis of the benzimidazole ketones, with synthetic route and yields reported below (Scheme 5.7 and Table 5.1).



Scheme 5.7. Reagents and conditions: (a) DMAP (0.1 eq.), DCM, room temperature, overnight (69% yield); (b) Pd(PPh₃)₄ (0.1 eq.), dioxane, sealed tube, 80 °C, overnight (15 – 53% yield); (c) SnCl₂ (10 eq.), ethanol, 65 °C, overnight, (39 – 95% Yield); (d) 1,3-Bis(methoxycarbonyl)-2-methyl-2-thiopseudourea (**26**) (1 eq.), acetic acid (2 M), methanol (0.4 M), sealed tube, 65 °C, overnight (30 – 71% yield).

Table 5.1. Percentage yields obtained for all compounds created within the ketone template, including intermediates and final products.

	R ¹	Step B % Yield (23)	Step C % Yield (24)	Step D % Yield (25)
25a	2-F	45	60	50
25b	2-F, 4-F	17	94	49
25c	4-Me	53	39	50
25d	4-Cl	29	62	71
25e	4-OMe	48	71	45
25f	3-OMe	15	76	17
25g	4-OCF ₃	29	50	36
25h	2-F, 5-F	23	88	53
25i	2-F, 3-F	19	95	46

5.2.1.2.1 Synthesis of Activated Pyridyl Ester

Firstly, we needed to synthesise a pyridine ester derivative (**21**) in order to trial this reaction. Initially, due to concerns with the double reduction of the nitro groups, 4-amino-3-nitrobenzoic acid was used, coupling with 2-hydroxypyridine using both EDC.HCl and HATU as coupling reagents, but neither condition produced the desired ester. This was thought to be a two-fold issue, whereby the carboxylic acid has proven to be quite unreactive when it has been employed in other reactions within the group. Secondly the 2-hydroxypyridine shows reduced reactivity as it is known to tautomerise (Figure 5.3A). This renders the hydroxyl groups less likely to be involved in nucleophilic attack, and 2 hydroxypyridine is also known to form dimers, which may further reduce reactivity (Figure 5.3B).^{20, 21}

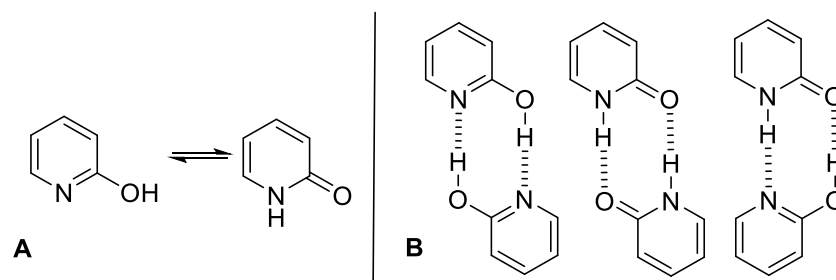


Figure 5.3. A. 2-hydroxypyridine tautomerisation to give pyridin-2(1H)-one. B. 2-hydroxypyridine tautomer dimers.

An alternative route involved using di(pyridin-2-yl) carbonate (**20**) and coupling with 3,4-dinitrobenzoic acid (**2**), which has been used in a number of synthetic routes during the project.²²⁻²⁴ The use of DMAP further accelerated this coupling process to give the desired product in around 56% yield. **21** was characterised by ¹H NMR noting the additional pyridine peaks observed when the ester is generated. This procedure involved a work-up which did result in some loss of product due to decomposition of the activated ester back to the acid, due to its high susceptibility to nucleophilic attack. This did result in some acid impurity in the product, however purification of **21** proved to be unsuccessful via column chromatography and it was easier to carry through crude into the next Suzuki coupling step. Furthermore, the 3,4-dinitrobenzoic acid (**2**) does not react in the next step, and can easily be removed.

5.2.1.2.2 Pyridyl Ester Suzuki Coupling Route

The next step involved a palladium mediated Suzuki style coupling between the activated ester (**21**) and a chosen boronic acid (**22**). It is proposed by Tatamidani *et. al.* that this reaction occurs via initial coordination of palladium to the pyridine nitrogen (**A**) (Figure 5.4). The palladium can then undergo attack on the carbonyl of the of the activated ester (**A**) to generate an unstable tetrahedral intermediate (**B**). This collapses to reform the carbonyl and an acylpalladium species (**C**), then undergoes transmetalation, with an boronic acid to give (**D**). Finally, a reductive elimination occurs, which produces the desired ketone (**23**), and regenerates the catalyst.

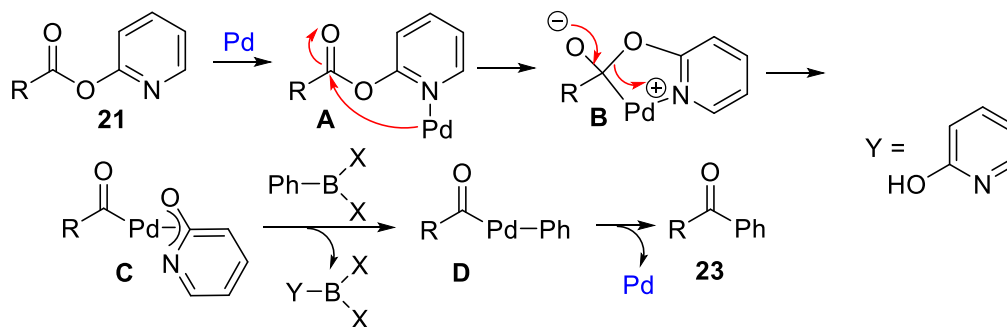


Figure 5.4. A Suzuki palladium catalysed reaction, following coordination, transmetalation and reductive elimination to give the desired ketones (**23**).

This reaction provided **23**, using only two synthetic steps and offered a moderately easy purification of the compound. However, these ketones were synthesised in variable yields (15 – 43 %). Firstly, remaining starting material from the first step as well as degradation of the activated ester, may have resulted in a smaller amount of product formation. To improve yields a number of changes to the reaction conditions were attempted (Table 5.2). This included placing the reactions in a sealed tube, rather than a round bottom flask fitted with a reflux condenser. The sealed tubes appeared to offer little to no improvement in yield, however allowed for a number of coupling reactions to be run in parallel, allowing for faster synthesis but also to allow more rapid use of the activated ester starting material in order to reduce its degradation upon storage. Furthermore, it was noted that in the paper, they used Pd(OAc)₂ and PPh₃, thus generating the catalyst in the reaction, rather than using the Pd(PPh₃)₄, initially used for the first few palladium couplings. However no change in yield was observed and it was easier to employ Pd(PPh₃)₄ in the reaction (Table 5.2).

Table 5.2. Altering the Suzuki condition on the *o*-F substrate revealed the a sealed tube and Pd(PPh₃)₄ showed slightly better yields and an ease of reaction set-up.

Entry	Catalyst	Reaction Container	Yield %
a	Pd(PPh ₃) ₄	Round bottom flask	43
b	Pd(PPh ₃) ₄	Sealed Tube	45
c	Pd(OAc) ₂	Sealed Tube	41

This showed success for a number of ketones within this project. The products were characterised by NMR, with ¹³C NMR proving to be the most useful, as the presence of a peak at around 190 ppm indicates the carbon of the ketone functionality has been installed. One compound of particular interest that was made was a morpholine derivative (**26**), this was successfully synthesised using these reaction conditions, however was only made in small amounts, so not enough was produced to carry through to the final ring closure reaction, and there was not enough time to complete a scale up (See Appendix, Figure 4A).

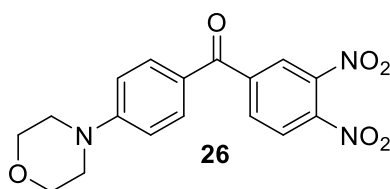


Figure 5.5. The morpholine derivative synthesised.

5.2.1.2.3 Tin (II) Chloride Dinitro reduction

There were concerns surrounding the success of the dinitro reduction. In the literature they discussed doubling equivalents of tin (II) Chloride in the reaction to ensure full reduction of the nitro groups. Ten equivalents were employed in the reaction and this resulted in an excellent yield being obtained for

the majority of the ketone compounds and generally better than other templates.²⁵⁻²⁸ A reaction was also tested using 5 eq of tin (II) chloride as seen with the other templates. Given that at these concentrations the tin was still in excess, there was potential for this to work whilst reducing tin (II) chloride use. However, after overnight reflux this resulted in incomplete reduction and an additional 5 eq of the tin (II) chloride was added, which ensured reaction completion.

¹H NMR analysis was used to confirm these compounds given the substantial up-field shift of the protons on the diamine core. This is due to the loss of two powerful electron withdrawing nitro groups and their conversion into two electron donating groups, causing this up-field shift (Figure 5.6) (See Appendix, Figure 4B).

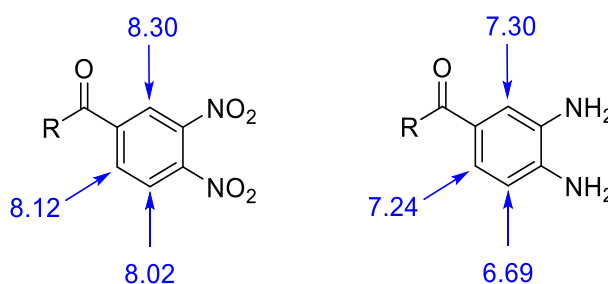


Figure 5.6. The ¹H NMR spectra for these the diamine shows a significant up-field shift for the protons on the rings bearing the diamine.

5.2.1.2.4 Acid Mediated Ring Closure to Establish the Benzimidazole Core

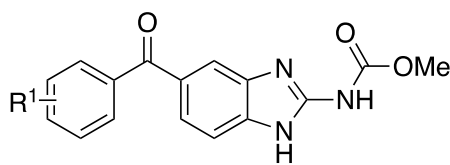
The final acid mediated ring closure steps occurred in variable yields for this reaction with the ketone (30 – 71%). Unlike other templates the ketones underwent ring closure reactions, and the precipitated solid was isolatable, even on very small-scale reactions, will the smallest scale observed being 15 mg. However, for these analogues obtaining full final data wasn't always easy due to a very small amount of product being formed. It was often difficult to get a full characterisable ¹³C NMR spectra, whereby all carbons, particularly quaternary carbons were actually visible (See Appendix, Figure 4C - E).

5.2.2 Biological Activity

Biological testing was carried out as stated in Section 3.2.2, Chapter 3. Data given in Table 5.3.

Minimum inhibitory testing was carried out on these analogues and it was found that these compounds possessed similar activity to the starting compound flubendazole (**1**) (0.125 mg/L). *Para* substituted derivatives appear to provide the best activity (**1**, **25c**, **25d** and **25e**), with *ortho* and *meta* derivatives giving similar values. As with all other templates the addition of an OCF₃ group (**25g**) results in a complete loss of activity. Double substitution of the fluorine on the ring also results in a drop in activity. When the substitution pattern is 2,4 as seen in compound **25b**, some activity is still maintained, giving a value of 1 mg/L, however the 3,5 compound (**25k**) shows a complete lack of activity.

Table 5.3. The ketone class of compound show generally good MIC testing data. **Green** – good - 0.015 – 0.25 mg/L, **yellow** – acceptable - 0.5 – 4 mg/L, **red** – poor - >4 mg/L. * j and k made by Dr Emma Shore. ATD – Awaiting Testing Data.



Compound	R ¹	MIC (mg/L)
1	4-F	0.125
25a	2-F	1
25b	2-F, 4-F	1
25c	4-Me	0.25
25d	4-Cl	0.25
25e	4-OMe	0.125
25f	3-OMe	0.5
25g	4-OCF ₃	>4
25h	2-F, 5-F	ATD
25i	2-F, 3-F	ATD
25j	3-F	1
25k	3-F, 5-F	>4

5.2.3 DMPK

5.2.3.1 Predicted DMPK

Predicted DMPK data for the ketone class showed overall favourable properties, apart from aqueous solubility showing no further improvement (Table 5.4). Log D for these compounds is lower than 4 with the majority below 3.5, which shows these compounds should have a good balance between solubility and permeability, meaning the compounds should have the best compromise of lipophilicity for oral absorption and cell membrane permeation. These compounds all show excellent values for metabolism, with all compounds highlighted in green. However, like the thiol class of compound, we need measured data to confirm that the predicted clearance values are identifying the reduction of the ketone as a possible metabolic route, especially as metabolites of this kind have been identified in the literature.

Table 5.4. Predicted DMPK data for the ketone class of compounds show good metabolic properties overall, but solubility is poor. Values are colour coded with a traffic light system according to how good or bad a particular value is. **Green** – good, **amber** – acceptable/medium, **red** – poor.

	LogD _{7.4}	CLogP	Aqueous Solubility (μM)	Rat Heps CLint (μl/min/mg)	Human Mics CLint (μl/min/mg)	MPO
25a	2.68	2.80	2.4	14	15	5.1
25b	2.89	2.94	1.0	11	13	5.1
25c	3.27	3.56	1.9	20	28	4.6
25d	3.39	3.82	0.5	15	20	4.4
25e	2.75	3.03	1.6	12	12	5.1
25g	3.73	4.14	0.4	7	9	4.1

Stardrop predictions were carried out for these compounds (Figure 5.7) and we observed that they are mostly metabolised by CYP3A4 and CYP2C9 as reported in the literature.²⁹ There is also the usual metabolic hit-point on the carbamate, metabolism of the aryl ring, and for the 4-OMe derivative **25e**, there is oxidation of the methoxy group. Interestingly, Stardrop does not indicate any metabolism of the ketone to the hydroxyl metabolite.^{30,31} This was a concern as the hydroxyl metabolite is known to show reduced efficacy. However, based on the Stardrop predictions and the measured and predicted DMPK data, this may not happen significantly or quickly, allowing for more efficacious concentrations of the drug to remain.

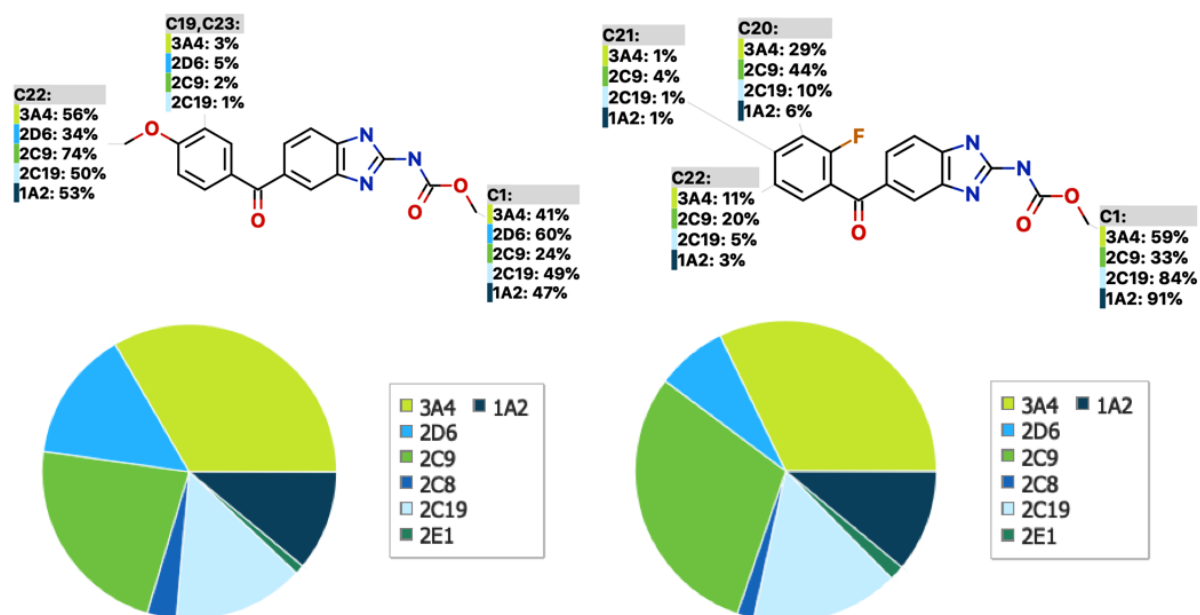


Figure 5.7. Metabolism predictions for two compounds from the ketone series. Calculations run on Stardrop.

5.2.3.2 Measured DMPK

The measured DMPK shows some differences versus what was predicted. Log D values are similar to both the ether and thiol templates, and show a lipophilicity that should be suitable for CNS penetration. As observed with other templates, the aqueous solubility is still very low, apart from **25g** which contains a OCF_3 group and may be an anomalous result. However, the biggest change observed is for the measured DMPK values which are larger than predicted for some of the analogues (Table 5.5). Compound **25a**, which is a 2-F derivative shows better DMPK than flubendazole (**1**) which is a 4-F derivative. It is believed that the 2-F is potentially acting as a steric block reducing metabolism at the carbonyl group.

Table 5.5. Measured DMPK data for the ketone class of compounds show good metabolic properties overall, but poorer clearance compared with other templates. Values are colour coded with a traffic light system according to how good or bad a particular value is. Green – good, amber – acceptable/medium, red – poor.

Compound	LogD _{7.4}	Aqueous Solubility (μM)	Rat Heps CLint (μl/min/mg)	Human Mics CLint (μl/min/mg)
1	2.9	0.8	39	44
25a	2.8	3	10	47
25d	3.6	2	169	71
25e	3	0.3	15	19
25g	3.8	145	24	8

Measured and predicted values were plotted against each other to understand if there was any correlation between values (Figure 5.8). Generally across the ketone class, there is good correlation

between measured and predicted values. The log D values show excellent correlation with an $R^2 = 0.98$, with numbers being almost identical. Aqueous solubility shows a negative correlation; however this was due to the 4-OCF₃ derivative (**25g**) having a much larger value than predicted. Rat hepatic clearance shows a generally positive correlation, however the measured clearance of the of the 4-Cl derivative (**25d**) was higher than expected and affects the correlation. Finally, the human microsomal clearance values show excellent correlation with $R^2 = 0.98$, and whilst the numbers aren't identical and are general slightly higher for the measured DMPK values, the increase or decrease observed for each compound is consistent. This could be used to predict whether a compound would likely increase or decrease this metabolism. This is only a small sample size, so more measured DMPK values would be required in order to further investigate the correlation between measured and predicted DMPK properties, but can be used as a reasonable guide for compound selection.

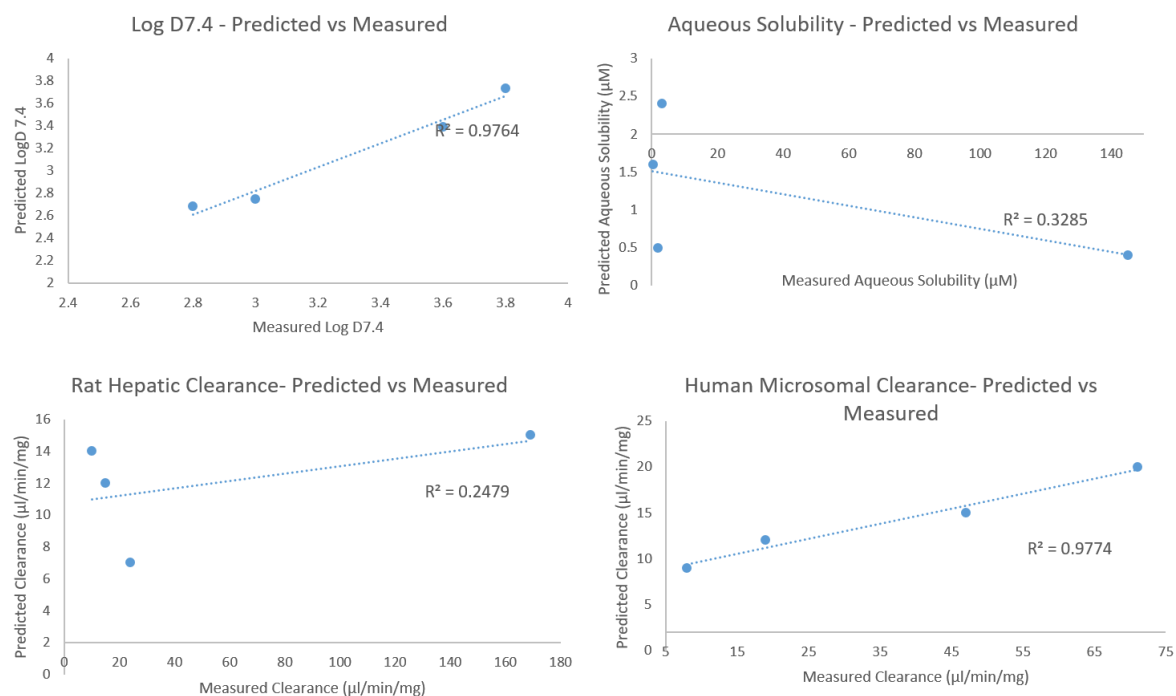


Figure 5.8. Each of the parameters obtained from measured DMPK testing was plotted against the numbers obtained from predicted DMPK analysis.

5.2.4 *In Vivo* Mouse Data

Flubendazole, the starting compound for this project, is a commercially available drug and thus was an ideal candidate for *in vivo* testing. A number of *in vivo* tests were carried out on flubendazole (**1**) assessing activity, choice of vehicle, administration route and dose. *In vivo* work was carried out by Suzy Gore.

From the data in Figures 5.9 – 5.11, we can see that flubendazole has excellent *in vivo* activity, which is observed through a significant log drop in fungal density in the brain, when compared with the

control and the other templates previously discussed. Furthermore, flubendazole was tested subcutaneously and orally at 150mg/kg and no significant difference between the dosing method was observed in terms of activity (Figure 5.9).

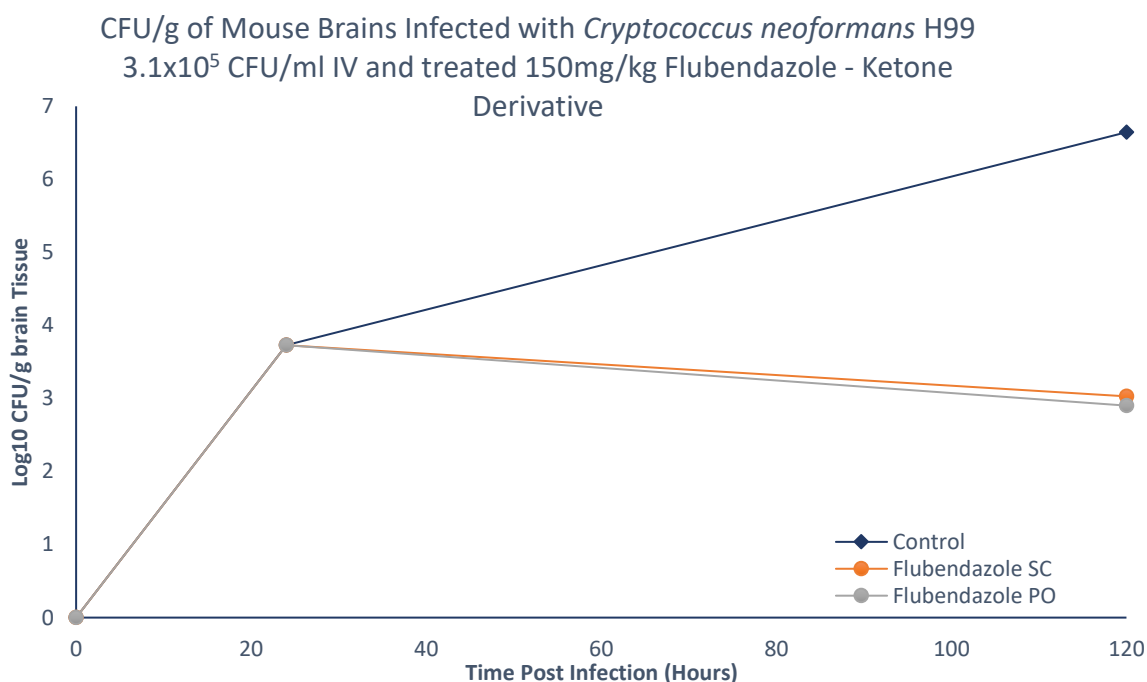


Figure 5.9. Flubendazole (**1**) was testing *in vivo* using 10% DMSO, 10% Tween and 80% PBS as the vehicle. Flubendazole shows a significant drop in fungal density in the brain, with similar results being observed, regardless of route of administration.

Different routes of administration were also investigated further along with dosage (Figure 5.10). The dose range chosen was 25 mg/kg to 150 mg/kg was chosen, with 150mg/kg chosen as the maximum due to higher risk of toxicity. Furthermore, above this dose solubility limitations mean the compound would precipitate out of solution. Figure 5.10 shows subcutaneous dosing at a range of concentration, whereby the drug is given once a day (q24) at four doses and shows no significant decrease in efficacy, even as the dose is lowered, with only a slightly smaller drop in fungal density observed at the lower dose of 25 mg/kg.

Interestingly, if we compare the once every 48-hour dose (q48), this showed a similar decrease in fungal density as dosing every 24 hours, even when the same dose of 150 mg/kg was used. Finally, **1** was also administered as a single dose, and whilst it showed the least significant drop in fungal density of all the doses tested, it still exhibited a significant drop in fungal density when compared with the control and with other analogues in the project, reducing fungal density to the same level after 24 hours of growth. This provides a potential opportunity for single dose, subcutaneous administration. This is attractive prospect given the need for novel antifungal drugs in areas with poor medical infrastructure.

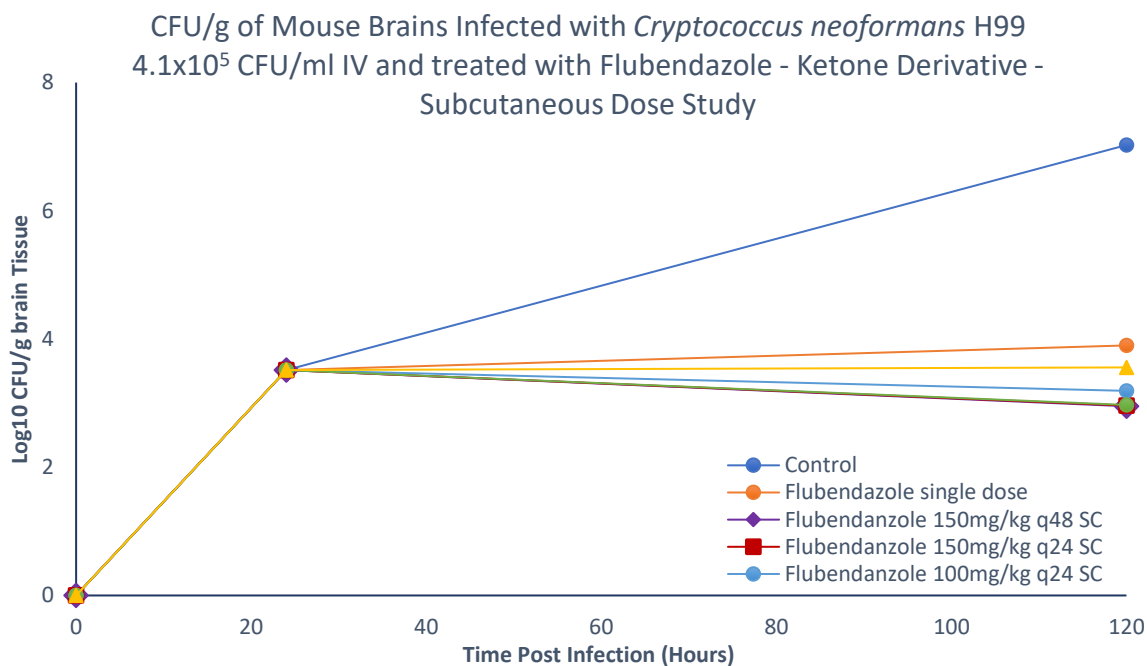


Figure 5.10. Flubendazole was tested subcutaneously at a range of doses and regimens, with no significant difference in fungal density being observed when dosing once a day at a range of concentrations. The single dose administration didn't reduce fungal density as much as the other examples, but still showed a significant decrease.

Figure 5.11 displays the dosage studies carried out when flubendazole was tested orally using 10% DMSO, 10% Tween and PBS as the vehicle. Oral dosing appeared to show a similar magnitude of decrease in fungal density as observed with subcutaneous administration. Oral administration showed no significant difference in efficacy when dosage was decreased from 150 mg/kg to 25 mg/kg once daily, with 25 mg/kg offering a substantial fungal density drop, but due to lower dose may prevent some of the toxicity issues present with benzimidazoles.

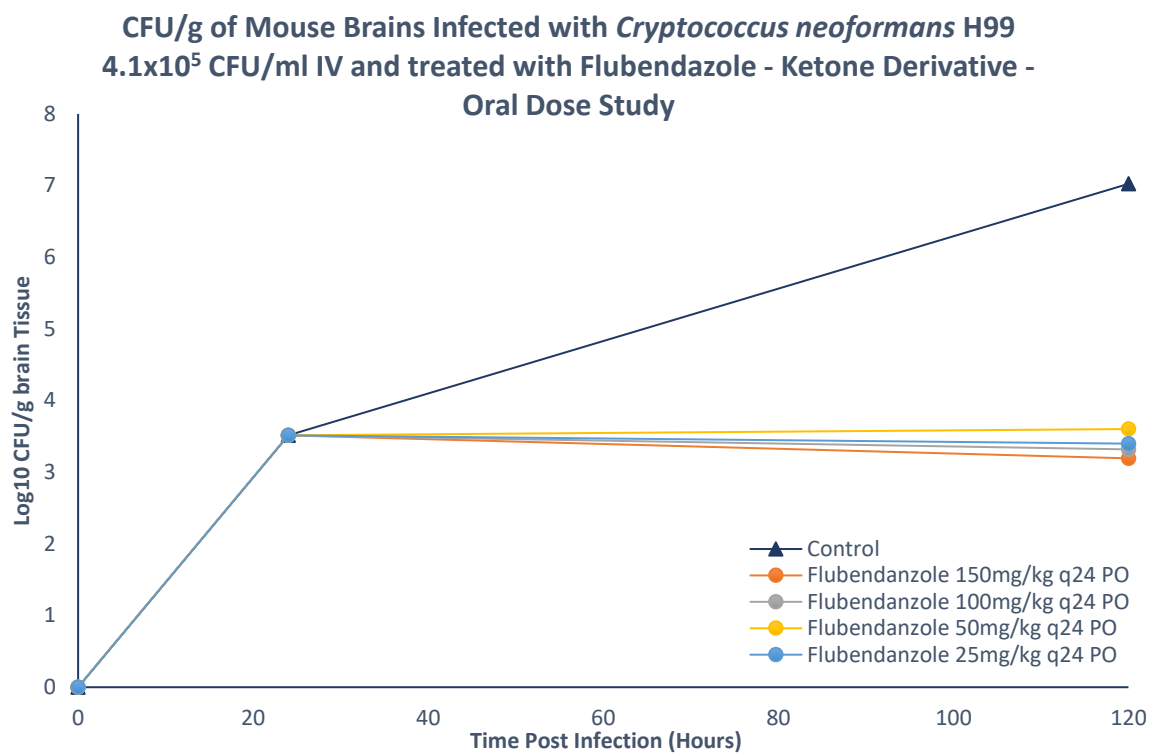


Figure 5.11. Flubendazole was extensively tested *in vivo* due to be the starting compound for the project and ready accessibility to commercially available material. The results show that efficacy of flubendazole *in vivo* is highly dependent on the vehicle used.

5.3 Conclusion

Derivatives of flubendazole (**1**) were important to make given its precedence as a medicinal compound. A number of synthetic routes were tried, with a new Suzuki based route developed and implemented. Biological data shows that these compounds have sub-optimal activity (0.125 - >4 mg/L) when compared the thioether and ether class (0.015 - >4 mg/L). Derivatives in the *para* position show better activity, apart from **25g**, which is a 4-OCF₃ derivative. Furthermore, the analogues synthesised have shown no improvement in solubility when compared with **1**. Metabolic clearance values however are generally improved when compared with flubendazole.

5.4 Future Work

Synthesis of other derivatives is important in order to allow for better development of an SAR profile (Figure 5.12). This includes different carbamate derivatives, different substituents in the R¹ position, substitution on the benzimidazole core and furnishing the aryl ring with a solubilising group, similar to the active morpholine derivative observed in Chapter 4.

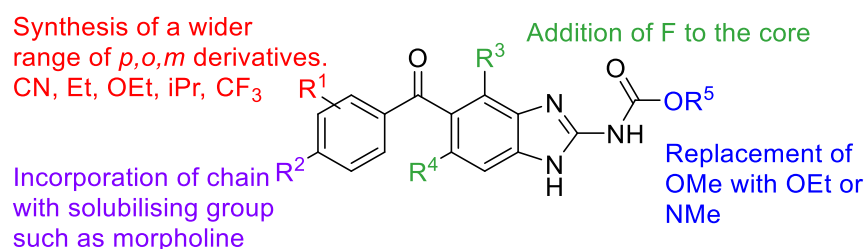


Figure 5.12. Design of future analogues to improve both activity and solubility.

Further work is also being carried out to look at the selectivity of these compounds. Work is ongoing to isolate the *C. neoformans* β -tubulin protein for use in an in-house selectivity assay. The human protein is not available, so porcine β -tubulin will be used instead as this is reported to be similar in structure to human β -tubulin. This will allow us to identify if flubendazole and other analogues are selective for *C. neoformans* β -tubulin over human β -tubulin, which may help to reduce toxicity.

5.5 Experimental

5.5.1 General Experimental Details

For general experimental details please see Section 3.5.1, Chapter 3. For synthesis of dimethyl ((methylthio)methylene)dicarbamate please see Section 3.5.2, Chapter 3.

5.5.1.1 HPLC

Flow rate 1 ml/min for 15 minutes using MeCN/Water with compounds dissolved in methanol. UV detector recorded signals at 254 nm. **HPLC Method A:** min, gradient: 2% MeCN hold to 1 min, 2-98% MeCN in 11 min, then hold at 98% MeCN to 15 min.

General Procedure A – Ketone Suzuki Coupling

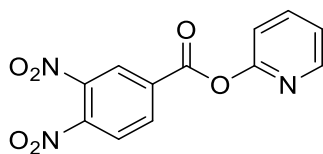
To a sealed tube at room temperature was added pyridin-2-yl 3,4-dinitrobenzoate (**21**) (1.0 eq.), the desired boronic acid (2.0 eq.), dioxane and Pd(PPh₃)₄ (0.1 eq.) and the reaction heated to 80 °C overnight. The reaction was then cooled to room temperature and diluted with ethyl acetate, washed with saturated aq. NaHCO₃ solution, water, brine, dried over magnesium sulphate and concentrated. The crude product was then purified via column chromatography, eluting with 100% *n*-hexane, increasing up to a maximum of 20% ethyl acetate in *n*-hexane.

General Procedure B – Dinitro SnCl₂ Reduction

To a flask at room temperature was added the desired (3,4-dinitrophenyl)(phenyl)methanone derivative (1.0 eq.), ethanol (0.15 M) and tin (II) chloride (10 eq.) and the reaction heated to 65 °C overnight. The reaction was then cooled to room temperature, concentrated, basified to pH 10 using 25% NaOH solution and the precipitate filtered off. The filtrate was then washed with water, brine, dried over magnesium sulfate, concentrated. The product was purified via column chromatography eluting with 50% ethyl acetate in *n*-hexane, increasing to 100% ethyl acetate.

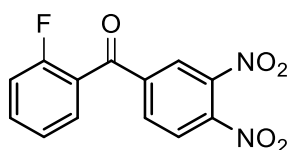
General Procedure C – Acid Mediated Ring Closure

To a flask at room temperature was added (3,4-diaminophenyl)(phenyl)methanone derivative (1.0 eq.), acetic acid (2 M), methanol (0.4 M), dimethyl ((methylthio)methylene)dicarbamate (1.0 eq.) and the reaction heated to 65 °C overnight. The reaction was cooled to room temperature and the resulting solid filtered using diethyl ether to give the final product.

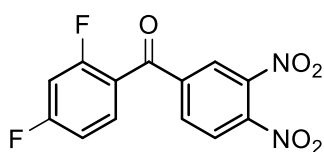
5.5.1.1 Synthesis of pyridin-2-yl 3,4-dinitrobenzoate (**21**)

To a flask at room temperature was added 3,4-dinitrobenzoic acid (**2**) (1 eq.), dichloromethane, di(pyridin-2-yl) carbonate (**20**) (1 eq.) and DMAP (0.1 eq.) and the reaction stirred at room temperature overnight. Reaction was then concentrated, diluted with ethyl acetate, washed with NaHCO₃, water, brine, dried over magnesium sulfate and concentrated. The product (**21**) was then continued crude into the next reaction (1.38 g, 69 % yield) as a cream solid. ¹H NMR (400 MHz, CDCl₃) δ 8.27 (d, 1H, *J* = 1.3 Hz), 8.10 (dd, 1H, *J* = 8.1 & 1.3 Hz), 8.02 (d, 1H, *J* = 8.1 Hz), 7.80 (d, 2H, *J* = 8.9 Hz), 7.03 (d, 2H, *J* = 8.9 Hz), 3.93 (s, 3H). ¹³C NMR (100 MHz, CDCl₃) δ 190.6, 164.5, 147.9, 143.0, 133.9, 132.7, 130.5, 127.8, 125.9, 125.5, 114.4, 55.6. HRMS: (Cl⁺, CH₄) *m/z* calculated for C₁₄H₁₁N₂O₆: 303.0612. Found [M+H]⁺: 303.0623 (Diff -3.86 ppm).

5.5.1.2 Synthesis of (3,4-dinitrophenyl)(phenyl)methanone Derivatives

(3,4-Dinitrophenyl)(2-fluorophenyl)methanone (23a)

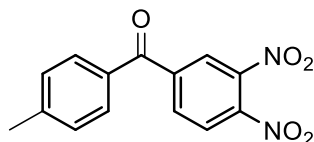
General Procedure A – Employed 2-fluorophenylboronic acid to give the title compound (**23a**) (0.14 g, 45% yield) as a white solid. ¹H NMR (400 MHz, CDCl₃) δ 8.34 (s, 1H), 8.16 (d, 1H, *J* = 8.3 Hz), 8.01 (d, 1H, *J* = 8.3 Hz), 7.71 – 7.67 (m, 2H), 7.39 – 7.37 (m, 1H), 7.24 – 7.21 (m, 1H). ¹³C NMR (100 MHz, CDCl₃) δ 189.2, 160.2 (d, *J* = 253.3 Hz), 149.5, 144.9, 141.7, 135.5 (d, *J* = 9.5 Hz), 134.0 (d, *J* = 1.9 Hz), 131.3 (d, *J* = 2.6 Hz), 125.8 (d, *J* = 2.0 Hz), 125.3 (d, *J* = 3.5 Hz), 124.5, 124.4 (d, *J* = 13.8 Hz), 116.8 (d, *J* = 21.3 Hz). HRMS: (Cl⁺, CH₄) *m/z* calculated for C₁₃H₈FN₂O₅: 291.0412. Found [M+H]⁺: 291.0425 (Diff - 4.68 ppm).

(2,4-Difluorophenyl)(3,4-dinitrophenyl)methanone (23b)

General Procedure A – Employed 2,4-difluorophenylboronic acid to give the title compound (**23b**) (0.073 g, 17% yield) as a yellow oil. ¹H NMR (400 MHz, CDCl₃) δ 8.32 (t, 1H, *J* = 1.5 Hz), 8.13 (dt, 1H, *J* =

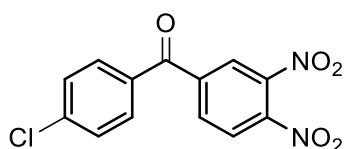
8.2 & 1.5 Hz), 8.01 (d, 1H, $J = 8.2$ Hz), 7.76 – 7.73 (m, 1H), 7.13 – 7.11 (m, 1H), 6.99 – 6.66 (m, 1H). HRMS (ES+) m/z $C_{16}H_{12}F_2N_3O_3$ Found 332.0840, Expected 332.0847 (Diff = -2.0 ppm).

(3,4-Dinitrophenyl)(*p*-tolyl)methanone (23c)



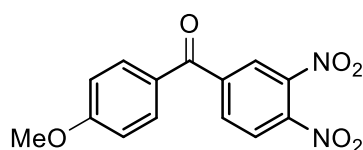
General Procedure A – Employed 4-methylphenylboronic acid to give the title compound **(23c)** (0.10 g, 53% yield) as a brown oil. 1H NMR (400 MHz, $CDCl_3$) δ 8.30 (d, 1H, $J = 1.7$ Hz), 8.12 (dd, 1H, $J = 8.2$ & 1.7 Hz), 8.02 (d, 1H, $J = 8.2$ Hz), 7.70 (d, 2H, $J = 7.9$ Hz), 2.48 (s, 3H). ^{13}C NMR (100 MHz, $CDCl_3$) δ 191.7, 145.5, 144.3, 142.6, 141.2, 134.2, 132.5, 130.3, 129.8, 136.1, 125.2, 21.9. HRMS: (CI+, CH_4) m/z calculated for $C_{14}H_{11}N_2O_5$: 287.0662. Found $[M+H]^+$: 287.0670 (diff – 2.60 ppm).

(4-Chlorophenyl)(3,4-dinitrophenyl)methanone (23d)

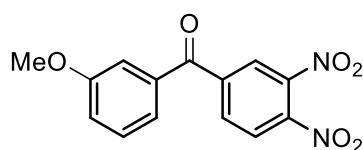


General Procedure A – Employed 4-chlorophenylboronic acid to give the title compound **(23d)** (0.092 g, 29% yield) as a white solid. 1H NMR (400 MHz, $CDCl_3$) δ 8.31 (d, 1H, $J = 1.5$ Hz), 8.13 (dd, 1H, $J = 8.3$ and 1.5 Hz), 8.04 (d, 1H, $J = 8.3$ Hz), 7.76 (d, 2H, $J = 8.7$ Hz), 7.55 (d, 2H, $J = 8.7$ Hz). ^{13}C NMR (100 MHz, $CDCl_3$) δ 190.9, 144.6, 142.7, 141.7, 141.0, 134.2, 133.5, 131.4, 129.5, 126.1, 125.4. HRMS: (CI+, CH_4) m/z calculated for $C_{13}H_8ClN_2O_5$: 307.0116. Found $[M+H]^+$: 307.0116 (Diff -0.17 ppm).

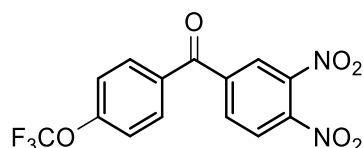
(3,4-Dinitrophenyl)(4-methoxyphenyl)methanone (23e)



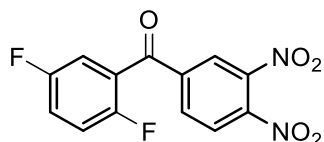
General Procedure A – Employed 4-methoxyphenylboronic acid to give the title compound **(23e)** (0.17 g, 48% yield) as a white solid. 1H NMR (400 MHz, $CDCl_3$) δ 8.27 (d, 1H, $J = 1.3$ Hz), 8.10 (dd, 1H, $J = 8.1$ & 1.3 Hz), 8.02 (d, 1H, $J = 8.1$ Hz), 7.80 (d, 2H, $J = 8.9$ Hz), 7.03 (d, 2H, $J = 8.9$ Hz), 3.93 (s, 3H). ^{13}C NMR (100 MHz, $CDCl_3$) δ 190.6, 164.5, 147.9, 143.0, 133.9, 132.7, 130.5, 127.8, 125.9, 125.2, 114.4, 55.6. HRMS: (CI+, CH_4) m/z calculated for $C_{14}H_{11}N_2O_6$: 303.0612. Found $[M+H]^+$: 303.0623 (Diff -3.86 ppm).

(3,4-Dinitrophenyl)(3-methoxyphenyl)methanone (23f)

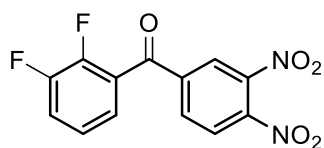
General Procedure A – Employed 3-methoxyphenylboronic acid to give the title compound (**23f**) (0.062 g, 15% yield) as a yellow solid. ^1H NMR (400 MHz, CDCl_3) δ 8.33 (d, 1H, $J = 1.6$ Hz), 8.15 (dd, 1H, $J = 8.2$ & 1.6 Hz), 8.03 (d, 1H, $J = 8.2$ Hz), 7.46 (dd, 1H, $J = 7.8$ & 8.6 Hz), 7.36 (dd, 1H, $J = 2.7$ & 1.7 Hz), 7.28 (ddd, 1H, $J = 7.7$, 1.7 & 0.9 Hz), 7.24 (ddd, 1H, $J = 8.3$, 2.7 & 0.9 Hz), 3.88 (s, 3H). ^{13}C NMR (100 MHz, CDCl_3) δ 191.8, 160.2, 149.3, 143.0, 142.1, 136.4, 134.3, 130.0, 126.2, 125.2, 122.8, 120.6, 114.2, 55.6. HRMS: (Cl^+ , CH_4) m/z calculated for $\text{C}_{14}\text{H}_{11}\text{N}_2\text{O}_6$: 303.0612. Found $[\text{M}+\text{H}]^+$: 303.0600 (Diff 3.84 ppm).

(3,4-Dinitrophenyl)(4-(trifluoromethoxy)phenyl)methanone (23g)

General Procedure A – Employed (4-(trifluoromethoxy)phenyl)boronic acid to give the title compound (**23g**) (0.14 g, 29% yield) as a yellow oil. ^1H NMR (400 MHz, CDCl_3) δ 8.32 (d, 1H, $J = 1.6$ Hz), 8.14 (dd, 1H, $J = 8.3$ & 1.6 Hz), 8.05 (d, 1H, $J = 8.3$ Hz), 7.88 (d, 2H, $J = 8.9$ Hz), 7.40 (d, 2H, $J = 8.9$ Hz). ^{13}C NMR (100 MHz, CDCl_3) δ 190.5, 153.3, 149.2, 144.6, 141.6, 134.2, 133.2, 132.1, 126.1, 125.4, 120.7. OCF_3 carbon not visible due to fluorine splitting. HRMS: (Cl^+ , CH_4) m/z calculated for $\text{C}_{14}\text{H}_8\text{F}_3\text{N}_2\text{O}_6$: 357.0329. Found $[\text{M}+\text{H}]^+$: 357.0339 (Diff – 2.72 ppm).

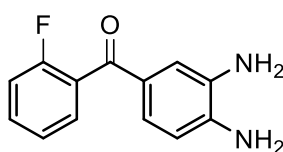
(2,5-Difluorophenyl)(3,4-dinitrophenyl)methanone (23h)

General Procedure A – Employed 2,5-difluorophenylboronic acid to give the title compound (**23h**) (0.099 g, 23% yield) as a pale yellow solid. ^1H NMR (400 MHz, CDCl_3) δ 8.35 (s, 1H), 8.16 (d, 1H, $J = 8.3$ Hz), 8.01 (d, 1H, $J = 8.3$ Hz), 7.44 – 7.33 (m, 2H), 7.22 (ddd, 1H, $J = 9.6$ & 9.1 and 4.0 Hz). HRMS: (Cl^+ , CH_4) m/z calculated for $\text{C}_{13}\text{H}_7\text{F}_2\text{N}_2\text{O}_5$: 309.0318. Found $[\text{M}+\text{H}]^+$: 309.0326 (Diff – 2.82 ppm).

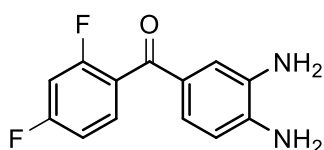
(2,3-Difluorophenyl)(3,4-dinitrophenyl)methanone (23i)

General Procedure A – Employed 2,3-difluorophenylboronic acid to give the title compound (**23i**) (0.080 g, 19% yield) as a pale yellow solid. ^1H NMR (400 MHz, CDCl_3) δ 8.36 (s, 1H), 8.17 (d, 1H, $J = 8.3$ Hz), 8.02 (d, 1H, $J = 8.3$ Hz), 7.54 – 7.40 (m, 2H), 7.37 – 7.29 (m, 1H). LRMS: (Cl^+ , CH_4) m/z calculated for $\text{C}_{13}\text{H}_7\text{F}_2\text{N}_2\text{O}_5$: 309.0318. Found $[\text{M}+\text{H}]^+$: 309.0.

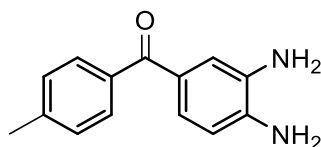
5.5.1.3 Synthesis of (3,4-diaminophenyl)(phenyl)methanone Derivatives

(3,4-Diaminophenyl)(2-fluorophenyl)methanone (24a)

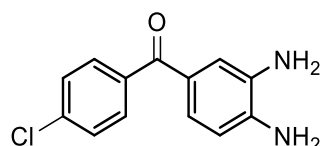
General Procedure B - Employed (3,4-dinitrophenyl)(2-fluorophenyl)methanone (**23a**) to give the title compound (**24a**) (0.066 g, 60% yield) as a white solid. ^1H NMR (400 MHz, CDCl_3) δ 7.48 - 7.44 (m, 2H), 7.34 (s, 1H), 7.23 – 7.21 (m, 2H, $J = 8.1$ Hz), 7.15 – 7.12 (m, 1H), 6.66 (d, 2H, $J = 8.1$ Hz). ^{13}C NMR (100 MHz, CDCl_3) δ 191.9, 159.8 (d, $J = 247.9$ Hz), 141.8, 139.5, 133.2, 132.0 (d, $J = 8.0$ Hz), 130.3 (d, $J = 3.6$ Hz), 128.8, 128.1 (d, $J = 16.1$ Hz), 124.0, 118.3, 116.0 (d, $J = 21.4$ Hz), 114.4. HRMS: (Cl^+ , CH_4) m/z calculated for $\text{C}_{13}\text{H}_{12}\text{FN}_2\text{O}$: 231.0928. Found $[\text{M}+\text{H}]^+$: 231.0934 (Diff -2.58 ppm).

(3,4-Diaminophenyl)(2,4-difluorophenyl)methanone (24b)

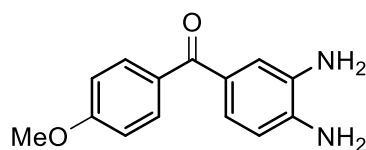
General Procedure B - Employed (2,4-difluorophenyl)(3,4-dinitrophenyl)methanone (**23b**) to give the title compound (**24b**) (0.049 g, 94% yield) as a yellow solid. ^1H NMR (400 MHz, CDCl_3) δ 7.52 – 7.45 (m, 1H), 7.32 (d, 1H, $J = 1.7$ Hz), 7.19 (dd, 1H, $J = 8.1$ & 1.7 Hz), 6.99 – 6.93 (m, 1H), 6.91 – 6.85 (m, 1H), 6.67 (d, 1H, $J = 8.1$ Hz), 3.99 (bs, 2H), 3.38 (bs, 2H). ^{13}C NMR (100 MHz, CDCl_3) δ 190.8, 164.3 (d, $J = 253.0$ Hz), 141.9, 133.2, 131.8 (dd, $J = 10.4$ & 9.9 Hz), 128.8, 125.4, 124.3, 118.3, 114.4, 111.6 (dd, $J = 21.4$ and 3.4 Hz), 104.4 (dd, $J = 25.7$ & 26.0 Hz) one C-F carbon not visible. HRMS: (ES^+) m/z calculated for $\text{C}_{13}\text{H}_{11}\text{F}_2\text{N}_2\text{O}$: 249.0834. Found $[\text{M}+\text{H}]^+$: 294.0844 (Diff -2.62 ppm).

(3,4-Diaminophenyl)(p-tolyl)methanone (24c)

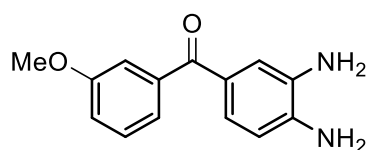
General Procedure B - Employed (3,4-dinitrophenyl)(p-tolyl)methanone (**23c**) to give the title compound (**24c**) (0.031 g, 39% yield) as a yellow solid. ^1H NMR (400 MHz, CDCl_3) δ 7.66 (d, 1H, $J = 7.8$ Hz), 7.30 (d, 1H, $J = 1.8$ Hz), 7.25 (d, 2H, $J = 7.8$ Hz), 7.24 (dd, 1H, $J = 8.4$ & 8.1 Hz), 6.69 (d, 1H, $J = 8.4$ Hz), 3.86 (s, 2H), 3.38 (s, 2H), 2.24 (s, 3H). ^{13}C NMR (100 MHz, CDCl_3) δ 185.4, 146.7, 143.8, 138.6, 136.6, 134.3, 130.2, 129.6, 120.8, 117.8, 115.1, 32.4. HRMS: (Cl^+ , CH_4) m/z calculated for $\text{C}_{14}\text{H}_{15}\text{N}_2\text{O}$: 227.1179. Found $[\text{M}+\text{H}]^+$: 227.1187 (Diff – 3.58 ppm).

(4-Chlorophenyl)(3,4-diaminophenyl)methanone (24d)

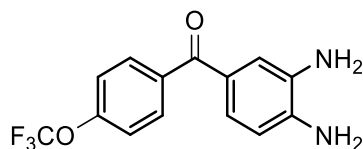
General Procedure B - Employed (4-chlorophenyl)(3,4-dinitrophenyl)methanone (**23d**) to give the title compound (**24d**) (0.046 g, 62% yield) as a yellow solid. ^1H NMR (400 MHz, CDCl_3) δ 7.68 (d, 2H, $J = 8.3$ Hz), 7.43 (d, 2H, $J = 8.3$ Hz), 7.29 (d, 1H, $J = 1.9$ Hz), 7.20 (d, 1H, $J = 8.0$ Hz), 6.69 (d, 1H, $J = 8.0$ Hz), 3.92 (s, 2H), 3.40 (s, 2H). ^{13}C NMR (100 MHz, CDCl_3) δ 194.4, 142.0, 139.8, 138.5, 137.1, 133.3, 131.0, 128.3, 125.2, 118.8, 114.4. HRMS: (Cl^+ , CH_4) m/z calculated for $\text{C}_{13}\text{H}_{12}\text{ClN}_2\text{O}$: 247.0633. Found $[\text{M}+\text{H}]^+$: 247.0637 (Diff 1.62 ppm).

(3,4-Diaminophenyl)(4-methoxyphenyl)methanone (24e)

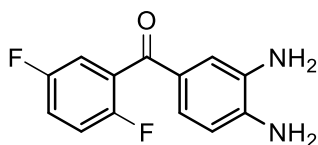
General Procedure B - Employed (3,4-dinitrophenyl)(4-methoxyphenyl)methanone (**23e**) to give the title compound (**24e**) (0.10 g, 71% yield) as a white solid. ^1H NMR (400 MHz, CDCl_3) δ 7.77 (d, 2H, $J = 8.9$ Hz), 7.27 (d, 1H, $J = 1.9$ Hz), 7.21 (dd, $J = 8.3$ & 1.9 Hz), 6.94 (d, 2H, $J = 8.9$ Hz), 6.69 (d, 1H, $J = 8.3$ Hz), 3.89 - 3.85 (m, 5H), 3.41 (s, 2H). ^{13}C NMR (100 MHz, CDCl_3) δ 194.7, 162.6, 140.2, 133.3, 132.1, 131.3, 129.5, 124.5, 118.9, 114.5, 113.3, 55.8. HRMS: (Cl^+ , CH_4) m/z calculated for $\text{C}_{14}\text{H}_{15}\text{N}_2\text{O}_2$: 243.1128. Found $[\text{M}+\text{H}]^+$: 243.1134 (Diff -2.63ppm).

(3,4-Diaminophenyl)(3-methoxyphenyl)methanone (24f)

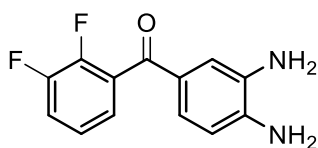
General Procedure B - Employed (3,4-dinitrophenyl)(3-methoxyphenyl)methanone (**23f**) to give the title compound (**24f**) (0.039 g, 76% yield) as an orange oil. ^1H NMR (400 MHz, CDCl_3) δ 7.31 – 7.15 (m, 5H), 7.10 – 6.95 (m, 2H), 3.85 (bs, 4H), 3.77 (s, 3H). ^{13}C NMR (100 MHz, CDCl_3) δ 194.4, 158.3, 139.8, 139.2, 138.0, 132.1, 128.0, 124.3, 121.1, 118.0, 116.7, 116.4, 113.3, 54.6. HRMS: (ES+) m/z calculated for $\text{C}_{14}\text{H}_{15}\text{N}_2\text{O}_2$: 243.1128. Found $[\text{M}+\text{H}]^+$: 243.1126 (Diff 0.67 ppm).

(3,4-Diaminophenyl)(4-(trifluoromethoxy)phenyl)methanone (24g)

General Procedure B - Employed (3,4-dinitrophenyl)(4-(trifluoromethoxy)phenyl)methanone (**23g**) to give the title compound (**24g**) (0.058 g, 50% yield) as a yellow solid. ^1H NMR (400 MHz, CDCl_3) δ 7.78 (d, 2H, $J = 8.8$ Hz), 7.30 (d, 1H, $J = 1.9$ Hz), 7.28 (d, 2H, $J = 8.8$ Hz), 7.21 (dd, 1H, $J = 8.10$ & 1.9 Hz), 6.70 (d, 1H, $J = 8.8$ Hz), 3.94 (s, 2H), 3.41 (s, 2H). ^{13}C NMR (100 MHz, CDCl_3) δ 194.0, 151.4, 141.0, 137.3, 133.3, 131.3, 128.3, 125.2, 120.4 (q, $J = 260.0$ Hz), 120.1, 118.8, 114.5. HRMS: (ES+) $\text{C}_{14}\text{H}_{12}\text{F}_3\text{N}_2\text{O}_2$: 297.0845. Found $[\text{M}+\text{H}]^+$: 297.0853 (Diff -2.67 ppm).

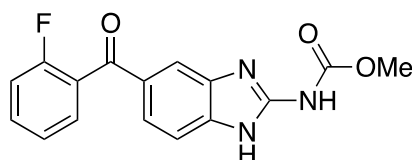
(3,4-Diaminophenyl)(2,5-difluorophenyl)methanone (24h)

General Procedure B - Employed (2,5-difluorophenyl)(3,4-dinitrophenyl)methanone (**23h**) to give the title compound (**24h**) (0.070 g, 88% yield) as a yellow solid. ^1H NMR (400 MHz, CDCl_3) δ 7.33 (d, 1H, $J = 1.3$ Hz), 7.20 (dd, 1H, $J = 8.2$ & 1.3 Hz), 7.17 – 7.07 (m, 3H), 6.66 (d, 1H, $J = 8.2$ Hz), 4.03 (s, 2H), 3.37 (bs, 2H). ^{13}C NMR (100 MHz, CDCl_3) δ 190.3, 158.2 (d, $J = 243.6$ Hz), 155.5 (d, $J = 249.4$ Hz), 142.3, 133.1, 129.1, 128.1, 125.6, 118.4, 118.3 (dd, $J = 24.1$ & 8.7 Hz), 117.4 (dd, $J = 24.7$ & 8.7 Hz), 116.6 (dd, $J = 25.2$ & 3.8 Hz), 114.4. HRMS: (CI+, CH_4) m/z calculated for $\text{C}_{13}\text{H}_{11}\text{F}_2\text{N}_2\text{O}$: 249.0834. Found $[\text{M}+\text{H}]^+$: 249.0834 (Diff -0.05 ppm).

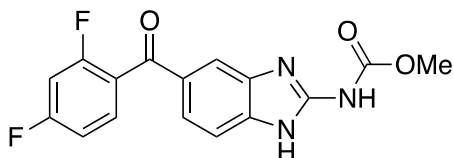
(3,4-Diaminophenyl)(2,3-difluorophenyl)methanone (24i)

General Procedure B - Employed (2,3-difluorophenyl)(3,4-dinitrophenyl)methanone (**23i**) using to give the title compound (**24i**) (0.062 g, 95% yield) as a yellow solid. ^1H NMR (400 MHz, CDCl_3) δ 7.25 (s, 1H), 7.23 – 7.18 (m, 1H), 7.16 – 7.06 (m, 3H), 6.59 (d, 1H, $J = 8.1$ Hz), 3.95 (s, 2H), 3.79 (s, 2H). ^{13}C NMR (100 MHz, CDCl_3) δ 190.5, 150.5 (dd, $J = 250.5$ Hz & 12.8 Hz), 147.8 (dd, $J = 268.4$ & 13.5 Hz), 142.3, 133.1, 130.2 (d, $J = 13.0$ Hz), 128.1, 125.7, 124.8 (dd, $J = 4.0$ & 3.8 Hz), 124.2 (dd, $J = 7.0$ & 6.5 Hz), 118.9 (d, $J = 17.2$ Hz), 118.3, 114.4. HRMS: (Cl^+ , CH_4) m/z calculated for $\text{C}_{13}\text{H}_{11}\text{F}_2\text{N}_2\text{O}$: 249.0834. Found $[\text{M}+\text{H}]^+$: 249.0830 (Diff 1.44 ppm).

5.651.4 Synthesis of Methyl (5-benzoyl-1H-benzo[d]imidazol-2-yl)carbamate Derivatives

Methyl (5-(2-fluorobenzoyl)-1H-benzo[d]imidazol-2-yl)carbamate (25a)

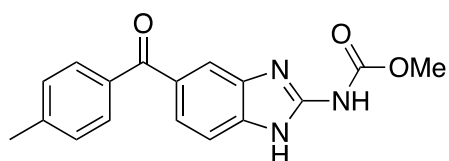
General Procedure C - Employed (3,4-diaminophenyl)(2-fluorophenyl) (**24a**) to give the title compound (**25a**) (0.040g, 50% yield) as a white solid. ^1H NMR (400 MHz, DMSO) δ 11.86 (s, 2H), 7.84 (s, 1H), 7.65 (m, 1H), 7.60 (d, 1H, $J = 8.2$ Hz), 7.55 (m, 1H), 7.51 (d, 1H, $J = 8.2$ Hz), 7.39 (m, 2H), 3.78 (s, 3H). ^{13}C NMR (100 MHz, DMSO) δ 190.5, 159.4 (d, $J = 244.0$ Hz), 154.8, 150.2, 143.0, 141.0, 133.1 (d, $J = 8.7$ Hz), 130.5 (d, $J = 2.6$ Hz), 130.2, 128.1 (d, $J = 15.2$ Hz), 125.1 (d, $J = 3.5$ Hz), 123.7, 118.9, 116.6 (d, $J = 22.4$ Hz), 114.5, 53.2. HRMS: (ES^+) m/z calculated for $\text{C}_{16}\text{H}_{13}\text{FN}_3\text{O}_3$: 314.0935. Found $[\text{M}+\text{H}]^+$: 314.0943 (Diff – 2.49 ppm). $\nu_{\text{max}}/\text{cm}^{-1}$ (solid); 3318 (s), 2980 (m), 2883 (m), 1730 (s), 1638 (s), 1459 (m), 1301 (s), 1287 (s). MP: 274 °C decomposed. Purity HPLC (Method A) 96.2%, $R_t = 8.27$ min.

Methyl (5-(2,4-difluorobenzoyl)-1H-benzo[d]imidazol-2-yl)carbamate (25b)

General Procedure C – Employed (3,4-diaminophenyl)(2,4-difluorophenyl)methanone (**24b**) to give the title compound (**25b**) (0.026 g, 49% yield) as a cream solid. ^1H NMR (400 MHz, DMSO) δ 11.92 (s, 2H), 7.84 (s, 1H), 7.65 (m, 1H), 7.58 (d, 1H, $J = 8.6$ Hz), 7.51 (d, 1H, $J = 8.6$ Hz), 7.46 (ddd, 1H, $J = 11.0$,

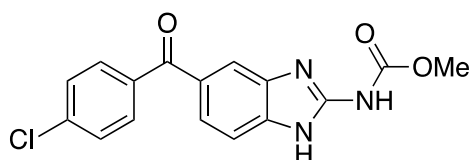
9.8 & 2.1 Hz), 7.27 (ddd, 1H, $J = 9.0, 8.3$ & 2.1 Hz), 3.78 (s, 3H). ^{13}C NMR (100 MHz, DMSO) δ 191.3, 164.0 (d, $J = 250.4$), 160.0 (d, $J = 244.9$), 153.1, 147.7, 141.0, 138.3, 132.4 (d, $J = 15.2$), 127.2, 125.0, 123.7 (d, $J = 14.8$), 120.3, 115.6, 112.5 (d, $J = 18.8$), 105.3 (d, $J = 25.6$), 53.2. HRMS: (ES+) m/z calculated for $\text{C}_{16}\text{H}_{12}\text{F}_2\text{N}_3\text{O}_3$: 332.0841. Found $[\text{M}+\text{H}]^+$: 332.0849 (Diff - 2.43 ppm). $\nu_{\text{max}}/\text{cm}^{-1}$: (solid) 3320 (s), 3051 (m), 2735 (m), 1725 (s), 1639 (s), 1595 (m), 1457 (m), 1276 (m). MP: 280°C decomposed. Purity HPLC (Method A) 98.8%, $R_t = 8.57$ min.

Methyl (5-(4-methylbenzoyl)-1H-benzo[d]imidazol-2-yl)carbamate (25c)

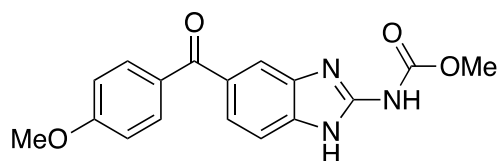


General Procedure C - Employed (3,4-diaminophenyl)(p-tolyl)methanone (**24c**) to give the title compound (**25c**) (0.020 g, 50% yield) as a white solid. ^1H NMR (400 MHz, DMSO) δ 12.04 (s, 1H), 7.64 (d, 2H, $J = 7.8$ Hz), 7.55 (d, 1H, $J = 8.2$ Hz), 7.5 (d, 1H, $J = 8.2$ Hz), 7.37 (d, 2H, $J = 7.8$ Hz), 3.78 (s, 3H), 2.42 (s, 3H). ^{13}C NMR (100 MHz, DMSO) δ 195.8, 151.5, 149.1, 142.6, 140.,5, 138.9, 136.1, 131.0, 130.1, 129.4, 124.0, 119.6, 113.9, 53.0, 21.6. HRMS: (ES+) m/z calculated for $\text{C}_{17}\text{H}_{16}\text{N}_3\text{O}_3$: 310.1186. Found $[\text{M}+\text{H}]^+$: 310.1172 (Diff 4.67 ppm). $\nu_{\text{max}}/\text{cm}^{-1}$ (solid); 3405 (s), 2956 (m), 2734 (m), 1715 (s), 1643 (s), 1452 (m), 1302 (s), 1242 (s). MP: 265 °C decomposed. Purity HPLC (Method A) 96.9%, $R_t = 8.76$ min.

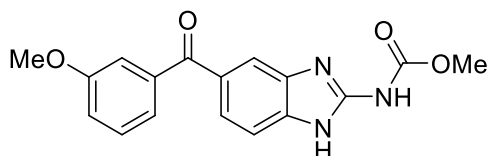
Methyl (5-(4-chlorobenzoyl)-1H-benzo[d]imidazol-2-yl)carbamate (25d)



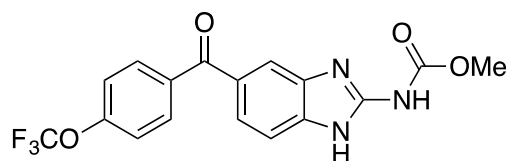
General Procedure C - Employed (4-chlorophenyl)(3,4-diaminophenyl)methanone (**24d**) to give the title compound (**25d**) (0.042 g, 71% yield) as a white solid. ^1H NMR (400 MHz, DMSO) δ 11.88 (s, 2H), 7.83 (s, 1H), 7.74 (d, 2H, $J = 8.3$ Hz), 7.63 (d, 2H, $J = 8.3$ Hz), 7.57 (d, 1H, $J = 8.5$ Hz), 7.52 (d, 1H, $J = 8.5$ Hz), 3.78 (s, 3H). ^{13}C NMR (100 MHz, DMSO) δ 194.9, 154.8, 149.9, 141.0, 137.7, 137.6, 137.1, 131.7, 131.6, 128.9, 124.4, 118.2, 116.6, 53.0. HRMS: (ES+) m/z calculated for $\text{C}_{16}\text{H}_{13}\text{ClN}_3\text{O}_3$: 330.0640. Found $[\text{M}+\text{H}]^+$: 330.0635 (Diff 1.59 ppm). MP: > 300 °C decomposed. Purity HPLC (Method A) 95.5%, $R_t = 9.14$ min.

Methyl (5-(4-methoxybenzoyl)-1H-benzo[d]imidazol-2-yl)carbamate (25e)

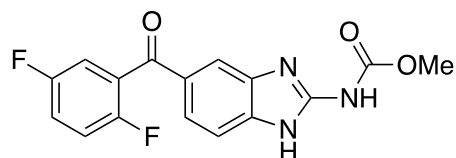
General Procedure C - Employed **(3,4-diaminophenyl)(3-methoxyphenyl)methanone (24e)** to give the title compound **(25e)** (0.058 g, 45% yield) as a cream solid. ^1H NMR (400 MHz, DMSO) δ 11.83 (s, 2H), 7.81 (s, 1H), 7.75 (d, 2H, $J = 8.7$ Hz), 7.52 (m, 2H), 7.10 (d, 2H, $J = 8.7$ Hz), 3.87 (s, 3H), 3.77 (s, 3H). ^{13}C NMR (100 MHz, DMSO) δ 194.9, 162.6, 149.6, 147.3, 141.1, 140.2, 132.4, 131.1, 130.3, 123.9, 119.6, 114.1, 110.5, 55.4, 53.1. HRMS: (ES+) m/z calculated for $\text{C}_{17}\text{H}_{16}\text{N}_3\text{O}_4$: 326.1135. Found $[\text{M}+\text{H}]^+$: 326.1142 (Diff -2.08 ppm). MP: 288 - 290 °C. Purity HPLC (Method A) 97.2%, $R_t = 8.21$ min.

Methyl (5-(3-methoxybenzoyl)-1H-benzo[d]imidazol-2-yl)carbamate (25f)

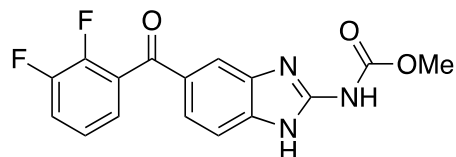
General Procedure C - Employed (3,4-diaminophenyl)(4-methoxyphenyl)methanone **(24f)** to give the title compound **(25f)** (0.007 g, 17% yield) as a cream solid. ^1H NMR (400 MHz, DMSO) δ 11.88 (s, 2H), 7.87 (s, 1H), 7.59 (d, 1H, $J = 8.3$ Hz), 7.52 (d, 1H, $J = 8.3$ Hz), 7.48 – 7.44 (m, 1H), 7.29 – 7.24 (m, 1H), 7.25 – 7.20 (m, 2H), 3.82 (s, 3H), 3.78 (s, 3H). ^{13}C NMR (100 MHz, DMSO) δ 195.6, 159.4, 154.9, 149.8, 140.3, 139.3, 138.0, 130.2, 130.0, 124.1, 122.2, 119.8, 118.1, 115.0, 114.6, 55.8, 53.1. HRMS: (ES+) m/z calculated for $\text{C}_{17}\text{H}_{16}\text{N}_3\text{O}_4$: 326.1135. Found $[\text{M}+\text{H}]^+$: 326.1141 (Diff -1.69 ppm). $\nu_{\text{max}}/\text{cm}^{-1}$: (solid) 33487 (m), 2980 (m), 2833 (m), 2651 (m), 1706 (s), 1627 (s). 1587 (m), 1449 (m), 1277 (s). MP: 289 - 291 °C.

Methyl (5-(4-(trifluoromethoxy)benzoyl)-1H-benzo[d]imidazol-2-yl)carbamate (25g)

General Procedure C - Employed (3,4-diaminophenyl)(4-(trifluoromethoxy)phenyl)methanone (**24g**) to give the title compound (**25g**) (0.022 g, 36% yield) as a pale yellow solid. ^1H NMR (400 MHz, DMSO) δ 11.86 (s, 2H), 7.86 (m, 3H), 7.59 (dd, 1H, J = 8.3 & 1.7 Hz), 7.54 (m, 3H), 3.78 (s, 3H). ^{13}C NMR (100 MHz, DMSO) δ 194.7, 154.9, 151.2, 150.1, 142.1, 137.9, 132.2, 129.8, 129.7, 124.2, 121.2, 121.1, 119.2, 113.9, 53.3. HRMS: (ES+) m/z calculated for $\text{C}_{17}\text{H}_{13}\text{F}_3\text{N}_3\text{O}_4$: 380.0853. Found $[\text{M}+\text{H}]^+$: 380.0863. $\nu_{\text{max}}/\text{cm}^{-1}$: (solid) 3304 (s), 2980 (m), 2709 (m), 1734 (s), 1645 (s), 1572 (m), 1459 (m), 1260 (m). MP 291 – 293°C. Purity HPLC (Method A) 96.9%, R_t = 8.76 min. Purity HPLC (Method A) 99.6%, R_t = 9.70 min.

Methyl (5-(2,5-difluorobenzoyl)-1H-benzo[d]imidazol-2-yl)carbamate (25h)

General Procedure C - Employed (3,4-diaminophenyl)(2,5-difluorophenyl)methanone (**24h**) to give the title compound (**25h**) (0.049 g, 53% yield) as a yellow solid. ^1H NMR (400 MHz, DMSO) δ 11.89 (s, 2H), 7.86 (s, 1H), 7.61 (d, 1H, J = 8.6 Hz), 7.52 (d, 1H, J = 8.6 Hz), 7.50 – 7.44 (m, 3H), 3.78 (s, 3H). ^{13}C NMR (100 MHz, DMSO) δ 191.2, 158.2 (d, J = 249.3 Hz), 155.4 (d, J = 236.7 Hz), 154.7, 150.4, 141.6, 139.6, 130.5, 125.4, 123.8, 119.6, 119.5, 118.4 (dd, J = 25.1 & 7.8 Hz), 116.8, 116.6 (dd, J = 25.6 & 3.7 Hz), 53.3. HRMS: (ES+) m/z calculated for $\text{C}_{16}\text{H}_{12}\text{F}_2\text{N}_3\text{O}_3$: 332.0841. Found $[\text{M}+\text{H}]^+$: 332.0846 (Diff – 1.54 ppm). ^{19}F NMR (376 MHz, DMSO) δ -117.9 (d, J = 18.2 Hz), -120.0 (d, J = 18.2 Hz). $\nu_{\text{max}}/\text{cm}^{-1}$: (solid) 3319 (s), 2980 (m), 2884 (m), 2710 (m), 1727 (s), 1638 (s), 1593 (m), 1460 (m), 1272 (s). MP - 280 °C decomposed. Purity HPLC (Method A) 95.2%, R_t = 8.61 min.

Methyl (5-(2,3-difluorobenzoyl)-1H-benzo[d]imidazol-2-yl)carbamate (25i)

General Procedure C - Employed (3,4-diaminophenyl)(2,3-difluorophenyl)methanone (**24i**) to give the title compound (**25i**) (0.036 g, 46% yield) as a pale yellow solid. ^1H NMR (400 MHz, DMSO) δ 11.85 (s, 2H), 7.87 (s, 1H), 7.75 – 7.65 (m, 1H), 7.63 (d, 1H, J = 8.5 Hz), 7.53 (d, 1H, J = 8.5 Hz), 7.53 (d, 1H, J =

8.5 Hz), 7.44 – 7.36 (m, 2H), 3.78 (s, 3H). ^{13}C NMR (100 MHz, DMSO) δ 191.0, 154.7, 150.4, 147.5 (d, J = 263.5 Hz), 139.4, 130.2 (d, J = 14.4 Hz), 129.7, 125.9, 125.6, 123.9, 120.1 (d, J = 17.4 Hz), 118.3, 116.6, 53.1. ^{19}F NMR (376 MHz, DMSO) δ -138.0 (d, J = 23.3 Hz), -140.6 (d, J = 23.3 Hz). HRMS: (ES+) m/z calculated for $\text{C}_{16}\text{H}_{12}\text{F}_2\text{N}_3\text{O}_3$: 332.0841. Found $[\text{M}+\text{H}]^+$: 332.0842 (Diff – 0.27 ppm). $\nu_{\text{max}}/\text{cm}^{-1}$: 3312 (m), 2980 (m), 2883 (m), 2712 (m), 1733 (s), 1646 (s), 1596 (m), 1476 (m), 1263 (s). MP 272 – 274 °C. Purity HPLC (Method A) 96.6%, R_t = 8.63 min.

5.6 References

1. S. Lachau-Durand, L. Lammens, B.-j. van der Leede, J. Van Gompel, G. Bailey, M. Engelen and A. Lampo, *PLOS Negl. Trop. Dis*, 2019, **13**, 1-26.
2. T. G. Geary, C. D. Mackenzie and S. A. Silber, *PLOS Negl. Trop. Dis*, 2019, **13**, 1-5.
3. R. Collins, Janssen Discontinues Development of Flubendazole Formulation to Treat Onchocerciasis, <https://www.jnj.com/media-center/press-releases/janssen-discontinues-development-of-flubendazole-formulation-to-treat-onchocerciasis>, (accessed June 2019).
4. Y. Fujikawa, F. Morisaki, A. Ogura, K. Morohashi, S. Enya, R. Niwa, S. Goto, H. Kojima, T. Okabe, T. Nagano and H. Inoue, *Chem. Commun.*, 2015, **51**, 11459-11462.
5. J. Zhang, L. Fu, M. Tian, H. Liu, J. Li, Y. Li, J. He, J. Huang, L. Ouyang, H. Gao and J.-h. Wang, *Bioorg. Med. Chem.*, 2015, **23**, 976-984.
6. H. Park, S. Hong, J. Kim and S. Hong, *J. Am. Chem. Soc.*, 2013, **135**, 8227-8237.
7. N. Thamban Chandrika, S. Shrestha, H. Ngo and S. Garneau-Tsodikova, *Bioorg. Med. Chem.*, 2016, **24**, 3680-3686.
8. S. Bhagwanth, A. G. Waterson, G. M. Adjabeng and K. R. Hornberger, *J. Org. Chem.*, 2009, **74**, 4634-4637.
9. G. F. Moore, M. Hamburger, G. Kodis, W. Michl, D. Gust, T. A. Moore and A. L. Moore, *J. Phys. Chem. B*, 2010, **114**, 14450-14457.
10. G. F. Moore, M. Hamburger, M. Gervaldo, O. G. Poluektov, T. Rajh, D. Gust, T. A. Moore and A. L. Moore, *J. Am. Chem. Soc.*, 2008, **130**, 10466-10467.
11. X. Han, R. L. Civiello, H. Fang, D. Wu, Q. Gao, P. V. Chaturvedula, J. E. Macor and G. M. Dubowchik, *J. Org. Chem.*, 2008, **73**, 8502-8510.
12. T. Tachikawa, N. Wang, S. Yamashita, S.-C. Cui and T. Majima, *Angew. Chem.*, 2010, **49**, 8593-8597.
13. M. Ikeda, H. Nakagawa, T. Suzuki and N. Miyata, *Bioorg. Med. Chem. Lett.*, 2012, **22**, 1949-1952.
14. C. Liu, J. Lin, S. Pitt, R. F. Zhang, J. S. Sack, S. E. Kiefer, K. Kish, A. M. Doweiko, H. Zhang, P. H. Marathe, J. Trzaskos, M. McKinnon, J. H. Dodd, J. C. Barrish, G. L. Schieven and K. Lefttheris, *Bioorg. Med. Chem. Lett.*, 2008, **18**, 1874-1879.
15. O. Labeeuw, P. Phansavath and J.-P. Genêt, *Tetrahedron Lett.*, 2004, **45**, 7107-7110.
16. J. Buchspies and M. Szostak, *Catalysts*, 2019, **53**, 1-23.
17. M. Haddach and J. R. McCarthy, *Tetrahedron Lett.*, 1999, **40**, 3109-3112.
18. T. Khotavivattana, S. Calderwood, S. Verhoog, L. Pfeifer, S. Preshlock, N. Vasdev, T. L. Collier and V. Gouverneur, *Org. Lett.*, 2017, **19**, 568-571.
19. H. Tatamidani, F. Kakiuchi and N. Chatani, *Org. Lett.*, 2004, **6**, 3597-3599.
20. H. I. Abdulla and M. F. El-Bermani, *Spectrochim. Acta A*, 2001, **57**, 2659-2671.
21. S. Mata, V. Cortijo, W. Caminati, J. Alonso, M. Sanz, J. López and S. Blanco, *J. Phys. Chem. A*, 2010, **114**, 11393-11398.
22. W. Kampe, *Angew. Chem.*, 1963, **75**, 641-641.
23. I. Um, Y. Song, M. Kim and J. Lee, *Bull. Korean Chem. Soc.*, 2013, **34**, 1525-1529.
24. K. Sunggak, I. L. Jae and K. K. Young, *Tetrahedron Lett.*, 1984, **25**, 4943-4946.
25. E. C. Cortés and L. A. A. Anaya, *J. Heterocycl. Chem.*, 1997, **34**, 745-748.
26. Y. Ogata, *J. Org. Chem.*, 1982, **47**, 3577-3581.
27. M. B. Smith and J. March, *March's Advanced Organic Chemistry: Reactions, Mechanisms, and Structure*, Wiley, 2001.
28. *Eur. Pat.*, KR20170098486, 2017.
29. Optibrium, *Stardrop*, 2018.
30. L. Ceballos, L. Alvarez, C. Mackenzie, T. Geary and C. Lanusse, *Int. J. Parasitol. Drugs. Drug. Resist.*, 2015, **5**, 178-184.
31. I. Vokřál, H. Bártíková, L. Prchal, L. Stuchlíková, L. Skálová, B. Szotáková, J. Lamka, M. Várady and V. Kubiček, *Parasitology*, 2012, **139**, 1309-1316.

Chapter 6

Synthesis and Biological Evaluation of Biphenyl Derivatives

6.1 Biphenyl Benzimidazole Derivatives

As previously reported in Chapter 2 there were concerns surrounding the metabolic stability of some compounds within the thiol and ketone classes, with the linking group between the two aryl rings thought to be the cause.¹⁻⁵ With this in mind, we decided to remove this linker atom and have two aryl rings joined directly together to create the biphenyl class (Figure 6.1).

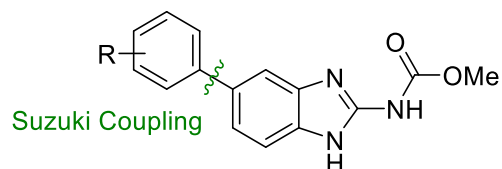


Figure 6.1. The new benzimidazole biphenyl template.

This template has not been reported in the literature before in terms of synthesis or biological activity. Therefore, a new synthetic route will need to be devised in order to obtain the desired product. A common way of connecting two aryl rings together is to carry out a palladium catalysed Suzuki coupling.⁶⁻⁸ Furthermore, there is wide commercial availability of boronic acids that can be used in Suzuki reactions, allowing for a wide range of derivatives to be explored (Figure 6.1).

The aims of the benzimidazole biphenyl project were;

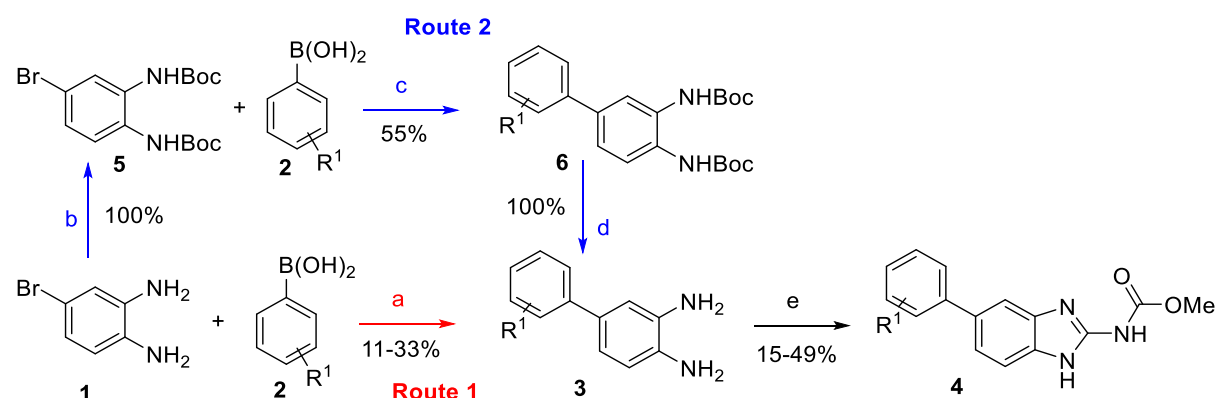
1. To design and optimise a synthetic route to allow for synthesis of a number of biphenyl compounds.
2. To subject novel compounds to MIC testing and DMPK testing to observe where activity or metabolic clearance is improved.
3. To incorporate a pyridine ring to increase solubility whilst maintaining activity.

6.2 Biphenyl Discussion

6.2.1 Synthesis

6.2.1.1 Suzuki Coupling Chemistry

Firstly, we tried the most direct route (Scheme 6.1, Route 1), which was to employ the commercially available 5-bromo-1,2-diaminobenzene (**1**), with the desired boronic acid (**2**) to give the diamine (**3**) necessary for ring closure. However, only two analogues, 2,4-difluoro (**3a**) and 2-Cl (**3b**), were synthesised and showed very poor yields of 11 and 33% respectively. A number of other analogues were tried with this set of conditions but there was no formation of product. For the two products produced, this allowed them to be carried into the ring closure step directly after purification to generate the final product (**4**).



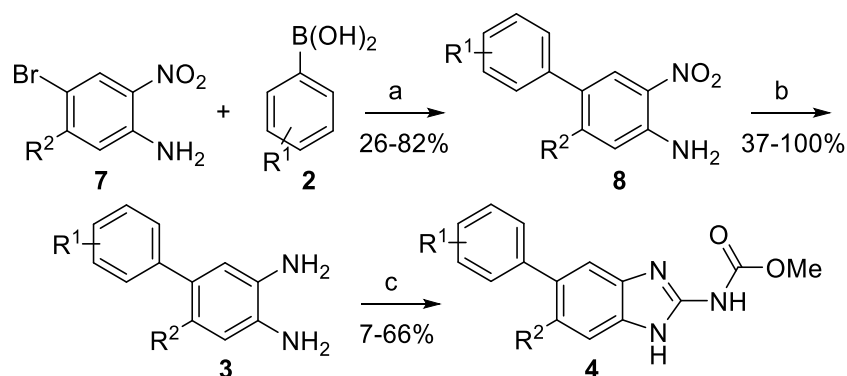
Scheme 6.1. Reagents and Conditions: (a) Cs₂CO₃ (1.8 eq), Pd(PPh₃)₄ (0.05eq), toluene, reflux, overnight (11-33% yield); (b) Boc₂O (2.4 eq), ethanol, room temperature, overnight (100 % yield); (c) Cs₂CO₃ (1.8 eq), Pd(dppf)Cl₂ (0.05eq), toluene, reflux, overnight 80 °C, overnight (55% yield); (d) DCM/TFA (1:1), room temperature, overnight (100 % yield); (e) 1,3-Bis(carbonyl)-2-methyl-2-thiopseudourea (1.0 eq), acetic acid (2 M), methanol (0.4 M), sealed tube, 65 °C, overnight (15 - 49% yield).

Table 6.1. Percentage yields obtained for all compounds created within the biphenyl template, including intermediates and final products produced from Scheme 6.1.

Compound	R ¹	R ²	R ³	X	Step a yield (%) (3)	Step b yield (%) (5)	Step c yield (%) (6)	Step d yield (%) (3)	Step yield (%) (4)
4a	2-F, 4-F	H	Me	CH	11	-	-	-	32
4b	2-Cl	H	Me	CH	33	-	-	-	15
4c	2-Me	H	Me	CH	-	100	55	100	49

It was realised that there was potential for the amines to interfere in the reaction, undergoing coupling themselves or making the 5-bromo-1,2-diaminobenzene (**1**) less reactive. Route 2 in Scheme 6.1 allowed for protection of the diamine (**1**), which was carried out through a double *tert*-butyl carbamate protection (**5**).^{9, 10} This prevented their interference in the reaction, and then employed the same Suzuki conditions as presented in the first route to generate the desired biphenyl (**6**). The

Boc protection was generally quantitative, with a brown solid being produced, and evidenced via the appearance of two peaks at around 1.5 ppm, with a combined integration of 18, suggesting the two Boc groups had been incorporated. The next step, which employed Suzuki coupling conditions occurred in better yield than observed when the diamine was not protected, and yields for the methyl derivative were improved to 55%. Boc deprotection with trifluoroacetic acid proved simple, and only required an aqueous workup and concentration to yield the product diamine (**3**), as discussed further in section 6.2.1.2.^{11, 12} Despite the addition of two further synthetic steps to Route 2, both steps occurred in quantitative yield and the Suzuki coupling step showed improved yields. However, when this new route was applied to other compounds, there was either no conversion of product observed on the TLC or too little to be isolated, resulting in the design of an alternative route.



Scheme 6.2. Optimised route for biphenyl synthesis. *Reagents and Conditions:* (a) K_2CO_3 (1.8 eq), $Pd(PPh_3)_4$ (0.05eq), DMF/Water (1:1), reflux, overnight (26 – 82% yield); (b) $SnCl_2$ (5.0 eq), ethanol, reflux, overnight (37 – 100% yield); (c) 1,3-Bis(carbonyl)-2-methyl-2-thiopseudourea (1.0 eq), acetic acid (2 M), methanol (0.4 M), sealed tube, 65 °C, overnight (7 - 66% yield).

Table 6.2. Percentage yields obtained for all compounds created within the biphenyl template, including intermediates and final products produced from Scheme 6.2.

	R ¹	R ²	R ³	X	Step a yield (%) (8)	Step b yield (%) (3)	Step c yield (%) (4)
4c	2-Me	H	Me	CH	100	91	27
4d	H	H	Me	CH	43	55	51
4e	3-F	H	Me	CH	26	43	40
4f	2-F	F	Me	CH	46	86	33
4g	2-F	F	Et	CH	46	86	14
4h	2-F	Me	Me	CH	46	63	29
4i	2-isopropyl	H	Me	CH	40	40	7
4j	4-OMe	H	Me	CH	57	55	66
4k	2-OMe, 6-OMe	H	Me	CH	42	37	30
4l	2-Me, 4-OMe	H	Me	CH	58	60	43
4m	3-OMe	H	Me	CH	57	67	61
4n	2-OMe	H	Me	CH	82	48	41
4o	2-CF ₃	H	Me	CH	23	51	37

Scheme 6.2 details the use of 4-bromo-2-nitroaniline undergoing a Suzuki coupling with the desired boronic acid.^{7, 13} The advantages of using **7** are cheap cost, availability and only possessing one nitro group, which should allow for easier reduction to the diamine. Finally, the amine lone pair, which may interfere with the Suzuki reaction, can be delocalised into the adjacent nitro group, making it less available for side-reactions, and thus protecting groups on the amine don't need to be employed. This Suzuki reaction proved to be successful, but did require optimisation in order to work consistently for a variety of analogues in improved yield.

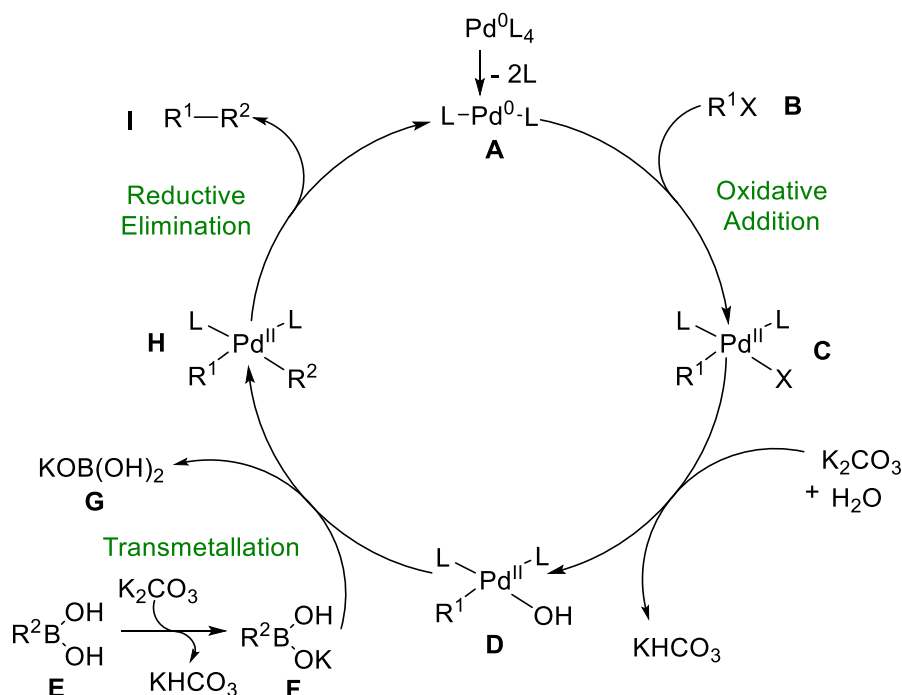


Figure 6.2. The mechanism of a Suzuki coupling of two aryl rings, R^1 and R^2 . Reproduced from; *Transition-metal-catalyzed Suzuki–Miyaura cross-coupling reactions: a remarkable advance from palladium to nickel catalysts*, Han, F et al.^{14, 15}

The mechanism of the Suzuki reaction is detailed in Figure 6.2. The active palladium catalyst (**A**) undergoes oxidative addition with the desired aryl halide (**B**), generating a organopalladium (II) intermediate, which can then undergo reaction with potassium carbonate to produce intermediate (**D**). The boronic acid (**E**) is converted to the activated salt (**F**), which can then undergo transmetallation with (**D**) to produce a salt (**G**) and the intermediate (**H**). This can then undergo reductive elimination to provide the biphenyl and regenerate the active catalyst.^{14, 15}

The reaction was initially carried out with the 5-chloro-2-nitroaniline derivative, as this had previously been used on other templates. We also tried potassium carbonate and caesium carbonate as bases, as well as toluene and a DMF/water mixture as the solvent, as reported in the literature (Table 6.3).¹⁶ Use of DMF/Water as the solvent mixture resulted in improved yields, and worked for all substrates

tested, even in cases where toluene did not. This is thought to be due to enhanced solubility of the starting materials in this mixture. Use of the bromo derivative also improved yields versus the chloro derivative, owing to bromine being a better coupling partner in Suzuki reactions.

The bromine analogue was used with DMF/Water as a solvent and potassium carbonate, with the reaction carried out on up to a 1 g scale successfully in a sealed tube. This was carried out for the 2-methyl derivative, due to requiring more material for *in vivo* testing. This reaction resulted in 100% yield, easy purification and only took one hour to go to completion, rather than overnight. Previously for the 1 g scale, the bromo derivative was used but with toluene and caesium carbonate and the reaction was unsuccessful.

Table 6.3. The Suzuki conditions for the biphenyl template required optimisation, this was carried out through changing the halogenated started material, base and solvent to give the desired product, with a reaction that worked more consistently.

Nitroaniline Starting material	Base	Solvent	Yield Range
5-chloro-2-nitroaniline	Cs ₂ CO ₃	Toluene	0 - 26%
5-chloro-2-nitroaniline	K ₂ CO ₃	DMF/Water	0 - 46%
4-bromo-2-nitroaniline	Cs ₂ CO ₃	Toluene	0 - 40%
4-bromo-2-nitroaniline	K ₂ CO ₃	DMF/Water	42 - 100%

2,6-difluorophenylboronic acid proved to be the only reactant that did not couple in any of the conditions above. When a Suzuki reaction occurs, we think of the boronic acid as being the 'nucleophilic' partner, and the bromonitroaniline as being the 'electrophile' at the carbon. In the case of 2,6-difluorophenylboronic acid, the two fluorines *ortho* to the carbon bearing the boron were very electron withdrawing, rendering that carbon less electron rich and thus less nucleophilic. The synthesis of compound **4k**, which possesses two methoxy groups *ortho* to the carbon bearing the boron, resulted in the product being obtained in 42% yield. Methoxy groups are electron donating, pushing more electron density onto the carbon, making it more nucleophilic. This means it is more likely to take place in the transmetallation step. The yield however is thought to be limited by the methoxy groups providing a partial steric block at both *ortho* positions, making it more difficult for the reaction to occur.

These analogues were identified by ¹H NMR, most notably observing downfield protons adjacent to the nitro group, regardless of which starting nitroaniline was used (See Appendix, Figure 5A).

6.2.1.2 Production of the Diamine

6.2.1.2.1 *Tert*-butyl carbamate deprotection to give diamine

Due to the diverse range of chemistry tried for the Suzuki coupling, there were a couple of different routes utilised to achieve the diamine. For those analogues that were Boc protected, trifluoroacetic acid and DCM was used to cleave off the *t*-butyl carbamate protecting groups. This was evidenced by the disappearance of the large Boc peaks at around 1.50 ppm. For the 2-Me derivative (**4c**) this was successfully carried out and a quantitative yield was obtained. Furthermore, purification was effected by the simple removal of the trifluoroacetic acid with a NaHCO₃ wash and required no further column purification before carrying through into the next step. Whilst this reaction does benefit from easy purification and high yields, it does result in a large loss of mass in one step. The removal of two *tert*-butyl carbamates results in a molecular weight loss of 200, which shows poor atom economy.

6.2.1.2.2 Tin (II) Chloride Nitro Reduction

Alternatively, for those analogues bearing a nitro group, the usual tin (II) chloride reduction was used (See Chapter 3, Section 3.2.1.2 for more detail), with a noticeable shift in the ¹H NMR spectrum being observed for the proton next to the nitro group regardless of the nitroaniline starting material used (Figure 6.4). Yields of 37 - 86% were obtained, with no noticeable difference observed between the nitro being in the 3 or 4 positions, due to the different initial starting materials used.¹⁷⁻¹⁹

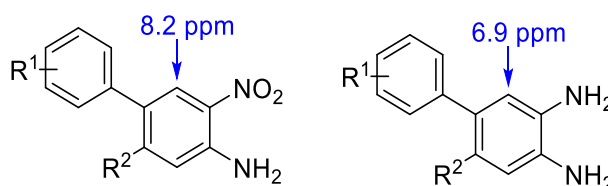


Figure 6.4. Due to the electron withdrawing nature of the nitro group, the neighbouring proton highlighted in blue is found downfield at 8.2 ppm. Reduction to the diamine results in an obvious ¹H NMR change to a more downfield position of 6.9 ppm.

A similar shift in protons is observed when the nitro reduction takes place as observed for the other templates. The proton adjacent to the nitro group, shows the most identifiable change, from around 8.2 ppm to 6.9 ppm for all analogues, regardless of the position of the nitro group on the ring. When this is combined with the appearance of a broad singlet, integrating to four protons at around 4.4 ppm, indicating the presence of the two amine groups and gives confidence the correct product has been produced (Figure 6.4) (See Appendix, Figure 5B).

6.2.1.3 Acid Mediated Ring Closure to Establish the Benzimidazole Core

A number of products (**4**) were produced through the usual ring closure method. However, there was often the requirement to repeat the synthetic route to generate the product (**4**) due to poor yields (7-66%) being observed in this final step. Measured DMPK shows the biphenyls have improved solubility versus other benzimidazoles in this project, which will be discussed in more detail in a subsequent section (Section 4.2.3.1). It was noticed during the reaction, that precipitation of the final product (**4**) did not occur as readily as observed with the other templates, especially at the reaction temperature (65 °C). Cooling of these reactions to room temperature, or even allowing further cooling in a fridge, often resulted in solid precipitating, which could then be isolated, albeit in sub-optimal yields.

Also, when carrying out HPLC purity analysis of these compounds, it was noted that the biphenyl compounds (**4**) more readily dissolved in methanol, which was used for sample preparation. The samples were also much more soluble in the NMR solvent DMSO, requiring little heat for dissolution. All this evidence is congruent with the biphenyl class having improved solubility, which is a desirable characteristic for potential future drug formulation, but is problematic in the ring closure step, which relies on its insolubility for isolation and purification. Nonetheless, a number of biphenyl analogues were obtained, which were easily identified via NMR and mass spectrometry, and showed excellent compound purity, which generally proved to be better than other templates (See Appendix, Figure 5C – E).

4.2.1.4 Compound Scale-Up

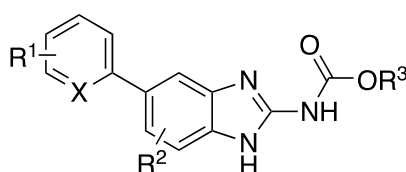
4c, a 2-Me derivative was taken forward for *in vivo* testing (discussed in Section 6.2.4). Compound scale-up was therefore required. Previously this analogue had been synthesised on a 0.3 g scale, but in order to synthesise enough for *in vivo* testing the scale was increased to 1.5 g of the starting 5-bromo-2-nitroaniline (**7**) and the route from Scheme 6.2 was employed. The first two steps of this sequence occurred in excellent yields of 100% and 91% for the Suzuki coupling and tin (II) chloride reduction respectively. The third step occurred in a low yield of 27%, which did allow for enough compound to be synthesised for *in vivo* testing, but would need to be optimised if this was to be made on a larger scale. This was carried out in a large sealed tube, but for reactions of this scale and larger round bottom flask would allow for better stirring and may increase compound yield.

6.2.2 Biological Activity

Biological testing was carried out as stated on Section 3.22, Chapter 3. Data shown in Table 6.4.²⁰⁻²²

The biphenyl template was sent for minimum inhibitory concentration testing, and in general the results for this compound class showed poor activity for the majority of analogues. Those analogues that did possess activity, showed sub-optimal activity when compared with the thiol, ether and ketone class.

Table 6.4. The biphenyl class of compound show generally good MIC testing data. **Green** – good - 0.015 – 0.25 mg/L, **yellow** – acceptable - 0.5 – 4 mg/L, **red** – poor - >4 mg/L. * Synthesis of compounds p-q was carried out by Ryan McBerney



Compound	R ¹	R ²	R ³	X	MIC (mg/L)
4a	2-F, 4-F	H	Me	CH	1
4b	2-Cl	H	Me	CH	0.5
4c	2-Me	H	Me	CH	1
4d	H	H	Me	CH	>4
4e	3-F	H	Me	CH	>4
4f	2-F	F	Me	CH	2
4g	2-F	F	Et	CH	>4
4h	2-F	Me	Me	CH	>4
4i	2-isopropyl	H	Me	CH	>4
4j	4-OMe	H	Me	CH	>4
4k	2-OMe, 6-OMe	H	Me	CH	>4
4l	2-OMe, 4-OMe	H	Me	CH	>4
4m	3-OMe	H	Me	CH	1
4n	2-OMe	H	ME	CH	1
4o	2-CF ₃	H	Me	CH	>4
4p	2-F	H	Me	CH	1
4q	H	H	Me	N	>16

General observations show that the 2-position is preferred, with only one 3-position analogue, **4m**, showing activity. Smaller groups are preferred in the 2-position, however double substitution in the *ortho*, as seen in compound **4k**, causes a complete loss of activity. This also applies to **4l**, which despite having a 2-OMe group, also possess a 4-OMe group and shows no biological activity (MIC = >4 mg/L). **4a**, which bears a 2-F, 4-F substitution pattern shows a good MIC result of 1 mg/L, despite being doubly substituted. It appears that the 2-F allows for activity, and the 4-F is not imposing any steric restrictions or electron restrictions, given the 2-F derivative (**4p**) possess the same activity. Compound **4i**, bearing

a 2-isopropyl, validates that larger groups in the 2-position diminish biological activity. The 2-Cl analogue compound **4b**, shows an unexpected result, which is actually the best in terms of the biphenyl class. This may be that chlorine is the optimal size for the binding pocket, enhancing binding interactions. This could also be a spurious result, however multiple repeats of the MIC testing confirmed and activity of 0.5 mg/L. Furthermore, a pyridine analogue (**4q**) was also synthesised to improve solubility, but like all other pyridine analogues possessed no biological activity. Overall, the SAR for this template proved to be flat, with multiple attempts at optimisation offering no improvement in activity.²³

6.2.3 DMPK Data

6.2.3.1 Predicted DMPK Data

Table 6.5. Predicted data shows the biphenyl class has acceptable metabolic properties but no further improvement in solubility. **Green** – good, **amber** – acceptable/medium, **red** – poor. ClogP calculated using Chemdraw.²⁴

	LogD _{7.4}	ClogP	Aqueous Solubility (μM)	Rat Heps CLint (μl/min/mg)	Human Mics CLint (μl/min/mg)	MPO Score
4a	3.75	3.88	1.4	10	12	4.5
4b	3.85	4.06	1.1	12	10	4.1
4c	3.93	3.80	2.4	27	25	4.3
4d	3.63	3.60	2.6	12	12	4.6
4e	4.28	3.74	1.9	29	41	4.0
4f	3.86	3.96	1.9	12	20	4.5
4g	4.20	4.49	1.8	20	36	4.1
4h	3.75	3.94	6.8	19	20	4.3
4i	3.80	4.72	2.8	14	11	4.5
4j	3.70	3.52	1.8	14	18	4.9
4k	3.38	3.05	0.6	18	21	4.9
4l	3.06	3.05	1.2	19	18	4.9
4m	3.60	3.52	1.6	18	21	4.9
4n	3.61	3.52	3.4	23	22	4.9
4o	3.99	4.48	1.0	16	23	3.8

Predicted DMPK showed that these compounds had generally very high log D values, which is due to the addition of the lipophilic benzene ring, with no additional heteroatoms. Predicted solubility is shown to be slightly improved upon most of the other templates, however no significant improvement is offered, with all compound predicted to have values <10 μM. However, metabolically these compounds look excellent, with only a couple of compounds showing slightly higher values. **4i** possesses an isopropyl group, which is known to have higher metabolic rates.²⁵ **4b**, which contains a 2-Cl group, was identified as being the most active compound within the template. It shows excellent

metabolic data, possessing much lower clearance values than flubendazole or fenbendazole. **4c**, which contains a 2-Me and possessed an MIC of 1 mg/L also showed excellent values and a modest increase in aqueous solubility (2.4 μ M). ClogP indicates these compounds have moderate lipophilicity which is important for CNS penetration, but may mean that these compounds are not very hydrophilic, meaning they may have difficulty during absorption from the intestines. All these ClogP values do obey Lipinski's rule of 5, whereby ClogP must be <5.²⁶

Metabolism predictions were also calculated using Stardrop's CYP450 metabolism prediction module, with the results represented in Figure 6.6.²⁷

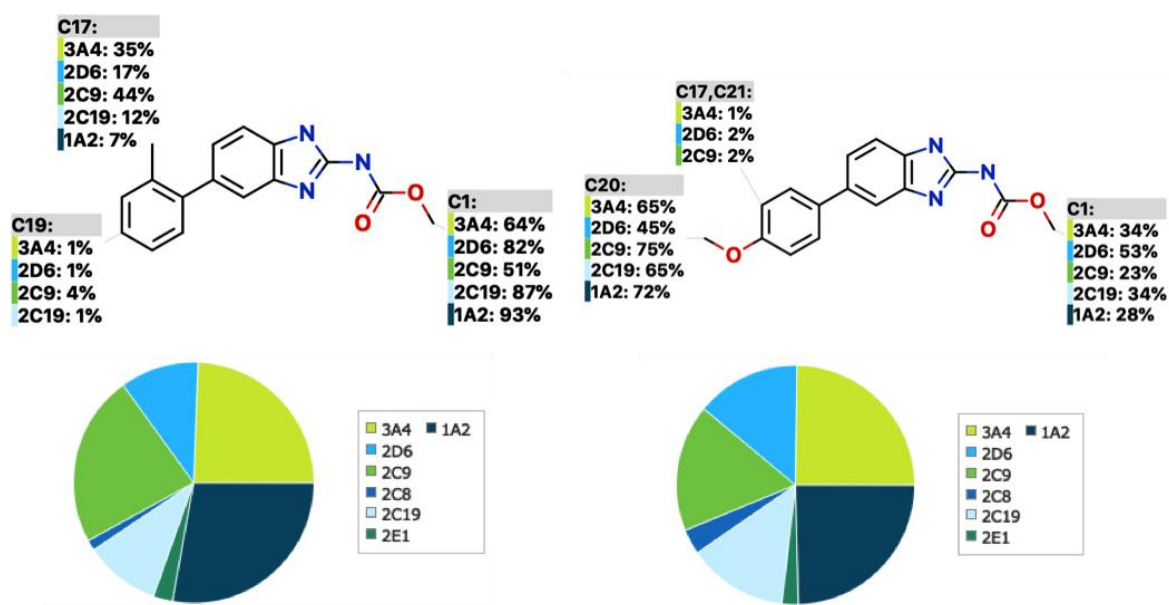


Figure 6.6. Metabolism predictions for two compounds from the ether series. Calculations run on Stardrop.²⁷

These yielded similar information to the other templates whereby CYP3A4 and CYP2C9, CYP1A2 are the main isoforms responsible for metabolism and agrees with what is reported in the literature.¹⁻⁵ The carbamate group is metabolised as expected, but not as significantly as observed in other templates. The most notable metabolism is derived from the substituents on the aryl ring. Here the methyl and methoxy groups are shown as being oxidised by CYP3A4 and 2C9. For the 4-OMe analogue (**4j**), this agrees with the measured rat hepatic clearance value of 64 μ l/min/mg, which is moderately high.

6.2.3.2 Measured DMPK Data

Measured DMPK data was obtained for four of the analogues as shown in Table 6.6.

Table 6.6. Predicted data shows the biphenyl class has acceptable metabolic properties but no further improvement in solubility. Green – good, amber – acceptable/medium, red – poor.

Compound	LogD _{7.4}	Aqueous Solubility (μM)	Rat Heps CLint (μl/min/mg)	Human Mics CLint (μl/min/mg)
Flubendazole	2.9	0.8	39	44
Fenbendazole	3.9	0.3	20	33
4c	3.8	58	26.1	12.5
4l	2.3	28	64	11
4m	3.5	10	35.9	37.4
4o	4.1	2	6	7

The most interesting data obtained was aqueous solubility, as it gave some unexpected results. The biphenyl class still maintains the carbamate group which is believed to be the main contributor to the poor aqueous solubility observed in other templates.^{28, 29} However, what we observed was a 100-fold increase in aqueous solubility when compared with the ether, ketone and thiol analogues. This presented the biphenyls as possessing the best solubility of all the benzimidazole templates. We proposed that this was due to the ability of the biphenyl group to twist around the bond between the two aryl rings at angles of between 45° and 90°. The angle was measured using Spartan³⁰ and obtained an angle of 53° for the unsubstituted biphenyl derivative **4d**, and 81° for the 2-Me substituted derivative **4c** (Figure 6.5). Aryl rings are known to pi-pi stack and this is easier when bigger groups can't impede these effects through sterics.³¹ This is more profound when there is an *ortho* substituent present, which agrees with the improved solubility value of 58 μM for compound **4c**.^{32, 33}

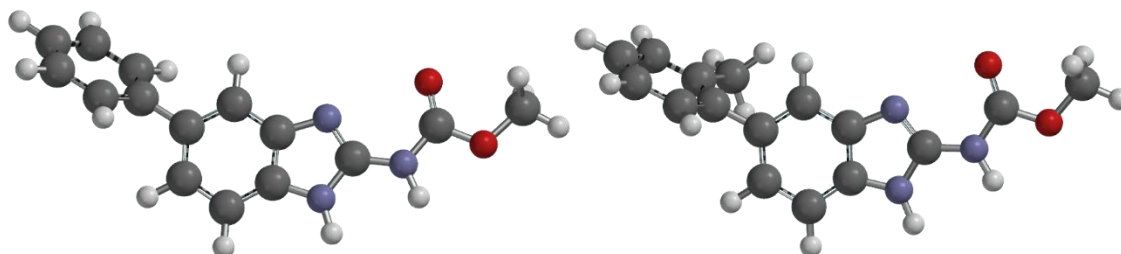


Figure 6.5. Biphenyls 'twist' in order to adopt an energetically favourable conformation.³⁰

6.2.4 *In Vivo* Mouse Data

Measured data showed a significant increase in solubility for one of the biphenyl molecules, **4c**, and it possessed a moderate activity value of 1 mg/L. Therefore, it was synthesised on an increased scale and subjected to *in vivo* testing (Figure 6.7). Subcutaneous dosing was carried out using 10% DMSO, 10% Tween and 80% PBS and showed no significant decrease in fungal density when compared with the control. This is believed to be an issue with gut penetration, as observed with some of the other templates, but further PK/PD studies are ongoing to understand the lack of *in vivo* activity.

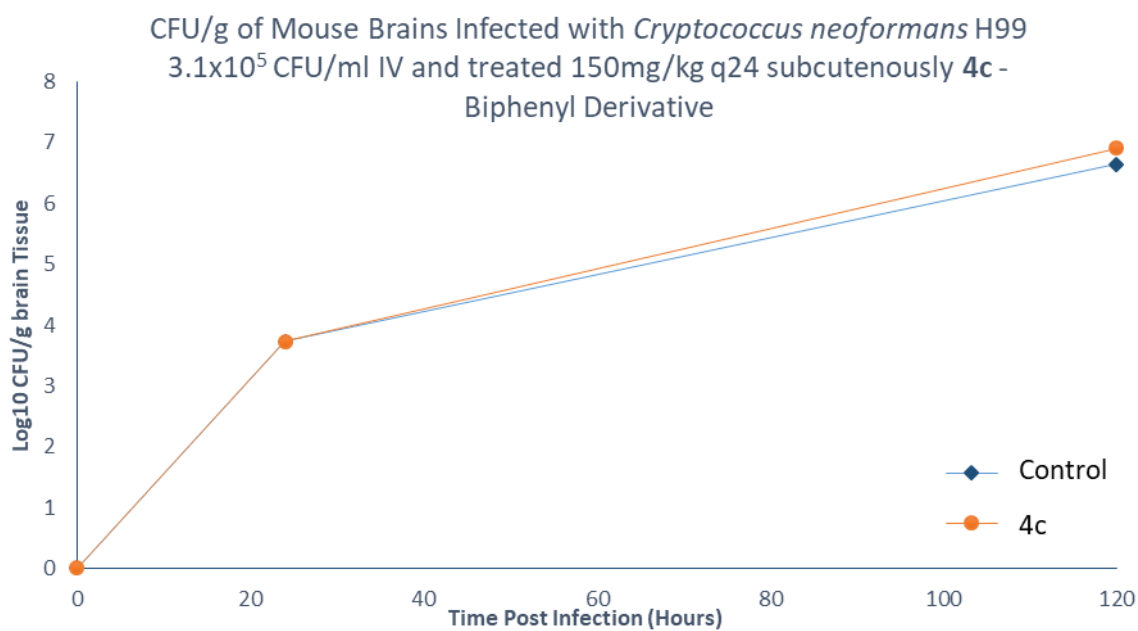


Figure 6.7. Compound **4c** was administered subcutaneously 150 mg/kg once daily, but showed no decrease in fungal density.

6.3 Conclusion

Establishment of a new synthetic route to synthesise a range of biphenyl derivatives was devised and optimised and a total of 17 analogues were synthesised, and a basic SAR profile developed (Figure 6.8). Whilst there is the presence of some activity, the most active compound has an MIC of 0.5 mg/L, which when compared to other benzimidazole templates is only acceptable. It also showed no observable reduction in fungal density in the *in vivo* mouse model. Furthermore, compared to other classes, the biphenyl class has increased measured metabolic clearance values. However, it does possess improved solubility, with the best measured solubility value recorded as 58 μ M, which is a significantly better than the flubendazole value of 0.8 μ M. Despite the improvement in solubility, this template was suspended due to reduced activity and metabolic clearance values.

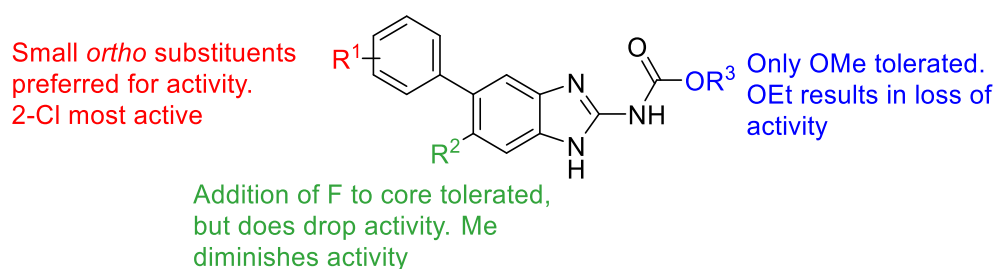


Figure 6.8. An overall SAR conclusion.

6.4 Future work

Due to the suspension of this template, there are currently no plans to carry out any further optimisation of these analogues due to suboptimal properties. However, addition of a morpholine solubilising group could be employed to identify if this helps further with aqueous solubility. Given that morpholine generally causes a reduction in activity, this is likely to completely diminish activity from the biphenyl class. Furthermore, it may be beneficial to test an active biphenyl analogue again in an *in vivo* mouse model, using a different vehicle or dosing route, so as to observe whether this helps with exposure. This should be further validated with PK/PD models to determine what happens to the compound after administration.

6.5 Experimental

6.5.1 General Experimental Details

For general experimental details please see Section 3.5.1, Chapter 3. For synthesis of dimethyl ((methylthio)methylene)dicarbamate please see Section 3.5.2, Chapter 3.

6.5.1.1 HPLC

Flow rate 1 ml/min for 15 minutes using MeCN/Water with compounds dissolved in methanol. UV detector recorded signals at 254 nm. **HPLC Method A:** min, gradient: 2% MeCN hold to 1 min, 2-98% MeCN in 11 min, then hold at 98% MeCN to 15 min.

6.5.2 General Procedures

General Procedure A – Suzuki Coupling of tert-butyl dicarbonate protected amine

To a sealed tube at room temperature was added Di-tert-butyl (4-bromo-1,2-phenylene)dicarbamate (1.0 eq.), cesium carbonate (2.0 eq.), a substituted boronic acid (1.2 eq.), Bis(triphenylphosphine)palladium(II) dichloride (0.1 eq.), toluene (4 ml) and the reaction stirred overnight at 80 °C. The reaction was cooled to room temperature, diluted with ethyl acetate, washed with saturated aq. NaHCO₃ solution, water and brine, dried over magnesium sulphate, concentrated and purified by column chromatography eluting with 5% ethyl acetate and *n*-hexane to afford the desired products (55% yield).

General Procedure B – Suzuki coupling of a 2-nitroaniline derivative with a boronic acid

To a flask at room temperature was added a halogenated 2-nitroaniline compound (1eq.), chosen carbonate base (1.8 eq.), a substituted boronic acid (1.2 eq.), Tetrakis(triphenylphosphine)palladium(0) (0.05 eq.) and chosen solvent and the reaction heated to 80 °C overnight. The reaction was then cooled to room temperature, diluted with ethyl acetate, washed with saturated aq. NaHCO₃ solution, water and brine, dried over magnesium sulphate and purified via column chromatography eluting with 10% ethyl acetate in *n*-hexane.

General Procedure C – tert-butyl carbamate deprotection

To a flask at room temperature was added the substituted di-tert-butyl [1,1'-biphenyl]-3,4-diyl dicarbamate (0.50 mmol, 1 eq.), DCM (5 ml) and trifluoroacetic acid (5 ml) and the reaction stirred at room temperature overnight. The reaction was then concentrated, diluted with ethyl acetate,

washed with saturated aq. NaHCO₃ solution,, water, brine, dried over magnesium sulphate and concentrated to give the desired product (100%).

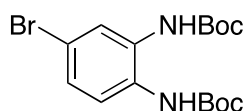
General Procedure D – Single Nitro reduction

To a flask at room temperature was added 3-nitro-[1,1'-biphenyl]-4-amine (1.0 eq.), EtOH (0.15 M) and SnCl₂ (5.0 eq.) and the reaction refluxed (65 °C) overnight. The reaction was then cooled to room temperature, concentrated, adjusted to pH 10 with 25% NaOH and filtered with water and ethyl acetate. The water layer was then washed twice more with ethyl acetate, the combined organic layers washed with brine, dried over magnesium sulphate and concentrated. The product was purified by column chromatography eluting with 50% Ethyl acetate in *n*-hexane, increasing to 100% Ethyl acetate, to elute the product.

General Procedure E – Acid Mediated Ring Closure

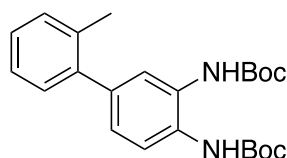
To a flask at room temperature was added 4-(Phenylthio)benzene-1,2-diamine derivative (1.0 eq.), acetic acid (2 M), MeOH (0.4 M), dimethyl ((methylthio)methylene)dicarbamate (1.0 eq.) and the reaction heated to 65 °C overnight. The reaction was allowed to cool to room temperature and the resulting solid filtered using diethyl ether to give the final product.

Synthesis of Di-tert-butyl (4-bromo-1,2-phenylene)dicarbamate (5)



To a flask at room temperature was added 4-bromo-1,2-diaminobenzene (**1**) (1.0 eq), ethanol (20 ml) and di-tert-butyl dicarbonate (2.4 eq) and the reaction stirred at room temperature overnight. The resulting reaction was concentrated under reduce pressure to yield the product (**5**) (4.37 g, 100% yield) as a brown solid. ¹H NMR (400 MHz, CDCl₃) δ 7.75 (d, 1H, *J* = 2.1 Hz), 7.32 (d, 1H, *J* = 7.0 Hz), 7.21 (dd, 1H, *J* = 7.0 & 2.1 Hz), 6.77 (bs, 1H), 6.59 (bs, 1H), 1.51 (s, 9H), 1.50 (s, 9H). ¹³C NMR (100 MHz, CDCl₃) δ 153.7, 153.3, 127.9, 126.8, 126.5, 125.7, 125.5, 118.9, 85.2, 81.3, 28.2, 27.4. HRMS (ES+) Calculated for C₁₆H₂₃N₂O₄²³Na⁷⁹Br: 409.0739. Found [M+Na]⁺: 409.0727 (Diff -2.9 ppm).

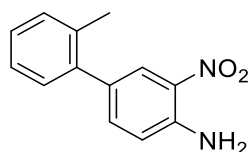
Di-tert-butyl (2'-methyl-[1,1'-biphenyl]-3,4-diyl)dicarbamate (6c)



General Procedure A - Employed 2-methylphenylboronic acid to yield the product (**6c**) (0.28 g, 55% yield) as a yellow solid. ^1H NMR (400 MHz, CDCl_3) δ 7.52 (d, 1H, $J = 8.2$ Hz), 7.45 (d, 1H, $J = 2.0$ Hz), 7.24 – 7.20 (m, 4H), 7.09 (dd, 1H, $J = 2.0$ Hz), 6.75 (s, 2H), 2.27 (s, 3H), 1.54 (s, 9H), 1.51 (s, 9H). ^{13}C NMR (100 MHz, CDCl_3) δ 153.9, 153.8, 140.9, 139.2, 135.4, 130.3, 129.8, 127.3, 126.2, 125.6, 125.7, 121.0, 80.9, 28.3, 28.2, 20.5. HRMS (ES+) Calculated for $\text{C}_{23}\text{H}_{30}\text{N}_2\text{O}_4^{23}\text{Na}$: 421.2013. Found $[\text{M}+\text{Na}]^+$: 421.2092 (Diff – 2.7 ppm).

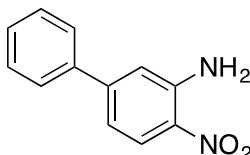
6.5.2.1 Synthesis of 3-nitro-[1,1'-biphenyl]-4-amines

2'-Methyl-3-nitro-[1,1'-biphenyl]-4-amine (**8c**)

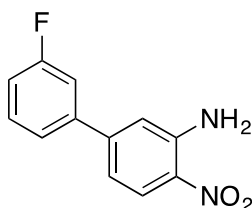


General Procedure B – Employed 4-bromo-2-nitroaniline and 2,4-dimethoxyphenylboronic acid, potassium carbonate in DMF/Water (1:1) to yield the product (**8c**) (1.58 g, 100% yield) as a yellow solid. ^1H NMR (400 MHz, CDCl_3) δ 8.11 (d, 1H, $J = 2.0$ Hz), 7.37 (dd, 1H, $J = 8.6$ & 2.0 Hz), 7.29 – 7.19 (m, 4H), 6.86 (d, 1H, $J = 8.6$ Hz), 6.10 (bs, 2H), 2.29 (s, 3H). ^{13}C NMR (100 MHz, CDCl_3) δ 143.5, 139.5, 136.9, 135.4, 132.0, 131.0, 130.6, 129.7, 127.6, 126.2, 126.1, 118.5, 20.5.

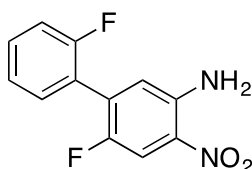
4-Nitro-[1,1'-biphenyl]-3-amine (**8d**)



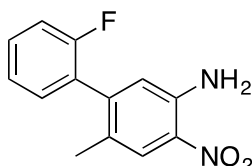
General Procedure B – Employed 5-chloro-2-nitroaniline and phenylboronic acid, potassium carbonate in DMF/Water (1:1) to yield the product (**8d**) (0.15 g, 43% yield) as a yellow solid. ^1H NMR (400 MHz, CDCl_3) δ 8.18 (d, 1H, $J = 8.6$ Hz), 7.59 - 7.55 (m, 2H), 7.47 - 7.44 (m, 3H), 6.98 (d, 1H, $J = 2.0$ Hz), 6.93 (dd, 1H, $J = 8.6$ & 2.0 Hz), 6.14 (s, 2H). ^{13}C NMR (100 MHz, CDCl_3) δ 148.6, 144.8, 138.9, 131.5, 129.0, 128.9, 127.2, 126.9, 116.5, 116.4. HRMS (Cl^+ , CH_4) Calculated for $\text{C}_{12}\text{H}_{11}\text{N}_2\text{O}_2$: 215.0815. Found $[\text{M}+\text{H}]^+$: 215.0819 (Diff -1.76 ppm).

3'-Fluoro-4-nitro-[1,1'-biphenyl]-3-amine (8e)

General Procedure B – Employed 5-chloro-2-nitroaniline and 3-fluorophenylboronic acid, cesium carbonate in Toluene (1:1) to yield the product **(8e)** (0.14 g, 26% yield) as a yellow solid. ^1H NMR (400 MHz, CDCl_3) δ 8.19 (d, 1H, $J = 8.9$ Hz), 7.44 – 7.42 (m, 1H), 7.35 (d, 2H, $J = 8.9$ Hz), 7.27 (d, 1H, $J = 8.5$ Hz), 7.13– 7.10 (m, 1H), 6.96 (d, 1H, $J = 2.1$ Hz), 6.91 (dd, 1H, $J = 8.5$ & 2.1 Hz), 6.15 (s, 2H). ^{13}C NMR (100 MHz, CDCl_3) δ 163.1 (d, $J = 247.3$ Hz), 147.2, 144.8, 130.5 (d, $J = 7.9$ Hz), 130.1, 127.0, 122.8 (d, $J = 3.2$ Hz), 116.7, 116.2, 115.7 (d, $J = 22.0$ Hz), 114.2 (d, $J = 22.0$ Hz). Not all quaternary carbons visible. HRMS (Cl^+ , CH_4) Calculated for $\text{C}_{12}\text{H}_{10}\text{FN}_2\text{O}_2$: 233.0721. Found $[\text{M}+\text{H}]^+$: 233.0722 (Diff -0.72 ppm).

2',6-Difluoro-4-nitro-[1,1'-biphenyl]-3-amine (8f/8g)

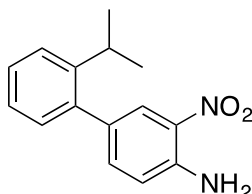
General Procedure B – Employed 5-chloro-4-fluoro-2-nitroaniline, 2-fluorophenylboronic acid, potassium carbonate in DMF/Water (1:1) to yield the product **(8f/8g)** (0.17 g, 46% yield) as a yellow solid. ^1H NMR (400 MHz, CDCl_3) δ 7.94 (d, 1H, $J = 10.2$ Hz), 7.44 – 7.42 (m, 1H), 7.39 – 7.37 (m, 1H), 7.23 – 7.20 (m, 2H), 6.85 (d, 1H, $J = 6.0$ Hz), 6.00 (s, 2H). ^{13}C NMR (100 MHz, CDCl_3) δ 159.6 (d, $J = 250.3$ Hz), 150.8 (d, $J = 244.2$ Hz), 141.1, 139.7 (d, $J = 22.6$ Hz), 133.0 (d, $J = 18.4$ Hz), 131.1 (d, $J = 8.1$ Hz), 131.1 (d, $J = 2.1$ Hz), 124.3 (d, $J = 3.6$ Hz), 121.6 (d, $J = 15.0$ Hz), 121.0 (d, $J = 2.4$ Hz), 116.1 (d, $J = 22.3$ Hz), 111.9 (d, $J = 28.5$ Hz). HRMS (Cl^+ , CH_4) Calculated for $\text{C}_{12}\text{H}_{10}\text{F}_2\text{N}_2\text{O}_2$: 251.0627. Found $[\text{M}+\text{H}]^+$: 251.0624 (Diff 1.23 ppm).

2'-Fluoro-6-methyl-4-nitro-[1,1'-biphenyl]-3-amine (8h)

General Procedure B – Employed 5-chloro-4-methyl-2-nitroaniline, 2-fluorophenylboronic acid, potassium carbonate in DMF/Water (1:1) to yield the product **(8h)** (0.18 g, 46% yield) as a yellow solid. ^1H NMR (400 MHz, CDCl_3) δ 8.03 (s, 1H), 7.40 – 7.38 (m, 1H), 7.23 – 7.20 (m, 2H), 7.16 – 7.14 (m, 1H),

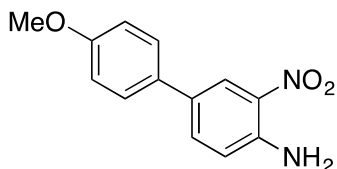
6.70 (s, 1H), 5.96 (s, 1H), 2.09 (s, 3H). ^{13}C NMR (100 MHz, CDCl_3) δ 159.1 (d, $J = 244.9$), 153.3, 144.4, 142.4, 130.6 (d, $J = 3.4$ Hz), 130.1 (d, $J = 7.9$ Hz), 127.2 (d, $J = 17.5$ Hz), 126.4, 125.1, 124.2, (d, $J = 3.3$ Hz), 120.2, 115.8 (d, $J = 21.9$ Hz), 18.8. HRMS (CI^+ , CH_4) Calculated for $\text{C}_{13}\text{H}_{12}\text{FN}_2\text{O}_2$: 247.0877. Found $[\text{M}+\text{H}]^+$: 247.0885 (Diff -3.25 ppm).

2'-Isopropyl-3-nitro-[1,1'-biphenyl]-4-amine (8i)



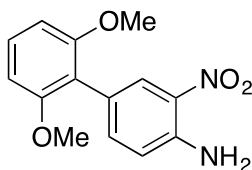
General Procedure B – Employed 4-bromo-2-nitroaniline and 2-isopropylphenylboronic acid, cesium carbonate in toluene to yield the product **(8i)** (0.19 g, 40% yield) as a yellow solid. ^1H NMR (400 MHz, CDCl_3) δ 8.08 (s, 1H), 7.37 – 7.33 (m, 3H), 7.22 - 7.20 (m, 1H), 7.15 (d, 1H, $J = 8.0$ Hz), 6.85 (d, 1H, $J = 8.6$ Hz), 6.09 (s, 2H), 3.02 (sep, 1H, $J = 6.8$ Hz), 1.17 (d, 6H, $J = 6.8$ Hz). ^{13}C NMR (100 MHz, CDCl_3) δ 146.6, 143.4, 138.6, 137.0, 133.4, 131.1, 130.0, 128.1, 126.2, 125.8, 125.6, 118.4, 29.5, 24.2. HRMS (CI^+ , CH_4) Calculated for $\text{C}_{15}\text{H}_{17}\text{N}_2\text{O}_2$: 257.1285. Found $[\text{M}+\text{H}]^+$: 257.1290 (Diff 1.94).

4'-Methoxy-3-nitro-[1,1'-biphenyl]-4-amine (8j)



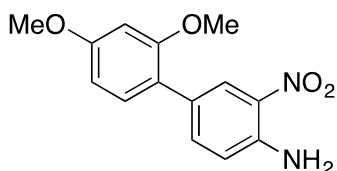
General Procedure B – Employed 4-bromo-2-nitroaniline and 4-methoxyphenylboronic acid, potassium carbonate in DMF/Water (1:1) to yield the product **(8j)** (0.25 g, 57% yield) as a yellow solid. ^1H NMR (400 MHz, CDCl_3) δ 8.31 (d, 1H, $J = 1.9$ Hz), 7.60 (dd, 1H, $J = 8.7$ & 1.9 Hz), 7.48 (d, 2H, $J = 8.9$ Hz), 6.97 (d, 2H, $J = 8.9$ Hz), 6.87 (d, 1H, $J = 8.7$ Hz), 6.07 (s, 2H), 3.84 (s, 3H). ^{13}C NMR (100 MHz, CDCl_3) δ 159.1, 143.3, 134.3, 131.4, 130.2, 127.4, 123.2, 119.3, 114.4, 55.4. HRMS (CI^+ , CH_4) Calculated for $\text{C}_{13}\text{H}_{12}\text{N}_2\text{O}$: 245.0921. Found $[\text{M}+\text{H}]^+$: 245.0929 (Diff -3.25 ppm).

2',6'-Dimethoxy-3-nitro-[1,1'-biphenyl]-4-amine (8k)



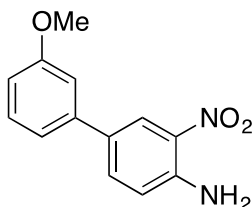
General Procedure B – Employed 4-bromo-2-nitroaniline and 2,6-dimethoxyphenylboronic acid, potassium carbonate in DMF/Water (1:1) to yield the product (**8k**) (0.21g, 42% yield) as a yellow solid. ^1H NMR (400 MHz, CDCl_3) δ 8.16 (d, 1H, $J = 1.9$ Hz), 7.39 (dd, 1H, $J = 8.5$ & 1.9 Hz), 7.28 (dd, 1H, $J = 8.5$ & 8.2 Hz), 6.82 (d, 1H, $J = 8.5$ Hz), 6.64 (d, 2H, $J = 8.2$ Hz), 6.06 (s, 2H), 3.76 (s, 6H). ^{13}C NMR (100 MHz, CDCl_3) δ 157.7, 143.5, 139.0, 131.7, 129.0, 128.3, 122.9, 117.8, 117.0, 104.1, 56.1.

2',4'-Dimethoxy-3-nitro-[1,1'-biphenyl]-4-amine (8l)

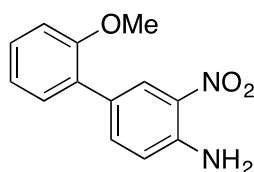


General Procedure B – Employed 4-bromo-2-nitroaniline and 2,4-dimethoxyphenylboronic acid, potassium carbonate in DMF/Water (1:1) to yield the product (**8l**) (0.29 g, 58% yield) as a yellow solid. ^1H NMR (400 MHz, CDCl_3) δ 8.25 (d, 1H, $J = 1.8$ Hz), 7.57 (dd, 1H, $J = 8.4$ & 1.8 Hz), 7.22 (d, 1H, $J = 8.0$ Hz), 6.82 (d, 1H, $J = 8.4$ Hz), 6.58 – 6.54 (m, 2H, $J = 8.0$ Hz), 6.06 (s, 2H), 3.85 (s, 3H), 3.81 (s, 3H). ^{13}C NMR (100 MHz, CDCl_3) δ 160.5, 157.5, 143.3, 137.3, 132.2, 130.7, 127.7, 126.0, 121.2, 118.2, 104.8, 99.0, 55.6, 55.5. HRMS (Cl^+ , CH_4) Calculated for $\text{C}_{14}\text{H}_{15}\text{N}_2\text{O}_4$: 275.1026. Found $[\text{M}+\text{H}]^+$: 275.1034 (Diff - 2.81 ppm).

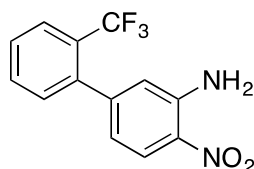
3'-Methoxy-3-nitro-[1,1'-biphenyl]-4-amine (8m)



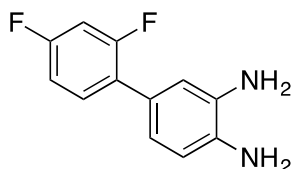
General Procedure B – Employed 4-bromo-2-nitroaniline and 3-methoxyphenylboronic acid, potassium carbonate in DMF/Water (1:1) to yield the product (**8m**) (0.25 g, 57% yield) as a yellow solid. ^1H NMR (400 MHz, CDCl_3) δ 8.37 (d, 1H, $J = 2.2$ Hz), 7.63 (dd, 1H, $J = 8.9$ & 2.2 Hz), 7.36 – 7.34 (m, 1H, $J = 8.6$ Hz), 7.14 (d, 1H, $J = 8.9$ Hz), 7.08 – 7.05 (m, 1H), 6.88 (d, 2H, $J = 8.6$ Hz), 6.11 (bs, 2H), 3.87 (s, 3H). ^{13}C NMR (100 MHz, CDCl_3) δ 160.2, 143.9, 140.3, 134.6, 132.5, 130.3, 130.0, 124.1, 119.3, 118.9, 112.7, 112.2, 55.4. HRMS (Cl^+ , CH_4) Calculated for $\text{C}_{13}\text{H}_{15}\text{N}_2\text{O}$: 215.1179. Found $[\text{M}+\text{H}]^+$: 215.1186 (Diff -3.91 ppm).

2'-Methoxy-3-nitro-[1,1'-biphenyl]-4-amine (8n)

General Procedure B – Employed 4-bromo-2-nitroaniline and 2-methoxyphenylboronic acid, potassium carbonate in DMF/Water (1:1) to yield the product (**8n**) (0.37 g, 82% yield) as a yellow solid. ^1H NMR (400 MHz, CDCl_3) δ 8.31 (d, 1H, $J = 2.3$ Hz), 7.61 (dd, 1H, $J = 8.7$ & 2.3 Hz), 7.33 – 7.30 (m, 2H), 7.04 – 7.02 (m, 1H, $J = 7.9$ Hz), 6.98 (d, 1H, $J = 7.9$ Hz), 6.83 (d, 1H, $J = 8.7$ Hz), 3.83 (s, 3H). ^{13}C NMR (100 MHz, CDCl_3) δ 156.4, 143.5, 137.3, 132.1, 130.2, 128.9, 128.3, 127.7, 126.4, 121.0, 118.2, 111.2, 55.6. HRMS (Cl^+ , CH_4) Calculated for $\text{C}_{13}\text{H}_{13}\text{N}_2\text{O}_3$: 245.0921. Found $[\text{M}+\text{H}]^+$: 245.0926 (Diff -2.25 ppm).

4-Nitro-2'-(trifluoromethyl)-[1,1'-biphenyl]-3-amine (8o)

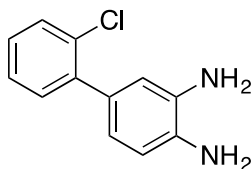
General Procedure B – Employed 5-chloro-2-nitroaniline and 2-trifluoromethylphenylboronic acid, potassium carbonate in DMF/Water (1:1) to yield the product (**8o**) (0.15 g, 23% yield) as a yellow solid. ^1H NMR (400 MHz, CDCl_3) δ 8.14 (d, 1H, $J = 8.8$ Hz), 7.76 (d, 1H, $J = 7.5$ Hz), 7.59 (dd, 1H, $J = 7.6$ Hz & 8.0 Hz), 7.52 (dd, 1H, $J = 7.4$ & 8.0 Hz), 7.31 (d, 1H, $J = 7.4$ Hz), 6.76 (s, 1H), 6.67 (d, 1H, $J = 8.8$ Hz), 6.11 (s, 2H). ^{13}C NMR (100 MHz, CDCl_3) δ 147.5, 143.9, 139.1, 131.7, 131.6, 131.0, 128.3, 126.3 (q, $J = 5.0$ Hz), 125.8, 125.3, 122.5 (q, $J = 234.5$ Hz), 119.1, 118.4. HRMS (Cl^+ , CH_4) Calculated for $\text{C}_{13}\text{H}_{10}\text{F}_3\text{N}_2\text{O}_2$: 283.0689. Found $[\text{M}+\text{H}]^+$: 283.0697 (Diff -3.04 ppm).

6.5.2.2 Synthesis of [1,1'-biphenyl]-3,4-diamines**2',4'-Difluoro-[1,1'-biphenyl]-3,4-diamine (3a)**

General Procedure D - Employed 4-bromo-1,2-diaminobenzene, 2,4-difluorophenylboronic acid and cesium carbonate in dioxane to yield the product (**3a**) (0.037 g, 11% yield) as an orange oil. ^1H NMR (400 MHz, CDCl_3) δ 7.46 – 7.42 (m, 1H), 6.90 – 6.65 (m, 4H), 6.76 (d, 1H, $J = 7.68$ Hz), 3.45 (s, 4H). ^{13}C NMR (100 MHz, CDCl_3) δ 165.7 (d, $J = 255.2$ Hz), 165.3 (d, $J = 252.5$ Hz), 139.1, 134.7, 131.0, 126.8,

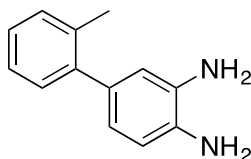
124.0, 121.0, 117.3, 116.5, 109.0 (d, $J = 14.6$ Hz), 102.4 (dd, $J = 26.5$ & 24.5 Hz). HRMS (CI+, CH₄) Calculated for C₁₂H₁₁F₂N₂: 221.0890. Found [M+H]⁺: 221.0885 (Diff – 2.26 ppm).

2'-Chloro-[1,1'-biphenyl]-3,4-diamine (3b)



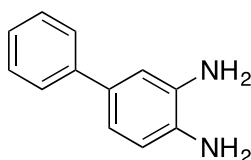
General Procedure D – Employed 4-bromo-1,2-diaminobenzene, 2-chlorophenylboronic acid and cesium carbonate in dioxane to yield the product **(3b)** (0.19 g, 33% yield) as an orange oil. ¹H NMR (400 MHz, CDCl₃) δ 7.42 (d, 1H, $J = 8.2$ Hz), 7.31 (dd, 1H, $J = 7.5$ & 1.6 Hz), 7.28 – 7.25 (m, 1H, $J = 1.6$ Hz), 7.21 (ddd, 1H, $J = 8.2, 7.5$ & 1.9 Hz), 6.83 – 6.80 (m, 2H), 6.77 (d, 1H, $J = 8.6$ Hz), 3.45 (s, 4H). ¹³C NMR (100 MHz, CDCl₃) δ 140.7, 134.5, 134.1, 132.5, 131.4, 129.9, 127.9, 126.7, 121.6, 118.0, 116.8, 116.2. HRMS (CI+, CH₄) Calculated for C₁₂H₁₂ClN₂: 219.0684. Found [M+H]⁺: 219.0690 (Diff -2.93 ppm).

2'-Methyl-[1,1'-biphenyl]-3,4-diamine (3c)

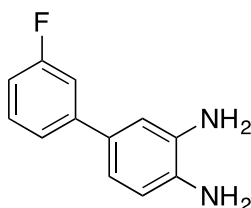


General Procedure C - Employed using di-tert-butyl (2'-methyl-[1,1'-biphenyl]-3,4-diyl)dicarbamate **(6c)** to yield the product **(3c)** (0.099 g, 100% yield) as an orange oil. ¹H NMR (400 MHz, CDCl₃) δ 7.23 – 7.19 (m, 4H), 6.74 (d, 1H, $J = 8.4$ Hz), 6.69 – 6.65 (m, 2H), 2.89 (s, 4H), 2.29 (s, 3H). ¹³C NMR (100 MHz, CDCl₃) δ 142.1, 135.5, 134.3, 134.2, 133.5, 130.2, 129.8, 126.7, 125.6, 121.2, 117.7, 116.4, 20.6. HRMS (CI+, CH₄) Calculated for C₁₃H₁₅N₂: 199.1235. Found [M+H]⁺: 199.1233 (Diff -1.00 ppm).

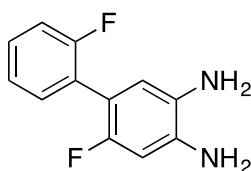
[1,1'-Biphenyl]-3,4-diamine (3d)



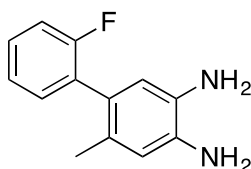
General Procedure D - Employed 4-nitro-[1,1'-biphenyl]-3-amine **(8d)** to yield the product **(3d)** (0.11 g, 55% yield) as an orange oil. ¹H NMR (400 MHz, CDCl₃) δ 7.52 (d, 2H, $J = 8.3$ Hz), 7.50 - 7.47 (m, 3H), 7.27 (d, 1H, $J = 7.5$ Hz), 6.96 (s, 1H), 6.76 (d, 1H, $J = 7.5$ Hz). ¹³C NMR (100 MHz, CDCl₃) δ 141.4, 134.9, 134.3, 133.5, 128.6, 126.6, 126.4, 119.1, 117.0, 115.5. HRMS (CI+, CH₄) Calculated for C₁₂H₁₃N₂: 185.1073. Found [M+H]⁺: 185.1077 (Diff -2.27 ppm).

3'-Fluoro-[1,1'-biphenyl]-3,4-diamine (3e)

General Procedure D - Employed 3'-fluoro-4-nitro-[1,1'-biphenyl]-3-amine (**8e**) to yield the product (**3e**) (0.047 g, 43% yield) as an orange oil. ^1H NMR (400 MHz, CDCl_3) δ 7.25 – 7.22 (m, 2H), 7.13 – 7.11 (m, 1H), 6.86 (d, 1H, $J = 7.8$ Hz), 6.85 – 6.82 (m, 2H), 6.66 (d, 1H, $J = 7.8$ Hz), 3.37 (s, 4H). ^{13}C NMR (100 MHz, CDCl_3) δ 163.0 (d, $J = 230.8$ Hz), 143.7, 143.6, 134.9, 132.0, 130.0 (d, $J = 9.0$ Hz), 122.1 (d, $J = 3.8$ Hz), 119.1, 116.9, 115.3, 113.2, (d, $J = 22.8$ Hz), 113.0 (d, $J = 21.4$ Hz). HRMS (Cl^+ , CH_4) Calculated for $\text{C}_{12}\text{H}_{12}\text{FN}_2$: 203.0979. Found $[\text{M}+\text{H}]^+$: 203.0984 (Diff -2.58 ppm).

2',6-Difluoro-[1,1'-biphenyl]-3,4-diamine (3f/3g)

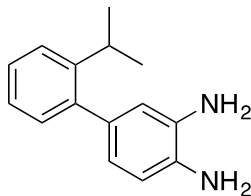
General Procedure D - Employed 2',6-difluoro-4-nitro-[1,1'-biphenyl]-3-amine (**8f/8g**) to yield the product (**3f/3g**) (0.13 g, 86% yield) as an orange oil. ^1H NMR (400 MHz, CDCl_3) δ 7.34 – 7.31 (m, 2H), 7.18 – 7.12 (m, 2H), 6.70 (d, 1H, $J = 6.7$ Hz), 6.52 (d, 1H, $J = 10.6$ Hz), 3.62 (s, 2H), 3.28 (s, 2H). ^{13}C NMR (100 MHz, CDCl_3) δ 159.9 (d, $J = 248.0$ Hz), 154.6 (d, $J = 239.3$ Hz), 137.2 (d, $J = 10.3$ Hz), 131.7 (dd, $J = 3.3$ & 2.1 Hz), 129.7 (d, $J = 2.3$ Hz), 128.9 (d, $J = 8.1$ Hz), 115.7 (d, $J = 22.4$ Hz), 113.3 (d, $J = 16.5$ Hz), 103.3 (d, $J = 26.9$). Not all quaternary carbons visible. HRMS (Cl^+ , CH_4) Calculated for $\text{C}_{12}\text{H}_{11}\text{F}_2\text{N}_2$: 221.0885. Found $[\text{M}+\text{H}]^+$: 221.0887 (Diff -1.21 ppm).

2'-Fluoro-6-methyl-[1,1'-biphenyl]-3,4-diamine (3h)

General Procedure D - Employed 2'-fluoro-6-methyl-4-nitro-[1,1'-biphenyl]-3-amine (**8h**) to yield the product (**3h**) (0.10 g, 63% yield) as an orange oil. ^1H NMR (400 MHz, CDCl_3) δ 7.32 – 7.27 (m, 1H), 7.24 – 7.20 (m, 1H), 7.17 – 7.14 (m, 1H), 7.13 – 7.08 (m, 1H), 6.62 (s, 1H), 6.59 (s, 1H), 3.36 (s, 4H), 2.06 (s, 3H). ^{13}C NMR (100 MHz, CDCl_3) δ 159.9 (d, $J = 245.1$ Hz), 137.0, 135.0, 132.0 (d, $J = 3.1$ Hz), 129.4 (d, J

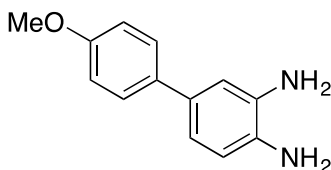
= 16.5 Hz), 128.5 (d, $J=7.9$ Hz), 127.1, 123.8 (d, $J=3.60$ Hz), 118.9, 118.0, 117.1, 115.3 (d, $J=23.5$ Hz), 19.1. HRMS (CI⁺, CH₄) Calculated for C₁₃H₁₄FN₂: 217.1136. Found [M+H]⁺: 217.1138 (Diff -1.08 ppm).

2'-Isopropyl-[1,1'-biphenyl]-3,4-diamine (**3i**)



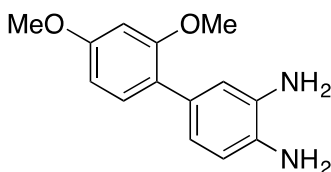
General Procedure D - Employed 2'-isopropyl-3-nitro-[1,1'-biphenyl]-4-amine (**8i**) to yield the product (**3i**) (0.096 g, 60% yield) as an orange solid. ¹H NMR (400 MHz, CDCl₃) δ 7.34 (d, 1H, $J=7.7$ Hz), 7.30 – 7.28 (m, 1H), 7.18 – 7.14 (m, 2H), 6.74 – 7.72 (m, 1H), 6.65 – 6.63 (m, 2H), 3.44 (s, 4H), 3.15 (sep, 1H, $J=6.8$ Hz), 1.15 (d, 6H, $J=6.8$ Hz). ¹³C NMR (100 MHz, CDCl₃) δ 146.6, 141.3, 134.4, 134.3, 133.4, 130.1, 127.2, 125.4, 125.1, 121.3, 117.8, 116.3, 20.5, 24.2. HRMS (CI⁺, CH₄) Calculated for C₁₅H₁₉N₂: 227.1543. Found [M+H]⁺: 227.1552 (Diff – 4.18 ppm).

4'-Methoxy-[1,1'-biphenyl]-3,4-diamine (**3j**)



General Procedure D - Employed 4'-methoxy-3-nitro-[1,1'-biphenyl]-4-amine (**8j**) to yield the product (**3j**) (0.12 g, 55% yield) as an orange oil. ¹H NMR (400 MHz, CDCl₃) δ 7.44 (d, 2H, $J=8.2$ Hz), 6.92 (d, 2H, $J=8.2$ Hz), 6.92 – 6.88 (m, 2H), 6.75 (d, 1H, $J=8.4$ Hz), 3.83 (s, 3H), 3.43 (s, 4H). ¹³C NMR (100 MHz, CDCl₃) δ 158.5, 135.0, 134.1, 133.7, 133.3, 127.6, 118.7, 117.1, 115.2, 114.0, 55.3. HRMS (CI⁺, CH₄) Calculated for C₁₂H₁₁F₂N₂: 215.1179. Found [M+H]⁺: 215.1183 (Diff -1.83 ppm).

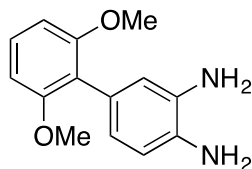
2',4'-Dimethoxy-[1,1'-biphenyl]-3,4-diamine (**3k**)



General Procedure D - Employed 2',4'-dimethoxy-3-nitro-[1,1'-biphenyl]-4-amine (**8k**) to yield the product (**3k**) (0.15 g, 60% yield) as an orange oil. ¹H NMR (400 MHz, CDCl₃) 7.19 (d, 1H, $J=8.2$ Hz), 6.89 – 6.84 (m, 2H), 6.73 (d, 1H, $J=8.2$ Hz), 6.55 – 6.51 (m, 2H), 3.83 (s, 3H), 3.78 (s, 3H), 3.34 (s, 4H). ¹³C NMR (100 MHz, CDCl₃) 159.7, 157.4, 134.2, 133.6, 131.0, 130.5, 123.9, 121.5, 118.1, 116.4, 104.4,

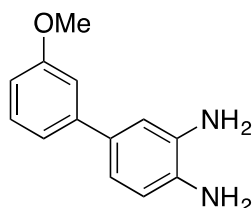
99.0, 55.6, 55.4. HRMS (CI+, CH₄) Calculated for C₁₄H₁₇N₂O₂: 245.1285. Found [M+H]⁺: 245.1290 (Diff - 2.78 ppm).

2',6'-Dimethoxy-[1,1'-biphenyl]-3,4-diamine (3l)



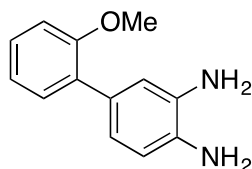
General Procedure D - Employed 2',6'-dimethoxy-3-nitro-[1,1'-biphenyl]-4-amine (**8l**) to yield the product (**3l**) (0.068 g, 37% yield) as an orange oil. ¹H NMR (400 MHz, CDCl₃) 7.22 (d, 1H, *J* = 8.5 Hz), 6.75 (m, 1H), 6.72 (m, 2H), 6.63 (d, 2H, *J* = 8.5 Hz), 3.73 (s, 6H), 3.40 (s, 4H). ¹³C NMR (100 MHz, CDCl₃) 157.9, 134.0, 133.8, 128.0, 125.7, 122.9, 121.1, 119.6, 116.4, 104.2, 56.0. HRMS (CI+, CH₄) Calculated for C₁₄H₁₇N₂O₂: 245.1285. Found [M+H]⁺: 245.1292.

3'-Methoxy-[1,1'-biphenyl]-3,4-diamine (3m)

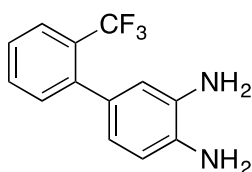


General Procedure D - Employed 3'-methoxy-3-nitro-[1,1'-biphenyl]-4-amine (**8m**) to yield the product (**3m**) (0.14 g, 67% yield) as an orange oil. ¹H NMR (400 MHz, CDCl₃) δ 7.30 (dd, 1H, *J* = 8.7 & 7.8 Hz), 7.11 (d, 1H, *J* = 7.8 Hz), 7.06 (d, 1H, *J* = 2.3 Hz), 6.99 - 6.95 (m, 2H, *J* = 8.2 Hz), 6.82 (dd, 1H, *J* = 8.2 & 2.3 Hz), 6.75 (d, 1H, *J* = 8.2 Hz), 3.86 (s, 3H), 3.45 (s, 4H). ¹³C NMR (100 MHz, CDCl₃) δ 159.9, 142.9, 134.9, 134.5, 133.4, 129.5, 119.2, 119.1, 116.9, 115.5, 112.3, 111.8, 55.1. HRMS (CI+, CH₄) Calculated for C₁₂H₁₁F₂N₂: 215.1179. Found [M+H]⁺: 215.1186 (Diff -3.42 ppm).

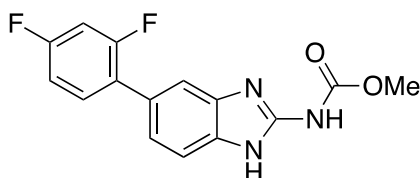
2'-Methoxy-[1,1'-biphenyl]-3,4-diamine (3n)



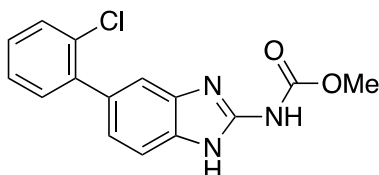
General Procedure D - Employed 2'-methoxy-3-nitro-[1,1'-biphenyl]-4-amine (**8n**) to yield the product (**3n**) (0.15 g, 48% yield) as an orange oil. ¹H NMR (400 MHz, CDCl₃) δ 7.29 - 7.24 (m, 2H), 6.99 (d, 1H, *J* = 7.4 Hz), 6.93 - 6.58 (m, 3H), 6.74 (d, 1H, *J* = 7.4 Hz), 3.79 (s, 3H), 3.41 (s, 4H). HRMS (CI+, CH₄) Calculated for C₁₃H₁₅N₂O: 215.1179. Found [M+H]⁺: 215.1186 (Diff -3.08 ppm).

2'-(Trifluoromethyl)-[1,1'-biphenyl]-3,4-diamine (3o)

General Procedure D - Employed 4-nitro-2'-(trifluoromethyl)-[1,1'-biphenyl]-3-amine (**8o**) to yield the product (**3o**) (0.082 g, 51% yield) as an orange oil. ^1H NMR (400 MHz, CDCl_3) δ 7.07 (d, 1H, $J = 7.4$ Hz), 7.50 (dd, 1H, $J = 8.6$ & 7.4 Hz), 7.40 (dd, 1H, $J = 8.6$ & 7.5 Hz), 7.32 (d, 1H, $J = 7.5$ Hz), 6.72 – 6.68 (m, 3H), 3.44 (s, 4H). ^{13}C NMR (100 MHz, CDCl_3) δ 144.5, 141.7, 134.2 (q, $J = 45.1$ Hz), 132.2, 132.0, 131.1, 126.7, 126.0 (q, $J = 6.3$ Hz), 124.5 (q, $J = 254.4$ Hz), 122.9, 121.1, 117.6, 116.0. HRMS (CI^+ , CH_4) Calculated for $\text{C}_{13}\text{H}_{12}\text{F}_3\text{N}_2$: 253.0947. Found $[\text{M}+\text{H}]^+$: 253.0949 (Diff – 0.88 ppm).

6.5.2.3 Synthesis of methyl (5-phenyl-1H-benzo[d]imidazol-2-yl)carbamates**Methyl (5-(2,4-difluorophenyl)-1H-benzo[d]imidazol-2-yl)carbamate (4a)**

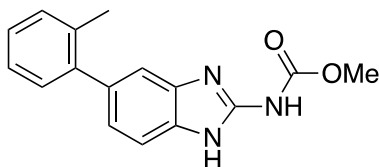
General Procedure E - Employed 2',4'-difluoro-[1,1'-biphenyl]-3,4-diamine (**3a**) to yield the product (**4a**) (0.13 g, 32% yield) as white solid. ^1H NMR (400 MHz, CDCl_3) δ 11.67 (s, 2H), 7.57 (dd, 1H, $J = 8.3$ & 2.0 Hz), 7.52 (s, 1H), 7.47 (d, 1H, $J = 8.3$ Hz), 7.34 – 7.32 (m, 1H), 7.23 – 7.20 (m, 1H), 7.17 – 7.14 (m, 1H), 3.77 (s, 3H). ^{13}C NMR (100 MHz, CDCl_3) δ 163.6 (d, $J = 252.3$ Hz), 158.0 (d, $J = 250.6$ Hz), 152.6, 149.1, 141.5, 134.6, 132.7, 132.6, 125.7 (d, $J = 16.0$ Hz), 112.4, 118.5, 113.1, 112.3 (d, $J = 20.8$ Hz), 105.0 (dd, $J = 26.9$ & 26.3 Hz), 52.9. HRMS (ES^+) Calculated for $\text{C}_{15}\text{H}_{12}\text{F}_2\text{N}_3\text{O}_2$: 304.0898 (Diff -1.20 ppm). Found $[\text{M}+\text{H}]^+$: 304.0894. $\nu_{\text{max}}/\text{cm}^{-1}$: (solid) 3372 (s), 1715 (s), 1511 (m), 1478 (m), 1274 (m). Purity HPLC (Method A) 92.6%, $R_t = 9.18$ min.

Methyl (5-(2-chlorophenyl)-1H-benzo[d]imidazol-2-yl)carbamate (4b)

General Procedure E - Employed 2'-chloro-[1,1'-biphenyl]-3,4-diamine (**3b**) to yield the product (**4b**) (0.020 g, 15% yield) as white solid. ^1H NMR (400 MHz, DMSO) δ 11.66 (s, 2H), 7.55 (d, 1H, $J = 8.0$ Hz), 7.47 – 7.42 (m, 4H), 7.38 – 7.36 (m, 1H), 7.11 (d, 1H, $J = 8.0$ Hz), 3.77 (s, 3H). ^{13}C NMR (100 MHz, DMSO)

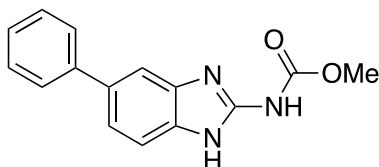
δ 156.1, 150.6, 141.2, 141.1, 132.2, 132.1, 132.0, 130.2, 129.1, 129.0, 127.8, 122.9, 117.2, 116.0, 52.9. HRMS (ES+) Calculated for $C_{15}H_{13}ClN_3O_2$: 302.0696. Found $[M+H]^+$: 302.0688 (Diff – 2.64 ppm). ν_{max}/cm^{-1} : (solid) 3330 (s), 2979 (m), 2882 (m), 1645 (s), 1460 (m), 1440 (m), 1256 (m), 761 (s). MP: >280 °C decomposed. Purity HPLC (Method A) 97.5%, R_t = 9.31 min.

Methyl (5-(*o*-tolyl)-1*H*-benzo[*d*]imidazol-2-yl)carbamate (4c)

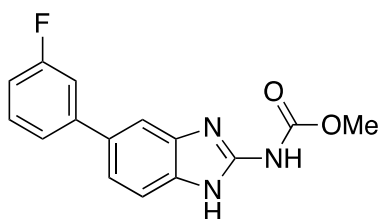


General Procedure E - Employed 2'-methyl-[1,1'-biphenyl]-3,4-diamine (**3c**) to yield the product (**4c**) (0.048 g, 49% yield) as white solid. 1H NMR (400 MHz, DMSO) δ 11.65 (bs, 2H), 7.44 (d, 1H, J = 8.2 Hz), 7.32 (d, 1H, J = 1.3 Hz), 7.30 – 7.26 (m, 1H), 7.26 – 7.20 (m, 3H), 7.03 (dd, 1H, J = 8.2 & 1.3 Hz), 3.75 (s, 3H), 2.24 (s, 3H). ^{13}C NMR (100 MHz, DMSO) δ 115.6, 148.5, 142.7, 135.3, 134.8, 133.5, 132.7, 130.7, 130.3, 127.2, 126.3, 122.9, 114.0, 113.4, 52.6, 20.5. HRMS (ES+) Calculated for $C_{16}H_{16}N_3O_2$: 282.1243. Found $[M+H]^+$: 282.1236 (Diff – 2.30 ppm). ν_{max}/cm^{-1} : (solid) 3328 (s), 3019 (m), 2952 (m), 1651 (s), 1469 (m), 1445 (m), 1262 (m). MP: 206 - 208 °C. Purity HPLC (Method A) 96.3%, R_t = 9.38 min.

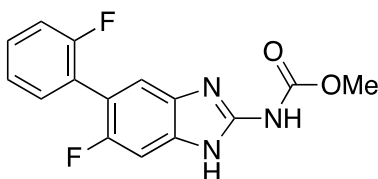
Methyl (5-phenyl-1*H*-benzo[*d*]imidazol-2-yl)carbamate (4d)



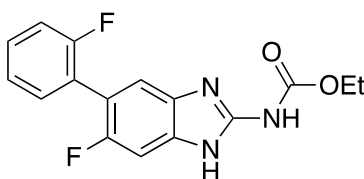
General Procedure E - Employed [1,1'-biphenyl]-3,4-diamine (**3d**) to yield the product (**4d**) (0.037 g, 51% yield) as white solid. 1H NMR (400 MHz, DMSO) δ 11.69 (s, 2H), 7.67 – 7.62 (m, 3H), 7.48 – 7.42 (m, 3H), 7.37 (d, 1H, J = 7.9 Hz), 7.32 (d, 1H, J = 7.9 Hz), 3.77 (s, 3H). ^{13}C NMR (100 MHz, DMSO) δ 155.5, 148.5, 141.8, 141.2, 134.1, 129.6, 126.3, 127.2, 127.0, 120.7, 117.8, 114.7. HRMS (ES+) Calculated for $C_{15}H_{14}N_3O_2$: 268.1086. Found $[M+H]^+$: 268.1084 (Diff -0.74 ppm). ν_{max}/cm^{-1} : (solid) 3361 (s), 2950 (m), 2683 (m), 1621 (m), 1588 (m), 1268 (s). MP: >280 °C decomposed. Purity HPLC (Method A) 97.1%, R_t = 8.90 min.

Methyl (5-(3-fluorophenyl)-1H-benzo[d]imidazol-2-yl)carbamate (4e)

General Procedure E - Employed 3'-fluoro-[1,1'-biphenyl]-3,4-diamine (**3e**) to yield the product (**4e**) (0.028g, 40 % yield) as white solid. ^1H NMR (400 MHz, DMSO) δ 11.67 (s, 2H), 7.69 (s, 1H), 7.50 – 7.56 (m, 3H), 7.47 – 7.42 (m, 2H), 7.15 – 7.13 (m, 1H), 3.77 (s, 3H). ^{13}C NMR (100 MHz, DMSO) δ 163.1 (d, J = 243.5 Hz), 155.4, 148.6, 144.4 (d, J = 7.6 Hz), 139.4, 135.6, 132.5, 131.2 (d, J = 8.6 Hz), 123.3 (d, J = 2.4 Hz), 120.7, 116.0, 114.3, 113.8 (d, J = 22.1 Hz), 113.6 (d, 21.2 Hz), 52.9. HRMS (ES+) Calculated for $\text{C}_{15}\text{H}_{13}\text{FN}_3\text{O}_2$: 286.0992. Found $[\text{M}+\text{H}]^+$: 286.0987 (Diff -1.75 ppm). $\nu_{\text{max}}/\text{cm}^{-1}$: (solid) 3371 (s), 2953 (m), 2682 (m), 1629 (s), 1460 (m), 1298 (s). MP: 282 °C decomposed. Purity HPLC (Method A) 97.3%, R_t = 9.14 min.

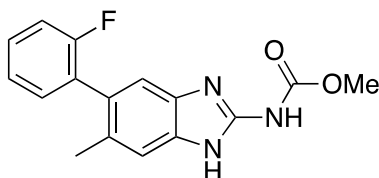
Methyl (6-fluoro-5-(2-fluorophenyl)-1H-benzo[d]imidazol-2-yl)carbamate (4f)

General Procedure E - Employed 2',6-difluoro-[1,1'-biphenyl]-3,4-diamine (**3f**) to yield the product (**4f**) (0.027 g, 33% yield) as white solid. ^1H NMR (400 MHz, DMSO) δ 11.93 (s, 1H), 11.53 (s, 1H), 7.48 – 7.45 (m, 2H), 7.39 (d, 1H, J = 6.9 Hz), 7.35 – 7.33 (m, 2H), 7.29 (d, 1H, J = 9.6 Hz), 3.78 (s, 3H). ^{13}C NMR (100 MHz, DMSO) δ 162.3 (d, J = 248.6 Hz), 157.3 (d, J = 256.9 Hz), 154.9, 149.0, 139.5, 132.5 (d, J = 2.7 Hz), 131.0 (dd, J = 21.4 & 12.0 Hz), 130.5 (d, J = 9.9 Hz), 130.3 (d, J = 8.0 Hz), 125.1 (d, J = 2.2 Hz), 124.6 (d, J = 16.3 Hz), 120.8 (dd, J = 28.4 & 7.7 Hz), 176.1 (d, J = 22.4 Hz), 130.8 (d, J = 16.7 Hz), 53.5. HRMS (ES+) Calculated for $\text{C}_{15}\text{H}_{12}\text{FN}_3\text{O}_2$: 304.0898. Found $[\text{M}+\text{H}]^+$: 304.0891 (Diff -2.30 ppm). $\nu_{\text{max}}/\text{cm}^{-1}$: (solid) 3393 (s), 2956 (m), 2668 (m), 1650 (s), 1581 (m), 1468 (m), 1262 (s). MP: 230 - 232 °C decomposed. Purity HPLC (Method A) 97.3%, R_t = 9.05 min.

Ethyl (6-fluoro-5-(2-fluorophenyl)-1H-benzo[d]imidazol-2-yl)carbamate (4g)

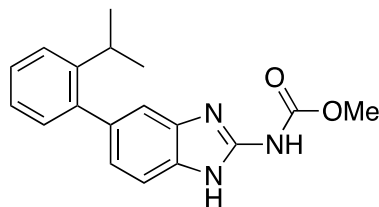
General Procedure E - Employed 2',6-difluoro-[1,1'-biphenyl]-3,4-diamine (**3g**) to yield the product (**4g**) (0.012 g, 14% yield) as white solid. ^1H NMR (400 MHz, DMSO) δ 11.91 (s, 2H), 7.47 – 7.44 (m, 2H), 7.37 (d, 1H, $J = 6.8$ Hz), 7.35 – 7.31 (m, 2H), 7.27 (d, 1H, $J = 10.3$ Hz), 4.22 (q, 2H, $J = 6.2$ Hz), 1.28 (t, 2H, $J = 6.2$ Hz). ^{13}C NMR (100 MHz, DMSO) δ 159.9 (d, $J = 247.5$ Hz), 158.0 (d, $J = 267.4$ Hz), 150.3, 146.7, 139.2 (d, $J = 10.2$ Hz), 132.5 (d, $J = 3.0$ Hz), 131.6 (d, $J = 8.7$ Hz), 131.1 (dd, $J = 33.4$ & 8.7 Hz), 130.2 (d, $J = 8.7$ Hz), 125.1 (d, $J = 3.3$ Hz), 124.6 (d, $J = 16.2$ Hz), 116.0 (d, $J = 22.4$ Hz), 114.2 (d, $J = 11.3$ Hz), 100.6 (d, $J = 17.1$ Hz), 61.6, 14.9. HRMS (ES+) Calculated for $\text{C}_{16}\text{H}_{14}\text{F}_3\text{N}_3\text{O}_2$: 318.1054. Found $[\text{M}+\text{H}]^+$: 318.1045 (Diff – 2.83 ppm). $\nu_{\text{max}}/\text{cm}^{-1}$: (solid) 3308 (m), 2028 (m), 2983 (m), 2944 (m), 1604 (s), 1526 (m), 1426 (m). MP: 294 - 296 °C decomposed. Purity HPLC (Method A) 96.5%, $R_t = 9.57$ min.

Methyl (5-(2-fluorophenyl)-6-methyl-1H-benzo[d]imidazol-2-yl)carbamate (4h)



General Procedure E - Employed 2'-fluoro-6-methyl-[1,1'-biphenyl]-3,4-diamine (**3h**) to yield the product (**4h**) (0.04 g, 29% yield) as white solid. ^1H NMR (400 MHz, DMSO) δ 11.62 (s, 2H), 7.44 – 7.42 (m, 1H), 7.31 – 7.27 (m, 4H), 7.20 – 7.18 (s, 1H), 3.75 (s, 3H), 2.15 (s, 3H). ^{13}C NMR (100 MHz, DMSO) δ 159.6 (d, $J = 245.5$ Hz), 156.2, 148.8, 148.4, 134.6, 132.5 (d, $J = 3.4$ Hz), 130.0, 129.8, 129.6 (d, $J = 8.1$ Hz), 129.0 (d, $J = 23.0$ Hz), 124.9 (d, $J = 2.6$ Hz), 116.7, 115.9 (d, $J = 22.8$ Hz), 113.2, 52.9, 20.4. HRMS (ES+) Calculated for $\text{C}_{16}\text{H}_{15}\text{FN}_3\text{O}_2$: 300.1148. Found $[\text{M}+\text{H}]^+$: 300.1143 (Diff -1.67 ppm). $\nu_{\text{max}}/\text{cm}^{-1}$: (solid) 3302 (s), 2984 (m), 2944 (m), 2846 (m), 1624 (s), 1594 (m), 1476 (m), 1274 (s). MP: >300 °C decomposed. Purity HPLC (Method A) 96.5%, $R_t = 9.27$ min

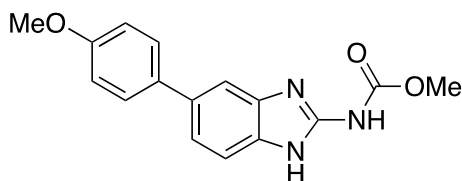
Methyl (5-(2-isopropylphenyl)-1H-benzo[d]imidazol-2-yl)carbamate (4i)



General Procedure E - Employed 2'-isopropyl-[1,1'-biphenyl]-3,4-diamine (**3i**) to yield the product (**4i**) (0.009 g, 7% yield) as white solid. ^1H NMR (400 MHz, DMSO) δ 11.54 (s, 2H), 7.37 (d, 1H, $J = 7.6$ Hz), 7.29 – 7.27 (m, 1H), 7.27 – 7.23 (m, 3H), 7.06 (d, 1H, $J = 1.3$ Hz), 6.71 (dd, 1H, $J = 7.6$ & 1.2 Hz), 3.54 (s, 3H), 3.16 (sep, 1H, $J = 6.9$ Hz), 1.11 (d, 6H, $J = 6.9$ Hz). ^{13}C NMR (100 MHz, DMSO) δ 157.6, 146.5, 142.9, 139.4, 136.5, 132.4, 130.6, 127.2, 125.7, 125.5, 123.3, 115.8, 114.1, 51.7, 29.2, 24.7. Not all quaternary

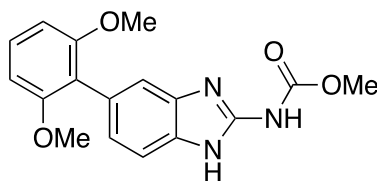
carbons visible. HRMS (ES+) Calculated for $C_{18}H_{20}N_3O_2$: 310.1556. Found $[M+H]^+$: 310.1556 (Diff 0.00 ppm). Not enough sample to obtain rest of data after MIC testing.

Methyl (5-(4-methoxyphenyl)-1H-benzo[d]imidazol-2-yl)carbamate (4j)



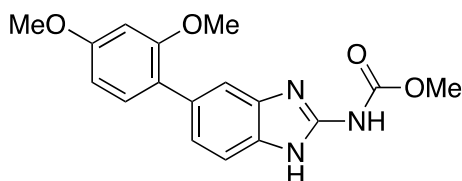
General Procedure E - Employed 4'-methoxy-[1,1'-biphenyl]-3,4-diamine (**3j**) to yield the product (**4j**) (0.083 g, 66 % yield) as white solid. 1H NMR (400 MHz, DMSO) δ 11.63 (s, 2H), 7.58 (d, 1H, $J = 1.5$ Hz), 7.56 (d, 2H, $J = 8.7$ Hz), 7.43 (d, 1H, $J = 8.3$ Hz), 7.32 (dd, 1H, $J = 8.3$ & 1.5 Hz), 7.01 (d, 2H, $J = 8.7$ Hz), 3.80 (s, 3H), 3.76 (s, 3H). ^{13}C NMR (100 MHz, DMSO) δ 158.8, 155.6, 145.5, 140.5, 134.3, 133.9, 131.8, 128.2, 120.4, 118.1, 115.2, 114.9, 55.6, 52.9. HRMS (ES+) Calculated for $C_{16}H_{14}F_3N_3O_2$: 298.1186. Found $[M+H]^+$: 298.1196 (Diff 3.35 ppm). ν_{max}/cm^{-1} : (solid) 3408 (s), 2958 (m), 2741 (m), 1637 (s), 1474 (m), 1275 (s). MP: >300 °C decomposed. Purity HPLC (Method A) 96.8%, $R_t = 9.84$ min.

Methyl (5-(2,6-dimethoxyphenyl)-1H-benzo[d]imidazol-2-yl)carbamate (4k)



General Procedure E - Employed 2',6'-dimethoxy-[1,1'-biphenyl]-3,4-diamine (**3k**) to yield the product (**4k**) (0.025 g, 30% yield) as white solid. 1H NMR (400 MHz, DMSO) δ 11.63 (s, 2H), 7.33 (d, 1H, $J = 8.7$ Hz), 7.28 (d, 1H, $J = 8.2$ Hz), 7.2 (d, 1H, $J = 1.5$ Hz), 6.88 (dd, 1H, $J = 8.2$ & 1.5 Hz), 6.73 (d, 2H, $J = 8.7$ Hz), 3.24 (s, 3H), 3.65 (s, 6H). ^{13}C NMR (100 MHz, DMSO) δ 163.4, 157.8, 148.3, 139.1, 135.1, 131.6, 1128.9, 124.5, 120.1, 116.5, 109.8, 104.9, 56.0, 52.7. HRMS (ES+) Calculated for $C_{17}H_{18}N_3O_4$: 328.1292. Found $[M+H]^+$: 328.1304 (Diff 3.66). MP: >300 °C. Purity HPLC (Method A) 98.0%, $R_t = 8.52$ min.

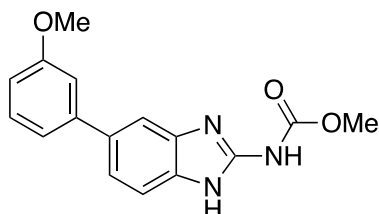
Methyl (5-(2,4-dimethoxyphenyl)-1H-benzo[d]imidazol-2-yl)carbamate (4l)



General Procedure E - Employed 2',4'-dimethoxy-[1,1'-biphenyl]-3,4-diamine (**3l**) to yield the product (**4l**) (0.041 g, 43% yield) as white solid. 1H NMR (400 MHz, DMSO) δ 11.72 (s, 2H), 7.26 (s, 1H), 7.19 –

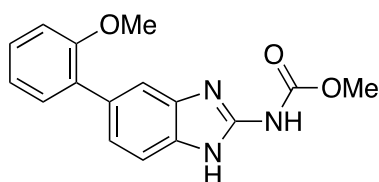
7.15 (m, 2H), 6.90 (d, 1H, $J = 8.4$ Hz), 6.62 (s, 1H), 6.58 (d, 1H, $J = 8.4$ Hz), 3.79 (s, 3H), 3.74 (s, 3H), 3.54 (s, 3H). ^{13}C NMR (100 MHz, DMSO) δ 161.9, 159.5, 157.5, 149.2, 140.6, 138.1, 131.4, 128.9, 125.1, 120.7, 115.1, 114.4, 105.5, 99.4, 55.9, 55.6, 51.6. HRMS (ES+) Calculated for $\text{C}_{17}\text{H}_{18}\text{N}_3\text{O}_4$: 328.1292. Found $[\text{M}+\text{H}]^+$: 328.1300 (Diff 2.43 ppm). MP: >300 °C. Purity HPLC (Method A) 97.7%, $R_t = 8.76$ min.

Methyl (5-(3-methoxyphenyl)-1H-benzo[d]imidazol-2-yl)carbamate (4m)

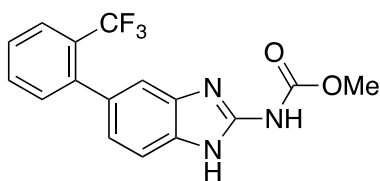


General Procedure E - Employed 3'-methoxy-[1,1'-biphenyl]-3,4-diamine (**3m**) to yield the product (**4m**) (0.049 g, 61% yield) as white solid. ^1H NMR (400 MHz, DMSO) δ 11.68 (s, 2H), 7.68 (s, 1H), 7.48 (d, 1H, $J = 8.4$ Hz), 7.41 – 7.39 (m, 1H), 7.37 (d, 1H, $J = 7.9$ Hz), 7.23 (d, 1H, $J = 7.9$ Hz), 7.17 (s, 1H), 6.92 (d, 1H, $J = 8.4$ Hz), 3.85 (s, 3H), 3.79 (s, 3H). ^{13}C NMR (100 MHz, DMSO) δ 160.2, 155.5, 152.1, 148.6, 143.4, 137.0, 133.9, 130.4, 120.8, 119.6, 118.0, 117.1, 112.7, 112.6, 55.5, 53.0. HRMS (ES+) Calculated for $\text{C}_{16}\text{H}_{14}\text{F}_3\text{N}_3\text{O}_3$: 298.1186. Found $[\text{M}+\text{H}]^+$: 298.1197 (Diff 3.69 ppm). MP: >300 °C decomposed.

Methyl (5-(2-methoxyphenyl)-1H-benzo[d]imidazol-2-yl)carbamate (4n)



General Procedure E - Employed 2'-methoxy-[1,1'-biphenyl]-3,4-diamine (**3n**) to yield the product (**4n**) (0.030 g, 41% yield) as white solid. ^1H NMR (400 MHz, DMSO) δ 11.61 (s, 2H), 7.49 (s, 1H), 7.39 (d, 1H, $J = 8.0$ Hz), 7.32 – 7.28 (m, 2H, $J = 8.0$ Hz), 7.16 (d, 1H, $J = 7.6$ Hz), 7.09 (d, 1H, $J = 7.6$ Hz), 7.03 – 7.01 (m, 1H), 3.76 (s, 6H). ^{13}C NMR (100 MHz, DMSO) δ 159.8, 156.6, 148.4, 138.2, 135.4, 131.6, 131.3, 131.1, 128.6, 123.1, 121.2, 116.9, 114.6, 112.2, 55.9, 52.8. HRMS (ES+) Calculated for $\text{C}_{16}\text{H}_{14}\text{F}_3\text{N}_3\text{O}_2$: 298.1186. Found $[\text{M}+\text{H}]^+$: 298.1192 (Diff 2.01 ppm). $\nu_{\text{max}}/\text{cm}^{-1}$: (solid) 3334 (s), 2955 (m), 2881 (m), 827 (m), 1653 (s), 1498 (m), 1263 (s). MP – 218 – 220 °C. Purity HPLC (Method A) 95.2%, $R_t = 12.60$ min

Methyl (5-(2-(trifluoromethyl)phenyl)-1H-benzo[d]imidazol-2-yl)carbamate (4o)

General Procedure E - Employed 2'-(trifluoromethyl)-[1,1'-biphenyl]-3,4-diamine (**3o**) to yield the product (**4o**) (0.041g, 37% yield) as white solid. ^1H NMR (400 MHz, DMSO) δ 11.71 (s, 2H), 7.82 (d, 1H, $J = 7.7$ Hz), 7.70 (d, 1H, $J = 8.6$ & 7.7 Hz), 7.60 (t, 1H, $J = 8.6$ Hz), 7.43 (d, 2H, $J = 8.3$), 7.34 (s, 1H), 7.01 (d, 1H, $J = 8.3$ Hz), 3.77 (s, 3H). ^{13}C NMR (100 MHz, DMSO) δ 155.3, 148.5, 142.3, 141.6, 133.1, 132.6, 129.3, 128.0, 127.7 (q, $J = 30.1$ Hz), 126.4 (q, $J = 6.0$ Hz), 126.1, 124.8 (q, $J = 272.7$ Hz), 122.4, 118.1, 114.3, 52.9. HRMS (ES+) Calculated for $\text{C}_{16}\text{H}_{13}\text{F}_3\text{N}_3\text{O}_2$: 336.0960. Found $[\text{M}+\text{H}]^+$: 336.0959 (Diff -0.29 ppm). $\nu_{\text{max}}/\text{cm}^{-1}$: (solid) 3391 (s), 2956 (m), 2760 (m), 1718 (s), 1471 (m), 1458 (m), 1248 (s), 1103 (s). MP – 211 - 213 °C decomposed. Purity HPLC (Method A) 95.1%, $R_t = 9.51$ min.

6.6 References

1. M. P. Marques, O. M. Takayanagui and V. L. Lanchote, *Braz. J. Med. Biol. Res.*, 2002, **35**, 261-269.
2. Q. A. McKellar, C. Gokbulut, K. Muzandu and H. Benchaoui, *Drug Metab. Dispos.*, 2002, **30**, 1230-1239.
3. M. Murray, A. M. Hudson and V. Yassa, *Chemical research in toxicology*, 1992, **5**, 60-66.
4. E. Syslová, P. Landa, L. R. Stuchlíková, P. Matoušková, L. Skálová, B. Szotáková, M. Navrátilová, T. Vaněk and R. Podlipná, *Chemosphere*, 2019, **218**, 662-669.
5. I. Vokřál, H. Bártíková, L. Prchal, L. Stuchlíková, L. Skálová, B. Szotáková, J. Lamka, M. Várady and V. Kubíček, *Parasitology*, 2012, **139**, 1309-1316.
6. Y. Ogino, N. Ohtake, Y. Nagae, K. Matsuda, M. Ishikawa, M. Moriya, M. Kanesaka, Y. Mitobe, J. Ito, T. Kanno, A. Ishihara, H. Iwaasa, T. Ohe, A. Kanatani and T. Fukami, *Bioorg. Med. Chem. Lett.*, 2008, **18**, 4997-5001.
7. N. Miyaura and A. Suzuki, *Bioorg. Med. Chem. Lett.*, 1995, **95**, 2457-2483.
8. A. Suzuki, *J. Organomet. Chem.*, 1999, **576**, 147-168.
9. *US Pat.*, WO2008US13865, 2008.
10. G. A. Molander and I. Shin, *Org. Lett.*, 2012, **14**, 4458-4461.
11. L. Wang, X. Yang, X. Wang and L. Sun, *Dyes Pigments*, 2015, **113**, 581-587.
12. *US Pat.*, US20080146637, 2007.
13. C. Baillie, W. Chen and J. Xiao, *Tetrahedron Lett.*, 2001, **42**, 9085-9088.
14. F.-S. Han, *Chem. Soc. Rev.*, 2013, **42**, 5270-5298.
15. A. J. J. Lennox and G. C. Lloyd-Jones, *Chem. Soc. Rev.*, 2014, **43**, 412-443.
16. L. Liu, W. Wang and C. Xiao, *J. Organomet. Chem.*, 2014, **749**, 83-87.
17. Y. Ogata, *J. Org. Chem.*, 1982, **47**, 3577-3581.
18. E. C. Cortés and L. A. A. Anaya, *J. Heterocycl. Chem.*, 1997, **34**, 745-748.
19. M. B. Smith and J. March, *March's Advanced Organic Chemistry: Reactions, Mechanisms, and Structure*, Wiley, 5th Edition edn., 2001.
20. EUCAST, European Committee on Antimicrobial Susceptibility Testing (EUCAST), <http://www.eucast.org/documents/sops/>, July 2019).
21. H. Nishikawa, Y. Fukuda, J. Mitsuyama, M. Tashiro, A. Tanaka, T. Takazono, T. Saijo, K. Yamamoto, S. Nakamura, Y. Imamura, T. Miyazaki, H. Kakeya, Y. Yamamoto, K. Yanagihara, H. Mukae, S. Kohno and K. Izumikawa, *J. Antimicrob. Chemother.*, 2017, **72**, 1709-1713.
22. T. Shibata, T. Takahashi, E. Yamada, A. Kimura, H. Nishikawa, H. Hayakawa, N. Nomura and J. Mitsuyama, *Antimicrob Agents Chemother*, 2012, **56**, 5892-5897.
23. Y. Hamada, in *Pyridine*, InTechOpen, 1st edn., 2018, DOI: 10.5772/intechopen.74719.
24. ChemDraw, *Perkin Elmer*, 2017.
25. G. Patrick, *An Introduction to Medicinal Chemistry* Oxford, 4th edn., 2009.
26. C. A. Lipinski, F. Lombardo, B. W. Dominy and P. J. Feeney, *Adv. Drug Deliv. Rev.*, 1997, **23**, 3-25.
27. Optibrium, *Stardrop*, 2018.
28. V. H. Freed, R. Haque and J. Verneti, *J. Agric. Food Chem.*, 1967, **15**, 1121-1123.
29. J. E. Cheong, M. Zaffagni, I. Chung, Y. Xu, Y. Wang, F. E. Jernigan, B. R. Zetter and L. Sun, *Eur. J. Med. Chem.*, 2018, **144**, 372-385.
30. Wavefunction, *Spartan*, 2017.
31. S. E. Wheeler, *J. Am. Chem. Soc.*, 2011, **133**, 10262-10274.
32. R. Karupnaswamy and P. Ganesan, *J. Chem. Sci.*, 2018, **130**, 82-89.
33. F. Grein, *J. Phys. Chem. A*, 2002, **106**, 3823-3827.

Chapter 7

Computational Evaluation of the Benzimidazole Scaffold

7.1 Computational Evaluation of the Benzimidazole Class

Synthetically, this project has allowed for the development and establishment of some successful routes to synthesise a number of different benzimidazole analogues. This has resulted in a large library of around 150 compounds being produced, with further synthesis ongoing. Within this template, there is room for much more optimisation and structure exploration and this presents synthetic chemists with a problem. With so many potential compounds that could be synthesised, how do we decide which ones should be prioritised?

In this chapter, we discuss the use of docking protocols and binding site visualisation, to understand how the molecules which have been synthesised are predicted to bind to the target protein. We will investigate the differences in binding between the classes, as well as any differences in binding between active and inactive compounds of the same class. Knowledge of binding poses and interactions can then be implemented in the design of future analogues.

Also, due to large number of compounds synthesised we can build a Quantitative Structure Activity Relationship (QSAR) model, which through a process of machine learning, will allow for a model to be built. The activity of new compounds can then be predicted, allowing for prioritisation of synthesis of new analogues.

7.2 Chapter Acknowledgements

Many thanks to Neil Berry for his guidance on how to use the programmes, develop the protocols and how to present the data. Thanks to Jack Simpson for the extra support with Pipeline Pilot and QSAR Modelling. Many thanks to Jaclyn Bibby who built the homology models for *C. neoformans* and Human β -tubulin, which are used for the docking protocols in this chapter.

7.3 Molecular Modelling

It was important to attempt to understand how the compounds we were synthesising were binding to the proposed target. This was carried out to aid understanding of the structure activity relationship. Whilst benzimidazoles are widely known to bind to β -tubulin, the precise binding poses within the active sites of *C. neoformans* and human β -tubulin are unknown due to no crystal structures being available. This meant that generation of a homology model was necessary in order to assess the binding of the molecules and understand the potential ligand-protein interactions.

7.3.1 Homology Models and Similarity

There are currently no crystal structures available for either *C. neoformans* or human β -tubulin. There is a crystal structure available for *Bos taurus*, also known as common cattle, which shows a high degree of similarity in amino sequence to both *C. neoformans* and of the human to *C. neoformans* (Table 7.1). This showed an 81% identity and 91% similarity of *Bos Taurus* to *C. neoformans* and the human showed a 90% similarity to *C. neoformans*. Work carried by Jaclyn Bibby in the University of Liverpool, Department of Chemistry allowed for homology models of both *C. neoformans* and human β -tubulin to be constructed from their amino acids sequences, based on the overall structure of *Bos taurus*.

Table 7.1. The identity and similarity of *Bos Taurus* and human β -tubulin when compared with *C. neoformans* β -tubulin. Identity relates to the number of amino acids that are identical. Similarity is amino acids that are similar.

With respect to <i>C. neoformans</i> β -tubulin	<i>Bos taurus</i> β -tubulin		Human β -tubulin	
	N ^o of Amino acid residues	Percentage %	N ^o of Amino acid residues	Percentage %
Identity	346/447	81.4		
Similarity	405/447	90.6	402/447	89.9

Molecular docking looks at how a ligand interacts with the target binding site. It does this in terms of conformation and orientation of a compound otherwise known as a pose. When looking at how a ligand binds we generally want to see what molecular interactions are present and how this impacts on activity. The process of docking starts by using docking algorithms to pose small molecules within the chosen active site of the protein, which is a challenge given that even small molecules can produce many different conformers and modes of binding. Scoring functions, which assess how strongly a given binding pose interacts with the protein are the objective function in the docking process.¹

Scoring functions rely on shape and what non-covalent interactions there could be, to evaluate how well a compound will 'fit'. If a particular conformer looks interesting, then it can be inspected in more

detail, looking at non-covalent interactions, including electrostatic, H-bonding and Van der Waals interactions.¹

It is possible to look for a correlation between predicted strength of binding (Score) with biological activity as it is hypothesised that those compounds with good activity, should also have good complementary binding and therefore more likely to possess good binding scores. This approach can then be applied to new molecules, which first can be docked and scored to see if they are likely to produce biological activity and then synthesised if they are believed to be a suitable candidate. This could save time and money as only compounds which are predicted to bind strongly would be prioritised for synthesis.^{1,2}

Docking involves looking at the space within the binding site and how a ligand, in its large number of orientations and conformations can be docked to find the most favourable pose. The docking algorithms look at this 'virtual space' within the binding site and evaluate exactly how the ligand can fit into the active site, given each ligand has a number of degrees of freedom, which leads to the vast number of possibilities. Programmes such as GOLD, used in this project, can also take into account some flexibility within the protein's active site, usually from some rotation of amino acids side chains and some further global energy minimisation, so give the lowest energy ligand-protein binding interaction. Scoring functions are then used to rank each of proposed ligand conformations and how tightly it binds to the active site. When using GOLD these binding scores used are known as CHEMPLP scores. CHEMPLP score performs a force-field based scoring function, which looks at H-bonding and Van der Waals interactions.^{1 3,4}

7.3.2 Identification of the Binding Site

Benzimidazoles are known to display a similar binding to colchicine so it was proposed that we would start by investigating the binding site of colchicine (**1**).⁵⁻⁷ Within the PDB databank there is a crystal structure of colchicine bound to β -tubulin, within the crystallised tubulin protein derived from *Bos taurus* in an *Escherichia coli* expression system.

The x-ray structure (PDB code 4O2A) shows the binding of colchicine to its binding site. From this, we identified the amino acid residues that are within 5 Å of colchicine, and this was used as our binding site for docking. The homology model, which was built in house from a known protein sequence was then aligned with this protein, to identify the binding site within both the *C. neoformans* and human β -tubulin structures. Looking at the comparison of the 4O2A binding sites, we can see that they adopt

a similar position (protein backbone), with some differences in amino acid residues, in the different species.

Within the colchicine binding site there is a LEU 252 amino acid, which was identified as a possible amino acid to be used as the residue to which new molecules are aligned to for their binding. This does not directly bind to colchicine, but is within close proximity (3.0- 3.5 Å). This was decided based on alignment of our homology models with 4O2A. The LEU 252 is exchanged for a LYS 252 in both *C. neoformans* and human β -tubulin and thus this amino acid was used as the binding site residue reference for docking.

There is evidence for drugs that destabilise tubulin and prevent cell division binding to the colchicine site, which is the proposed site for benzimidazoles to bind (Figure 7.2) (See Chapter 2, Page 34 for more on benzimidazoles and tubulin). BAL27862 (**2**) is a novel microtubule destabilising drug, which is implicated in the treatment of ovarian and breast cancers. It also has a benzimidazole moiety within the core, which helps to give greater confidence to the potential of our own benzimidazoles binding at this site.⁸ Podophyllotoxin (**3**) is also known to bind to the colchicine site and destabilise β -tubulin and is used in a wide range of medical applications including as an anthelmintic, antitumor and antiviral agent, amongst many other applications.⁹⁻¹¹

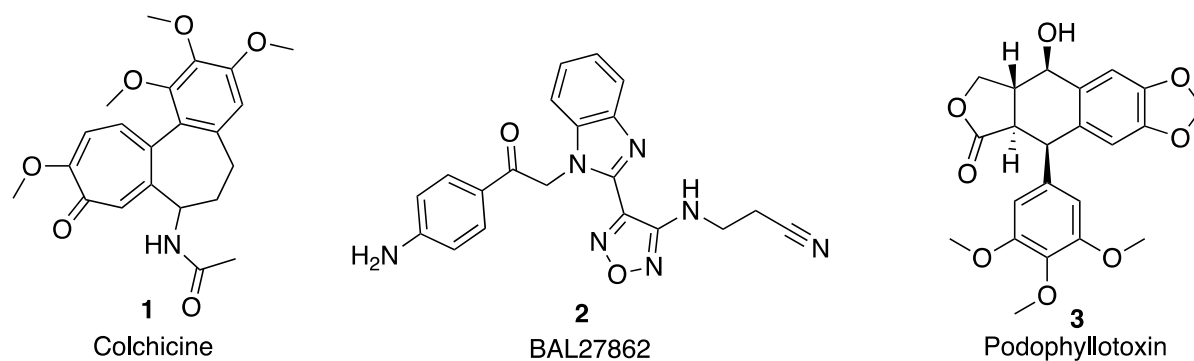


Figure 7.1. Colchicine (**1**) is a known β -tubulin binder, which binds at the colchicine site. BAL27862 (**2**) and Podophyllotoxin (**3**) are also bound at the same site, as identified within crystal structures.

7.4 Comparison of Binding Sites

Comparison of the binding sites of *C. neoformans* and human β -tubulin can tell us a lot about what sort of compounds may be able to bind preferentially to *C. neoformans* rather than human β -tubulin. This was carried out by looking at all of the amino acid residues within 5 Å of the bound molecule Flubendazole (Table 7.2).

Table 7.3. Identified amino acids in the *C. neoformans* and human β -tubulin binding site. Not Present* means not identified as being part of the binding site. **Green** – conserved in both binding sites. **Yellow** – Found in only one binding site. **Red** – different between the two binding sites.

<i>C. neoformans</i>	Human
GLY 235	Not Present*
VAL 236	Not Present*
CYS 239	CYS 239
GLN 245	GLN 245
LEU 246	LEU 246
Not Present*	ASN 247
Not Present*	ALA 248
Not Present*	ASP 249
LYS 252	LYS 252
LEU 253	LEU 253
ASN 256	ASN 256
MET 257	Not Present*
ALA 314	ALA 314
CYS 315	ALA 315
TYR 316	VAL 316
SER 350	LYS 350
ALA 351	THR 351
ALA 352	ALA 352

In total, there are 15 amino acids identified for both the *C. neoformans* and human binding sites (Table 7.2). There are a number of residues that are conserved between the binding sites. There are four amino acid residues that are different, which could prove important for promoting selective binding, as well as three residues that are present in one binding site, but not in the other. This produces a similarity between the binding sites of 53.3%, based on having 8/15 amino acid residues conserved.

The cysteine 315 residue that is present in the *C. neoformans* binding site has been replaced by an alanine in the human binding site (Figure 7.2). Cysteine has a polar neutral side chain versus alanine which has an aliphatic hydrophobic side chain.¹²⁻¹⁴ There is a small change in size of the amino acids as the cysteine has the additional larger sulphur atom off the side chain. This sulphur atom is also key as it can form disulphide bridges in the protein, but importantly could form an S-S bond with a molecule when it binds. This could be exploited as a way of designing compounds that are selective for *C. neoformans* tubulin.

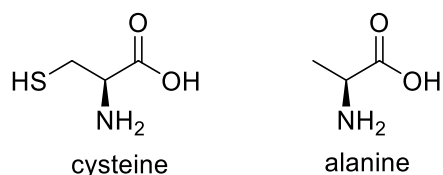


Figure 7.2. Cysteine 315 in the *C. neoformans* binding site is swapped for Alanine 315 in the human binding site.

In *C. neoformans* a tyrosine 316 residue has been swapped for a valine residue in the human binding site (Figure 7.3). This shows an exchange of a hydrophobic aromatic residue for a hydrophobic aliphatic residue, showing no change in hydrophathy.¹²⁻¹⁴ This does show some change in size due to the bigger aromatic ring being swapped for a smaller *iso*-propyl group. The phenol group of the tyrosine can also act as a H-bond donor or acceptor, this is lost when changed to valine and could affect binding.

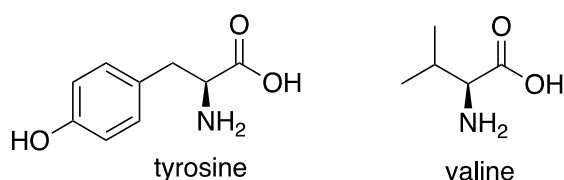


Figure 7.3. Tyrosine 316 in the *C. neoformans* binding site is swapped for valine 316 in the human binding site.

In the *C. neoformans* binding site the serine 350 has been swapped for a lysine residue within the human binding site (Figure 7.4). This an exchange of the polar neutral side chain of serine 350 for a charged basic side chain of the human lysine 350 at pH 7.¹²⁻¹⁴ This changes the charge at this point within the pocket. This is no change from aliphatic to aromatic, however lysine shows an elongated side chain versus serine, which may affect the shape of the binding pocket. The OH of the serine can undergo both H-bond acceptation and donation. The lysine can H-bond accept and donate as well, however it has two hydrogen donors versus serine's 1.

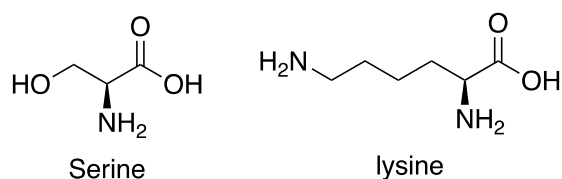


Figure 7.4. Serine 350 in the *C. neoformans* binding site is swapped for lysine 350 in the human binding site.

In the *C. neoformans* the alanine 351 residue has been mutated to a threonine 351 residue in human (Figure 7.5). This shows an exchange of a hydrophobic side aliphatic side chain for a polar neutral side chain.¹²⁻¹⁴ Not a large difference in size as the threonine side chain has only been expanded by one carbon. However, threonine has a side chain OH, which can act as both H-bond donor and acceptor, unlike the alanine of the *C. neoformans* binding site, which may change binding properties.

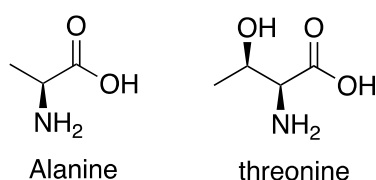


Figure 7.5. Alanine 351 in the *C. neoformans* binding site is swapped for threonine 351 in the human binding site.

The identification of these amino acid residues is crucial. Given that it is well established that benzimidazole toxicity derives from its binding to human β -tubulin, design of analogues that can selectively bind or interact with the residues indicated above that are present only in the *C. neoformans* binding site. The residues of particular interest are CYS 315, TYR 316 and SER 350 may lead to future design of a selective compound with reduced toxicity, which is out of the scope of this current work.

7.5 Benzimidazole Tautomerisation

Literature investigation showed that the benzimidazoles are regularly shown in two different tautomeric forms, with their structures being used interchangeably. For this project, it was important to understand any tautomeric binding differences, as different docking interactions may be observed. Density Functional Theory (DFT) calculations have been employed to see if any energy difference can be seen between the benzimidazole tautomers (Table 7.3).

Table 7.3. Energies calculated for the different tautomers of benzimidazoles, in order to determine the energy minimum.

Tautomer	DFT (au)	DFT (kcal mol ⁻¹)	Relative Energies
	-702.065177	-440552.644	0
	-702.064864	-440552.448	0.68
	-702.061361	-440550.249	2.40

DFT calculations were set up in water as the solvent and values quoted are calculated Gibbs free energies (Table 7.3). DFT calculation show that tautomer 1 possesses the lowest energy, meaning it is the most stable. Tautomer 2 shows a relative energy difference of 0.68, which is not significantly

different and supports the theory that both of these tautomers are energetically favourable, and interconvert readily. Tautomer 3 shows a greater relative energy difference of 2.40, indicating that it is less likely to be present.

Due to the small energy differences between tautomers 1 and 2, tautomeric forms of our benzimidazoles need to be taken into consideration when docking our compounds into the active site, as in theory they could bind in either tautomeric form.

7.6 Docking Protocol

The crystal structure for both *C. neoformans* and human β -tubulin were unavailable. The sequence for *Bos taurus* β -tubulin was most similar to both *C. neoformans* and human β -tubulin and thus was used to create homology models of them both.

Table 7.4. Protocol used for docking.

Feature	Protocol
Protonation	Hydrogens added to the protein
Waters	No addition or extraction of waters as no waters incorporated into the homology model
Ligands	Ligands added as .sdf file, after energy minimisation
Binding Site	LYS 252 identified as being a residue in the binding site of Colchicine, so this was selected. Binding site identified within 5 Å
Search Efficiency	200% efficiency
Number of GA runs	10 –terminated before this if 3 solutions found within 1.5 Å RMSD
Lone Pairs	Lone pairs not saved
Output	Output poses saved as individual files to allow better inspection of each pose
Scoring Function	CHEMPLP score

A database was built containing all of the benzimidazoles produced on the project, and they were separated into the different sub-templates. Each sub template was then subjected to a protocol to produce the other tautomer using a protocol within pipeline pilot, which is discussed in the experimental section (Figure 7.31, Section 7.14.3) and allowed for fast generation of tautomers for all compounds with the project. All the compounds for each sub-template and their tautomers were then docked into the active site of the protein using the docking programme GOLD.¹⁵

Molecules were then subjected to the docking protocol highlighted in Table 7.4. The binding pose with the highest CHEMPLP score was then selected and visualised in PyMol (Table 7.12, Section 7.14.2).

Potential interactions were identified using PyMol¹⁶ and ZincPharmer.¹⁷ Hydrogen bond distances were measured as heavy atom to heavy atom.

7.7 Docking Studies

7.7.1 Flubendazole

7.7.1.1 Benzimidazole Sub-templates

Investigation of whether the other sub-templates bound in a similar manner to flubendazole was also essential. Based on biological activity testing the thioether (MIC = 0.015 - >4 mg/L) and ether (0.06 - >4 mg/L) classes of compounds some had improved activity over the starting compound flubendazole (MIC = 0.125 mg/L). The biphenyl compounds had reduced activity (MIC = 0.5 - >4 mg/L) compared with flubendazole. Identification of binding interaction differences between these sub templates could help aid design of other analogues.

7.7.1.2 Flubendazole *C. neoformans* Binding Site

Given that flubendazole was the starting point for the project, we wanted to investigate its interactions in the binding site of β -tubulin, in order to aid design of new ketone analogues as well as new sub templates. As previously mentioned, the binding site has been found using flubendazole (**4**), so with that already established we were able to look at the binding site interactions for both flubendazole tautomers, in both *C. neoformans* and human β -tubulin.

As shown in Figure 7.6A, **4** interacts through a H-bond donor interaction to the carbonyl of the ASN 256 side chain. This is proposed to be a strong interaction as indicated by the short distance of 1.6 Å. There is also a H-bond acceptor interaction from the NH₂ of the side chain of the ASN 256 residue at a distance of 3.2 Å. There is also an additional acceptor interaction from a SER 350 residue with a distance of 3.0 Å. Finally, we can also observe an intramolecular H-bond between the carbonyl of the carbamate and the NH of the benzimidazole core. This forms a pseudo six membered ring and may help to lock the conformation, providing better binding interactions. For this tautomer, all poses displayed similar binding scores, with the highest being 54.5, an average of 54.0 and a standard deviation of 0.56. Visually, all binding poses looked very similar, with extensive superposition observed. Furthermore, this binding pose shows the 'tail' or substituted aryl part of the molecule buried in the hydrophobic pocket, which is observed for all analogues described in the following sections.

Looking at Figure 7.6B, we can see the proposed binding interactions observed for the other flubendazole tautomer (**4'**) with in the *C. neoformans* binding site. We can see that the SER 350 acceptor interaction is identical to **4**, with an identical length, which suggests it may be a key binding interaction. However, for this tautomer interaction to ASN 256 are no longer observed, instead we see interactions with LYS 252. There is an acceptor interaction from the carbonyl of the carbamate to the NH₂ of the LYS 252 side chain, with a distance of the 2.7 Å. There is also an acceptor interaction from the N of the sp² nitrogen of the benzimidazole core, with a distance of 2.6 Å. Both of the distances indicate moderate strength H-bonding interactions. What is noticeable is due to the conformational change there is no intramolecular H-bond in the carbamate region of the molecule. Whilst it may not be necessary for activity, and for **4'** we are still seeing some binding interactions, it may bind less in this tautomeric form and may be more favourable to bind as tautomer **4**. For this tautomer, visual inspection of the binding poses showed almost complete overlap, the highest CHEMPLP score being 58.1, the average 57.8 and a standard deviation of 0.33. It is worth noting that only when there is score difference of over 10 is this considered significant.¹⁸

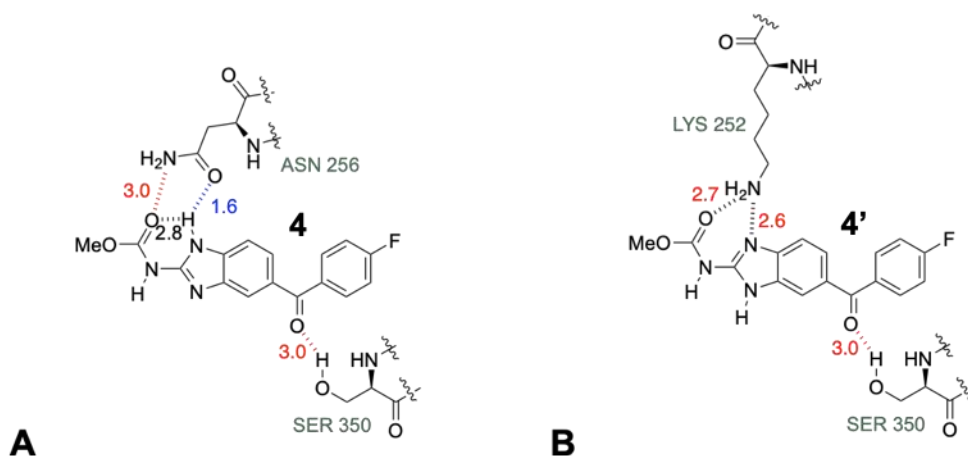
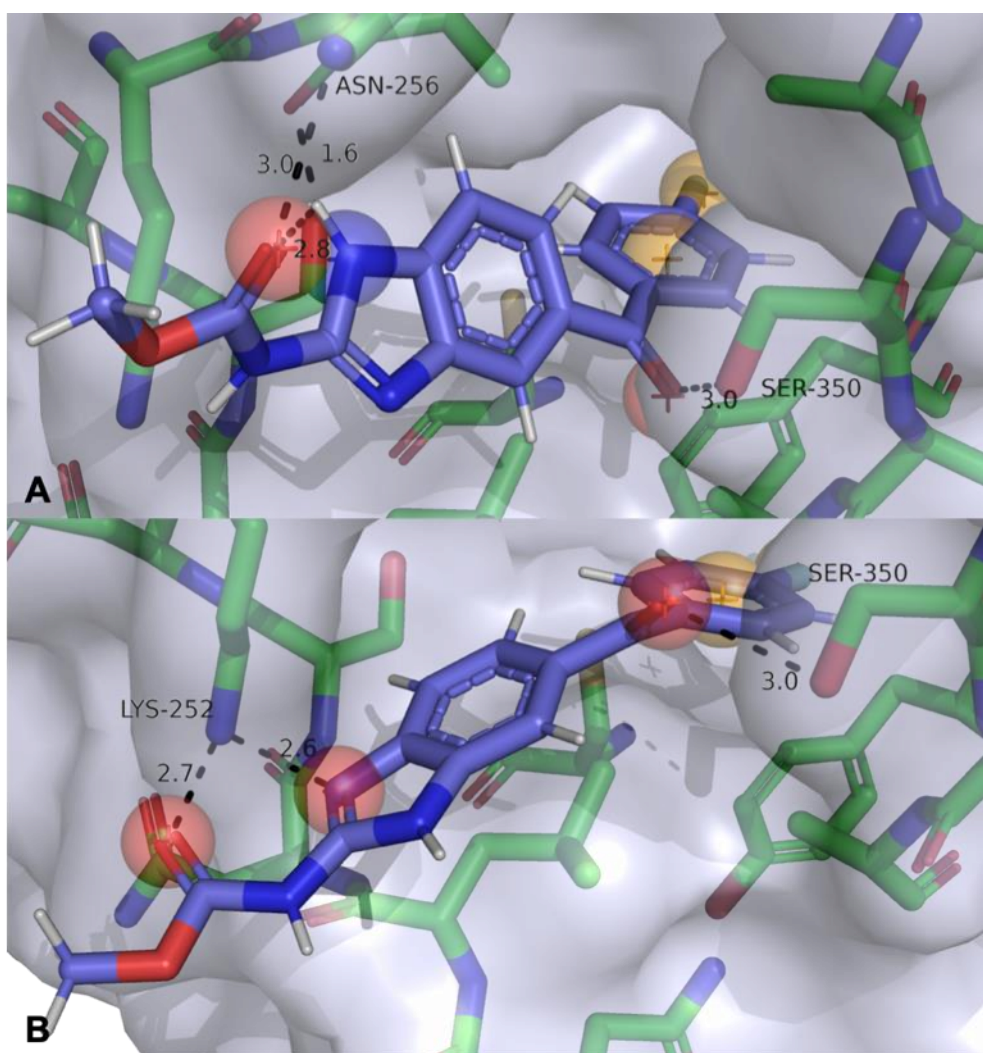


Figure 7.6. Red – H-bond acceptors, blue – H-bond donors. Docking pose is visualized with PyMol. Protein is shown as a surface representation coloured 40% transparent light blue. Compounds **4** and **4'** are represented as sticks where carbon – Light Blue, hydrogen – white, nitrogen – dark blue, oxygen – red, sulphur – yellow, fluorine – cyan. Binding site residues selected around 5 Å, represented as sticks where carbon – green, nitrogen – blue, oxygen – red, sulfur – yellow. Red sphere – H-bond acceptor, blue sphere – H-bond donor, yellow sphere – hydrophobic interaction.

7.7.1.3 Flubendazole Human Binding Site

Flubendazole (**4**) was also docked into the human β -tubulin binding site. This was carried out to identify any potential binding difference that could be exploited to achieve selectivity. Benzimidazoles have been identified as having potential toxicity issues due to their binding to human β -tubulin, which is a problem in areas of the body where there is rapid cell division, such as the lining of the intestine, resulting in gut toxicity, such as diarrhoea being observed.¹⁹ If there are differences in the binding sites, then compounds could potentially be designed that are selective for *C. neoformans* β -tubulin, over human β -tubulin, which may provide selectivity and reduce toxicity.

Figure 7.8A shows the first tautomer within the active site. We can see an acceptor interaction from the carbonyl of the carbamate to the NH₂ of the LYS 252 side chain, with a distance of 2.9 Å. This shows potential issues with selectivity due to also being found in *C. neoformans* binding site, and appears to be an essential binding amino acid residue for some of the templates. There is also a donor interaction of the NH of the benzimidazole core to the side chain carbonyl of ASN 247, another residue which is conserved from *C. neoformans*. Finally, there is also a strong interaction, with a distance of 2.2 Å, from the N-H of the carbamate to the backbone carbonyl of LEU 246, which is also implicated in being important for activity in the binding of other templates. Furthermore, there is also a strong intramolecular H-bond present, which may help to lock the conformation of flubendazole within the human binding site. The binding pose for **4** shown has a CHEMPLP score of 53.7, an average of 53.5 (from 10 docking solutions) and a small standard deviation of 0.33. Visual inspection of the binding poses showed good overlap, with only small differences in the position of the ketone.

We can also compare the second tautomer (**4'**) in Figure 7.8B, which also shows a number of strong binding interactions. The acceptor interaction to LYS 252 and donor interactions to LEU 246 and ASN 247 still being present, despite the tautomerism. However, the tautomerism has resulted in a loss of the pseudo six-membered ring that allowed for formation of the intramolecular H-bond. This tautomer possessed an average value of 50.8, and highest CHEMPLP score of 53.2 and a relatively large standard deviation of 1.44. From inspection of the binding; poses, it is clear to see why there is a large difference in standard deviation. Whilst the position of the aryl ring bearing the fluorine is similar in all poses, the position of the ketone, benzimidazole core and carbamate does vary in orientation between the poses, even though the area within the binding site remains the same.

So far, all the interactions highlighted indicate that achieving selectivity between the binding site of human *C. neoformans* β -tubulin may be challenging. However, the human binding site is missing one

key amino acid residue, SER 350, which was implicated in the binding of the ketone carbonyl of flubendazole in the *C. neoformans* binding site. In the human binding site this has been replaced by a LYS 350 residue. As discussed lysine is a more flexible side chain which, though having the potential to undergo H-bonding with the ketone, isn't ideally placed to do so. Furthermore, it is important to understand what additional binding site interactions the human tubulin may have over *C. neoformans*. The N-H of the carbamate appears to offer strong H-bonding in the human binding site, but no interactions in the *C. neoformans* binding site. Removal of the N-H could result in some loss of binding to human tubulin.

One proposed method of achieving this, was to methylate N-H, to produce compound **5**. This was attempted, however wasn't synthetically possible via the normal method described in Chapter 2 for producing the pseudo urea compound and ring closure. We attempted a methylation of the N-H of the carbamate to produce **5**, via synthesis of the appropriate urea. Whilst synthesis of the urea was successful, the ring closure reaction wasn't and thus the final product was not made.

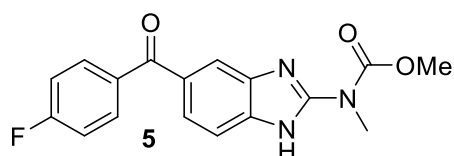


Figure 7.7. Compound **5** was proposed as an analogue that would more selectively bind to *C. neoformans* tubulin over human tubulin, potentially reducing toxicity.

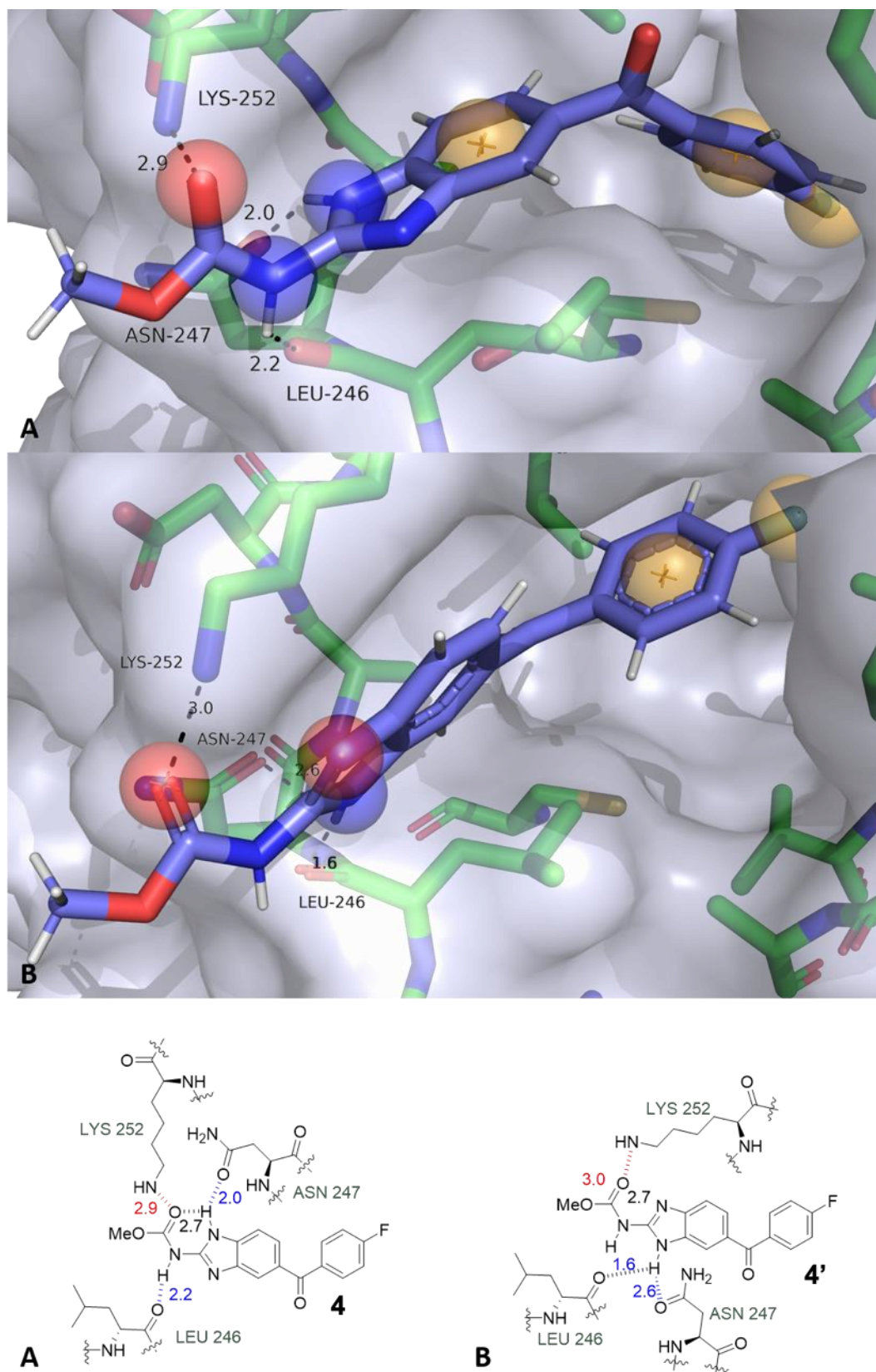


Figure 7.8. Red – H-bond acceptors, blue – H-bond donors. Docking pose is visualized with PyMol. Protein is shown as a surface representation coloured 40% transparent light blue. Compounds **4** and **4'** are represented as sticks where carbon – Light Blue, hydrogen – white, nitrogen – dark blue, oxygen – red, sulphur – yellow, fluorine – cyan. Binding site residues selected around 5 Å, represented as sticks where carbon – green, nitrogen – blue, oxygen – red, sulfur – yellow. Red sphere – H-bond acceptor, blue sphere – H-bond donor, yellow sphere – hydrophobic interaction.

7.7.2 Thioethers

Given the excellent biological activity of some compounds within the thioether class, it was important to understand the predicted binding and use this to rationalise the activity observed. This would allow for easier design of future analogues, without having to synthesise all the compounds of interest.

Compound **6** is shown in Figure 7.9, having both of its tautomers docked into the binding site of *C. neoformans* tubulin. For the first tautomer (Figure 7.9A) we can see a H-bond acceptor interaction to the side chain NH₂ of the LYS 252 residue of the binding site, with a distance of 2.9 Å. There are also two H-bond donor interactions observed, firstly the N-H of the benzimidazole core binding to the backbone carbonyl of the LEU 246 with a strong interaction distance of 2.6 Å. There is also a H-bond donor interaction to the GLN 245 backbone carbonyl at a distance of 3.6 Å. This wasn't initially identified as an interaction through PyMol, but was identified when looking at interactions through Zinc Pharmer, and so the polar interaction range for PyMol was increased to encompass this. It is worth noting that once H-bond is beyond the 3.2 Å point, it is considered weak.^{20, 21} Given the interaction between the N-H of the carbamate and the GLN 245 residue has a distance of 3.6 Å, it is considered a weak interaction.

There is an additional intramolecular interaction between the N-H of the benzimidazole core and the carbonyl of the carbamate, which aids in the formation of a pseudo six membered ring, which may help to lock the compound into a more favourable binding pose. There are also a number of hydrophobic interactions in the pocket of the binding site, which are identified through ZincPharmer and are found in all of the compounds being discussed. This compound showed an average CHEMPLP score of 54.4, with the pose shown possessing a score of 55.1 and a high standard deviation of 1.23. This proved interesting, as there was near perfect overlap of the poses observed in the binding site.

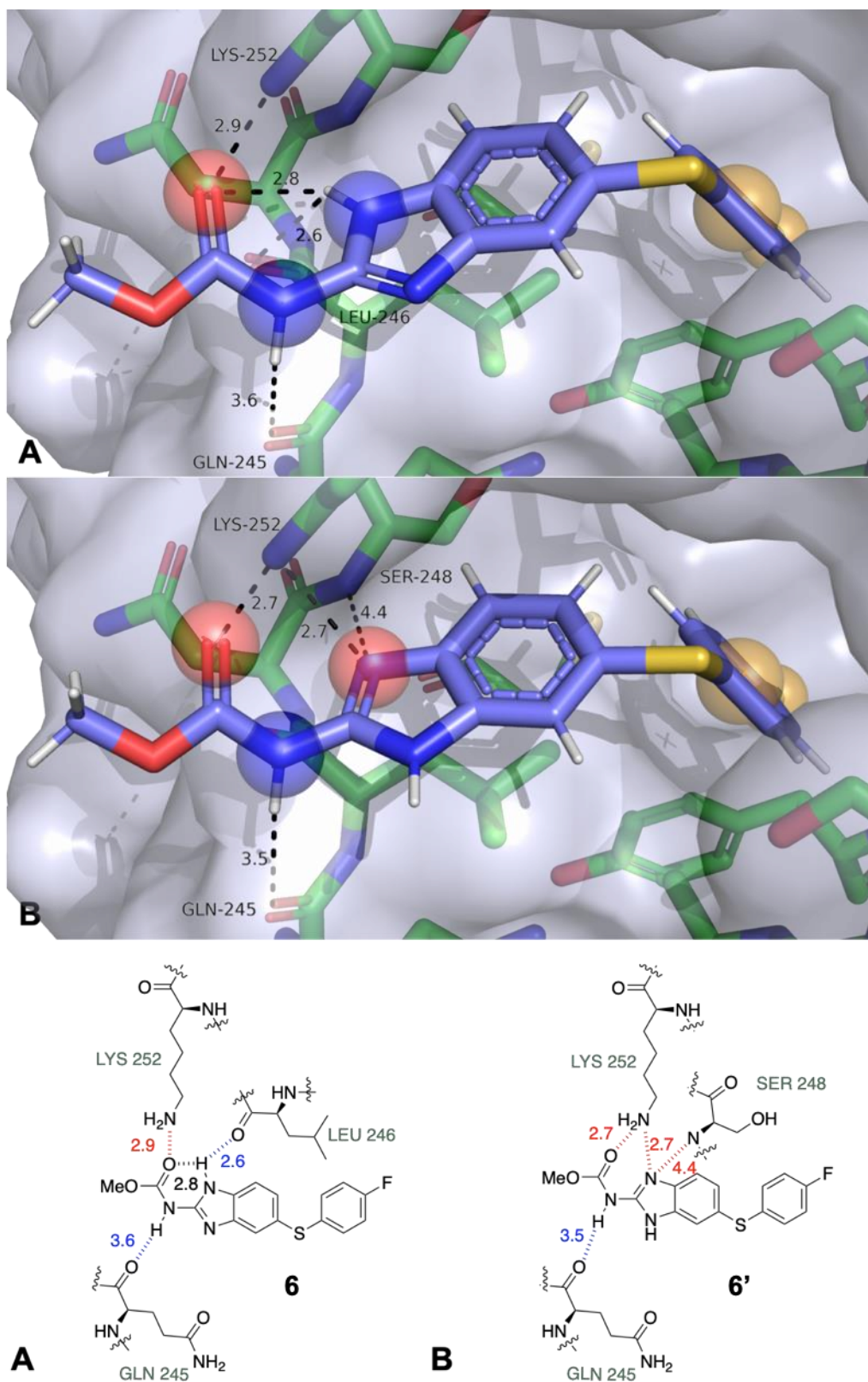


Figure 7.9. Red – H-bond acceptors, blue – H-bond donors. Docking pose is visualized with PyMol. Protein is shown as a surface representation coloured 40% transparent light blue. Compounds **6** and **6'** are represented as sticks where carbon – Light Blue, hydrogen – white, nitrogen – dark blue, oxygen – red, sulphur – yellow, fluorine – cyan. Binding site residues selected around 5 Å, represented as sticks where carbon – green, nitrogen – blue, oxygen – red, sulfur – yellow. Red sphere – H-bond acceptor, blue sphere – H-bond donor, yellow sphere – hydrophobic interaction.

Figure 7.9B, shows the same compound, but with the alternative tautomer (**6'**) docked in. It is observed that the acceptor interaction for the carbamate carbonyl from LYS 252 and the donor interaction of the carbamate N-H to the GLN 245 is conserved from the initial tautomer binding. New interactions include two H-bond acceptor interactions on the N of the benzimidazole core, one to the LYS 252 side chain, with a moderate distance of 2.7 Å and one to the SER 248 backbone NH with a very weak distance of 4.4 Å. The binding posed observed possessed a CHEMPLP score of 51.7, with an average score of 50.8 and a standard deviation of 0.84. Visually, all of the poses showed similar binding, with some small differences observed in the position of the sulphur atom.

We also wanted to dock an inactive compound to see if anything about binding and activity could be deduced. **7** was chosen with an MIC of >4 mg/L. Initially, similar binding interactions observed but there is a difference in strength of these interactions. Figure 7.10A shows the same binding interactions for **7** as seen for **6** Figure 7.9A. Table 7.5 shows the differences in bond strength for most of the bonds are not significant, apart from for GLN 245, whereby it is 3.6 Å for **6** and 4.3 Å for **7**. This bonding interaction for **7** is very weak and could influence activity. The pose observed had the highest binding score of 57.1, with an average score of 56.7 and a standard deviation of 0.39. Visual inspection showed identical overlap of all of the binding poses.

Table 7.5. Hydrogen bond distance comparison for Compounds **6** and **7** for tautomer A.

Interaction with Amino Acid	Acceptor/Donor (to Compound)	Compound 6 Distance (Å)	Compound 7 Distance (Å)
LYS 252	Acceptor	2.9	3.0
LEU 246	Donor	2.6	2.4
GLN 245	Donor	3.6	4.3
Intramolecular	-	2.8	2.6

For **7'**, the same binding site comparison can be carried out and again all the interactions are similar, showing similar H-bond distances, apart from the interactions at GLN 245, which are shorter for **6'** and thus stronger. This may indicate the necessity for this interaction for the thioether class to have activity. The pose observed showed the highest CHEMPLP score of 55.4, with an average of 54.8 and a standard deviation of 0.78. Visually, all of the poses possess similar binding positions, but there does appear to be some difference in the position of the sulphur, which results in moderate twisting of the benzimidazole core and carbamate within the binding site.

Table 7.6. Hydrogen bond distance comparison for Compounds **6'** and **7'** for tautomer A.

Interaction with Amino Acid	Acceptor/Donor (to Compound)	Compound 6' Distance (Å)	Compound 7' Distance (Å)
LYS 252	Acceptor	2.7	2.9
LYS 252	Acceptor	2.7	2.8
SER 248	Acceptor	4.4	4.5
GLN 245	Donor	3.5	4.5

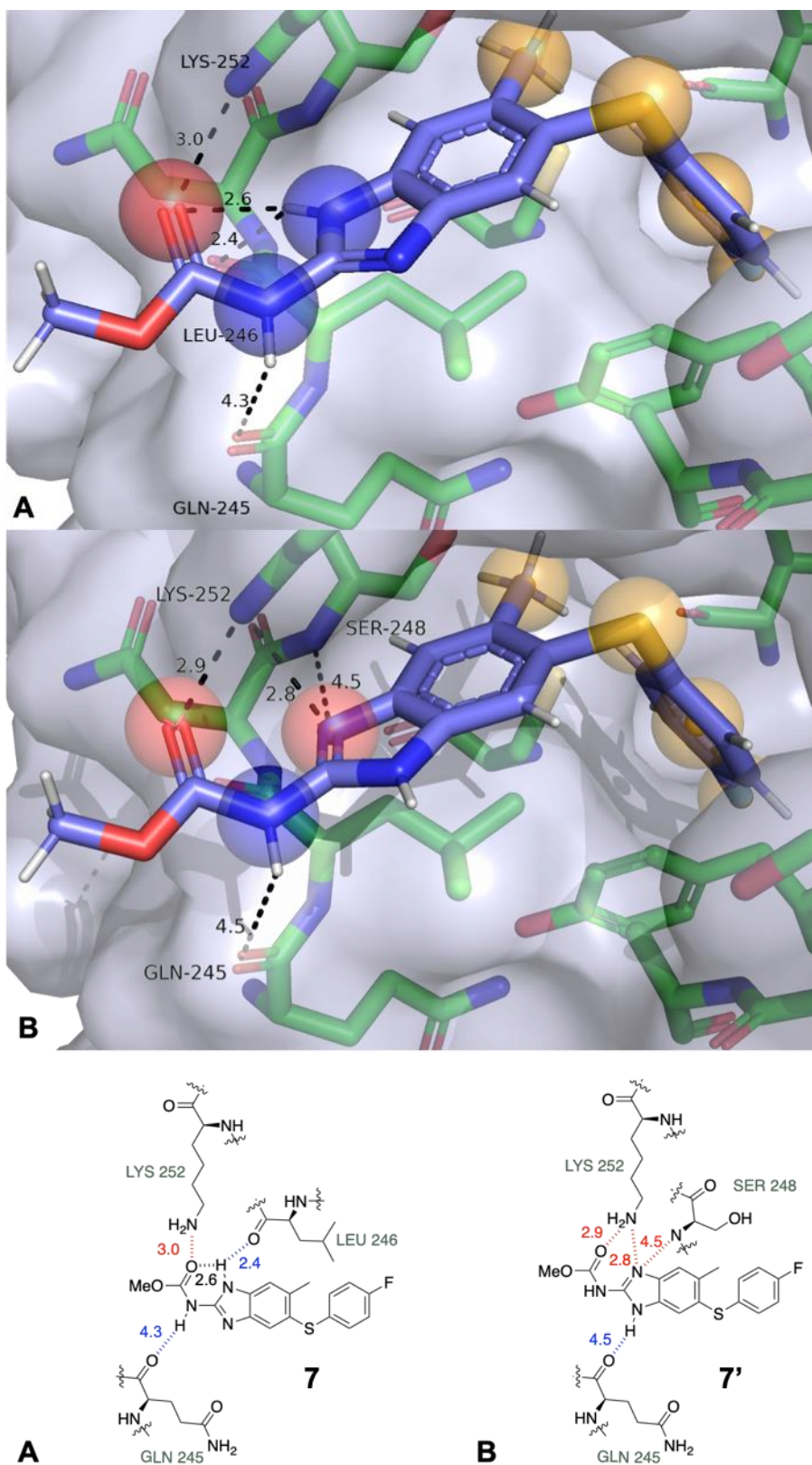


Figure 7.10. Red – H-bond acceptors, blue – H-bond donors. Docking pose is visualized with PyMol. Protein is shown as a surface representation coloured 40% transparent light blue. Compounds **7** and **7'** are represented as sticks where carbon – Light Blue, hydrogen – white, nitrogen – dark blue, oxygen – red, sulphur – yellow, fluorine – cyan. Binding site residues selected around 5 Å, represented as sticks where carbon – green, nitrogen – blue, oxygen – red, sulfur – yellow. Red sphere – H-bond acceptor, blue sphere – H-bond donor, yellow sphere – hydrophobic interaction.

7.7.3 Ethers

The ether class of compound was made as a direct comparison to the thioether class, in order to derive analogues which would hopefully possess similar activity, with potential metabolism of the sulphur negated. Whilst the ether class did produce compounds with good activity, they often proved to be reduced when compared with the thioether class overall. Binding was carried out to compare these classes to attempt to rationalise this difference in binding.

Figure 7.11A shows **8**, which possessed an excellent MIC value of 0.06 mg/L. As seen with the thioethers, we can observe an intramolecular H-bond between the carbamate and the NH of the core, which may help to arrange the compound in the correct binding conformation. This compound shows two H-bond acceptor interactions to the side chain of the LYS 252 and the OH of the SER 350 residue, with distances of 2.9 Å and 4.1 Å respectively. A distance of 2.9 Å shows a strong interaction between the carbamate carbonyl and the NH₂ of LYS 252. This was also observed for the thioether class, and for one of the tautomers of flubendazole, indicating it could be a key interaction. The SER 350 interaction of 4.1 Å is considered a weak interaction, but has proven to be a key binding interaction for the ketone class, and is an amino acid residue missing from the human binding site and could be exploited for selectivity. There are also two NH donation interactions to the backbone carbonyl of both LEU 246 and GLN 245, at distances of 3.1 Å and 4.5 Å respectively. A distance of 3.1 Å shows a moderate strength interaction, and the LEU 246 has also been implicated in binding with the thioether class, however the distance observed was shorter, indicating a stronger interaction. A distance of 4.5 Å, indicates a very weak interaction to GLN 245, much weaker than the 3.6 Å interaction observed for the thioether analogue. It is possible that the reason for the thioether class showing improved activity versus the ether class could derive from the strong interactions with GLN 245 and LEU 246. For **8** the pose observed had a CHEMPLP score of 51.4, with an average of 51.0 and a standard deviation of 0.34. Visually, all poses showed almost identical overlap.

Figure 7.11B shows compound **9**, which is an inactive ether (MIC of >4 mg/L). Overall, the binding interactions observed are similar to the active ether **8** (Table 7.7). The interaction with the SER 350 OH, shows a shorter distance of 3.1 Å, which indicates a stronger interaction than observed with **8**. However, there is no interaction of the core NH to LEU 246, which indicates that for the ether class this could be important for activity. Targeting LEU 246 could be problematic as is present in the human β -tubulin binding site

Table 7.7. Hydrogen bond distance comparison for Compounds **8** and **9**.

Interaction with Amino Acid	Acceptor/Donor (to Compound)	Compound 8 Distance (Å)	Compound 9 Distance (Å)
GLN 245	Donor	4.5	4.2
LEU 246	Donor	3.1	-
SER 350	Acceptor	4.1	3.1
LYS 252	Acceptor	2.9	2.9

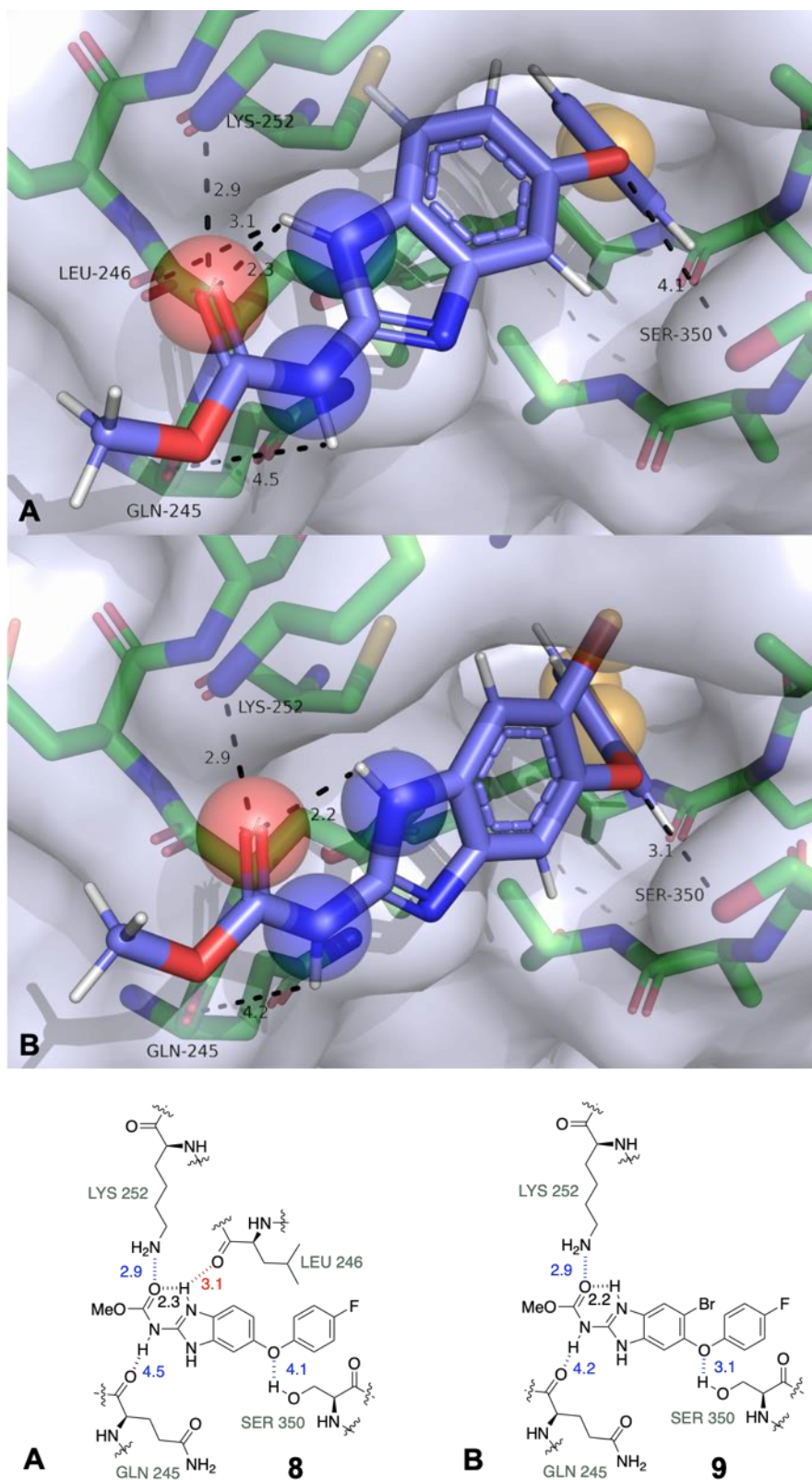


Figure 7.11. Red – H-bond acceptors, blue – H-bond donors. Docking pose is visualized with PyMol. Protein is shown as a surface representation coloured 40% transparent light blue. Compounds **8** and **9** are represented as sticks where carbon – Light Blue, hydrogen – white, nitrogen – dark blue, oxygen – red, sulphur – yellow, fluorine – cyan. Binding site residues selected around 5 Å, represented as sticks where carbon – green, nitrogen – blue, oxygen – red, sulfur – yellow. Red sphere – H-bond acceptor, blue sphere – H-bond donor, yellow sphere – hydrophobic interaction.

7.7.4 Morpholine Derivatives

The ether derivatives were extended on the aryl ring to give an elongated side chain with the addition of a group to enhance water solubility. The morpholine derivative (**10**) showed initial activity in the MIC assay (0.25 mg/L) and good *in vivo* activity in mouse models, exhibiting over a 3 log drop in fungal density. Therefore, it was important to see if any binding interactions could be predicted.

This image below (Figure 7.12) is observed from a different view point due to a small difference in the binding position of the morpholine derivative (**10**). Firstly, we can observe some H-bond acceptor interactions to ASN 256 and SER 350, which have previously been implicated in the binding of flubendazole (**4**). The NH₂ of the ASN 256 side chains shows two interactions to the carbamate carbonyl and the sp² N of the benzimidazole core, with distances of 4.1 Å and 4.0 Å respectively. This shows two weaker interactions compared with **4**. The SER 350 interaction is also weaker than observed in **4** at 3.9 Å. **10** shows two other H-bond donor interactions to THR 312 from the NH of the carbamate and NH of the benzimidazole core, with distances of 4.7 Å and 3.2 Å respectively. Whilst a distance of 4.7 Å shows a very weak interaction, 3.2 Å shows a stronger interaction, which may be important for the morpholine class and binding. The pose show for **10** has a score of 59.6 and the average binding score of 54.8 and a large standard deviation of 2.75. When visually inspecting the binding poses calculated, 7 out of 10 possess a similar binding position, however three out of ten show different binding positions, particularly regarding the carbamate, which accounts for the large standard deviation.

Notably, the morpholine derivatives are thought to bind in a similar manner to the other analogues with the aryl ring, ethyl chain and morpholine fitting into the pocket of the active site due to a good spatial fit between size and shape of the morpholine and the pocket. The carbamate is also more exposed to the edge of the pocket, due to the extended length of the morpholine derivative when compared with other analogues.

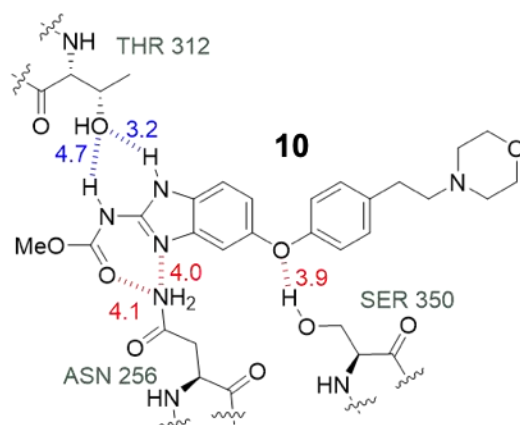
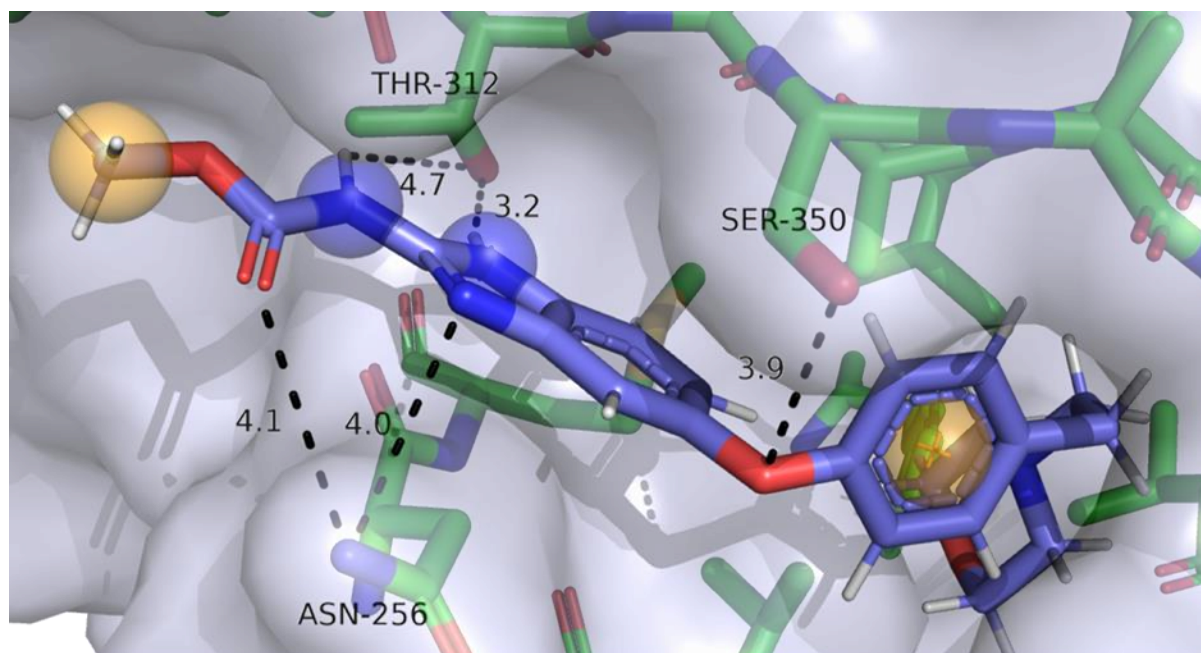


Figure 7.12. Red – H-bond acceptors, blue – H-bond donors. Docking pose is visualized with PyMol. Protein is shown as a surface representation coloured 40% transparent light blue. Compound **10** is represented as sticks where carbon – Light Blue, hydrogen – white, nitrogen – dark blue, oxygen – red, sulphur – yellow, fluorine – cyan. Binding site residues selected around 5 Å, represented as sticks where carbon – green, nitrogen – blue, oxygen – red, sulfur – yellow. Red sphere – H-bond acceptor, blue sphere – H-bond donor, yellow sphere – hydrophobic interaction..

7.7.5 Ketones

Whilst flubendazole binding has been extensively investigated at the beginning of this chapter, we also investigated binding of both an active and inactive ketone, as observed in Figure 7.13. Compound **11**, a 4-methoxy, derivative possessed an identical MIC value to flubendazole (**4**) of 0.125 mg/L. **11** shows identical binding to **4**, with acceptor and donator interactions to ASN 256, with distances of 3.0 Å and 1.6 Å being identical to those shown in **4**. The hydrogen acceptor interaction from the ketone to the OH of the SER 350 side chain is maintained at a distance of 3.0 Å and there is an intramolecular H-bond present that has previously been observed. This binding pose is conserved amongst the active analogues docked. The pose observed in Figure 7.13A possessed score of 55.9, average pose score of 50.7 and a standard deviation of 4.20. Visual inspection of the binding pose showed that whilst the functionalised aryl ring was bound similarly in all examples, the carbamate showed significantly different binding across the poses.

Figure 7.13B shows the binding of an inactive ketone, **12**, which has an MIC of >4 mg/L. The binding interaction to the SER 350 residue is maintained, with a moderate strength interaction at a distance of 3.0 Å. There is still binding to the ASN 256 residue, however rather than observing two interactions with the side chain of this residue, instead only one donor interaction is observed to the backbone carbonyl of ASN 245, through a strong interaction (2.0 Å). The pose observed has a high CHEMPLP score of 63.7, and average for the binding poses of 61.6 with a standard deviation of 1.53. This large standard deviation can be accounted for when the binding poses are inspected, whereby 7 out of 10 of the poses are similar to that observed in the Figure 7.13B, however 3 of the poses shows binding more similar to that usually observed for the ketones, but have the lowest CHEMPLP scores in the range. There are a reduced number of interactions present for the inactive analogue, and it gives rise to the hypothesis that extent of binding to the side chain of ASN 256 may be essential for ketone activity.

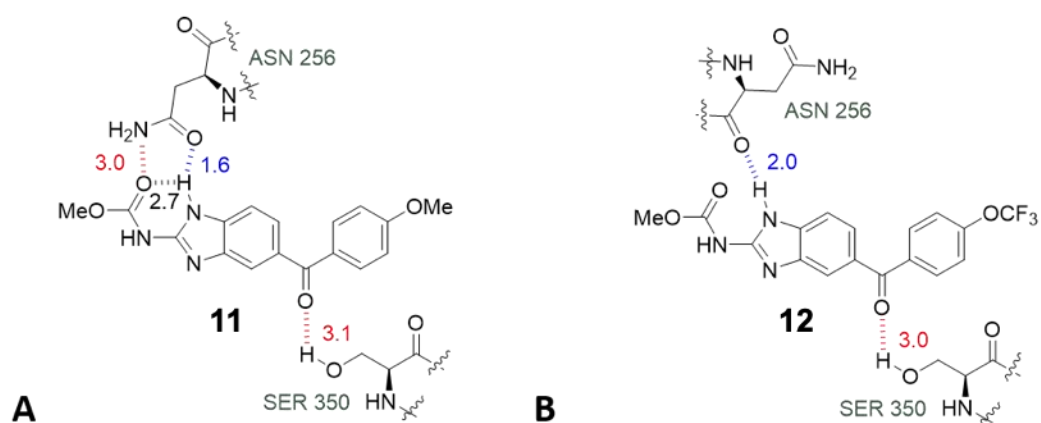
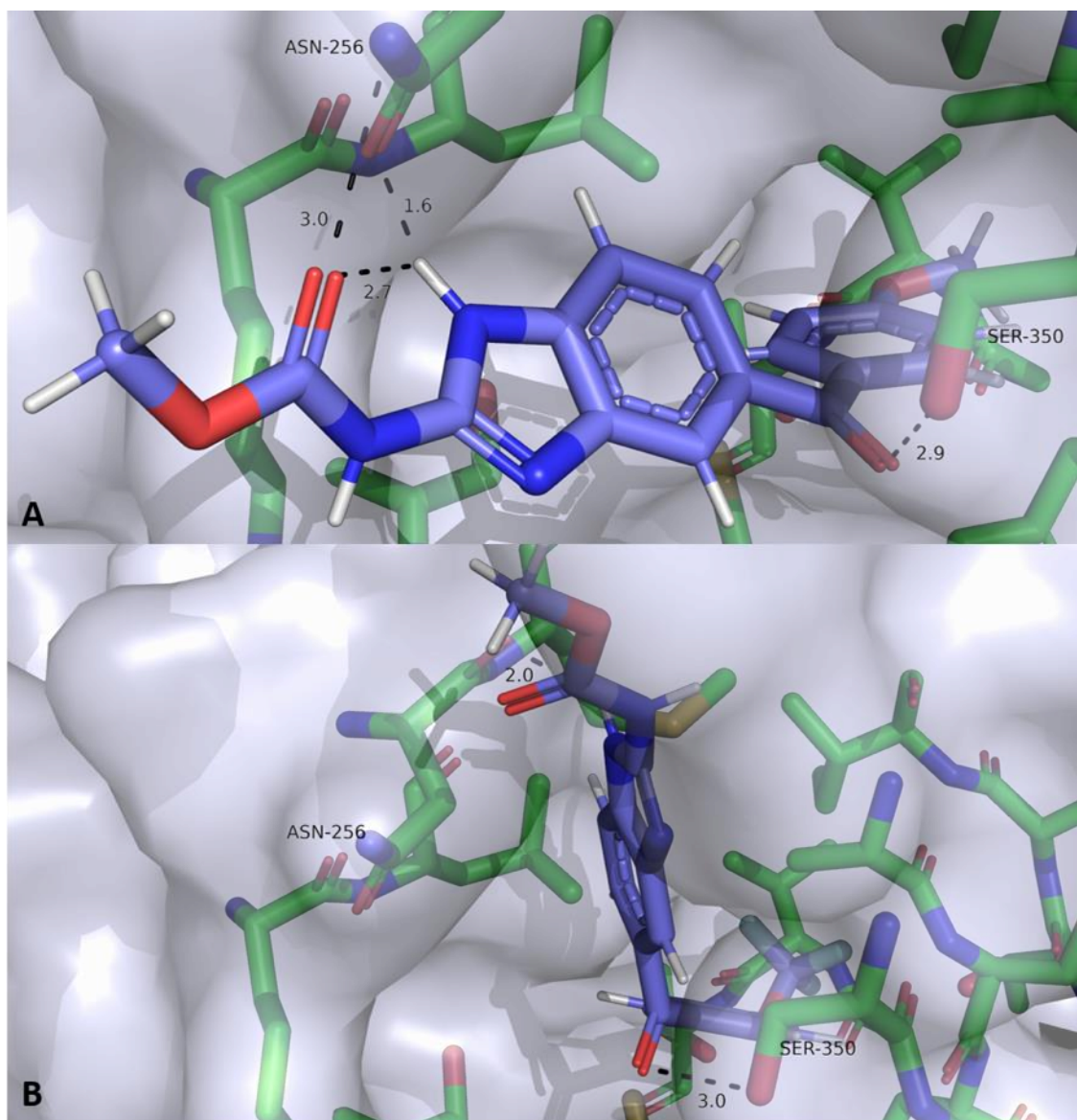


Figure 7.13. Red – H-bond acceptors, blue – H-bond donors. Docking pose is visualized with PyMol. Protein is shown as a surface representation coloured 40% transparent light blue. Compounds **11** and **12** are represented as sticks where carbon – Light Blue, hydrogen – white, nitrogen – dark blue, oxygen – red, sulphur – yellow, fluorine – cyan. Binding site residues selected around 5 Å, represented as sticks where carbon – green, nitrogen – blue, oxygen – red, sulfur – yellow. Red sphere – H-bond acceptor, blue sphere – H-bond donor, yellow sphere – hydrophobic interaction.

7.7.6 Biphenyls

The biphenyl class shows lower MIC values (0.5 - >4 mg/L) when compared with other classes, however does possess improved solubility. It was important to understand the binding interactions this class possesses so that improved analogues could be designed for better activity. Investigation of the binding site for the biphenyls, showed that size and position of substituents led to larger variations in binding interactions when compared with other classes. This can be rationalised as the benzimidazole core and derivatised aryl ring do not have a rotatable bond linking them. This results in less flexibility within the molecule, so more dramatic changes in binding are observed to accommodate the different groups. To exemplify the potential differences in binding, two active analogues and two inactive analogues have been docked.

7.7.6.1 Active Biphenyls

Figure 7.14A shows the binding pose for **13**. This 2-F biphenyl (**13**) possesses an MIC of 1 mg/L, which normally is considered good activity for *C. neoformans*, but isn't as biologically active as other templates within this project. There are two H-bond donor interactions that can be observed to the side chain of ASN 256 and the backbone carbonyl of LYS 252 at distances of 1.9 Å and 4.0 Å respectively. The interaction with ASN 256 is considered a strong interaction, and is observed for a number of other templates. There are also three potential acceptor interactions to ASN 256, LYS 252 and SER 350 of distances 4.5 Å, 4.6 Å and 5.0 Å respectively, all of which are very weak interactions. The pose shown possesses a binding core of 51.0, with an average score of 49.4 and a standard deviation of 1.78, which is quite large considering all of the binding poses line up, with no significant difference in the orientations observed.

If we look at Figure 7.14B, we can see the binding of **14**, a 2-Me analogue which also showed an MIC of 1 mg/L. We observe some conservation of the binding interactions seen with **13** (Table 7.8). There is still the presence of two LYS 252 interactions, which show shorter interaction distances of 3.1 Å and 3.9 Å when compared with the same interactions in **13**. The donor interaction at a distance of 2.0 Å is still present, however the acceptor interaction is not. Furthermore, there is also no interaction with SER 350 in **14**, although this was a very weak interaction in **13**. This also seems to be congruent with other templates. Notably, given that the images in Figure 1.14 are from the same view point, we can see that due to the larger 2-Me group, the rest of the molecule must twist slightly within the binding pocket in order to accommodate the larger group. Given the pocket is considered hydrophobic, the additional methyl group on **14** may facilitate additional hydrophobic interactions, improving activity.

The pose visualised possessed a CHEMPLP score of 46.6, with a pose average of 46.3 and a standard deviation of 0.27. All binding poses showed almost identical binding for this analogue.

Table 7.8. Hydrogen bond distance comparison for Compounds **13** and **14**.

Interaction with Amino Acid	Acceptor/Donor (to Compound)	Compound 13 Distance (Å)	Compound 14 Distance (Å)
SER 350	Acceptor	5.0	-
LYS 252	Acceptor	4.6	3.1
LYS 252	Donor	4.0	3.9
ASN 256	Acceptor	4.5	-
ASN 256	Donor	1.9	2.0

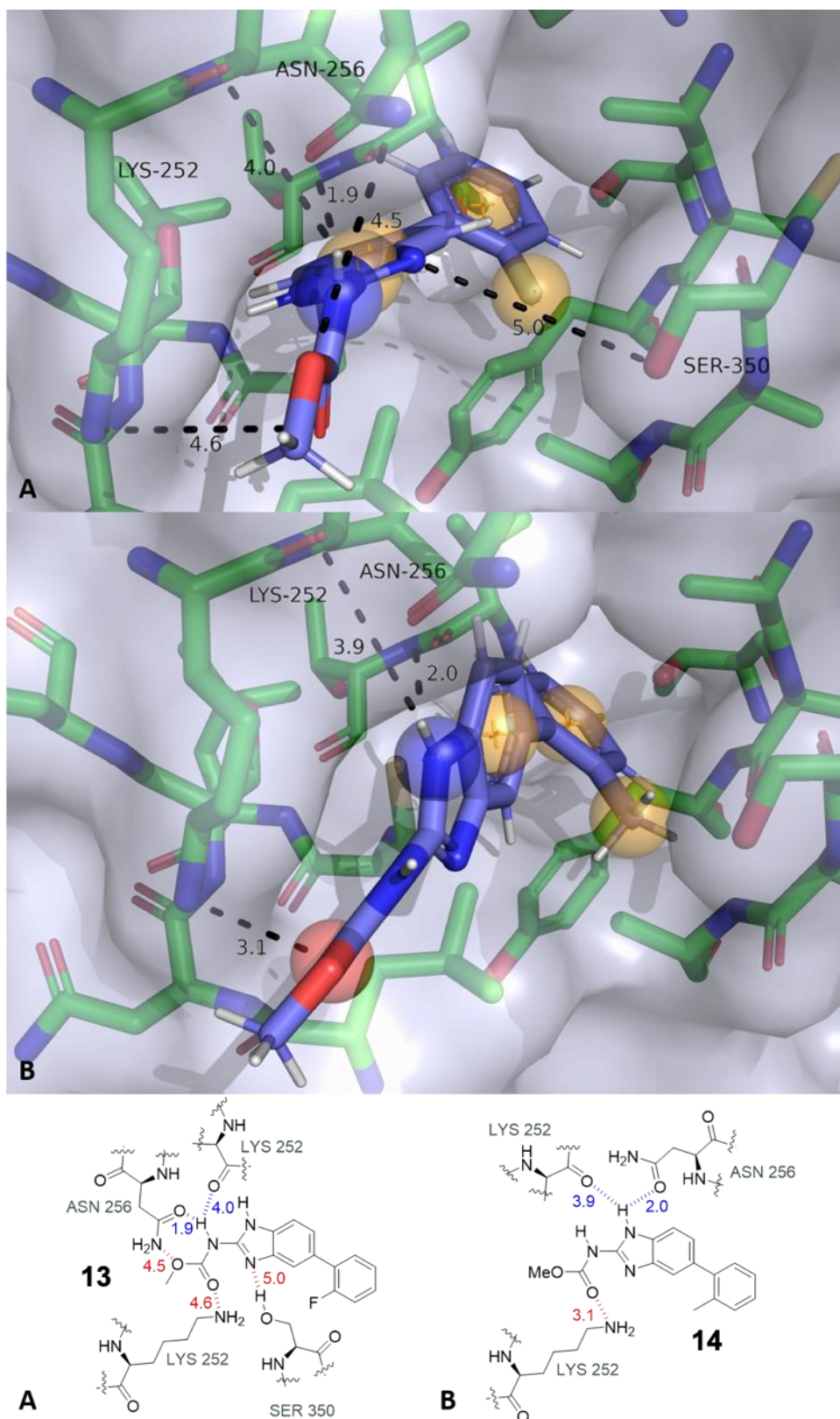


Figure 7.14. Red – H-bond acceptors, blue – H-bond donors. Docking pose is visualized with PyMol. Protein is shown as a surface representation coloured 40% transparent light blue. Compounds **13** and **14** are represented as sticks where carbon – Light Blue, hydrogen – white, nitrogen – dark blue, oxygen – red, sulphur – yellow, fluorine – cyan. Binding site residues selected around 5 Å, represented as sticks where carbon – green, nitrogen – blue, oxygen – red, sulfur – yellow. Red sphere – H-bond acceptor, blue sphere – H-bond donor, yellow sphere – hydrophobic interaction.

7.7.6.2 Inactive Biphenyl Derivatives

To assess what amino acids might be essential for binding, an investigation into the binding poses of inactive biphenyls was undertaken. Figure 7.15A shows **15**, a 3-F derivative which possessed an MIC of >4 mg/L. It still maintains an interaction with LYS 252 at distance of 4.0 Å, a weak interaction, but is a shorter distance than the same interaction in **13**. There is also an interaction with SER 350 at a distance of 2.3 Å, which is also shorter than that observed in the active analogue **13**. However, this interaction is now a donor interaction from the core NH, rather than an acceptor interaction that is observed for all other templates binding at SER 350. We also observed an additional acceptor interaction from the backbone NH of SER 248, which is a very weak interaction at a distance of 4.8 Å. Comparing the binding of **13** to **15** in the binding site, we can see that **15** lies “flat” within the binding pocket, whereas **13** which is active, twists more due to accommodating 2-F into the binding pocket. The average CHEMPLP score for the binding poses was 48.7, with a standard deviation of 3.19 and the pose observed having a score of 54.4. The binding poses show almost perfect overlap, with only some small changes in the orientation of the carbamate end.

Figure 7.15B shows a 2-iPr derivative, **16**, which also has an MIC of >4 mg/L. Compared with the 2-Me derivative **14**, this group is a lot bigger and in order to accommodate the aryl ring in the pocket there is a large change in conformation. This changes the binding interactions substantially, so now there are only two H-bond acceptor interactions to the ASN 256 side chain NH₂ at moderate strength distances of 3.1 Å and 3.2 Å. The binding pose shown has a CHEMPLP score of 54.9, an average of 51.9 and a standard deviation of 2.10. Inspection of the binding poses for **16** show nine poses that are almost identical, with only small changes in the carbamate and one that shows completely different binding, with none of the molecule sitting in the binding pocket. Binding evaluation of actives (**13** and **14**) and inactives (**15** and **16**) appears to indicate that interactions with both LYS 252 and ASN 256 are essential to activity. Furthermore, substituents of the correct size also ensure the correct binding conformation, meaning biological activity is achieved.

Table 7.9. Hydrogen bond distance comparison for Compounds **15** and **16**.

Interaction with Amino Acid	Acceptor/Donor (to Compound)	Compound 15 Distance (Å)	Compound 16 Distance (Å)
SER 248	Acceptor	4.8	-
SER 350	Donor	2.3	-
LYS 252	Acceptor	4.1	-
ASN 256	Acceptor	-	3.1 and 3.2

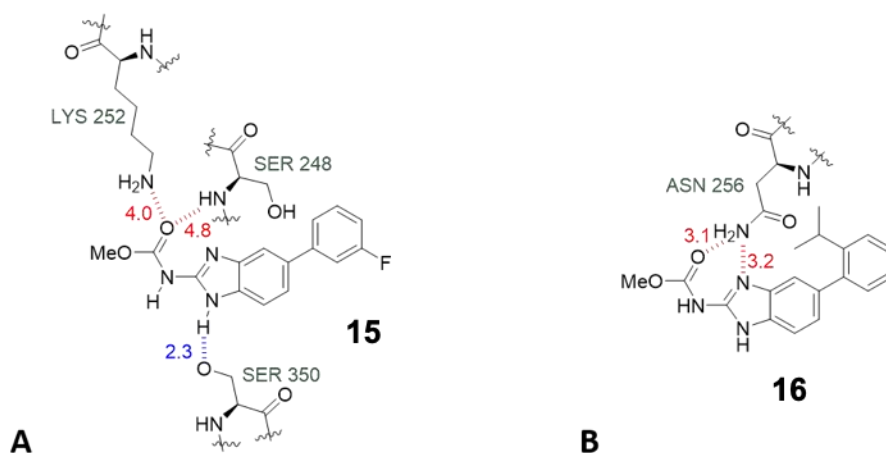
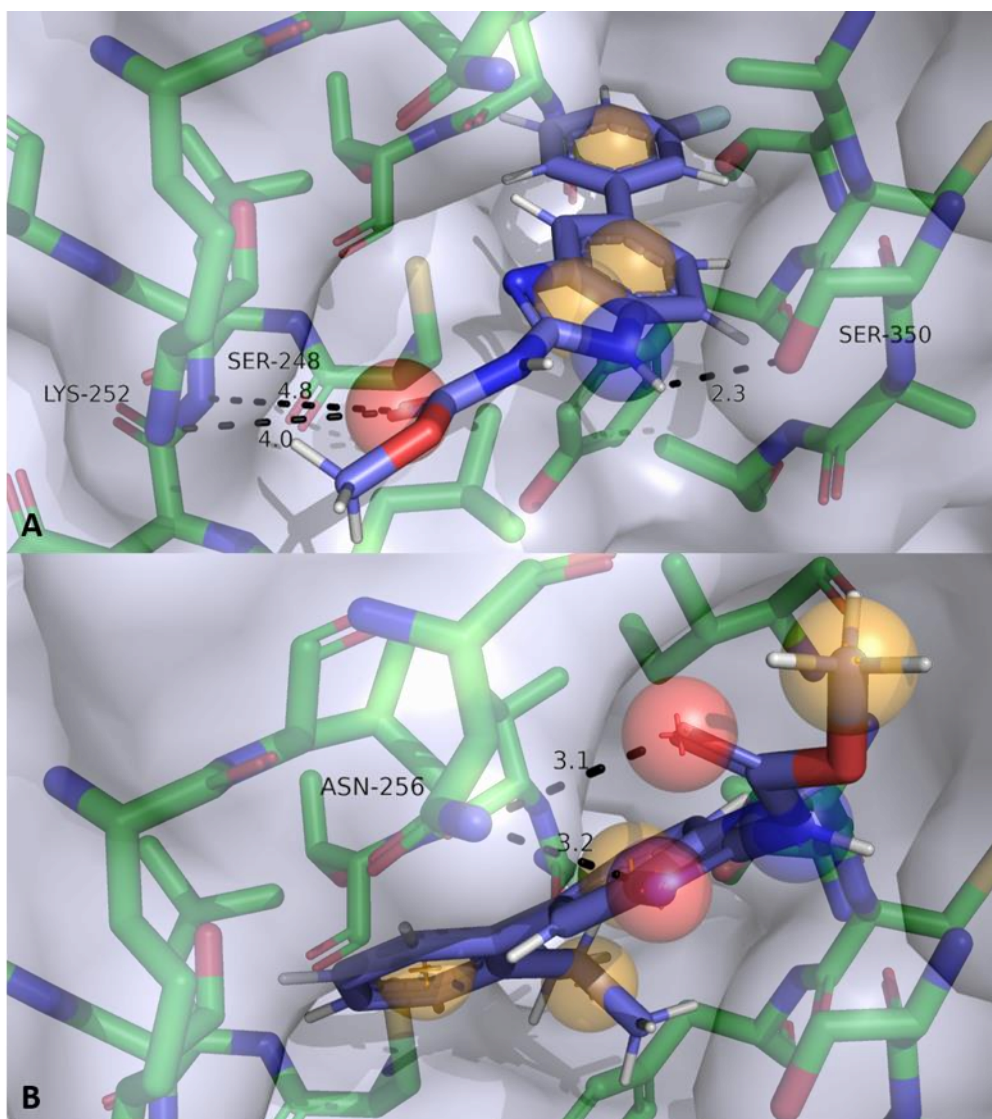


Figure 7.15. Red – H-bond acceptors, blue – H-bond donors. Docking pose is visualized with PyMol. Protein is shown as a surface representation coloured 40% transparent light blue. Compounds **15** and **16** are represented as sticks where carbon – Light Blue, hydrogen – white, nitrogen – dark blue, oxygen – red, sulphur – yellow, fluorine – cyan. Binding site residues selected around 5 Å, represented as sticks where carbon – green, nitrogen – blue, oxygen – red, sulfur – yellow. Red sphere – H-bond acceptor, blue sphere – H-bond donor, yellow sphere – hydrophobic interaction.

7.8 Correlation between Activity and CHEMPLP Score

We investigated if there was a correlation between CHEMPLP docking score and activity for the different compound classes. This involved turning our minimum inhibitory concentration values into more useful numbers by converting into molar units, and then converting into 1/molar. This was then plotted against CHEMPLP score. This was carried out for both the thioether and ether class, with the thioether class plot displayed below (Figure 7.16). It is clearly observed that there is no correlation between activity and CHEMPLP score, with a R^2 value of 0.0002 for the thioether class and 0.0006 for the ether class. This also didn't show any further correlation when individual tautomers were investigated.

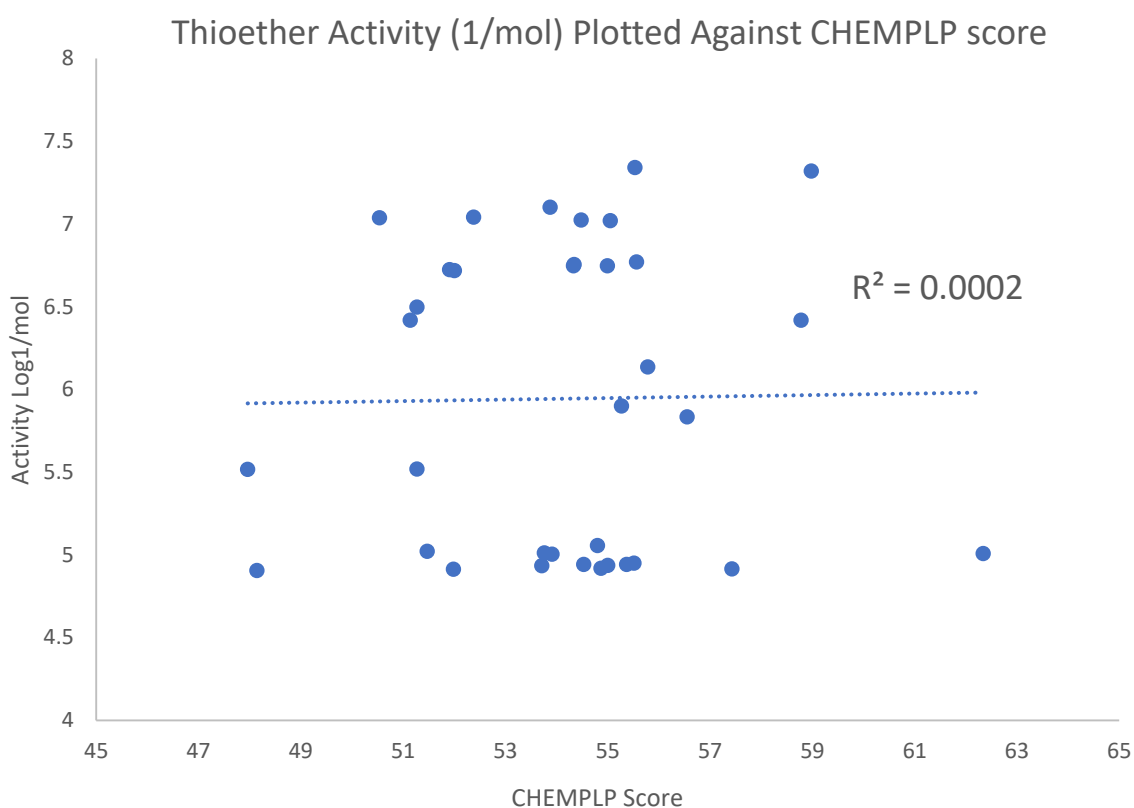


Figure 7.16. Activity was plotted against average CHEMPLP score for each compound, and it was clear that there was no correlation observed.

7.9 Binding Overview

It is worth noting that this section on binding offers a qualitative overview of expected binding of benzimidazole with *C. neoformans* and human β -tubulin. Crystal structures would be required to gain a more accurate understanding of the binding poses, which could then inform decisions about the design of new analogues. This could be used to rationally design new and improved analogues, which may allow for the addition of solubilising groups, without affecting activity. This is assuming that the crystal structures obtained capture the pharmacologically relevant interactions.

From the binding of all the templates we can see a number of amino acids residues which appear to be important to activity, including GLN 245, LEU 246, SER 350, LYS 252 and ASN 256. These amino acids appear to show important binding interactions across a number of the templates. Furthermore, SER 350, which is shown as a binding interaction in the ketones, ethers and biphenyls, is changed to a LYS 350 in the human binding site. In the future, design of new analogues could exploit this difference to create compounds that more selectively bind to *C. neoformans* β -tubulin.

7.10 Quantitative Structure Activity Relationship Studies

7.10.1 What is QSAR Modelling?

QSAR stands for Quantitative Structure Activity Relationship. This explores the relationship between biological activity and chemical structure, in order to help understand the molecular features that are important for activity and aid the design of new drug candidates.^{22, 23} Chemical structure is related to properties of the molecule which include electronic features, lipophilicity and steric parameters.²⁴ QSAR involves statistical analysis of sets of data to develop a model that can accurately predict biological activity of a novel candidate, providing it falls within the “applicability domain” that the model was built on.

Building of a QSAR model involves using statistical and mathematical methods to determine 2D relationships and it does this using the following;

$$P_i = k'(D_1, D_2, \dots, D_n)$$

P_i is the biological activity of the molecules. The D coefficients are either experimental or calculated structural properties and these are often referred to as molecular descriptors. K' is a mathematical transformation which is applied to the descriptors for all of the molecules. QSAR modelling is then used to see if a trend in the molecular descriptors determined can be correlated to biological activity.²² QSAR doesn't concern how the ligand binds within the active site and what pose it has. This falls more into the realms of molecular modelling, and isn't always completely accurate as analogues can bind very differently in the crystal structure than what was predicted. Instead, we look at how different structural features can influence activity.²⁴

QSAR methodologies can be classified depending on the way the descriptor values are derived and used to observe correlation (Table 7.10). There are also 4D, 5D and 6D QSAR methodologies, which take into account additional “dimensions” such as conformation.²⁵

Table 7.10. Different QSAR Models that can be used.²⁵

QSAR Methodology	Description
1D-QSAR	The correlation of biological activity and calculated/experimental properties such as pK _a , molecular weight or logP
2D-QSAR	The correlation of biological activity with structural patterns such as 2D pharmacophores, but not taking into account any 3D representation
3D-QSAR	The correlation of biological activity with interaction fields surrounding the molecules that are non-covalent in nature.

7.10.2 Why do we want to undertake QSAR studies?

QSAR is used often in medicinal chemistry projects for a number of reasons. Firstly, when starting a project, large numbers of compounds are often investigated. Prioritisation of what compounds should be screened and synthesised as starting points is essential if a new project is to move forward quickly. Secondly, once compounds are being synthesised, biological data can often lead to the design of numerous other analogues. Using models that can predict which of the compounds will have the best activity, prioritisation of these compounds can occur, meaning only the candidates that are likely to be successful are synthesised. If QSAR can predict what molecules should be made as a priority, this can be hugely efficient, saving both time and money.²⁵

Not only could QSAR help the organic and medicinal chemists, but also biologists. Biological assays possess their own issues. They are time consuming, not always completely applicable to the disease model, costly and ethically are problematic as most biological assays require some animal sacrifice. This involves either testing the compounds directly in animals, or through growth of the disease in animals, to be used in *in vivo* and *in vitro* assays.²⁵ We need to be able to link biological activity with molecular descriptors. Methods that allow for determination of this link are discussed in the following sections. The flow diagram in Figure 7.17 gives an overview of the QSAR process, with the following sections discussing this in more detail.

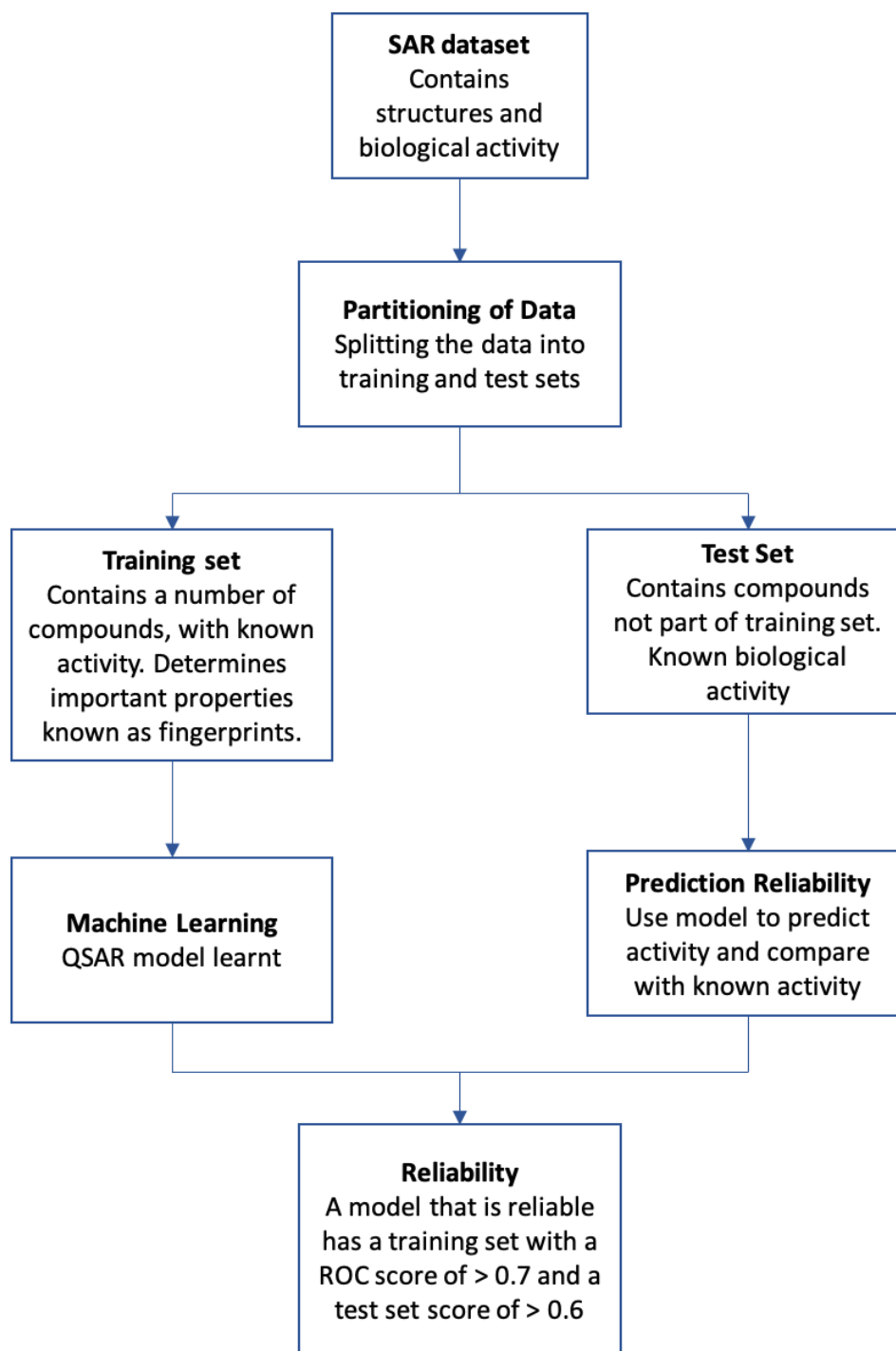


Figure 7.17. The training and testing of the model is displayed in a simple flow diagram and discussed in more detail in subsequent sections.

7.10.3 Molecular Fingerprints

Molecular fingerprints are a way of encoding the structure elements of a molecule into numerical data. They allow for screening of large chemical databases via the representation of chemical substructures, but are also used for analysis tasks including classification and similarity searching. For this project, we are more interested in a specific type of fingerprint known as Extended-connectivity

fingerprints (ECFPs) and they look specifically at the relationship between molecular features and activity, which in this case is biological activity. This can then be used to determine whether substructure can be used to predict activity.

ECFPs exhibit a number of important properties that allow for their use in structure activity modelling. Firstly, they can be very rapidly calculated. This is important when handling large sets of data and when large numbers of molecular fingerprints need to be calculated. They represent molecular structure via circular fingerprint, which looks at the surrounding atoms. This therefore takes into account local structural information, not just what is directly connected to an atom.²⁶⁻²⁹ Importantly, they give information that denotes whether a substructure will allow for activity, or whether it inhibits activity. This is important as for a more complete understanding of SAR, both are required. They are also not predefined meaning they can represent an infinite number of features, depending on the data set the ECFPs are learned from. This also means that stereochemical information can be obtained, which is particularly important in medicinal chemistry projects.

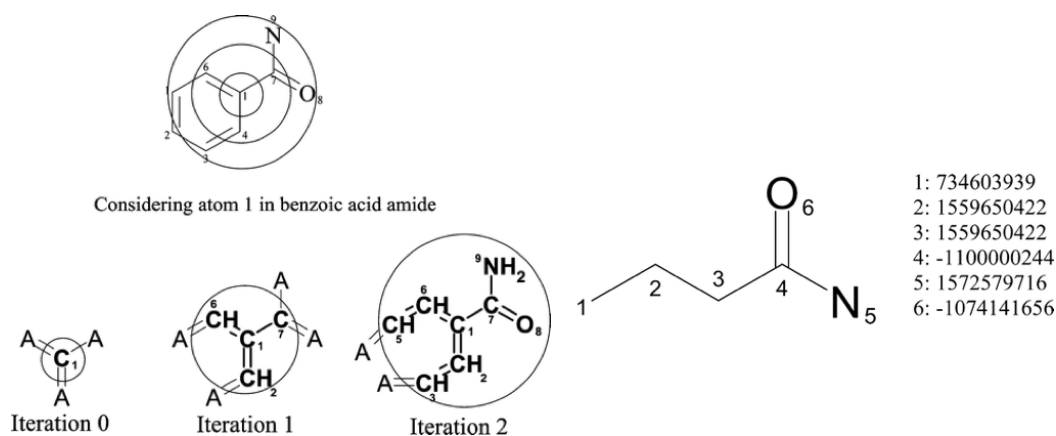


Figure 7.18. Circular fingerprints take into account local structural information. Reproduced from; *Extended-Connectivity Fingerprints*, D. Rogers et al.

The generation of ECFPs is a three-step process, which first involves assigning each atom a number (identifier) which forms the initial fingerprint set. Each atom then gathers its own identifier along with identifiers from neighbouring atoms. They then simplify this information back into a single integer identifier, which now contains information about the original identifiers, with the new information attached. This information is then added to the atom in a sequence of numbers known as a hash string and this is shown in Figure 7.18. This is then repeated through a number of iterations. Once this 'training' part is done, they then remove duplicates and then the integers that are left give the ECFP set. These ECFPs are structural features that are left as fingerprints for this project, given the non-trivial nature of conversion of these fingerprints into usable, defined structures.^{27, 30}

7.10.4 Applicability Domains

The applicability domain is a theoretical area which defines a level of confidence on any given molecule's predicted property. This is based on how similar a new structure is compared to the compounds the model was built on. This is important because how reliable a QSAR model is depends on the confidence of predicting activity for compounds that fall within the applicability domain.^{31, 32} A restrictive applicability domain implies that the model learned will be reliable at predicting activity for a limited number of compounds that will be closely related to the training set.

Within Pipeline pilot, during the learning process the applicability domain can be defined. It can do this in two ways; firstly by tracking the property ranges, whereby it can detect any out of range values, and allows for indication of the models domain of applicability. The learning process can also perform an OPS (optimum prediction space) analysis where it determines the optimum prediction space in which the model can reliably make prediction. This imposes tighter criteria on the prediction than simply tracking property ranges.³³

7.10.5 Random Forest Model

A random Forest is described as an ensemble of classification trees created from bootstrap samples of a set of training data and looking at the importance of a random set of descriptors and then a prediction is made when the outcomes of these trees are added together. In order to understand the process that is occurring here some processes and terminology needs to be defined.

The term bootstrapping, in relation to decision trees, means to take a smaller sample of data from a larger set of data. This larger set of data, when we start running a random forest model is known as a training set. A training set of data is a series of compounds with known descriptors and data for the property you are looking to predict, in this case whether something will be biologically active or not. We then also use test sets, which are smaller set of compounds that we use to test the accuracy of the model produced, where their activity is known, but crucially were not part of the training set. This allows us to validate the accuracy of the model built.³⁴

Random forest models are formed from a number of decision trees, which are the building blocks of this model. Decision trees individually can handle high-dimensional data and can ignore irrelevant descriptors, but individually have a low level of accuracy when it comes to predicting outcome. Individually, a decision tree can only learn from the data we give it, and this gives a propensity to overfitting the data, which can therefore lead to inaccurate predictions. However, the random forest

model, a supervised machine learning model, relies on an *ensemble* of decision trees. The Random Forest model has proved to be the most robust method due to its built-in ability to measure prediction accuracy and measure the importance of molecular descriptors.^{23, 35, 36}

During the Random Forest Model, each decision tree will be based on a randomly selected bootstrapped sample of data, and the tree will grow until it reaches a maximum size, where no further splits are possible. Further randomness is incorporated because at each node in the tree a split is based on a randomly selected subset of descriptors, rather than attempting to choose the best split from all the descriptors. This additional randomness of the best splitting at nodes ensures no overfitting of the data occurs. There is then repetition of the growth of the decision trees, so that n trees are grown. We then take all of the decision trees together, and a majority vote of all the trees is taken at the end to give the classification. (Figure 7.19).³⁵⁻³⁷

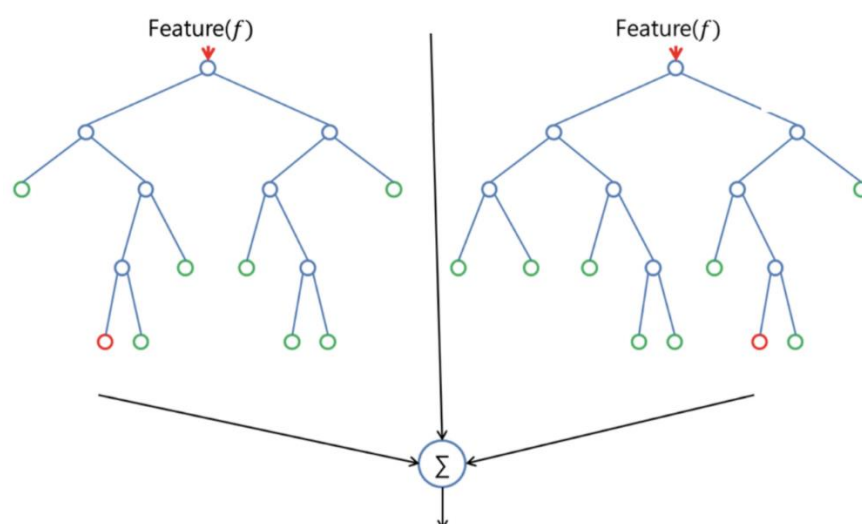


Figure 7.19. The random forest model builds a number of decision trees and then combines them together to provide a stable predictive model. Blue circles are decision nodes. Red and Green circles are terminal nodes. Reproduced from; *Tuning the parameters of your Random Forest model*, T. Srivastava.³⁷

The important thing about the Random Forest model is that it provides an assessment of the performance of the model produced, as it is producing the model. Ideally, if this was done using a large number of compounds, for example around 1000, we would use 900 for the training set and 100 as the test set. Unfortunately, the majority of academic and even some industry based projects don't have the luxury of 100s of compounds, rather have only around 100. Instead on the 100 compounds we have, we need to carry out some cross validation to gain some understanding how accurate this model is. Random Forest conveniently carries out its own cross validation as it carries out the training step. This is known as an Out-of-Bag (OOB) estimate of performance. During bootstrapping, as described above, some molecules are left out of the training samples, and these are what form the

OOB sample, and these are what are used to estimate the prediction performance of the decision tree ensemble and thus the model.

We also need to be wary of the applicability domain for any model produced. We build our data on a test set of compounds and when we use our model we are bound by the prediction restrictions based on that. In a very simplified way, if our training set contained only compounds between 200 and 500 molecular weight, we wouldn't necessarily expect an accurate prediction for activity for a compound that has a molecular weight of 150 or 600. This also applies to a number of other molecular descriptors, and needs to be considered when any output is given, but also how we curate the training set data.³⁸

7.10.6 Receiver Operator Characteristic Curves

A ROC curve employs a two-alternative forced choice (2AFC), also known as a binary classification. For the project described, this is active or inactive.³⁹ A receiver operator characteristic (ROC) curve shows the plot of the true positive rate against the false positive rate in a binary classification system.^{38, 40} The ROC score obtained from a ROC plot is a measure of how good a model is at classifying molecules correctly. For this project, it would be classifying them correctly as active or inactive.

The true positive rate is known as sensitivity or probability of detection. This is determined as a number between 0 and 1 and is based on the ratio of the number of identified actives or true positives (TP) to the total number of actives. The total number of actives is a combination of true positives and false negatives (FN). This can be given by the equation (Figure 7.20);^{38, 41}

$$\text{Sensitivity} = \frac{N_{\text{selected actives}}}{N_{\text{total actives}}} = \frac{\text{TP}}{\text{TP} + \text{FN}}$$

Figure 7.20. The equation that determines sensitivity, which is based on the number of positives identified versus the total number of actives

The false positive rate indicates how specific the model is, and relates to the percentage of truly inactive compounds that are identified. This is given by the equation (Figure 7.21);⁴¹

$$\text{Specificity} = \frac{N_{\text{discarded inactives}}}{N_{\text{total inactives}}} = \frac{\text{TN}}{\text{TN} + \text{FP}}$$

Figure 7.21. The equation that determines specificity, which is based on the number of true negatives (TN) and the total number of inactives.

We can then plot this as a curve with ROC space (Figure 7.22). This is plotted as sensitivity as a function of 1-specificity. From this curve, we can calculate the area under the curve (AUC), which provides with a ROC score and enables us to quantify the performance of the model. The perfect classification, or one that has 100% specificity and sensitivity would cross through coordinates (0,1) and would possess an AUC of 1. A diagonal line that runs through the middle of the graph, through (0,0), (0.5,0.5) and (1,1) shows the outcome if the prediction was just a random guess of whether a compound would be active or inactive. This should be the curve produced upon flipping an un-biased coin as there should be a 50/50 probability of obtaining head or tails and possesses an AUC of 0.5. In Figure 7.22, **A** shows a classification where there is a low number of false positives, however it shows reduced sensitivity so isn't detecting all of the true positives. **B** shows a completely random performance. **C** indicates a prediction worse than random. This could mean it is determining useful information, but it isn't applying the information towards prediction in the correct way. **C'** is better than **A** and much better than random, but still isn't perfect. In reality, most curves lie in between the line for random guess and the perfect classification. The closer the curve is to the perfect classification, the more reliable the model should be at predicting the outcome. If this is applied to our project, it should be more reliable at predicting whether a compound is active or inactive.⁴¹

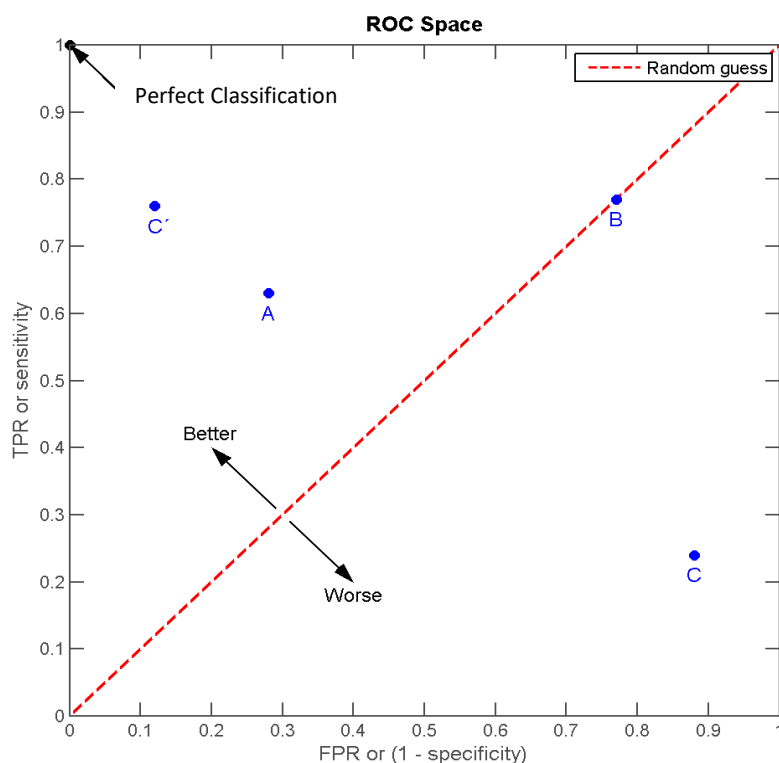


Figure 7.22. A receiver operator characteristic curve plots the true positive rate against the false positive rate. The curve given has a value which indicates how accurate the model is at predicting whether a compound is active or not. Reproduced from; ROC Space work by K. Walz.⁴²

7.11 Design and Testing of a QSAR Model

7.11.1 Pipeline Pilot Protocol

Pipeline pilot was used as the software to carry out machine learning (Figure 7.23). First of all, a database of compounds was compiled with MICs and compounds classified as active or inactive based on an MIC cut off value. For most of the templates this activity cut off is 0.5 mg/L, i.e. <0.5 is classified as active as some classes of the benzimidazoles show excellent activity. For the biphenyl class the cut off was set at 2 mg/L due to this class being less active overall and if set as the original cut off, would have resulted in no active compounds. The next stage involved the calculation of molecular weight and molecular fingerprints. These molecular fingerprints are parts of the molecule that correspond to a structural motif.²⁸⁻³⁰

Finally, the last stage is the machine learning protocol. This is where the random forest protocol is used to produce a model, using the molecular weight and fingerprints. This can then be used to predict the activity of novel compounds, classifying them in a binary manner. There are also extra functions which mainly concern data processing that produces tables confirming the classification of the compounds, the ROC plot and ROC score and importance rankings for particular features.

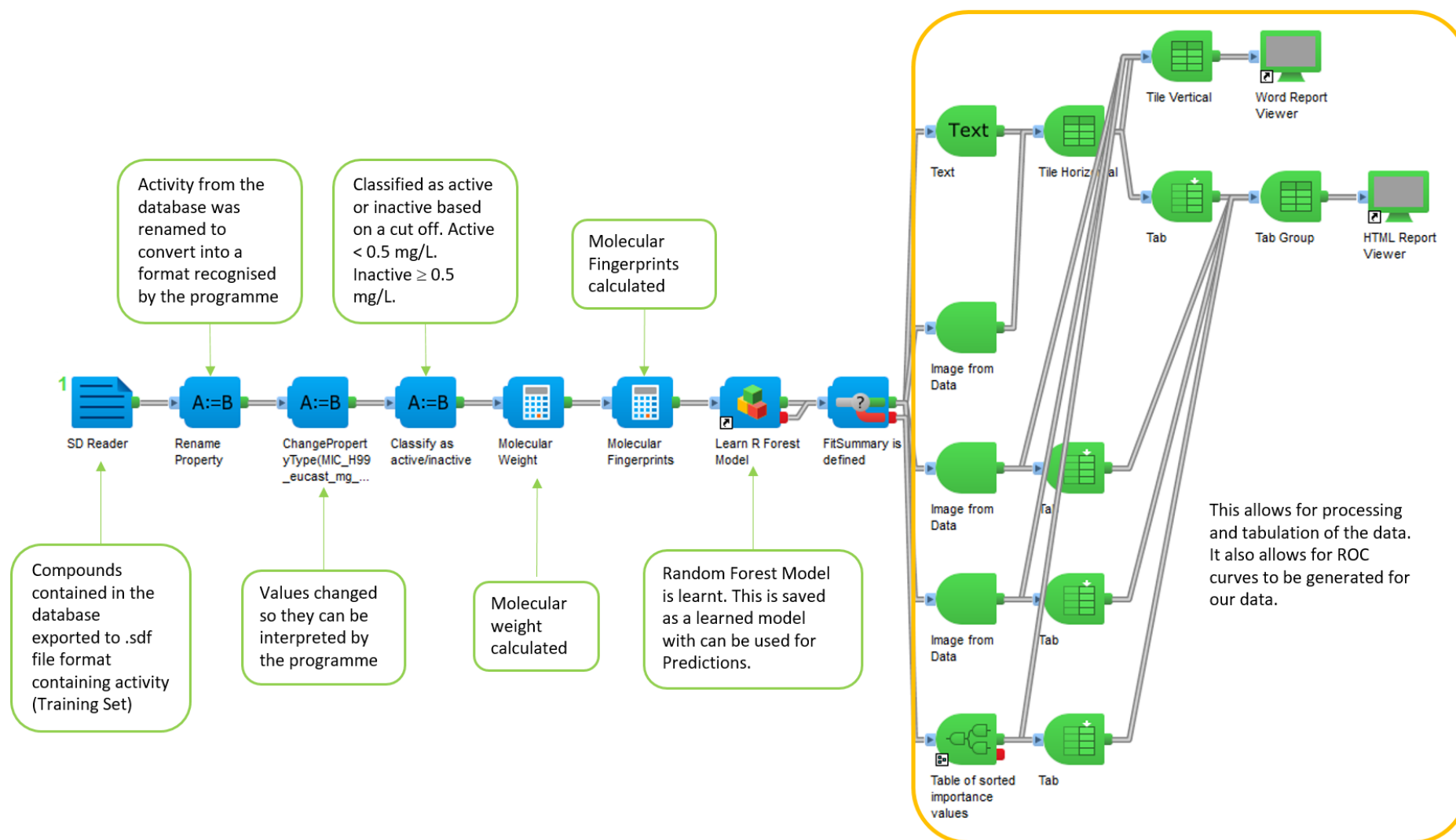


Figure 7.23. The protocol used for generating the Random Forest Model. This learned model can then be used to predict whether a compound is likely to be active or not, which may help to aid future design and synthesis of new compounds

7.11.2 Pipeline Pilot Results - Training

7.11.2.1 Complete Benzimidazole Library

Our own database of 134 compounds was subjected to the pipeline protocol listed above. The protocol produced a ROC curve based a total number of 500 decision trees, with 15 random variables tried at each split. The ROC curve generated had a score of 0.85 (Figure 7.24). This is much higher than a score of 0.5, which is very good performance but not a perfect classification. We can also see there is a reasonable balance between the number of predicted actives and inactives. This suggests that the model produced should have an 85% chance of being able to distinguish between an active and inactive class. It is important to note that within this data set there are compounds included from the thioether, ether, biphenyl and ketone classes, as well as a number of other compounds that don't belong to a particular class due to differences in side chain structure. This gives a wider data set for the machine learning process. This also helps to increase the ROC score and increase the likelihood of the model predicting accurately whether new compounds are active. The balance of actives: inactives is also important when constructing the training set. If it is too heavily weighted to either side, then the model could generate biased predictions. In this database there are more inactives to actives (81 : 53).

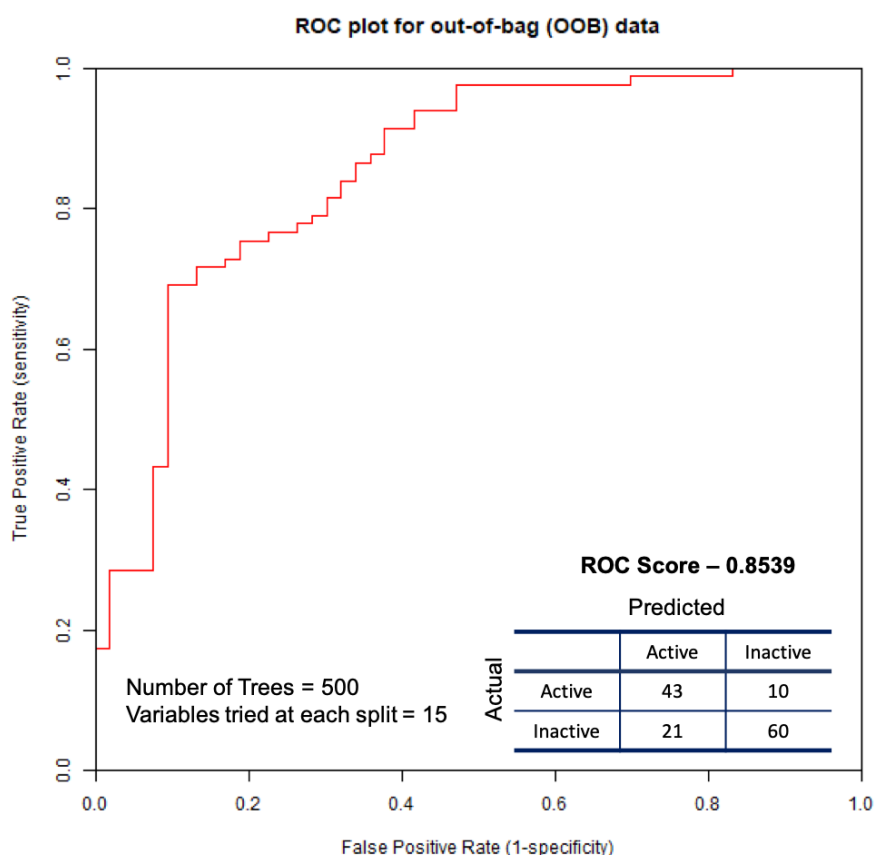


Figure 7.24. The ROC curve produced when a training set of 134 benzimidazoles was screened against a Random Forest Protocol.

Figure 7.25 shows the property importance. We can see that molecular weight is the most important property, followed by a number of molecular fingerprints. These fingerprints are ranked in accordance to how important they are in correctly predicting the activity of a compound. It isn't possible to map the fingerprints onto molecular fragments, but the power of the approach is in future virtual screening and prioritisation of molecules. For compounds we want to synthesise, application of this model will use the molecular fingerprints generated from the new compounds and align them to what the model has learnt, allowing for prediction of activity.

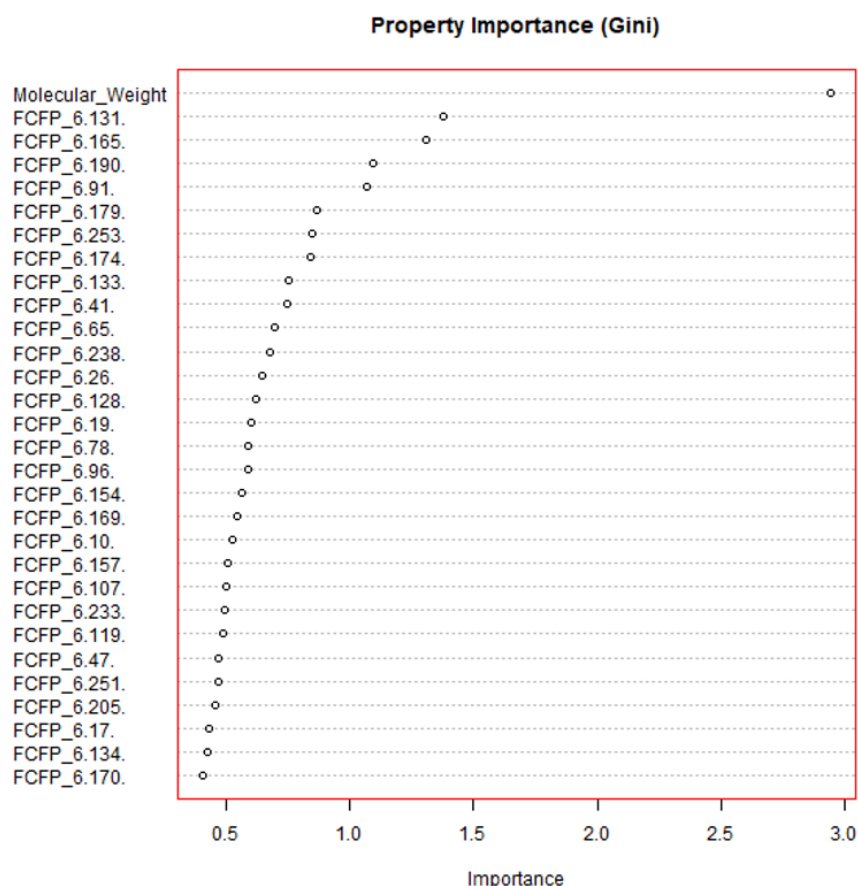


Figure 7.25. The molecular fingerprint importance plot produced when a random forest model is built for the whole benzimidazole class.

7.11.2.2 Thioether ROC Score

The thioether class was subjected to the pipeline pilot protocol (Figure 7.26). This was carried out for 32 compounds in the database, all of which possessed measured biological activity. We can see from the results that the ROC score for this dataset is 0.61, this indicates it is better than simply randomly guessing, but is not as good at predicting activity as when the whole class of benzimidazoles is screened together as seen in Figure 7.25. The number of decision trees for this screening was increased from 500 to 1000, to see if this would help to generate a better model with an improved ROC score. Only a small increase was observed from 0.6 to 0.61. There was also only 10 variables tried

at each node. Given that extra computer power must be dedicated to building extra decision trees, the outcome is not significantly different and perhaps does not warrant the addition computational time.

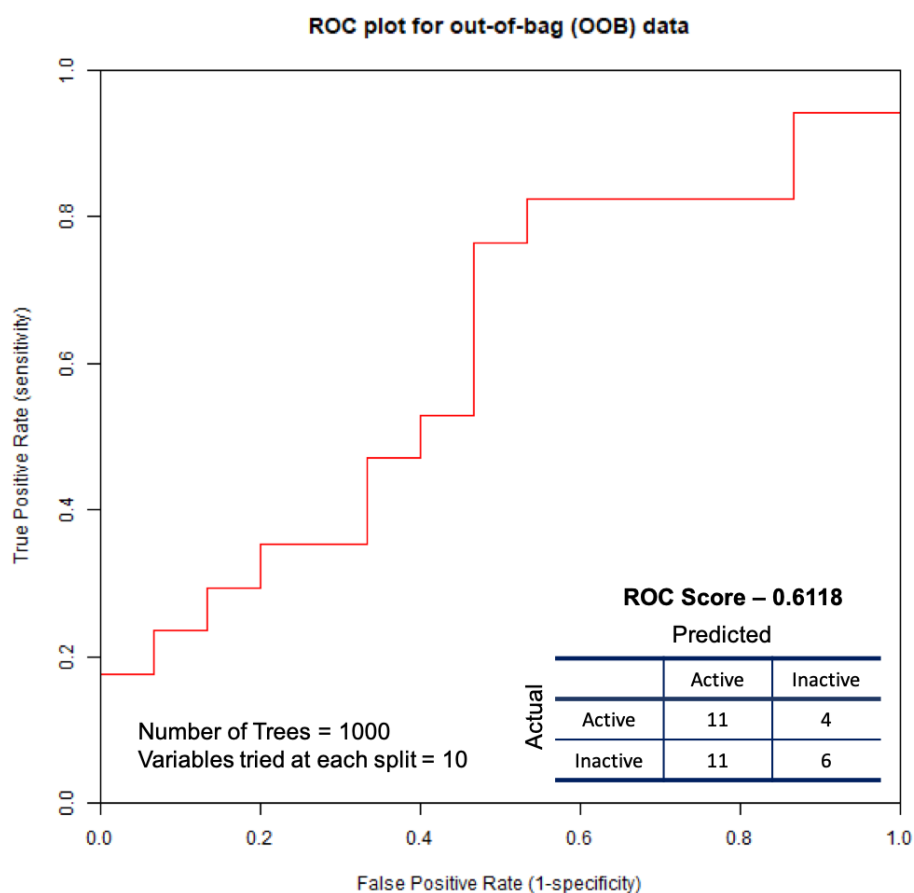


Figure 7.26. The ROC curve produced when A training set of 32 thioethers were screened against a Random Forest Protocol.

7.11.2.3 Ether ROC Score

The ether class was also subject to the modelling and showed a ROC score of 0.83, when a total of 42 ether compounds were screened, which also included the morpholine ethers (Figure 7.27). A ROC score of 0.83 is considered good and gives a higher chance that the model will predict any new compounds activity correctly. There is also a good balance of actives to inactives (22 : 20), with only a small number of false positives and negatives being observed. This was carried out using 500 decision trees with 10 variables tried at each split. The importance plot showed molecular weight as being the most important factor.

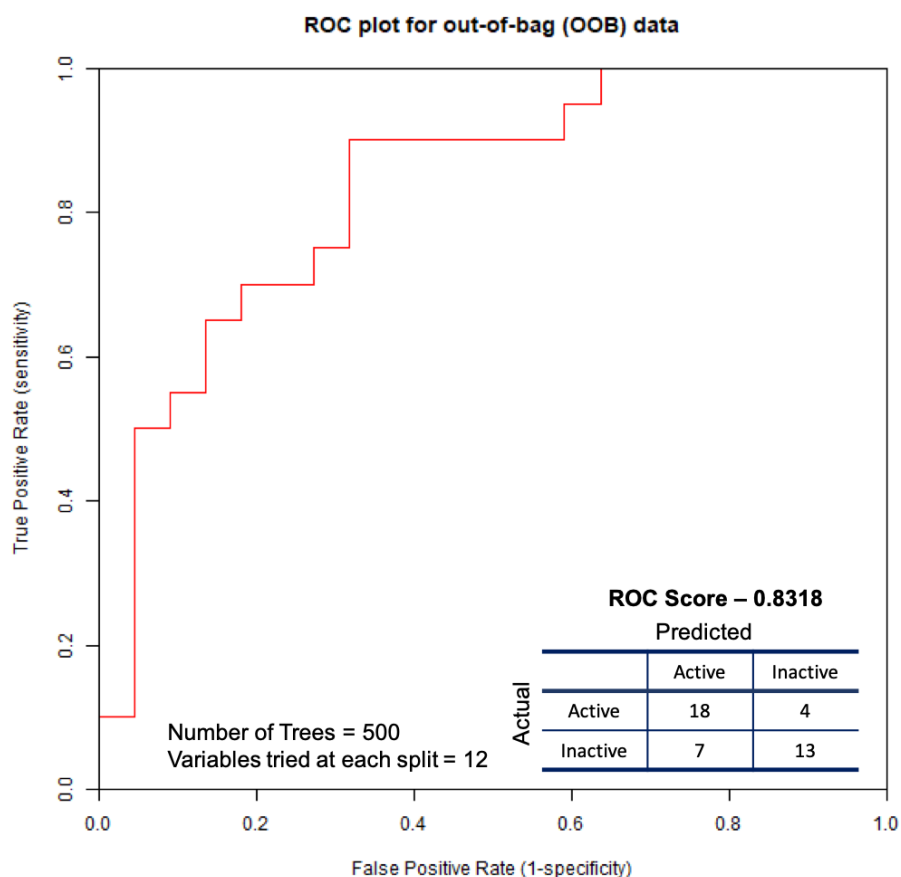


Figure 7.27. The ROC curve produced when A training set of 42 ethers were screened against a Random Forest Protocol.

7.11.2.4 Biphenyl QSAR

The biphenyl class, which contains 18 compounds was also subjected to the protocol. The cut off value for the classification of activity had to be changed from 0.5 mg/L to 2mg/L given the biphenyl class has inherently lower activity and in order to give more balance to the ratio of actives: inactives (7:11). The ROC plot produced showed a curve that sat closer to the line indicated for random guess, though with a ROC score of 0.60, it does indicate that the model should be better at predicting whether compounds are active than pulling results out of a bag. Again, molecular weight was of the highest importance.

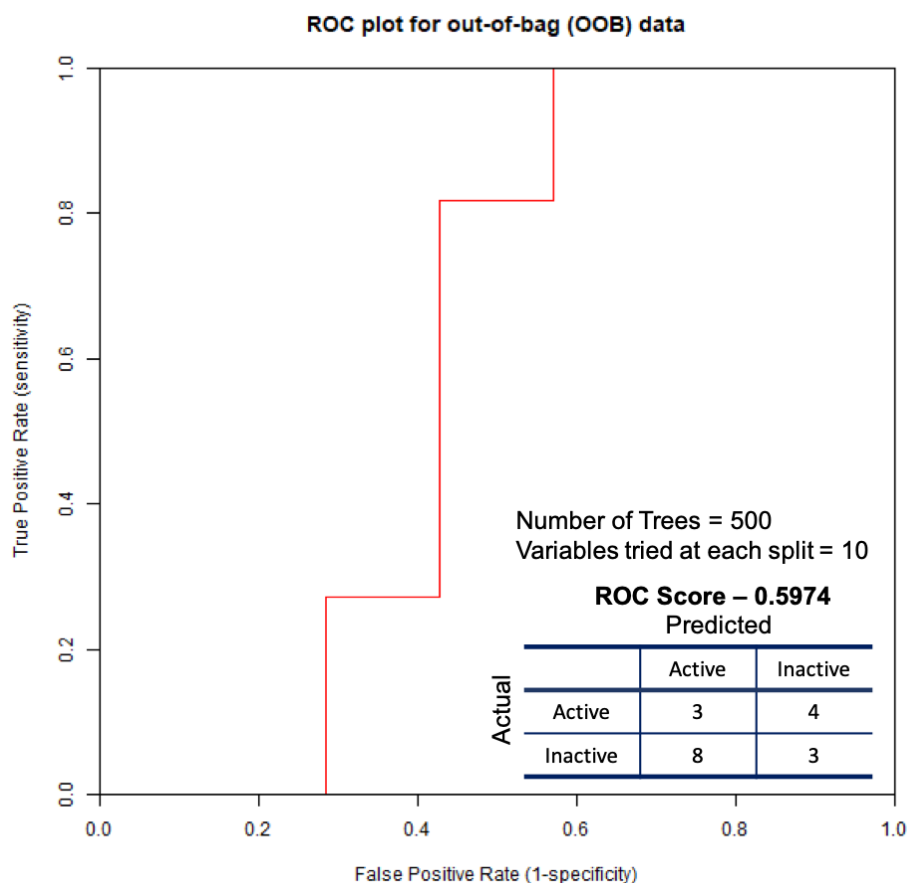


Figure 7.28. The ROC curve produced when A training set of 18 biphenyls were screened against a Random Forest Protocol.

7.11.3 Pipeline Pilot Results – Test

With our benzimidazole model built for the benzimidazole class from our training set, we now needed to carry out a test of model to see how accurate it is a predicting new compound activity for molecules that the model had not seen. This is done through a test set of compounds that haven't been a part of the set the model was trained on. These compounds used for validation of the model, need to have activity associated with them.

7.11.3.1 Test Protocol

The test set containing a different set of compound was saved with information determining whether these compounds were active or inactive, based on the activity cut off of 0.5 mg/L used for building the model. We then use the model that was built to classify the test set of compounds as active or inactive. The classification model evaluation then decides whether the model have correctly predicted the activity of each compound and generates a ROC score based on the accuracy of the model's prediction from the test set of compounds (Figure 7.29).

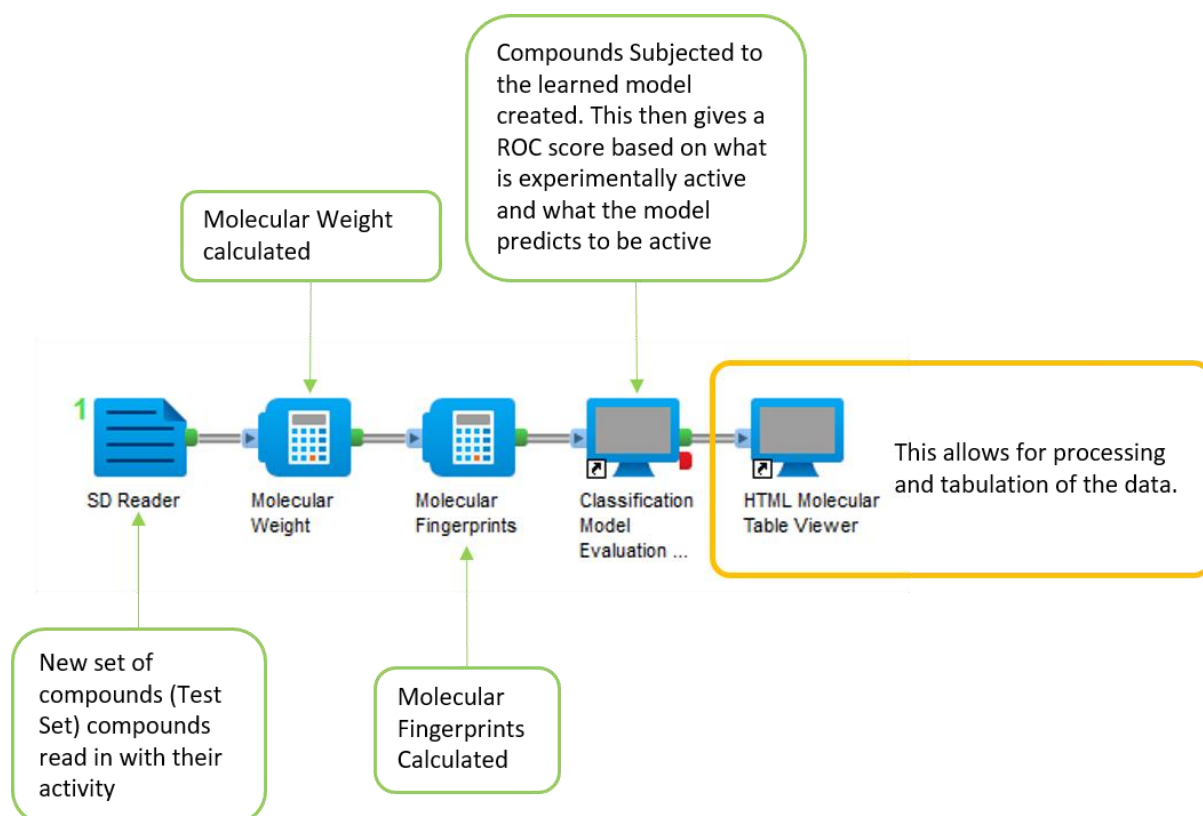


Figure 7.29. The protocol used for testing the model produced from the training protocol highlighted above.

7.11.3.2 Test Results

The test set investigated contained 12 compounds of known activity and were subjected to the model learnt from the training set. It produced a good ROC score of 0.69, which in combination with the shape of the graph shows this model is significantly better at predicting a compound's activity than just drawing activity from a bag. When we use a test set of data and for our compounds we will want to test in future, we need to consider the applicability domain. A researcher cannot give an accurate prediction of a compound's properties if it is significantly different to the compounds that the model was built on.⁴³ The benzisothiazolinones and benzoxaboroles (Discussed in Chapters 8 and 9) have a distinctly different structure and would not lie in the applicability domain of this model, which means any activity predictions would be unreliable. The colours of the lines on the graph indicate which compounds fall within the applicability domain. Those in green do, those in red don't and we can see that all of the compounds that formed part of our test set fell within the applicability domain. This means the ROC score produced for the test set, isn't biased by compounds the model can't predict activity for.

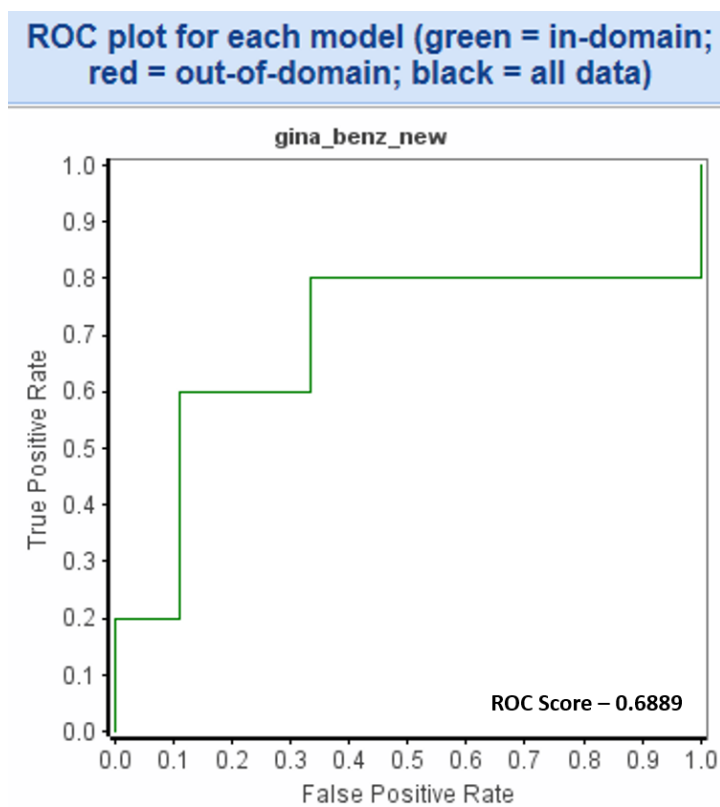


Figure 7.30. The ROC curve produced when A test set of 12 benzimidazoles were screened against the Random Forest Model learned from the training set.

7.12 Conclusion

The computational aspect of the project has identified the binding site for *C. neoformans* and human β -tubulin, noting some differences in the binding sites, which may allow for the development of *C. neoformans* selective analogues. A protocol for binding and visualisation of benzimidazoles was established using GOLD and PyMol. We have also identified some key binding site interactions that may determine why some compounds and classes are more active than others. Investigation into whether CHEMPLP score was linked to activity, showed no correlation, for either the thioether or ether class.

A quantitative structure activity relationship model was built and tested based on a library of benzimidazoles and preliminary tests show that this model could prove reliable for predicting activity of future analogues, which could lead to earlier prioritisation of potentially active analogues.

7.13 Future Work

For the computational modelling studies a crystal structure is necessary to validate the homology models and binding poses we have proposed. This crystal structure along with bound crystal structures of our own analogues will allow for full confirmation of binding pose.

For the QSAR analysis we have been investigating binary classification based on active or inactive. Work should be carried out to investigate whether a model can be built that will reliably predict activity based on MIC values. A project like the benzimidazoles has many synthetic options to choose from, and even a binary classification may not be enough to prioritise compounds enough. Regression QSAR modelling will allow for prediction of these activities, which will allow for better prioritisation.

Furthermore, the input of additional data into the model when it is built, may further help with predicting active compounds. Additional data could include predicted DMPK properties, pK_a , MPO score or binding scores. The prioritisation of molecules with better predicted potency and optimal binding scores could then be carried out, to give a higher likelihood of compound success.

7.14 Experimental

7.14.1 Docking Protocol

Table 7.11. Protocol used for docking.

Feature	Protocol
Protonation	Hydrogens added to the protein
Waters	No addition or extraction of waters as no waters incorporated into the homology model
Ligands	Ligands added as .sdf file, after energy minimisation
Binding Site	LYS 252 identified as being a residue in the binding site of Colchicine, so this was selected
Efficiency	200% efficiency
Number of GA runs	10 –terminated before this if 3 solutions found within 1.5 Å RMSD
Lone Pairs	Lone pairs not saved
Output	Output poses saved as individual files to allow better inspection of each pose
Scoring Function	CHEMPLP score

7.14.2 Generation of PyMol images

Table 7.12. Protocol to Generate PyMol images.¹⁶

Feature	Protocol
Pose Selection	Pose selected for visualisation was based on highest CHEMPLP score.
Protein	Surface Representation with Blue-white tint. 40% transparency.
Ligand	Stick Representation. Carbon – Light Blue, hydrogen – white, nitrogen – dark blue, oxygen – red, sulphur – yellow, fluorine – cyan
Binding Site Amino Acid Residues	Stick Representation. Carbon – green, nitrogen – blue, oxygen – red, sulfur – yellow
Spheres	Radius 0.5. 40% transparency. Red – H-bond acceptor, blue H-bond donor, yellow – hydrophobic interaction

7.14.3 Tautomer Generation

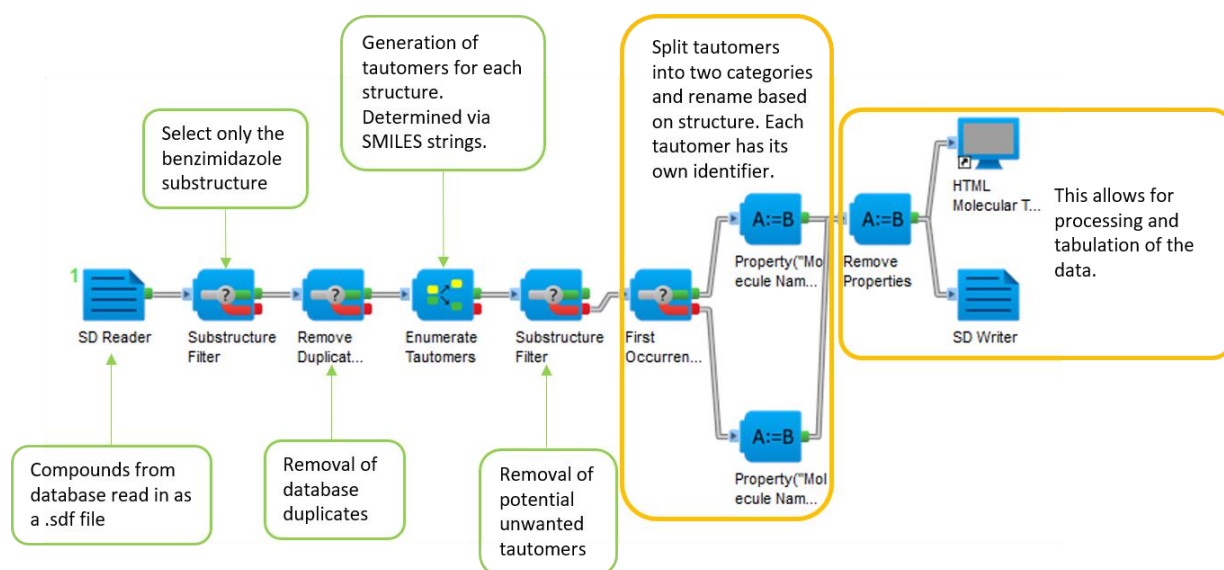


Figure 7.31. Generation of tautomers for each compound in pipeline pilot

7.14.4 Model Testing Protocol – Creation of data file

The test set containing a different set of compound was saved with information determining whether these compounds were active or inactive, based on the activity cut off of 0.5 mg/L used for building the model, this was done either by exporting these compounds into a separate database file, or by editing to the text within the .sdf file directly. This was then read into the SD reader and as previously observed, molecular weight and molecular fingerprints were calculated.

7.15 References

1. D. B. Kitchen, H. Decornez, J. R. Furr and J. Bajorath, *Nat. Rev. Drug Discov.*, 2004, **3**, 935-949.
2. V. Zoete, A. Grosdidier and O. Michielin, *J. Cell. Mol. Med.*, 2009, **13**, 238-248.
3. S.-Y. Huang, S. Z. Grinter and X. Zou, *Phys. Chem. Chem. Phys.*, , 2010, **12**, 12899-12908.
4. M. K. Annamala, K. K. Inampudi and L. Guruprasad, *Bioinformatics*, 2007, **1**, 339-350.
5. Y. Lu, J. Chen, M. Xiao, W. Li and D. D. Miller, *Pharm Res*, 2012, **29**, 2943-2971.
6. J. Wolff and L. Knipping, *J. Biol. Chem.* , 1995, **270**, 16809-16812.
7. R. Aguayo-Ortiz, O. Méndez-Lucio, J. L. Medina-Franco, R. Castillo, L. Yépez-Mulia, F. Hernández-Luis and A. Hernández-Campos, *J. Mol. Graph. Model.*, 2013, **41**, 12-19.
8. M.-A. Esteve, S. Honore, N. Mckay, F. Bachmann, H. Lane and D. Braguer, *Cancer Res.*, 2010, **70**, 1977-1977.
9. R. B. Ravelli, B. Gigant, P. A. Curmi, I. Jourdain, S. Lachkar, A. Sobel and M. Knossow, *Nature*, 2004, **428**, 198-202.
10. M. Gordaliza, P. A. García, J. M. Miguel del Corral, M. A. Castro and M. A. Gómez-Zurita, *Toxicol*, 2004, **44**, 441-459.
11. Y. Damayanthi and J. W. Lown, *Curr. Med. Chem.*, 1998, **5**, 205-252.
12. S. Al-Karadaghi, The 20 Amino Acids and Their Role in Protein Structures, <https://proteinstructures.com/Structure/Structure/amino-acids.html>, (accessed June, 2019).
13. Aldrich, Amino Acids Reference Chart, <https://www.sigmaaldrich.com/life-science/metabolomics/learning-center/amino-acid-reference-chart.html>, (accessed June, 2019).
14. J. Cooper, AMINO ACID SIDE CHAINS. PART III, http://www.cryst.bbk.ac.uk/PPS95/course/2_primary/primary3.html, (accessed June, 2019).
15. CCDC, *GOLD*, 2013.
16. S. LCC, *The PyMOL Molecular Graphics System*, 2018.
17. ZincPharmer, 2019.
18. N. Berry, *Personal Communication*, 2019.
19. P. Girard, Y. Pansart, I. Lorette and J. M. Gillardin, *Dig. Dis. Sci.*, 2003, **48**, 770-774.
20. J. J. Dannenberg, *J. Am. Chem. Soc.*, 1998, **120**, 5604-5604.
21. E. Martz, Help, Index & Glossary for Protein Explorer (PE), http://www.umass.edu/microbio/chime/pe_beta/pe/protexpl/igloss.htm, (accessed June 2019).
22. A. Tropsha, *Mol. Inform.*, 2010, **29**, 476-488.
23. B. Chen, R. P. Sheridan, V. Hornak and J. H. Voigt, *J. Chem. Inf. Model.*, 2012, **52**, 792-803.
24. G. Grant and W. Richards, G, *Computational Chemistry*, OUP, 1995.
25. V. Jitender, M. K. Vijay and C. C. Evans, *Curr. Top. Med. Chem.*, 2010, **10**, 95-115.
26. N. M. O'Boyle, M. Banck, C. A. James, C. Morley, T. Vandermeersch and G. R. Hutchison, *J. Cheminformatics*, 2011, **3**, 33.
27. R. Todeschini and V. Consonni, *Handbook of Molecular Descriptors*, Wiley, 2008.
28. R. C Glem, A. Bender, C. Hasselgren, L. Carlsson, S. Boyer and J. Smith, *IDrugs : the investigational drugs journal*, 2006, **9**, 199-204.
29. ChemAxon, Extended Connectivity Fingerprint ECFP <https://docs.chemaxon.com/display/docs/Extended+Connectivity+Fingerprint+ECFP#ExtendedConnectivityFingerprintECFP-Introduction>, (accessed June 2019).
30. D. Rogers and M. Hahn, *J. Chem. Inf. Model.*, 2010, **50**, 742-754.
31. K. Roy, S. Kar and P. Ambure, *Chemom. Intell. Lab. Syst.*, 2015, **145**, 22-29.
32. F. Sahigara, *Molecular Descriptors*, 2019.
33. Accelrys, *Pipeline Pilot*, 2016.
34. R. Veerasamy, H. Rajak, A. Jain, S. Sivadasan, P. V. Christapher and R. K. Agrawal, *Int J Drug Design and Discov*, 2011, **2**, 511-519.

35. V. Svetnik, A. Liaw, C. Tong, J. C. Culberson, R. P. Sheridan and B. P. Feuston, *J. Chem. Inf. Comput. Sci.*, 2003, **43**, 1947-1958.
36. A. Liaw and M. Wiener, *Classification and Regression by RandomForest*, Merck, 2001.
37. T. Srivastava, Tuning the parameters of your Random Forest model, <https://www.analyticsvidhya.com/blog/2015/06/tuning-random-forest-model/>, (accessed June 2019).
38. H. Sun, H. Veith, M. Xia, C. P. Austin, R. R. Tice and R. Huang, *Mol. Inform.*, 2012, **31**, 783-792.
39. J. A. Hanley and B. J. McNeil, *Radiology*, 1982, **143**, 29-36.
40. A. Pérez-Garrido, A. Helguera, F. Borges, N. Cordeiro, V. Rivero and A. Garrido Escudero, *J. Chem. Inf. Mod.*, 2011, **51**, 2746-2759.
41. N. Triballeau, F. Acher, I. Brabet, J. P. Pin and H. O. Bertrand, *J. Med. Chem.*, 2005, **48**, 2534-2547.
42. K. Walz, ROC Space, https://en.wikipedia.org/wiki/Receiver_operating_characteristic#/media/File:ROC_space-2.png, (accessed June 2019).
43. I. Sushko, S. Novotarskyi, R. Körner, A. K. Pandey, A. Cherkasov, J. Li, P. Gramatica, K. Hansen, T. Schroeter, K.-R. Müller, L. Xi, H. Liu, X. Yao, T. Öberg, F. Hormozdiari, P. Dao, C. Sahinalp, R. Todeschini, P. Polishchuk, A. Artemenko, V. Kuz'min, T. M. Martin, D. M. Young, D. Fourches, E. Muratov, A. Tropsha, I. Baskin, D. Horvath, G. Marcou, C. Muller, A. Varnek, V. V. Prokopenko and I. V. Tetko, *J. Chem. Inf. Model.*, 2010, **50**, 2094-2111.

Chapter 8

Synthesis and Biological Evaluation of the Benzisothiazolinone Class

8.1 An Introduction to Benzisothiazolinones

8.1.1 Properties of Benzisothiazolinones

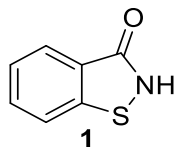


Figure 8.1. The structure of 1,2-benzisothiazol-3(2H)-one.

The compound 1,2-benzisothiazol-3(2H)-one (**1**) (Figure 8.1) is a commercially available off-white solid. Of all of the sulphur and nitrogen containing heterocycles, it is considered one of the most important due to its use in medicine, agriculture and the food industry.¹ The BIZT core is known for exhibiting fungicidal and microbiocidal properties, as well as being used as a preservative in emulsion paints, home cleaning and agriculturally in pesticides. In paint based products **1** is often used in combination with other isothiazolinone core based compounds, including methylisothiazolinone (**2**).²⁻

4

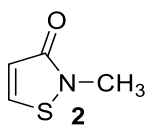


Figure 8.2. The structure of the biocide methylisothiazolinone (**2**).

The molecule is a fusion of benzene and an isothiazolinone, and the molecule retains some of the properties of isothiazolinones. The tautomerisation of isothiazolinones also translates to the benzisothiazolinones, whereby depending on solvent and groups attached to the molecules, it can exist in keto or enolic forms (Figure 8.2). In solvents like chloroform, it is thought the molecule exists primarily in the keto form, as substantiated by ¹³C NMR spectroscopic analysis due to a change in the position of the carbonyl peak. In solvents like dimethylsulphoxide the molecules exists primarily in the enolic form.^{5,6} At 25 °C the pK_a of the NH proton is 7.3 in water, meaning it is readily deprotonated by a number of bases including potassium carbonate and sodium hydride.^{7,8}

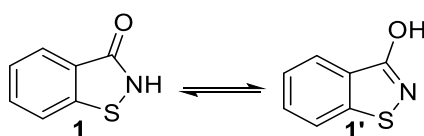


Figure 8.2. Tautomerisation of 1,2-benzisothiazol-3(2H)-one (**1**).

8.1.2 Previous Uses of Benzisothiazolinones

8.1.2.1 Saccharin

Saccharin is a benzisothiazolinone, where the sulphur has been oxidised to generate a sulphone.

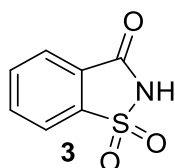


Figure 8.3. Saccharin (**3**) has a structure which is similar to that of the BIZT core being investigated.

3 is an artificial sweetener that is around 300 – 500 times as sweet as sucrose depending on concentration and is used commonly in the food industry for sweetening cake and diet soft drinks.⁹ In rats, an association between in-take of **3** has shown an increase in urinary tumours, however testing in humans has failed to show any similar association.¹⁰

8.1.2.2 MEP Pathway Inhibitors

Through an in-house drug discovery programme, the benzisothiazolinones were also identified as potential novel antimalarial treatments. The methylerythritol phosphate (MEP) pathway does not occur in mammals, but is an essential pathway found in malaria parasites.¹¹ Isoprenoid biosynthesis is an essential metabolic pathway in the malaria parasite, with the isoprenoids being essential for a number of cellular activities including electron transport.¹² Mammals synthesise their isoprenoids via the mevalonate (MVA) pathway.¹³ Due to these pathways being biologically distinct, inhibitors can be designed that inhibit the MEP pathway selectively, with no inhibition of the MVA pathway, minimising the risk to the patient.^{14, 15}

Identification of the BIZT core came about using a combinatorial approach of both high-throughput enzymatic screening and chemoinformatics and from this a series of compounds, including **4** and **5** were synthesised and identified as potential new antimalarials.

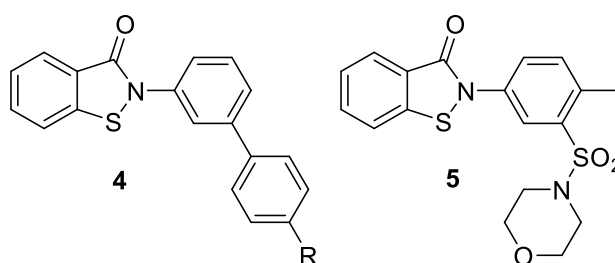


Figure 8.4. The chemical structures of the lead BIZT core compounds (**4** and **5**) produced as IspD inhibitors of the MEP pathway.¹³

8.1.3 Discovery as a Potential *C. neoformans* Treatment

Screenings of an in-house library at the Department of Chemistry, Wichita State University, led to the identification of a compound of the benzisothiazolinone class;¹⁶

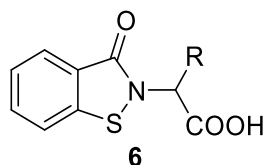
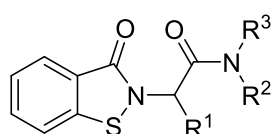


Figure 8.5. The general structure of the compounds synthesised and tested against *Candida* and eventually *C. neoformans*.

Of a number of compounds tested, some showed activity against two *Candida* strains. Compound **6j** (Table 8.1) showed the best activity (MIC 1.6 mg/L) and was further tested against a larger number of *Candida* strains, as well as *Aspergillus fumigatus* and *C. neoformans*.

Table 8.1 shows that those compounds that are substituted at the R¹ position show a decline in activity and those compounds that feature benzyls rather than phenyls also perform better. From this the best performing compound **6j** was then tested against a number of other fungal strains including other *Candida* species, *A. fumigatus* and *C. neoformans*. Activity for compound **6j** is conserved across all of the *Candida* species tested, unlike the traditional treatment fluconazole, which shows varying activity. In *A. fumigatus* we see a decrease in activity, which is comparable to that of fluconazole, and in *C. neoformans* a dramatic increase in activity is observed (Table 8.2).¹⁶

Table 8.1. A number of benzisothiazolinone compounds were synthesised and tested against two *Candida* strains. Compound **6j** showed good activity against both *Candida* strains and thus was further tested.¹⁶



	R ¹	R ²	R ³	MIC ₅₀ (mg/L)	
				<i>C. albicans</i>	<i>C. glabrata</i>
6a	H	H	Phenyl	6.4	6.4
6b	H	H	(<i>o</i> -COOCH ₃)phenyl	6.4	12.5
6c	H	H	(<i>m</i> -COOCH ₃)phenyl	12.5	25
6d	H	Methyl	Phenyl	>50	>50
6e	H	H	Benzyl	3.2	6.4
6f	H	H	(<i>m</i> -OCH ₃)benzyl	3.2	6.4
6g	H	H	(<i>p</i> -OCH ₃)benzyl	3.2	3.2
6h	H	H	(<i>p</i> -F)benzyl	1.6	3.2
6i	Methyl	H	Benzyl	>50	>50
6j	H	Methyl	Benzyl	1.6	1.6
6k	Methyl	Methyl	Benzyl	25	25

6l	H	Ethyl	Benzyl	6.4	12.5
6m	H	Ethyl	Ethyl	>50	>50
6n	H	H	(S)CH(CH ₃)Ph	6.4	12.5
6o	H	H	(R)CH(CH ₃)Ph	6.4	6.4
6p	H	H	(CH ₂) ₂ Ph	>50	>50
6q	H	H	1-adamantyl	3.2	6.4
6r	H	H	2-thiazoyl	>50	>50
6s	H	H	(CH ₂) ₂ morpholino	>50	>50

Table 8.2. The data shows conservation of activity across the candida species. What is apparent is the large increase in activity of compound **6j**, when compared with fluconazole, a standard fungal treatment.¹⁶

Fungus	MIC ₅₀ (µg/mL)	
	Compound 6j	Fluconazole
<i>Candida albicans</i> (CAF-2)	1.6	0.2
<i>Candida glabrata</i>	1.6	3.2
<i>Candida tropicalis</i>	1.6	16
<i>Candida parapsilosis</i>	1.6	0.4
<i>Candida lusitanae</i>	1.6	3.2
<i>Candida guilliermondii</i>	1.6	6.4
<i>Candida apicola</i>	1.6	0.2
<i>Aspergillus fumigatus</i> (AF-298)	12.5	16
<i>Cryptococcus neoformans</i> (H-99)	1.6	>64
<i>Cryptococcus neoformans</i> (JEC-21)	1.6	>64

8.1.4 Biological Effects of Benzisothiazolinones

8.1.4.1 Genetics Based Approach

Identification of benzisothiazolinone activity against *C. neoformans* resulted in mode of action studies. ‘Amino Acid-Derived 1,2-benzisothiazolinone Derivatives as Novel Small-Molecule Antifungal Inhibitors’¹⁷ highlights the use of their analogue, DFD-VI-15, which possesses the same structure as compound **6j**. This mode of action study involved the combined use of a genetics-based approach, utilising a homozygous deletion of a large number of *Saccharomyces* mutants, which allowed for the identification of a number of hypersensitive and resistant mutants.

Susceptibility assays were then used to identify resistant and hypersensitive mutants. This screen yielded a number of hypersensitive mutants, of which a large number lacked mitochondrial or mitochondrion related encoding genes. A number of other categories were identified whereby genes that were lacking included; amino acid biosynthesis, protein sorting, iron utilisation and stress adaptation. From the resistant mutants one was identified as lacking ACE2. This has been implicated in a number of functions including positively regulating glycolysis.¹⁷

Down-regulation of glycolytic metabolism genes and genes responsible for adenosine triphosphate (ATP) synthesis, oxidative phosphorylation and Tricarboxylic Acid (TCA) cycle was noted. Resistance may be explained by mitochondrial functions being elevated by a compensatory mechanism that leads to the survival of treated cells. Phenotypic data suggests that benzisothiazolinones inhibit mitochondrial respiration, leading to an increased production of reactive oxygen species (ROS) and membrane depolarisation can occur.^{17, 18}

This is promising, as inhibition of mitochondrial functions is an alluring target in antifungal drug discovery. Firstly, if inhibition of fungal-specific proteins occurs within the mitochondria, the essential process of energy production will be affected, which could have a number of 'knock-on' effects on other cellular activities, leading to fungal cell death.¹⁸ Secondly, most fungi have alternative respiration pathways, which are the Alternative Oxidase Pathway (AOX) and the Parallel Pathway (PAR), both of which are not present in mammalian cells making for an ideal selective target.

8.1.4.2 A Comparison to Ebselen

Ebselen (**7**) is considered to function by mimicking glutathione peroxidase and providing cytoprotective, anti-inflammatory and anti-oxidant activity (Figure 8.5). Glutathione peroxidases are part of a class of peroxidase enzymes which help to turn the cytotoxic compound hydrogen peroxide into water. **7** is very good at sequestering hydrogen peroxide in cells, stopping oxidative damage occurring when hydrogen peroxide is produced.¹⁹

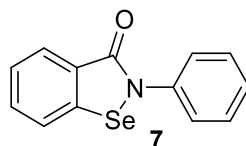


Figure 8.5. The structure of ebselen (**7**) is similar to that of the benzisothiazolinone core with a simple replacement of sulphur with selenium.

The compound has been indicated in a number of diseases such as ischemic heart disease, hearing loss and bipolar disorder. We can also learn something about the potential mechanism of action of BIZT compounds from the extensive work carried out on **7**. One of the main proposed mechanism of action for ebselen is the reduction of peroxide based compounds, which results in a reduction of oxidative stress in a cell (Figure 8.6).^{19, 20}

The mechanism starts with ebselen (**7**), which through a process of glutathione conjugation, produces a selenium-sulphur bonded derivative known as selenyl sulphide (**8**), via a five-membered ring opening mechanism. For our own compounds this would create a disulphide compound instead. A second molecule of glutathione can then remove the sulphur linkage to produce a selenol compound (**9**). This then can react with hydrogen peroxide or other peroxide derivatives, allowing for its conversion into

water and the production of selenic acid (**10**), which with a second loss of water can undergo a 5-membered ring closure to regenerate **7**. It is also hypothesised that **10** can undergo glutathione conjugation to reform intermediate **8**, providing a short cut to the cycle.^{19, 21, 22}

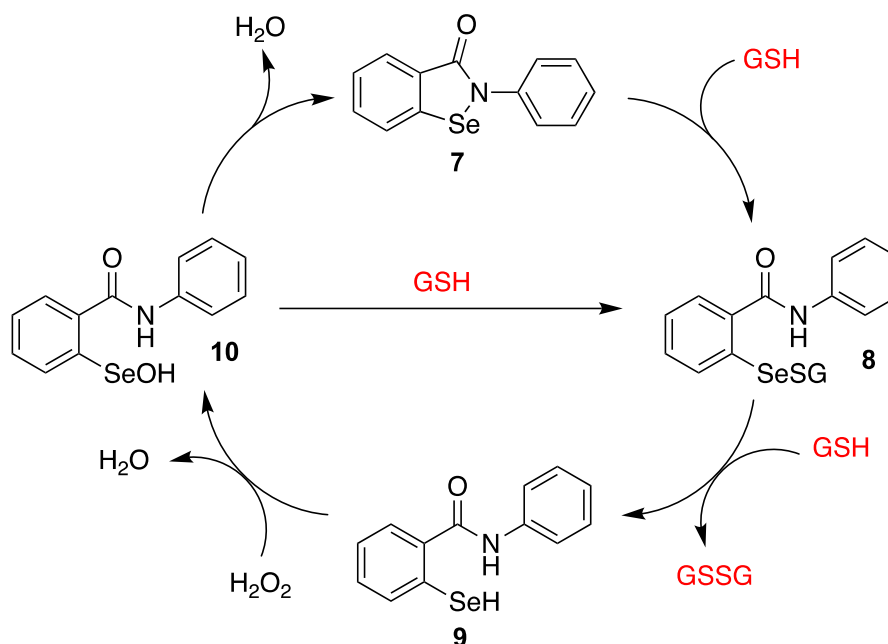


Figure 8.6. The proposed mechanism of glutathione conjugation within the cell for the commercially available drug ebselen (**7**). From this we can see how the generation of active intermediate selenium derivatives of ebselen (**7**) can allow for reduction in the amount of hydrogen peroxide, leading to a reduced level of oxidative stress. Reproduced from; *In vitro glutathione peroxidase mimicry of ebselen is linked to its oxidation of critical thiols on key cerebral suphydryl proteins – A novel component of its GPx-mimic antioxidant mechanism emerging from its thiol-modulated toxicology and pharmacology*, I, Kade *et al.*²¹

8.1.4.3 A comparison to the IspD Mechanism

Previous work within the department of chemistry allowed for discovery of a number of analogues of the benzisothiazolinones that were tested against malaria and the IspD pathway. A mechanism of action was proposed that involves the sulphur of a cysteine residue behaving as a nucleophile, attacking the sulphur of the benzisothiazolinone core, generating a disulphide bond. This causes ring opening of the BIZT core, generating a negative charge on the nitrogen, which is now part of an amide functionality (Figure 8.7).²³⁻²⁵

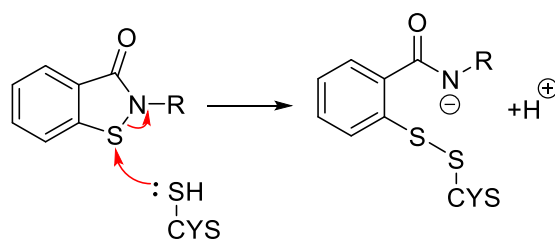


Figure 8.7. A hypothesised mechanism, showing the interactions of the core sulphur with a cysteine in the binding site.²³⁻²⁵

Despite not knowing the target of BIZTs within *C. neoformans*, it can be easily envisaged that the same mechanism can be applied to the hypothetical target. Suggesting that the molecule binds with a cysteine residue within the active site of the target, which suggests the necessity of the N-S bond. However, whilst the N-S bond does appear to be essential for activity, due to its susceptibility to attack by nucleophiles, this does make it weak, and could present problems metabolically. This N-S/N-Se bond cleavage is observed in metabolism of these compounds and is discussed in the next section.²³⁻

25

8.1.5 Benzisothiazolinone Metabolism

The metabolism of benzisothiazolinones is relatively under discussed in the literature. However, there is data surrounding the metabolism of ebselen (**7**). Along with the glutathione conjugation mechanism described in Figure 8.8, other metabolism of this core involves glucuronidation, hydroxylation and methylation.

A study looking at these metabolic pathways employed the use of ¹⁴C labelled (**7**), whereby two major metabolites were discovered in high concentrations in plasma and bile. They then isolated these metabolites and subjected them to structure elucidation. The metabolites Se(O)Me (**11**) and SeOx (**12**) (Se-Oxide), as highlighted in the blue boxes in the image below have been confirmed via spectroscopic analysis. The SeMe (**B**) product is produced, when methylation and ring opening of (**7**) occurs, generating this intermediate, which is then oxidised to give the identified metabolite Se(O)Me (**11**). When the SeOx metabolite is left for a prolonged period of time, it undergoes glutathione conjugation to the intermediate **D**, which then undergoes ring closure to regenerate ebselen, and helps to verify the reformation of ebselen, both metabolically and mechanistically, in terms of its mode of action.

Ebselen itself can also undergo direct oxidation of the selenium, to give an oxide SeOx (**12**), which can undergo a ring opening reaction, from the addition of water to give intermediate A. This reaction is reversible and SeOx can be reformed upon the loss of water. SeOx can then react with glutathione to create an Se-S bond (**D**), as observed in the mechanism of action described for **7**, which can then be

cleaved, via a second reaction with glutathione to give intermediate **C** which can lose water to give ebselen. It is proposed that the same metabolism can be envisaged for the BIZT core.²⁶

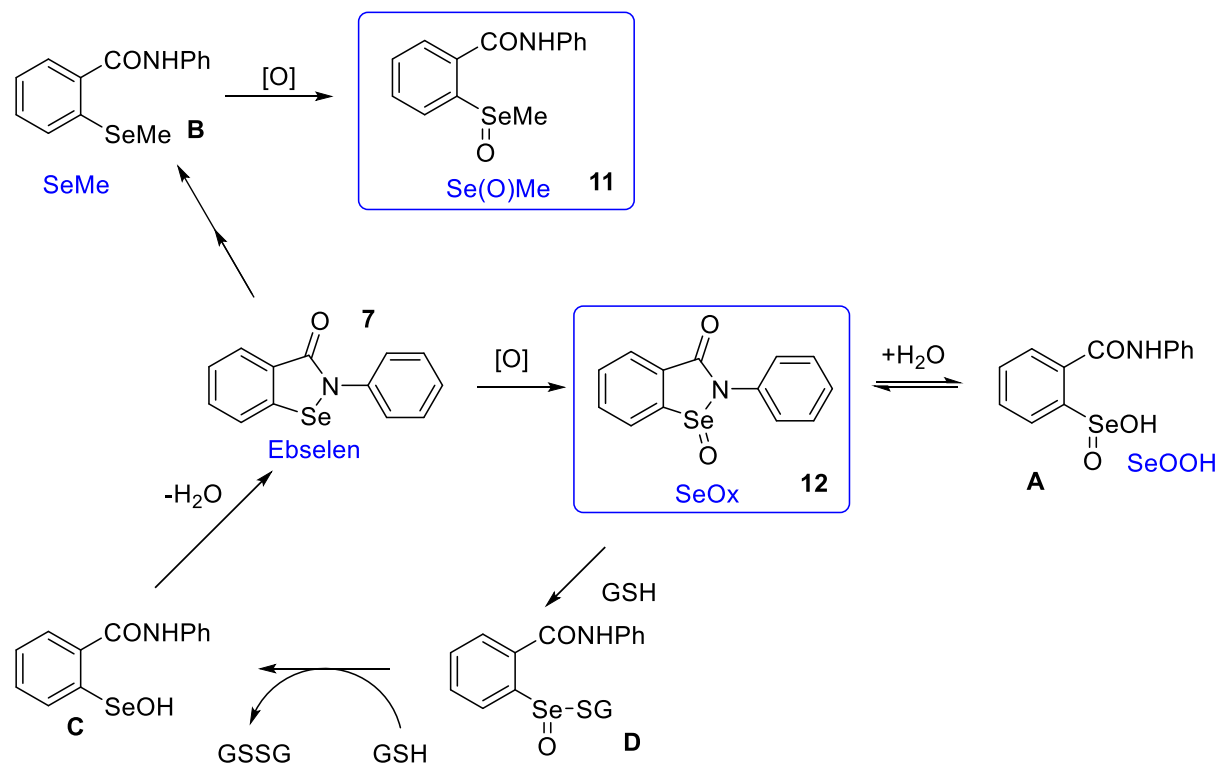


Figure 8.8. The metabolism of ebselen has identified through ¹⁴C labelled Ebselen to follow the pathway described, Compounds in blue boxes have been confirmed via spectroscopic analysis. Reproduced from; *Metabolism of ebselen (dr-3305) : relation to the antioxidant activity*, H, Masumoto, et al.²⁶

There is also a proposed mechanism of metabolism which describes a similar route as for ebselen, whereby a number of metabolic derivatives are produced. This includes the analogous *o*-methylthiobenzamide (**C**) formed via methylation and the sulphoxide metabolite (**D**) formed via oxidation (Figure 8.9).²⁷

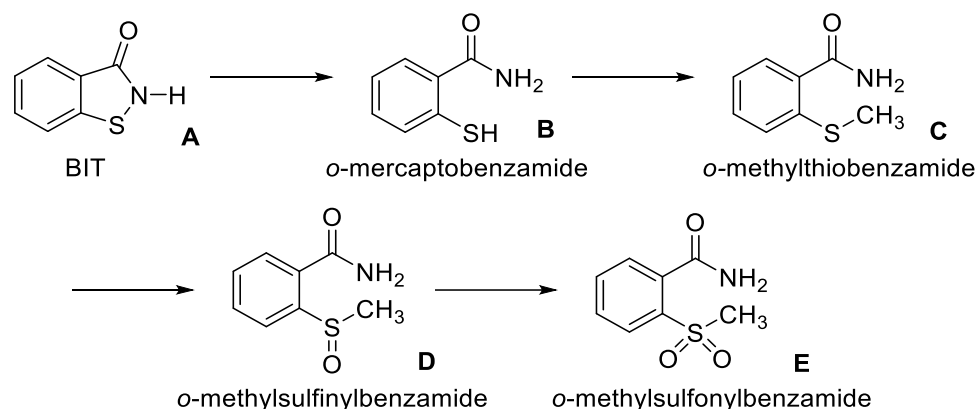


Figure 8.9. The proposed metabolic route for the BIZT core.²⁷

8.1.6 This Project: The Benzisothiazolinone Core

The benzisothiazolinone core presents as a promising starting point. There are synthetic routes already established in the literature, and some previous work done within the group. There is evidence in the literature of antifungal activity, but there is only limited evidence of activity against *C. neoformans* specifically. We can also use ebselen (**7**) to draw comparisons from when attempting to understand mechanisms of action and metabolism due to similarity in structure. However, synthetically and biologically there is scope for improvement. The paper doesn't test any other analogues against *C. neoformans*, so work will be carried out to make more analogues. This is important for understanding biological activity.

From this aims for this project were decided;

1. To resynthesise the hit from the paper to confirm biological activity.
2. To design and synthesise other benzisothiazolinone analogues in order to explore the SAR relationship, and use this to design more efficacious analogues in the future (Figure 8.10).
3. Obtain DMPK data to understand the extent of the metabolism of these analogues, particularly the impact of the N-S bond.

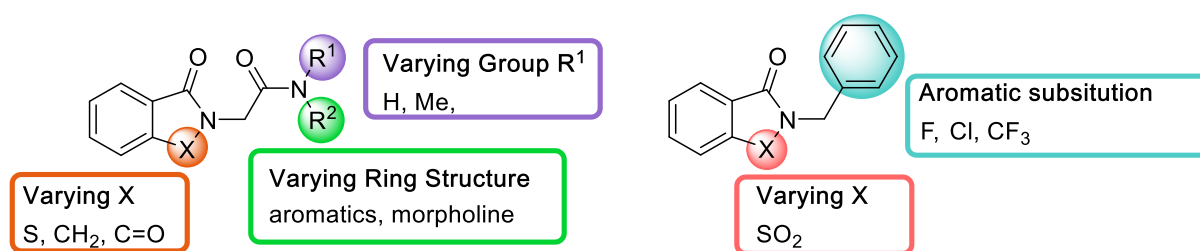


Figure 8.10. The benzisothiazolinone class presents a large number of compound derivatives that could be synthesised in order to explore the SAR of this compound class as a treatment for *C. neoformans*.

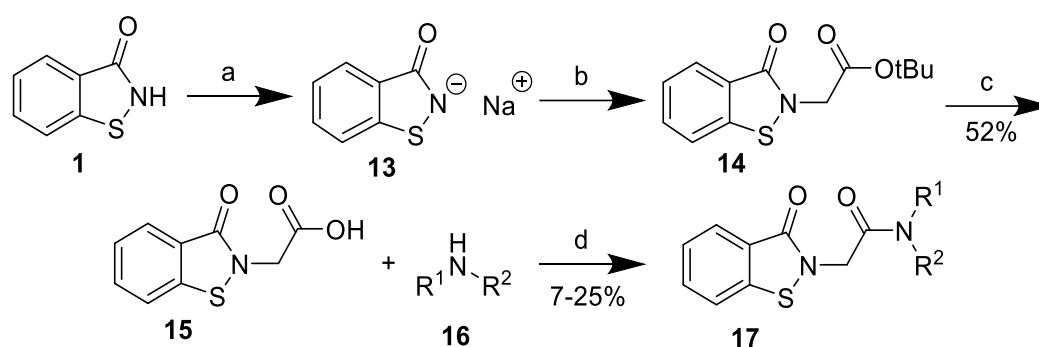
8.2 Results and Discussion

8.2.1 BIZT Core Amides

8.2.1.1 Synthesis

Given that a number of analogues needed to be synthesised, a route was implemented which only underwent divergence in the last step.

8.2.1.1.1 Divergent Acid Synthetic Route



Scheme 8.1. Reagents and conditions: (a) NaH (1.2), THF, 0 °C, 15mins; (b) *t*-butylbromoacetate (1.0 eq), 2,2,2-trifluoroethanol, 0 °C to reflux, 1 hour; (c) TFA, DCM, room temperature, overnight, 52% yield; (d) *N*-methylbenzylamine (1.0 eq.), EDC.HCl (1.2 eq.), pyridine (4.0 eq.), DMF, room temperature, overnight (7 – 25% yield).¹⁶

Table 8.3. Percentage yields obtained for all compounds created within the BIZT core amide template.

Compound	R ¹	R ²	Step D % yield
17a	Me	C ₆ H ₅	17
17b	H	4-phenoxyaniline	15
17c	H	4-(4-fluorophenoxy)aniline	13
17d	H	4-(4-chlorophenoxy)aniline	7
17e	H	4-(3-chlorophenoxy)aniline	24
17f		4-benzylpiperidine	25
17g		4-fluoropiperidine	19

Initially, the hit compound (**17a**) from the paper was resynthesized to check activity against *C. neoformans*. This was done by following the same route (Scheme 8.1) as that described in the paper, with some minor alterations to the reagents used. The first step involved the deprotonation of the acidic core N-H proton using sodium hydride in tetrahydrofuran at 0 °C to give the reactive sodium salt of the BIZT core (**13**). Isolation of **13** was brought about via removal of the THF solvent, allowing it to be used crude in the next step. The second step of this synthetic route involved the alkylation of the BIZT core using *t*-butylbromoacetate, using 2,2,2-trifluoroethanol at 0 °C and then refluxed to give **14** as a pink solid that was continued crude into the next reaction. Next, we wanted to isolate the free acid (**15**), which could be used as our divergent point for a series of amide couplings. The presence of

the *t*-butyl ester allows for an easy deprotection which was carried out using trifluoroacetic acid, in dichloromethane, to give the desired acid as a white solid in a moderate yield of 52%.¹⁶ Steps a and b were generally carried through crude, however **14** was isolated and ¹H NMR confirms the product via the appearance of the Boc protons at 1.49 ppm. The acid (**15**) was confirmed via mass spectrometry and ¹H NMR showed a distinct peak at 4.59 ppm, which is indicative of the CH₂ aliphatic peak. There was also the presence of a broad singlet at 13.09 ppm, which corresponds to the OH of the acid. Focusing on the key peaks with in the ¹³C NMR we can detect the presence of two downfield peaks at 169.8 ppm and 165.4 ppm, indicating the presence of the two carbonyl groups of the BIZT core and the acid handle.

The next step in this sequence involved an amide coupling between **15** and the desired amine (**16**) to give compound **17**. When synthesising the hit compound (**17a**), the yield for this reaction was quite poor at only 17%. This is thought to be due to the bulky nature of the secondary amine coupling into the acid, however a small amount of final compound was synthesised as indicated by mass spectrometry and the presence of additional aromatic protons. Initial analysis of this compound proved to be difficult due to the presence of *cis* and *trans* isomers of the compound, which results in a more complicated ¹H NMR spectrum (See Appendix, Figure 6A&B for general NMR data).

Most secondary amide bonds adopt the *trans* conformation as this means the substituted groups are furthest away from each other, minimising steric interactions.^{28, 29} For tertiary amides, this changes and we observe an increase in the *cis*-amide population. This is because there is a lower energy barrier between the *cis* and *trans* configurations.³⁰⁻³² The stability of *cis* versus *trans* is derived from the position of the groups attached to the amide and their steric interactions with the carbonyl and the other groups attached. In the case of the *N*-benzylmethylamine derivate (**17a**), the *trans* amide is considered more stable due to exhibiting reduced steric clashes of the benzyl group with the carbonyl, whereas the *cis* show greater steric clashes. The methyl on the amide also provides some steric clashes and whilst this impacts upon the carbonyl less, it is still substantial enough to result in a mixture of the *trans* and *cis* isomer forming.^{31, 33}

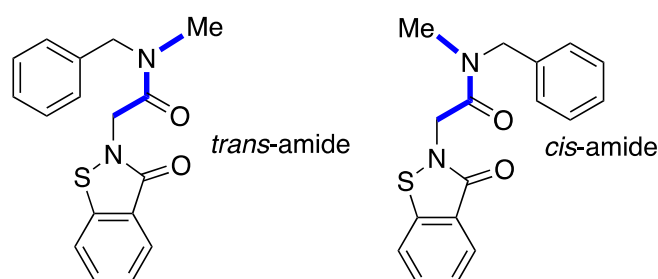


Figure 8.11. Tertiary amides can exist as *trans* and *cis* isomers.

This is most observable when studying the ^1H NMR spectrum (Figure 8.12). This shows the aromatic protons, with only one being distinguishable from a multiplet at around 8.05 ppm, and clearly shows two doublets, with different integrations. The rest of the aromatic protons are in complicated multiplets, due to coupling to each other and different peaks for *cis/trans* isomers. The most profound evidence of this *cis/trans* isomerisation derives from the CH_2 peaks at around 4.76 & 4.67 ppm. These CH_2 peaks should be singlets, but instead initially appear as doublets. However, rather than doublets there are individual singlets for each of the two isomers. Their relative integrations show a difference in the ratio of the two isomers, with the *trans* likely to dominate with a ratio of 1:0.66, based on literature evidence.²⁸⁻³²

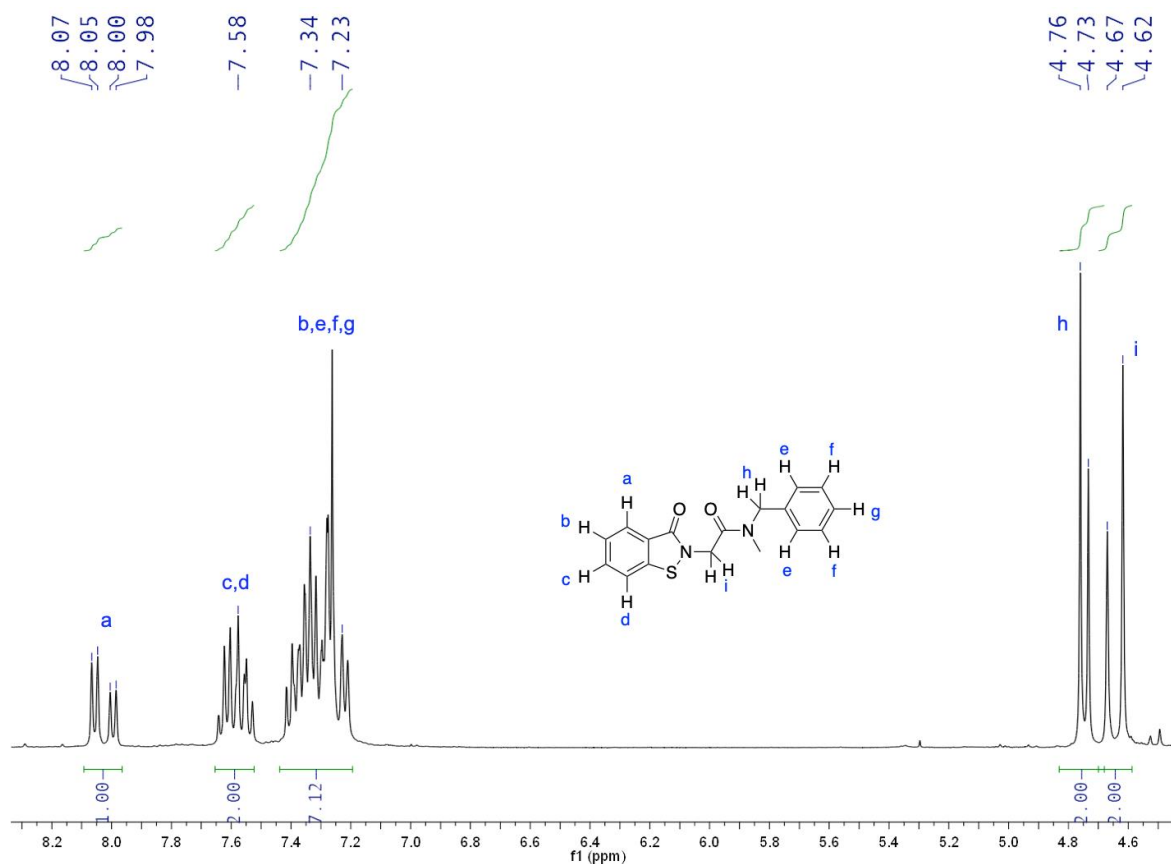


Figure 8.12. The ^1H NMR spectra of the *N*-Benzylmethylamine derivative **17a**. It is clearly observed the presence of two peaks for each proton, correlating with the *cis* and *trans* isomers of the amide.

Due to the poor yields we sought to improve the reaction conditions by changing the amide coupling conditions used.

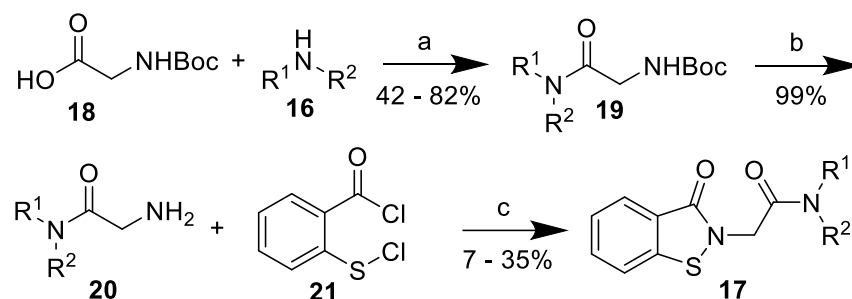
Table 8.4. A number of different conditions were used to promote amide bond formation, however using this route only reaction one produced the desired product and this was done in poor yield.

	Amide Coupling Reagent	Eq.	Base	Eq.	Yield (%)
1	EDC.HCl	1.2	Pyridine	4	17
2	EDC.HCl	1.2	Pyridine	2	0
3	HATU	1.5	K_2CO_3	4	0
4	HATU	1.3	DIPEA	1.5	0

Firstly, we started off by using EDC.HCl and four equivalents of base, this gave poor yields of 17% for **17a**. We then tried to reduce the equivalents of base, to ensure the pyridine was not interfering in the reaction. Reduction to two equivalents of pyridine resulted in no product observed via TLC. HATU was also employed with the bases potassium carbonate and DIPEA, but still resulted in no conversion to the product. These reactions were repeated many times, using a variety of amines, but only EDC.HCl provided any final compound.

8.2.1.1.2 Ring Closing Benzisothiazolinone Synthetic Route

In the initial stages of this project, the synthesis of the initial hit **17a** proved to be poor yielding, so an alternative route was devised (Scheme 8.2).



Scheme 8.2. Reagents and conditions: (a) *N*-benzylmethylamine (1.0 eq.), EDC.HCl (2.0 eq.), pyridine (2.0 eq.), DMF, room temperature, overnight, 42 - 82% yield; (b) TFA: DCM (3:7), room temperature, 2 hours, 99% yield; (c) Et₃N (1.0 eq.), DCM, room temperature, overnight, 7 - 35% yield.²³

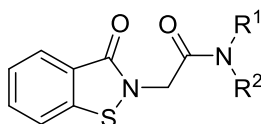
This involved *t*-butyl carbonyl protected glycine (**18**) and carrying out an amide coupling with the desired amine (**16**) (*N*-Benzylmethylamine or phenoxyaniline), using EDC.HCl and pyridine to give the intermediate **19** in moderate yields.^{34, 35} Confirmation of this product was carried out by lack of OH proton from the carboxylic acid, which is predicted to be at approximately 13.0 ppm. Further proof was derived from the ¹H and ¹³C NMR spectra which suggested the presence of *cis/trans* isomers due to the formation of the tertiary amide. This was most profound for the Boc group protons at 1.46 ppm which should be a singlet, but due to the two isomers have ended up as two separate peaks. All other protons in the NMR spectra also show two peaks for each environment, confirming the two isomers.

The next step involved a trifluoroacetic acid deprotection of the Boc group from the amine of the glycine portion of the molecule, and quantitative yields for this reaction were observed.^{36, 37} The free amine (**20**) generated from the deprotection reaction was then subjected to a ring closure reaction to produce the final BIZT compound (**17**).³⁸ The first step involves addition of the primary amine into the acid chloride (**21**) to generate one molecule of HCl, followed by a second addition of the amine into the S-Cl bond to produce a second molecule of HCl, completing the ring closure, with final compounds being identified as previously described.

8.2.1.2 Biological Activity

Biological testing carried out as stated in Chapter 3, Section 3.2.3 and data given in Table 8.5.

Table 8.5. Biological activity obtained in the form of minimum inhibitory concentration shows the compounds with a sulphur core and amide arm showed poor biological activity. **Green** – good - 0.015 – 0.25 mg/L, **yellow** – acceptable - 0.5 – 4 mg/L, **red** – poor - >4 mg/L. *17i-17k made by Caroline Vermeiren.



Compound	R ¹	R ²	<i>C. neoformans</i> MIC (mg/L)
17a	Me	CH ₂ -C ₆ H ₅	>4
17b	H	4-phenoxyaniline	>4
17c	H	4-(4-fluorophenoxy)aniline	>4
17d	H	4-(4-chlorophenoxy)aniline	>4
17e	H	4-(3-chlorophenoxy)aniline	>4
17f		4-benzylpiperidine	4
17g		4-fluoropiperidine	>4
17h	Me	CH ₂ -2-F-C ₆ H ₄	4
17i	Me	CH ₂ -3-F-C ₆ H ₄	4
17j	Me	CH ₂ -4-F-C ₆ H ₄	4
17k	H	CH ₂ -4-F-C ₆ H ₄	>4

The start of this project involved remaking the hit **17a** and reassessing its biological activity against *C. neoformans* through an in-house minimum inhibitory concentration assay. When subjected to our own assay **17a** was found to have an MIC of >4 mg/L, meaning no activity was observed. This was different to what was proposed in the initial paper which suggested that this compound possessed an MIC of 1.6 mg/L. Some fluorinated derivatives (**17h**, **17i** and **17j**) of this compound were synthesised, and all possessed an MIC value of 4 mg/L, which does show some moderate activity and suggests that the aryl ring needs to be fluorinated for activity. Furthermore, **17k** showed that the removal of the methyl from the amine, producing a secondary amide rather than a tertiary amide, resulting in a loss of activity (MIC >4 mg/L), when compared with the methylated derivative (**17j**) (MIC 4mg/L).

An initial phenoxyaniline **17b** was synthesised due to availability of the compound and wanting to see if a larger group was potentially tolerated. Initial MIC testing values for this compound, showed a good value of 0.5 mg/L and thus fluoro (**17c**) and chloro phenoxyaniline (**17d** and **17e**) derivatives were also synthesised. These compounds showed a lack of activity in the assay and lead to the re-testing of the initial phenoxyaniline, which came back this time inactive and was more in line with the other results for the phenoxyaniline derivatives we observed.

Compound **17f** was also synthesised at the same time. The rationale behind this was to provide a molecule with a similar shape to the phenoxyaniline (**17b**) which was initially thought to be active. This allowed reduction of the high lipophilicity of the extra benzene ring and introduced some more sp³ centres, which are thought to lead to a more ‘drug-like’ compound. This gave an activity value of 4 mg/L; whilst this may not be a potent compound, it does show some activity has been established.

It was also desirable to introduce solubilising groups into the scaffold to improve the compounds aqueous solubility and also to increase the number of sp³ centres, something which had previously give a minor improvement in activity with **17f**. This was done via the introduction of a 4-fluoropiperidine group (**17g**), this however resulted in no observable activity.

8.2.1.3 DMPK

8.2.1.3.1 Predicted DMPK

Table 8.6. Predicted DMPK data for the benzisothiazolinone amide derivatives show poor properties overall. Values are colour coded with a traffic light system according to how good or bad a particular value is. Green – good, amber – acceptable/medium, red – poor.

	Log D _{7.4}	CLogP	Aqueous Solubility (μM)	Human Mics CLint (μl/min/mg)	Rat Heps CLint (μl/min/mg)	MPO
17a	2.31	2.73	266.4	67.4	136.8	5.6
17b	4.02	4.55	5.9	67.1	213.6	4.0
17c	4.09	4.69	6.6	64.9	187.5	3.9
17d	4.67	5.26	1.6	55.7	150.6	3.5
17e	4.31	5.26	4.8	79.4	157.1	3.5
17f	3.02	3.88	40.7	57.0	127.6	4.0
17g	1.44	1.63	4558	47.8	45.6	6.0

Predicted DMPK data was obtained for these compounds (Table 8.6). The initial hit (**17a**), which was described as active in the literature, showed good Log D and aqueous solubility, which was an improvement over the benzimidazole class. However metabolic clearance was high, in particular in the rat hepatocytes, where the compound is extensively metabolised. Derivatives containing a phenoxyaniline side chain **17b-e**, showed high Log D, poor solubility and very high metabolic clearance rates. The benzyl piperidine derivative (**17f**) showed a modest improvement in solubility, but again suffered from poor metabolic clearance. Finally, the 4-fluoropiperidine derivative (**17g**) showed excellent aqueous solubility with a value of 4558 μM and acceptable metabolic clearance values.

Stardrop predictions have also been analysed and indicate the main CYP450 isoforms involved in metabolism are 3A4 and 2C9. For the *N*-benzylmethylamine derivative **17a**, there is extensive oxidation on the unsubstituted benzene ring and methyl group of the amide. Interestingly, the

nitrogen and sulphur atoms have also been indicated, but do exhibit reduced metabolism. The phenoxyaniline derivative (**17b**) shows less metabolism across the molecule, but much more extensive metabolism on the substituted aryl ring, which accounts for the high predicted metabolism for this derivative.³⁹

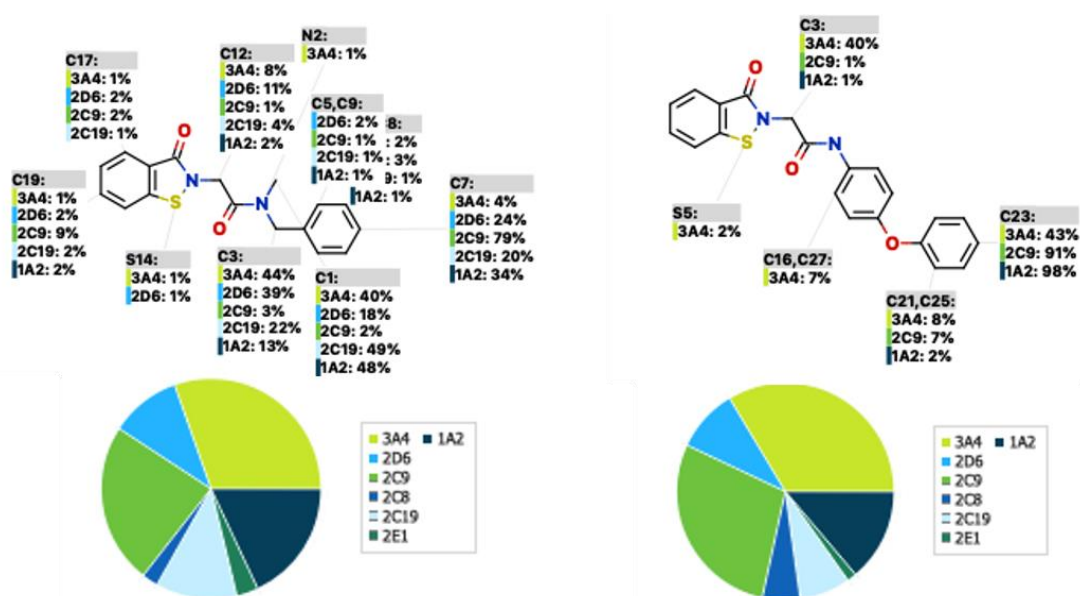


Figure 8.13. Metabolism predictions for four compounds from the BIZT amide series. Calculations run on Stardrop.

8.2.1.3.2 Measured DMPK

Table 8.7. Measured DMPK data for the benzisothiazolinone amide class of compounds show good to acceptable metabolic properties overall, but poor solubility. Values are colour coded with a traffic light system according to how good or bad a particular value is. Green – good, amber – acceptable/medium, red – poor. *could not detect after second-time point.

Compound	LogD _{7.4}	Aqueous Solubility (μM)	Human Mics CLint (μl/min/mg)	Rat Heps CLint (μl/min/mg)
17a	2.2	1000	81.5	No Value*
17b	>4.4	<0.90	No value*	No value*
17d	3.5	0.3	No value*	>300
17h	2.4	687	66.5	No value*
17i	2.4	909	53.2	No value*

The measured DMPK results (Table 8.7) showed good agreement with the predictive DMPK data. However, the measured metabolic values were even poorer than that predicted, whereby the majority of the compounds couldn't be measured due to such rapid metabolism and they couldn't be detected at a second-time point. In some examples one clearance value was obtained, but the other not, indicating this class may possess issues with metabolic clearance, which does not make for an ideal future drug candidate.

Amide metabolism was thought to be one possible route.⁴⁰ Amides can be hydrolysed, however this process is generally very slow. Oxidative α -hydroxylation is instead a possibility and this could occur via hydroxylation of the C-H bond, as indicated by the Stardrop predictions. Metabolic oxidation of the phenoxyaniline scaffold has been reported in the literature through the analysis of Polybrominated diphenyl ethers (PDBE), whereby brominated and mono and poly chlorinated compounds showed oxidation via CYP450 2B6, which also causes oxidation of around 10% of all drugs including efavirenz and artemisinin.^{41, 42} This explains the poor metabolic stability of the derivatives containing phenoxyaniline groups (**17b-e**).

As mentioned in the introductory section discussing BIZT metabolism in Section 8.1.5, the N-S bond is thought to be the major route of metabolism. This is due to oxidation of the sulphur to the sulfoxide and sulphone resulting in cleavage of this bond to generate the ring opened compound. It is already evidenced in the literature that ring open compounds possess no biological activity. This can be observed for the original hit compound (**17a**), which reportedly possessed an MIC = 1.6 mg/L, whereas the ring opened derivative (**22**) possessed no biological activity (Figure 8.14). This is important because the N-S bond seems to be integral to the biological activity of these compounds, but also appears to be a metabolic weakness, which may prevent the compounds from reaching biological relevant concentrations.

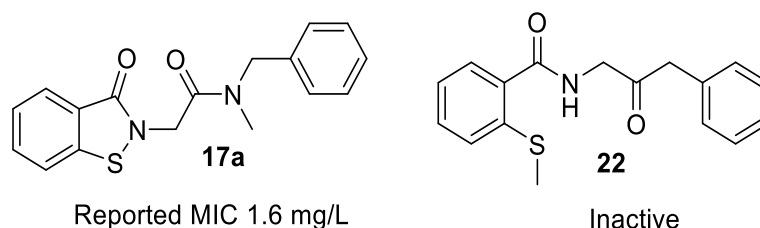


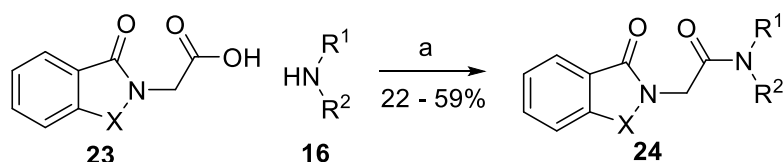
Figure 8.14. The hit compound **17a** was reported to possess a MIC = 1.6 mg/L, but the open chain version (**22**) shows no antifungal activity.

Owing to the lack of stability of these types of compounds, it was decided that no more of these amide derivatives should be made until investigation of core and amide modification allowed for an improvement in activity, metabolic stability or ideally both.

8.2.2 BIZT Core Alternatives

8.2.2.1 Synthesis

Removal of the sulphur from the BIZT core was studied for two reasons. Firstly, removing the sulphur can help elucidate whether the sulphur atom is essential to the mechanism of action. Secondly, DMPK testing of sulphur containing BIZT compounds has shown that they are metabolically unstable. Removal of the sulphur, which is thought to be the metabolic weak point, may increase this stability, leading to a compound with improved drug-like characteristics.



Scheme 8.6. Reagents and conditions: (a) amine (1.0 eq.), EDC.HCl (1.2 eq.), pyridine (4.0 eq.), DMF, room temperature, overnight (7 – 25% yield).

Table 8.8. Percentage yields obtained for all compounds created within the BIZT core alternatives template.

Compound	R ¹	R ²	X	Step A % yield
24a	Me	C ₆ H ₅	C=O	34
24b	H	4-phenoxyaniline	C=O	59
24c	H	4-(4-chlorophenoxy)aniline	C=O	44
24d		4-fluoropiperidine	C=O	29
24e		morpholine	C=O	22
24f	Me	C ₆ H ₅	CH ₂	44
24g	H	4-phenoxyaniline	CH ₂	43
24h	H	4-(4-chlorophenoxy)aniline	CH ₂	27
24i		morpholine	CH ₂	44

Synthesis was carried out via a one-step procedure due to the starting acids (**23**) being both commercially available and inexpensive. The C=O core replacement was characterised by the presence of a carbonyl peak at 168 ppm, and the highly symmetrical nature of the phthalimide core giving rise to only two doublet of doublets in the aromatic region of the ¹H NMR, rather than the 4 individual aromatic peaks observed with the other cores. Simplistically we would expect just two doublets in the aromatic region, however the apparent doublet of doublet is commonly reported for phthalimides, due to second order NMR effects (Figure 8.15) (See Appendix, Figures 6C&6D).⁴³⁻⁴⁵

For the CH₂ replacement on the core, this was easily identified by the presence an additional CH₂ peak at around 4.4 ppm in the ¹H NMR spectrum and in the ¹³C NMR spectrum there is an additional aliphatic peak at around 50 ppm, signifying the desired product (See Appendix, Figures 6E&6F).

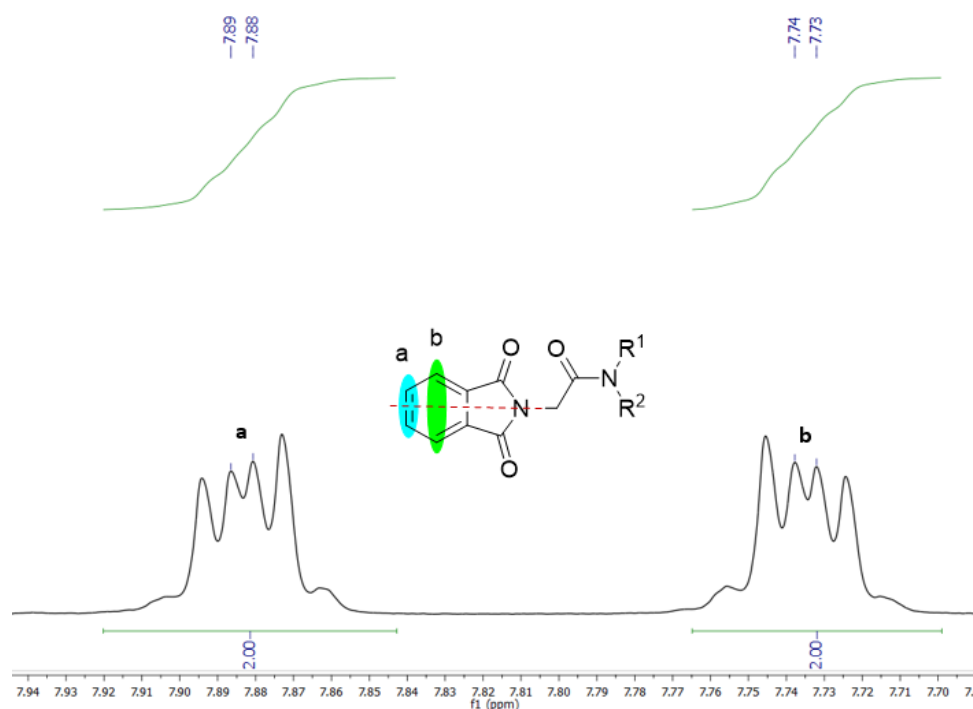


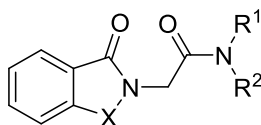
Figure 8.15. The ^1H NMR spectra for the phthalimide core shows unexpected coupling patterns due to second order effects and can be used to identify whether the final compound has been obtained.

Yields of under 50% were observed for these reactions, which can be explained in a few ways. Often, there was incomplete conversion of the starting carboxylic acid to the amide, as detected via TLC. Secondly, the amines being used all had reduced nucleophilicity to react with the EDC activated carboxylic acid. For the addition of the phenoxyanilines, the NH_2 will be able to delocalise its lone pair of electron into the benzene ring, so may not be as nucleophilic. For the morpholine and *N*-benzylmethylamine compounds, a secondary amine is being used, which often results in reduced yields for amide couplings predominantly due to steric effects.⁴⁶ Furthermore, for the morpholine derivatives a large increase in polarity was observed. This made these compounds more difficult to purify via column chromatography. Instead for a lot of these compounds, trituration with diethyl ether was used instead, however this meant a sacrifice in yield, to gain improved purity.

8.2.2.2 Biological Activity

A number of different analogues were synthesised, mimicking those that had been produced as part of the previous template. For these compounds no activity was observed, even when the counterpart BIZT core analogue did give some activity (Table 8.9). The rationale for this observation is that the alternative cores no longer have the N-S bond, which suggests that this bond is essential for interaction with the target. The typical bond dissociation energy for a N-S bond is $469 \pm 24 \text{ kJ mol}^{-1}$, which is significantly lower than the reported C-N bond dissociation energy of $750 \pm 2.9 \text{ kJ mol}^{-1}$. Due to the higher bond dissociation energy of the C-N bond, is unlikely to ring open, unless subjected to much more forcing conditions and thus no interaction with a target within *C. neoformans*.^{47, 48}

Table 8.9. Substitution of the N-S bond for a C-N bond results in a complete loss of activity. **Green** – good - 0.015 – 0.25 mg/L, **yellow** – acceptable - 0.5 – 4 mg/L, **red** – poor - >4 mg/L.



Compound	R ¹	R ²	X	<i>C. neoformans</i> MIC (mg/L)
24a	Me	C ₆ H ₅	C=O	>4
24b	H	4-phenoxyaniline	C=O	>4
24c	H	4-(4-chlorophenoxy)aniline	C=O	>4
24d		4-fluoropiperidine	C=O	>4
24e		morpholine	C=O	>4
24f	Me	C ₆ H ₅	CH ₂	>4
24g	H	4-phenoxyaniline	CH ₂	>4
24h	H	4-(4-chlorophenoxy)aniline	CH ₂	>4
24i		morpholine	CH ₂	>4

8.2.2.3 DMPK

8.2.2.3.1 Predicted DMPK

Table 8.10. Predicted DMPK data for the BIZT core alternative class of compounds show good metabolic properties overall, but poor solubility and Log D values. Values are colour coded with a traffic light system according to how good or bad a particular value is. **Green** – good, **amber** – acceptable/medium, **red** – poor.

	LogD _{7.4}	ClogP	Aqueous Solubility (μM)	Human Mics CLint (μl/min/mg)	Rat Heps CLint (μl/min/mg)	MPO
24a	1.95	2.55	13.3	24.4	39.9	5.6
24b	3.62	4.37	0.35	25.5	65.5	4.3
24c	4.18	5.08	0.07	21.4	50.5	3.5
24d	1.09	0.97	119.7	15.3	13.3	6.0
24e	0.45	1.45	303.3	5.32	7.77	6.0
24f	2.12	2.32	239.1	22.1	35.2	5.7
24g	3.61	4.15	4.10	23.7	53.4	4.4
24h	4.20	4.86	1.11	19.1	41.8	3.7
24i	0.62	0.74	7230	4.9	6.1	6.0

These compounds showed greatly improved DMPK properties, when compared with the previous sulphur based compounds (Table 8.10). Metabolism for these compounds was generally very good with some of the compounds showing slightly high hepatic clearance, which is mostly likely due to CH₂ groups, which can be easily metabolised and in the case of compounds **24b**, **24c**, **24g** and **24h** the presence of phenoxyaniline derivatives results in more metabolism.^{41, 42} However, with these values being reduced, it does suggest that the predictive screen may be identifying some sulphur oxidation, which is why the BIZT core thiols have poor values. Overall Log D is good for these compounds, with

compounds containing the phenoxylaniline moiety driving the lipophilicity and thus Log D higher, but all other compounds fall within an acceptable range. Solubility is mixed, with derivatives containing *N*-Benzylmethylamine, morpholine and 4-fluoropiperidine groups showing excellent solubility (**24a**, **24d-f** and **24i**). The derivatives containing phenoxyaniline groups (**24b**, **24c**, **24g** and **24h**) show poor aqueous solubility, due to the lipophilic nature of the multiple aryl rings.

Stardrop predictions (Figure 8.16) indicated a number of sites for metabolism, with CYP3A4, 2C9 and 2C19 being indicated as the biggest metabolising isoforms. The sites for metabolism are indicated as the *N*-benzylmethylamine group, both on the aryl ring and the CH₂ and methyl groups. The phthalimide derivative has greater metabolism indicated on the core aryl ring than CH₂ derivative, which shows metabolism at the core CH₂ group instead.

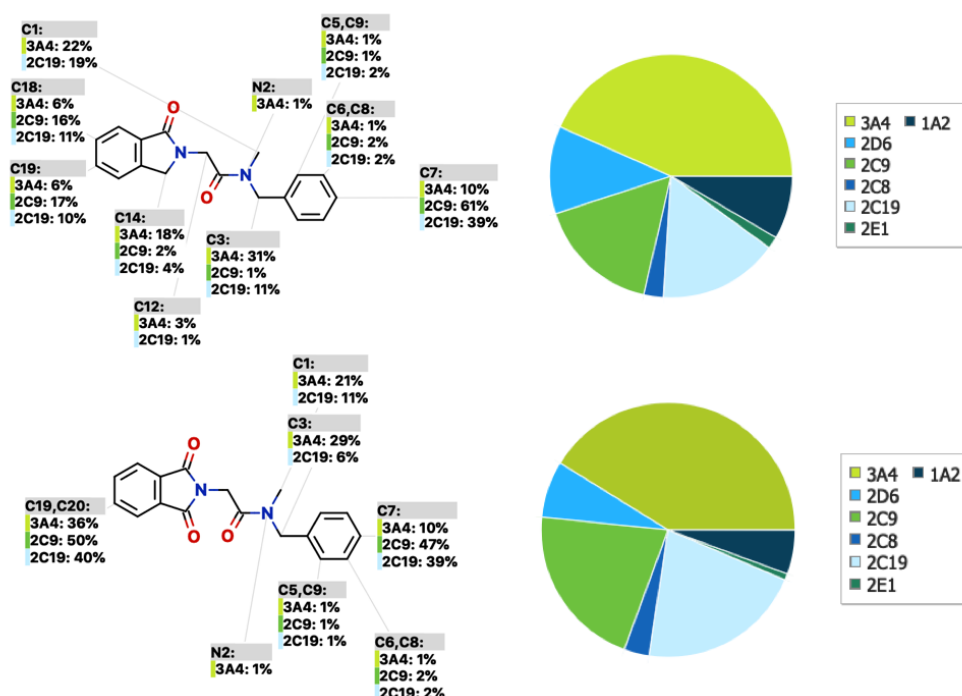


Figure 8.16. Metabolism predictions for two compounds from the BIZT alternative core series. Calculations run on Stardrop.

8.2.2.3.2 Measured DMPK

Measured DMPK for these compounds shows a significant improvement on that of the BIZT core, and is comparable if not better than the predicted data (Table 8.10 versus Table 8.11). Only two compounds (**24a** and **24d**) have been submitted for measured DMPK testing due to possessing poor MIC results (MIC >4 mg/L). We can see for both compounds **24a** and **24d** that their overall profiles are excellent. Metabolic clearance values are as expected, proving to be significantly better than the N-S analogues. This confirms the theory that the N-S bond is crucial to the metabolism of this template and its poor clearance values.

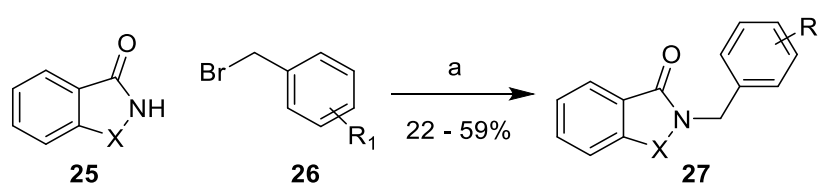
Table 8.11. Predicted DMPK data for the BIZT core alternative class of compounds show good metabolic properties overall, but poor solubility and Log D values. Values are colour coded with a traffic light system according to how good or bad a particular value is. **Green** – good, **amber** – acceptable/medium, **red** – poor.

Compound	LogD _{7.4}	Aqueous Solubility (μM)	Human Mics CLint (μl/min/mg)	Rat Heps CLint (μl/min/1mg)
24a	2.1	106	7	42
24d	1	577	3	13

8.2.3 Benzyl BIZT Core Derivatives

It was identified in the Stardrop metabolism predictions that the amide group of the benzisothiazolinone amide series (**17**) could also be metabolised. Investigation of this was carried out via direct *N*-alkylation of the BIZT core. Synthesis of these compounds allowed for understanding of SAR. Furthermore, removal of the amide could indicate whether this is the main site of metabolism or the N-S bond.

8.2.3.1 Synthesis



Scheme 8.7. Reagents and conditions: (a) benzyl bromide (1.0 eq.), Potassium Carbonate (2.5 eq.), THF, **27a-i** room temperature, **27j** reflux, Overnight, 22 – 59% yield;

Table 8.12. Percentage yields obtained for all compounds created within the BIZT benzyl template.

Compound	R ¹	X	Step A % yield
27a	H	S	34
27b	4-F	S	59
27c	3-F	S	59
27d	2-F	S	25
27e	4-Cl	S	47
27f	4-CF ₃	S	22
27g	3-OMe	S	34
27h	4-Br	S	56
27i	4-COOMe	S	41
27j	4-F	SO ₂	50

This was carried out by stirring 1,2-benzisothiazol-3(2H)-one with potassium carbonate and the desired benzyl bromide at room temperature. This allowed for the alkylation reaction to occur and a number of compounds to be generated, typically as yellow solids and in moderate yields (Table 8.12).⁴⁹ This is characterised by the appearance of a CH₂ peak at around 5 ppm and additional aromatic

protons as well as a carbon peak at around 40 – 55 ppm. There was an ease of purification for these reactions, with the only spots being visible the two starting materials and the product. The variation in the reactions yields was rationalised to be due to the reactivity of NH of the BITZ core. Whilst having an acidic proton, the lone pair of the nitrogen after deprotonation can be delocalised into the carbonyl of the core, rendering the nitrogen less available for the *N*-alkylation reaction (Figure 8.17).⁵⁻⁸

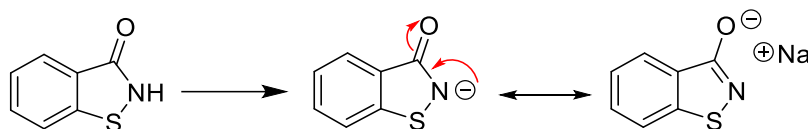


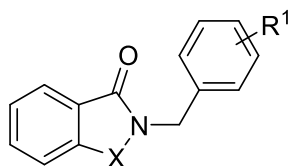
Figure 8.17. The BITZ core could potential undergo delocalisation of its charged amine into the carbonyl, resulting in tautomers, resulting in a lower yielding *N*-alkylation.

Compound **27j**, whereby the sulphur of the core has been replaced with a sulphone group, proved much more difficult to synthesise. Several attempts at synthesising compounds eventually resulted in refluxing the reaction in order for conversion to the product to occur, which eventually generated the desired compound in a moderate yield of 50%. This may be due to the further ability of the deprotonated nitrogen to delocalise its negative charge into the sulphone groups, making the negative charge less available for the *N*-alkylation reaction (See Appendix, Figure 6G&6H).

8.2.3.2 Biological Activity

The benzyl derivatives were synthesised in order to remove the amide, previously seen in the other templates, to rule this bond out as a metabolic issue, whilst still retaining the N-S bond, which is thought to be essential for activity. In total, ten compounds were synthesised, most of which provided improved activity versus the previous BITZ sub-templates, though still possessed insufficient activity when compared with the benzimidazoles.

Table 8.13. MIC data for the benzisothiazolinone benzyl derivatives showed improved MIC data when compared with other BIZT derivatives. **Green** – good - 0.015 – 0.25 mg/L, **yellow** – acceptable - 0.5 – 4 mg/L, **red** – poor - >4 mg/L.



Compound	R ¹	X	<i>C. neoformans</i> MIC (mg/L)
a	H	S	2
b	4-F	S	2
c	3-F	S	2
d	2-F	S	2
e	4-Cl	S	2
f	4-CF ₃	S	4
g	3-OMe	S	4
h	4-Br	S	2
i	4-COOMe	S	2
j	4-F	SO ₂	>4

The SAR for these compounds is relatively flat. With a variety of groups, both electron donating and withdrawing in nature being tolerated and only 3-CF₃ (**27f**) and 3-OMe (**27g**) showing poor activity. One compound was made, whereby the sulphur of the core was replaced with a sulphone (**27j**), as observed in the molecule saccharin and this showed no activity, despite the sulphur analogue (**27i**) showing an MIC value of 2 mg/L.

8.2.3.3 DMPK

8.2.3.3.1 Predicted DMPK

Predicted DMPK measurements were obtained (Table 8.14) and showed that this class of compound suffered similar issues with metabolism and the original BIZT core amide template, with both microsomal and hepatic metabolism being slightly high. The lack of amide and phenoxyaniline groups did help to reduce the metabolism and activity is generally better for this class, making them a more promising candidate. Log D and aqueous solubility overall are good with only a few analogues (**27e**, **27f** and **27h**) showing poor aqueous solubility, due to the additional of more lipophilic halogen based groups such as Cl, Br and CF₃.

Table 8.14. Predicted DMPK data for the BIZT benzyl class of compounds show good metabolic properties overall, but poor solubility and Log D values. Values are colour coded with a traffic light system according to how good or bad a particular value is. **Green** – good, **amber** – acceptable/medium, **red** – poor.

	LogD _{7.4}	CLogP	Aqueous Solubility (μM)	Human Mics CLint (μl/min/mg)	Rat Heps CLint (μl/min/mg)	MPO
27a	2.89	2.90	61.3	48.9	81.0	4.4
27b	2.98	3.05	68.8	44.3	71.2	4.4
27c	2.99	3.05	123.6	40.1	88.2	4.4
27d	2.98	3.05	66.2	51.2	105.7	4.4
27e	3.57	3.62	18.9	53.8	67.1	3.8
27f	3.68	3.79	16.5	36.1	46.1	3.6
27g	2.82	2.82	97.2	68.5	125.9	4.9
27h	3.60	3.77	5.1	58.8	132.0	3.8
27i	3.01	2.87	64.1	93.4	140.9	5.5
27j	1.82	2.46	23.1	31.5	78.5	6.0

Stardrop predictions were also obtained. For this class, no metabolism was indicated on the sulphur atom of the core and no N-S bond cleavage was identified. CYP3A4 is indicated as being a major metaboliser, particularly on the aromatic ring. For the sulphur derivative **27b**, CYP1A2 and 2C9 are indicated in metabolism of the aryl rings. For the saccharin derivative **27i**, CYP2C9 and CYP2C19 appear to be the major isoforms, particularly on the aryl ring.

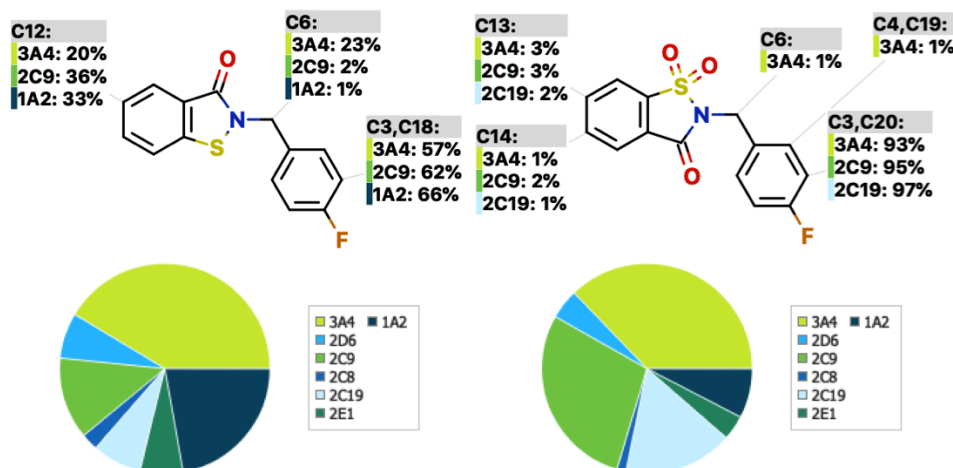


Figure 8.18. Metabolism predictions for two compounds from the BIZT benzyl series. Calculations run on Stardrop.

8.2.2.3.2 Measured DMPK

Measured DMPK data was obtained for three compounds. They possess moderate Log D and good aqueous solubility values. Human microsomal clearance is good, however rat hepatic clearance data is very high, with compound **27a** not detectable after the second time point, due to such extensive metabolism, and compounds **27b** and **27c** showing poor values of >300 μl/min/mg. This further validates the N-S bond being the major site of metabolism, and not the amide from compound **17a**,

which was also predicted to undergo metabolism. This presents a problem given the extensive metabolism, as it is highly likely that not enough drug will remain intact to achieve biologically relevant concentrations.

Table 8.15. Predicted DMPK data for the BIZT benzyl class of compounds show good metabolic properties overall, but poor solubility and Log D values. Values are colour coded with a traffic light system according to how good or bad a particular value is. **Green** – good, **amber** – acceptable/medium, **red** – poor. *could not detect after second time -point.

Compound	LogD _{7.4}	Aqueous Solubility (μM)	Human Mics CLint (μl/min/mg)	Rat Heps CLint (μl/min/mg)
27a	3.5	357	36.9	No Value*
27b	3.2	325	33.9	>300
27c	3.2	85	21.7	>300

8.3 Conclusion

A number of BIZT core analogues were made during this project, however biological activity and DMPK properties were not suitable for continuing forward. Compounds containing the BIZT scaffold showed poor activity when compared with the literature and metabolically were very unstable, with some analogues too unstable to determine measured values.

Replacement of the BIZT core with CH₂ and C=O alternatives, were easily synthesised from commercially available starting materials in moderate yields. They showed a great improvement in metabolic stability, but unfortunately they were completely inactive against *C. neoformans*, but could prove to be promising drug candidates for another disease. This also highlighted the need for the N-S bond, as it seems this is involved in the mechanism of action. It appears that the metabolic weak point of the structure is the component essential for activity (Figure 8.19).

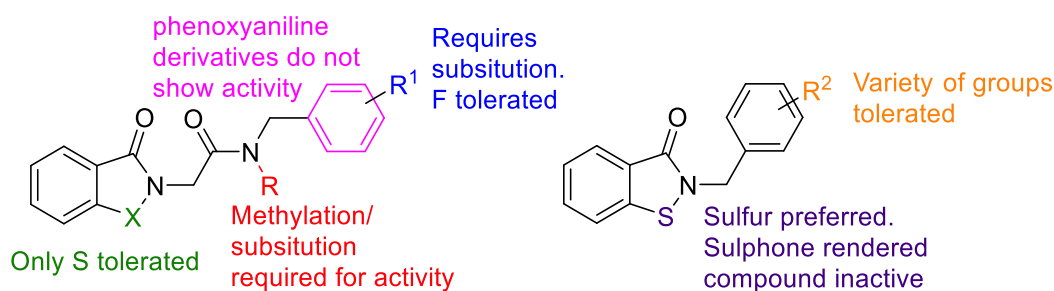


Figure 8.19. An overall SAR conclusion.

8.4 Future Work

Whilst synthetically we don't wish to continue with this project, there is still biological investigation that needs to be carried out. Given that one of the mechanisms of action reported in literature is mitochondrial based, work is currently on going to devise an assay to test whether this is a likely mechanism of action. This is done by investigating the growth of the fungus in different carbon sources. Dextrose is a fermentable carbon source, whereas glycerol is not. If the BIZT core inhibits mitochondrial function, then if the fungus was grown in the two media, it would grow in the dextrose solution but not in the glycerol, as it is not fermentable. A procedure similar to the MIC method is used to determine the growth.⁵⁰

8.5 Experimental

8.5.1 General Experimental Details

For general experimental details please see Section 3.5.1, Chapter 3. 2-(chlorocarbonyl)phenyl hypochlorothioite obtained pure from Matthew Pye.

8.5.1.1 NMR

^1H and ^{13}C NMR assignment of amide isomers give as; isomer 1 – I1, isomer 2 – I2, mixed isomers – I1&2. For splitting, app. means apparent splitting from the NMR spectra but it should show something different in theory.

8.5.1.2 HPLC

Flow rate 1 ml/min for 15 minutes using MeCN/Water with compounds dissolved in methanol. UV detector recorded signals at 254 nm. Method A: min, gradient: 2% MeCN hold to 1 min, 2-98% MeCN in 11 min, then hold at 98% MeCN to 15 min.

8.5.2 General Procedures

General Procedure A – Amide coupling conditions for final products

To a flask at room temperature was added 2-(3-oxobenzod[*d*]isothiazol-2(3*H*)-yl)acetic acid (1.0 eq.), DMF (5 ml) EDC.HCl (1.2 eq.) and pyridine (2.0 eq.). The flask was left to stir for 15 minutes followed by the addition of the desired amine (1.0 eq.) and further pyridine (2.0 eq.) and the reaction stirred overnight at room temperature. The reaction was then diluted with ethyl acetate (30 ml), acidified with 1 M HCl (20 ml), basified with 1 M NaOH (20 ml), washed with water, brine, dried over magnesium sulphate and concentrated to yield the crude product, which was purified via column chromatography eluting with 20% ethyl acetate in hexane to afford the desired compound.

General Procedure B - Synthesis of *Tert*-butyl (2-oxoethyl)carbamate derivatives via amide

To a flask at room temperature was added (*tert*-butoxycarbonyl)glycine (1.0 eq.), DMF (10 ml), pyridine (2.0 eq.), EDC.HCl (2 eq.) and the reaction stirred at room temperature for 15 minutes. Desired amine (1 eq.) and further pyridine (2.0 eq.) were added and the reaction stirred overnight at room temperature. The reaction was then diluted with ethyl acetate, acidified with 1 M HCl, basified with 1 M NaOH, washed with water, brine, dried over magnesium sulphate and concentrated. The reaction was then purified via column chromatography eluting with 20% ethyl acetate in hexane to give the product. (35% - 82% yield).

General Procedure C – Trifluoroacetic acid deprotection

To a flask at room temperature was added the desired *tert*-butyl (2-oxoethyl)carbamate derivative (1.0 eq.) and DCM and TFA as a 3:7 mixture and was then reacted overnight at room temperature. The reaction was then concentrated to yield the product (99% yield).

General Procedure D – BIZT core ring closure

To a flask at room temperature was added 2-(chlorocarbonyl)phenyl hypochlorothioite (1.2 eq.), DCM, the desired 2-amino-*N*-acetamide analogue (1.0 eq.) and triethylamine (1.0 eq.) and the reaction stirred at room temperature overnight. The reaction was then diluted with ethyl acetate, washed with water, NaHCO₃, brine, dried over magnesium sulphate and concentrated. The reaction was then purified via column chromatography eluting with 20% ethyl acetate in hexane to give the product.

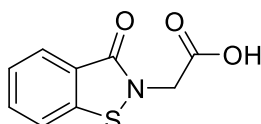
General Procedure E – Amide coupling to give 2-(1isoindolin-2-yl)acetamide Derivatives

To a flask at room temperature was added 2-(1-oxoisindolin-2-yl)acetic acid derivative (1.0 eq.), DMF, EDC.HCl (1.5 eq.), pyridine (2.5 eq.), and the desired amine (1.0 eq.) and the reaction stirred at room temperature overnight. The reaction was then diluted with ethyl acetate, acidified with 1M HCl, basified 1M NaOH, washed with water, brine, dried over magnesium sulphate, concentrated and purified by trituration with ethyl acetate or column chromatography to give the final product.

General Procedure F – Alkylation of the BIZT core using benzyl bromides

To a flask at room temperature was added benzo[*d*]isothiazol-3(2*H*)-one (1eq.), THF, potassium carbonate (2.5 eq.) and the desired benzyl bromide (2.0 eq.), and the reaction stirred at room temperature overnight. The reaction was then concentrated, diluted with ethyl acetate, washed with a saturated NaHCO₃ solution, water, brine, dried over magnesium sulphate, concentrated and purified via column chromatography eluting with 12.5% ethyl acetate in *n*-hexane.

8.5.3 BZT Core Amides

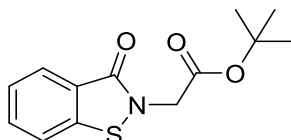
2-(3-Oxobenzo[*d*]isothiazol-2(3*H*)-yl)acetic acid (15)

To a flask was added 1,2-benzisothiazol-3(2*H*)-one (1.0 eq.) in THF (15 ml) and sodium hydride (1.2 eq.) was added portion-wise and the reaction stirred at 0 °C for 15 minutes. The solvent was then removed and 2,2,2-trifluoroethanol added at 0 °C, along with *tert*-butylbromoacetate (1.0 eq.) and

the reaction refluxed for 1 hour. The solvent was then removed and the reaction diluted with ethyl acetate, acidified with 1 M HCl, basified with 1 M NaOH, washed with brine, dried over magnesium sulphate and concentrated to give the crude material as a pink solid. On one occasion this intermediate was also purified and tested. Data given below as compound **14**.

To the solid was added dichloromethane (10 ml) and trifluoroacetic acid (20 ml) and the reaction stirred overnight at room temperature. The reaction was then evaporated to dryness and washed with ethyl acetate (3 x 20 ml), to give the title compound (**15**) (3.58 g, 52% yield) as a white solid. ^1H NMR (400 MHz, CDCl_3) δ 13.06 (bs, 1H), 7.99 (d, 1H, $J = 8.0$ Hz), 7.89 (d, 1H, $J = 8.0$ Hz), 7.71 (t, 1H, $J = 7.4$ Hz), 7.45 (t, 1H, $J = 7.4$ Hz), 4.59 (s, 2H). ^{13}C NMR (100 MHz, CDCl_3) δ 169.8, 165.4, 141.8, 132.5, 126.12, 125.9, 122.8, 122.3, 44.7. HRMS (CI^+ , NH_3) Calculated for $\text{C}_9\text{H}_7\text{NO}_3\text{S}$: 164.0165. Found $[\text{M}+\text{H}]^+$: 164.0167 (Diff -1.67 ppm).

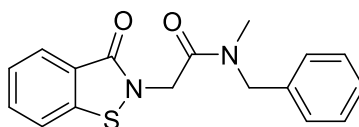
Tert-butyl 2-(3-oxobenzo[d]isothiazol-2(3H)-yl)acetate (14)



^1H NMR (400 MHz, CDCl_3) δ 8.05 (d, 1H, $J = 8.1$ Hz), 7.62 (dd, 1H, $J = 8.2$ & 7.0 Hz), 7.55 (d, 1H, $J = 8.2$ Hz), 7.40 (dd, 1H, $J = 8.1$ & 7.0 Hz), 4.51 (s, 2H), 1.49 (s, 9H). ^{13}C NMR (100 MHz, CDCl_3) δ 166.7, 165.8, 140.9, 132.2, 126.9, 125.5, 123.6, 120.3, 83.0, 45.3, 28.0. HRMS (ES^+) Calculated for $\text{C}_{13}\text{H}_{15}\text{NO}_3\text{NaS}$: 288.0670. Found $[\text{M}+\text{H}]^+$: 288.0668 (Diff -1.67 ppm). $\nu_{\text{max}}/\text{cm}^{-1}$: (solid) 2998 (m), 2982 (m), 2935 (m), 1740 (s), 1660 (s), 1624 (s), 1459 (m), 1257 (m). MP: 68 - 70 °C Microanalysis: Calculated C(58.85%), H(5.70%); N(5.28%), Obtained C(58.69%), H(5.64%), N(5.15%).

8.5.3.1 2-(3-oxobenzo[d]isothiazol-2(3H)-yl)acetamide Derivatives

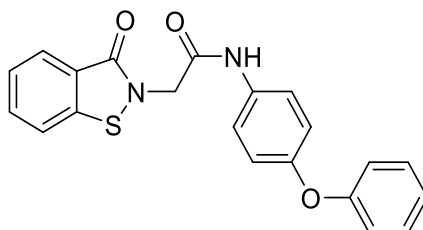
N-benzyl-N-methyl-2-(3-oxobenzo[d]isothiazol-2(3H)-yl)acetamide (17a)



General Procedure A - Employed *N*-benzylmethylamine to obtain the title compound (**17a**) (0.051 g, 17% yield) as yellow oil and as a mixture of two isomers 1:0.65. ^1H NMR (400 MHz, CDCl_3) δ 8.03 (l1, d, 1H, $J = 7.92$ Hz), 7.99 (l2, 1H, $J = 7.92$ Hz), 7.59 – 7.56 (l1&2, m, 2H), 7.37 – 7.31 (l1&2, m, 6H), 4.76 (l1, s, 2H), 4.73 (l2, s, 2H), 4.67 (l2, s, 2H), 4.62 (l1, s, 1H), 3.02 (l1, s, 3H), 3.01 (l2, s, 3H). ^{13}C NMR (100 MHz, CDCl_3) δ 167.1 (l2), 166.6 (l1), 166.0 (l2), 165.8 (l1), 141.5 (l2), 136.5 (l1), 135.7 (l2), 132.1 (l1), 132.0 (l2), 129.1 (l2), 128.7 (l1), 128.3 (l1), 127.9 (l2), 127.1 (l1), 126.8 (l1), 126.74 (l2), 126.3 (l1&2), 125.4 (l2), 123.5 (l1), 123.4 (l2), 120.3 (l1), 120.3 (l1), 53.1 (l2), 51.4 (l1), 45.0 (l1), 44.9 (l2), 34.5 (l2),

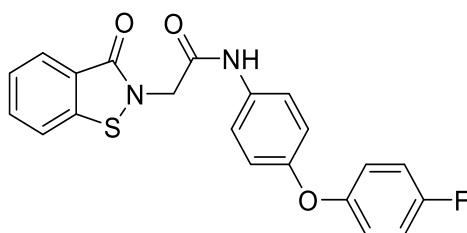
34.1 (I1). HRMS (ES+) Calculated for $C_{17}H_{16}N_2O_2S$: 335.0830. Found $[M+Na]^+$: 335.0827 (Diff – 0.90 ppm). MP: 151–153 °C. Purity HPLC (Method A) 97.7%, R_t = 8.58 min.

2-(3-Oxobenzo[d]isothiazol-2(3H)-yl)-N-(4-phenoxyphenyl)acetamide (17b)

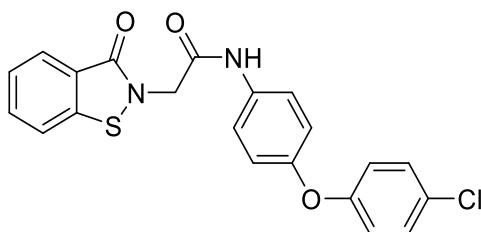


General Procedure A - Employed 4-phenoxyaniline to obtain the title compound (**17b**) (0.059 g, 15% yield) as a white solid. 1H NMR (400 MHz, DMSO) δ 10.35 (s, 1H), 7.98 (d, 1H, J = 8.1 Hz), 7.89 (d, 1H, J = 7.8 Hz), 7.71 (t, 1H, H = 7.1 Hz), 7.60 (d, 2H J = 8.1 Hz), 7.45 (t, 1H, J = 7.8 Hz), 7.37 (t, 2H, J = 7.5 Hz), 7.10 (t, 1H, J = 7.5 Hz), 7.00 – 6.96 (m, 4H), 4.67 (s, 2H). HRMS (ES+) Calculated for $C_{21}H_{16}N_2O_3S^{23}Na$: 399.0779. Found $[M+Na]^+$: 399.0768 (Diff -2.76 ppm). ν_{max}/cm^{-1} : (solid) 3657 (s), 3065 (m), 2980 (m), 1686 (s), 1661 (m), 1504 (m), 1445 (m), 1288 (m). MP: 175 – 178 °C. Purity HPLC (Method A) 95.3%, R_t = 10.04 min.

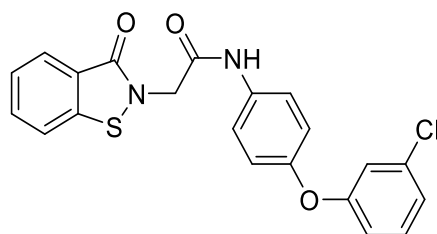
N-(4-(4-Fluorophenoxy)phenyl)-2-(3-oxobenzo[d]isothiazol-2(3H)-yl)acetamide (17c)



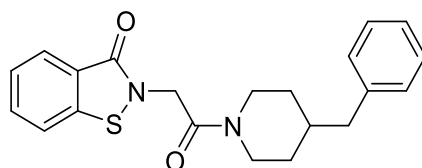
General Procedure A - Employed 4-(4-fluorophenoxy)aniline to obtain the title compound (**17c**) (0.075 g, 13% yield) as a white solid. 1H NMR (400 MHz, $CDCl_3$) δ 8.76 (s, 1H), 8.05 (d, 1H, J = 7.9 Hz), 7.70 – 7.68 (m, 1H), 7.65 (d, 1H, J = 8.1 Hz), 7.49 – 7.45 (m, 3H), 7.03 – 7.00 (m, 2H), 6.96 – 6.91 (m, 4H), 4.63 (s, 2H). ^{13}C NMR (100 MHz, $CDCl_3$) δ 166.5, 165.1, 154.2, 141.1, 132.8, 132.7, 126.8, 126.0, 123.2, 121.8, 120.5, 120.1, 120.0, 119.0, 116.4, 116.1, 49.2. HRMS (ES+) Calculated for $C_{21}H_{15}N_2O_3FS^{23}Na$: 417.0685. Found $[M+Na]^+$: 417.0673 (Diff – 2.88 ppm). ν_{max}/cm^{-1} : (solid) 3267 (m), 3076 (m), 2924 (m), 1686 (s), 1631 (d), 1495 (m), 1407 (m), 1290 (m). MP: 202–204 °C. Microanalysis: Calculated C(63.95%), H(3.83%), N(7.10%); Obtained C(64.17%), H(4.13%), N(6.79%).

***N*-(4-(4-Chlorophenoxy)phenyl)-2-(3-oxobenzo[*d*]isothiazol-2(3*H*)-yl)acetamide (17d)**

General Procedure A - Employed 4-(4-chlorophenoxy)aniline to obtain the title compound (**17d**) (0.043 g, 7% yield) as a white solid. ^1H NMR (400 MHz, CDCl_3) δ 8.79 (s, 1H), 8.08 (d, 1H, $J = 7.7$ Hz), 7.68 (dd, 1H, $J = 7.6$ & 7.9 Hz), 7.60 (d, 1H, $J = 7.6$ Hz), 7.49 (d, 2H, $J = 8.8$ Hz), 7.45 (dd, 1H, $J = 7.7$ & 7.9 Hz), 7.25 (d, 2H, $J = 8.8$ Hz), 6.93 (d, 2H, $J = 8.7$ Hz), 6.87 (d, 2H, $J = 8.7$ Hz), 4.63 (s, 2H). ^{13}C NMR (100 MHz, CDCl_3) δ 166.7, 166.5, 156.2, 153.3, 141.1, 133.2, 133.1, 132.7, 129.7, 128.1, 126.9, 126.0, 121.8, 120.5, 119.6, 49.3. Not all quaternary carbons visible. HRMS (ES+) Calculated for $\text{C}_{21}\text{H}_{15}\text{N}_2\text{O}_3\text{ClS}^{23}\text{Na}$: 433.0390. Found $[\text{M}+\text{Na}]^+$: 433.0377 (Diff -3.00 ppm). $\nu_{\text{max}}/\text{cm}^{-1}$: (solid) 3281 (m), 3063 (m), 2980 (m), 1694 (s), 1669 (m), 1485 (m), 1400 (m), 1266 (m). MP: 175-177 °C.

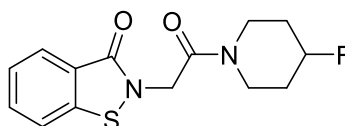
***N*-(4-(3-Chlorophenoxy)phenyl)-2-(3-oxobenzo[*d*]isothiazol-2(3*H*)-yl)acetamide (17e)**

General Procedure A - Employed 4-(3-chlorophenoxy)aniline to obtain the title compound (**17ec**) (0.14 g, 24% yield) as a white solid. ^1H NMR (400 MHz, CDCl_3) δ 8.99 (s, 1H), 8.06 (d, 1H, $J = 7.8$ Hz), 7.65 (dd, 1H, $J = 7.3$ & 7.9 Hz), 7.59 (d, 1H, $J = 7.9$ Hz), 7.44 (dd, 1H, $J = 7.3$ & 7.8 Hz), 7.52 (d, 2H, $J = 8.9$ Hz), 7.20 (dd, 1H, $J = 8.0$ Hz, & 8.2 Hz), 7.02 (d, 1H, $J = 8.0$ Hz), 6.94 (d, 2H, $J = 8.9$ Hz), 6.91 (s, 1H), 6.82 (d, 1H, 8.2 Hz), 4.67 (s, 2H). ^{13}C NMR (100 MHz, CDCl_3) δ 166.5, 165.2, 158.6, 156.7, 141.2, 135.0, 133.7, 132.6, 130.5, 126.8, 126.0, 123.2, 123.0, 121.8, 120.5, 120.1, 118.3, 116.2, 49.0. HRMS (ES+) Calculated for $\text{C}_{21}\text{H}_{15}\text{N}_2\text{O}_3\text{ClS}^{23}\text{Na}$: 433.0390. Found $[\text{M}+\text{H}]^+$: 433.0832 (Diff -1.85 ppm). $\nu_{\text{max}}/\text{cm}^{-1}$: (solid) 3660 (s), 3074 (m), 2929 (m), 1684 (s), 1631 (d), 1503 (m), 1444 (m), 1297 (m). MP 174 - 176 °C. Microanalysis: Calculated C(61.39%), H(3.68%), N(6.82%); Obtained C(61.07%), H(3.71%), N(6.66%).

***2*-(2-(4-Benzylpiperidin-1-yl)-2-oxoethyl)benzo[*d*]isothiazol-3(2*H*)-one (17f)**

General Procedure A - Employed 4-benzylpiperidine to obtain the title compound (**17f**) (0.13 g, 25% yield) as a white solid. ^1H NMR (400 MHz, CDCl_3) δ 8.03 (d, 1H, $J = 8.0$ Hz), 7.62 – 7.60 (m, 1H), 7.55 (d, 1H, $J = 8.0$ Hz), 7.40 – 7.38 (m, 1H), 7.29 (d, 2H, $J = 7.1$ Hz), 7.23 – 7.21 (m, 1H), 7.11 (d, 1H, $J = 7.1$ Hz), 4.74 (d, 1H, $J = 16.1$ Hz), 4.63 (d, 1H, $J = 16.1$ Hz), 3.92 – 3.91 (m, 1H), 3.04 – 3.02 (m, 1H), 2.60 – 2.59 (m, 1H), 2.55 – 2.54 (m, 1H), 2.54 – 2.52 (m, 2H), 1.75 – 1.73 (m, 3H), 1.20 – 1.17 (m, 2H). ^{13}C NMR (100 MHz, CDCl_3) δ 174.5, 173.6, 150.3, 148.5, 140.8, 137.8, 137.14, 135.6, 135.5, 134.9, 134.2, 134.1, 132.3, 129.0, 54.3, 53.6, 51.6, 46.8, 40.3. HRMS (CI^+ , CH_4) Calculated for $\text{C}_{21}\text{H}_{23}\text{N}_2\text{O}_2\text{S}$: 367.1475. Found $[\text{M}+\text{H}]^+$: 367.1490 (Diff -4.19 ppm). $\nu_{\text{max}}/\text{cm}^{-1}$: (solid) 3026 (m), 2926 (m), 1669 (s), 1633 (s), 1494 (m), 1284 (m). MP: 175 – 176 °C. Microanalysis: Calculated C(68.83%), H(6.05%), N(7.64%); Obtained C(68.63%), H(6.03%), N (7.60%).

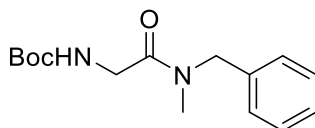
2-(2-(4-Fluoropiperidin-1-yl)-2-oxoethyl)benzo[d]isothiazol-3(2H)-one (**17g**)



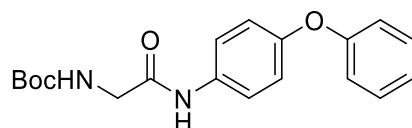
General Procedure A - Employed 4-fluoropiperidine hydrochloride to obtain the title compound (**17g**) (0.13 g, 19% yield) as a white solid. ^1H NMR (400 MHz, CDCl_3) δ 8.04 (d, 1H, $J = 7.9$ Hz), 7.63 (app. t, 1H, $J = 8.1$ Hz), 7.56 (d, 1H, $J = 7.9$ Hz), 7.40 (app. t, 1H, $J = 8.1$ Hz), 4.97 – 4.80 (m, 2H), 4.62 (d, 1H, $J = 16.0$ Hz), 3.97 – 3.95 (m, 1H), 3.65 – 3.63 (m, 2H), 3.48 – 3.47 (m, 1H), 1.88 – 1.84 (m, 4H). ^{13}C NMR (100 MHz, CDCl_3) δ 165.7, 165.0, 141.4, 132.2, 126.8, 125.5, 123.5, 120.4, 87.1 ($J = 172.2$ Hz), 45.0, 41.3 ($J = 4.9$ Hz), 38.2 ($J = 4.2$ Hz), 31.4 ($J = 18.6$ Hz), 30.9 ($J = 17.7$ Hz). HRMS (CI^+ , CH_4) Calculated for $\text{C}_{14}\text{H}_{15}\text{FN}_2\text{O}_2\text{S}$: 295.0911. Found $[\text{M}+\text{H}]^+$: 295.0917 (Diff -1.99 ppm). Predicted C(57.13%), H(5.14%), N(9.52%); Obtained C(56.82%), H(5.02%), N (9.44%). $\nu_{\text{max}}/\text{cm}^{-1}$: (solid) 2974 (m), 2937 (m), 1637 (s), 1596 (s), 1450 (m), 1252 (m). MP: 94 – 97 °C. Purity HPLC (Method A) 90.5%, $R_t = 7.88$ min.

8.5.3.2 General Synthesis of *Tert*-butyl (2-oxoethyl)carbamate derivatives

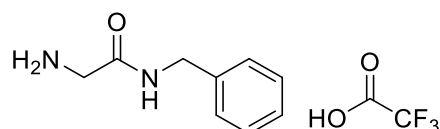
Tert-butyl (2-(benzyl(methyl)amino)-2-oxoethyl)carbamate (**19a**)



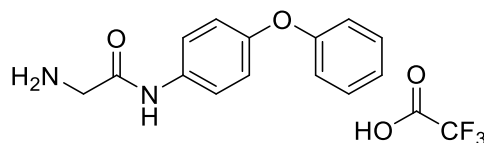
General Procedure B - Employed *N*-benzylmethylamine to obtain the title compound (**19a**) (0.66 g, 42% yield) as a yellow oil. ^1H NMR (400 MHz, CDCl_3) δ 7.35 – 7.32 (l1&2, m, 3H), 7.22 (l1, d, 1H, $J = 7.24$ Hz), 7.14 (l2, d, 1H, $J = 7.24$ Hz), 5.58 (l1&2, bs, 1H), 4.60 (l1, s, 2H), 4.46 (l2, s, 2H), 4.01 – 3.99 (l1&2, m, 2H), 2.98 (l2, s, 3H), 2.88 (l1, s, 3H), 1.46 (l1, s, 9H), 1.44 (l2, s, 9H); ^{13}C NMR (100 MHz, CDCl_3) δ 168.8, 155.9, 136.6, 129.1, 128.7, 128.0, 71.9, 51.2, 42.4, 33.5, 28.3. HRMS (ES^+) calculated for $\text{C}_{15}\text{H}_{22}\text{N}_2\text{O}_3\text{Na}$ 301.1528; $[\text{M}+\text{Na}]^+$ found 301.1524 (Diff -1.33 ppm).

Tert-butyl (2-oxo-2-((4-phenoxyphenyl)amino)ethyl)carbamate (19b)

General Procedure B - Employed 4-phenoxyaniline to obtain the title compound **(19b)** (0.80 g, 82% yield) as an orange/brown oil. ^1H NMR (400 MHz, CDCl_3) δ 8.25 (bs, 1H) 7.46 (d, 2H, $J = 8.88$ Hz), 7.32 (t, 2H, $J = 7.56$ Hz), 7.08 (app. t, 1H, $J = 7.4$ Hz), 6.97 (app. d, 4H, $J = 8.88$ Hz) 5.33 (bs, 1H), 3.93 (d, 2H, $J = 5.8$ Hz), 1.48 (s, 9H). HRMS (ES+) calculated for $\text{C}_{19}\text{H}_{22}\text{N}_2\text{O}_4\text{Na}$ 365.1477; $[\text{M}+\text{Na}]^+$ found 365.1466 (Diff -3.01 ppm).

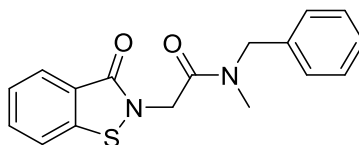
8.5.3.3 General Synthesis of 2-Amino-*N*-acetamide Analogues***2-Amino-N-benzylacetamide 2,2,2-trifluoroacetate (20a)***

General Procedure C - Employed *tert*-butyl (2-(benzyl(methyl)amino)-2-oxoethyl)carbamate **(19a)** (0.88 g) to give the title compound **(20a)** (0.78 g, 99% yield) as a yellow oil and as a mixture of isomers in a ratio 1: 0.46. ^1H NMR (400 MHz, CDCl_3) δ 8.08 (l1&2, bs, 2H), 7.27 – 7.24 (l1&2, m, 3H), 7.09 – 7.06 (l1&2, m, 2H), 4.47 (l1, s, 2H), 4.31 (l2, s, 2H), 3.92 (l1&2, s, 2H), 2.83 (l2, s, 3H), 2.77 (l1, s, 3H). ^{13}C NMR (100 MHz, CDCl_3) δ 166.23 (l1&2, 135.32 (l1), 134.18 (l2), 129.17 (l2) 128.86 (l1) 128.30 (l2), 127.38 (l1), 126.50 (l2), 52.35 (l2), 40.38 (l1&2), 33.95 (l2), 33.61 (l1); HRMS (Cl^+ , CH_4) calculated for $\text{C}_{10}\text{H}_{15}\text{N}_2\text{O}$ 179.1179; $[\text{M}+\text{H}]^+$ found 179.1183 (Diff -2.06 ppm).

2-Amino-N-(4-phenoxyphenyl)acetamide 2,2,2-trifluoroacetate (20b)

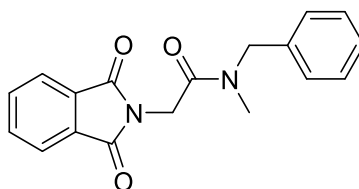
General Procedure C - Employed *tert*-butyl (2-oxo-2-((4-phenoxyphenyl)amino)ethyl)carbamate **(19b)** (0.80 g) to give the title compound **(20b)** (0.78g, 99% yield) as a white/grey solid. Telescoped into next reaction crude. LRMS (Cl^+ , CH_4) calculated for $\text{C}_{14}\text{H}_{14}\text{N}_2\text{O}_2$; Loss of $\text{C}_6\text{H}_5+2\text{H}^+$ obtained $[(\text{C}_8\text{H}_7\text{N}_2\text{O}_2)+^{23}\text{Na}]^+$ found 186.

8.5.3.4 General Synthesis of 3-Oxobenzo[d]isothiazol-2(3H)-yl)acetamides

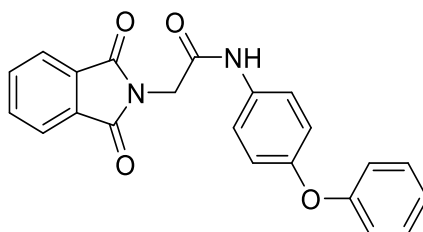
***N*-Benzyl-2-(3-oxobenzo[d]isothiazol-2(3H)-yl)acetamide (17a)**

General Procedure D - Employed 2-amino-*N*-benzylacetamide 2,2,2-trifluoroacetate (**20a**) to give the title compound (**17a**) (0.11 g, 35% yield) as a yellow solid. ¹H NMR (400 MHz, CDCl₃) δ 8.05 (l1, 1H, *J* = 7.88 Hz), 7.99 (l2, d, 1H, *J* = 7.88 Hz), 7.58 – 7.56 (l1&2, m, 2H), 7.36 – 7.31 (l1&2, m, 6H), 4.76 (l1, s, 2H) 4.73 (l2, s, 2H), 4.67 (l2, s, 2H), 4.62 (l1, s, 2H), 3.02 (l1, s, 3H), 3.01 (l2, s, 3H); ¹³C NMR δ (100 MHz, CDCl₃) δ 167.1 (l2), 166.6 (l1), 166.0 (l2), 165.8 (l1), 141.6 (l1), 141.5 (l2), 136.5 (l1), 135.7 (l2), 132.1 (l1), 132.0 (l2), 129.1 (l2), 128.7 (l1), 128.3 (l1), 127.9 (l2), 127.1 (l1), 126.8 (l1), 126.7 (l2), 126.3 (l1&2), 125.4 (l2), 123.5 (l1), 123.5 (l2), 120.3 (l1&2), 53.0 (l2), 51.4 (l1), 45.0 (l1), 44.9 (l2), 34.5 (l2), 34.1 (l1); HRMS (ES⁺) calculated for C₁₇H₁₆N₂O₂SNa 335.0830; [M+Na]⁺ found 335.0827 (Diff -0.90 ppm); Microanalysis: Calculated C(65.36%), H(5.20%), N(8.97%), S(10.26%); Obtained C(63.42%), H(5.46%), N(8.58%), S(9.09%).

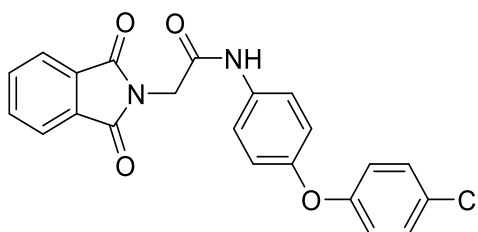
8.5.4 Synthesis of 2-(1,3-dioxoisindolin-2-yl)acetamide Derivatives

***N*-benzyl-2-(1,3-dioxoisindolin-2-yl)-*N*-methylacetamide (24a)**

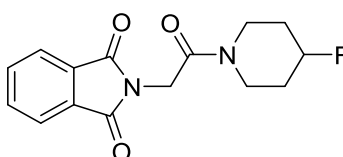
General Procedure E - Employed 2-(1,3-dioxoisindolin-2-yl)acetic acid and *N*-methyl-1-phenylmethanamine to obtain the title compound (0.10 g, 34% yield) as a white solid and a mixture of two isomers (1 : 0.59). ¹H NMR (400 MHz, CDCl₃) δ 7.89 - 7.86 (m, 2H), 7.74 – 7.72 (m, 2H), 7.45 – 7.42 (m, 2H), 7.34 – 7.30 (m, 3H), 7.26 – 7.23 (m, 2H), 4.61 (l2, s, 2H), 4.59 (l1, s, 2H), 4.56 (l2, s, 2H), 4.54 (l1, s, 2H), 3.01 (l1, s, 3H), 2.967 (l2, s, 3H). ¹³C NMR (100 MHz, CDCl₃) δ 168.1 (l1&2), 165.9 (l2), 165.6 (l1), 136.5 (l1), 135.4 (l2), 134.1 (l1), 132.3 (l2), 129.2 (l2), 128.7 (l1), 128.2 (l1), 128.0 (l2), 127.6 (l1), 126.4 (l2), 123.6 (l1), 123.0 (l2), 52.6 (l2), 51.5 (l1), 39.3 (l1), 39.2 (l2), 34.3 (l2), 33.8 (l1). HRMS (Cl⁺, CH₄) Calculated for C₁₇H₁₉N₂O₃: 309.1234. Found [M+H]⁺: 309.1245 (Diff -3.79 ppm). *v*_{max}/cm⁻¹: (solid) 3670 (s), 2980 (m), 2888 (m), 1768 (s), 1709 (s), 1659 (s), 1495 (m), 1454 (m), 1270 (m). MP: 147 – 149 °C. Purity HPLC (Method A) 96.9%, R_t = 9.24 min

2-(1,3-Dioxoisindolin-2-yl)-N-(4-phenoxyphenyl)acetamide (24b)

General Procedure E - Employed 2-(1,3-dioxoisindolin-2-yl)acetic acid and 4-phenoxyaniline to obtain the title compound **(24b)** (0.16 g, 59% yield) as a white solid. ^1H NMR (400 MHz, DMSO) δ 10.35 (s, 1H), 7.92 (m, 4H), 7.57 (d, 2H, $J = 8.3$ Hz), 7.37 (app. t, 2H, $J = 8.3$ & 7.9 Hz), 7.10 (app. t, 1H, $J = 7.9$ Hz), 6.99 (d, 2H, $J = 8.6$ Hz), 6.97 (d, 2H, $J = 8.6$ Hz), 4.44 (s, 2H). ^{13}C NMR (100 MHz, DMSO) δ 168.0, 165.1, 157.7, 152.6, 135.2, 134.8, 132.1, 130.4, 123.8, 128.5, 121.4, 119.9, 118.5, 41.2. HRMS (CI⁺, CH₄) Calculated for C₂₂H₁₇N₂O₄: 373.1183. Found [M+H]⁺: 373.1190 (Diff -3.85 ppm). $\nu_{\text{max}}/\text{cm}^{-1}$: (solid) 3261 (s), 2979 (m), 2889 (m), 1775 (s), 1723 (s), 1658 (s), 1464 (m), 1266 (m). MP: 201 – 203 °C. Purity HPLC (Method A) 95.1%, $R_t = 10.41$ min.

N-(4-(4-chlorophenoxy)phenyl)-2-(1,3-dioxoisindolin-2-yl)acetamide (24c)

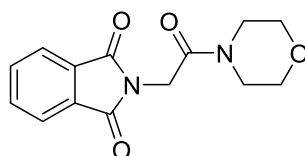
General Procedure E - Employed 2-(1,3-dioxoisindolin-2-yl)acetic acid and 4-(4-chlorophenoxy)aniline to obtain the title compound **(24c)** (0.17 g, 44% yield) as a white solid. ^1H NMR (400 MHz, DMSO) δ 10.38 (s, 1H), 7.95 – 7.93 (m, 2H), 7.93 – 7.90 (m, 2H), 7.60 – 7.57 (m, 2H), 7.43 – 7.40 (m, 2H), 7.04 – 7.01 (m, 2H), 7.00 – 6.97 (m, 2H), 4.45 (s, 2H). ^{13}C NMR (100 MHz, DMSO) δ 168.0, 165.2, 165.1, 156.7, 152.1, 135.1, 132.1, 130.3, 127.2, 123.7, 121.5, 121.4, 120.1, 120.0. HRMS (CI⁺, CH₄) Calculated for C₂₂H₁₆N₂O₄Cl: 407.0793. Found [M+H]⁺: 407.0810 (Diff -4.24 ppm). $\nu_{\text{max}}/\text{cm}^{-1}$: (solid) 3659 (s), 3272 (m), 2980 (m), 2888 (m), 1771 (s), 1715 (s), 1662 (s), 1504 (m), 1464 (m), 1233 (m). MP: 184 – 185 °C. Purity HPLC (Method A) 93.3%, $R_t = 11.06$ min.

2-(2-(4-Fluoropiperidin-1-yl)-2-oxoethyl)isoindoline-1,3-dione (24d)

General Procedure E - Employed 2-(1,3-dioxoisindolin-2-yl)acetic acid and 4-fluoropiperidine hydrochloride to obtain the title compound **(24d)** (0.081 g, 29% yield) as a white solid. ^1H NMR (400

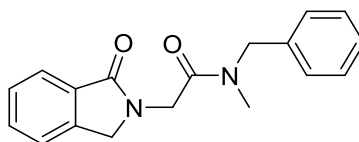
MHz, CDCl₃) δ 7.89 – 8.86 (m, 2H), 7.44 – 7.42 (m, 2H), 4.51 (s, 2H), 4.93 – 4.91 (m, 1H), 3.94 – 3.94 (m, 1H), 3.65 – 3.63 (m, 1H), 3.57 – 3.56 (m, 1H), 3.48 – 3.46 (m, 1H), 1.99 – 1.94 (m, 4H). ¹³C NMR (100 MHz, CDCl₃) δ 168.1, 163.9, 134.1, 132.2, 123.6, 87.2 (d, *J* = 172.1 Hz), 39.0, 40.7 (d, *J* = 5.2 Hz), 38.2 (d, *J* = 4.7 Hz), 31.4 (d, *J* = 20.1 Hz), 30.6 (d, *J* = 20.3 Hz). *v*_{max}/cm⁻¹: (solid) 2990 (m), 2875 (m), 1771 (s), 1706 (s), 1645 (s), 1451 (m), 1262 (m). Purity HPLC (Method A) 96.5%, *R*_t = 7.88 min.

2-(2-Morpholino-2-oxoethyl)isoindoline-1,3-dione (24e)

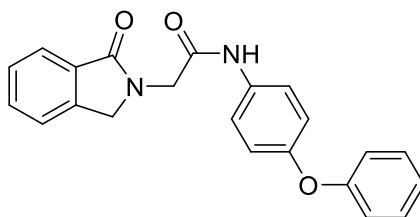


General Procedure E - Employed 2-(1,3-dioxisoindolin-2-yl)acetic acid and morpholine hydrochloride to obtain the title compound (**24e**) (0.043 g, 22% yield) as a white solid. ¹H NMR (400 MHz, CDCl₃) δ 7.88 (m, 2H), 7.73 (m, 2H), 4.49 (s, 2H), 3.74 (m, 4H), 3.58 (m, 4H). ¹³C NMR (100 MHz, CDCl₃) δ 168.0, 164.2, 134.1, 132.3, 123.6, 66.7, 66.3, 45.2, 42.5, 39.0. HRMS (CI⁺, CH₄) Calculated for C₁₄H₁₅N₂O₄: 275.1026. Found [M+H]⁺: 275.1030 (Diff 1.45 ppm). *v*_{max}/cm⁻¹: (solid) 2990(m), 2854(m), 1780(s), 1706(s), 1640(s), 1441(m), 1294 (m). MP: 182 – 185 °C. Microanalysis: Calculated C(61.31%), H(5.15%), N(10.21%); Obtained C(60.53%), H(5.11%), N(10.16%). Purity HPLC (Method A) 97.1%, *R*_t = 6.68 min.

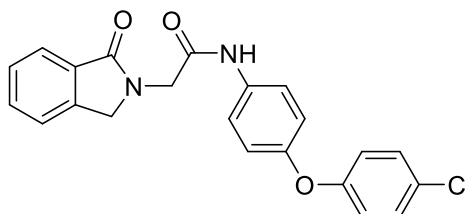
N-benzyl-*N*-methyl-2-(1-oxisoindolin-2-yl)acetamide (24f)



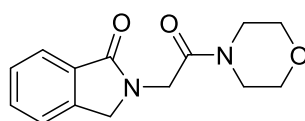
General Procedure E - Employed 2-(1-oxisoindolin-2-yl)acetic acid and *N*-benzylmethylamine to obtain the title compound (**24f**) (0.14 g, 44% yield) as a white solid and a mixture of two isomers. ¹H NMR (400 MHz, CDCl₃) δ 7.79 (l1, d, 1H, *J* = 8.0 Hz), 7.75 (l2, d, 1H, *J* = 8.0 Hz), 7.47 – 7.45 (m, 1H), 7.38 – 7.35 (m, 2H), 7.27 – 7.23 (m, 3H), 7.18 – 7.15 (m, 2H), 4.59 (l2, s, 2H), 4.55 (l1, s, 2H), 4.52 (l1, s, 2H), 4.50 (l2, s, 2H), 4.43 (l1, s, 2H), 4.42 (l2, s, 2H), 2.94 (l1, s, 3H), 2.91 (l2, s, 3H). ¹³C NMR (100 MHz, CDCl₃) δ 169.0 (l1), 168.8 (l2), 168.3 (l1), 167.9 (l2), 141.9 (l1), 141.8 (l2), 136.7 (l1), 136.1 (l2), 132.0 (l1), 131.6 (l2), 129.0 (l2), 128.7 (l1), 128.2 (l1), 127.9 (l1), 127.8 (l2), 127.7 (l2), 127.6 (l1), 126.3 (l2), 123.9 (l1), 53.4 (l2), 58.0 (l2), 51.3 (l1), 50.9 (l2), 44.0 (l1), 43.9 (l2), 34.3 (l2). HRMS (CI⁺, CH₄) Calculated for C₁₈H₁₉N₂O₂: 296.1441. Found [M+H]⁺: 295.1449 (Diff 2.70 ppm). *v*_{max}/cm⁻¹: (solid) 3667 (s), 2980 (m), 2927 (m), 1684 (s), 1646 (s), 1473 (m), 1424 (m), 1261 (m). MP: 121 – 124 °C. Purity HPLC (Method A) 100%, *R*_t = 8.30 min.

2-(1-Oxoisoindolin-2-yl)-N-(4-phenoxyphenyl)acetamide (24g)

General Procedure E - Employed 2-(1-oxoisoindolin-2-yl)acetic acid and 4-phenoxyaniline to obtain the title compound (**24g**) (0.12 g, 43 % yield) as a white solid. ^1H NMR (400 MHz, DMSO) δ 10.23 (s, 1H), 7.72 (d, 1H, $J = 7.4$ Hz), 7.62 (d, 1H, $J = 7.8$ Hz), 7.61 (d, 1H, $J = 8.9$ Hz), 7.55 – 7.50 (m, 1H), 7.37 (dd, 2H, $J = 8.1$ & 7.9 Hz), 7.10 (t, 1H, $J = 7.4$ Hz), 6.99 (d, 2H, $J = 8.9$ Hz), 6.96 (d, 2H, $J = 8.1$ Hz), 4.59 (s, 2H), 4.40 (s, 2H). ^{13}C NMR (100 MHz, DMSO) δ 168.4, 167.1, 157.7, 152.4, 142.8, 135.1, 132.4, 132.0, 130.4, 128.3, 124.0, 123.5, 123.3, 121.4, 119.9, 118.4, 51.1, 45.7. HRMS (ES+) Calculated for $\text{C}_{22}\text{H}_{18}\text{N}_2\text{O}_3^{23}\text{Na}$: 381.1215. Found $[\text{M}+\text{Na}]^+$: 381.1208 (Diff -1.84 ppm). $\nu_{\text{max}}/\text{cm}^{-1}$: (solid) 3306 (s), 3042 (m), 2959 (m), 1666 (s), 1617 (s), 1455 (m), 1228 (m). MP: 185 – 187 °C. Microanalysis: Calculated C(73.73%), H(5.06%), N(7.82%): Obtained C(73.36%), H(5.00%), N(7.69%).

N-(4-(4-chlorophenoxy)phenyl)-2-(1-oxoisoindolin-2-yl)acetamide (24h)

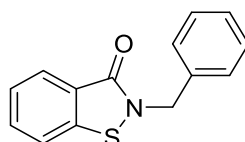
General Procedure E - Employed 2-(1-oxoisoindolin-2-yl)acetic acid and 4-(4-chlorophenoxy)aniline to obtain the title compound (**24h**) (0.11 g, 27% yield) as a white solid. ^1H NMR (400 MHz, DMSO) δ 10.26 (s, 1H), 7.76 – 7.74 (m, 1H), 7.69 – 7.63 (m, 4H), 7.55 – 7.54 (m, 1H), 7.45 – 7.42 (m, 2H), 7.05 (d, 2H, $J = 8.7$ Hz), 7.01 (d, 2H, $J = 8.7$ Hz), 4.59 (s, 2H), 4.40 (s, 2H). ^{13}C NMR (100 MHz, DMSO) δ 168.4, 167.2, 156.8, 151.9, 142.8, 135.4, 132.3, 132.0, 130.3, 128.3, 127.2, 123.9, 123.3, 121.4, 120.1, 120.0, 51.1, 45.7. HRMS (CI+, CH_4) Calculated for $\text{C}_{22}\text{H}_{18}\text{N}_2\text{O}_3\text{Cl}$: 393.0999. Found $[\text{M}+\text{H}]^+$: 393.0999 (Diff 0.00 ppm). $\nu_{\text{max}}/\text{cm}^{-1}$: (solid) 3658 (s), 2989 (m), 2930 (m), 1666 (s), 1621 (m), 1503 (m), 1455 (m), 1288 (m). MP: 222 – 223 °C. Microanalysis: Calculated C(67.26%), H(4.36%), N(7.13%): Obtained C(66.90%), H(4.28%), N(6.96%).

2-(2-Morpholino-2-oxoethyl)isoindolin-1-one (24i)

General Procedure E - Employed 2-(1-oxoisindolin-2-yl)acetic acid and morpholine to obtain the title compound (**24i**) (0.088g, 44% yield) as a white solid. ^1H NMR (400 MHz, CDCl_3) δ 7.85 (d, 1H, $J = 7.5$ Hz), 7.55 (app. t, 1H, $J = 7.7$ Hz), 7.46 (app. t, 2H, $J = 7.5$ & 7.7 Hz), 4.55 (s, 2H), 4.45 (s, 2H), 3.71 – 3.67 (m, 4H), 3.63 – 3.58 (m, 4H). ^{13}C NMR (100 MHz, CDCl_3) δ 168.7, 166.5, 141.8, 131.8, 131.7, 128.0, 128.9, 122.8, 66.8, 66.6, 50.8, 45.7, 43.9, 42.2. HRMS (Cl^+ , CH_4) Calculated for $\text{C}_{24}\text{H}_{17}\text{N}_2\text{O}_3$: 261.1242. Found $[\text{M}+\text{H}]^+$: 261.1234 (Diff -3.18 ppm). $\nu_{\text{max}}/\text{cm}^{-1}$: (solid) 2920 (m), 2842 (m), 1683 (s), 1656 (s), 1468 (m), 1270 (m). Purity HPLC (Method A) 93.7%, $R_t = 6.012$ min. MP: 140 – 142 °C. Purity HPLC (Method A) 94.6%, $R_t = 6.02$ min.

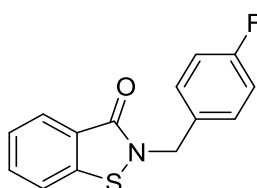
8.5.5 2-benzylbenzo[d]isothiazol-3(2H)-one Derivatives

2-Benzylbenzo[d]isothiazol-3(2H)-one (**27a**)

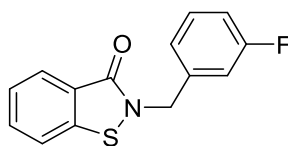


General Procedure F - Employed benzyl bromide to obtain the title compound (**27a**) (0.11 g, 34% yield) as pale yellow solid. ^1H NMR (400 MHz, CDCl_3) δ 8.07 (d, 1H, $J = 7.9$ Hz), 7.58 (dd, 1H, $J = 8.2$ & 7.2 Hz), 7.48 (d, 1H, $J = 8.1$ Hz), 7.40 (dd, 1H, $J = 7.9$ & 7.2 Hz), 7.38 – 7.33 (m, 5H), 5.06 (s, 2H). ^{13}C NMR (100 MHz, CDCl_3) δ 165.4, 140.4, 136.3, 131.9, 128.8, 128.5, 128.3, 126.8, 125.5, 124.5, 120.4, 47.6. HRMS (Cl^+ , CH_4) Calculated for $\text{C}_{14}\text{H}_{12}\text{NOS}$: 242.0634. Found $[\text{M}+\text{H}]^+$: 242.0643 (Diff -3.63 ppm). $\nu_{\text{max}}/\text{cm}^{-1}$: (solid) 3077 (m), 3021 (m), 2923 (m), 1656 (s), 1454(m), 1242 (m). MP: 68 – 71 °C. Purity HPLC (Method A) 95.3%, $R_t = 9.43$ min.

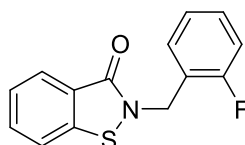
2-(4-Fluorobenzyl)benzo[d]isothiazol-3(2H)-one (**27b**)



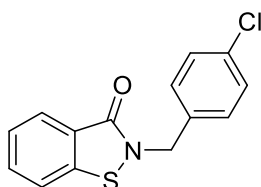
General Procedure F - Employed 4-fluorobenzyl bromide to obtain the title compound (**27b**) (0.20 g, 59% yield) as pale yellow solid. ^1H NMR (400 MHz, CDCl_3) δ 8.06 (d, 1H, $J = 7.7$ Hz), 7.60 – 7.58 (m, 1H, $J = 8.1$ Hz), 7.51 (d, 1H, $J = 8.1$ Hz), 7.42 – 7.40 (m, 1H, $J = 7.7$ Hz), 7.36 – 7.32 (m, 2H), 7.06 – 7.03 (m, 2H), 5.02 (s, 2H). ^{13}C NMR (100 MHz, CDCl_3) δ 165.3, 140.3, 132.0, 131.9, 130.2, 126.9, 125.6, 124.4, 120.4, 115.9, 115.7, 46.8. HRMS (Cl^+ , CH_4) Calculated for $\text{C}_{14}\text{H}_{11}\text{FNOS}$: 260.0540. Found $[\text{M}+\text{H}]^+$: 260.0550 (Diff -4.04 ppm). $\nu_{\text{max}}/\text{cm}^{-1}$: (solid) 2921 (m), 2851 (m), 1632 (s), 1444 (m), 1235 (m), 745 (m). MP: 78 – 80 °C. Purity HPLC (Method A) 96.6%, $R_t = 9.57$ min.

2-(3-Fluorobenzyl)benzo[d]isothiazol-3(2H)-one (27c)

General Procedure F - Employed 3-fluorobenzyl bromide to obtain the title compound (**27c**) (0.20 g, 59% yield) as pale yellow solid. ^1H NMR (400 MHz, CDCl_3) δ 8.07 (d, 1H, $J = 7.8$), 7.62 – 7.60 (m, 1H), 7.51 (d, 1H, $J = 8.3$ Hz), 7.42 – 7.40 (m, 1H), 7.33 – 7.31 (m, 1H), 7.13 (d, 1H, $J = 7.8$ Hz), 7.06 – 7.04 (m, 1H), 7.00 (d, 1H, $J = 8.6$ Hz), 5.04 (s, 2H). ^{13}C NMR (100 MHz, CDCl_3) δ 165.4, 164.2, 161.8, 140.3, 138.6, 132.0, 130.4, 126.9, 125.6, 124.2, 123.8, 120.5, 115.3, 47.0. HRMS (Cl^+ , CH_4) Calculated for $\text{C}_{14}\text{H}_{11}\text{FNOS}$: 260.0540. Found $[\text{M}+\text{H}]^+$: 260.0545 (Diff -2.05 ppm). $\nu_{\text{max}}/\text{cm}^{-1}$: (solid) 3050 (m), 2979 (m), 1847 (s), 1486 (m), 1263 (s), 733 (s). MP: 67 – 69 °C. Purity HPLC (Method A) 97.8%, $R_t = 9.59$ min.

2-(2-Fluorobenzyl)benzo[d]isothiazol-3(2H)-one (27d)

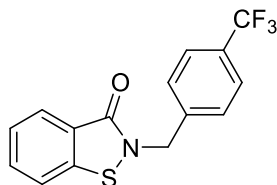
General Procedure F - Employed 2-fluorobenzyl bromide to obtain the title compound (**27d**) (0.085 g, 25% yield) as pale yellow solid. ^1H NMR (400 MHz, CDCl_3) δ 7.98 (D, 1H, $J = 7.8$ Hz), 7.51 (m, 1H), 7.42 (d, 1H, $J = 7.8$ Hz), 7.31 (m, 2H), 7.21 (m, 1H), 7.02 (m, 2H), 5.05 (s, 2H). ^{13}C NMR (100 MHz, CDCl_3) δ 165.4, 160.8 (d, $J = 247.8$ Hz), 140.5, 131.9, 130.8 (d, $J = 3.5$ Hz), 130.2 (d, $J = 8.2$ Hz), 126.8, 125.5, 124.6 (d, $J = 3.4$ Hz), 124.3, 123.3 (d, $J = 14.6$ Hz), 102.4, 115.5 (d, $J = 21.3$ Hz), 41.0. HRMS (Cl^+ , CH_4) Calculated for $\text{C}_{14}\text{H}_{11}\text{FNOS}$: 260.0540. Found $[\text{M}+\text{H}]^+$: 260.0544 (Diff – 1.52 ppm). $\nu_{\text{max}}/\text{cm}^{-1}$: (solid) 3056 (m), 3015 (m), 2932 (m), 1652 (s), 1488 (m), 1356 (s). MP: 98 -100 °C. Purity HPLC (Method A) 97.6%, $R_t = 9.55$ min.

2-(4-Chlorobenzyl)benzo[d]isothiazol-3(2H)-one (27e)

General Procedure F - Employed 4-chlorobenzyl bromide to obtain the title compound (**27e**) (0.17 g, 47% yield) as yellow solid. ^1H NMR (400 MHz, CDCl_3) δ 8.06 (d, 1H, $J = 7.9$ Hz), 7.60 – 7.58 (m, 1H), 7.50 (d, 1H, $J = 7.9$ Hz), 7.41 – 7.39 (m, 1H), 7.33 – 7.28 (m, 4H), 5.01 (s, 2H). ^{13}C NMR (100 MHz, CDCl_3) δ 165.4, 140.3, 134.7, 134.2, 132.0, 129.8, 129.0, 126.9, 125.6, 124.3, 120.5, 46.8. HRMS (Cl^+ , CH_4) Calculated for $\text{C}_{14}\text{H}_{11}\text{ClNOS}$: 276.0244. Found $[\text{M}+\text{H}]^+$: 276.0250 (Diff -2.09 ppm). $\nu_{\text{max}}/\text{cm}^{-1}$: (solid)

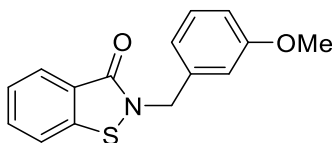
3056 (m), 928 (m), 1655 (s), 1459 (m), 1285 (m), 735 (s). MP: 64 - 66 °C. Microanalysis: Calculated C(60.98%), H(3.66%), N(5.08%); Obtained C(60.81%), H(3.63%), N(4.85%).

2-(4-(Trifluoromethyl)benzyl)benzo[d]isothiazol-3(2H)-one (27f)



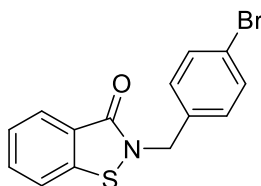
General Procedure F - Employed 4-(trifluoromethyl)benzyl bromide to obtain the title compound (**27f**) (0.086 g, 22% yield) as yellow solid. ^1H NMR (400 MHz, CDCl_3) δ 8.08 (d, 1H, $J = 7.9$ Hz), 7.62 (m, 3H, $J = 7.6$ & 8.3 Hz), 7.52 (d, 1H, $J = 7.9$ Hz), 7.46 (d, 2H, $J = 8.3$ Hz), 7.42 (d, 1H, $J = 7.6$ Hz), 5.12 (s, 2H). ^{13}C NMR (100 MHz, CDCl_3) δ 165.5, 140.3, 132.2, 130.6, 130.3, 128.5, 127.0, 125.9, 125.7, 125.3, 124.1, 120.5, 46.9. HRMS (CI^+ , CH_4) Calculated for $\text{C}_{15}\text{H}_{11}\text{F}_3\text{NOS}$: 310.0508. Found $[\text{M}+\text{H}]^+$: 310.051743 (Diff - 3.05 ppm). $\nu_{\text{max}}/\text{cm}^{-1}$: (solid) 3067 (m), 2917 (m), 2853 (m), 1636 (s), 1443 (m), 1246 (m), 781 (s). MP: 82 - 84 °C. Microanalysis: Calculated C(58.25%), H(4.83%), N(5.16%); Obtained C(58.20%), H(4.77%), N(4.92%).

2-(3-Methoxybenzyl)benzo[d]isothiazol-3(2H)-one (27g)



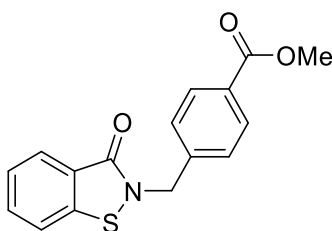
General Procedure F - Employed 4-(methoxy)benzyl bromide to obtain the title compound (**27g**) (0.12 g, 34% yield) as cloudy oil that solidified to a yellow solid on standing. ^1H NMR (400 MHz, CDCl_3) δ 8.06 (d, 1H, $J = 7.8$ Hz), 7.59 (app. t, 1H, $J = 7.2$ & 8.0 Hz), 7.49 (d, 1H, $J = 8.0$ Hz), 7.40 (app. t, 1H, $J = 7.2$ & 7.8 Hz), 7.27 (app. t, 1H, $J = 8.0$ & 7.6 Hz), 6.94 (d, 1H, $J = 7.6$ Hz) 6.88 - 6.85 (m, 2H, $J = 8.0$ Hz), 5.03 (s, 2H), 3.79 (s, 3H). ^{13}C NMR (100 MHz, CDCl_3) δ 165.3, 160.0, 140.4, 137.7, 131.9, 129.9, 126.8, 125.5, 124.5, 120.7, 120.4, 113.9, 113.8, 55.3, 47.5. HRMS (CI^+ , CH_4) Calculated for $\text{C}_{15}\text{H}_{14}\text{NO}_2\text{S}$: 273.0740. Found $[\text{M}+\text{H}]^+$: 273.0738 (Diff 0.81 ppm). $\nu_{\text{max}}/\text{cm}^{-1}$: (solid) 2919 (m), 1637 (s), 1455 (m), 1229 (m). MP: 44 - 46 °C. Purity HPLC (Method A) 100%, $R_t = 9.44$ min.

2-(4-Bromobenzyl)benzo[d]isothiazol-3(2H)-one (27h)



General Procedure F - Employed 4-bromobenzyl bromide to obtain the title compound (**27h**) (0.60 g, 56% yield) as yellow solid. ^1H NMR (400 MHz, CDCl_3) δ 8.06 (d, 1H, $J = 7.9$ Hz), 7.60 (dd, 1H, $J = 7.2$ & 8.1 Hz), 7.50 (d, 1H, $J = 8.1$ Hz), 7.47 (d, 2H, $J = 8.4$ Hz), 7.41 (app. t, 1H, $J = 7.2$ & 7.9 Hz), 7.22 (d, 2H, $J = 8.4$ Hz), 5.00 (s, 2H). ^{13}C NMR (100 MHz, CDCl_3) δ 165.4, 140.3, 135.2, 132.1, 132.0, 130.1, 126.9, 125.7, 124.3, 122.4, 120.5, 46.1. HRMS (Cl^+ , CH_4) Calculated for $\text{C}_{14}\text{H}_{11}\text{BrNOS}$: 319.9739. Found $[\text{M}+\text{H}]^+$: 319.9739 (Diff 0.16 ppm). $\nu_{\text{max}}/\text{cm}^{-1}$: (solid) 2978 (m), 2928 (m), 1657 (s), 1446 (m), 1234 (m), 736 (m). MP: 103 – 105 °C. Microanalysis: Calculated C(52.51%), H(3.15%), N(4.37%); Obtained C(51.86%), H(3.09%), N(4.17%).

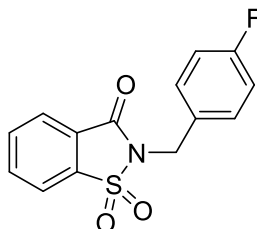
Methyl 4-((3-oxobenzo[d]isothiazol-2(3H)-yl)methyl)benzoate (27i)



General Procedure F - Employed 4-(bromomethyl)benzoate to obtain the title compound (**27i**) (0.24 g, 41% yield) as yellow solid. ^1H NMR (400 MHz, CDCl_3) δ 8.08 (d, 1H, $J = 7.9$ Hz), 8.02 (d, 2H, $J = 8.3$ Hz), 7.61 (app. t, 1H, $J = 7.1$ & 8.1 Hz), 7.51 (d, 1H, $J = 7.9$ Hz), 7.40 (m, 3H, $J = 8.3$ & 7.1 Hz), 5.12 (s, 2H), 3.91 (s, 3H). ^{13}C NMR (100 MHz, CDCl_3) δ 166.6, 165.4, 141.2, 140.3, 132.1, 130.1, 130.0, 128.2, 126.9, 125.7, 124.2, 120.5, 52.2, 47.1 HRMS (Cl^+ , CH_4) Calculated for $\text{C}_{14}\text{H}_{14}\text{NOS}$: 242.0634 (Diff -3.72 ppm). Found $[\text{M}+\text{H}]^+$: 242.0643. $\nu_{\text{max}}/\text{cm}^{-1}$: (solid) 2979 (m), 2890 (m), 1713 (s), 1652 (s), 1455 (m), 1252 (m). MP: 115 - 117 °C. Microanalysis: Predicted C(64.20%), H(4.38%), N(4.68%); Obtained C(63.92%), H(4.35%), N (4.60%).

8.5.6 Synthesis of 2-benzo[d]isothiazol-3(2H)-one 1,1-dioxide Derivatives

2-(4-Fluorobenzyl)benzo[d]isothiazol-3(2H)-one 1,1-dioxide (27j)



General Procedure F - Employed 4-fluorobenzyl bromide and benzo[d]isothiazol-3(2H)-one 1,1-dioxide, refluxing overnight, to obtain the title compound (**27j**) (0.24 g, 50% yield) as yellow solid. ^1H NMR (400 MHz, CDCl_3) δ 8.05 (d, 1H, $J = 7.0$ Hz), 7.91 (d, 1H, $J = 7.3$ Hz), 7.87 (m, 2H, $J = 7.3$ & 7.0 Hz), 7.51 (d, 2H, $J = 8.5$ Hz), 7.04 (d, 2H, $J = 8.5$ Hz), 4.87 (s, 2H). ^{13}C NMR (100 MHz, CDCl_3) δ 162.7 (d, $J = 247.2$ Hz), 158.9, 137.7, 134.9, 134.4, 130.8 (d, $J = 8.9$ Hz), 130.3 (d, $J = 4.0$ Hz), 127.2, 125.3, 121.1,

115.6 (d, $J = 22.0$ Hz), 42.0. HRMS (CI⁺, NH₃) Calculated for C₁₄H₁₄FN₂O₃S: 309.0704. Found [M+NH₄]⁺: 309.0713 (Diff -3.1 ppm). $\nu_{\max}/\text{cm}^{-1}$: (solid) 2980 (m), 1723 (s), 1504 (m), 1255 (m), 750 (s). MP: 116 – 119 °C. Microanalysis: Calculated C(57.73%), H(3.46%), N(4.81%): Obtained C(58.02%), H(3.47%), N(4.51%).

References

1. A. Li, Z. Chen, Q.-Y. Wu, M.-H. Huang, Z.-Y. Liu, P. Chen, L.-C. Mei and H.-Y. Hu, *Chem. Eng. J.*, 2016, **300**, 376-383.
2. J. F. Schwensen, M. D. Lundov, R. Bossi, P. Banerjee, E. Gimenez-Arnau, J.-P. Lepoittevin, C. Lidén, W. Uter, K. Yazar, I. R. White and J. D. Johansen, *Contact Dermatitis*, 2015, **72**, 127-138.
3. E. Garcia-Hidalgo, V. Sottas, N. von Goetz, U. Hauri, C. Bogdal and K. Hungerbühler, *Contact Dermatitis*, 2017, **76**, 96-106.
4. U. F. Friis, T. Menné, M.-A. Flyvholm, J. P. E. Bonde, J.-P. Lepoittevin, C. J. Le Coz and J. D. Johansen, *Contact Dermatitis*, 2014, **71**, 65-74.
5. M. Birsa, S. Braverman, Y. Charalambides, M. Cherkinsky and C. Diaper, *Science of Synthesis: Houben-Weyl Methods of Molecular Transformations* Georg Thieme Verlag, 2014.
6. A. Rafoth, S. Gabriel, F. Sacher and H.-J. Brauch, *J. Chromatogr. A*, 2007, **1164**, 74-81.
7. D. Chen, T. Li, L. Yang, K. Ni, Z. Shi and F. Li, *Org. Biomol. Chem.*, 2016, **14**, 6297-6303.
8. S. Scientific Committee of Consumer Safety – and A. M. Giménez-Arnau, *Regul. Toxicol. Pharmacol.*, 2016, **76**, 211-212.
9. J. F. Lawrence, in *Encyclopedia of Food Sciences and Nutrition (Second Edition)*, ed. B. Caballero, Academic Press, Oxford, 2003, DOI: <https://doi.org/10.1016/B0-12-227055-X/01033-6>, pp. 5033-5035.
10. M. J. Prival, in *Encyclopedia of Food Sciences and Nutrition (Second Edition)*, ed. B. Caballero, Academic Press, Oxford, 2003, DOI: <https://doi.org/10.1016/B0-12-227055-X/00155-3>, pp. 799-804.
11. A. R. Odom, *PLOS Pathog.*, 2011, **7**, e1002323.
12. M. B. Cassera, F. C. Gozzo, F. L. D'Alexandri, E. F. Merino, H. A. del Portillo, V. J. Peres, I. C. Almeida, M. N. Eberlin, G. Wunderlich, J. Wiesner, H. Jomaa, E. A. Kimura and A. M. Katzin, *J. Biol. Chem.*, 2004, **279**, 51749-51759.
13. K. E. Price, C. M. Armstrong, L. S. Imlay, D. M. Hodge, C. Pidathala, N. J. Roberts, J. Park, M. Mikati, R. Sharma, A. S. Lawrenson, N. H. Tolia, N. G. Berry, P. M. O'Neill and A. R. John, *Sci. Rep.*, 2016, **6**, 1-12.
14. I. Hale, P. M. O'Neill, N. G. Berry, A. Odom and R. Sharma, *Med. Chem. Commun.*, 2012, **3**, 418-433.
15. M. Rodriguez-Concepcion, *Curr. Pharm. Des.*, 2004, **10**, 2391-2400.
16. D. Dou, D. Alex, B. Du, K.-C. Tiew, S. Aravapalli, S. R. Mandadapu, R. Calderone and W. C. Groutas, *Bioorg. Med. Chem.*, 2011, **19**, 5782-5787.
17. D. Alex, F. Gay-Andrieu, J. May, L. Thampi, D. Dou, A. Mooney, W. Groutas and R. Calderone, *Antimicrob. Agents Chemother.*, 2012, **56**, 4630-4639.
18. M. P. Murphy, *Biochem. J.*, 2009, **417**, 1-13.
19. G. K. Azad and R. S. Tomar, *Mol. Biol. Rep.*, 2014, **41**, 4865-4879.
20. M. J. Parnham, S. Leyck, P. Kuhl, J. Schalkwijk and W. B. van den Berg, *Int. J. Tissue React.*, 1987, **9**, 45-50.
21. I. J. Kade, B. D. Balogun and J. B. T. Rocha, *Chem.-Biol. Interact.*, 2013, **206**, 27-36.
22. E. E. Alberto, V. d. Nascimento and A. L. Braga, *J. Braz. Chem. Soc.*, 2010, **21**, 2032-2041.
23. M. Pye, Doctor in Philosophy, University of Liverpool, 2017.
24. N. J. Roberts, Doctor in Philosophy, University of Liverpool, 2016.

25. A. C. Joice, M. T. Harris, E. W. Kahney, H. C. Dodson, A. G. Maselli, D. C. Whitehead and J. C. Morris, *Int. J. Parasitol. Drugs Drug. Resist.*, 2013, **3**, 154-160.
26. H. Masumoto, K. Hashimoto, M. Nakaoka and H. Hakusui, *Drug Metab. Pharmacokinet.*, 1995, **10**, 158-161.
27. Wiley, in *The MAK-Collection for Occupational Health and Safety*, Wiley-VCH, 2012, DOI: 10.1002/3527600418.mb263433kske0002, pp. 222-230.
28. S. Wawra and G. Fischer, Wiley VCH, 2006, DOI: 10.1002/9783527609338, ch. 9, pp. 167-193.
29. A. E. Tonelli, *J. Am. Chem. Soc.*, 1971, **93**, 7153-7155.
30. L. Escobar, A. Díaz-Moscoso and P. Ballester, *Chem. Sci.*, 2018, **9**, 7186-7192.
31. G. Fischer, *Chem. Soc. Rev.*, 2000, **29**, 119-127.
32. J. S. Laursen, J. Engel-Andreasen, P. Fristrup, P. Harris and C. A. Olsen, *J. Am. Chem. Soc.*, 2013, **135**, 2835-2844.
33. C. Dugave and L. Demange, *Chem. Rev.*, 2003, **103**, 2475-2532.
34. Y. Pang, M. Guan, R. Zeng and Y. Zhao, *Org. Chem. Front*, 2017, **4**, 2408-2411.
35. Y. Cao, T.-X. Xiang and B. D. Anderson, *Mol. Pharmaceutics*, 2008, **5**, 371-388.
36. M.-C. Frantz, L. P. Pellissier, E. Pflimlin, S. Loison, J. Gandía, C. Marsol, T. Durroux, B. Mouillac, J. A. J. Becker, J. Le Merrer, C. Valencia, P. Villa, D. Bonnet and M. Hibert, *J. Med. Chem.*, 2018, **61**, 8670-8692.
37. R. Sharma and S. S. Soman, *Synth. Commun.*, 2016, **46**, 1307-1317.
38. M. Pietka-Ottlik, P. Potaczek, E. Piasecki and J. Mlochowski, *Molecules*, 2010, **15**, 8214-8228.
39. S. Mehta, Phase I Metabolism- Oxidative Reactions- Oxidation of Aromatic compounds, <https://pharmaxchange.info/2014/02/phase-i-metabolism-oxidative-reactions-oxidation-of-aromatic-compounds/>, (accessed July 2019).
40. B. Testa and J. M. Mayer, in *Hydrolysis in Drug and Prodrug Metabolism*, eds. B. Testa and J. M. Mayer, Wiley-VCH, 2006, DOI: 10.1002/9783906390444.ch4, pp. 81-162.
41. C. Chen, J. Liu, J. R. Halpert and P. R. Wilderman, *Biochemistry*, 2018, **57**, 817-826.
42. G. Thomas, *Medicinal Chemistry: An Introduction*, John Wiley & Sons, 2011.
43. R. C. Howell, S. H. Edwards, A. S. Gajadhar-Plummer, I. A. Kahwa, G. L. McPherson, J. T. Mague, A. J. P. White and D. J. Williams, *Molecules*, 2003, **8**, 565-592.
44. W. Grzesiak and B. Brycki, *Molecules*, 2012, **17**, 12427-12448.
45. G. Facey, Chemical and Magnetic Equivalence <http://u-of-o-nmr-facility.blogspot.com/2008/08/chemical-and-magnetic-equivalence.html>, (accessed July 2019).
46. F. Brotzel, Doctor in Philosophy, Ludwig-Maximilians-Universität München, 2008.
47. Y. Lu, Bond dissociation energies, <http://staff.ustc.edu.cn/~luo971/2010-91-CRC-BDEs-Tables.pdf>, (accessed July 2019).
48. Y. Lu, *Comprehensive Handbook of Chemical Bond Energies*, CRC Press, Boca Raton, 1 edn., 2007.
49. D. Liu, Z. Tian, Z. Yan, L. Wu, Y. Ma, Q. Wang, W. Liu, H. Zhou and C. Yang, *Bioorg. Med. Chem.*, 2013, **21**, 2960-2967.
50. T. Shibata, T. Takahashi, E. Yamada, A. Kimura, H. Nishikawa, H. Hayakawa, N. Nomura and J. Mitsuyama, *Antimicrob. Agents. Chemother.*, 2012, **56**, 5892-5897.

Chapter 9

Synthesis of Benzoxaboroles as Novel
Treatments for *C. neoformans*

9.1 Benzoxaborole Introduction

9.1.1 Benzoxaborole Overview

As detailed in earlier chapters, the benzimidazoles, with the exception of lead morpholine derivative described in Chapter 4, possessed promising activity, but lacked the desired *in vivo* data and solubility required for an optimal drug candidate. The benzisothiazolinones, whilst soluble, showed inadequate activity when compared with other templates and possessed poor metabolic properties. In order to provide a suitable back-up template to the morpholine benzimidazole series a new class of compounds was required. Benzoxaboroles became known to the group when working on a project which allowed for screening of an Anacor library as part of the AWOL (anti-wolbachia consortium) project.¹⁻³ At this point they were known to possess some antifungal activity, moderate DMPK properties and a good toxicity profile. For these reasons, it was decided that the benzoxaborole class would form the third template within the *C. neoformans* project.

9.1.2 Benzoxaborole Structure and Reactivity

Benzoxaboroles (Figure 9.1) are the fusion of the benzene ring with a five-membered oxaborole ring. They were synthesised and characterised as early as 1957 and are also known as 1-hydroxy-1,3-dihydrobenzoxaboroles. They are known to show a strong resistance to hydrolytic cleavage in comparison to their boronic acid counterparts and the five-membered ring itself is very stable. Furthermore, boronic acids are known for being poorly water soluble, however the oxaborole ring helps to improve this solubility, making them more feasible as drug like molecules.⁴

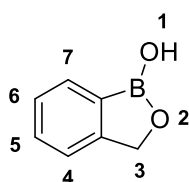


Figure 9.1. Benzoxaboroles are the fusion of the benzene ring and a five-membered boron containing ring.

9.1.2.1 Benzoxaboroles pK_a

Benzoxaboroles behave in a similar manner to phenyl boronic acids in that they behave as Lewis acids, rather than Brønsted acids.⁵ Benzoxaboroles show greater acidity ($pK_a = 7.3$) than phenyl boronic acids ($pK_a = 8.8$). This is because coordination or addition of a nucleophilic species to the Lewis acidic boron reduces ring strain that is present from the five-membered heterocyclic ring, via formation of a tetrahedral species.^{6,7}

We can also draw a correlation between aromatic substituent values and the pK_a of the benzoxaboroles. The substituent constant (σ) is a measure of the total polar effect exerted by a particular substituent on the reaction centre, which in this case is the boron. This is related to pK_a by the following equation (Figure 9.2);

$$\sigma = -(pK_a - pK_a(H))$$

Figure 9.2. the equation that relates substituent constant to pK_a .

The pK_a of an unsubstituted oxaborole is 7.4. As the σ becomes more positive, the pK_a decreases, which is due to a more electron withdrawing group being present. This is because there will be more electron density present on the boron, meaning it will be more susceptible to nucleophilic attack. This occurs with substituents such a fluorine and more profoundly with CF_3 , which is particularly electron withdrawing and reduces the pK_a to 6.3. As σ becomes more negative, we see an increase in pK_a , becoming less acidic. This is seen with electron donating groups such as methyl, which is inductively electron withdrawing and increases pK_a to 7.7, and even more profound with methoxy, which is mesomerically electron donating which increases pK_a to 7.9. This shows a negative correlation between σ and pK_a (Figure 9.3).⁷

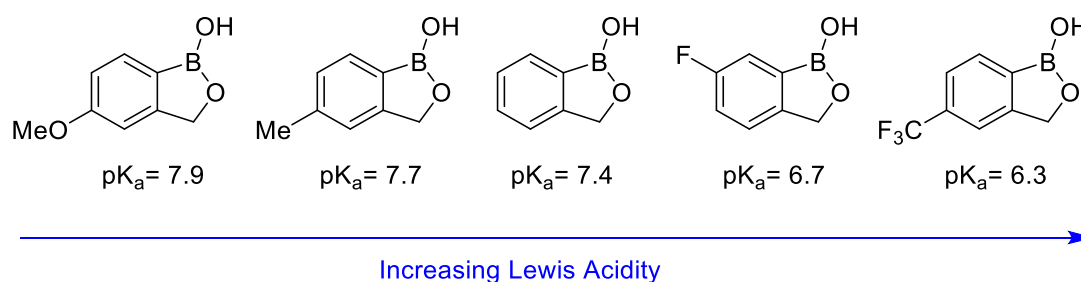


Figure 9.3. Different substituents can affect benzoxaborole pK_a , which affects Lewis acidity.

9.1.2.2 Structural Properties

As observed with phenyl boronic acids, most benzoxaboroles occur in a dimeric form, when in the solid state. The dimers are produced when hydrogen bonds form at a distance of 2.73 Å between the OH of one molecule and the oxygen of the other as shown in Figure 9.4.^{4,8}

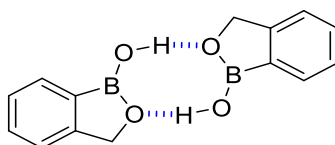


Figure 9.4. Oxaborole form dimers in the solid state.^{4,8}

9.1.3 Oxaborole Previous and Current Use

Boron containing compounds are well known to have biological activity and interact specifically with the active sites of enzymes through esterification and the formation of a tetrahedral intermediates which prevents the enzyme from exerting its biological effect.^{4, 9, 10} A major target for the benzoxaboroles has been identified at the leucyl-tRNA synthetases (LeuRS). These are enzymes that aid protein biosynthesis and work via attachment of amino acid residues to the tRNA molecules, which can then undergo translation. Benzoxaboroles have shown activity against a number of different leucyl-tRNA synthetases, including fungal, bacterial and protozoal.⁹⁻¹¹

Benzoxaboroles have also been shown to exhibit activity against other classes of enzymes, including selective inhibition of β -lactamases, some serine proteases and phosphodiesterases.^{10, 12} One example of a phosphodiesterase inhibitor is Crisaborole (**1**), trademarked as Eucrisa (Figure 9.5). It is an anti-inflammatory inhibitor of phosphodiesterase 4 (PDE4). It is used as a topical treatment of atopic dermatitis, also known as eczema, which causes the skin to become very red and itchy. Currently, there is no precise mechanism of action known as to how **1** exerts its anti-inflammatory effect, however they do see that PDE4 is inhibited, which increases intracellular cAMP, a second messenger. Through a series of signals this leads to inhibition of cytokine production which is known to cause inflammation.¹³

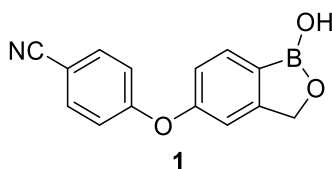


Figure 9.5. Crisaborole is a Benzoxaborole analogue used for the treatment of atopic dermatitis.

There are other less therapeutic uses for benzoxaboroles. Recognition of carbohydrates at physiologically relevant conditions is important. Oligonucleotides have been shown to be functionally important in mediating cell-cell interactions, which includes infection by pathogens, such as bacteria and viruses.¹⁴ It was found that simple benzoxaboroles, such as **2**, are known to bind to carbohydrates and could be used to design oligomeric receptors and sensors, which could aid in the understanding of infection.¹⁵⁻¹⁷ Benzoxaboroles have also found use as plastic biocides (**3**), which prevent microbial growth within the plastic, improving longevity.^{17, 18} Finally, benzoxaboroles have also found use in blue dyes (**4**) and pigments (Figure 9.6).¹⁹

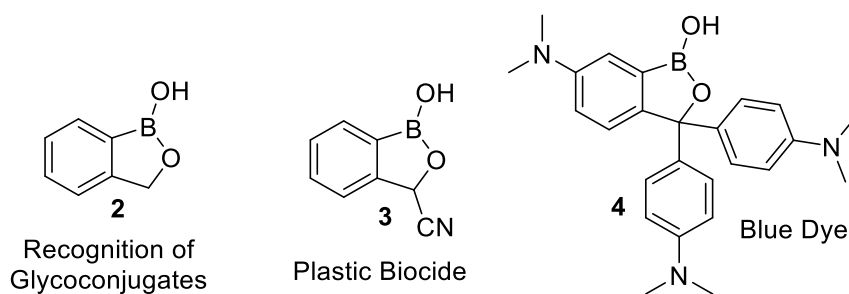


Figure 9.6. The use of benzoxaboroles expands beyond medicinal chemistry.¹⁶

9.1.4 Identification of Oxaboroles as Antifungals

Benzoxaboroles have been identified as having anti-fungal activity. One of the leading fungicides AN2690 (**5**) has a mode of action which involves the inhibition of fungal leucyl-tRNA synthetase (Figure 9.7).

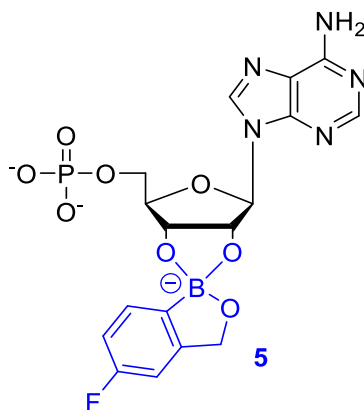


Figure 9.7. The spiro ester adduct formed from **5** which inhibits LeuRS and prevents fungal protein synthesis.²⁰

It has also been established that the benzoxaboroles are better for antifungal activity than phenylboronic acid derivatives. This was carried out by investigating the fungicidal activity of 3-piperazine-bis(Benzoxaborole) (**6**) and 3-piperazine-bis(phenylboronic acid) (**7**) (Figure 9.8). A total of five filamentous fungal strains were investigated to understand the difference in activity between the two analogues. The bis(Benzoxaborole) analogue, **6**, was found to not only have better activity than its boronic acid counterpart, but even higher inhibitory activity than the antifungal drug amphotericin B, which is one of the current front line treatments for *C. neoformans* and was discussed in more detail in Chapter 1. The mechanism of action for these bis(benzoxaborole) analogues has still not been elucidated.^{4,21}

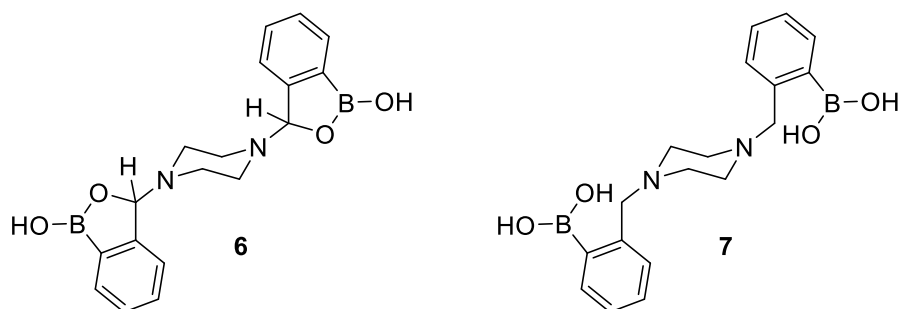


Figure 9.8. Bis(Benzoxaboroles) (**6** and **7**) have proven to have enhanced activity over their bis(phenylboronic acid) counterparts.²¹

Furthermore, when benzoxaboroles are mixed with α - or β -hydroxy carboxylic acids, they produced formulations, which were stable and could be used in the treatment of fungal nail infections, which is clinical referred to as onychomycosis. They are used as a topical nail treatment and in this manner they interact with hydroxyl acids and act as a drug delivery system, with the hydroxy acids performing the role of antifungal carriers. They also established that these oxaboroles could be used as antimicrobials in plant and meat protection.^{4, 22, 23}

In 2014 the FDA approved the first oxaborole antifungal drug, Tavaborole (**5**) under the trade name 'Kerydin'. This drug is used to treat onychomycosis. They have identified it acting as a LeuRS synthetase inhibitor, which leads to inhibition of fungal cell growth. Tavaborole can be used topically, which is an advantage as it reduces the change of systemic effect. It also showed little inhibition of CYP450 enzymes, so less chance of drug-drug interaction occurring and shows a similar safety and efficacy profile to other marketed topical antifungals.²⁴

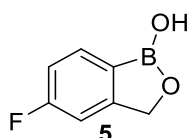


Figure 9.9. Tavaborole is the first FDA approved Benzoxaborole agent.

In a paper published in 2006 by Baker, *et al*, they investigated a number of oxaborole analogues and tested them against a number of fungal strains including *C. neoformans*. They found that **5** showed a MIC of 0.25 mg/L against *C. neoformans*, which shows a potential starting point for good activity.²⁵

9.1.5 Benzoxaboroles Mode of Action

Aminoacyl-tRNA synthetases allow for the attachment of an amino acid to a tRNA molecule (**A**) (Figure 9.10). This is done in the presence of ATP and via the formation of an enzyme-amino acid-AMP complex (**B**). The specific tRNA molecule for that amino acid binds to the complex, forms a new

covalent bond between the tRNA and the amino acid and releases AMP to give an enzyme-amino acid-tRNA complex (C). The tRNA-amino acid complex then detaches from the enzyme for use (D). During protein synthesis, it is tRNA molecules, with their corresponding amino acids, that are essential for protein synthesis, during the translation step of gene expression.²⁶ Blocking the active site of these enzymes can prevent gene translation via blockage of protein biosynthesis. Compound **5** was found to block the active site of this enzyme via the formation of a spiro ester adduct (Figure 9.7) with a tRNA molecule that is bound with the LeuRS. This binding prevents the enzyme's catalytic cycle from occurring, which blocks protein synthesis within the fungus.²⁰

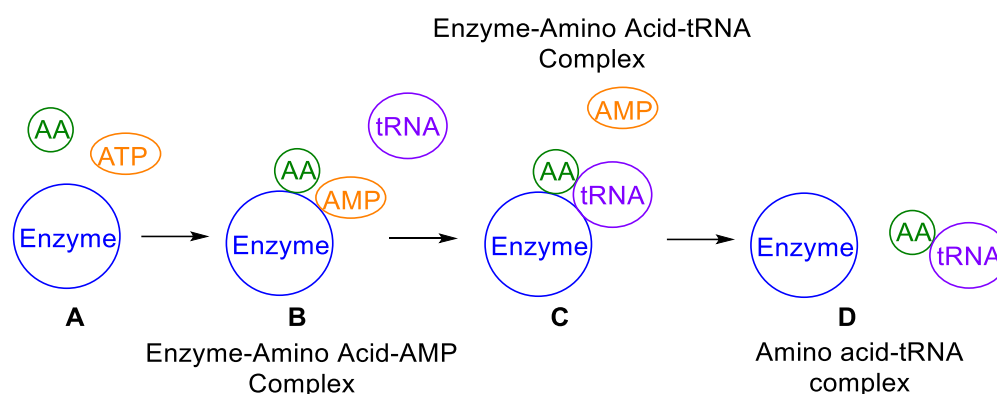


Figure 9.10. The synthesis of amino acid-tRNA complex using the enzyme LeuRS transferase. AA- amino acid.

However, one paper by Nocentini, *et al.*, highlights benzoxaborole binding to carbonic anhydrases (CAs) as being another potential mechanism of action. Here we discuss this mechanism of action in more detail, given the paper specifically evidences its mechanism of action in *C. neoformans*.²⁷ Carbonic anhydrases are Zinc metalloproteins that catalyse the reversible hydration of carbon dioxide to bicarbonate, via the removal of a proton.²⁸ Carbonic anhydrases present as attractive anti-infective targets for antibiotics and antifungals, and don't appear to possess issues of resistance seen with other drugs. Initially, there was an investigation into boronic acids as carbonic anhydrase inhibitors, and they noticed the boronic acid acted as a zinc binding group.²⁹ A marketed boronic acid peptidomimetic drug, Bortezomib, **8**, was shown to inhibit carbonic anhydrases in fungi and bacteria (Figure 9.11).²⁷ From this Nocentini, *et al* reported a benzoxaborole scaffold, that proved to bind to carbonyl anhydrases.³⁰

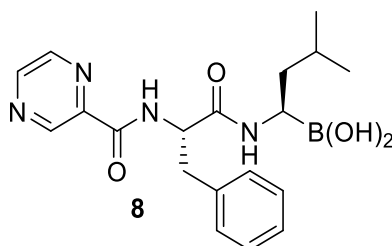


Figure 9.11. Bortezomib (**8**) is a marketed peptidomimetic drug, which has been found to inhibit carbon anhydrases.^{27, 29}

Within the active site of the *C. neoformans* carbonic anhydrases (Can2), it was observed that there were a large number of interactions of the benzoxaborole with both binding site residues and active site associated zinc ion (Figure 9.12).^{27,31} There are key interactions of the Zn^{2+} ion to three amino acid residues within the binding site, HIS 124, CYS 127 and CYS 68. There are also interactions from the boronic acid functionality to GLY 128, GLY 129, GLU 59 and ASP 70. Finally, there is also a pi-pi stacking interaction from the aryl ring of the benzoxaborole to the aromatic ring of TYR 109.

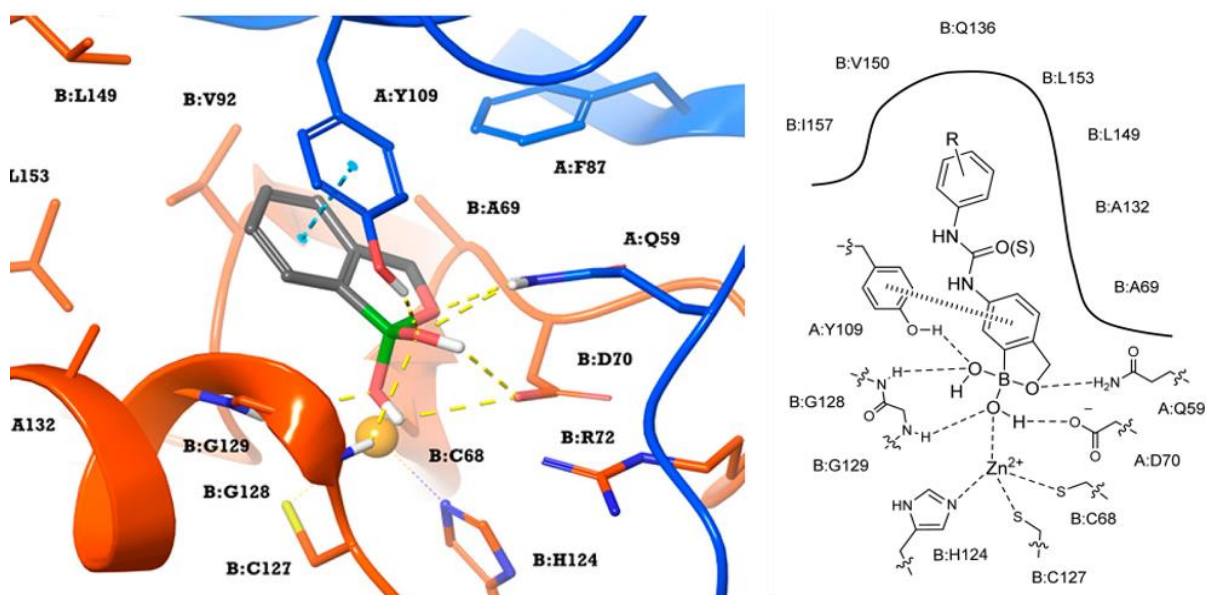


Figure 9.12. A representation of the binding mode of a benzoxaborole in the Can2 binding site. Reproduced from; *Benzoxaboroles as Efficient Inhibitors of the β -Carbonic Anhydrases from Pathogenic Fungi: Activity and Modeling Study*, Nocentini, A, et al.^{27,31}

9.1.6 Oxaborole Metabolism

Literature reveals very little information about the metabolic routes of benzoxaboroles, with more sources stating that Tavaborole, **5**, is extensively metabolised as has been proven by ^{14}C labelling.³² The 'Office of Clinical Pharmacology Review' does however propose a biotransformation pathway (Figure 9.13),³³ the results of which were gained from the topical administration of this drug onto mice. Not all of these metabolites have been confirmed in humans, however some have been identified through a radiolabelling study in a pharmacokinetic trial and are highlighted in blue. Based on this Tavaborole undergoes extensive metabolism.

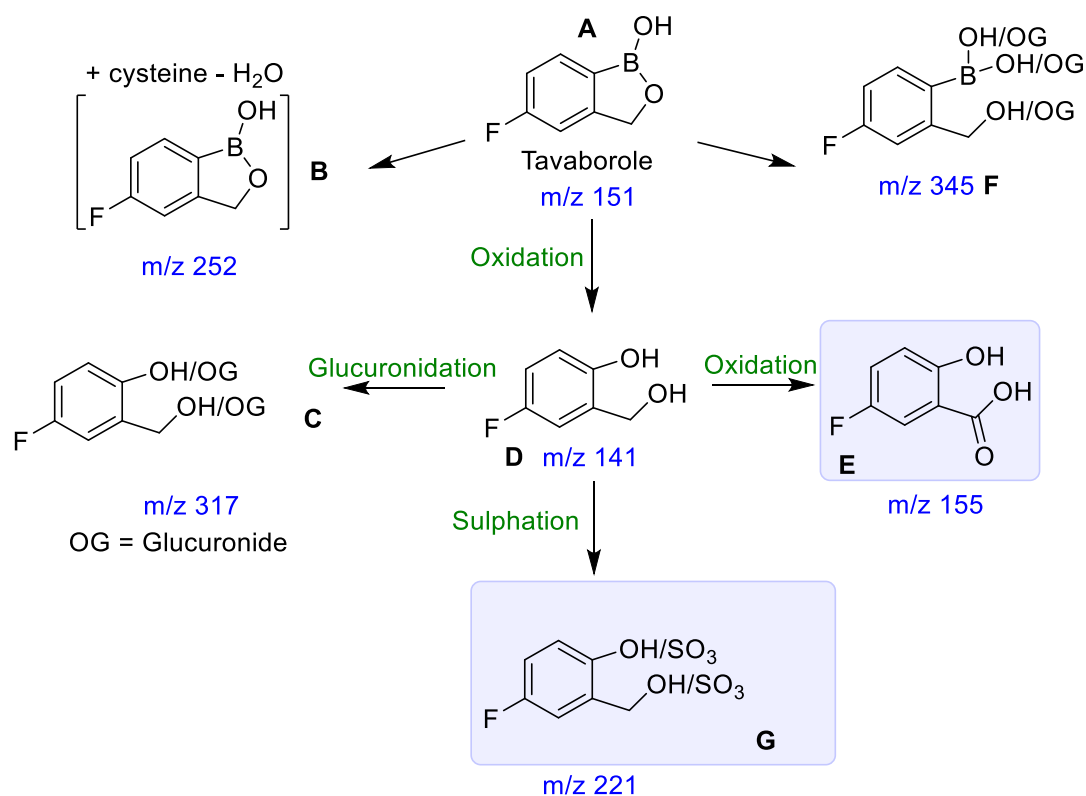


Figure 9.13. Tavaborole, a commercially available oxaborole is extensively metabolised. For structures **B,F,C** and **G** there is covalent attachment but precise structure is not known.

In vitro findings by Anacor suggested that the Cytochrome P450 (CYP450) enzymes were the main route of metabolism for the formation of the major metabolite, **D**, which is carried out through oxidation.³ There is also the further involvement of Flavinmonooxygenases (FMO) in the formation of metabolite **D**. *In vivo* studies which were carried out using ¹⁴C labelling revealed the metabolic profiles in both mice and rats showed that following administration there is oxaborole ring cleavage, as observed through the oxidation pathway described, and then sulphation **G** and glucuronidation **C**. They also identified a further metabolic product, which was an oxidation of the primary alcohol of **D** to a benzoic acid metabolite **E**, which was carried out through an oxidation pathway. In mice, they discovered all of these metabolites were at significant concentration in the blood and the most predominant metabolite excreted in the urine was the sulphur conjugate **G** at up to 35% of the dose. In rats the same metabolites were observed, with again the sulphur conjugate being the predominant metabolite observed at 62% of the dose.^{33, 34}

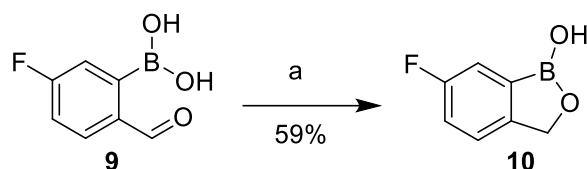
9.2 Results and Discussion

Due to the confirmed activity of benzoxaboroles against *C. neoformans* (MIC = 0.5 mg/L), it was decided that a series of analogues should be made in order to carry out in-house MIC testing.

9.2.1 Synthesis

9.2.1.1 Synthesis of 6-fluorobenzo[c][1,2]oxaborol-1(3H)-ol

This reaction was carried out via a step conversion of the (5-fluoro-2-formylphenyl)boronic acid (**9**), to the product, 6-fluorobenzo[c][1,2]oxaborol-1(3H)-ol (**10**). This reaction was carried out via a sodium borohydride reduction of the aldehyde in tandem with a ring closure of the resulting alcohol to generate a new five-membered heterocyclic ring. This reaction occurred in a moderate yield of 59% and gave the pure product as a white solid, which only required an aqueous/organic separation to purify, with microanalysis confirming that good purity was obtained.



Scheme 9.1. Reagents and Conditions: (a) NaBH₄ (1.0 eq.), ethanol/THF (4:1), 0 °C to room temperature, Overnight (59% yield);

There were a number of reasons to synthesise this compound. Firstly, to create a simple benzoxaborole derivative that could be tested for activity. Secondly, to prove that this ring closure could be carried out on a boronic acid, rather just boronic esters, as proposed in the literature. Finally, to have an example compound which could be used for comparative analysis of future analogues.

Confirmation of this product came from NMR data, with the ¹H NMR spectrum being particularly useful. We wanted to confirm that the peak observed at 9.35 ppm, which integrated to a single proton was the OH attached to the boron and not a potential impurity. Furthermore, the peak at 5.02 ppm, we wanted to confirm belonged to the CH₂ group, and wasn't the 2 OH protons of the unreacted starting material, which was predicted to be around 5 ppm. For this a D₂O shake was carried out, with the addition of deuterated water, to confirm the presence of exchangeable protons. In addition, absence of the aldehyde proton at around 10.4 ppm indicating loss of the aldehyde proton, further indicates conversion to the product has occurred (Figure 9.14).

Sample in DMSO

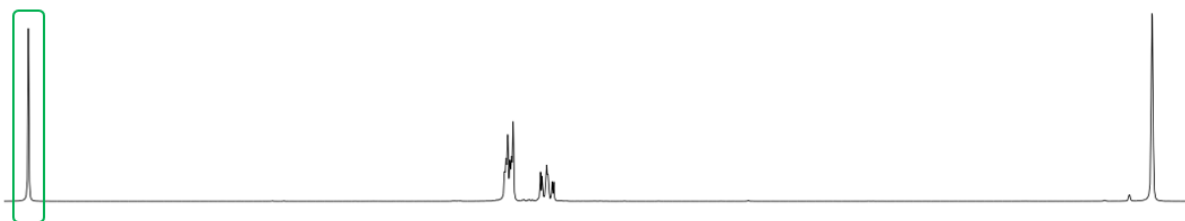
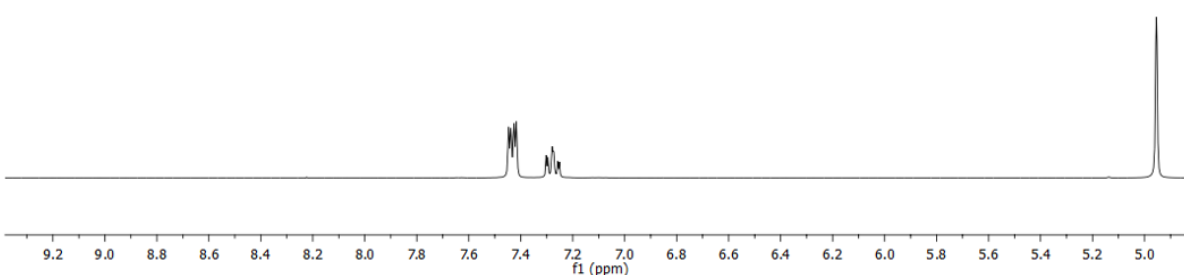
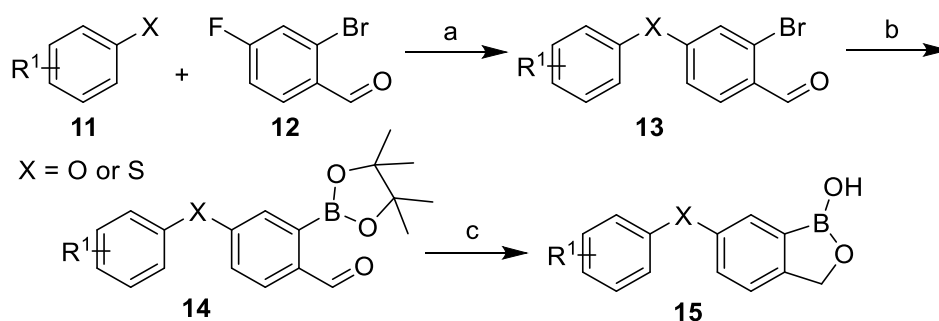
Sample in DMSO + D₂O

Figure 9.14. Stacked ¹H NMR spectra which show the presence of an exchangeable proton, which is proposed to be the OH attached to the boron atom.

This analogue was then tested for biological activity, but gave an MIC of >4 mg/L. Further literature investigation of this compound showed it had been synthesised previously and presented with an MIC of 32 mg/L, which explains why no activity was observed as it was beyond the cut-off set for our own assay.³

9.2.1.2 Synthesis of 2-bromo-4-phenoxybenzaldehyde and 2-bromo-4-(phenylthio)benzaldehyde Derivatives



Scheme 9.2. Proposed three step synthesis *Reagents and Conditions:* (a) K₂CO₃ (2.0 eq.), DMF, reflux, overnight); (b) Bis(pinacol-diboron (1.3 eq.), KOAc (2.0 eq.), dioxane, reflux, overnight); (c) NaBH₄ (1.0 eq.), ethanol/THF (4:1), 0 °C to room temperature, Overnight.³⁵

For this project, we started by making derivatives of a similar design to the Crisaborole structure seen in Figure 9.5. These compounds have reported synthetic routes in the literature. Initially, the first route tried was a three step synthesis (Scheme 9.2).³⁵

This proposed route was tried using both ether and thiol derivatives and resulted in no compound (**15**) being produced. The first step of the route (**13**), which will be discussed in more detail in a subsequent section, generally occurred in good yield. However, it was the second step, which involved a palladium catalysed borylation (**14**) did not proceed as expected. Whilst there was full consumption of the starting material, the TLC showed a very messy set of products. Even when column purification was attempted, which was very difficult due to the very non-polar nature of the compound, isolation of what appeared to be single spot, resulted in a mixture of two or more products by NMR.

The borylation conditions were checked by synthesising compound **16** (Figure 9.15). This reaction occurred in a moderate yield, with confirmation of the product via NMR and mass spec, where there was no bromine isotopic pattern present. A ring closure was attempted on this using the NaBH₄ reduction method indicated above, however purification was difficult due to polarity of the compound and number of products formed. However, NMR did indicate that the correct product had been formed, and that this route was worth pursuing.

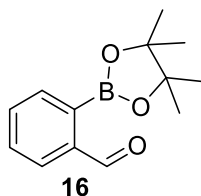
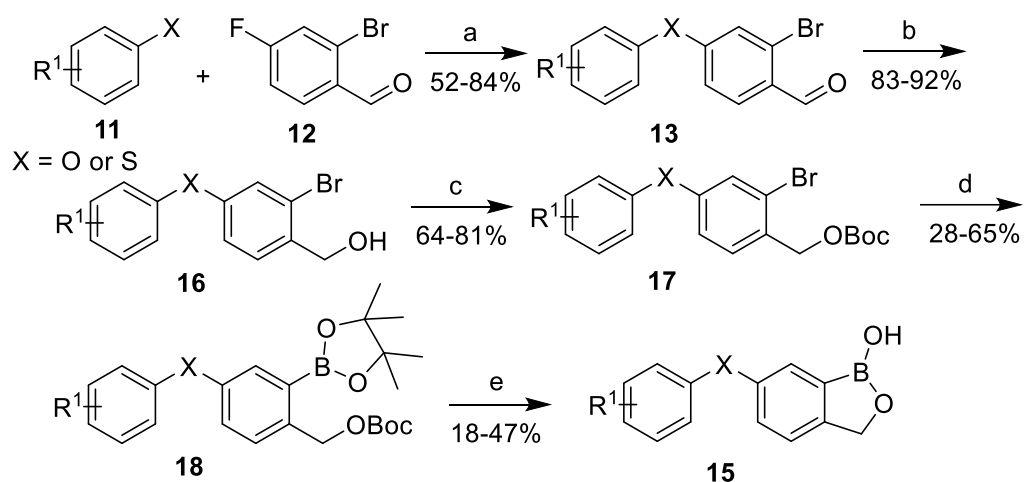


Figure 9.15. Compound **16** was synthesised to confirm the conditions for the borylation were suitable.

Despite not being able to confirm the synthesis of intermediate **14**, we decided to take the crude material and perform the aldehyde reduction to see if the product (**15**) could be isolated at the final step. For these reactions, full consumption of the starting material (**14**) was not observed, and further numerous products were also observed, meaning purification and analysis of the product was difficult.

A new route need to be established (Scheme 9.3). What we learnt from the previous route is that the first S_NAr step generally worked very well and that carrying out the borylation under the correct conditions could be a useable step.



Scheme 9.3. New five step synthesis. *Reagents and Conditions:* (a) K_2CO_3 (2.0 eq.), DMF, reflux, overnight (52 – 84% yield); (b) $NaBH_4$ (1.0 eq.), ethanol/THF (4:1), 0 °C to room temperature, overnight (83 – 92% yield); (c) Boc_2O (1.0 eq.), Et_3N (1.0 eq.) DMAP (0.1 eq.), DCM, room temperature, overnight (64 - 81% yield); (d) Bis(pinacol-diboron (1.3 eq.), KOAc (3.0 eq.), Pd(dppf)Cl₂ (0.05 eq) Dioxane, reflux, overnight (28 – 65% yield); (e) Acetone/ 2M HCl (1:1), 40 °C, overnight (18 – 47% yield).³⁵

9.2.1.3 Synthesis of 2-bromo-4-phenoxybenzaldehyde and 2-bromo-4-(phenylthio)benzaldehyde Derivatives

Making compound **13** involved a nucleophilic aromatic substitution (S_NAr) of the desired thiol or phenol (**11**) with the 2-bromo-4-fluorobenzaldehyde starting material (**12**).^{3, 35, 36} Overall this reaction occurred in good yield (52 – 84%) with no notable differences observed between using thiols or phenols (Table 9.1). This was also somewhat comparable to yields of around 90% that are reported in the literature, with small reductions in yield being attributable to protodeborylation or other palladium catalysed side reactions, giving rise to small amounts of unidentifiable products.³⁵

Table 9.1. Derivatives of compound **13** and their percentage yields.

	R ₁	X	Yield (%)
13a	4-F	O	65
13b	2-F	O	84
13c	2-OMe	O	52
13d	4-F	S	78
13e	2-F	S	82
13f	4-OMe	S	59
13g	3-OMe	O	58

The use of potassium carbonate as a base and DMF as a solvent is widely reported in the literature, with reports of reaction times generally decreasing as temperature is increased.^{37, 38} Another base

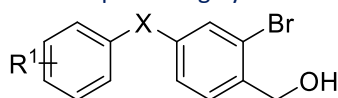
commonly used is NaH and is sometimes used when reactions with potassium carbonate fail and a stronger base is required. This reaction uses the electron withdrawing ability of the aldehyde *para* to the fluorine atom to allow for addition of a nucleophile. This generates a reactive Meisenheimer intermediate, which undergoes re-aromatisation with the loss of fluoride to give the desired product.³⁹

The reactions were generally very clean with only two product spots produced and the desired compound, which was the least polar spot, could be easily isolated. Confirmation of the product was carried out via ¹H NMR analysis, with additional aromatic peaks being observed (See Appendix, Figure 7A). ¹⁹F NMR was used to check for the absence of additional fluorine peaks in the derivatives, which proved the correct product had been made and confirmed purity. The 2-OMe (**13d**) derivative was more difficult to purify, with an additional spot sitting very close to the desired product spot, which was very difficult to separate. For this reason, it was continued crude into the next step.

9.2.1.4 Synthesis of (2-bromo-4-phenoxyphenyl)methanol and (2-bromo-4-(phenylthio)phenyl)methanol derivatives

This step involved a sodium borohydride reduction of the aldehyde (**13**) to produce a primary alcohol (**16**) and fortunately did not require the use of more reactive hydride sources, such as lithium aluminium hydride. Also, literature investigation of 2-bromobenzaldehyde derivatives showed that NaBH₄ was the favoured reagent for reduction, especially in analogues similar in structure to our own.^{3, 35, 40, 41} The reaction worked well when carried out in an ethanol/tetrahydrofuran mixture (4:1) for the solvent and then left overnight at room temperature.

Table 9.2. Derivatives of compound **16** and their percentage yields.



	R ₁	X	Yield (%)
16a	4-F	O	92
16b	2-F	O	83
16c	2-OMe	O	84
16d	4-F	S	96
16e	2-F	S	90

Excellent yields were observed for this reaction, with the sulfides proving to have slightly better yields than the ether derivatives. The reaction also occurred cleanly, with only a 1M NaOH based work up required to quench the NaBH₄ and remove the HCl salt produced. The lack of requirement for column

purification helped increase yields and synthesis time. For this reaction, it was simple to track formation for the product through TLC, by staining with KMnO_4 as the alcohol stains with a very yellow colour, whereas the aldehyde does not. From this method of monitoring the reaction, we could see that the reaction had almost gone to completion in only a couple of hours, however was left overnight to ensure full consumption of the starting material.

Identification of the product proved simple from the NMR due to some major shifts in peaks in both ^1H and ^{13}C NMR spectra, which are compared in figure 9.16. The aldehyde proton which occurs at 10.24 ppm in the starting material disappears and is replaced by the CH_2 proton at 4.67 ppm, with an integration of two protons. In the ^{13}C NMR spectrum we can also see the disappearance of the aldehyde carbon peak at 190.4 ppm, which is replaced by an aliphatic carbon of the primary alcohol at 64.6 ppm (See Appendix, Figure 7B).

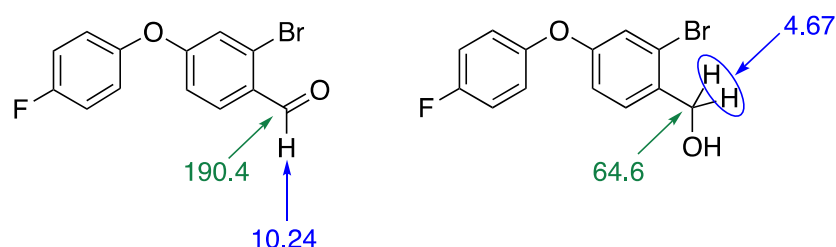
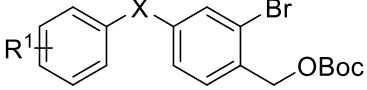


Figure 9.16. Significant changes found in the NMR spectra, confirming the synthesis of the product. ^1H NMR values highlighted in blue. ^{13}C NMR shifts highlighted in green.

9.2.1.5 Synthesis of 2-bromo-4-phenoxybenzyl tert-butyl carbonate and 2-bromo-4-(phenylthio)benzyl tert-butyl carbonate derivatives

Initially, the borylation step was attempted on the alcohol (**16**) intermediate directly. This resulted in incomplete conversion of the starting materials and formation of a number of products, which could not be identified. This was believed to be due to the presence of the free primary alcohol, which may interfere in the reaction. It is often reported that for Suzuki coupling reactions and Miyaura borylations that alcohols and amines are protected before the reaction occurs.^{40,42} A patent detailing the synthesis of crisaborole shows the acetate protection of the alcohol before carrying out the formylation step.⁴³

With this in mind, we decided to protect the alcohol using di-*tert*-butyl dicarbonate (Boc_2O). This is a common protecting group that is normally used in the protection of amines, but there is literature precedence for its use as an alcohol protecting group. Conditions similar to that described in a paper by Shang, *et. al* were used, which described the use of Boc_2O , trimethylamine, 4-Dimethylaminopyridine (DMAP) in DCM allowing for an overnight room temperature reaction.⁴⁴

Table 9.3. Derivatives of compound **17** and their percentage yields.


	R ₁	X	Yield (%)
17a	4-F	O	66
17b	2-F	O	79
17c	2-OMe	O	81
17d	4-F	S	64
17e	2-F	S	73

This reaction proceeds in generally good yield (64 – 81%) and the desired protected alcohol (**17**) was afforded after a simple work up to remove DMAP and column purification. This product was confirmed by the appearance of a distinctive *t*-butyl carbamate peak at around 1.50 ppm for all analogues. The ¹³C NMR spectra also showed 3 additional peaks at around 153, 82 and 27 ppm (see Appendix, Figure 7C).

9.2.1.6 5 Synthesis of tert-butyl (4-phenoxy-2-(4,4,5,5-tetramethyl-1,3,2-dioxaborolan-2-yl)benzyl) carbonate and tert-butyl (4-(phenylthio)-2-(4,4,5,5-tetramethyl-1,3,2-dioxaborolan-2-yl)benzyl) carbonate Derivatives

With the *t*-butyl carbamate protected analogues (**17**) in hand, the bromine could now be used to carry out a standard Miyaura borylation reaction. These conditions required a boron source, which was chosen as bis(pinacolato)diboron, which is a cheap and extensively used reagent, and within the group we had observed success with this reagent for producing boronic esters.⁴⁵ The reaction used potassium acetate as the base, Pd(dppf)Cl₂ as the catalyst and dioxane as the solvent. In this reaction, it is essential to use correct base otherwise a competing Suzuki reaction can occur causing homocoupling of the product (Figure 9.17).⁴⁵⁻⁴⁷

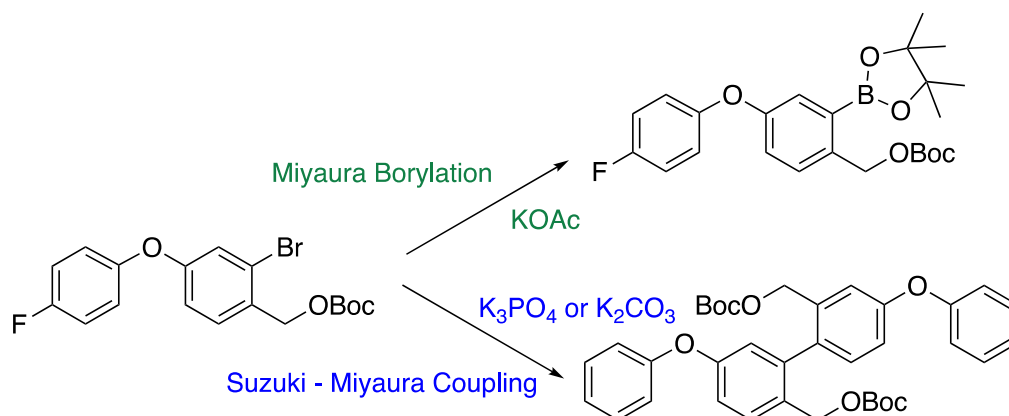


Figure 9.17. Selection of the correct base is essential during a borylation reaction, otherwise production of the undesired homocoupled product can occur.

This reaction occurs via a palladium (0) catalysed mechanism (Figure 9.18). The catalyst used was Pd(dppf)Cl₂, which is converted to the active Pd(0) catalyst **(A)** in order to take part in the catalytic cycle. Firstly, in the oxidative addition step, there is coordination of the aryl halide **(B)** to the Pd(0) catalyst to generate a Pd(II) species **(C)**. The species then undergoes ligand exchange with acetate to produce an acetoxypalladium intermediate **(D)**. This intermediate is very reactive and readily undergoes transmetalation with bis(pinacolato)diboron **(F)**. One of the boron atoms forms a dative covalent bond with the alkoxy anion **(G)**, which allows for the other boron to act as a nucleophile towards the palladium metal and coordinate **(H)**. Finally, the last reductive elimination step produces the desired arylboronate **(I)** and allows for the Pd(0) catalyst **(A)** to be regenerated.^{46,48}

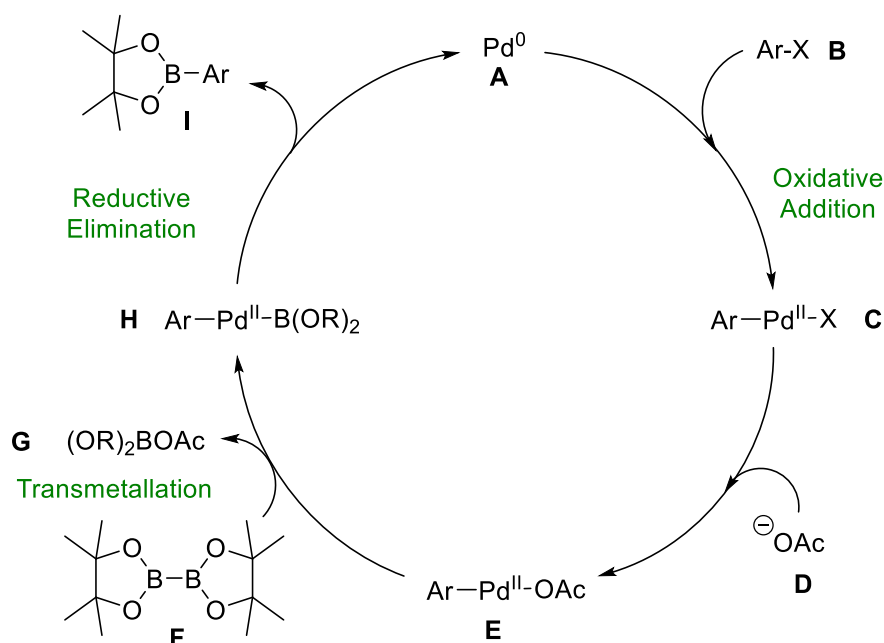
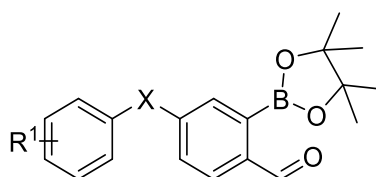


Figure 9.18. The Miyaura Borylation catalytic cycle. Reproduced from; *A decade advancement of transition metal-catalyzed borylation of aryl halides and sulfonates*, W. Chow et al.^{14,48}

Table 9.4. Derivatives of compound **18** and their percentage yields.



	R ₁	X	Yield (%)
18a	4-F	O	28
18b	2-F	O	62
18c	2-OMe	O	26
18d	4-F	S	65
18e	2-F	S	46

The reaction was carried out successfully, using the conditions described above. Yields for this reaction showed a decrease when compared with the previous step, but overall were acceptable (Table 9.4).

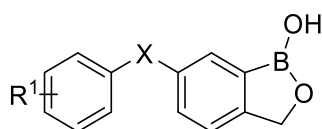
The reaction was generally clean, but it was difficult to observe whether the starting material had been fully consumed due to overlapping R_f values. If starting material was present this made column purification difficult as separation of the starting material and product resulted in mixed fractions and reduced yields in order to obtain a purer product.

Confirmation of the product (**18**) was carried out by NMR analysis and mass spectrometry. In the ^1H NMR spectrum we observed a large peak at around 1.33 ppm, which indicates the presence of the twelve pinacol protons, this is also accompanied by peaks at 84.1 and 24.8 ppm in the ^{13}C NMR spectra for the pinacol group carbons. Furthermore, mass spectrometry showed no bromine isotopic splitting pattern, confirming its absence in the product (See Appendix, Figure 7D).

9.2.1.7 Synthesis of 6-phenoxybenzo[*c*][1,2]oxaborol-1(3H)-ol and 6-(phenylthio)benzo[*c*][1,2]oxaborol-1(3H)-ol Derivatives

The last step of this sequence involved a tandem deprotection and ring closure mechanism. Initially, we considered the use of standard trifluoroacetic acid conditions to deprotect the *t*-butyl carbonate protecting group to generate the free alcohol.⁴⁹⁻⁵¹ This would mean that the boron pinacol ester would have to be cleaved in a separate step. In the literature, there are numerous examples of pinacol ester cleavage using sodium metaperiodate to cleave the ester and produce the boronic acid.⁵²⁻⁵⁵ Whilst sodium metaperiodate itself is relatively stable despite being hypervalent, it's the sodium iodate by-product that is formed that causes issues due to being heat, shock and friction explosive and may cause asthma.

There is however literature precedence for the removal of the boronate ester via HCl and acetone conditions, which would provide tandem deprotection conditions for the boc group, removing a step.⁵⁶ This was trialled using 2M HCl and acetone in a 1:1 ratio to obtain the product (**15**). The precise mechanism of this is not known.

Table 9.5. Derivatives of compound **15** and their percentage yields.

	R ₁	X	Yield (%)
15a	4-F	O	Not Completed
15b	2-F	O	35
15c	2-OMe	O	47
15d	4-F	S	Not Completed
15e	2-F	S	18

For this final step three products have been obtained so far with yields ranging from 18 – 47%. For compounds **15a** and **15d**, the reaction was successfully carried out, but in the ¹H NMR spectrum there appeared to be the presence of some of the Boc- deprotected starting material which was difficult to separate from the starting material, particularly due to the “streaky” nature of the final benzoxaborole product on the TLC plate. Identification of the product was carried out thanks to the disappearance of the twelve methyl protons of the pinacol groups from the ¹H NMR spectra at 1.33 ppm.

Compounds **15a** and **15d**, were not finished as the final step occurred in low yield and isolation of the pure product could not be obtained. The synthetic route needs to be repeated in order to obtain these compounds for testing.

9.2.2 Biological Data

Biological testing carried out as stated in Chapter 3, Section 3.2.3 and data given in Table 9.6.

Table 9.6. MIC data obtained for the Benzoxaborole class.

	R ₁	X	MIC (mg/L)
15a	4-F	O	-
15b	2-F	O	>4
15c	2-OMe	O	>4
15d	4-F	S	-
15e	2-F	S	0.25

Due to time constraints, it was difficult to synthesise a significant number of these compounds. Only one of the compounds synthesised so far showed any activity against *C. neoformans*, which was a sulfide (**15e**), whereas two ether compounds showed no activity at all. It is important to note that this isn't a huge sample size of compounds, so isn't indicative of how the classes of compounds will behave

as a whole. However, the MIC data obtained for **15e** is promising and warrants further investigation into this class as a novel template.

9.2.3 Predicted Metabolism

Table 9.10 Predicted data shows the benzoxaborole class has excellent DMPK properties. Values are colour coded with a traffic light system according to how good or bad a particular value is. Green – good, amber – acceptable/medium, red – poor.

	LogD _{7.4}	ClogP	Aqueous Solubility (μM)	Rat Heps CLint (μl/min/mg)	Human Mics CLint (μl/min/mg)	MPO
10	0.87	1.24	4209	112	6	5.2
15a	2.10	3.14	215	31	9	5.2
15b	2.11	3.14	195	33	8	5.2
15c	1.86	2.77	116	35	19	5.3

These compounds were submitted for predicted DMPK assessment and show excellent values (Table 9.10). These compound show a good LogD implying better gut penetration, however this may result in poorer CNS penetration. The aqueous solubility for these compounds is excellent and greatly improved upon the benzimidazole class. Metabolic clearance values are good overall and much improved compared with the benzisothiazolinone class.

When these compounds were set for measured DMPK assessment, no data was obtained due to an unknown error. However, we did obtain some predicted metabolic data through StarDrop. Unsurprisingly, for both compounds observed below, CYP3A4 carries out the most extensive metabolism of these compounds. It is the most abundant isoform that is expressed mainly in the liver and gastrointestinal tract and is known to be promiscuous in its metabolism. It metabolises a very diverse range of compounds and carries out an oxidation process in over half of all drugs that are administered.^{57, 58} Other CYP450 isoforms that show extensive metabolism of these compounds include 2C9 and 1A2.

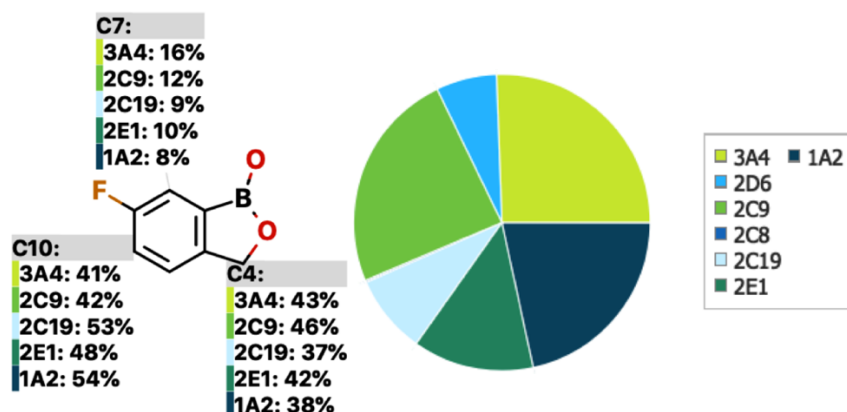


Figure 9.19. Predicted sites and extent of metabolism by CYP450 isoforms for Compound 10.

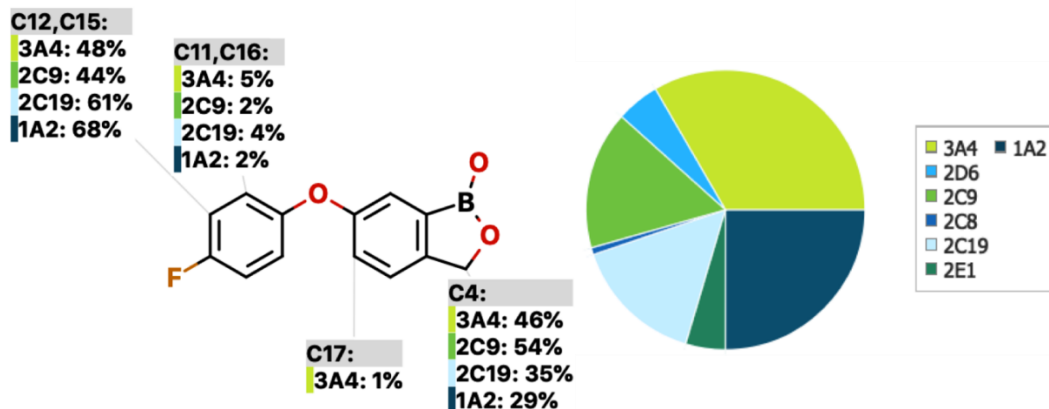


Figure 9.20. Predicted sites and extent of metabolism by CYP450 isoforms for Compound 15a.

9.3 Conclusion

A potential new class of *C. neoformans* agents has begun preliminary investigation. Work so far has established a new synthetic route, which allows for all intermediates to be purified easily and fully characterised, with removal of some potentially dangerous chemicals. Five analogues have been synthesised, with two awaiting further purification or re-synthesis to obtain the final product in improved purity. Compound 15e has shown a promising activity of 0.25 mg/L, which is comparable with the active benzimidazole class. No DMPK data has been obtained for these compounds, mainly due to them not having a suitable method to analyse the metabolism. Further work is required to address the final step, for the Boc deprotection, pinacol cleavage and ring closure, to ensure that occurs in higher yield with improved purity.

9.4 Future Work

In order to better assess the activity of these compounds against *C. neoformans*, work needs to be carried out to generate more analogues of both the thiol and ether classes, to allow for an improved understanding of the SAR. In the literature, there are also many reported routes of functionalisation of benzoxaboroles, which could be interesting to pursue for the development of other oxaboroles derivatives, in order to investigate whether substitution elsewhere on the core is tolerated in terms of biological activity.

Utilising the aldehyde functionality of the starting material we can add nucleophiles such as morpholine in a reductive amination style reaction. This would be followed by a ring closure to install the five-membered ring, in a single step, under mild conditions. This also generates a stereogenic centre, which could be biologically interesting for comparing activity of different enantiomers.^{8, 59}

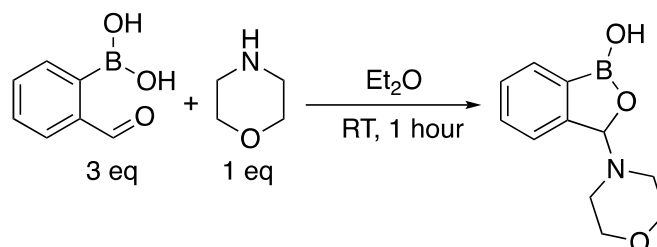


Figure 9.21. Reductive amination style conditions can be used to functionalise the 3-position of the benzoxaborole scaffold.⁵⁹

Also reported is the aryl functionalisation of the 3-position by taking 2-bromo-4-fluorobenzaldehyde and subjecting it to a Grignard reagent to generate a functionalised alcohol. Treatment with NaH, BuLi and B(OiPr)₃ allowed for the borylation at the 2-bromo position. The isopropyl groups are then cleaved under acidic conditions, generating the free boronic acid, which rapidly undergoes cyclisation to give the final oxaborole product.¹⁶

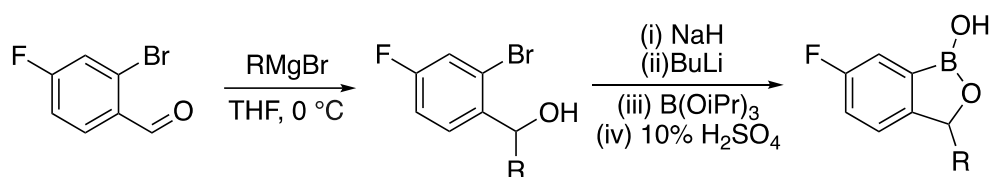


Figure 9.22. Grignard conditions to generate functionalised alcohol, followed by borylation and cyclisation can lead to functionalisation of the 3-position of the benzoxaborole scaffold.¹⁶

Furthermore, development of a more reliable final pinacol cleavage reaction is important to ensure better yields and purity. Two routes are of particular interest to attempt. Firstly, a paper by Sun *et al* highlights a two-step procedure for the deprotection of alkylpinacol boronate esters, by first creating a diethanolamine (DEA) adduct, which is then much more readily hydrolysed to the boronic acid.^{60, 61}

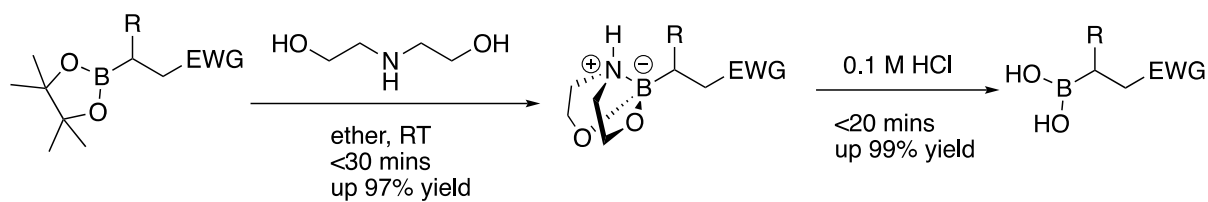


Figure 9.23. Cleavage of a pinacol boronate ester can be achieved via conversion into a more readily hydrolysed boronate ester.^{60, 61}

Another option is to carry out a transesterification using a simple boronic acid such as a phenyl boronic acid and using the aryl group as ‘sacrificial’ acceptor of the boronic ester, allowing the attachment of the boronic acid to the desired group.^{61, 62}

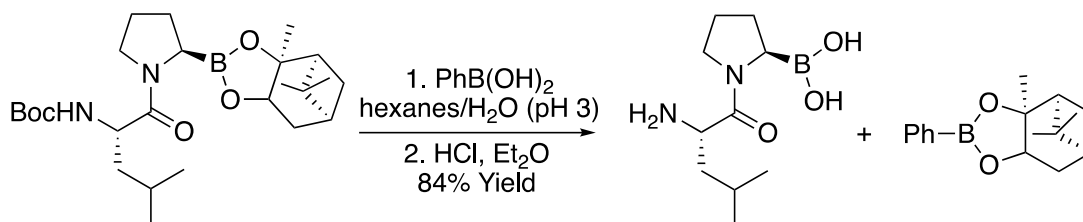


Figure 9.24. Cleavage of the boronic ester can also occur via a biphasic transesterification method in hexane and water.^{61, 62}

9.5 Experimental

9.5.1 General Experimental Details

For general experimental details please see Section 3.5.1, Chapter 3.

General Procedure A – S_NAr Coupling

To a flask at room temperature was added 2-bromo-4-fluorobenzaldehyde (1.0 eq.), DMF (0.64 M), potassium carbonate (2.0 eq.) and the desired phenol or thiol derivative (1.2 eq.) and the reaction refluxed overnight. The reaction was then cooled to room temperature, diluted with ethyl acetate, washed with saturated aq. NaHCO_3 solution, water and brine. Dried over magnesium sulphate and concentrated. The crude material was purified by column chromatography, eluting with 2% ethyl acetate in n-hexane to give the desired product.

General Procedure B – Reduction of aldehyde to alcohol

To a flask at 0 °C was added the desired 2-bromo-4-phenoxybenzaldehyde or 2-bromo-4-(phenylthio)benzaldehyde derivative (1.0 eq.), ethanol and THF (4:1) and sodium borohydride was added portion wise. The reaction was then stirred for 30 minutes at 0 °C, acidified carefully to pH 3 and then left to stir at room temperature overnight. The reaction was then quenched with NaHCO_3 , diluted with ethyl acetate, washed with saturated aq. NaHCO_3 solution, water, brine and dried over magnesium sulphate and concentrated to give the product, which was carried through into the next step with no further purification.

General Procedure C – di-*tert*-butyl carbamate protection of alcohol

To a flask at room temperature was added the desired (2-bromo-4-phenoxyphenyl)methanol or (2-bromo-4-(phenylthio)phenyl)methanol derivative (1.0 eq.), DCM, di-*tert*-butyl dicarbonate (1.0 eq.), trimethylamine (1.0 eq.) and DMAP (0.1 eq.) and the reaction stirred at room temperature overnight. The reaction was then cooled to room temperature, diluted with DCM, washed with water and brine, dried over magnesium sulphate and concentrated. The crude material was purified by column chromatography, eluting with 100% hexane to give the product.

General Procedure D – Suzuki Miyaura borylation

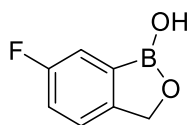
To a sealed tube at room temperature was added the desired 2-bromo-4-phenoxybenzyl *tert*-butyl carbonate or 2-bromo-4-(phenylthio)benzyl *tert*-butyl carbonate derivative (1.0 eq.), Dioxane, Bis(4,4,5,5-tetramethyl-[1,3]dioxolan-2-yl)borane (1.3 eq.), potassium acetate (3.0 eq.) and [1,1'-Bis(diphenylphosphino)ferrocene]dichloropalladium(II) (0.05 eq.) and the reaction heated to 80 °C

overnight. The reaction was then cooled to room temperature, diluted with ethyl acetate and filtered through celite. The filtrate was then washed with saturated aq. NaHCO₃ solution, water and brine, dried over magnesium sulphate and concentrated. The crude material was purified by column chromatography eluting with 100% hexane.

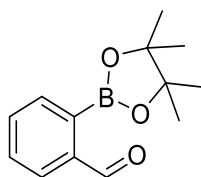
General Procedure E - Synthesis of 6-phenoxybenzo[c][1,2]oxaborol-1(3H)-ol and 6-(phenylthio)benzo[c][1,2]oxaborol-1(3H)-ol Derivatives

To a flask at room temperature was added the desired (4-phenoxy-2-(4,4,5,5-tetramethyl-1,3,2-dioxaborolan-2-yl)benzyl) carbonate or tert-butyl (4-(phenylthio)-2-(4,4,5,5-tetramethyl-1,3,2-dioxaborolan-2-yl)benzyl) carbonate derivative (1.0 eq.) acetone and 2M HCl and the reaction heated to 55 °C overnight. The reaction was then cooled to room temperature, diluted with ethyl acetate, washed with water and brine, dried over magnesium sulphate and concentrated. The crude product was purified via column chromatography eluting with 10% ethyl acetate in n-hexane to yield the product as a white solid.

6-Fluorobenzo[c][1,2]oxaborol-1(3H)-ol (**10**)

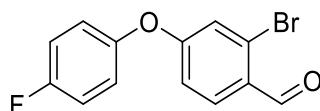


To a flask at 0 °C was added (5-fluoro-2-formylphenyl)boronic acid (1 eq.), ethanol and THF (4:1) and sodium borohydride (1 eq.) was added portion wise. The reaction was then stirred for 1 hour at 0 °C, acidified carefully to pH 3 and then left to stir at room temperature overnight. The reaction was then quenched with NaHCO₃, diluted with ethyl acetate, washed with saturated aq. NaHCO₃, water, brine and dried over magnesium sulphate and concentrated to give the product, which was carried through into the next step with no further purification to yield the product (**10**) (0.16 g, 59% yield) as a white solid. ¹H NMR (400 MHz, DMSO) δ 9.35 (s, 1H), 7.52 – 7.47 (m, 2H), 7.38 – 7.32 (m, 1H), 5.02 (s, 2H). ¹³C NMR (100 MHz, CDCl₃) δ 162.2 (d, *J* = 241.5 Hz), 150.0 (d, *J* = 1.9 Hz), 133.6, 123.9 (d, *J* = 8.2 Hz), 118.5 (d, *J* = 22.9 Hz), 116.4 (d, *J* = 20.0 Hz), 70.3. ¹⁹F NMR (376 MHz, CDCl₃) δ -116.8. HRMS (CI+, CH₄) Calculated for C₇H₇BFNO₂: 152.0554. Found [M+H]⁺: 152.0551 (Diff 2.18 ppm). ν_{max}/cm⁻¹: (solid) 3301 (m), .058 (m), 2959 (m), 2890 (m), 1476 (m), 1295 (m). MP: 112 – 114 °C. Predicted C(55.34%), H(3.98%); Obtained C(55.18%), H(3.93%).

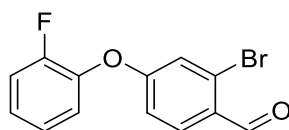
2-(4,4,5,5-Tetramethyl-1,3,2-dioxaborolan-2-yl)benzaldehyde (16)

To a flask at room temperature were added 2-bromobenzaldehyde (1.0 eq.), dioxane, Bis(4,4,5,5-tetramethyl-[1,3]dioxolan-2-yl)borane (2.0 eq.), potassium acetate (3.0 eq.) and bis(triphenylphosphine)palladium(II) dichloride (0.1 eq.), under a nitrogen atmosphere and the reaction was heated to 80 °C overnight. The reaction was then cooled to room temperature, diluted with ethyl acetate and filtered through celite. The filtrate was then washed with saturated aq. NaHCO₃, water and brine, dried over magnesium sulphate and concentrated. The crude material was purified by column chromatography eluting with 100% hexane to yield the product **(16)** (0.25 g, 40% yield) as a white solid. ¹H NMR (400 MHz, CDCl₃) δ 10.54 (s, 1H), 7.98 – 7.94 (m, 1H), 7.88 – 7.84 (m, 1H), 7.62 – 7.53 (m, 2H), 1.40 (s, 12H). ¹³C NMR (100 MHz, CDCl₃) δ 194.7, 141.3, 135.5, 132.9, 130.8, 128.0, 84.4, 24.9. One quaternary carbon not visible. HRMS (CI+, NH₃) Calculated for C₁₃H₁₈BO₃: 233.1344. Found [M+H]⁺: 233.1350 (Diff -2.59 ppm).

9.5.2.1 Synthesis of 2-bromo-4-phenoxybenzaldehyde and 2-bromo-4-(phenylthio)benzaldehyde Derivatives

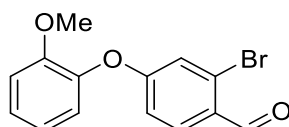
2-Bromo-4-(4-fluorophenoxy)benzaldehyde (13a)

General procedure A - Employed 4-fluorophenol to yield the product **(13a)** (1.12 g, 65% yield) as a white solid. ¹H NMR (400 MHz, CDCl₃) δ 10.24 (s, 1H), 7.89 (d, 1H, *J* = 8.6 Hz), 7.13 (m, 3H), 7.06 (m, 2H), 6.95 (dd, 1H, *J* = 8.6 & 2.6 Hz). ¹³C NMR (100 MHz, CDCl₃) δ 190.4, 163.3, 160.0 (d, *J* = 243.5 Hz), 150.2 (d, *J* = 3.2 Hz), 131.6, 128.5, 128.3, 122.2 (d, *J* = 8.4 Hz), 121.3, 117.0 (d, *J* = 23.7 Hz), 116.4. ¹⁹F NMR (376 MHz, CDCl₃) δ -116.8. HRMS (CI+, CH₄) Calculated for C₁₃H₉BrFO₂: 294.9764. Found [M+H]⁺: 294.9971 (Diff -2.22 ppm).

2-Bromo-4-(2-fluorophenoxy)benzaldehyde (13b)

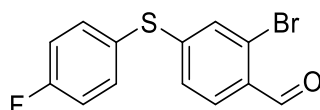
General procedure A - Employed 2-fluorophenol to yield the product **(13b)** (1.21 g, 84% yield) as a white solid. ^1H NMR (400 MHz, CDCl_3) δ 10.25 (s, 1H), 7.90 (d, 1H, $J = 8.7$ Hz), 7.30 – 7.22 (m, 2H), 7.22 – 7.17 (m, 2H), 7.16 (d, 1H, $J = 2.4$ Hz), 6.96 (dd, 1H, $J = 8.7$ & 2.4 Hz). ^{13}C NMR (100 MHz, CDCl_3) δ 190.4, 162.7, 154.5 (d, $J = 250.7$ Hz), 141.2 (d, $J = 13.0$ Hz), 131.5, 128.5 (d, $J = 5.5$ Hz), 127.0 (d, $J = 6.7$ Hz), 125.3 (d, $J = 4.1$ Hz), 123.3, 121.2, 117.6 (d, $J = 18.3$ Hz), 115.6. Not all carbons visible. HRMS (Cl^+ , CH_4) Calculated for $\text{C}_{13}\text{H}_9\text{BrFO}_2$: 294.9764. Found $[\text{M}+\text{H}]^+$: 294.9774 (Diff – 3.38 ppm).

2-Bromo-4-(2-methoxyphenoxy)benzaldehyde (13c)



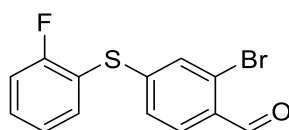
General procedure A - Employed 2-methoxyphenol to yield the product **(13c)** (0.79 g, 52% yield) as a white solid. Carried through crude into next step.

2-Bromo-4-((4-fluorophenyl)thio)benzaldehyde (13d)

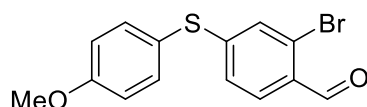


General procedure A - Employed 4-fluorothiophenol to yield the product **(13d)** (1.20 g, 78% yield) as a white solid. ^1H NMR (400 MHz, CDCl_3) δ 10.23 (s, 1H), 7.75 (d, 1H $J = 8.3$ Hz), 7.54 (dd, 2H, $J = 8.7$ & 7.3 Hz), 7.25 (s, 1H), 7.17 (dd, 2H, $J = 9.7$ & 8.7 Hz), 7.05 (d, 1H, $J = 8.7$ Hz). ^{13}C NMR (100 MHz, CDCl_3) δ 190.8, 163.7 (d, $J = 249.9$ Hz), 149.0, 137.2 (d, $J = 8.5$ Hz), 130.6, 130.3, 129.9, 127.7, 125.4, 125.2 (d, $J = 3.6$ Hz), 117.4 (d, $J = 21.9$ Hz).

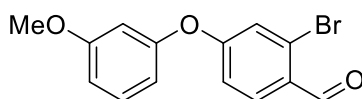
2-Bromo-4-((2-fluorophenyl)thio)benzaldehyde (13e)



General procedure A - Employed 2-fluorothiophenol to yield the product **(13e)** (0.94 g, 82% yield) as a yellow solid. ^1H NMR (400 MHz, CDCl_3) δ 10.24 (s, 1H), 7.76 (d, 1H, $J = 8.4$ Hz), 7.59 – 7.53 (m, 1H), 7.52 – 7.46 (m, 1H), 7.32 (s, 1H), 7.23 – 7.20 (m, 2H), 7.10 (d, 1H, $J = 8.4$ Hz). ^{13}C NMR (100 MHz, CDCl_3) δ 190.9, 162.7 (d, $J = 250.5$ Hz), 146.9, 140.4, 135.8, 132.4 (d, $J = 8.0$ Hz), 130.9, 130.0, 127.6, 125.7, 125.4 (d, $J = 4.0$ Hz), 117.3 (d, $J = 18.8$ Hz), 116.9 (d, $J = 23.1$ Hz). HRMS (Cl^+ , CH_4) Calculated for $\text{C}_{13}\text{H}_{11}\text{BrFO}_2\text{S}$: 324.9693. Found $[\text{M}+\text{H}]^+$: 324.9696 (Diff – 1.16 ppm).

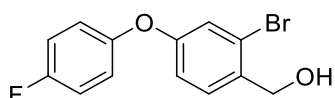
2-Bromo-4-((4-methoxyphenyl)thio)benzaldehyde (13f)

General procedure A - Employed 4-methoxythiophenol to yield the product **(13f)** (1.13 g, 59% yield) as a cream solid. ^1H NMR (400 MHz, CDCl_3) δ 10.22 (s, 1H), 7.72 (d, 1H, $J = 8.1$ Hz), 7.48 (d, 2H, $J = 8.7$ Hz), 7.21 (d, 1H, $J = 8.7$ Hz), 7.04 – 7.01 (m, 2H), 6.99 (d, 1H, $J = 8.7$ Hz), 3.87 (s, 3H). ^{13}C NMR (100 MHz, CDCl_3) δ 190.9, 161.1, 150.7, 137.1, 132.6, 130.2, 129.8, 129.6, 127.7, 119.8, 114.6, 55.5. HRMS (Cl^+ , CH_4) Calculated for $\text{C}_{14}\text{H}_{12}\text{BrO}_2\text{S}$: 322.9736. Found $[\text{M}+\text{H}]^+$: 322.9736 (Diff – 0.06 ppm).

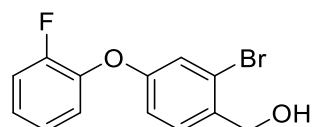
2-Bromo-4-(3-methoxyphenoxy)benzaldehyde (13g)

General procedure A - Employed 3-methoxyphenol to yield the product **(13g)** (0.44 g, 58% yield) as a white solid. ^1H NMR (400 MHz, CDCl_3) δ 10.25 (s, 1H), 7.89 (d, 1H, $J = 8.8$ Hz), 7.32 (dd, 1H, $J = 8.4$ & 8.1 Hz), 7.18 (d, 1H, $J = 2.3$ Hz), 6.99 (dd, 1H, $J = 8.4, 2.4$ & 0.5 Hz), 6.80 (ddd, 1H, $J = 8.1, 2.6$ & 0.5 Hz), 6.63 (dd, 1H, $J = 2.4$ & 2.6 Hz), 6.58 - 6.56 (m, 1H), 3.81 (s, 3H). ^{13}C NMR (100 MHz, CDCl_3) δ 190.5, 163.1, 161.3, 155.5, 131.5, 130.7, 128.5, 128.3, 121.7, 116.8, 112.5, 111.1, 106.6, 55.5.

9.5.2.2 Synthesis of (2-bromo-4-phenoxyphenyl)methanol and (2-bromo-4-(phenylthio)phenyl)methanol derivatives

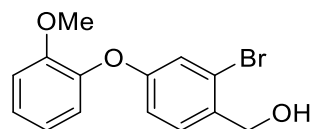
(2-Bromo-4-(4-fluorophenoxy)phenyl)methanol (16a)

General procedure B - Employed 2-bromo-4-(4-fluorophenoxy)benzaldehyde **(13a)** to yield the product **(16a)** (1.01 g, 92% yield) as a white solid. ^1H NMR (400 MHz, CDCl_3) δ 7.40 (d, 1H, $J = 8.5$ Hz), 7.15 (d, 1H, $J = 1.9$ Hz), 7.05 (m, 2H), 6.98 (m, 2H), 6.91 (dd, 1H, $J = 8.5$ & 1.9 Hz), 4.67 (s, 2H). ^{13}C NMR (100 MHz, CDCl_3) δ 159.2 (d, $J = 244.5$ Hz), 157.8, 152.0 (d, $J = 2.6$ Hz), 134.3, 130.1, 123.1, 122.0, 121.0 (d, $J = 8.0$ Hz), 117.1, 116.6 (d, $J = 23.6$ Hz), 64.6. HRMS (Cl^+ , CH_4) Calculated for $\text{C}_{13}\text{H}_{11}\text{BrFO}_2$: 296.9921. Found $[\text{M}+\text{H}]^+$: 296.9920 (Diff – 1.19 ppm).

(2-Bromo-4-(2-fluorophenoxy)phenyl)methanol (16b)

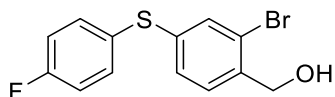
General procedure B – Employed 2-bromo-4-(2-fluorophenoxy)benzaldehyde (**13b**) to yield the product (**16b**) (1.21 g, 83% yield) as a white solid. ^1H NMR (400 MHz, CDCl_3) δ 7.42 (d, 1H, $J = 8.5$ Hz), 7.23 – 7.06 (m, 5H), 6.93 (dd, 1H, $J = 8.5$ & 2.1 Hz). ^{13}C NMR (100 MHz, CDCl_3) δ 157.5, 154.4 (d, $J = 247.0$ Hz), 142.9, 134.4, 130.0, 125.7 (d, $J = 6.5$ Hz), 124.9 (d, $J = 3.7$ Hz), 123.1, 122.4, 121.1, 121.0, 117.3 (d, $J = 18.9$ Hz), 64.5.

(2-Bromo-4-(2-methoxyphenoxy)phenyl)methanol (16c)



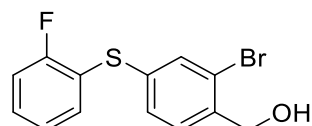
General procedure B – Employed 2-bromo-4-(2-methoxyphenoxy)benzaldehyde (**13c**) to yield the product (**16c**) (0.69 g, 84% yield) as a white solid. ^1H NMR (400 MHz, CDCl_3) δ 7.41 (d, 1H, $J = 8.5$ Hz), 7.27 – 7.22 (m, 1H), 7.21 (d, 1H, $J = 2.2$ Hz), 6.98 (dd, 1H, $J = 8.5$ & 2.2 Hz), 6.72 – 6.67 (m, 1H), 6.60 – 6.56 (m, 2H), 4.72 (s, 2H), 3.78 (s, 3H). ^{13}C NMR (100 MHz, CDCl_3) δ 161.1, 157.6, 157.3, 134.5, 130.3, 130.0, 123.0, 122.7, 117.8, 111.3, 109.6, 105.3, 64.6, 55.4. HRMS (Cl^+ , CH_4) Calculated for $\text{C}_{14}\text{H}_{14}\text{BrO}_2$: 309.0121. Found $[\text{M}+\text{H}]^+$: 309.0129 (Diff -2.75 ppm).

(2-Bromo-4-((4-fluorophenyl)thio)phenyl)methanol (16d)



General procedure B – Employed 2-bromo-4-((4-fluorophenyl)thio)benzaldehyde (**16d**) to yield the product (**16d**) (1.26g, 96% yield) as a white solid. ^1H NMR (400 MHz, CDCl_3) δ 7.43 – 7.35 (m, 4H), 7.17 (dd, 1H, $J = 8.1$ & 1.8 Hz), 7.08 – 7.03 (m, 2H), 4.69 (s, 2H). ^{13}C NMR (100 MHz, CDCl_3) δ 162.8 (d, $J = 248.8$ Hz), 138.3, 138.1, 134.9 (d, $J = 8.2$ Hz), 132.6, 129.3, 218.8, 128.4, 123.0, 116.7 (d, $J = 22.4$ Hz), 64.6. HRMS (Cl^+ , NH_3) Calculated for $\text{C}_{13}\text{H}_8\text{BrFS}$: 294.9587. Found $[\text{M}-\text{H}_2\text{O}+\text{H}]^+$: 297.9589 (Diff -1.63 ppm).

(2-Bromo-4-((2-fluorophenyl)thio)phenyl)methanol (16e)

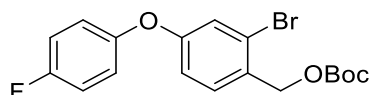


General procedure B – Employed 2-bromo-4-((2-fluorophenyl)thio)benzaldehyde (**13e**) to yield the product (**16e**) (0.85 g, 90% yield) as a white solid. ^1H NMR (400 MHz, CDCl_3) δ 7.47 (s, 1H), 7.41 (d, 1H, $J = 7.4$ Hz), 7.34 (m, 2H), 7.25 (m, 1H), 7.14 (m, 1H), 7.12 (d, 1H, $J = 7.4$ Hz), 4.72 (s, 2H). ^{13}C NMR (100

MHz, CDCl₃) δ 138.6, 136.1, 134.4, 133.4, 130.3 (d, J = 8.0 Hz), 129.3 (d, J = 7.2 Hz), 124.9 (d, J = 3.8 Hz), 122.9, 121.1 (d, J = 17.2 Hz), 116.3 (d, J = 22.3 Hz), 64.8. not all quaternary carbons visible.

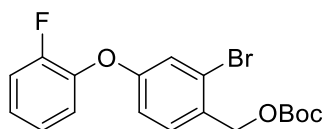
9.5.2.3 Synthesis of 2-bromo-4-phenoxybenzyl tert-butyl carbonate and 2-bromo-4-(phenylthio)benzyl tert-butyl carbonate derivatives

2-bromo-4-(4-fluorophenoxy)benzyl tert-butyl carbonate (17a)



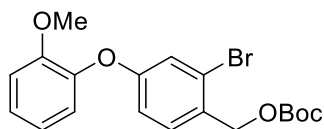
General procedure C – Employed (2-bromo-4-(4-fluorophenoxy)phenyl)methanol (**16a**) to yield the product (**17a**) (0.88 g, 66% yield) as a white solid. ¹H NMR (400 MHz, CDCl₃) δ 7.38 (d, 1H, J = 8.5 Hz), 7/15 (d, 1H, J = 2.2 Hz), 7.06 (m, 2H), 6.99 (m, 2H), 6.90 (dd, 1H, J = 8.5 & 2.2 Hz), 5.15 (s, 2H), 1.50 (s, 9H). ¹³C NMR (100 MHz, CDCl₃) δ 159.4 (d, J = 242.9 Hz), 158.4, 153.3, 151.8 (d, J = 2.6 Hz), 131.9, 129.6, 124.1, 121.9, 121.1 (d, J = 8.0 Hz), 116.8 (d, J = 15.2 Hz), 116.5, 82.7, 67.3, 27.8.

2-Bromo-4-(2-fluorophenoxy)benzyl tert-butyl carbonate (17b)

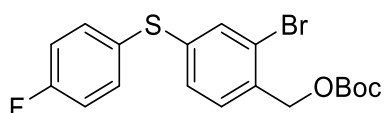


General procedure C – Employed (2-bromo-4-(2-fluorophenoxy)phenyl)methanol (**16b**) to yield the product (**17b**) (1.07 g, 79% yield) as a white solid. ¹H NMR (400 MHz, CDCl₃) δ 7.38 (d, 1H, J = 8.4 Hz), 7.23 – 7.06 (m, 5H), 6.91 (dd, 1H, J = 8.4 & 2.5 Hz), 5.15 (s, 2H), 1.50 (s, 9H). ¹³C NMR (100 MHz, CDCl₃) δ 158.1, 154.4 (d, J = 251.5 Hz), 153.3, 142.6 (d, J = 11.7 Hz), 131.1, 129.6, 125.8 (d, J = 6.9 Hz), 124.9 (d, J = 3.8 Hz), 124.1, 122.5, 121.0, 117.3 (d, J = 18.2 Hz), 115.9, 82.6, 67.6, 27.8. HRMS (ES+) Calculated for C₁₈H₁₈BrFNaO₄: 419.0265. Found [M+Na]⁺: 419.0259 (Diff 1.27 ppm).

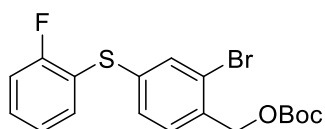
2-Bromo-4-(2-methoxyphenoxy)benzyl tert-butyl carbonate (17c)



General procedure C – Employed (2-bromo-4-(2-methoxyphenoxy)phenyl)methanol (**17b**) to yield the product (**17c**) (0.74 g, 81% yield) as a white solid. ¹H NMR (400 MHz, CDCl₃) δ 7.39 (d, 1H, J = 8.5 Hz), 7.26 – 7.21 (m, 2H), 6.96 (dd, 1H, J = 8.5 & 2.5 Hz), 6.73 – 6.69 (m, 1H), 6.60 – 6.56 (m, 2H), 5.16 (s, 2H), 3.79 (s, 3H), 1.51 (s, 9H). ¹³C NMR (100 MHz, CDCl₃) δ 161.1, 157.8, 157.3, 153.2, 131.1, 130.3, 129.7, 124.0, 122.6, 117.6, 11.4, 109.9, 105.4, 82.5, 67.8, 55.4, 27.8. HRMS (ES+) Calculated for C₁₉H₂₁BrNaO₅: 431.0465. Found [M+Na]⁺: 431.0479 (Diff -3.44 ppm).

2-Bromo-4-((4-fluorophenyl)thio)benzyl tert-butyl carbonate (17d)

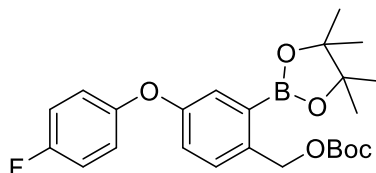
General procedure C – Employed (2-bromo-4-((4-fluorophenyl)thio)phenyl)methanol (**16d**) to yield the product (**17d**) (1.07 g, 64% yield) as a white solid. ^1H NMR (400 MHz, CDCl_3) δ 7.45 – 7.40 (m, 2H), 7.38 (d, 1H, $J = 1.8$ Hz), 7.31 (d, 1H, $J = 8.1$ Hz), 7.13 (dd, 1H, $J = 8.1$ & 8.1 Hz), 7.10 – 7.05 (m, 2H), 5.13 (s, 2H), 1.50 (s, 9H). ^{13}C NMR (100 MHz, CDCl_3) δ 162.9 (d, $J = 251.2$ Hz), 153.2, 139.5, 135.3 (d, $J = 8.8$ Hz), 133.2, 132.4, 130.0, 128.4 (d, $J = 3.4$ Hz), 127.9, 123.8, 116.8 (d, $J = 21.8$ Hz), 82.7, 67.6, 27.8. HRMS (ES+) Calculated for $\text{C}_{18}\text{H}_{18}\text{BrFNaO}_3\text{S}$: 435.0036. Found $[\text{M}+\text{Na}]^+$: 435.0027 (Diff 2.13 ppm).

2-Bromo-4-((2-fluorophenyl)thio)benzyl tert-butyl carbonate (17e)

General procedure C – Employed (2-bromo-4-((2-fluorophenyl)thio)phenyl)methanol (**16e**) to yield the product (**17e**) (0.82 g, 73% yield) as a white solid. ^1H NMR (400 MHz, CDCl_3) δ 7.45 (s, 1H), 7.35 (m, 3H), 7.20 (d, 1H, $J = 8.3$ Hz), 7.13 (m, 2H), 5.15 (s, 2H), 1.50 (s, 9H). ^{13}C NMR (100 MHz, CDCl_3) δ 161.7 (d, $J = 245.9$ Hz), 153.2, 137.3, 134.8, 133.7, 133.2, 130.6 (d, $J = 7.6$ Hz), 130.1, 128.7, 125.0 (d, $J = 3.7$ Hz), 123.6, 120.8, 116.3 (d, $J = 21.4$ Hz), 82.8, 67.6, 27.8.

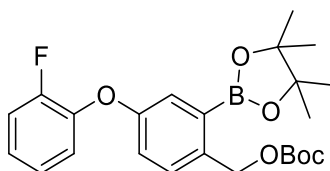
9.5.2.4 Synthesis of tert-butyl (4-phenoxy-2-(4,4,5,5-tetramethyl-1,3,2-dioxaborolan-2-yl)benzyl) carbonate and tert-butyl (4-(phenylthio)-2-(4,4,5,5-tetramethyl-1,3,2-dioxaborolan-2-yl)benzyl) carbonate Derivatives

Tert-butyl (4-(4-fluorophenoxy)-2-(4,4,5,5-tetramethyl-1,3,2-dioxaborolan-2-yl)benzyl) carbonate (18a)



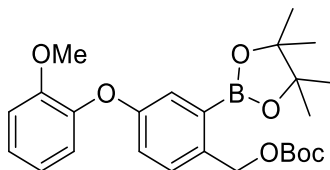
General procedure D – Employed 2-bromo-4-(4-fluorophenoxy)benzyl tert-butyl carbonate (**17a**) to yield the product (**18a**) (0.27 g, 28% yield) as a clear oil. ^1H NMR (400 MHz, CDCl_3) δ 7.45 (d, 1H, $J = 2.5$ Hz), 7.35 (d, 1H, $J = 8.4$ Hz), 6.99 (m, 3H), 6.93 (m, 2H), 5.32 (s, 2H), 1.49 (s, 9H), 1.32 (s, 12H). ^{13}C NMR (100 MHz, CDCl_3) δ 158.6 (d, $J = 238.1$ Hz), 156.6, 153.5, 153.2 (d, $J = 2.6$ Hz), 136.4, 130.5, 126.0, 120.9, 120.1 (d, $J = 8.5$ Hz), 118.1, 116.2 (d, $J = 23.0$ Hz), 84.0, 81.8, 68.1, 27.8, 24.8. HRMS (ES+) Calculated for $\text{C}_{24}\text{H}_{30}^{11}\text{BF}^{23}\text{NaO}_6$: 467.2012. Found $[\text{M}+\text{Na}]^+$: 467.2019 (Diff -1.46 ppm).

Tert-butyl (4-(2-fluorophenoxy)-2-(4,4,5,5-tetramethyl-1,3,2-dioxaborolan-2-yl)benzyl) carbonate (18b)



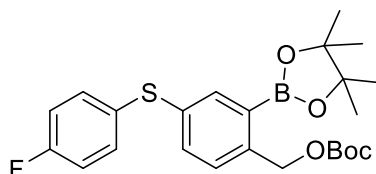
General procedure D – Employed 2-bromo-4-(2-fluorophenoxy)benzyl tert-butyl carbonate (**17b**) to yield the product (**18b**) (0.74 g, 62% yield) as a white solid. ^1H NMR (400 MHz, CDCl_3) δ 7.50 (d, 1H, $J = 2.8$ Hz), 7.35 (d, 1H, $J = 8.5$ Hz), 7.20 – 7.14 (m, 1H), 7.10 – 7.05 (m, 2H), 7.01 – 6.95 (m, 2H), 5.33 (s, 2H), 1.49 (s, 9H), 1.32 (s, 12 H). ^{13}C NMR (100 MHz, CDCl_3) δ 156.4, 154.2 (d, $J = 248.3$ Hz), 153.5, 144.1 (d, $J = 11.4$ Hz), 136.4, 130.5, 125.3, 124.6 (d, $J = 3.9$ Hz), 124.5 (d, $J = 6.8$ Hz), 121.3, 119.8, 117.8, 117.0 (d, $J = 19.1$ Hz), 84.0, 81.7, 68.1, 27.9, 24.8. HRMS (ES+) Calculated for $\text{C}_{24}\text{H}_{30}\text{BFNaO}_6$: 466.2048. Found $[\text{M}+\text{Na}]^+$: 466.2049 (Diff – 0.29 ppm).

Tert-butyl (4-(2-methoxyphenoxy)-2-(4,4,5,5-tetramethyl-1,3,2-dioxaborolan-2-yl)benzyl) carbonate (18c)



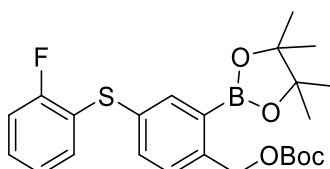
General procedure D – Employed 2-bromo-4-(2-methoxyphenoxy)benzyl tert-butyl carbonate (**17c**) to yield the product (**18c**) (0.11 g, 26% yield) as a white solid. ^1H NMR (400 MHz, CDCl_3) δ 7.52 (d, 1H, $J = 1.8$ Hz), 7.37 (d, 1H, $J = 8.4$ Hz), 7.20 (dd, 1H, $J = 9.0$ & 8.5 Hz), 7.05 (dd, 1H, $J = 8.4$ & 1.8 Hz), 6.63 (d, 1H, $J = 8.5$ Hz), 6.55 – 6.51 (m, 2H), 5.33 (s, 2H), 3.77 (s, 3H), 1.50 (s, 9H), 1.32 (s, 12H). ^{13}C NMR (100 MHz, CDCl_3) δ 160.9, 158.7, 155.9, 153.4, 136.6, 135.3, 130.5, 130.0, 126.8, 121.6, 110.5, 108.8, 104.3, 83.9, 81.7, 68.1, 55.3, 27.9, 24.8, 25.0. HRMS (ES+) Calculated for $\text{C}_{25}\text{H}_{33}\text{BNaO}_7$: 479.2212. Found $[\text{M}+\text{Na}]^+$: 479.2214 (Diff -0.56 ppm).

Tert-butyl (4-((4-fluorophenyl)thio)-2-(4,4,5,5-tetramethyl-1,3,2-dioxaborolan-2-yl)benzyl) carbonate (18d)



General procedure D – Employed 2-bromo-4-((4-fluorophenyl)thio)benzyl tert-butyl carbonate (**17d**) to yield the product (**18d**) (0.68 g, 65% yield) as a white solid. ^1H NMR (400 MHz, CDCl_3) δ 7.83 (d, 1H, $J = 2.0$ Hz), 7.34 – 7.27 (m, 4H), 7.03 – 6.97 (m, 1H), 5.33 (s, 2H), 1.49 (s, 1H), 1.33 (s, 12H). ^{13}C NMR (100 MHz, CDCl_3) δ 162.3 (d, $J = 246.9$ Hz), 153.4, 140.6, 138.0, 135.4, 133.4 (d, $J = 8.2$ Hz), 133.1, 131.3, 130.7 (d, $J = 3.2$ Hz), 129.2, 116.3 (d, $J = 22.0$ Hz), 84.1, 81.9, 68.0, 27.9, 24.9. HRMS (CI+, CH_4) Calculated for $\text{C}_{24}\text{H}_{30}\text{BFNaO}_5\text{S}$: 482.1820. Found $[\text{M}+\text{Na}]^+$: 482.1800 (Diff - 0.04 ppm).

Tert-butyl (4-((2-fluorophenyl)thio)-2-(4,4,5,5-tetramethyl-1,3,2-dioxaborolan-2-yl)benzyl) carbonate (18e)

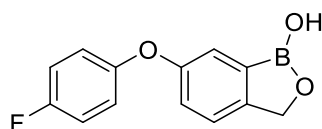


General procedure D – Employed 2-bromo-4-((2-fluorophenyl)thio)benzyl tert-butyl carbonate (**17e**) to yield the product (**18e**) (0.42 g, 46% yield) as a white solid. ^1H NMR (400 MHz, CDCl_3) δ 7.90 (s, 1H), 7.35 (s, 2H), 7.27 – 7.19 (m, 1H), 7.18 – 7.13 (m, 1H), 7.10 – 7.01 (m, 2H), 5.34 (s, 2H), 1.49 (s, 9H), 1.33

(s, 12H). ^{13}C NMR (100 MHz, CDCl_3) δ 171.0, 160.8 (d, $J = 247.6$ Hz), 153.4, 141.1, 139.1, 134.1, 132.9, 132.8 (d, $J = 19.1$ Hz), 132.7 (d, $J = 1.2$ Hz), 129.2, 128.9 (d, $J = 7.7$ Hz), 124.1 (d, $J = 3.8$ Hz), 123.3 (d, $J = 17.8$ Hz), 115.8 (d, $J = 22.1$ Hz), 84.1, 83.5, 27.8, 24.8. HRMS (ES+) Calculated for $\text{C}_{24}\text{H}_{30}\text{BFNaO}_5\text{S}$: 483.1783. Found $[\text{M}+\text{H}]^+$: 483.1787 (Diff – 0.81 ppm).

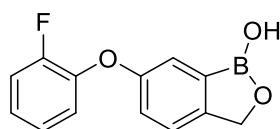
9.5.2.5 Synthesis of 6-phenoxybenzo[*c*][1,2]oxaborol-1(3*H*)-ol and 6-(phenylthio)benzo[*c*][1,2]oxaborol-1(3*H*)-ol Derivatives

6-(4-Fluorophenoxy)benzo[*c*][1,2]oxaborol-1(3*H*)-ol (**15a**)



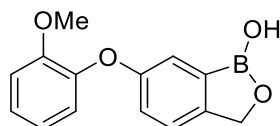
General procedure E – Employed *tert*-butyl (4-(4-fluorophenoxy)-2-(4,4,5,5-tetramethyl-1,3,2-dioxaborolan-2-yl)benzyl) (**18a**) carbonate to yield the product (**15a**) (0.039 g, 35% yield) as a white solid. ^1H NMR (400 MHz, CDCl_3) δ 7.27 (s, 1H), 7.23 (d, 1H, $J = 8.1$ Hz), 7.12 – 7.01 (m, 2H), 6.57 (d, 1H, $J = 8.1$ Hz), 6.52 – 6.47 (m, 2H), 5.85 (s, 1H), 5.01 (s, 2H), 3.69 (s, 3H). ^{13}C NMR (100 MHz, CDCl_3) δ 161.0, 158.7, 156.6, 148.5, 130.2, 122.9, 122.5, 120.2, 110.9, 108.9, 104.9, 71.1, 55.4. LRMS (Cl^+ , CH_4) Calculated for $\text{C}_{13}\text{H}_{18}\text{BO}_3$: 244.03. Found $[\text{M}+\text{NH}_4]^+$: 244.10. $\nu_{\text{max}}/\text{cm}^{-1}$: (solid) 3309 (m), 3058 (m), 2980 (m), 2935 (m), 1498 (m), 1266 (m). MP: 120 – 123 °C.

6-(2-Fluorophenoxy)benzo[*c*][1,2]oxaborol-1(3*H*)-ol (**15b**)



General procedure E – Employed *tert*-butyl (4-(2-fluorophenoxy)-2-(4,4,5,5-tetramethyl-1,3,2-dioxaborolan-2-yl)benzyl) carbonate (**18b**) to yield the product as a crude white solid (**15b**) that could not be purified fully. Larger scale synthesis required to isolate compound.

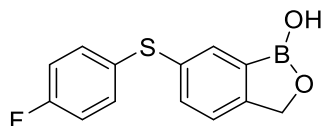
6-(2-Methoxyphenoxy)benzo[*c*][1,2]oxaborol-1(3*H*)-ol (**15c**)



General procedure E – Employed *tert*-butyl (4-(2-methoxyphenoxy)-2-(4,4,5,5-tetramethyl-1,3,2-dioxaborolan-2-yl)benzyl) carbonate (**18c**) to yield the product (**15c**) (0.013 g, 46% yield) as a white solid. ^1H NMR (400 MHz, CDCl_3) δ 7.27 (s, 1H), 7.23 (s, 1H), 7.18 – 7.07 (m, 2H), 6.57 (d, 1H, $J = 8.1$ Hz), 6.52 – 6.47 (m, 2H), 5.85 (s, 1H), 5.01 (s, 2H), 3.69 (s, 3H). ^{13}C NMR (100 MHz, CDCl_3) δ 161.0, 158.7,

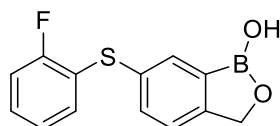
156.6, 148.5, 130.2, 122.9, 122.5, 120.2, 110.9, 108.9, 104.9, 71.1, 55.4. Not all carbons visible. HRMS (CI+, CH₄) Calculated for C₁₄H₁₄BO₄: 257.0980. Found [M+H]⁺: 257.0982 (Diff – 1.08 ppm).

6-((4-Fluorophenyl)thio)benzo[*c*][1,2]oxaborol-1(3*H*)-ol (15d)



General procedure E – Employed tert-butyl (4-((4-fluorophenyl)thio)-2-(4,4,5,5-tetramethyl-1,3,2-dioxaborolan-2-yl)benzyl) carbonate (**18d**) to yield the product as a crude white solid (**15d**) that could not be purified fully. Larger scale synthesis required to isolate compound.

6-((2-Fluorophenyl)thio)benzo[*c*][1,2]oxaborol-1(3*H*)-ol (15e)



General procedure E – Employed tert-butyl (4-((2-fluorophenyl)thio)-2-(4,4,5,5-tetramethyl-1,3,2-dioxaborolan-2-yl)benzyl) carbonate (**18e**) to yield the product (**15e**) (0.043 g, 18% yield) as a white solid. ¹H NMR (400 MHz, CDCl₃) δ 7.72 (s, 1H), 7.50 (d, 1H, *J* = 8.1 Hz), 7.30 (d, 1H, *J* = 8.1 Hz), 7.28 – 7.22 (m, 2H), 7.12 – 7.03 (m, 2H), 5.09 (s, 2H), 5.07 (s, 1H). ¹³C NMR (100 MHz, CDCl₃) δ 161.1 (d, *J* = 245.7 Hz), 153.0, 147.1, 134.0, 133.4, 133.3 (d, *J* = 3.1 Hz), 129.4 (d, *J* = 8.0 Hz), 124.8 (d, *J* = 3.7 Hz), 122.9 (d, *J* = 17.5 Hz), 122.1, 116.0 (d, *J* = 23.4 Hz), 71.0. Carbon attached to boron not visible. ν_{max}/cm⁻¹: (solid) 3391 (m), 2980 (m), 2885 (m), 1640 (s), 1429 (m), 1381 (m), 1268 (s). MP: 122 – 125 °C. Purity HPLC (Method A) 97.1%, R_t = 10.08 min.

9.6 References

1. A.WOL, Anti-Wolbachia Consortium, <https://awol.lstmed.ac.uk/>, June 2019).
2. B. Nare, S. Wring, C. Bacchi, B. Beaudet, T. Bowling, R. Brun, D. Chen, C. Ding, Y. Freund, E. Gaukel, A. Hussain, K. Jarnagin, M. Jenks, M. Kaiser, L. Mercer, E. Mejia, A. Noe, M. Orr, R. Parham, J. Plattner, R. Randolph, D. Rattendi, C. Rewerts, J. Sligar, N. Yarlett, R. Don and R. Jacobs, *Antimicrob. Agents Chemother.*, 2010, **54**, 4379-4388.
3. *US Pat.*, US7582621B2, 2006.
4. A. Adamczyk-Woźniak, K. M. Borys and A. Sporzyński, *Chem. Rev.*, 2015, **115**, 5224-5247.
5. A. Adamczyk-Woźniak, M. Jakubczyk, A. Sporzyński and G. Żukowska, *Inorg. Chem. Comm.*, 2011, **14**, 1753-1755.
6. J. Sravan Kumar, M. A. Alam, S. Gurrapu, G. Nelson, M. Williams, M. A. Corsello, J. L. Johnson, S. C. Jonnalagadda and V. R. Mereddy, *J. Heterocycl. Chem.*, 2013, **50**, 814-820.
7. J. W. Tomsho, A. Pal, D. G. Hall and S. J. Benkovic, *ACS Med. Chem. Lett.*, 2011, **3**, 48-52.
8. A. Adamczyk-Woźniak, I. Madura, A. H. Velders and A. Sporzyński, *Tetrahedron Lett.*, 2010, **51**, 6181-6185.
9. S. J. Baker, J. W. Tomsho and S. J. Benkovic, *Chem. Soc. Rev.*, 2011, **40**, 4279-4285.
10. P. C. Trippier and C. McGuigan, *Med. Chem. Commun.*, 2010, **1**, 183-198.
11. Q.-H. Hu, R.-J. Liu, Z.-P. Fang, J. Zhang, Y.-Y. Ding, M. Tan, M. Wang, W. Pan, H.-C. Zhou and E.-D. Wang, *Sci. Rep.*, 2013, **3**, 2475-2475.
12. Y. Xia, K. Cao, Y. Zhou, M. R. K. Alley, F. Rock, M. Mohan, M. Meewan, S. J. Baker, S. Lux, C. Z. Ding, G. Jia, M. Kully and J. J. Plattner, *Bioorg. Med. Chem. Lett.*, 2011, **21**, 2533-2536.
13. S. M. Hoy, *Am. J. Clin. Dermatol.*, 2017, **18**, 837-843.
14. A. Davis and T. James, in *Functional Synthetic Receptors*, Wiley-VCH, 2019, DOI: 10.1002/352760572X, pp. 45-109.
15. M. Dowlut and D. G. Hall, *J. Am. Chem. Soc.*, 2006, **128**, 4226-4227.
16. D. S. Gunasekera, D. J. Gerold, N. S. Aalderks, J. S. Chandra, C. A. Maanu, P. Kiprof, V. V. Zhdankin and M. V. R. Reddy, *Tetrahedron*, 2007, **38**, 9401-9405.
17. J. S. Kumar, C. M. Bashian, M. A. Corsello, S. C. Jonnalagadda and V. R. Mereddy, *Tetrahedron Lett.*, 2010, **51**, 4482-4485.
18. *Eur. Pat.*, WO1995GB01206, 1995.
19. *US Pat.*, US5512246A, 1993.
20. F. L. Rock, W. Mao, A. Yaremchuk, M. Tukalo, T. Crépin, H. Zhou, Y.-K. Zhang, V. Hernandez, T. Akama, S. J. Baker, J. J. Plattner, L. Shapiro, S. A. Martinis, S. J. Benkovic, S. Cusack and M. R. K. Alley, *Science*, 2007, **316**, 1759-1761.
21. A. Adamczyk-Woźniak, K. M. Borys, I. D. Madura, S. Michałek and A. Pawełko, *Tetrahedron*, 2013, **69**, 8936-8942.
22. A. B. Shapiro, N. Gao, L. Hajec and D. C. McKinney, *Analytical Biochemistry*, 2012, **431**, 48-53.
23. *US Pat.*, US201461991821P, 2015.
24. N. Sharma and D. Sharma, *J. Pharmacol. Pharmacother.*, 2015, **6**, 236-239.
25. S. J. Baker, Y.-K. Zhang, T. Akama, A. Lau, H. Zhou, V. Hernandez, W. Mao, M. R. K. Alley, V. Sanders and J. J. Plattner, *J. Med. Chem.*, 2006, **49**, 4447-4450.
26. V. Rajendran, P. Kalita, H. Shukla, A. Kumar and T. Tripathi, *Int. J. Biol. Macromol.*, 2018, **111**, 400-414.
27. A. Nocentini, R. Cadoni, S. del Prete, C. Capasso, P. Dumy, P. Gratteri, C. T. Supuran and J.-Y. Winum, *ACS Med. Chem. Lett.*, 2017, **8**, 1194-1198.
28. C. T. Supuran, *Nat. Rev. Drug Discov.*, 2008, **7**, 168-181.
29. J.-Y. Winum, A. Innocenti, A. Scozzafava, J.-L. Montero and C. T. Supuran, *Bioorg. Med. Chem. Lett.*, 2009, **17**, 3649-3652.
30. V. Alterio, R. Cadoni, D. Esposito, D. Vullo, A. D. Fiore, S. M. Monti, A. Caporale, M. Ruvo, M. Sechi, P. Dumy, C. T. Supuran, G. D. Simone and J.-Y. Winum, *Chem. Commun.*, 2016, **52**, 11983-11986.
31. C. Schlicker, R. A. Hall, D. Vullo, S. Middelhaufe, M. Gertz, C. T. Supuran, F. A. Mühlischlegel and C. Steegborn, *J. Mol. Biol.*, 2009, **385**, 1207-1220.
32. A. K. Gupta and S. G. Versteeg, *Expert Rev. Clin. Pharmacol.*, 2016, **9**, 1145-1152.

33. Anacor, Kerydin, https://www.accessdata.fda.gov/drugsatfda_docs/nda/2014/204427Orig1s000MedR.pdf).
34. B. Hill, Pharmacology and Toxicology review of Kerydin, https://www.accessdata.fda.gov/drugsatfda_docs/nda/2008/022157s000PharmR.pdf, June 2019).
35. D. Ding, Y. Zhao, Q. Meng, D. Xie, B. Nare, D. Chen, C. J. Bacchi, N. Yarlett, Y.-K. Zhang, V. Hernandez, Y. Xia, Y. Freund, M. Abdulla, K.-H. Ang, J. Ratnam, J. H. McKerrow, R. T. Jacobs, H. Zhou and J. J. Plattner, *ACS Med. Chem. Lett.*, 2010, **1**, 165-169.
36. *Eur. Pat.*, WO201409555A1, 2013.
37. E. Dubost, V. Babin, F. Benoist, A. Hébert, P. Barbey, C. Chollet, J.-P. Bouillon, A. Manrique, G. Pieters, F. Fabis and T. Cailly, *Org. Lett.*, 2018, **20**, 6302-6305.
38. B. D. Palmer, H. S. Sutherland, A. Blaser, I. Kmentova, S. G. Franzblau, B. Wan, Y. Wang, Z. Ma, W. A. Denny and A. M. Thompson, *J. Med. Chem.*, 2015, **58**, 3036-3059.
39. F. Terrier, *Modern Nucleophilic Aromatic Substitution* Wiley-VCH, 2013.
40. *US Pat.*, US8039450B2, 2009.
41. T. Akama, S. J. Baker, Y.-K. Zhang, V. Hernandez, H. Zhou, V. Sanders, Y. Freund, R. Kimura, K. R. Maples and J. J. Plattner, *Bioorg. Med. Chem. Lett.*, 2009, **19**, 2129-2132.
42. C. Liskey, unpublished work.
43. *Eur. Pat.*, WO2018224923A1, 2018.
44. R. Shang, Z. Huang, X. Xiao, X. Lu, Y. Fu and L. Liu, *Adv. Synth. Catal.*, 2012, **354**, 2465-2472.
45. G. A. Molander, S. L. J. Trice, S. M. Kennedy, S. D. Dreher and M. T. Tudge, *J. Am. Chem. Soc.*, 2012, **134**, 11667-11673.
46. T. Ishiyama, M. Murata and N. Miyaura, *J. Org. Chem.*, 1995, **60**, 7508-7510.
47. C. C. Johansson Seechurn, M. O. Kitching, T. J. Colacot and V. Snieckus, *Angew. Chem. Int. Ed. Engl.*, 2012, **51**, 5062-5085.
48. W. Kin Chow, O. Ying Yuen, P. Choy, C. So, C. Po Lau, W. Tak Wong and F. Y. Kwong, *RSC Adv.*, 2013, **3**, 12518-12539.
49. S. Saito and S. Kobayashi, *J. Am. Chem. Soc.*, 2006, **128**, 8704-8705.
50. D. Uraguchi, M. Torii and T. Ooi, *ACS Catal.*, 2017, **7**, 2765-2769.
51. *US Pat.*, US2009068827, 2009.
52. C. C. Tzschucke, J. M. Murphy and J. F. Hartwig, *Am. Chem. Soc.*, 2007, **9**, 761-764.
53. T. Yamamoto, A. Ishibashi and M. Sugimoto, *Org. Lett.*, 2017, **19**, 886-889.
54. J. M. Murphy, C. C. Tzschucke and J. F. Hartwig, *Org. Lett.*, 2007, **9**, 757-760.
55. N. Zhang, T. Wang, X. Wu, C. Jiang, F. Chen, W. Bai and R. Bai, *RSC Adv.*, 2018, **8**, 3803-3808.
56. Y. Xiong, J. Guo, M. R. Candelore, R. Liang, C. Miller, Q. Dallas-Yang, G. Jiang, P. E. McCann, S. A. Qureshi, X. Tong, S. S. Xu, J. Shang, S. H. Vincent, L. M. Tota, M. J. Wright, X. Yang, B. B. Zhang, J. R. Tata and E. R. Parmee, *J. Med. Chem.*, 2012, **55**, 6137-6148.
57. I. F. Sevrioukova and T. L. Poulos, *Dalton Trans.*, 2013, **42**, 3116-3126.
58. F. P. Guengerich, *Annu. Rev. Pharmacol. Toxicol.*, 1999, **39**, 1-17.
59. A. Sporyński, M. Lewandowski, P. Rogowska and M. K. Cyrański, *Appl. Organometal. Chem*, 2005, **19**, 1202-1203.
60. J. Sun, M. T. Perfetti and W. L. Santos, *J. Org. Chem.*, 2011, **76**, 3571-3575.
61. D. G. Hall, *Boronic Acids: Preparation and Applications in Organic Synthesis and Medicine*, Wiley-VCH, 2005.
62. D. Matteson, in *Boronic Acids*, Wiley-VCH, 2006, DOI: 10.1002/3527606548, ch. 8, pp. 305-342.

Appendix

1. Thioether Data

Figure 1A - ^1H NMR - $\text{S}_{\text{N}}\text{Ar}$ Nitroaniline Example

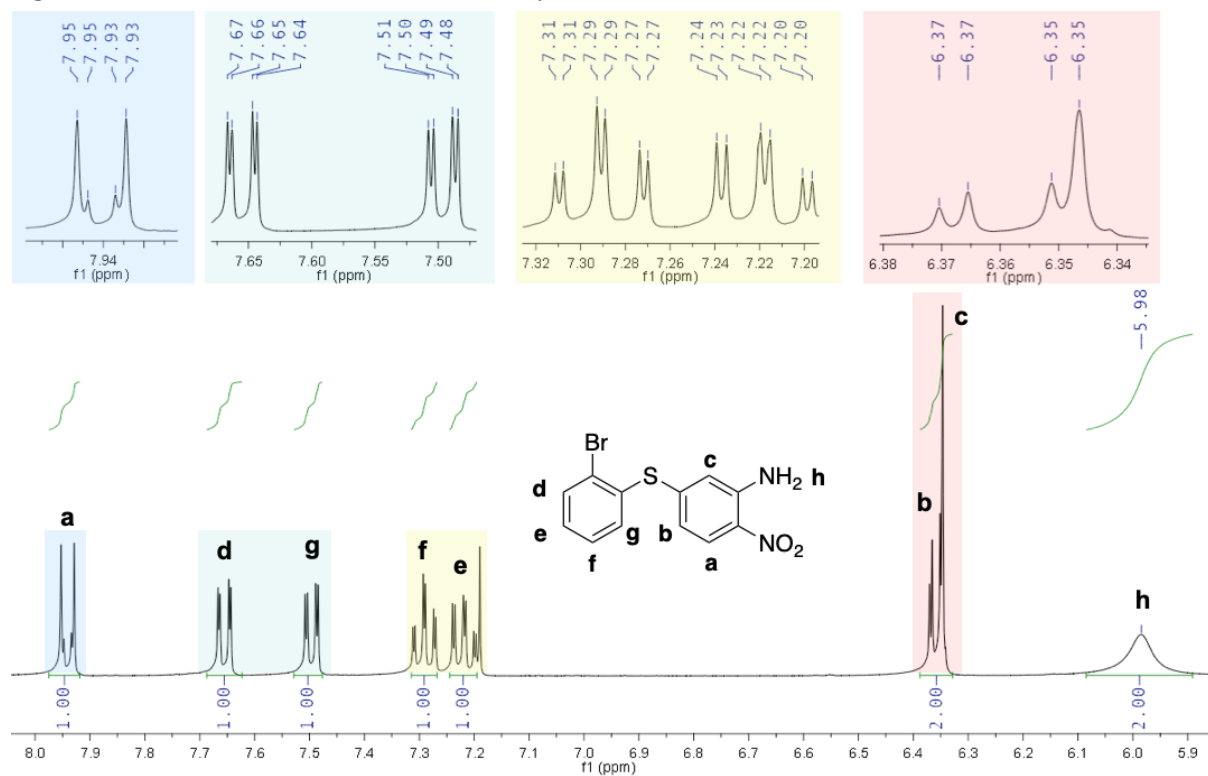


Figure 1B - ^1H NMR - SnCl_2 Reduction Example

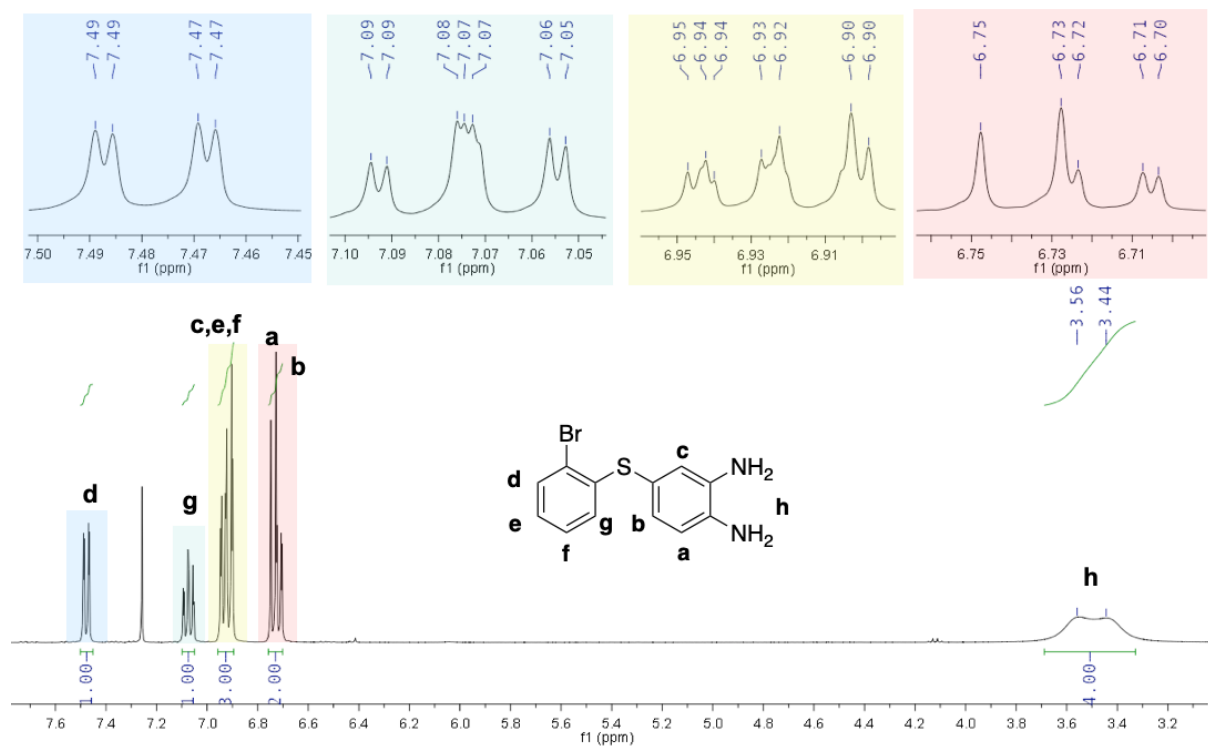


Figure 1C – ¹H NMR - Final Ring Closure Product

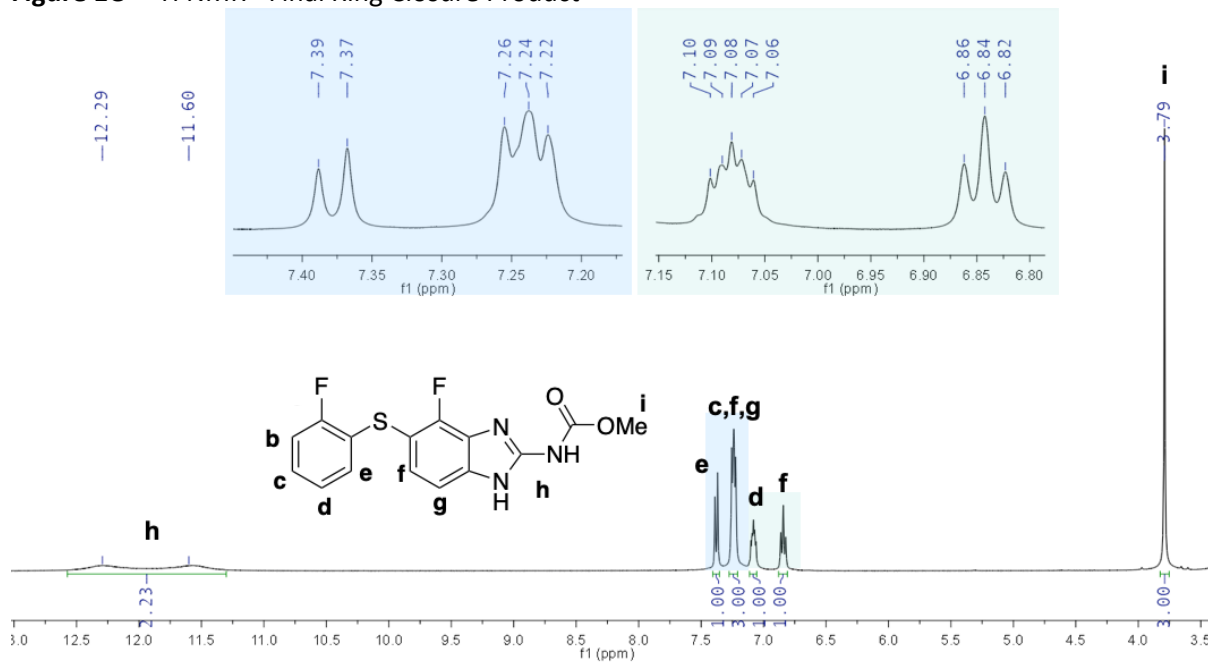


Figure 1D – ¹³C NMR

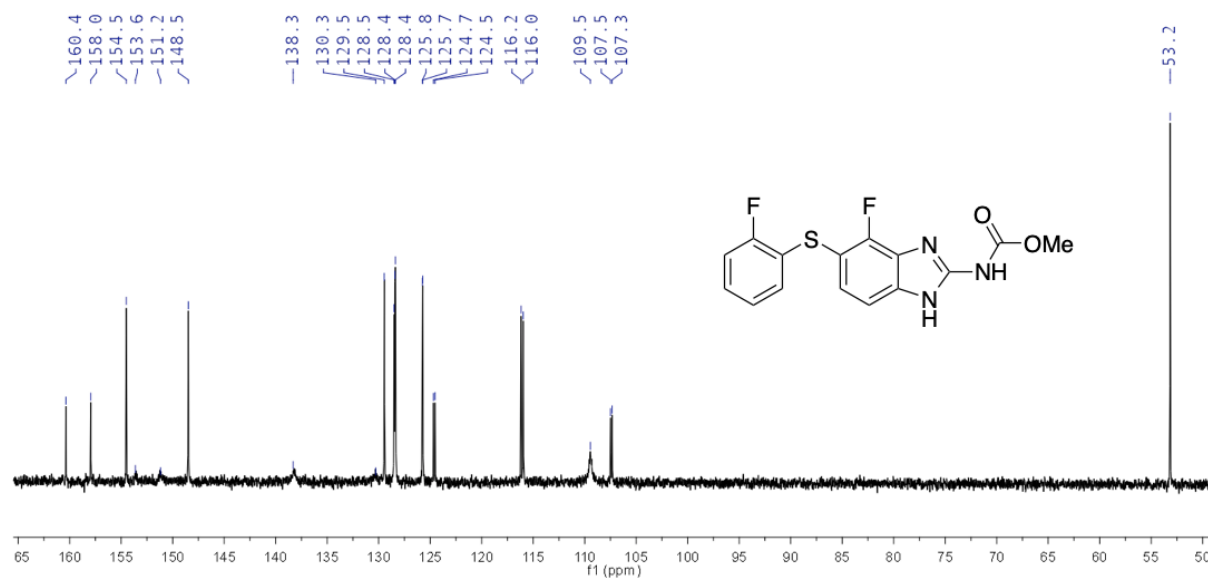
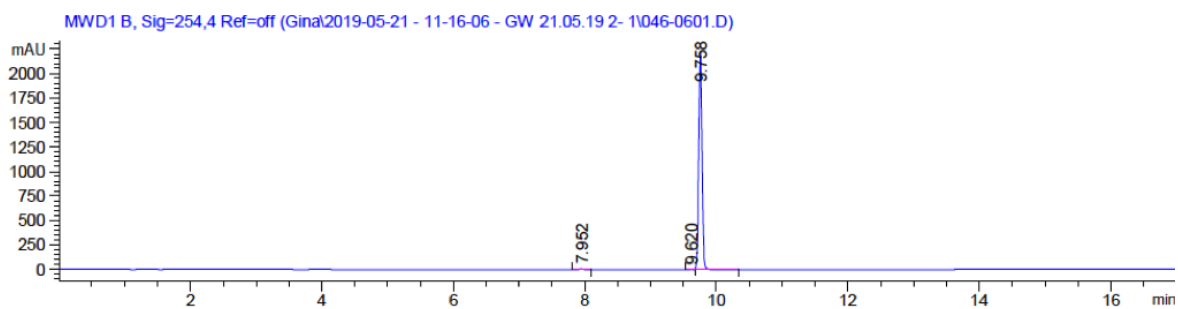


Figure 1E – Example Thioether HPLC



2. Ether Data

Figure 2A – ^1H NMR - $\text{S}_{\text{N}}\text{Ar}$ Nitroaniline Example

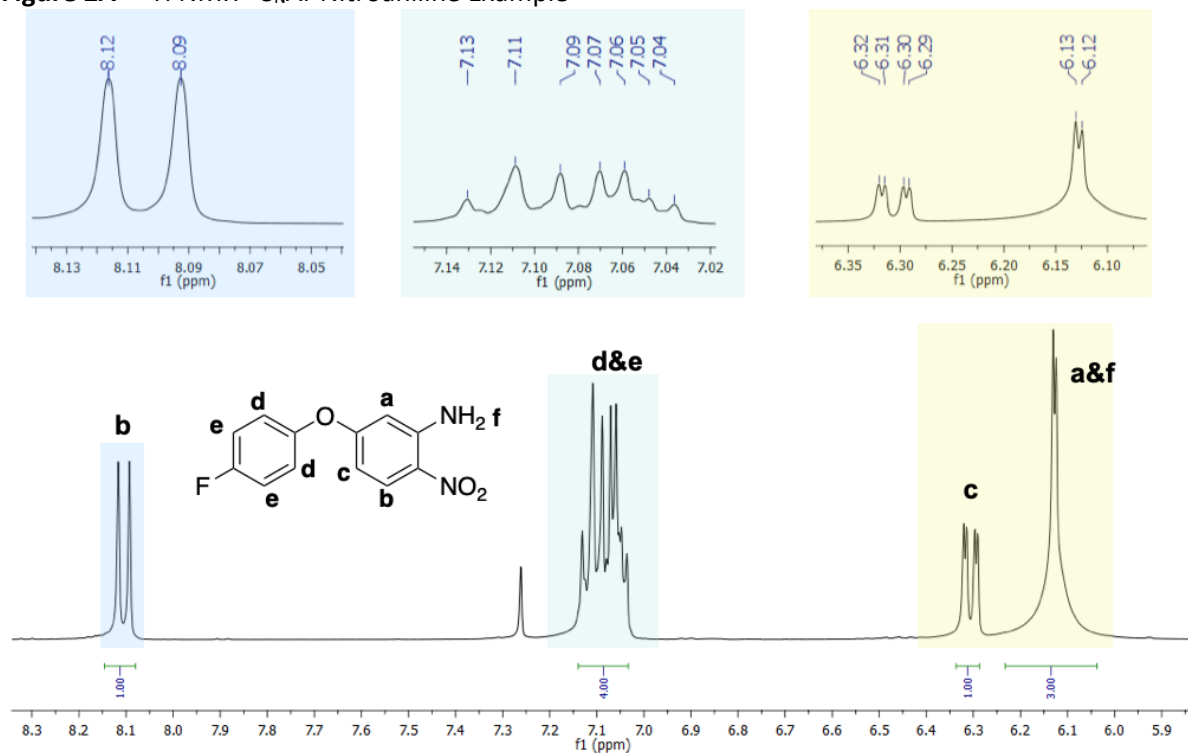


Figure 2B - ^1H NMR - SnCl_2 Reduction Example

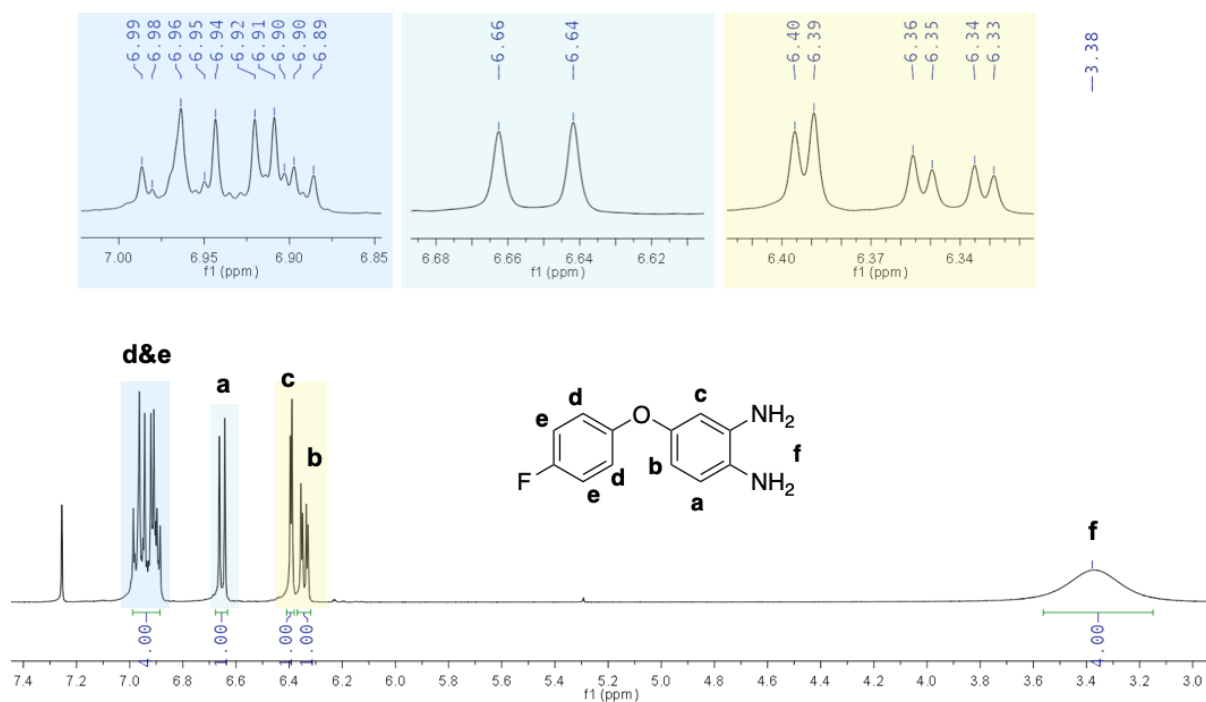


Figure 2C – ^1H NMR - Final Ring Closure Product

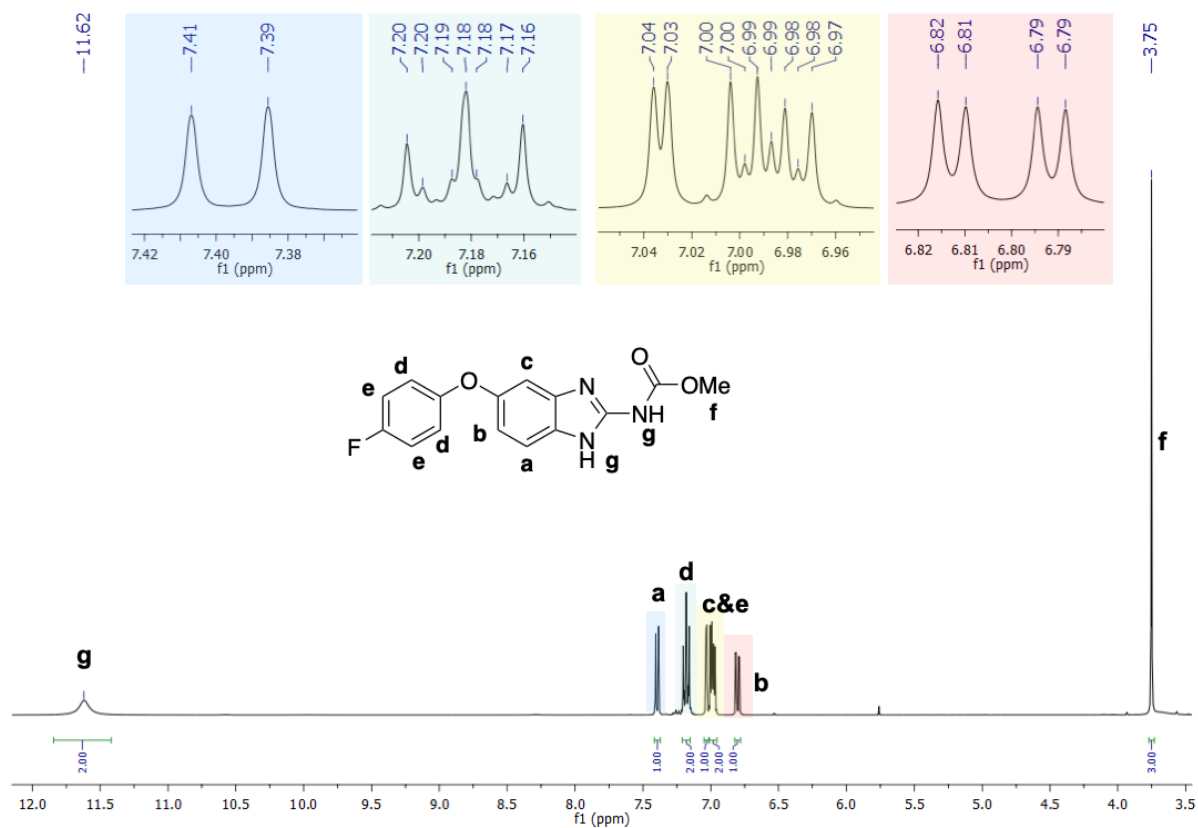


Figure 2D – ^{13}C NMR

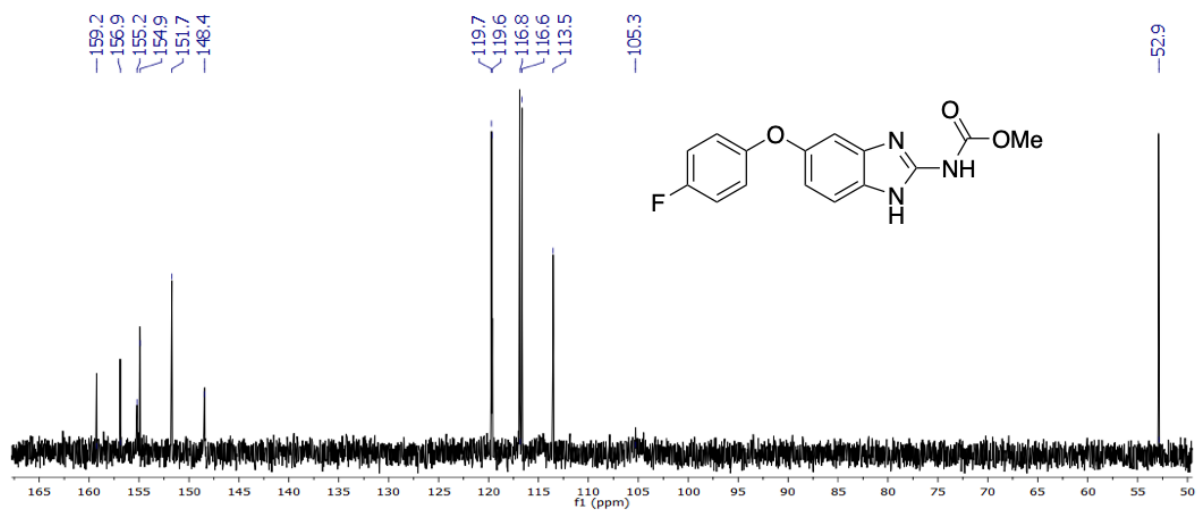
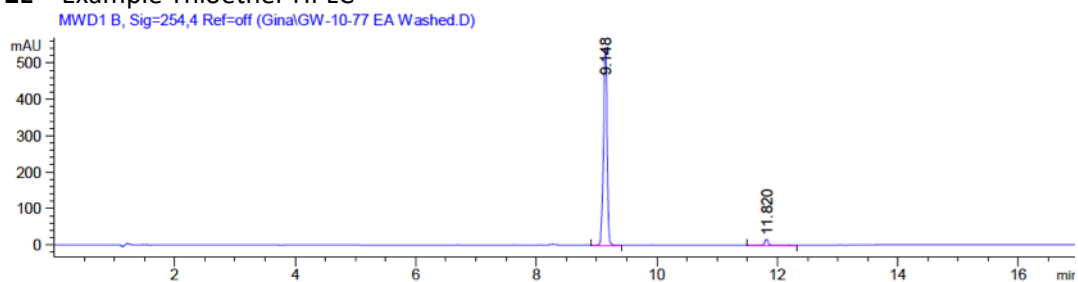


Figure 2E – Example Thioether HPLC



3. Morpholine Derivatives

Figure 3A – Morpholine Nucleophilic Substitution Product ^1H NMR

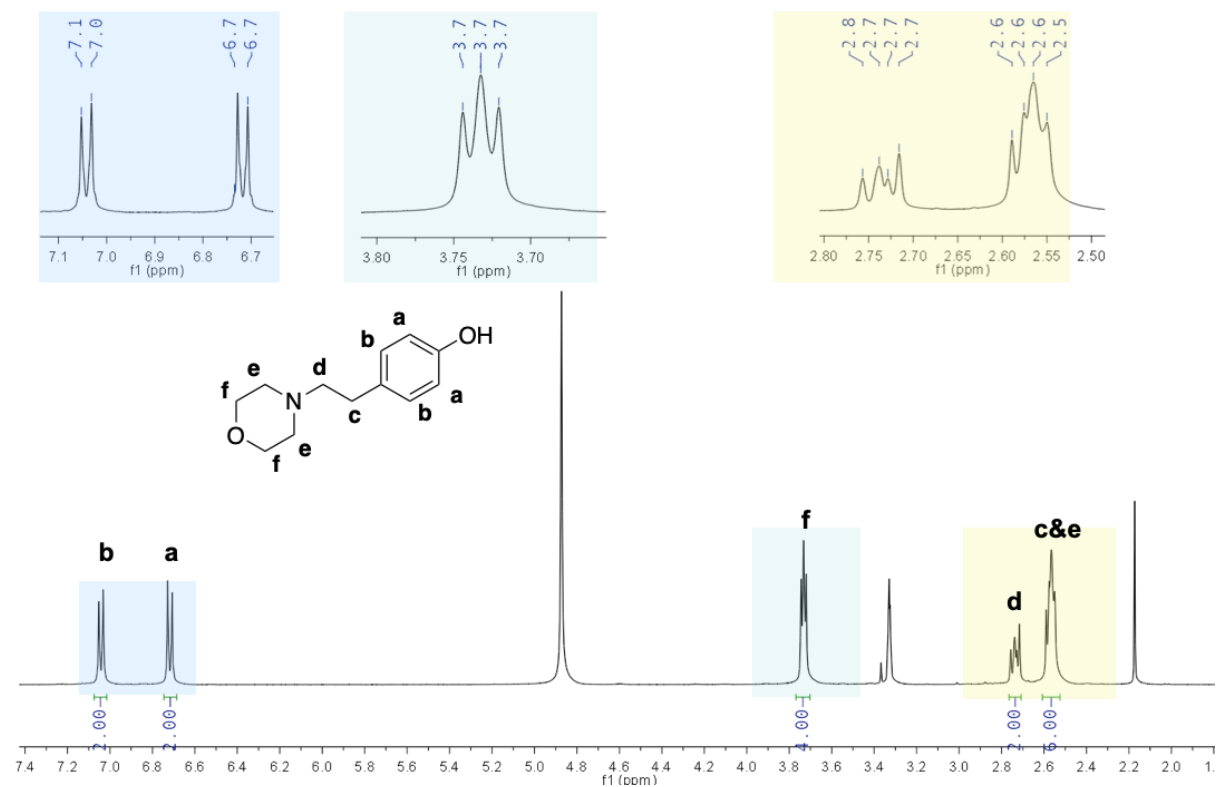


Figure 3B – Morpholine Aromatic Substitution Product ^1H NMR

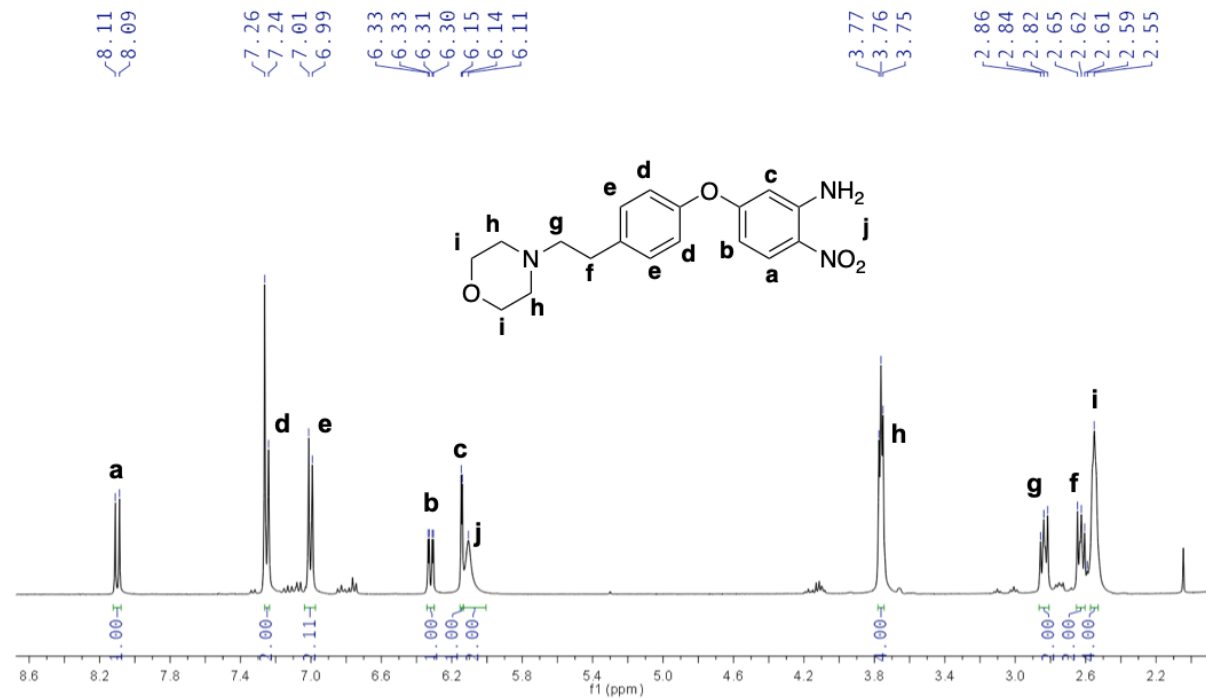


Figure 3C – Morpholine Tin (II) Chloride Product ¹H NMR

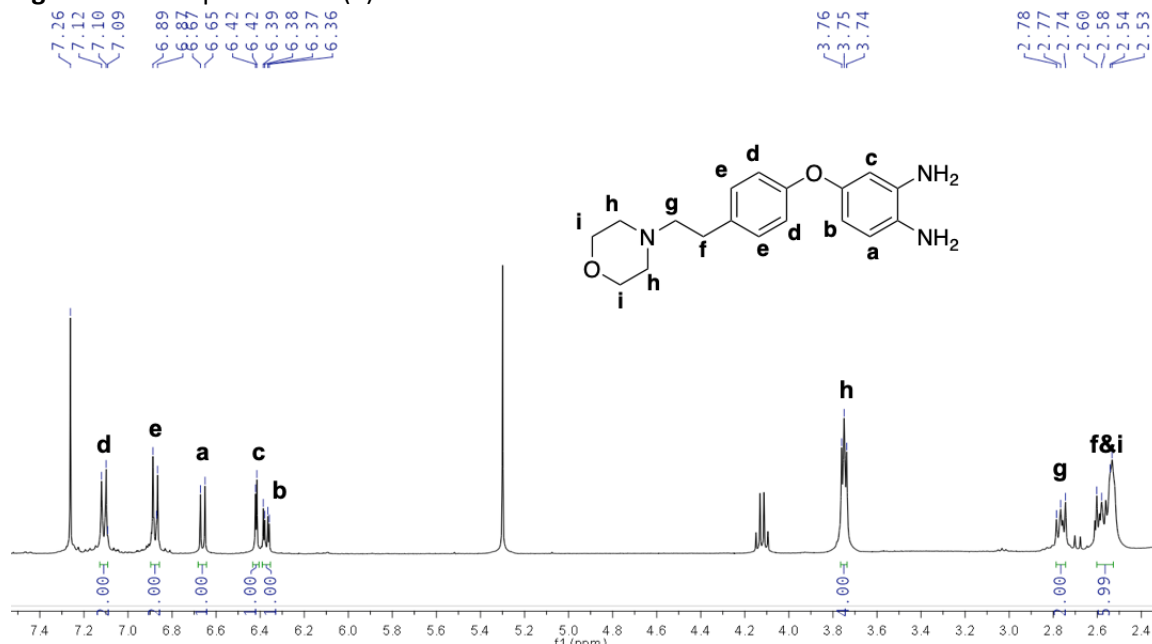


Figure 3D – Morpholine Ring Closure Product ¹H NMR

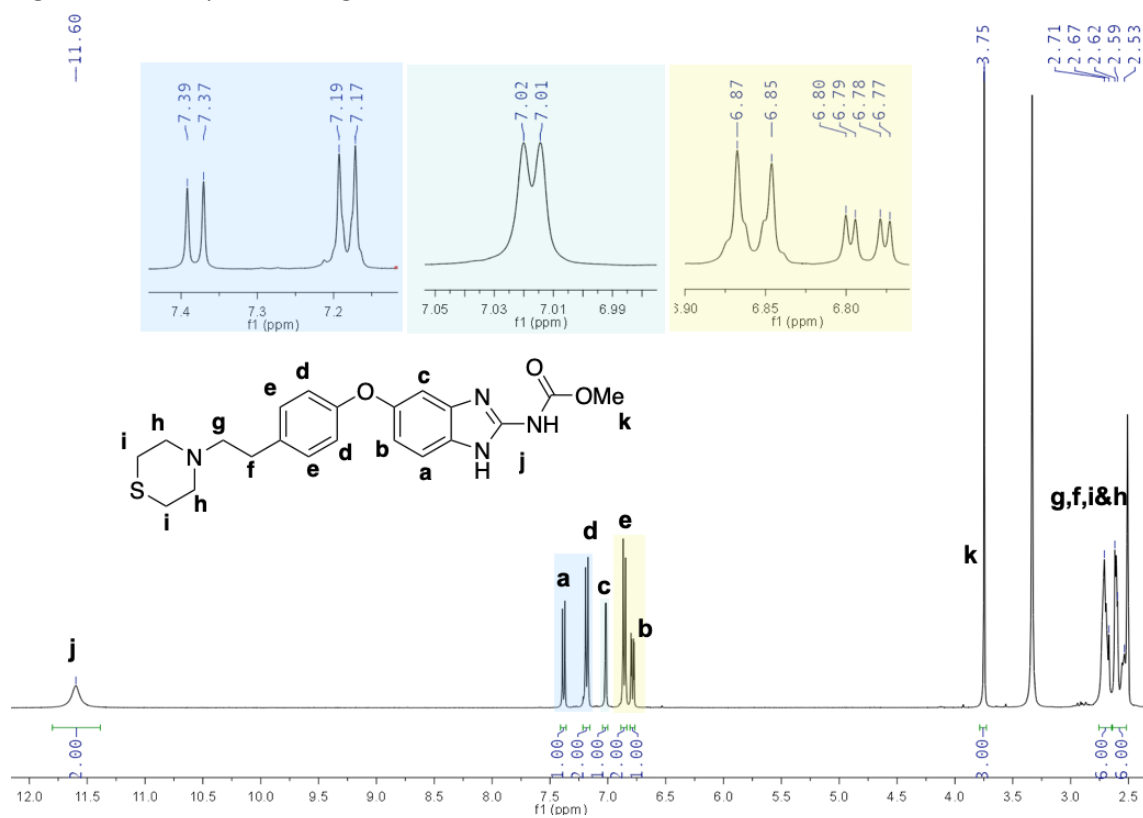


Figure 3E – Morpholine Ring Closure Product ¹H NMR

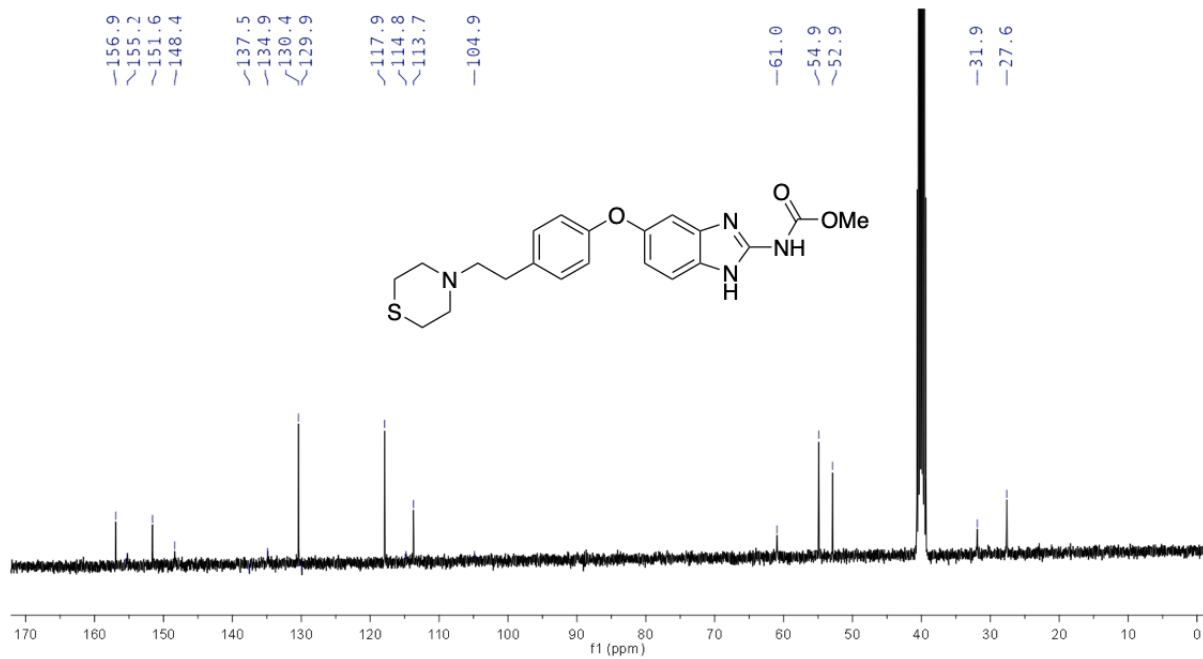
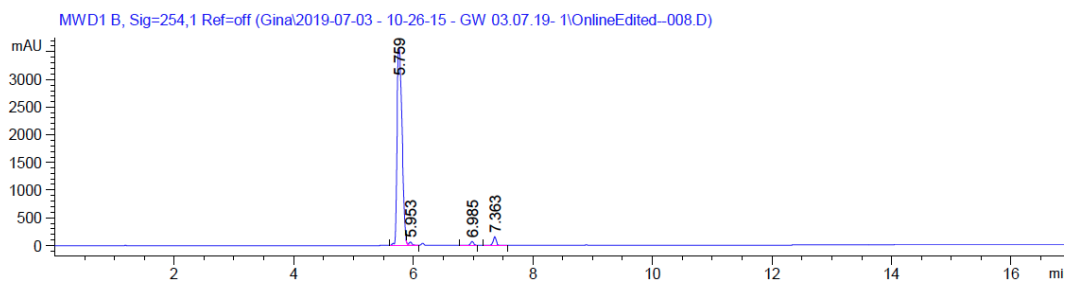


Figure 3F – Morpholine Final HPLC



4. Ketones

Figure 4A – ^1H NMR – Ketone Suzuki Example

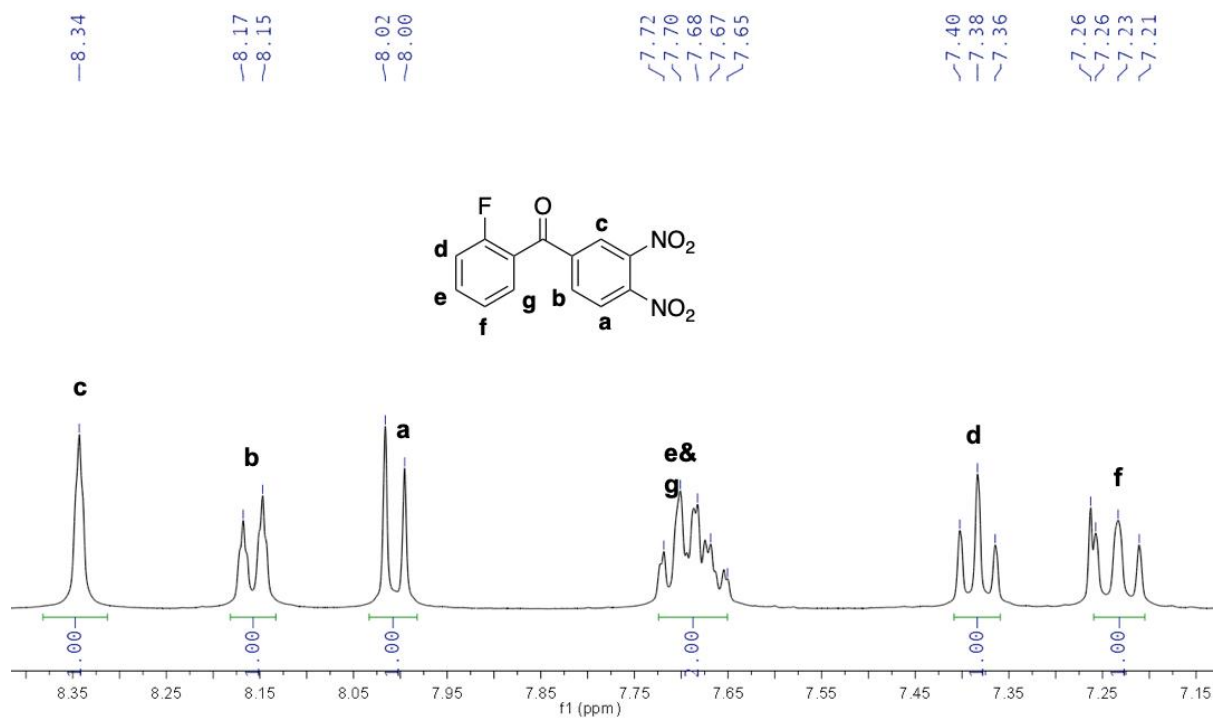


Figure 4B - ^1H NMR - SnCl_2 Reduction Example

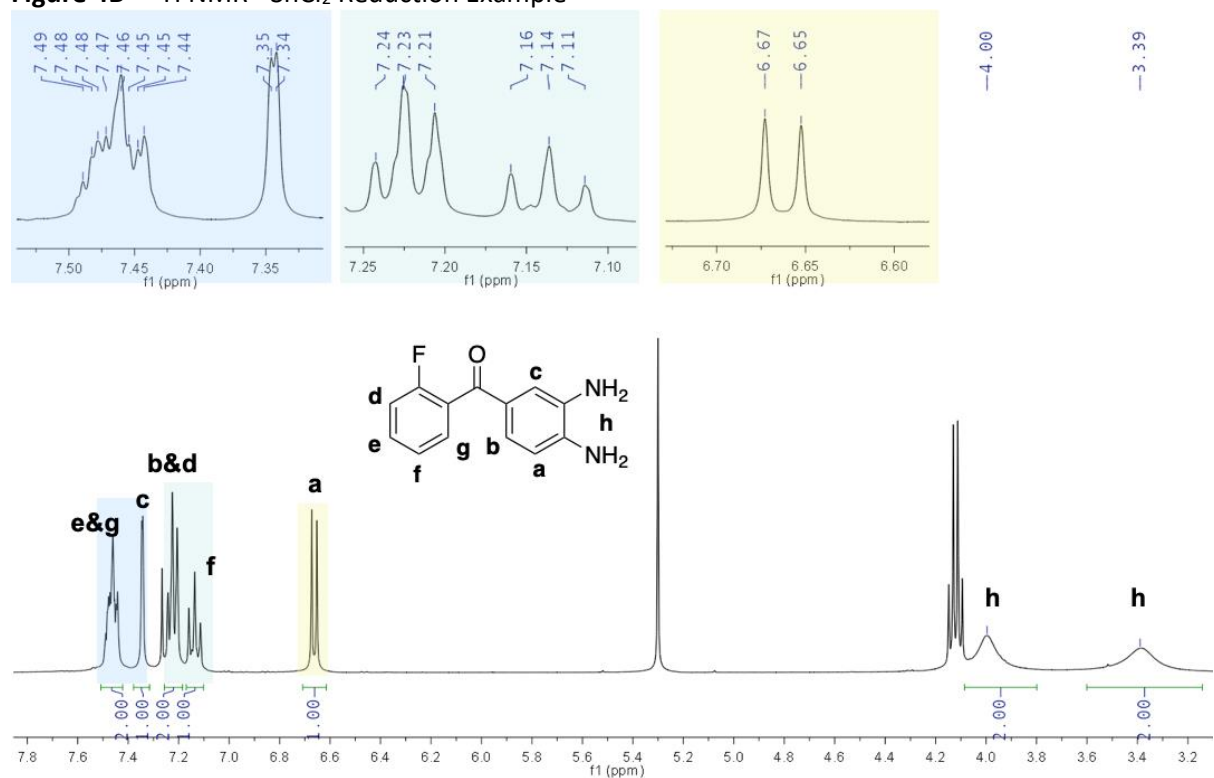


Figure 4C – ¹H NMR - Final Ring Closure Product

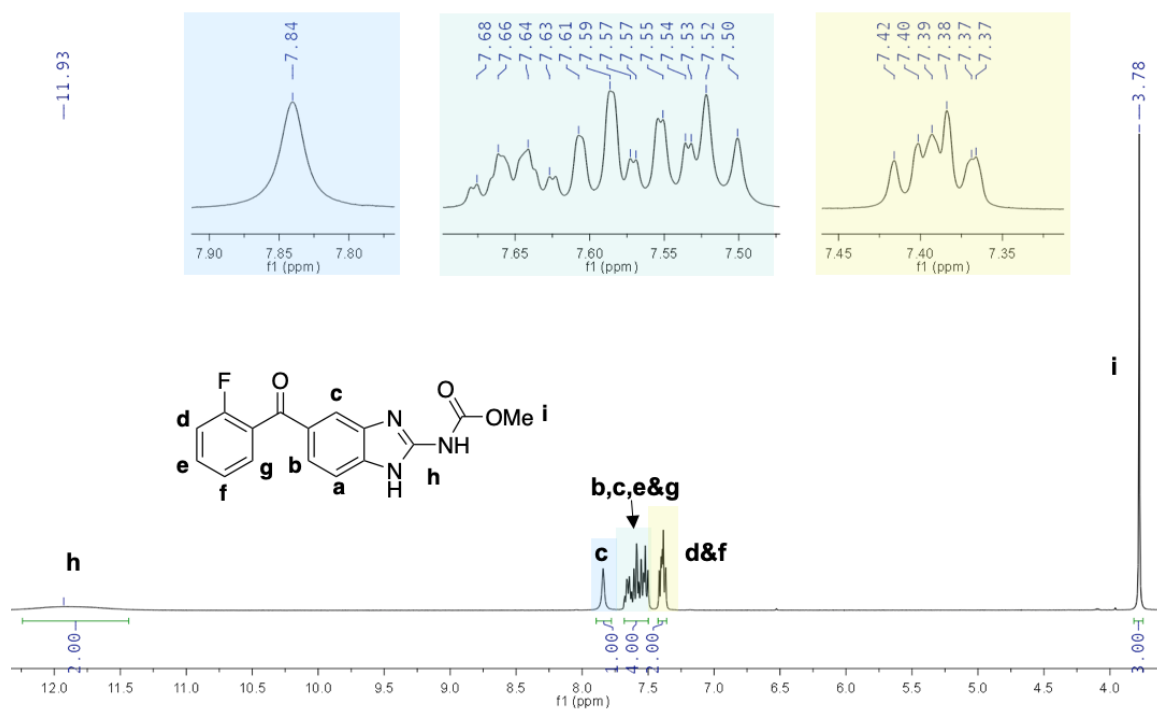


Figure 4D – ¹³C NMR

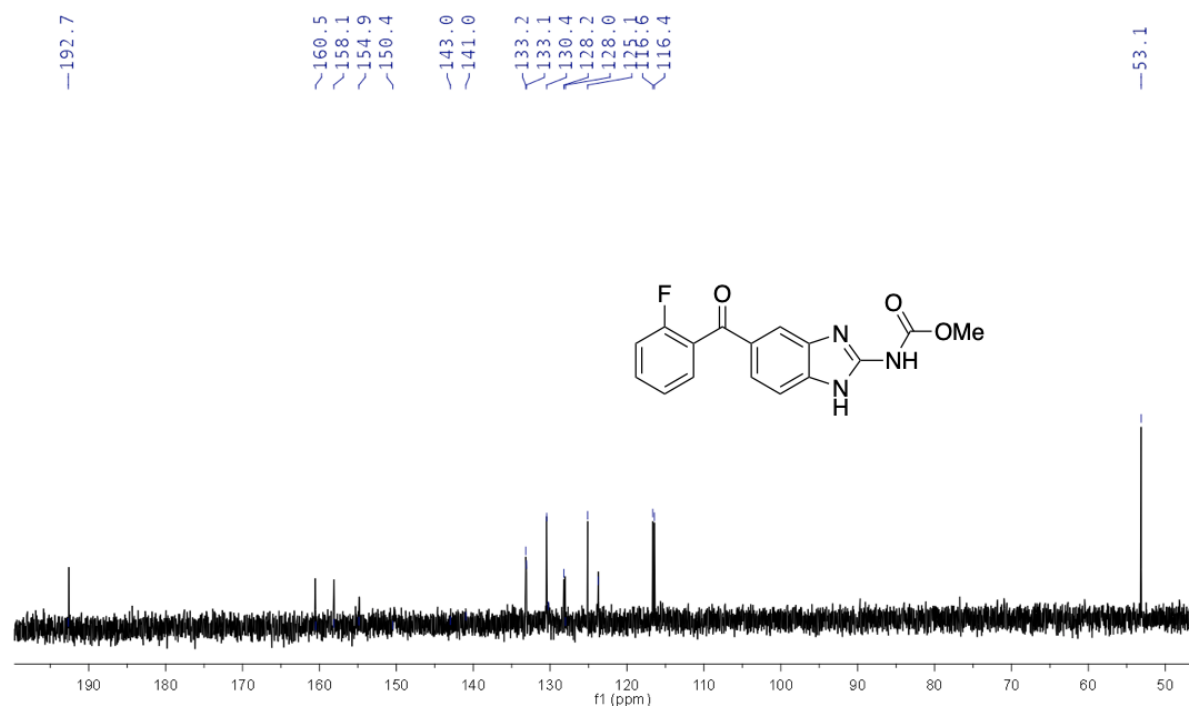
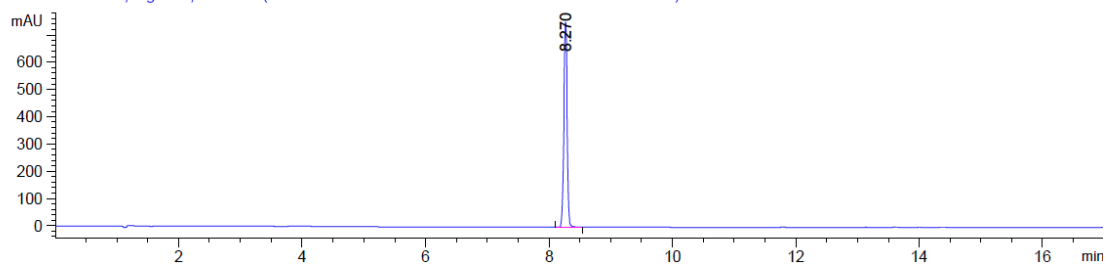


Figure 4E – Example Ketone HPLC

MWD1 B, Sig=254,4 Ref=off (Gina2019-04-11 - 13-28-59 - GW 10.04.19 - 1\045-0201.D)



5. Biphenyl Derivatives

Figure 5A – ^1H NMR – Suzuki Example

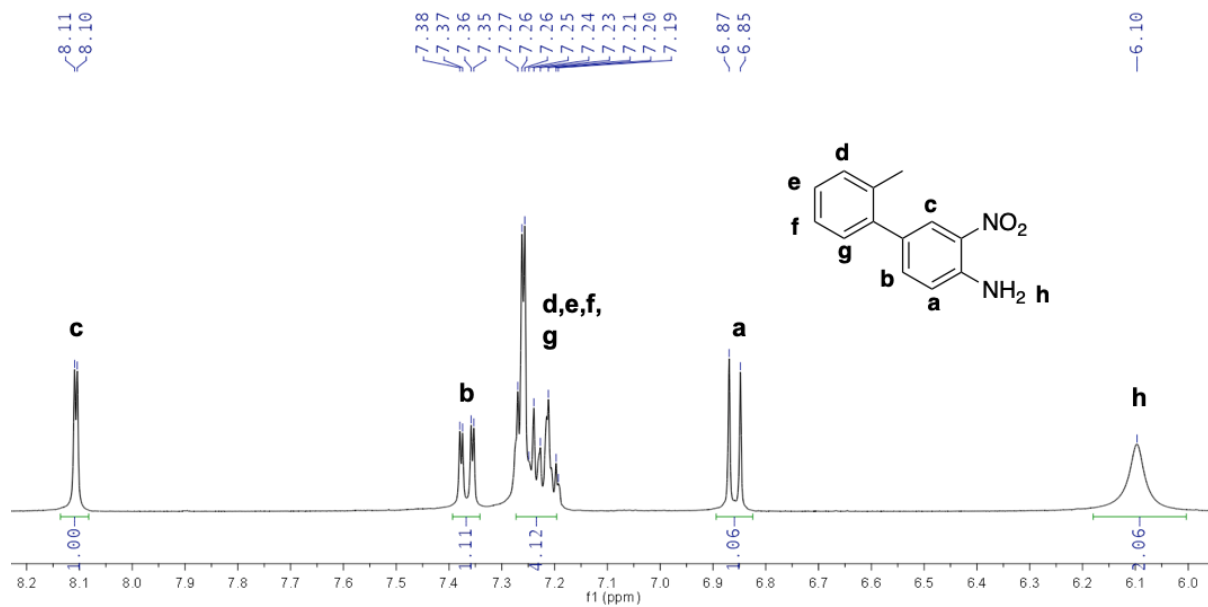


Figure 5B – ^1H NMR - SnCl_2 Reduction Example

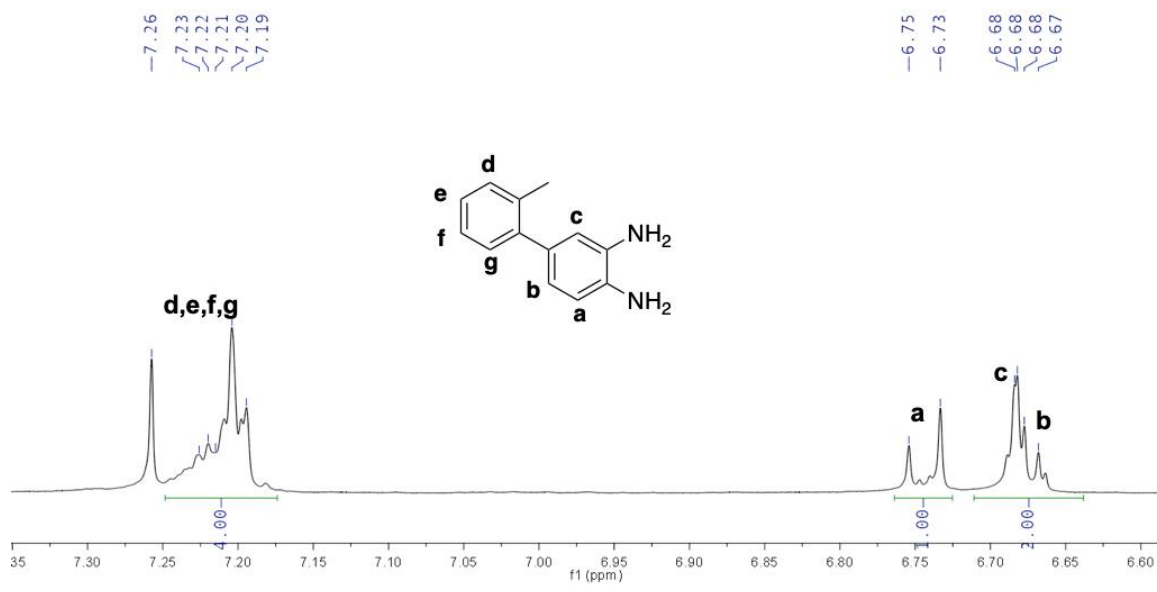


Figure 5C – ¹H NMR - Final Ring Closure Product

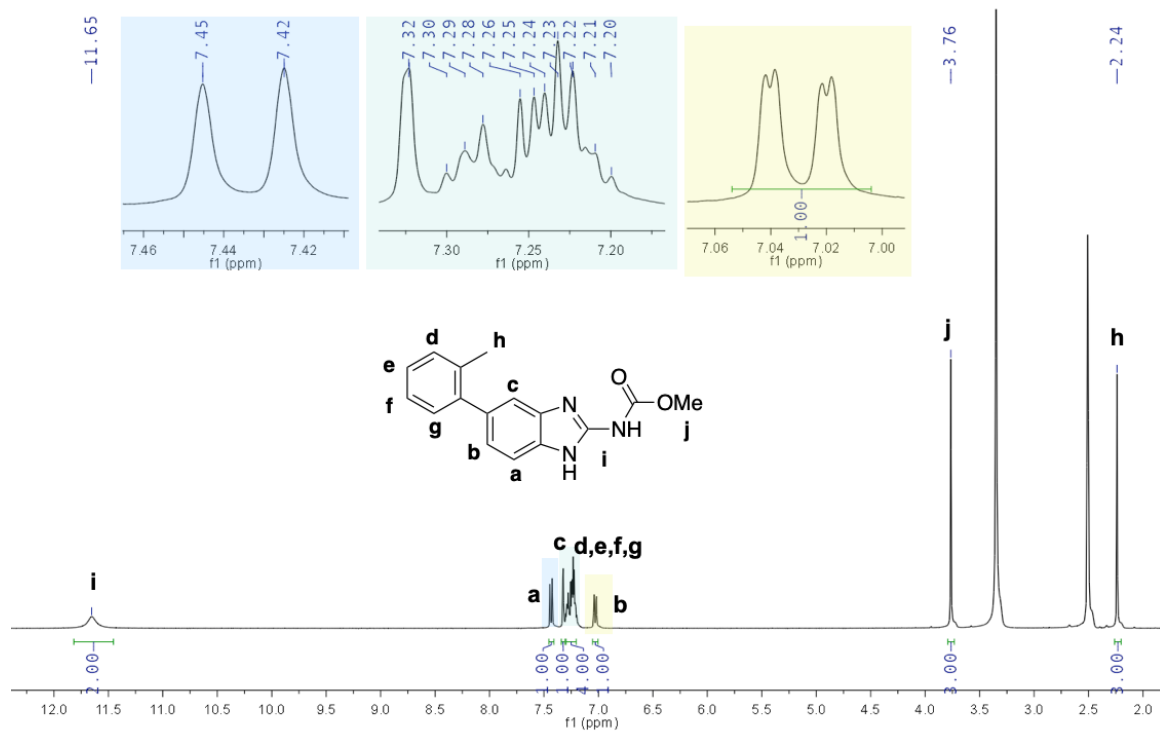


Figure 5D – ¹³C NMR

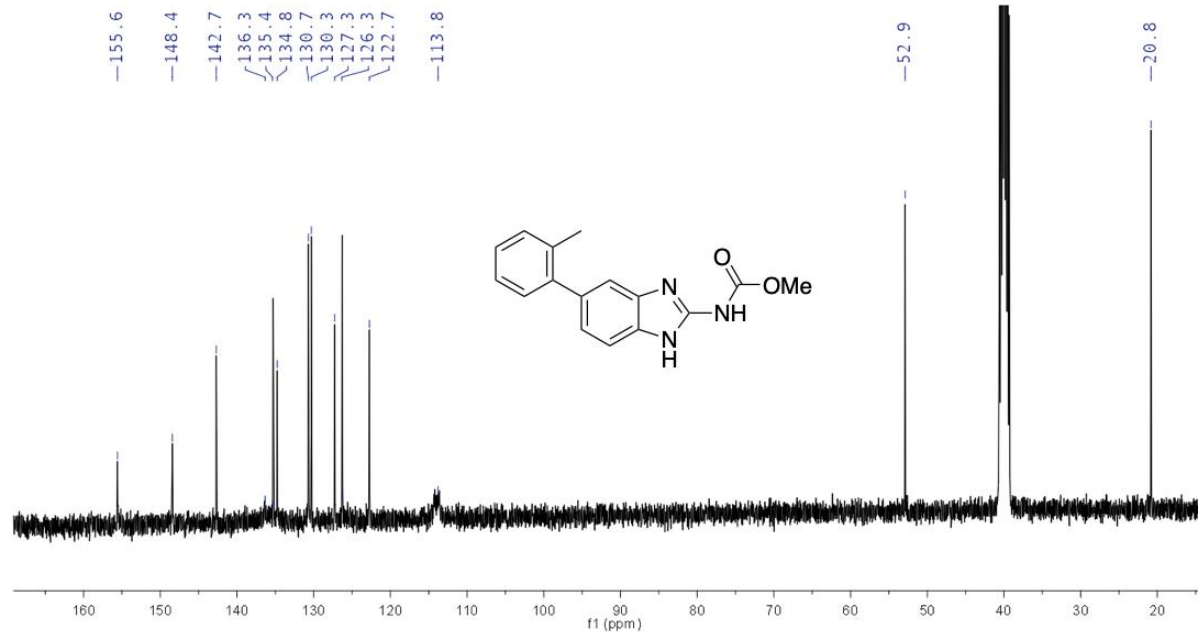
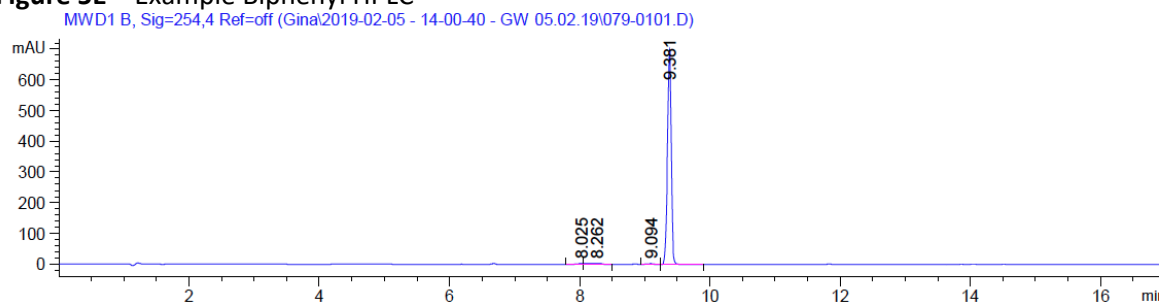


Figure 5E – Example Biphenyl HPLC



6. Benzisothiazolinones

Figure 6A – BIZT Core Amide ^1H NMR Example

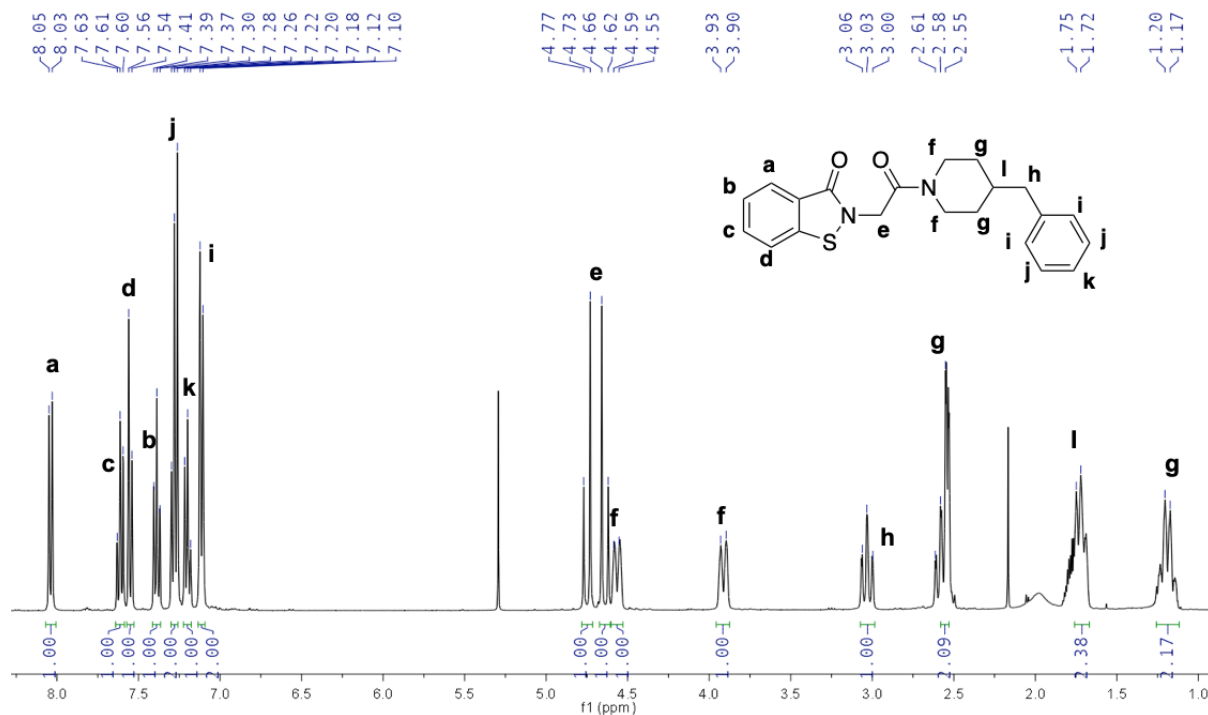


Figure 6B – BIZT Core Amide ^{13}C NMR Example

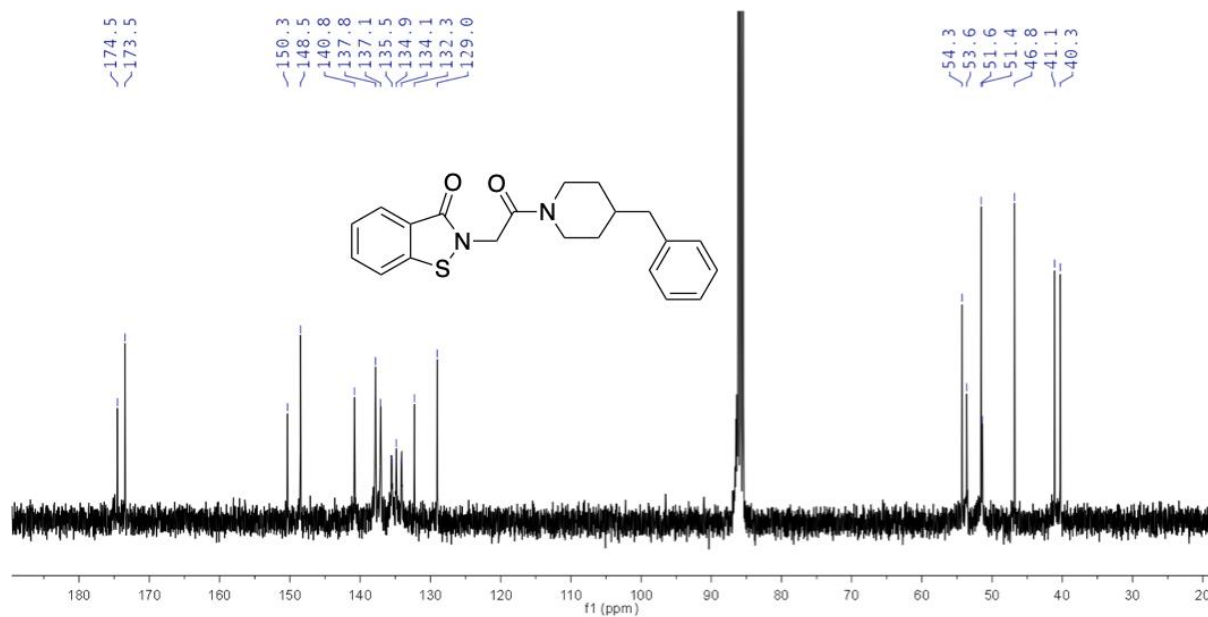


Figure 6C – BIZT Core Alternative C=O ¹H NMR Example

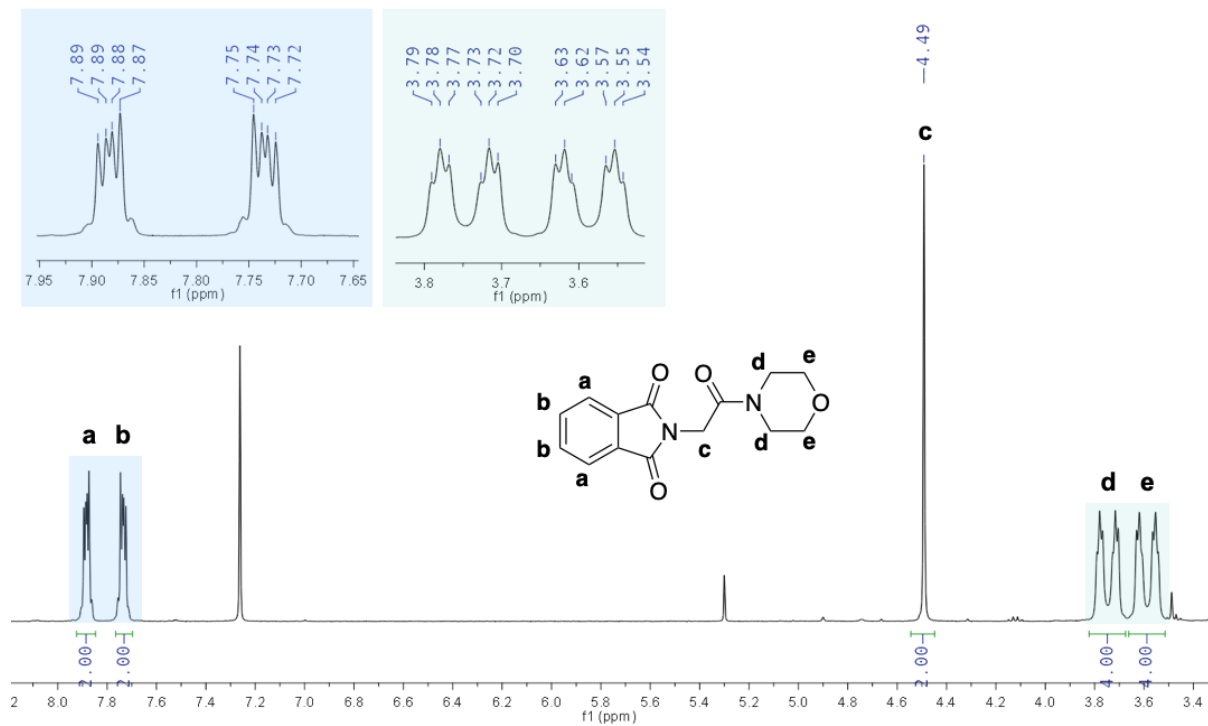


Figure 6D – BIZT Core Alternative C=O ¹³C NMR Example

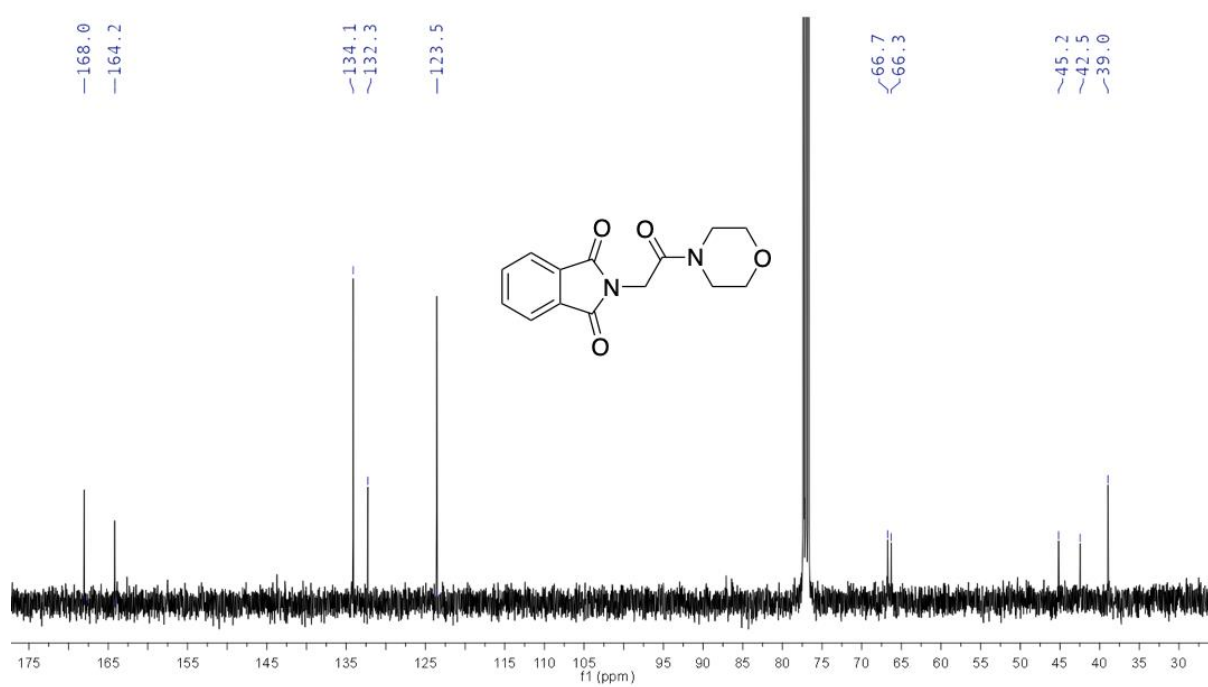


Figure 6E – BIZT Core Alternative CH₂ ¹H NMR Example

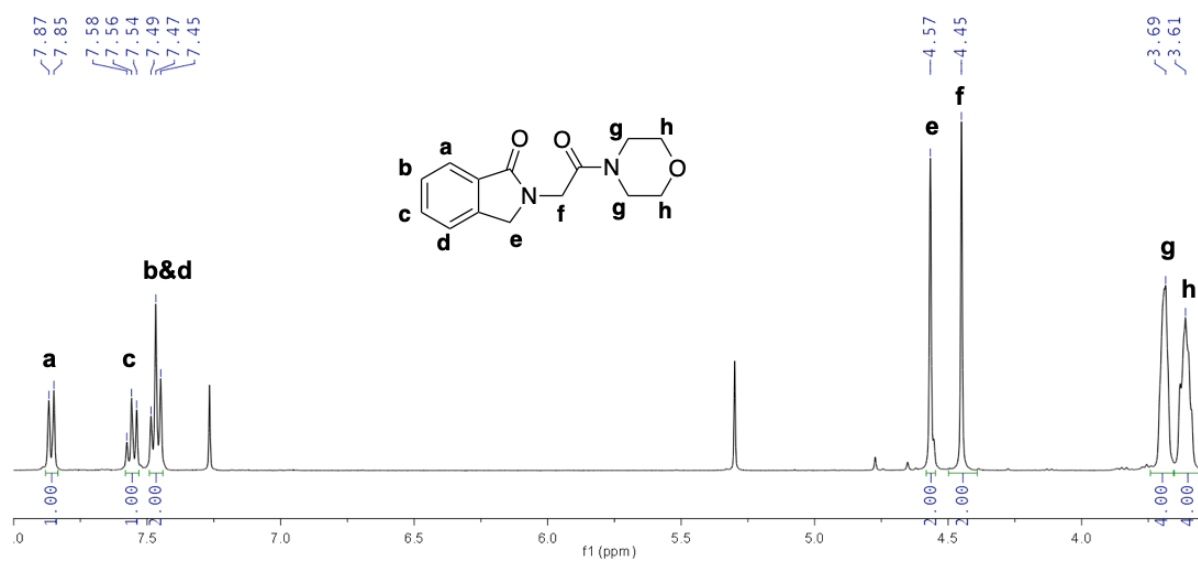
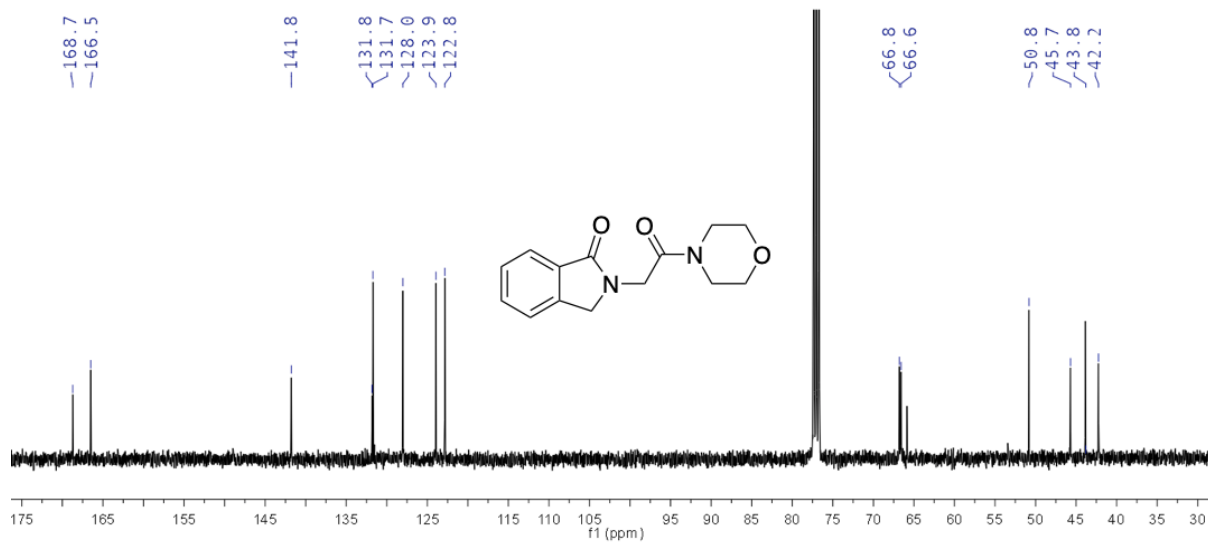


Figure 6F – BIZT Core Alternative CH₂ ¹³C NMR Example



7. Benzoxaborole Data

Figure 7A – Nucleophilic Aromatic Substitution ¹H NMR

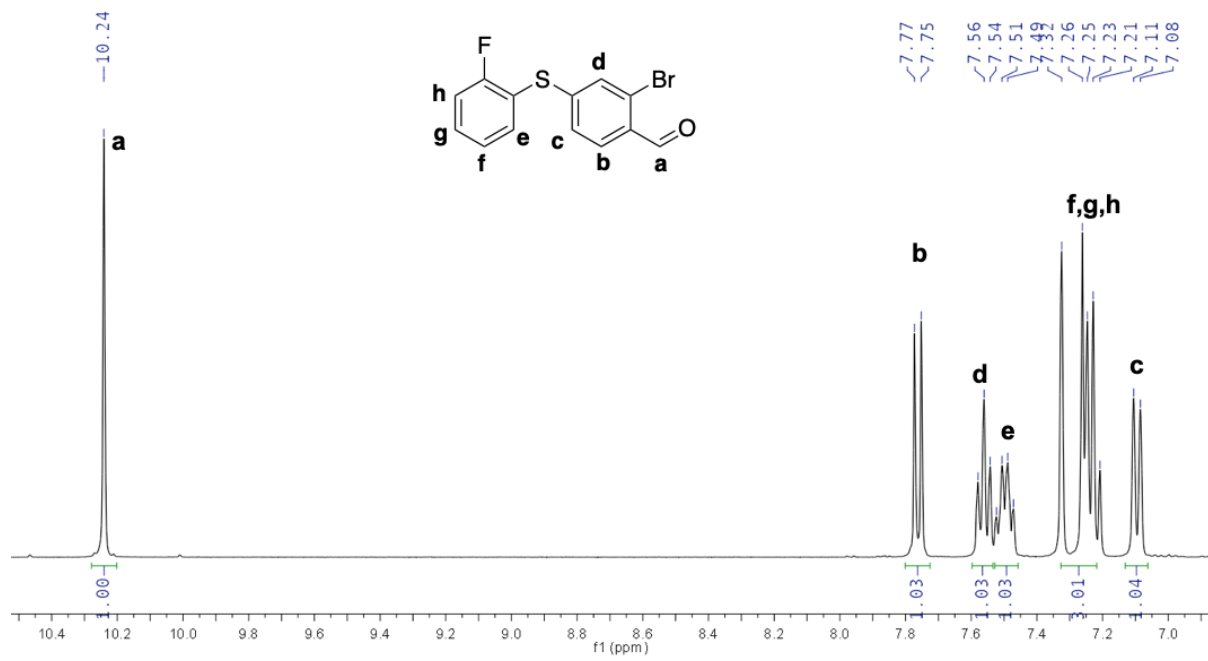


Figure 7B – Reduction ¹H NMR

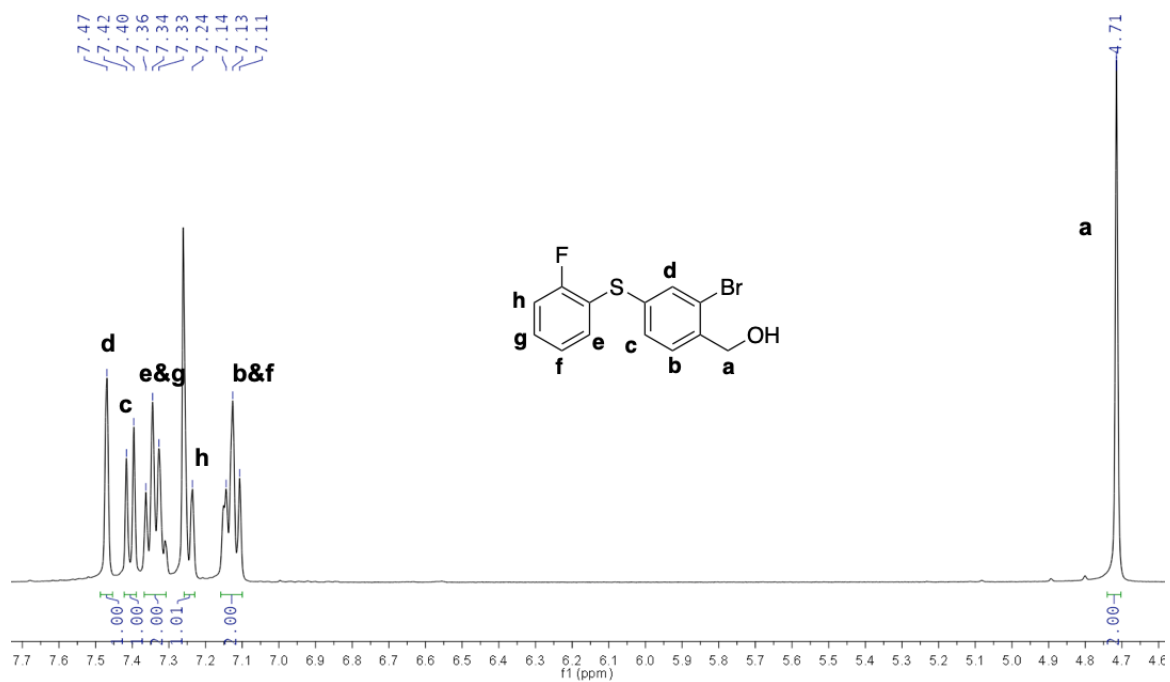


Figure 7C – Boc Protection ^1H NMR

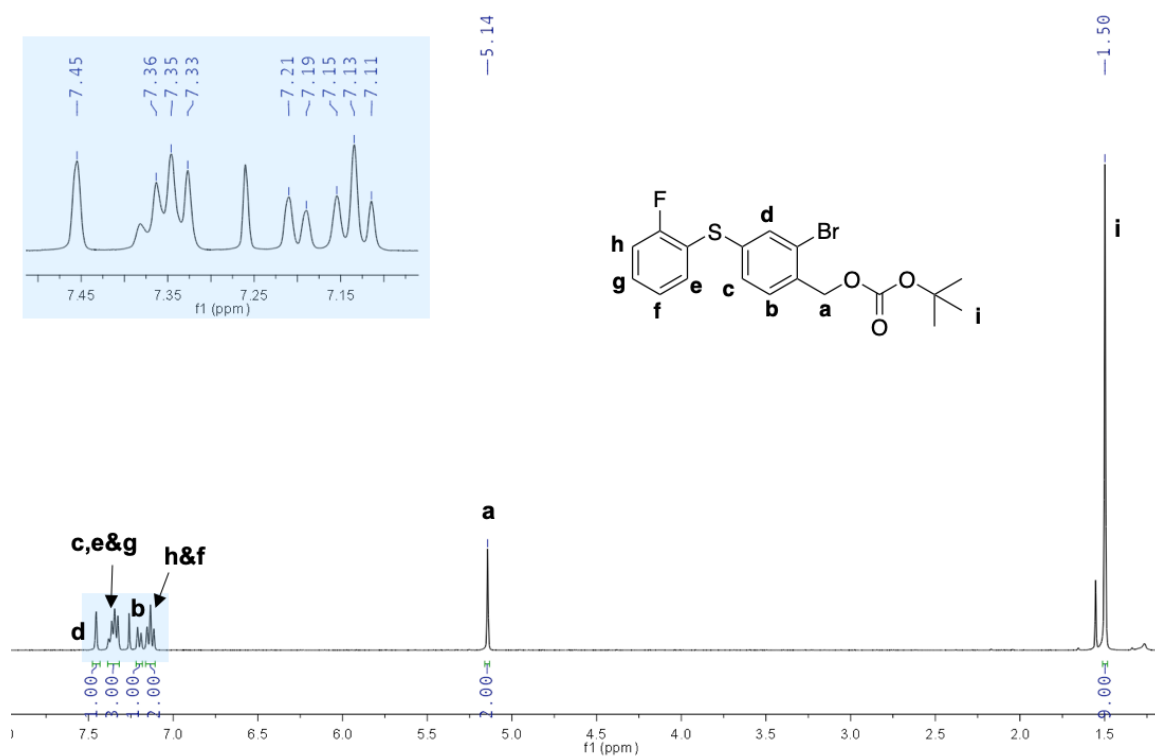


Figure 7D – Borylation ^1H NMR

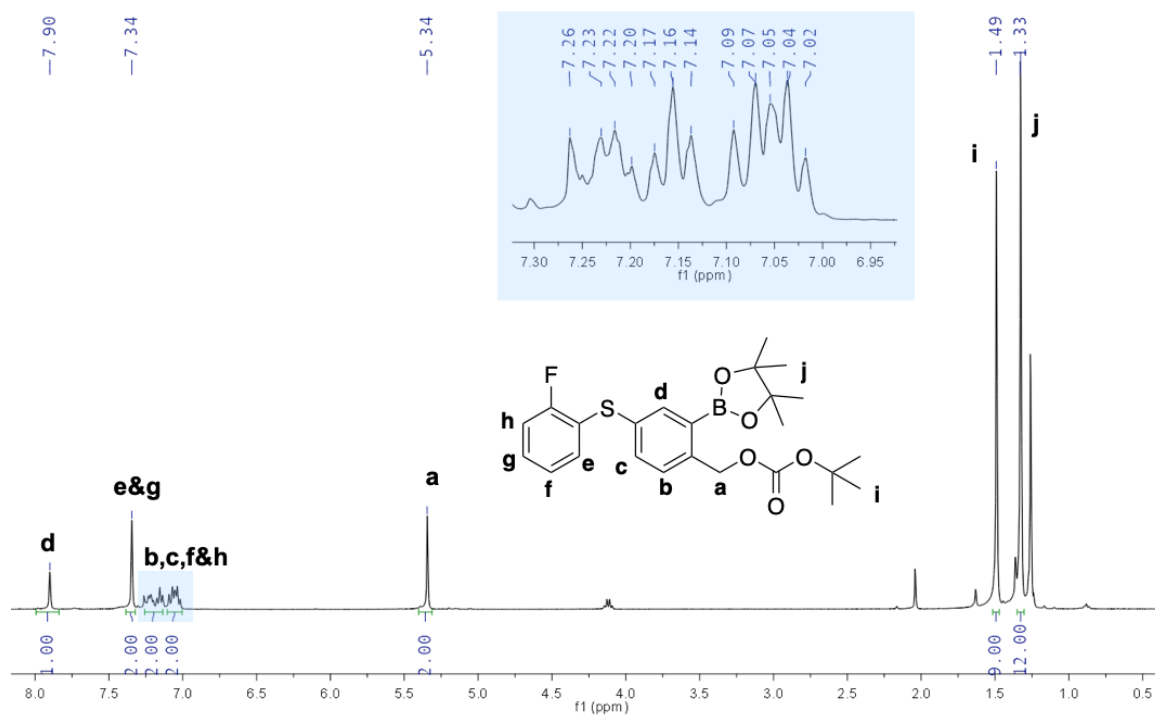


Figure 7E – Ring Closure ¹H NMR

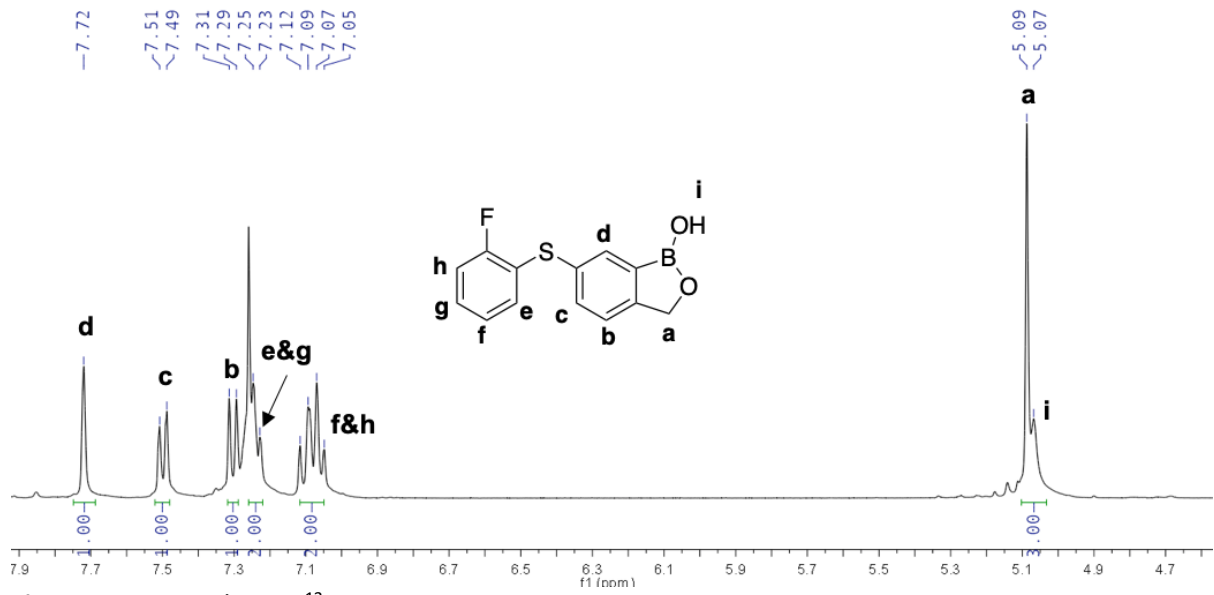


Figure 7F – Ring Closure ¹³C NMR

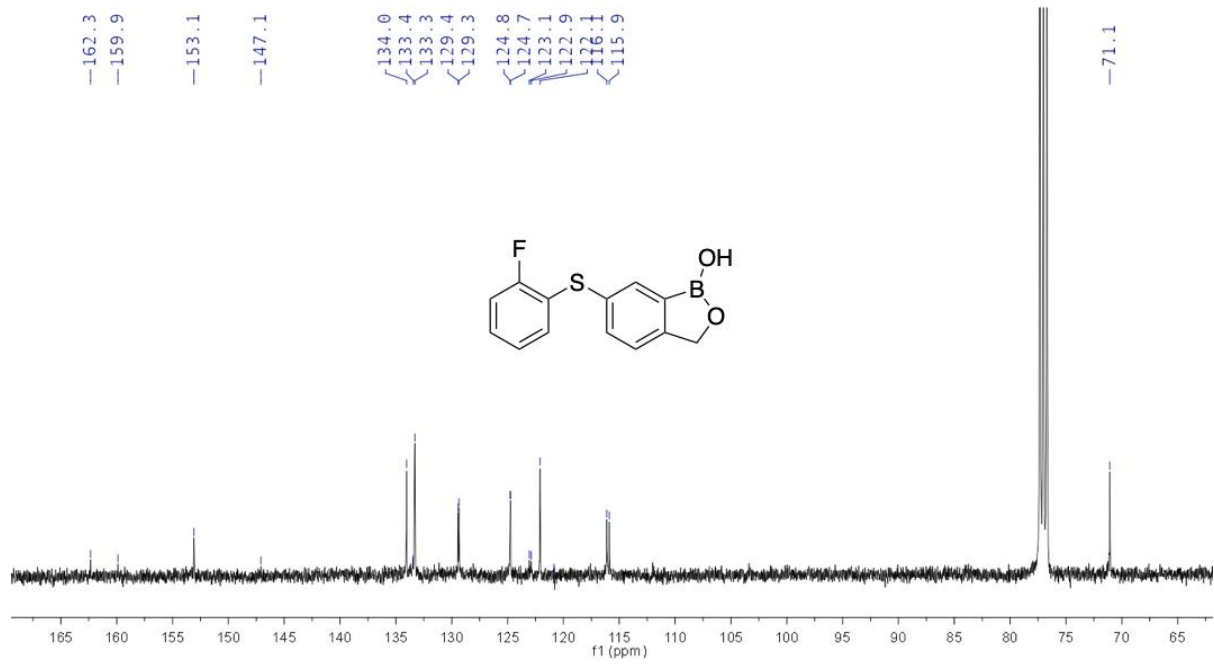


Figure 7G – Example HPLC

